Externally Venting Flames (EVF) dynamics and development in non-orthogonal geometries

by

Anoop Subramania Warrier

A thesis submitted in partial fulfilment for the requirements for the degree of Doctor of Philosophy at the University of Lancashire

November 2025

RESEARCH STUDENT DECLARATION FORM

Type of Award Doctor of Philosophy

School School of Engineering and Computing

1. Concurrent registration for two or more academic awards

I declare that while registered as a candidate for the research degree, I have not been a registered candidate or enrolled student for another award of the University or other academic or professional institution

2. Material submitted for another award

I declare that no material contained in the thesis has been used in any other submission for an academic award and is solely my own work

3. Collaboration

Where a candidate's research programme is part of a collaborative project, the thesis must indicate in addition clearly the candidate's individual contribution and the extent of the collaboration. Please state below:

4. Use of a Proof-reader

No proof-reading service was used in the compilation of this thesis.

Signature of Candidate

Print name: Anoop Subramania Warrier

Abstract

The building industry is increasingly favouring green building initiatives resulting in increased use of different façade materials and systems, including materials with combustible characteristics, to meet stringent energy standards. This trend has highlighted the need to address the evolving fire safety challenges associated with modern and sustainable buildings. Particularly in high-rise buildings exterior fire spread and heat transfer caused by Externally Venting Flames (EVF) pose significant challenges as evidenced by the increased number of façade fire incidents worldwide. This present work aims to progress the current state of the art by investigating EVF characteristics and development in non-orthogonal curvilinear geometries. A database of recent façade fire incidents based on type of geometries was developed, indicating that curvilinear and/or nonorthogonal structures were involved in 43% of the reported fires. An experimental investigation was conducted to examine the effects of forced draught conditions on fully developed mediumscale rectilinear and curvilinear compartment with an emphasis on EVF behaviour. Aiming at better understanding the effect of wind on fire and EVF dynamics under different ventilation conditions a parametric study has been performed investigating the influence of wind with different fire compartment opening dimensions. Experimental results indicate that in forced draught conditions there is less thermal impact on a façade wall as the wind forces EVF outward increasing its projection and decreasing its height. A complementary numerical investigation using computational fluid dynamics (CFD) was performed in curvilinear and orthogonal geometries to identify key factors influencing EVF development and their impact on the façade. A parametric study was undertaken by altering the geometry (curvilinear, rectilinear, and number of openings), ventilation conditions, and heat release rate. Sixteen different fire scenarios have been considered to investigate the accuracy of currently available empirical correlations in predicting EVF characteristics. Additionally, velocity, temperature and oxygen concentration spatial distributions were analysed in the interior and exterior of the fire compartment. Numerical results enabled assessing EVF development indicating that geometry, ventilation conditions and fire load may significantly affect fire characteristics and impact on the facade. This work provides a deeper insight into how EVF is influenced by façade design and environmental conditions advancing current understanding of EVF in the context of curvilinear non-orthogonal façade geometries. The research findings contribute to improved fire risk assessment and could potentially inform future fire safety design practices and guidelines.

Keywords: Externally venting flames; façade fire; flame spread; complex geometries; modelling; CFD.

Contents

Resear	rch Student Declaration Form	Error! Bookmark not defined.
Abstra	ict	V
Conter	nts	vii
Author	r's List of Achievements, Publications, and Submissions	xiii
Ackno	wledgements	XV
List of	Figures	xvii
List of	f Tables	xxvi
Abbre	viations	xxviii
Nome	nclature	xxx
1 IN	NTRODUCTION	1
1.1	Externally Venting Flames (EVF)	1
1.2	Façade fire incident database	2
1.3	Regulatory framework	5
1.4	Aims and Objectives of the project	6
1.5	Structure of the Thesis	7
2 L	ITERATURE REVIEW	12
2.1	Major past studies and research on EVF	12
2.2	Enclosure Fire Dynamics	20
2.3	Effect of Ventilation	21
2.	.3.1 Fuel controlled versus Ventilation controlled Fire	21
2.	.3.2 Forced Draught and No Forced Draught	22
2.	.3.3 The influence of Wind or Forced Draught on Exte	ernally Venting Flame22
2.4	The effect of building characteristics	25
2.	.4.1 Opening Characteristics	26
2.	.4.2 Architectural features and their influence on EVF	29
2.5	Concluding remarks	33

		D DRAUGHT IMPACT ON EXTERNALLY VENTING FLAMES:	
EXPER	IMEN	TAL AND NUMERICAL INVESTIGATION	36
3.1	Intro	oduction	36
3.2	Exp	erimental and Numerical Investigation	36
3.2	.1	Experimental setup	36
3.3	Nun	nerical setup	43
3.3	.1	Computational Domain	44
3.3	.2	Grid independence	45
3.3	.3	Turbulence model	46
3.3	.4	Validation of Numerical Simulation	47
3.4	Res	ult and Discussion	49
3.4	.1	Effect of opening size on EVF thermal characteristics	49
3.4	2	Effect of opening size on the façade	54
3.4	.3	Developed thermal field	55
3.4	.4	Effect of wind velocity on EVF development	56
3.4	.5	Oxygen Concentration	60
3.5	Con	clusions	61
4 EF	FECT	S OF BUILDING FEATURES ON THE DEVELOPMENT OF EXTERNAL	LLY
VENTI		FLAMES: EXPERIMENTAL AND NUMERICAL INVESTIGATION	
RECTII		AR AND CURVED GEOMETRIES	
4.1	Intro	oduction	64
4.2	Exp	erimental and Numerical Investigation	65
4.2	1	Experimental Setup	65
4.2	2	Sensors and data acquisition system	66
4.2	3	Experimental Test Scenarios	67
4.2	.4	Repeatability Study	68
4.2	5	Numerical Simulation Details	69
4.3	Effe	ect of material on compartment fire development	76

4.4	Е	xperimental Investigation: Results and Discussion	78
4.	4.1	Fuel mass loss	78
4.	4.2	Air supply rate and Global Equivalence ratio	82
4.	4.3	Thermal characteristics	85
4.	4.4	Heat flux at the façade surface	93
4.5	C	omparison of Indoor versus Outdoor experiments	95
4.6	C	onclusions from experimental investigations	97
4.7	N	fumerical investigation: Results and Discussion	98
4.	7.1	Effect of geometry on fire development and EVF	98
	a.	Compartment gas temperature	99
	b.	Opening temperature	100
	c.	EVF average temperature	101
	d.	Temperature field	103
	e.	EVF Gas mixture velocity	104
	f.	Oxygen concentration	105
4.	7.2	Effect of Opening Size on Fire Development and Externally Venting Fla	mes106
	a.	Interior gas temperature	106
	b.	Opening temperature	108
	c.	EVF average temperature	109
	d.	Temperature field	111
	e.	EVF Gas mixture velocity.	113
	f.	Oxygen Concentration	115
4.	7.3	Effect of ventilation conditions on fire development and EVF	117
	a.	Interior gas temperature	117
	b.	Opening temperature	119
	c.	EVF average temperature	120
	đ.	Temperature field	122

e. EV	VF gas mixture velocity
f. O	xygen concentrations
4.7.4	Additional Analysis with Rectilinear and Curvilinear Geometry127
a. Velo	city Flow field127
b. Tem	perature field
c. Oxyg	gen concentration field
4.8 Cond	clusion from Numerical investigations
	AL VENTING FLAMES FROM CURVILINEAR ENCLOSURES: A
	AND EXPERIMENTAL INVESTIGATION ON THE EFFECTS OF N
	duction
	e Scale Experimental Setup
	Measuring devices and Data acquisition
5.2.2	Simulation details
5.3 Resu	lt and Discussion137
5.3.1	Fuel mass loss and HRR
5.3.2	Interior gas temperature
5.3.3	Heat Flux
5.3.4	EVF temperature
5.3.5	EVF Centreline temperature contours
5.3.6	EVF Thermal Field
5.3.7	EVF gas mixture velocity flow field149
5.3.8	Oxygen Concentration
5.3.9	Conclusion
	metric Study: Numerical Investigation of the Effect of Ventilation Conditions and ometrical Features on the Development of Externally Venting Flames
5.4.1	Fire Engineering design correlation related to EVF
5.4.2	Numerical simulation 154

a.	Description of the geometry	154
b.	Computational domain	155
c.	Grid Sensitivity	156
5.4	Examined test cases	157
5.5	Result and discussion	158
5.5	Effect of ventilation condition on EVF development	158
á	a. Velocity Flow field	158
1	b. Temperature field	159
(c. Oxygen Concentration	160
5.5	5.2 Effect of building geometrical features	161
ä	a. Velocity field	161
1	b. Temperature field	162
(c. Oxygen concentration field	163
5.5	EVF geometric characteristics	164
5.5	Validation of Numerical Result with Engineering Correlation	166
ä	a. EVF Temperature analysis	168
5.6	Conclusion	171
6 CC	ONCLUSION & FUTURE WORKS	173
6.1	Conclusion	173
6.2	Limitations	177
6.3	Recommendation for Future Works	177
7 RE	EFERENCES	181
APPEN	DIX A: INFLUENCE OF TURBULENCE MODELLING IN FDS ON	FORCED
DRAUG	GHT CONDITIONS AND EVF IN COMPARTMENT FIRES	192
A.1 I	ntroduction	192
A.2 T	Furbulence Modelling	193
A.2	2.1 Turbulence Modelling Approaches	193

A.3 Fire Dynamic Simulator (FDS)	194
A.3.1 Turbulence models in FDS	195
A.3.2 Models for the Turbulent Viscosity (SGS Models)	195
A.4 Turbulence model and forced draught impact on EVF	197
A.4.1 Temperature at the opening with different turbulence models	197
A.4.2 Temperature at the Façade with different turbulence model	199
A.4.3 EVF flow and velocity field with different turbulence models	199
A.5 Conclusion	200
Appendix A: References	201
APPENDIX B: Fire Incident Register	203
APPENDIX C: FDS Input File	222

Author's List of Achievements, Publications, and Submissions

Research Grants and Achievements

- Awarded a research grant of approximately £6,500 (3,000 Omani Rial by The Research Council (TRC) of the Sultanate of Oman, funded by the Ministry of Higher Education, Research and Innovation, for the project titled "Experimental investigation of fire behavior and smoke flow pattern in unevenly shaped compartment ceiling" (2021).
- Recipient of the 2022 SFPE Foundation Research Grant of 5,000 USD for the study titled "Externally Venting Flames (EVF) dynamics and development in non-orthogonal geometries".
- Awarded the below internal research grants through the Research and Ethics Committee of the International College of Engineering and Management (Oman):
 - "Geometric Characteristics of Externally Ventilating Flames (EVF) Dynamics" of approximately £1,665 (800 Omani Rial)
 - "Development of Liquid Vaporization Model for Compartment Fire" of approximately £1,040 (500 Omani Rial)

Journal Articles (Submitted)

- "Forced draught impact on Externally Venting Flames: An experimental and numerical investigation", authored by **Anoop Warrier**, Jan Smolka, Kamila Kempna, Meet Panchal, Tony Graham, and Eleni Asimakopoulou submitted to Fire and Materials Journal (Manuscript ID: FAM-24-0190: under revision).
- "Effects of Building Features on the Development of Externally Venting Flames: Experimental and Numerical Investigation in Rectilinear and Curved Geometries", authored by **Anoop Warrier**, Meet Panchal, Tony Graham and Eleni Asimakopoulou – submitted to Fire Technology, currently under review.

Conference Presentations

- **Warrier A.,** Khan K., Nasriani H.R., Ndlovu S., Chamchine A., Graham T.L., Asimakopoulou E., "Numerical investigation of the effect of ventilation conditions of Externally Venting Flames on curvilinear geometries," 10th International Seminar on Fire and Explosion Hazards, 22–27 May 2022, Oslo, Norway.
- Warrier A., Khan K., Nasriani H.R., Ndlovu S., Chamchine A., Graham T.L., Asimakopoulou E., "Effect of ventilation conditions on Externally Venting Flames development on curvilinear geometries," 14th SFPE International Conference on Performance-Based Codes and Fire Safety Design Methods, 23–25 March 2022 (Virtual).
- **Anoop Warrier,** "Risk Reduction Approaches for Existing Façade Systems in High-Rise Buildings," presented at the International Workshop on Design Adaptation Strategies to Reduce the Societal Impact of Climate Change and Coastal Hazards, University of Central Lancashire, UK, 11–12 May 2023.
- **Anoop Warrier,** "A Computational Study of the Effect of Building Geometrical Features on the Development of Externally Venting Flames", presented at the International Conference on Advances in Health, Safety, Fire, Environment, Allied Sciences and

Sustainability (HSFEAS) 2023, GD Goenka University, Haryana, India, 29–30 November 2023.

Poster Presentations

Two posters to the 14th International Symposium on Fire Safety Science (IAFSS2023), Tsukuba, Japan (22–27 October 2023):

- Warrier A., Khan K., Nasriani H.R., Ndlovu S., Chamchine A., Graham T.L., Asimakopoulou E., "Forced Draught Impact on Externally Venting Flames: An Experimental and Numerical Investigation"
- Warrier A., Smolka J., Kempna K., Panchal M., Graham T., Asimakopoulou E., "A Computational Study of the Effect of Building Geometrical Features on the Development of Externally Venting Flames"

Newsletter Feature

An article authored by **Anoop Warrier**, Khalid Khan, Nasriani Hamid, Shephard Ndlovu, Tony Graham, Eleni Asimakopoulou, University of Central Lancashire, UK titled "Effect of Building Geometrical Features on the Development of Externally Venting Flames" was published in the SFPE Europe Digital Newsletter (Q4 2023 Issue 32). Available at: https://www.sfpe.org/publications/periodicals/sfpeeuropedigital/sfpeeurope32/europeissue32feature4

Acknowledgements

First and foremost, I would like to express my deepest gratitude to my supervisor, Dr. Eleni Asimakopoulou, for her unwavering support, guidance, and mentorship throughout my PhD journey. Her encouragement and commitment have been instrumental in helping me stay focused and continuously progress toward my research goals, even while I was engaged in demanding professional commitments. Her ability to provide timely advice and motivation has made a lasting impact on my academic and personal growth.

I am also sincerely thankful to Dr. Tony Graham for his invaluable insights and for consistently helping me understand the scientific underpinnings of my results. His support has deepened my appreciation for the subject and enriched the quality of my work.

My heartfelt thanks go to my father & mother and brothers (Dileep, Sudheep and Swaroop), whose unconditional support and encouragement have always been my strength. I am also grateful to my father-in-law and mother-in-law, for their constant love, support, and help throughout this journey.

I would also like to extend my appreciation to the International College of Engineering and Management (ICEM), my previous employer, for providing me with the opportunity and resources to conduct my experimental work. I am grateful to the fire safety department staffs (Amal, Sivi, Sabra & Khan) and undergraduate students—particularly Fatema Al Shehhi, Malika, and Miysaa—who assisted in various stages of the research. A special mention goes to Meet Panchal, whose tireless dedication and technical support were pivotal to the successful execution of both large- and medium-scale experiments. I am also thankful to Sathik for his significant contributions in the preparation of compartments, fabrication, and equipment setup.

I would like to acknowledge my friends Mohammed Shibin, Zuno Verghese and Sabin K G for their constant encouragement and readiness to help whenever needed.

I am equally grateful to Ahmed Shaheen, Samuel Rojas, Asad Salah and entire staffs of Xeluxe Fire Safety Consultancy, whose support in the workplace ensured that I could continue my research without disruptions.

Last but by no means least, I extend my deepest love and gratitude to my wife (Anjana) and children Adwaith (Unnikuttan) and Aadith (Kunju), whose patience, understanding, and unwavering belief in me have been the foundation of this achievement. Their presence has been my greatest motivation throughout this journey.

List of Figures

Figure 1: Formation of EVF in a compartment fire (Asimakopoulou, 2016)
Figure 2: Exponential increase of fire incident (Bonner et al., 2020)
Figure 3: Global façade fire incident 1990-2022.
Figure 4: Schematic representation of interconnected research themes of the current thesis 8
Figure 5: Structure of the thesis.
Figure 6: External flame geometry under through or FD conditions. These images have been extracted from EC1 (EN 1991-1-2, 2002).
Figure 7: Effect of wall projections on fire plume. The images have been extracted from (Yung & Oleszkiewicz, 1988)
Figure 8: Stages of compartment fire (Karlsson and Quintiere, 2000)
Figure 9: Schematic of general EVF shape in NoFD and FD conditions (Asimakopoulou et al., 2016).
Figure 10: High-rise building fire spread aggravated by wind and combustible cladding (Hardy et al.,2019; BBC, 2016).
Figure 11: EVF under different external boundary condition (Sun et al., 2023)26
Figure 12: Compartment fire and façade with casement window (Sun et al. 2020)28
Figure 13: Façade flame with top hung window (Zhang et al., 2022)29
Figure 14: Experimental setup of incline eave (Fang et.al 2024).
Figure 15: Model-scale utility tunnel platform for investigating the flame extension Pan et al. (2022)
Figure 16: Dimensions of curvilinear tunnel setup (Sturdy and Johansson, 2025)
Figure 17: Reduced scale tests to investigate the flame extension under curved ceilings (Sturdy and Johansson, 2025)
Figure 18: Front view of the experimental setup (dimensions in mm)
Figure 19: Thermocouples layout at the experimental configuration
Figure 20: Thermocouples and BDVP location at the openings
Figure 21: Numerical (left) and experimental (right) setup

Figure 22: Computational domain and relevant dimensions of the model NoFD (left) and FD (right)
Figure 23: Grid sensitivity analysis for FD-20×20 through the temporal distribution of the temperature (a) and velocity (b) at centre of outlet opening for NoFD (left) and FD (right) conditions.
Figure 24: Temporal distribution for FD-20×20 of the temperature (a) and velocity (b) at centre of the outlet opening for different LES models for NoFD (left) and FD (right) conditions47
Figure 25: Validation based on predicted velocity at centre of outlet opening for NoFD 20×20.47
Figure 26: Validation based on predicted temperature at centre of outlet and temperature distribution at horizontal distances of 10 mm to 900 mm
Figure 27: Temperature measurement at the opening for the case of NoFD 20×2050
Figure 28: Non dimensional vertical distribution of the temperature profile at the outlet opening for NoFD (left) and FD (right) conditions.
Figure 29: Temperature profile versus the horizontal distance at the center of the outlet opening for NoFD (left) and FD (right) conditions.
Figure 30: Vertical distribution of the temperature profile at the centreline of the outlet façade with fibre cement board for NoFD (left) and FD (right) conditions
Figure 31: Spatial distribution of gaseous temperature 150 s and 200 s after fire initiation under NoFD (a) and (c) and FD (b) and (d) conditions; 20 cm (top) and 40 cm (bottom) opening size.
Figure 32: Gas mixture velocity and EVF 150 s and 200 s after fire initiation under NoFD (a) and (c) and FD (b) and (d) conditions; 20 cm (top) and 40 cm (bottom) opening size
Figure 33: Gas mixture velocity and EVF at 200 s after fire initiation under FD condition with different wind velocities.
Figure 34: Non dimensional vertical distribution of the temperature at the outlet opening with different wind speed
Figure 35: Vertical distribution of the temperature at the facade with different wind speed 60
Figure 36: Spatial distribution of oxygen concentration 150 s and 200 s after fire initiation under NoFD (a) and (c)and FD (b) and (d) conditions; 20 cm (top) and 40 cm (bottom) opening size. 61
Figure 37: Experimental setup indoor (top) and outdoor (bottom)

Figure 38: Schematic drawing of the experimental facility and sensor locations for curvilinear (left) and rectilinear (right)
Figure 39: Fuel mass loss (left) and gas temperature inside the fire compartment (right) measurements obtained in the repeatability tests
Figure 40: Schematic of Extended computational domain, dimensions in mm71
Figure 41: Extended Computational domain in FDS
Figure 42: Temporal evolution of the temperature at the centreline of opening for the different meshes used
Figure 43: Validation based on predicted temperature at centre of the opening
Figure 44: Validation based on the predicted temperature at the centre of the opening (left) and interior compartment temperature (right) under FD conditions
Figure 45: Validation based on the predicted temperature at the centre of the opening (left) and interior compartment temperature (right) under NoFD conditions
Figure 46: Interior temperature profiles of the curvilinear compartment constructed with steel and Monolux.
Figure 47: Fuel mass loss for curvilinear and rectilinear geometries
Figure 48: Fuel mass loss for curvilinear geometry with different opening size80
Figure 49: Fuel mass loss in compartments with varying fuel burner height locations under FD conditions (left) and NoFD conditions (right)
Figure 50: Temporal evolution of incoming flow to the fire compartment for rectilinear and curvilinear geometries
Figure 51: Temporal evolution of incoming flow to the fire compartment curvilinear geometries with different opening sizes.
Figure 52: Temporal evolution of incoming flow to the fire compartment with different fuel burner height location for FD (left) and NoFD condition (right)
Figure 53: Calculated GER for curvilinear and rectilinear geometries (left) and for curvilinear geometries with different opening sizes (right).
Figure 54: Temporal evolution of interior fire compartment temperature for rectilinear and curvilinear geometries.

Figure 55: Temporal evolution of interior fire compartment temperature for curvilinear geometry
with different opening sizes
Figure 56: Temporal evolution of interior fire compartment temperature with varying fuel burner
height location for FD (left) and NoFD condition (right)
Figure 57: Temporal evolution of opening temperature for rectilinear and curvilinear geometries.
Figure 58: Temporal evolution of opening temperature for curvilinear geometry with different opening sizes
Figure 59: Temporal evolution of opening temperature with varying fuel burner height location
for FD condition(left) and NoFD condition (right)
Figure 60: Time averaged EVF temperatures for curvilinear and rectilinear geometries in FD and NoFD conditions.
Figure 61: Time averaged EVF temperatures for curvilinear geometry with different opening sizes.
Figure 62: Temporal evolution of heat flux on the facade for rectilinear and curvilinear geometries.
Figure 63: Temporal variation of façade heat flux: comparison between experiment and FDS for
rectilinear (left) and curvilinear (right) geometries
Figure 64: Fuel mass loss (left) and temporal evolution of incoming flow to the fire compartment (right) for rectilinear and curvilinear geometry.
Figure 65: Temporal evolution of interior compartment temperature (left) and opening temperature (right) for rectilinear and curvilinear geometries
Figure 66: Interior temperature profiles for curvilinear and rectilinear compartments: experimental vs. FDS results.
Figure 67: Temporal temperature profile at the centre of the opening for curvilinear and rectilinear compartments: experimental vs. FDS results
Figure 68: Time averaged EVF temperatures for curvilinear and rectilinear geometry from FDS.
Figure 69: Time averaged EVF temperatures for curvilinear and rectilinear geometry from experiment

Figure 70: Spatial distribution of gaseous temperature 600 s and 400 s after fire initiation with curvilinear (left)and rectilinear (right) compartment under FD conditions
Figure 71: Gas mixture velocity and EVF 600 s and 400 s after fire initiation with curvilinear (left)and rectilinear (right) compartment under FD conditions
Figure 72: Spatial distribution of oxygen concentration 600 s and 400 s after fire initiation with curvilinear (left)and rectilinear (right) compartment under FD conditions
Figure 73: Interior temporal profiles of the curvilinear compartment (left) and rectilinear compartment (right) with different opening dimension for experiment and numerical analysis.
Figure 74: Opening temporal profiles the curvilinear compartment (left) and rectilinear compartment (right) with different opening dimension for experiment and numerical analysis.
Figure 75: Time averaged EVF temperatures for curvilinear geometry with different opening dimension for both experiment and FDS.
Figure 76: Time averaged EVF temperatures for rectilinear geometry with different opening dimension for both experiment and FDS.
Figure 77: Spatial distribution of gaseous temperature 600 s & 1150s after fire initiation with 25W x 40H cm (top) and 25W x 20H cm (bottom) conditions for curvilinear (left) and 400 s and 1050s after fire for rectilinear (right)
Figure 78: Gas mixture velocity and EVF 600 s & 1150s after fire initiation with 25W x 40H cm (top) and 25W x 20H cm (bottom) conditions for curvilinear (left) and 400 s & 1050s after fire for rectilinear (right).
Figure 79: Spatial distribution of oxygen concentration 600 s & 1150s after fire initiation with 25W x 40H cm (top) and 25W x 20H cm (bottom) conditions for curvilinear (left) and 400 s & 1050s after fire for rectilinear (right).
Figure 80: Interior temporal profiles of the curvilinear compartment (left) and rectilinear compartment (right) with different ventilation conditions for experiment and numerical analysis.
Figure 81: Opening temporal profiles of the curvilinear compartment with different ventilation conditions for experiment and numerical analysis

Figure 82: Time averaged EVF temperatures for curvilinear geometry with different ventilation condition for both experiment and FDS
Figure 83: Time averaged EVF temperatures for rectilinear geometry with different ventilation condition for both experiment and FDS
Figure 84: Spatial distribution of gaseous temperature 600 s & 810s after fire initiation with 25W x 40H cm (top) and 25W x 20H cm (bottom) conditions for curvilinear (left) and 400 s & 590s after fire for rectilinear (right)
Figure 85: Gas mixture velocity and EVF 600 s & 810s after fire initiation with 25W x 40H cm (top) and 25W x 20H cm (bottom) conditions for curvilinear (left) and 400 s & 590s after fire for rectilinear (right).
Figure 86: Spatial distribution of oxygen concentration 600 s & 810s after fire initiation with 25W x 40H cm (top) and 25W x 20H cm (bottom) conditions for curvilinear (left) and 400 s & 590s after fire for rectilinear (right)
Figure 87: Gas mixture velocity 600 s after fire initiation for curvilinear (left) and 400s after fire initiation for rectilinear (right).
Figure 88: Spatial distribution of gaseous temperature 600 s after fire initiation for curvilinear (left) and 400 s after fire initiation for rectilinear (right)
Figure 89: Oxygen concentration 600 s after fire initiation for curvilinear (left) and 400s after fire initiation for rectilinear (right).
Figure 90: Indicative photos of fire test configuration and the experimental setup
Figure 91: Schematic drawings of the large-scale test setup
Figure 92: Indicative photos of fire test configuration and the experimental setup
Figure 93: Fuel pan height located 0.3 m from the floor
Figure 94: Indicative photos of fire test configuration and the experimental setup
Figure 95: Fuel mass loss and measured heat release rate for FD condition
Figure 96: Fuel mass loss and measured heat release rate for NoFD condition
Figure 97: Temporal evolution of temperature at the interior of the compartment
Figure 98: Temporal evolution of heat flux to the façade wall, at a height 0.3 m from the opening
for experiment (left) and for FDS cases (right)

Figure 99: Time averaged EVF centreline temperature for experimental values FD and NoFD cases for 300 seconds (left) and 600 seconds (right)
Figure 100: Time averaged EVF centreline temperature for experimental values compares with EC1 for FD and NoFD cases for 900 seconds (left) and 1200 seconds (right)
Figure 101: Time averaged EVF centreline temperature for experimental values FD case and numerical values (FDS) for 300 seconds (left) and 600 seconds (right)
Figure 102: Time averaged EVF centreline temperature for experimental values FD case and numerical values (FDS) for 900 seconds (left) and 1200 seconds (right)
Figure 103: Time averaged EVF centreline temperature for experimental values FD case and numerical values (FDS) for 1350 seconds.
Figure 104: Time averaged EVF centreline temperature for experimental values NoFD case and numerical values (FDS) for 300 seconds (left) and 600 seconds (right)
Figure 105: Time averaged EVF centreline temperature for experimental values NoFD case and numerical values (FDS) for 900 seconds (left) and 1200 seconds (right)
Figure 106: Spatial distribution of gaseous temperature 1100 s after fire initiation for FD case (left) and 1150s after fire initiation for NoFD case (right).
Figure 107: Gas mixture velocity 1100 s after fire initiation for FD case (left) and 1150s after fire initiation for NoFD case (right).
Figure 108: Oxygen Concentration 1100 s after fire initiation for FD case (left) and 1150s after fire initiation for NoFD case (right)
Figure 109: Geometry and location of measuring devices, all dimensions are in mm
Figure 110: Openings of the fire compartment front (left) and top (right) view155
Figure 111: Extended computational domain used in this study
Figure 112: Temporal evolution of the temperature at the centerline of Door 1 of Geometry 2, 1.8 m height from the ground for the different meshes used
Figure 113: Gas mixture velocity and flame locations predictions for FD-1.5 (bottom left), NoFD-1.5 (top left) FD-2.0 (top middle), NoFD-2.0(bottom middle), FD-4.0 (top right) and NoFD-4.0 (top right) 500 s after fire initiation

Figure 114: Spatial distribution of gaseous temperature 500 s after fire initiation for FD-1.5MW (bottom left), No FD-1.5MW (top left) FD-2.0 MW (bottom middle), NoFD-2.0 MW (top middle) and FD-4.0 MW (bottom right), NoFD-4.0MW (top right)
Figure 115: Spatial distribution of oxygen concentration 500 s after fire initiation for FD-1.5MW (bottom left), No FD-1.5MW (top left) FD-2.0 MW (bottom middle), NoFD-2.0MW(top middle) and FD-4.0 MW (bottom right), NoFD-4.0MW (top right)
Figure 116: Gas mixture velocity 500 s after fire initiation for NoFD (top) and FD (bottom) conditions for both rectilinear (left) and curvilinear (right) 4 MW cases
Figure 117: Spatial distribution of gaseous temperature 500 s after fire initiation NoFD (top) and FD (bottom) conditions for both rectilinear (left) and curvilinear (right) 4 MW cases
Figure 118: Oxygen concentration 500 s after fire initiation NoFD (top) and FD (bottom) conditions for both rectilinear (left) and curvilinear (right) 4 MW cases
Figure 119: Side view of the flame intermittency contours for NoFD (top) and FD (bottom) conditions for both rectilinear (left) and curvilinear (right) 4 MW cases
Figure 120: Mean flame height NoFD and FD 4 MW
Figure 121: Mean flame width for NoFD and FD 4 MW
Figure 122: Vertical distribution of averaged temperature at the exterior of the fire compartment; effect of ventilation conditions FD (left) and NoFD (right)
Figure 123: Vertical distribution of the averaged centerline temperature at the exterior of the fire compartment for NoFD conditions for the rectilinear cases
Figure 124: Vertical distribution of the averaged centerline temperature at the exterior of the fire compartment for NoFD conditions for the curvilinear cases
Figure 125: Vertical distribution of temperature at the exterior of the fire compartment for NoFD and FD conditions for the 4 MW rectilinear and curvilinear cases
Figure 126: Heat flux at the facade for NoFD and FD conditions for the 4 MW rectilinear and curvilinear cases
Figure 127: Non dimensional vertical distribution of the temperature profile at the outlet opening with turbulence models.
Figure 128: Vertical distribution of the temperature profile at the centerline of the outlet façade with different turbulence models

Figure 129: Gas mixture velocity and EVF at 200 s after fire initiation under F	D conditions for 40
cm opening size with different turbulence models.	200

List of Tables

Table 1: Fires classified based on geometry of building involved	3
Table 2: Summary of key experimental investigations related to EVF	19
Table 3: Selected research work on wind-driven medium scale fires	24
Table 4: Main parameters of the test setup and the corresponding full-scale experiment.	39
Table 5: Experimental test scenarios	43
Table 6: Medium scale experimental test scenarios	68
Table 7: Summary of main operational parameters used in the repeatability tests	69
Table 8: Medium scale experimental test scenarios considered for numerical simulations	70
Table 9: Full scale experimental test scenarios.	137
Table 10: Empirical correlations for EVF shape and centerline temperature	153
Table 11: Examined test cases	157
Table 12: EVF geometrical characteristics according to empirical correlations	167
Table 13: Turbulence model test scenarios	197



Abbreviations

EVF Externally Venting Flames

NoFD No Forced Draught

FD Forced Draught

GER Global Equivalence Ratio

FDS Fire Dynamic Simulator

CFD Computational Fluid Dynamics

HRR Heat Release Rate

HRRPUV Heat Release Rate Per Unit Volume

MLR Mass Loss Rate

LES Large Eddy Simulations

VLES Very Large Eddy Simulations

SVLES Simply Very Large Eddy Simulations

CFL Courant-Friedrichs-Lewy

IFE Intermittent Flame Ejection

CEF Consistent External Flaming

RTE Radiative Transport Equation

VF Ventilation Factor

EC1 EN 1991-1-2: Euro code 1: Actions on Structures, Part 1-2 –

General Actions – Actions on Structures Exposed to Fire

BDVP Bi-directional velocity probe

FVM Finite Volume Method

TC1 & TC2 Thermocouple tress 1 and 2.



Nomenclature

SYMBOL	QUANTITY	UNITS
$A_{\mathcal{V}}$	Total area of vertical opening on all walls of	m^2
	the compartment	
A_O	Opening area	m^2
C_s	Smagorinsky Constant	0.2
C_{ve}	Specific heat of the target material	J/kg °C
D^*	Characteristic fire diameter	m
D_{v}	Hydraulic diameter of the opening	m
d_x	Nominal size of a mesh cell	m
g	Gravitational acceleration	9.18m/s^2
H_O	Opening height	m
h_{eq}	Weighted average of opening heights on	m
**	wall	W// 0G
K_{ve}	Thermal conductivity of target material	W/m. °C
L_L	Height of EVF	m
L_H	Projection of EVF	m
L_f	Flame length	m
l_x	Length along the EVF centerline,	m
1 11	originating at the opening	
l_p and l_m	Physical dimension of the prototype and	m
1.6	model system	
Ma	Mach number	1 /
m_a	Mass flow rate of incoming air to the	kg/s
$\dot{m_f}$	Fuel Mass Loss Rate	kg/s
m_f	Fuel mass	kg
m_{o2}	Oxygen mass flux	kg/s
N_{λ}	Empirically derived constant	-
P_r	Prandtl number	-
Q	Heat release rate	MW
RH	Ambient relative humidity	%
r	Fuel to oxygen stoichiometric ratio	-
T_g	Upper gas layer temperature	°C
T_{in}	Temperature inside	°C
T_o	Ambient temperature	°C
T_{out}	Temperature Outside	°C
T_{ve}	Temperature of the surface of the target	°C
	object	
T_{w}	Window opening temperature	K
T_{wall}	Façade wall temperature	K
T_Z	EVF centerline temperature in relation to	K
	height from the opening soffit.	

SYMBOL	QUANTITY	UNITS
U_{ve}	Function of both the geometry of the setup	-
	and thermal characteristics of the surface	
	material	
u	Velocity	m/s
V	External wind speed	m/s
Wv	Opening width	m
w_t	Sum of opening width on all walls of the	m
	burning room	
w_f	EVF width	m
X_{O_2}	Oxygen concentration	mol/mol
Y_{O2}	Oxygen mass fraction in ambient air	0.23
β	Empirically derived constant	-
$ ho_{amb}$	Air density at ambient condition	1.204 kg/m^3
ho500o C	Air density at 500 °C	0.45 kg/m^3
$ ho_{ m g}$	Density of hot combustible products	kg/m^3
$ ho_{ve}$	Density of the target material	kg/m^3
λ_{ve}	Material specific modifier	-



1 INTRODUCTION

1.1 Externally Venting Flames (EVF)

In a compartment fire scenario, following ignition, burning gases such as flames or hot unburnt combustion gases may exit through the compartment openings (doors, windows, etc.) and burn outside when this gaseous fuel mixes with ambient air. This rapid combustion can take place regardless of whether the internal fire-origin room environment is under ventilated- or well-ventilated. This phenomenon is called an Externally Venting Flame (EVF), or more commonly known as a façade fire (Asimakopoulou et al., 2020). In well-ventilated fire scenarios, during the growth stage of the fire, flames spread long enough through the ceiling jet to reach the windows and building openings which traverse to the outside atmosphere resulting in EVF, Figure 1. In under ventilated fires, unburnt fuel in vapor form traverse via the ceiling jet to the windows and building openings and develop EVF at that point when the external atmosphere offers sufficient air to support flaming combustion.

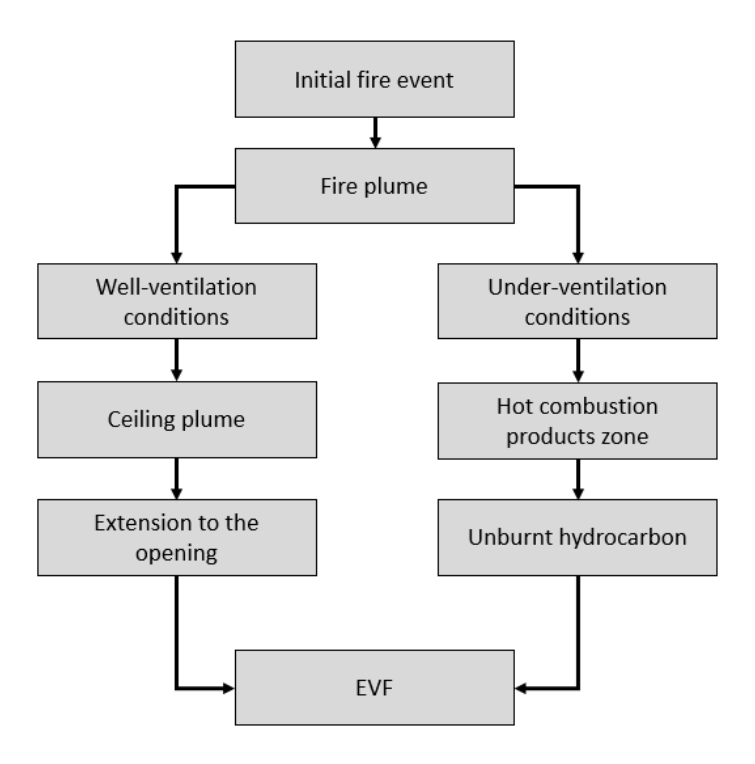


Figure 1: Formation of EVF in a compartment fire (Asimakopoulou, 2016).

1.2 Façade fire incident database

Modern day aesthetics and green building initiatives demand the use of different façade materials, including materials with combustible characteristics, which support façade fires from EVF which has the risk potential to envelope multiple stories of the building with fire. This is typically true and has major impact in case of façade fires in high rise buildings (White and Delichatsios, 2015).

Recent fire incidents associated with high rise buildings highlight the necessity to study the risk of external fire spread. With an exponential increase of fire incidents around the globe on high rise buildings (Bonner et al., 2020), Figure 2, it is important to study and understand the behaviour of façade fire which has been a major contributor in the flame spread on these fires.

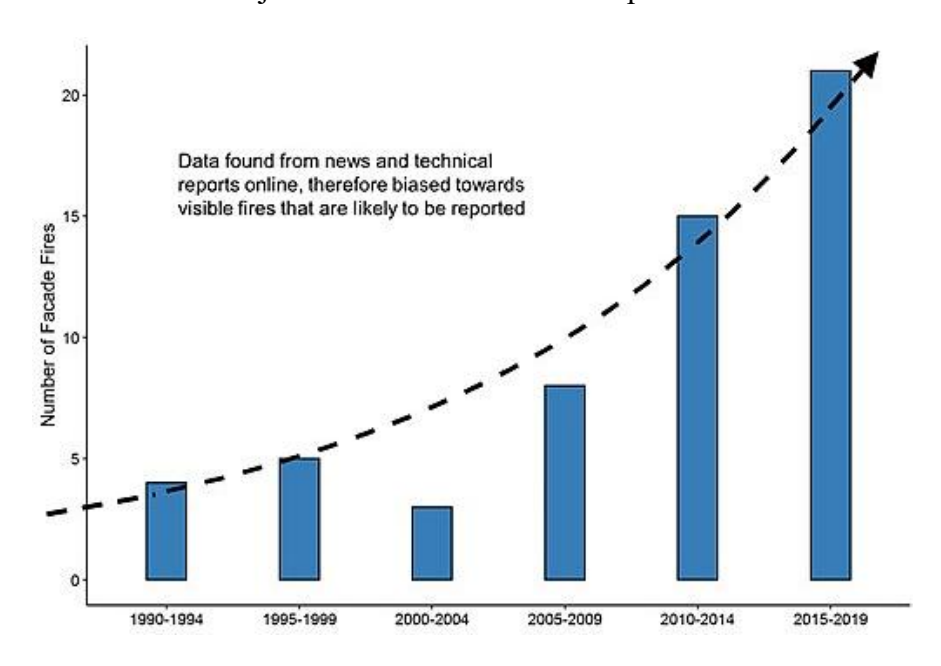


Figure 2: Exponential increase of fire incident (Bonner et al., 2020).

Analysing the images and videos of major fire incidents which happened in the past, it is found that most of the damages occur over the exterior façade of the building while the damages on the interior of the building is very minimal. This causes additional risk of falling debris and flying brands from the ignited façade cladding material which is a risk to the public and firefighters potentially causing additional damage or secondary fires.

There is a modern architecture and current construction trend to build non- orthogonal buildings rather than traditionally built rectilinear buildings. New engineering technologies and advanced manufacturing techniques have enabled the construction of new façade systems, e.g., curved glass façade systems. Further, non-orthogonal, curvilinear or "free form" geometries are widely used in building façade designs, and they pose a significant challenge for the fire safety design of the building as the emphasis on aesthetics many a times results in the use of non-conventional building materials which aggravates and enhances the fire spread in such constructions (White and

Delichatsios, 2015). Though there has been a multitude of studies on facade fires in orthogonal or rectilinear geometries, the influence of non-orthogonal geometry upon the EVF is not thoroughly investigated.

A database of façade fire incidents has been developed as a part of this work to showcase the research need on façade fires on non-orthogonal geometries as the exterior fire spread, façade fire, has become a growing concern and fire incidents have increased exponentially around the globe (Bonner et al., 2020). The developed registry capitalized on the previous database developed by Boner et.al., covering fire incidents from 1990-2019 (Bonner and Rein., 2020). That registry was further developed to include recent incidents from 2019-2022 around the globe, based on authenticated data and information received through reliable resources, including media reports. Based on this data analysis, fire incidents are categorized as per different types of geometries and are presented in Table 1. The developed incident registry specifically focuses on fire events in high-rise buildings. During the data collection process, it was observed that incident data from several regions, including South America, Africa, and many other parts of the world, were not readily available from reliable or verifiable sources. Consequently, these regions are underrepresented in the dataset, introducing a potential geographical bias. Furthermore, differences in reporting standards, verification processes, and definitions of 'high-rise buildings' across jurisdictions contribute additional variability. It is also recognized that reporting tends to emphasize severe or high-profile events, potentially leading to a selection bias. These limitations have been acknowledged and considered in interpreting the registry outcomes. The complete developed registry is appended in this thesis as Appendix B.

Table 1: Fires classified based on geometry of building involved.

No	Geometry of the building	Number of façade fire incidents	% Incidents
1	Rectilinear	48	58 %
2	Curvilinear	21	25 %
3	Non-Orthogonal	14	17 %

It was revealed that 42% of buildings were either curvilinear or non-orthogonal buildings; a substantial number that clearly indicates the necessity of the proposed research. Trend analysis developed from the data base indicates that most of the façade fires had engulfed multiple stories and indicates the need for increased legal and design regulations especially in developing countries which lack specifications on façade requirements. Figure 3 shows the major façade fire incidents recorded around the globe during 1990-2022.

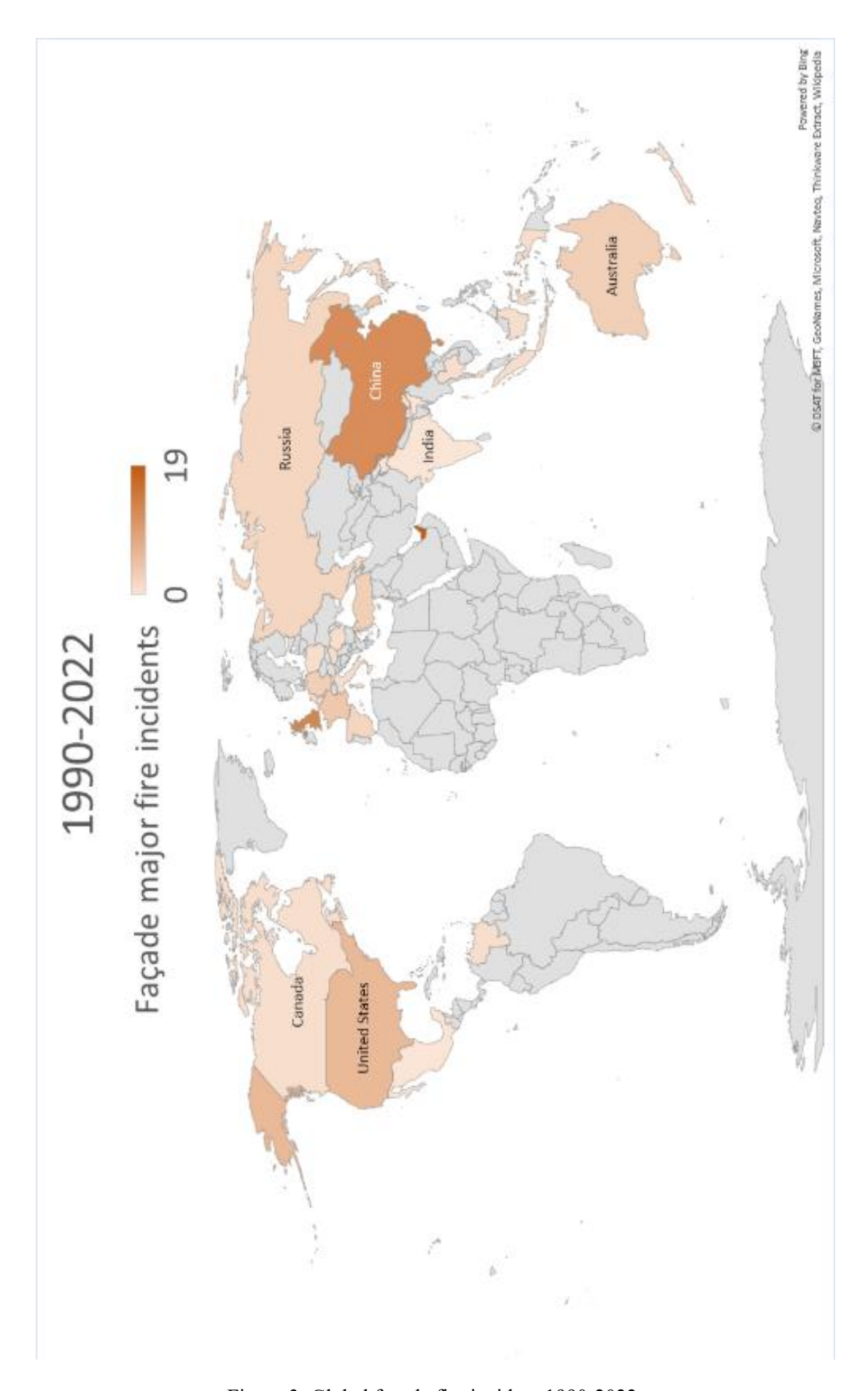


Figure 3: Global façade fire incident 1990-2022.

1.3 Regulatory framework

Exterior fire spread and heat transfer through the structures from EVF are major challenges during high-rise building fires. The severity of these fires is predominantly dependent on the building geometry, presence of combustible materials in the façade, and external weather conditions such as wind and temperature (Hirschler, 2020). Most developed countries have stringent requirement on using combustible façades and the regulations are often bound to this "combustibility" aspect only. The validation of combustibility is done via testing standards/requirements on façade assembly. However, the majority of current fire safety regulations and codes, worldwide, lacks specific methodologies to evaluate the risk associated with EVF. Although the need for regulations has gained importance, many international design guidelines do not adequately account for EVF characteristics (EN 1991-1-2, 2002). A majority of the studies on EVF characteristics are conducted on orthogonal structures and subsequently, existing testing standards for the façade assembly are also predominantly based on orthogonal geometries.

In her final report on the independent review of building regulation and fire safety, Dame Judith Hackitt puts forth several fundamental recommendations, which include the introduction of a new regulatory framework that places the utmost priority on the safety of residents. This framework would entail adopting a more risk-based approach to fire safety and enhancing the availability of fire safety information and guidance. The report emphasizes the need for significant changes in building regulations and fire safety practices to prevent future tragedies. The review's recommendations aim to create a safer built environment by promoting a culture of responsibility, competence, and resident engagement. This report was presented to Parliament by the secretary of state for housing, communities, and local government by command of Her Majesty (Hackitt, 2018).

It is of utmost importance to understand that in past studies the design correlation or design methodology developed were for simple geometries such as a cubic-like enclosure or simple rectilinear geometries. Very limited data and studies exist for complex geometries such as non-orthogonal, curvilinear geometries which are commonly used in modern architectural buildings.

This research aims to cover the current construction trend where multiple buildings with non-orthogonal structure (curvilinear, free form etc.) are becoming increasingly common and EVF and flame spread characteristics on such buildings are least studied. This research also aims to simulate results from realistic fire conditions to achieve the best output. Incorporation of design aspects in

these structures, such as life safety, property protection and further prevention measures, and the development of design methodologies underlies the important motivation of this study.

1.4 Aims and Objectives of the project

The critical analysis of the current state of research on compartment fire dynamics and EVF development, particularly in the context of non-orthogonal building geometries, reveals several significant knowledge gaps: (1) there remains a scarcity of systematic research on the influence of forced draught (FD) ventilation on the temperature profile and the characteristics of EVF and the resulting thermal impact on building façades, affected by different ventilation condition due to the various opening sizes within the compartments, (2) there are limited studies comparing the fire dynamics and EVF behaviour between rectilinear and curvilinear compartments through integrated experimental and numerical methods, (3) the detailed understanding of EVF flow fields, thermal fields, and external flame dynamics in compartments of varying geometrical configurations, remain under explored, (4) there is still a lack of large-scale experimental research focusing on the influence of ventilation (FD and NoFD) on EVF behaviour emerging from curvilinear enclosures, (5) there is a lack of comprehensive parametric studies investigating the effects of critical fire parameters—such as heat release rate (HRR), ventilation conditions, and opening dimensions—on EVF development across different geometrical forms, (6) the validation of existing fire engineering predictive correlations for parameters such as flame height, flame projection distance, external flame temperature, and façade heat flux against detailed numerical simulations in non-orthogonal geometries has not been systematically addressed.

In the context of this thesis, the classification of small-, medium-, and large-scale investigations is primarily based on the physical dimensions of the compartment and the associated heat release rate (HRR). As there is no universally standardised definition in the literature, this distinction is typically made based on the experimental setup and the energy scale of the fire. For instance, Lee and Delichatsios (2007) conducted small-scale compartment experiments with volumes on the order of 1 m³ and HRR values below 100 kW, which are widely regarded as representative of small-scale studies (Lee, Delichatsios and Silcock, 2007). Medium-scale experiments, such as those conducted in the present work, correspond to intermediate compartment sizes with HRRs in the range of a few hundred kilowatts, enabling detailed observation of EVF behaviour under controlled yet realistic conditions. In contrast, large-scale investigations generally follow standardized façade fire test methodologies such as ISO 13785, BS 8414, ISO 834, ASTM E119, and ISO 9705 – Room corner test, which involve full- or near-full-scale compartments and HRRs in the megawatt range, representing realistic building-level fire scenarios. This classification

provides context for interpreting the scale and applicability of the experimental and numerical work undertaken in this thesis.

In response to these identified gaps, this thesis aims to advance the understanding of EVF development under varying ventilation and geometrical conditions, through a combined experimental and numerical framework, addressing the following core objectives:

- (1) To experimentally and numerically investigate the influence of forced draught ventilation on externally venting flame characteristics in rectilinear compartments.
- (2) To perform a comparative study on the development and behaviour of EVF between rectilinear and curvilinear compartments at medium scale.
- (3) To conduct detailed numerical analyses of the internal compartment and EVF flow field and associated thermal impacts in the facades in compartments of varying geometries.
- (4) To undertake large-scale experimental investigations into the behaviour of EVF from curvilinear enclosures under different ventilation conditions.
- (5) To carry out a comprehensive parametric numerical study assessing the influence of HRR, ventilation conditions, and compartment opening characteristics on EVF behaviour for both rectilinear and curvilinear geometries.
- (6) To evaluate and critically assess the applicability and accuracy of existing fire engineering design correlations in predicting EVF parameters within compartments featuring non-orthogonal geometrical configurations.

1.5 Structure of the Thesis

This thesis is structured into eight chapters, each designed to progressively build the foundation, experimental evidence, and analytical insight into the development of EVF in relation to building geometrical features and ventilation conditions.

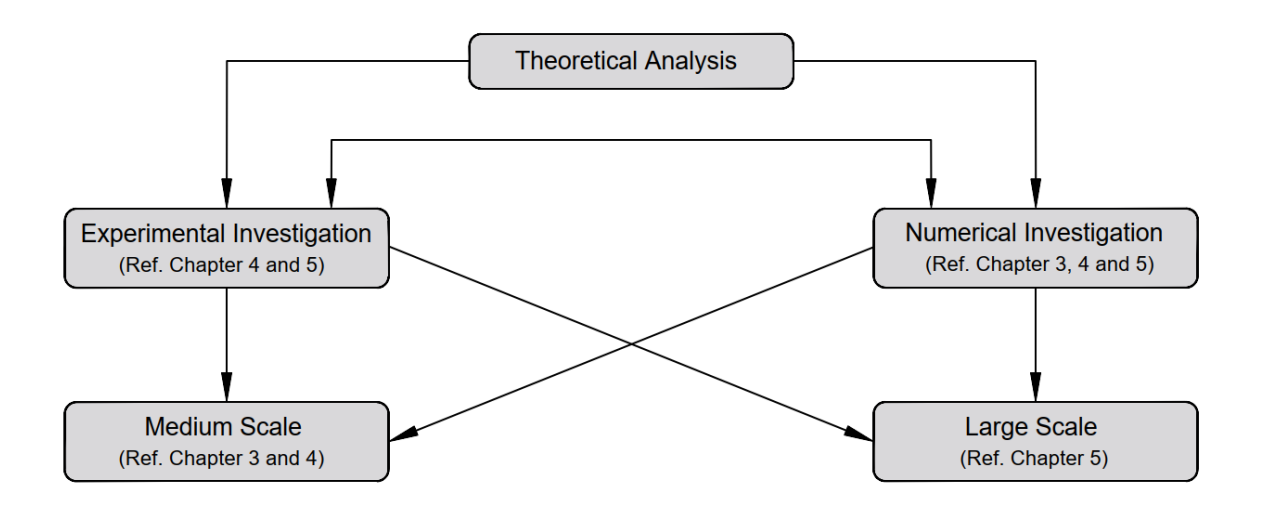


Figure 4: Schematic representation of interconnected research themes of the current thesis.

The research combines experimental and numerical methodologies across various scales to investigate the physical mechanisms behind EVF behaviour and assess the influence of architectural and fire engineering design parameters.

• Chapter 1 – Introduction

This chapter introduces the research context and significance, with a specific focus on façade fire risks and EVF behaviour. It includes a review of global façade fire incident databases, research motivations, and defines the main objectives and scope of the study.

• Chapter 2 – Literature Review

A comprehensive review of past studies on façade fire spread, EVF behaviour, and key building design features is presented. This chapter also reviews fire engineering design correlations used in the design and prediction of EVF characteristics.

• Chapter 3 – Forced Draught Impact on EVF

This chapter focuses on an experimental and numerical study investigating the influence of FD conditions on EVF. The purpose of this study is to investigate the impact of FD conditions on fully developed medium-scale compartment fires with an emphasis on EVF development. CFD using FDS numerical tool has been used to investigate EVF development and temperature characteristics under wind-driven conditions in medium scale compartments.

• Chapter 4– Medium-Scale Experimental and Numerical Investigation

The influence of building features—particularly geometry (rectilinear vs. curvilinear)—

on the development of EVF is explored through a series of medium-scale fire experiments. The aim of the current work is to progress the current state of the art by investigating effects of building features on the development of Externally Venting Flames (EVF) characteristics and development. An experimental investigation is conducted in curvilinear and orthogonal geometries to help identify the key factors influencing EVF development and their impact on the façade. Complementing with a detailed FDS-based numerical simulation of medium-scale experiments. The focus is on comparing predicted temperatures, velocities, and EVF behaviour to experimental results, and assessing the model's accuracy.

• Chapter 5 – Large-Scale Investigation on Curvilinear Geometries

This chapter discusses the results of both numerical and large-scale experimental studies on EVF development in curvilinear compartments. This high-fidelity investigation bridges the gap between lab-scale studies and realistic architectural configurations. Additionally, a broader parametric investigation is conducted to examine the combined effects of ventilation configurations (FD vs. NoFD) and building geometry on EVF formation. Numerical simulations are used to quantify the relationship between fuel load, airflow, and external flame dynamics.

• Chapter 6 – Conclusions and Recommendations

This final chapter summarizes the key findings across all phases of the research. It offers conclusions on the impact of geometrical and ventilation parameters on EVF behaviour and outlines recommendations for fire safety design and future research directions.

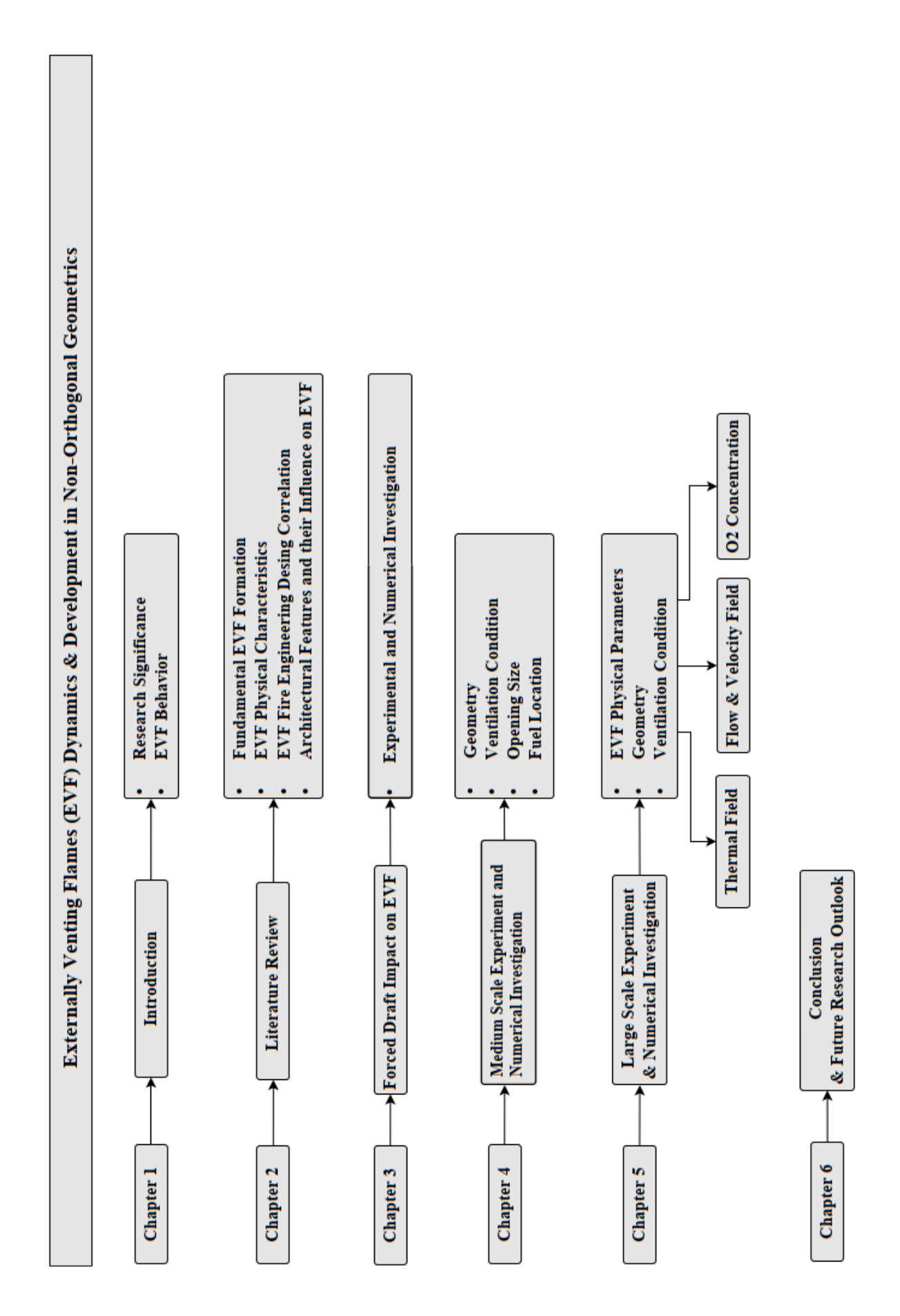


Figure 5: Structure of the thesis.

2 LITERATURE REVIEW

2.1 Major past studies and research on EVF

The study of EVF was first conducted by Yokoi in the 1960s (Yokoi, 1960) to understand the associated risk of EVF from window openings and further vertical fire spread above openings in the buildings. He started his investigation on temperature and velocity distribution of plume of hot gases initially from alcohol-based fuel. Based on this study, Yokoi further conducted a few full-scale tests in a concrete building with different compartment dimensions and opening sizes, used wood as the fuel source with varying fuel load densities. He investigated and analysed flame (considered as hot current) venting through the window opening. The major outcome of his study was the identification that aspect ratio of the window (n = 2w/h); where w is the width and h is the height in meters) was an important parameter along with the presence of a vertical wall above the window related the vented flame projection. As for the lower value of aspect ratio the flame tends to project further away from the wall and for a higher value, the plume is adhered to the wall. Similarly, he noticed that with the presence of a vertical wall above the window opening, the wall will absorb the heat from the flame, and it also prevents the air entrainment on the back of the vented plume. This will result the plume to adhere and travel along the wall (Yokoi, 1960).

In developing a correlation for the temperature of the external plume, Yokoi used a characteristic length scale to represent the external plume heat source as the area of the opening corresponding to the outflow of hot gases. This opening area is expressed in terms of the radius of a circle of equivalent area, such as the characteristic length scale of the heat source.

$$r_o = \sqrt{\frac{hw}{2\pi}} \tag{2.1}$$

Yokoi also used a non-dimensional temperature parameter to collate the plume temperature data.

$$\Theta = \frac{(T_z - T_o)r_o^{5/3}}{\sqrt[3]{\frac{\dot{Q}^2 T_a}{c^2 \rho^2 g}}}$$
 (2.2)

Where T_z is the temperature at a certain point along the external plume axis, T_o is the temperature of the plume at its axis and at its point of origin on the opening plane and Q is the rate of convective heat flow at the opening. Plotting the data collected from his model scale fire tests, using the non – dimensional temperature parameter against the vertical distance from the opening soffit, normalized against the characteristic length scale of the heat source, Yokoi obtained a very good

match between the data pertaining to tests with different opening aspect ratios. Yokoi also investigated the effect of EVF in presence of balcony or horizontal projection above window opening to study the risk of vertical spread. He found that flame will deflect and move away from the wall in the presence of horizontal projection, however beyond the projection the flame tends to deflect back to its original path. Further, Yokoi suggested the guidance to provide necessary vertical separation distance between vertical windows (spandrel length) and the length of horizontal projection above a window.

Webster *et al.* conducted a series of primarily model-scale experimental investigations aimed at quantifying the behaviour of externally venting flames (EVF) from compartment fires. In these experiments, flame heights were visually estimated for a range of conditions using cubical compartments, configured with one fully open wall and no façade wall above the opening, with wood cribs serving as the fuel source. The study provided valuable early insights into the influence of compartment geometry and opening configuration on external flame extension. Following Webster's work, Thomas employed dimensional analysis to correlate the experimental data with fundamental parameters such as heat release rate and ventilation conditions, extending the interpretability of the findings. The work also aligned with that of Yokoi, who related external plume temperature measurements to equivalent flame height. Specifically, Yokoi proposed that the point along the plume centreline where the gas temperature decreases to approximately 500 °C corresponds to the flame tip, as radiation emission becomes negligible beyond this point (Webster, Raftery and Smith, 1961), (Webster and Smith, 1964).

Seigel conducted a series of test Seigel conducted a series of large-scale fire experiments at Underwriters Laboratories (UL), where air was forcibly supplied to compartment fires to simulate both natural and forced-draught ventilation conditions to study the effect of EVF by studying flame height images and predicted their size by considering the plume as a horizontal jet (Seigel, 1969). The experiments systematically varied opening size and aspect ratio, using wood cribs as the primary fuel source. Flame height and temperature were recorded, with the flame tip defined at a measured temperature of approximately 540°C, consistent with the point where radiant emission becomes negligible. The study demonstrated that under forced-draught conditions (with airflow up to 2.25 m³/s), the flames behaved as forced horizontal jets, widening and projecting outward from the entire opening area, while buoyancy effects were excluded.

Thomas and Law in 1972 re-examined the experimental data of Yokoi, Webster and Seigel in 1960s. Experimental data were compared with Yokoi's data for the flow of hot current from the

window openings, by taking into consideration the differences and similarities in their test. From the analysis, they developed a correlation for external flame (Thomas and Law, 1972).

$$(z+h) = 18.6 \left(\frac{\dot{m}}{w}\right)^{\frac{2}{3}}$$
 (2.3)

where z represents the vertical component of the flame height above the opening, h is the opening height, \dot{m} the mass burning rate, and w the width of the opening. Despite the limited data and necessary estimations due to incomplete measurements from Seigel's experiments, this correlation effectively captured the general behavior of externally venting flames across multiple scales, whether treated as buoyant plumes or forced jets (Thomas and Law, 1972).

In 1978, Law developed a comprehensive methodology to assess the fire safety of external structural elements based on EVF characteristics (Law, 1978). This method considered a separate heat balance equation for two different scenarios of steel members engulfed and not engulfed in flames. The model considered two distinct fire situations, called "No through draft" and "Through draft conditions". For both conditions, empirical EVF correlation for flame height, width, and depth (projection), were developed and it is noteworthy that these correlations were mainly dependent on the parameters such as mass burning rate, window dimension (area, length and height) and wind speed / air supply velocity for the case of through draft (Law and O'Brien, 1989). The Law Model adopts empirically calibrated correlations derived from experimental data (Yokoi, Webster, Seigel and others) to account for flame geometry, emissivity, and heat flux distributions. Law model assumes steady-state condition for the heat transfer process as they lead to maximum steel temperature, as this is the area of interest and this applicable only for a simple right-angled cuboid shaped compartment. The Law model focuses on the effect of flame on structural steel members only, and the same methodology have been adopted in the Eurocode 1 for the assessment of temperature of external structural steel member from EVF and compartment fire (EN 1991-1-2, 2002).

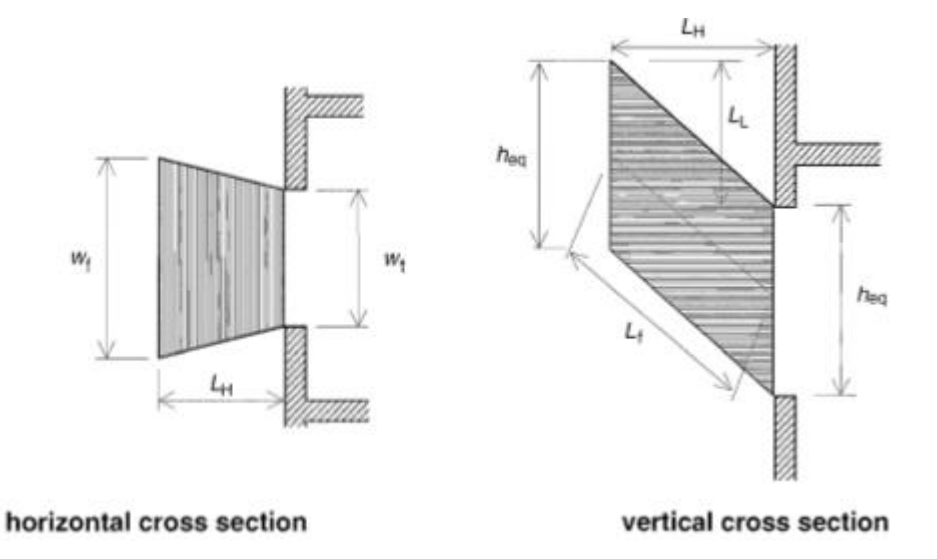


Figure 6: External flame geometry under through or FD conditions. These images have been extracted from EC1 (EN 1991-1-2, 2002).

EC1 methodology (EN 1991-1-2, 2002) majorly depends on the opening area (Ao), opening width (Wv), flame length (Lf) and rate of heat release (Q). The EVF flame height L_L is estimated using Equations 2.4 and 2.5 for NoFD and FD conditions, respectively (EN 1991-1-2, 2002).

$$L_{L} = \max \left[0; h_{eq} \left[2.37 \left[\frac{Q}{A_{\nu} \rho_{g} (h_{eq} g)^{\frac{1}{2}}} \right]^{\frac{2}{3}} - 1 \right] \right]$$
 (2.4)

$$L_L = \left[1.366 \left(\frac{1}{u} \right)^{0.43} \frac{Q}{A_p^{\frac{1}{2}}} \right] - h_{eq}$$
 (2.5)

Similarly, EVF temperature along the centreline is estimated using equation 2.6 for NoFD and 2.7 for FD conditions.

$$T_Z = (T_w - T_o) \left\{ 1 - \left[0.4725 \left(\frac{L_x W_t}{Q} \right) \right] \right\} + T_o \text{ where } \frac{L_x W_t}{Q} < 1$$
 (2.6)

$$T_z = (T_w - T_o) \left\{ 1 - \left[0.3325 \left(\frac{L_x \sqrt{A_v}}{Q} \right) \right] \right\} + T_o \text{ where } \frac{L_x \sqrt{A_v}}{Q} < 1$$
 (2.7)

Oleszkiewicz conducted a series of experiments in the late 1980s and 1990s to study the influence of compartment geometry, opening size, and fire source characteristics on external flame behaviour and façade heat flux. Yung and Oleszkiewicz (1988) conducted a comprehensive experimental study to investigate the mechanisms of fire spread along and between exterior walls of buildings. Their research identified three principal modes of vertical fire spread: internal spread through cracks at floor–wall junctions, window-to-window leap-frogging ignition caused by flames emerging from lower openings, and surface spread along combustible façades. Full-scale experiments were carried out using a compartment measuring 2.4 m (height) × 3.6 m (width) × 2.4 m (depth), with a 1.1 m² window opening on the front wall, which was extended to 6 m in height and 3.6 m in width to simulate a building façade. Wood cribs were used as the fuel source to achieve post-flashover conditions, producing severe flame exposure from the window opening. The study concluded that horizontal and vertical projections have opposite effects on fire spread — horizontal projections deflect flames away from upper openings, reducing fire spread, while vertical projections channel flames upward, intensifying vertical spread.

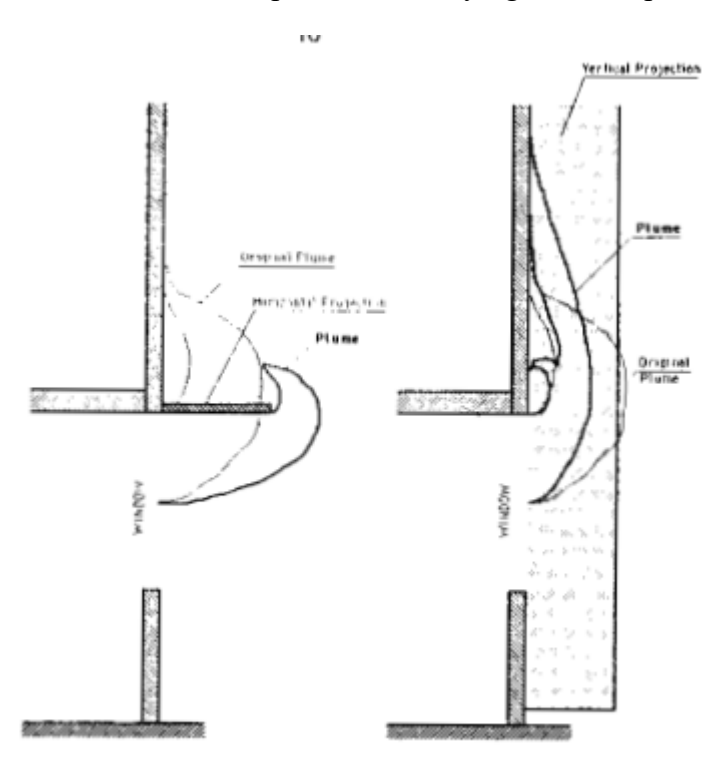


Figure 7: Effect of wall projections on fire plume. The images have been extracted from (Yung & Oleszkiewicz, 1988)

The results from smaller-scale tests were consistent with full-scale experiments, and it was also observed that fire spread between combustible façades can escalate rapidly, developing into a full-scale fire within five minutes of ignition (Yung & Oleszkiewicz, 1988). Further, Oleszkiewicz conducted investigation with single compartment configuration, with variations

applied to the opening size and aspect ratio. Measurements focused on the external heat flux to the wall surfaces above the openings (Oleszkiewicz, 1990). In some tests, propane gas burners were employed with variable flow rates, revealing that the external heat flux to the façade increased with higher gas flow rates. The heat flux above the opening, however, was observed to decrease with vertical distance from the soffit. These findings supported earlier observations by Yokoi, confirming that opening geometry significantly affects the shape of external flames and correlates with Law's model for determining façade heat flux. Further experiments using wood cribs produced higher heat fluxes compared to those using propane gas, attributed to the higher emissivity of wood flames. Oleszkiewicz also examined the effects of façade obstructions and projections on flame trajectory and façade exposure. Horizontal projections were found to reduce façade heat flux due to deflection of the flame path, whereas vertical projections near openings enhanced façade heating as flames elongated upward (Oleszkiewicz, 1991). Additionally, Oleszkiewicz highlighted the importance of adequate spandrel wall height above openings to mitigate vertical fire spread between storeys. He also proposed refinements to the constant flame-thickness assumption in Law's model, recommending a tapered, triangular flame profile for calculating flame emissivity and heat flux at specific axial positions. This adjustment aimed to produce more realistic correlations for flame radiation compared to the conservative assumptions used in earlier models. (Oleszkiewicz, 1990).

Similarly, the suggestion on external combustion near an opening from Oleszkiewicz, in the 1970s Bullen and Thomas found that an increase in external combustion further increased the exposure to the façade wall. They have suggested the concept of an excess fuel factor to calculate external combustion (Bullen and Thomas, 1979). Later, Ohmiya (1998-2003) investigated the phenomenon of external combustion and its influence on façade fire spread. Through a series of model-scale tests with varying opening dimensions similar to those used by Yokoi, it was observed that Yokoi's method may underestimate the risk of external fire spread, as it does not account for the heat release rate from external combustion (Ohmiya et al. 2000). Ohmiya proposed a predictive model for estimating the heat release rate resulting from external burning of excess fuel and reported that external flames can occur not only under ventilation-controlled conditions but also under fuel-controlled conditions, where flames from within the compartment extend out of the openings. The study highlighted that the risk of external fire spread due to external combustion is a complex function of opening geometry, compartment size, fire load, and fire location. Furthermore, Ohmiya emphasized that the uniform fuel distribution assumed in the Law model may not accurately represent real fire conditions, as spatial variations in fuel and combustion can significantly affect external flame behavior. Ohmiya et al. (2003) also developed a flame height

correlation based on experimental results from 0.5 m small-scale cubic compartment fire tests with varying opening sizes and fuel supply rates. In this study, the flame height was measured from the flame base (neutral plane) and normalized by the width of the opening (W) instead of its height. This approach provided a better correlation than using the opening height (H) or Yokoi's equivalent radius correlation. Furthermore, Ohmiya *et al.* introduced a virtual origin correction (Δz) to refine Yokoi's correlation and defined a dimensionless vertical temperature (Θ) as a function of $(z + \Delta z)/r_o$ (Ohmiya *et al.* 2003).

Klopovic and Turan (1990s–2000s) conducted a series of eight full-scale compartment fire tests in a 3.6 × 5.3 × 2.4 m enclosure with 2.4 × 1.5 m window openings and 0.8 × 2 m doors to examine the effects of ventilation (forced draught, no forced draught, and wind) on EVF and its impact on heat flux to façade wall focus on window breakage and suggested the risk of secondary fire on the story above. Furniture was used as fuel, providing a wood-equivalent fire load density of approximately 23–29 kg/m². The recorded flame dimensions, determined at a flame axis temperature of 540°C, exceeded predictions from the Law model correlation. In all tests, the glass in the upper-storey window failed, despite the spandrel wall height being nearly three times that recommended by Yokoi for preventing vertical fire spread. These findings indicate that earlier studies may have underestimated the risk of vertical flame spread under realistic fire conditions. The discrepancy is likely attributable to the use of non-cellulosic fuels, differing from the wood cribs used in developing many Law model correlations. Additionally, the distribution of fuel within the compartment, coupled with enhanced external combustion, may have contributed to elevated façade heat fluxes (Klopovic and Turan, 2001).

Lee et al. conducted a series of model-scale fire tests to investigate the internal and external heat release rates (HRR) and temperature distributions, with a focus on external flame height and façade heat flux to the spandrel wall above the opening. Using a gas burner, Lee systematically varied the compartment dimensions, opening sizes, and burner locations, and found that the burner position had no significant influence on the resultant external heat exposure. The experiments verified previous correlations between air inflow and heat release rate, showing uniform internal temperature conditions within the compartment. Based on these observations, Lee proposed a new characteristic length scale defined by the effective outflow area and the length after which the external plume changes from horizontal to vertical orientation under the influence of buoyancy. These parameters were incorporated into a new correlation for predicting flame height and façade heat flux above an opening (Lee, Delichatsios and Silcock, 2007).

Over the years, there were many research developments and knowledge transfer on the topic of EVF. The Law model remains the most comprehensive approach for linking internal compartment parameters with the characteristics of external flames and the resulting heat flux to surrounding structures. Later in 2010, Empis revisited this model to perform a detailed sensitivity analysis of the parameters considered within it and this further enables the identification of the parameters that have the greatest influence on the resultant external heat exposure (Abecassis, 2010). Asimakopoulou et al. also investigated the most common fire engineering design correlation used to describe the EVF geometry and thermal characteristics and concluded that many of the current design correlation had an inconsistent behaviour and thus suggesting that there is a need to improve the fire engineering design correlation (Asimakopoulou et al., 2017).

The present study examines the applicability of existing fire engineering correlations in accurately characterizing EVF systems in complex geometries, particularly those with curvilinear buildings. Additionally, this research investigates the thermal and geometrical characteristics of EVF within such complex geometries.

Table 2: Summary of key experimental investigations related to EVF

Ref	Fuel Type	EVF Characteristics
Yokoi (1960)	Timber	Plume temperature data
Webster and Smith, 1964	Wood cribs of sticks 24.5	EVF flame height
	mm	
Oleszkiewicz,	Propane Gas	Heat flux on the facade
1989	Wood cribs	
Ohmiya et al. 2000	Methane gas burner	EVF dimension, temperature
Klopovic and	Real furniture's	EVF dimensions, EVF
Turan, 2001a;		temperature, Heat flux on the
Klopovic and		façade
Turan, 2001b)		
(Lee, Delichatsios and Silcock,	Propane and methane	EVF dimensions, EVF
2007)	burners	temperature, Heat flux on the
		façade
Empis, 2010	Real furniture's	Heat flux on the facade
Asimakopoulou et al., 2017	Heptane	EVF dimensions, EVF
		temperature, Heat flux on the
		façade
Current thesis	Heptane	EVF dimensions, EVF
	Diesel	temperature, Heat flux on the
		façade

2.2 Enclosure Fire Dynamics

A compartment fire is a combustion process that develops within an enclosure, where the interaction between fuel, ventilation, and boundary materials governs its thermal and chemical behavior. The development of a compartment fire can be divided into distinct stages: ignition, growth, flashover, fully developed fire, and decay.

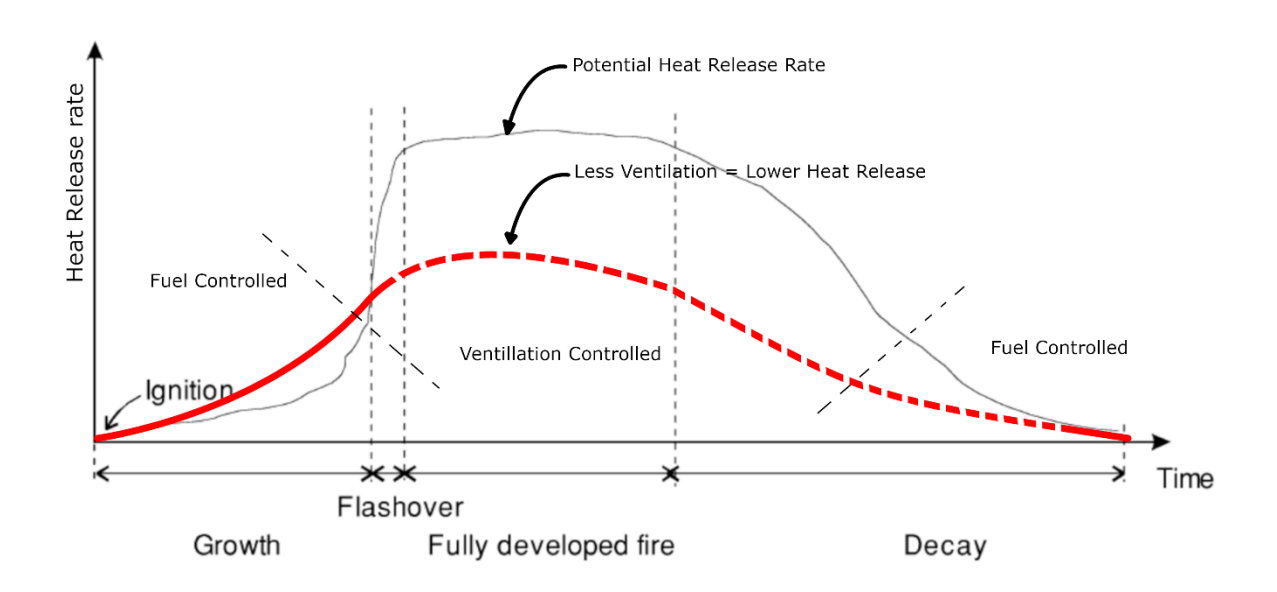


Figure 8: Stages of compartment fire (Karlsson and Quintiere, 2000).

Ignition marks the onset of a self-sustained exothermic reaction, occurring either through piloted ignition (e.g., a flame or spark) or spontaneous ignition due to heat accumulation in the fuel. Once ignited, the growth phase is characterized by an increasing heat release rate (HRR), influenced by the fuel characteristics, enclosure geometry, and available oxygen. The combustion may occur in either a smoldering or flaming mode, with the latter resulting in rapid flame spread and faster energy release.

The flashover stage represents a critical transition, where the compartment temperature rapidly increases to approximately 500–600 °C, or when the radiative heat flux to the floor exceeds 15–20 kW/m². This leads to near-simultaneous ignition of all combustible surfaces, transitioning the fire from the pre-flashover to the fully developed phase. In this stage, the HRR reaches its maximum and is typically limited by the available oxygen, signifying a shift from fuel-controlled to ventilation-controlled burning. The gas temperature within the enclosure may exceed 700–1200 °C, and unburnt gases may ignite upon exiting the openings, forming externally venting flames (Karlsson and Quintiere, 2000).

As the fuel is consumed and oxygen is depleted, the decay phase ensues, characterized by a declining HRR and compartment temperature.

The evolution of compartment fires is influenced by several parameters: ignition source characteristics, fuel type and configuration, enclosure geometry, opening size and position, and the thermal properties of the boundary materials. Understanding these factors is fundamental for predicting fire behavior and developing effective fire safety and structural design strategies (Karlsson and Quintiere, 2000).

2.3 Effect of Ventilation

In the initial stage of a fire, its growth can be determined by either the availability of fuel or the ventilation. This depends on factors such as the geometry (size, shape and number) of the openings, heat release rate and ventilation conditions and the sheer volume of the internal envelope as an air store.

This section primarily focuses on examining the impact of ventilation on compartment fire behaviour. Further, the subsequent sections will provide detailed explanations regarding the distinctions between fuel-controlled fires and ventilation-controlled fires. Additionally, the differences between forced draught and no forced draught conditions with respect to the externally venting flames will be explored. Finally, the influence of wind on EVF will be investigated in detail. Through this literature review, a comprehensive understanding of the intricate relationships between ventilation, compartment fire behaviour, and external factors will be attained.

2.3.1 Fuel controlled versus Ventilation controlled Fire.

Global equivalence ratio (GER) is the parameter used to differentiate the compartment fire ventilation condition which is under ventilated or well ventilated. GER is defined as the ratio of the fuel mass flux (m_f) to the oxygen mass flux entering the compartment (m_{o2}), divided by the fuel-to-oxygen stoichiometric ratio (r) in Equation 1 (Hurley, 2016; Quintiere, 2006).

$$GER = \frac{m_f}{rm_{o2}} \tag{2.8}$$

$$m_{o2} = \begin{cases} 0.5 \, Y_{o2,air} A_O \sqrt{H_O}, natural \ ventilation \\ 0.23 \, \rho_{amb} V, mechanical \ ventilation. \end{cases}$$
 (2.9)

The mass flow rate of the oxygen entering the compartment can be estimated using an empirical correlation Equation 2 (Hurley, 2016; Quintiere, 2006). When the value of GER exceeds unity, the fire is considered as fuel-controlled (well ventilated); when GER is less than one, the fire is considered as ventilation-controlled (under-ventilated).

2.3.2 Forced Draught and No Forced Draught.

EN 1991-1-2, defines draught conditions as No Forced Draught (NoFD) when openings are present only on one side of the compartment and Forced Draught (FD) when there are openings on opposite sides of the fire compartment and thus additional air is being fed to the fire from another source. Figure 4 depicts the schematic of EVF shape in FD and NoFD conditions in a building fire (EN 1991-1-2, 2002).

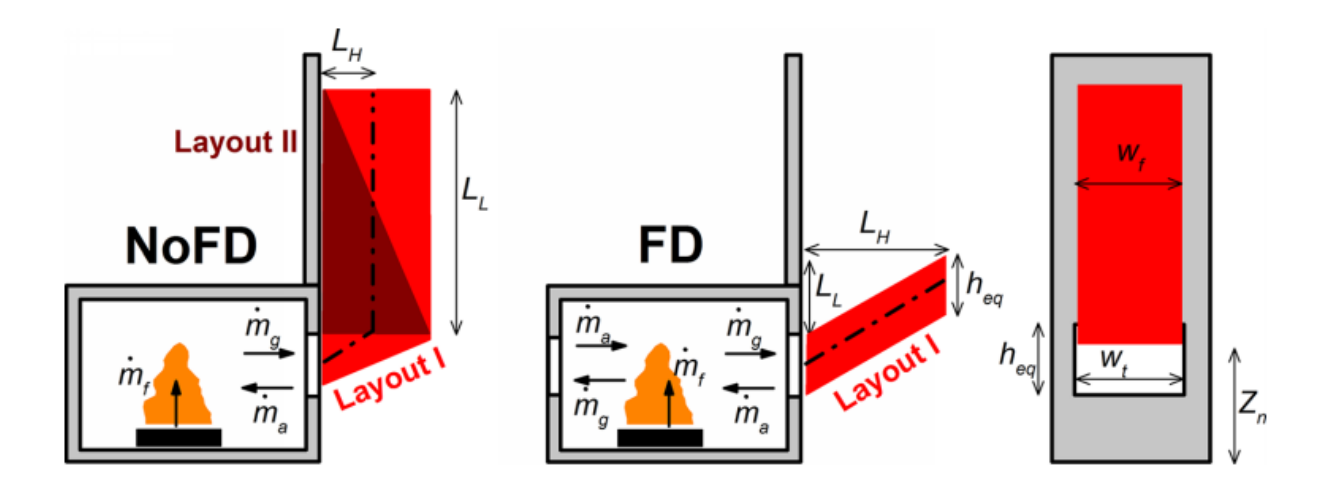


Figure 9: Schematic of general EVF shape in NoFD and FD conditions (Asimakopoulou et al., 2016).

In NoFD conditions (Layout II) EVF is found to be with constant flame thickness, and the flame is projected from the opening at an angle of 45⁰ and then bends upwards and exhibits a constant flame thickness. However, in FD conditions, one should observe a triangular shaped flame (Layout I). In FD conditions, EVF ejecting from the opening like a jet form and vent away from the façade through the entire height of the opening showing a constant flame thickness (Asimakopoulou et al., 2016).

2.3.3 The influence of Wind or Forced Draught on Externally Venting Flame.

A large amount of research has been conducted in the past to study the influence of wind on building fires (Li et al., 2017; Huang et al., 2009; Ji et al., 2015) and it is well understood that in many past fire incidents, wind conditions have played a significant role in the spread of fire and smoke. A few such cases were reported such as, Marina Torch Tower in 2015 and 2017 (BBC, 2017); Address downtown in 2015 (Hanna et al., 2015), in Dubai, United Arab Emirates. Figure 5 depicts the reported incidents where large fires have resulted in the flame spread over buildings in the neighbourhood or community in which wind could have been a critical aiding factor and aggravated by the presence of combustible building façade materials, which is usually wood or

combustible cladding (Hardy et al., 2019; BBC, 2016). A few of the reported instances of such fires are Lærdal fire in Norway (2014) (Steen-Hansen et al., 2016) and Cohoe fire in New York (2017) (J. Fahd, 2017).





Figure 10: High-rise building fire spread aggravated by wind and combustible cladding (Hardy et al.,2019; BBC, 2016).

Understanding the interaction of wind and fire on building façades is critical for improving building fire safety, as this may dictate the behaviour of façade fire propagation (Asimakopoulou et al., 2016). International building codes and regulations, in the context of fire and life safety, include methods and measures to ensure maximum fire prevention and protection against structural fires. Studies conducted by Yousef et. al. (Abu-Zidan et al., 2022) suggest that both wind speed and direction have a considerable influence on the façade fire propagation.

However, faster vertical propagation of fire was noticed for the case of no wind but with minimum lateral spread. Research concluded that the when the fire is fully developed, the presence of wind can increase the risk of fire spread along the multiple façade surfaces of the building (Abu-Zidan et al., 2022). To investigate the influence of wind on fire and smoke, research has been conducted considering different fuels sources including propane gas burners (Li et al., 2017; Li et al., 2013; Hu et al., 2017; Li et al., 2021), heptane pool fires (Huang et al., 2009; Ji et al., 2015; Gao, et al. 2021; Chen et al., 2011) or wood cribs (Loneermark et al., 2007; McAllister et al., 2016).

Table 2 tabulates selected medium-scale experiments from recent literature along with the relevant wind velocity ranges, compartment dimensions, measured quantitates (such as temperature at the interior, T_{in} , or exterior, T_{out} , of the fire compartment and heat flux at the façade, HF), parametric studies and number of openings tested. From those studies, it has been established that increased wind velocity (u) can affect EVF in largely two ways. First, it affects EVF height (EVF height) and projection (EVF projection), and second, it also affects Heat Release Rate (HRR) and fuel Mass Loss Rate (MLR).

Table 3: Selected research work on wind-driven medium scale fires.

<i>u</i> [m/s]	Fuel	Comp. dim. [mm]	Measurements	Par. Study	Open	Reference
0 - 6.0	C ₃ H ₈	800 x 800 x 800	Tin, Tout, u	u, HRR	2	Li et al., (2017)
0 - 3.6	C ₃ H ₈	800 x 800 x 800	T _{in} , u	u, HRR	2	Li et al., (2017)
0 - 3.0	C7H16	600 x 600 x 600	T_{in}, T_{out}, u, HF	и	2	Huang et al., (2009)
0 - 3.0	C7H16	1000x1000x1000	T_{in}, T_{out}, u, m_f	u, pan size	2	Ji et al., (2015)
0-2.0	C ₃ H ₈	400 x 400 x 400	Tin, Tout, u, EVF _{height}	u, op. size	1	Hu et al., (2017)
0 - 2.0	C ₃ H ₈	400 x 400 x 400	T_{in} , T_{out} , u , HRR	-	1	Hu et al., (2017)
0 - 2.0	LPG	400 x 400 x 400	Tin, Tout, u	<i>u</i> , op. size	1	Hu et al., (2017)
0 - 3.5	C7H16	580 x 580 x 580	T_{in} , T_{out} , u , HF	<i>u</i> , op. size, fuel posit.	2	Gao et al., (2016)
0 - 3.0	C7H16	600 x 600 x 600	T _{in} , T _{out} , u, MLR, HRR	и	2	Chen et al., (2011)
0-4.4	C ₂ H ₆ O	900 x 900 x 900	Tin, Tout, u, mf	-	2	Ji et al., (2015)
0 - 2.9	C7H16	900 x 600 x 600	$T_{in}, T_{out}, u, m_f,$ EVF	u, op. size	2	Smolka (2022)

Hu et. al. (Hu et al., 2017) studied the influence of opening sizes, HRR and u on the EVF and concluded that the EVF height decreases with increasing wind speed. However, it is important to note that this study consider a single opening at the centre of the side wall of the fire compartment (Chen et al., 2011). Also, Li et. al. (Li et al., 2017) studied the wind effect on EVF projection probability from a compartment with an opposing opening of different sizes (considers as a door and window) and concluded that when considering a "no wind" case or wind with very low velocities there are both inflow and outflow from the openings. However, with increased wind velocities such bidirectional flow will become unidirectional flow at low fuel supply rate and at high wind velocities, only unidirectional flow can be seen at the openings regardless of fuel supply rate. In his study, the wind tunnel was capable of producing a steady airflow varying from 0 to 15 m/s. However, for the experiments, wind velocities in the range of 0–3 m/s were applied, with an incremental increase of 0.6 m/s. According to the scaling laws adopted in the study, this corresponds to a full-scale equivalent wind speed range of approximately 0-6 m/s. (Li et al., 2017). Both studies were considering external wind normal to the opening (Li et al., 2017; Hu et al., 2017). However, Hu et.al. investigated the influence of wind on EVF where wind is introduced parallel to the façade and concluded that facade flame height decreased with an increase in sideward wind speed. Additionally, horizontal flame distance increased for larger opening and decreased for relatively smaller openings with an increase inside ward wind speed (Hu et al., 2019). Thus, we can conclude that the influence of wind and its direction has significant impact on the thermal and geometrical characteristics of EVF.

2.4 The effect of building characteristics

The characteristics of a building, such as its height, shape, and construction materials, have been found to have a significant impact on the spread and intensity of facade fires. Hu et, al. suggest that compared to a normal compartment fire, fire behaviour in high-rise buildings is more complex due to the special features involved in high rise buildings which include complex building structures and larger surface areas with extensive use of external façade insulation materials (Hu et al., 2017).

There have been many studies and research conducted on the influence of various building features on external venting flames, such as the effect of adjacent buildings or side wall structures and the effect of horizontal barriers such as balconies, window eaves, etc. Lee et al. conducted a series of experiments in small-scale compartments by varying the geometry of the compartment, opening dimensions, heat release rates, burner locations, etc. and investigating relations between façade flame height and the resultant heat flux from a façade fire. Based on these experiments and the flow development in the compartment they have developed two length scales l_1 and l_2 ; l_1 is related to the convective flow at the opening and used to correlate the flame height and l_2 is related to the buoyancy and momentum flux at the opening and used to correlate the heat flux on the façade from the fire (Lee et al., 2007).

To study the effect of a facing wall on an external venting flame, Lee et al. investigated the physics of the flame behaviour, flame heights, and heat fluxes on a building facade where an opposite parallel wall representing a building wall was installed through a series of small-scale experiments. This research provides valuable information on the separation distance between the building's external walls, and a new characteristic length scale was developed that gives the length after which the flames turn from horizontal to vertical (Lee et al., 2007). Similarly, Yanagisawa et al. also conducted similar research and examined the heat release rate at which flames occurred from the opening, the temperature distribution in ejected flames, and the heat flux from ejected flames with and without an opposite wall, concluding that the facing wall does not affect the burning inside the enclosure at under-ventilated conditions regardless of its distance from the opening (Yanagisawa et al., 2008).

Lu et al. investigated the influence of side wall length, which means the wall is located normal to the facade direction, on the ejected facade flame from a window of an under-ventilated compartment fire. It was observed that the window-ejected flame was very high in the narrow vertical channel formed by the two parallel side walls. Further to this, it was observed that the effects of the side wall length on the mean flame height are larger as the side wall distance decreases, leading to flame heights much higher than those without sidewalls (Lu, 2014).

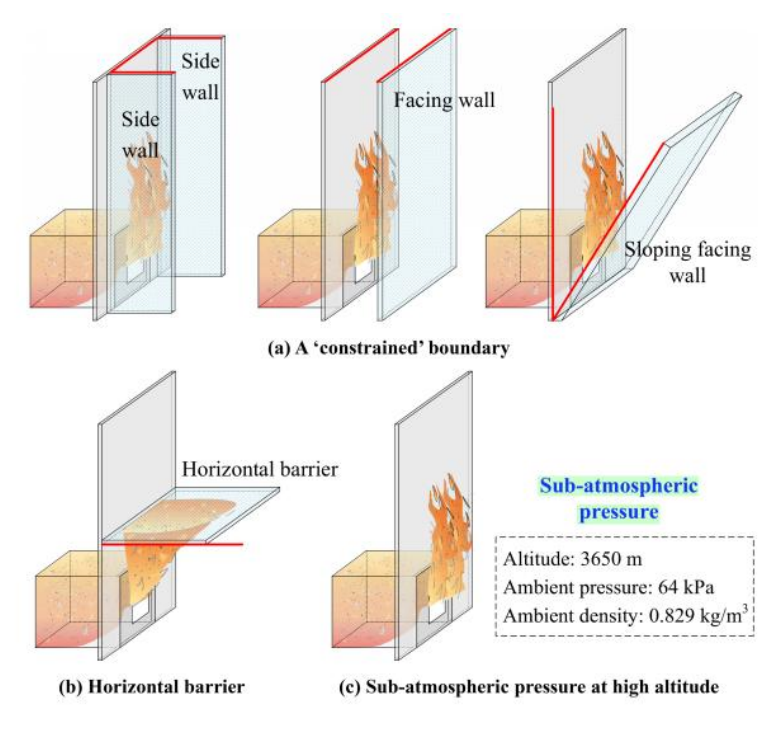


Figure 11: EVF under different external boundary condition (Sun et al., 2023).

In general, it was observed that an external venting flame originating from an opening with an opposite building facing wall or side wall reduces the air entrainment in the plume, which leads to larger flame heights and an increase in temperature. Due to this phenomenon, the external flame will have pushed closer to the façade and resulted in increased heat transfer and heat flux impact. If the façade is combustible in nature, this will cause increased fire to spread. However, in the case of horizontal barriers such as balconies, eaves, etc., this will result in increased air entrainment, and the presence of barriers above will stop the upward momentum of EVF and result in a decreased flame height. But this can lead to intense heat transfer to the horizontal barrier itself (Sun et al., 2023).

2.4.1 Opening Characteristics

a. Multiple opening

There have been many studies in the past on the characteristics of the window or opening through which EVF is ejected (Lu et al., 2015; Sun et al., 2020; Zhang et al., 2022). However, it is worth

noting that most of the studies in the past have studied EVF in single cubic-like enclosures with a single opening. However, in real-world scenarios, building typically feature more than one window, which can significantly influence the ventilation conditions within the compartment. Multiple openings can lead to complex phenomena such as turbulent combustion behaviour, increased inflow of fresh air, and altered EVF dynamics. Despite its importance, limited research has focused on the effects of multiple compartment openings and the mechanisms behind merging EVF. Such flame merging can lead to larger fire sizes and can further intensify the thermal and physical impact on the building façade.

Lu et al. investigated the EVF from two parallel windows, where they considered different window dimensions, different separation distances between the two parallel windows, and different HRRs. In this study, it was observed that based on the ejected flame from the opening, three different ranges, named continuous merging, intermittent merging, and non-merging flames, have been identified based on the different separation distances between the two windows. If the separation distance between the two windows is small, the external flame from the opening will merge continuously. When the smaller window separation distance is gradually increased to a moderate distance, then flames will merge intermittently, and finally, if the separation distance between windows is large, there is no merging flame behaviour (Lu et al., 2015).

b. Different opening shapes and their influence on External venting flame

Casement window

Sun et al. investigated façade flame evolution with a casement window of various opening angles. Experiments were conducted in a model-scale fire compartment with different heat release rates and a casement window of various dimensions and opening angles. It was found that the critical heat release rate for flame ejection as well as the external facade flame height decrease with increasing the window opening angle to less than 60 degrees ($\theta < 60^{\circ}$). Then, all these quantities change little as the window opening angle is further increased ($\theta \ge 60^{\circ}$). Further to this, they have also developed a new characteristic length scale to quantify the flame height based on the window dimension and opening angle of the casement window (Sun et al. 2020).

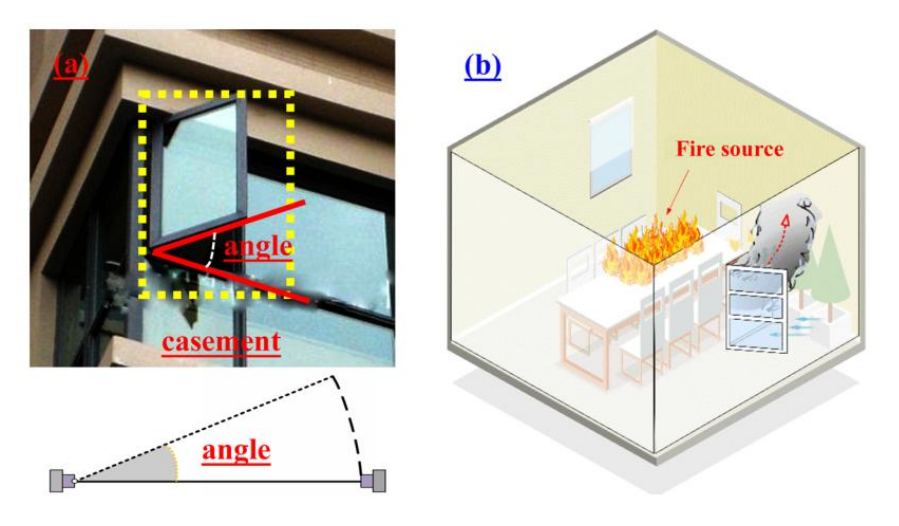


Figure 12: Compartment fire and façade with casement window (Sun et al. 2020).

Top hung window

Zhang et al. investigated the ejected facade flame behaviour from a top-hung window. Experiments were performed in a cubic-scale model compartment with a top-hung window with four opening angles and four dimensions under various heat release rates. In these experiments, they quantified the ejected facade flame's geometrical characteristics, such as vertical height and horizontal depth (normal to the facade). It is found that the position of the neutral plane between the inflow and outflow at the top-hung window increases with opening angle while being smaller as the window width is larger or the window height is smaller. The critical HRR for flame ejection is higher as the top-hung window opening angle is larger. The facade flame depth increases while the flame height decreases with the increasing opening angle of the top-hung window. Further to this, they have also developed a new characteristic length scale to determine the flame height based on the top-hung window dimensions and window opening angle (Zhang et al., 2022).

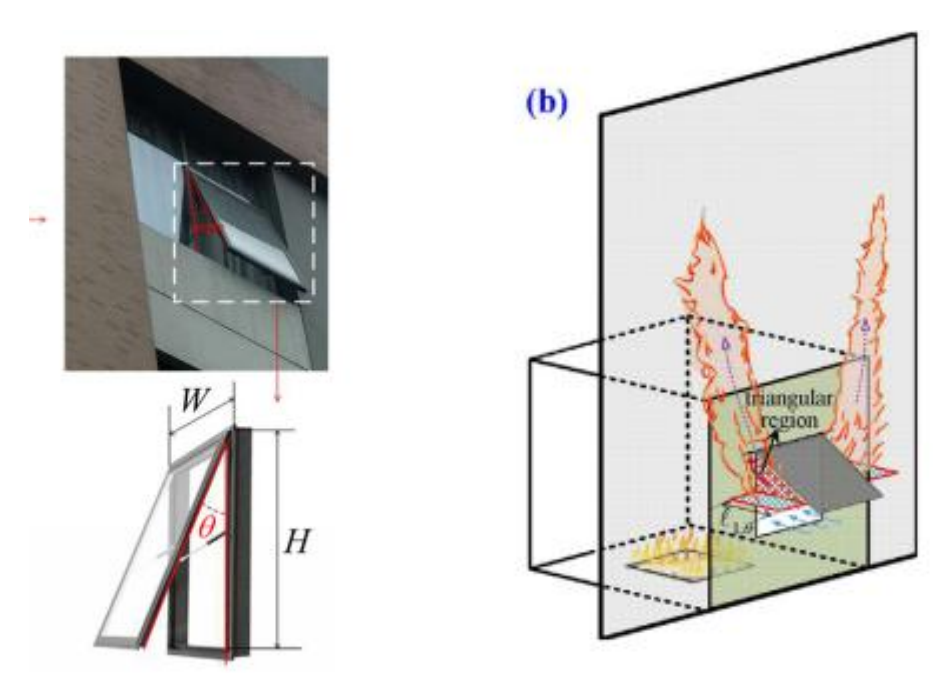


Figure 13: Façade flame with top hung window (Zhang et al., 2022).

Circular Windows

Zhang et al. investigated the façade flame for compartment fires involving circular openings and revealed that with the same opening dimensions, the maximum heat release rate inside the compartment with a circular opening is larger than that of a square opening. Also, for relatively large circular openings, façade flame tends to form as ceiling jet extension for lower HRR, and for increased HRR, it was observed that initially façade flame tends to form as ceiling jet extension, and then this will convert to a spill fire plume. Further to this, Zhang et al. developed a non-dimensional correlation to characterize the façade flame heights for both ceiling jet flame extension and spill fire plumes originating from a circular opening (Zhang et al. 2020).

Triangular Windows

Zhang et al. investigated the façade flame for compartment fires from triangular openings constrained by a vertically facing wall. The results revealed that the vertical facing wall has little effect on the hot gas temperature inside the compartment, and the facade flame height is independent of the vertical facing wall when the distance between the triangular opening and the vertical facing wall (D) is relatively large, while the facade flame height is increased at a relatively small D (Zhang et al., 2023).

2.4.2 Architectural features and their influence on EVF.

a. Cladding materials

The use of various combustible materials in exterior wall assemblies has become increasingly common due to their benefits in energy performance, moisture protection, and design flexibility.

Among the most widely employed systems are Exterior Insulation Finish Systems (EIFS), Metal Composite Materials (MCM), High-Pressure Laminates (HPL), Structural Insulated Panels (SIPS), Rain Screen Cladding (RSC), Weather-Resistive Barriers (WRB), and external timber panelling (White and Delichatsios, 2014). Modern architectural trends favour innovative cladding materials and curtain wall systems for their aesthetic and functional benefits. However, these features can significantly influence the behaviour of fires on building exteriors.

b. Sloped/Incline ceiling and flame extensions

Fang et al., (2024) investigated how an inclined eave structure above an opening alters façade fire plume behaviour compared to flat façade conditions. The research aims to understand the physical mechanism driving this extension and to develop prediction models for flame extension lengths. Their experiments revealed that the inclination angle of the eave plays a important role in altering flame dynamics. As the eave inclination increases, the upstream flame extension length grows due to enhanced buoyant momentum aiding the flame's propagation along the eave, while the downstream flame extension reduces because the opposing buoyancy weakens the flame momentum. It was observed that the upstream flame consistently extended further than the downstream flame for all inclination angles considered (0°–20°), and the difference in extension lengths became more pronounced with steeper inclinations. The study also analysed the flame extension mechanism through momentum and energy analysis of the facade flame. Feng et, al concluded that their findings and models can be applied to predict flame extension in building fires and inform building safety design, such as determining the critical eave length to prevent fire spread to upper rooms and thus underlining the necessity of accounting for architectural geometry in façade fire safety design (Fang et al., 2024).

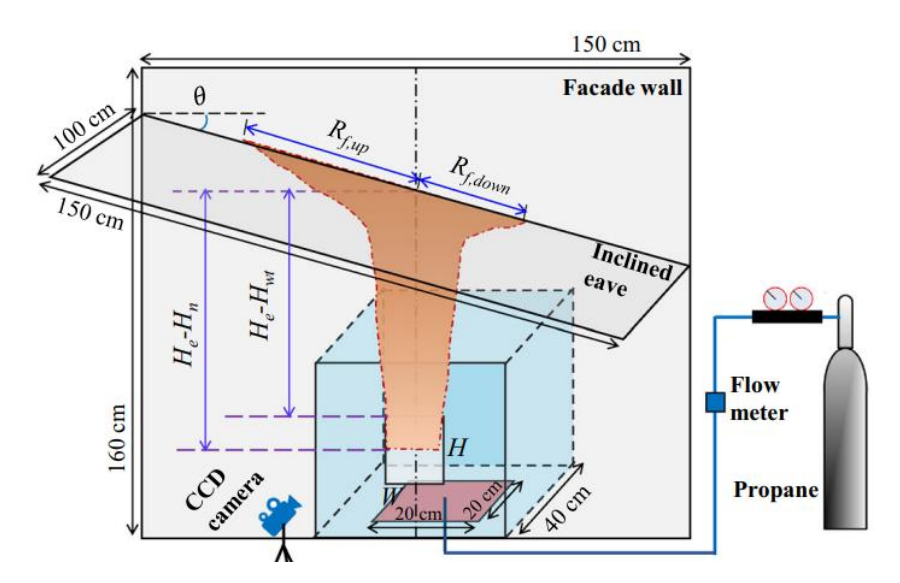


Figure 14: Experimental setup of incline eave (Fang et.al 2024).

c. Curved ceiling and flame extensions

Recent studies have highlighted that the curvature of ceilings and sidewalls significantly changes fire dynamics. Pan et al. (2022) experimentally and theoretically investigated the extension flame length of buoyancy induced fire plumes beneath curved ceilings in a utility tunnel. It was observed that curved surfaces affect flame extension by modifying the buoyancy and entrainment processes, leading to longer flame spread due to unburnt fuel mass flow after ceiling impingement. A new global equation for flame extension length beneath the curved ceiling was proposed to account for these effects, validated against experimental data with an error margin of less than 15%, highlighting the necessity to consider ceiling curvature in fire protection engineering design for the utility tunnel.





Figure 15: Model-scale utility tunnel platform for investigating the flame extension Pan et al. (2022).

To study the impact of curved side wall on the fire shape and temperature beneath ceiling centreline, another study conducted by Pan et al. (2020). It was found that curved walls bend the flame without directed contact with the curved ceiling, and once the flames touched the curved ceiling, flame extension along the ceiling increased evidently. A new correlation was developed to predict maximum temperatures, incorporating the concept of characteristic angles and accounting for smoke accumulation. The proposed models showed good agreement with experimental results, emphasizing that curved geometries strongly influence both flame development and thermal environments in enclosed spaces Pan et al. (2020).

Similarly, Sturdy and Johansson (2025) further investigate the influence of ceiling geometry on flame extension, using experiment with reduced scale tests with test setup's ratio is in between 1:11 and 1:15 depending on which the tunnel dimensions. Dimension of the test setup shown in the figure 16. They have studied the flame behaviour under curved ceilings with a propane gas burner and a heptane pool fire and found significant differences compared to traditional flat ceiling configurations.

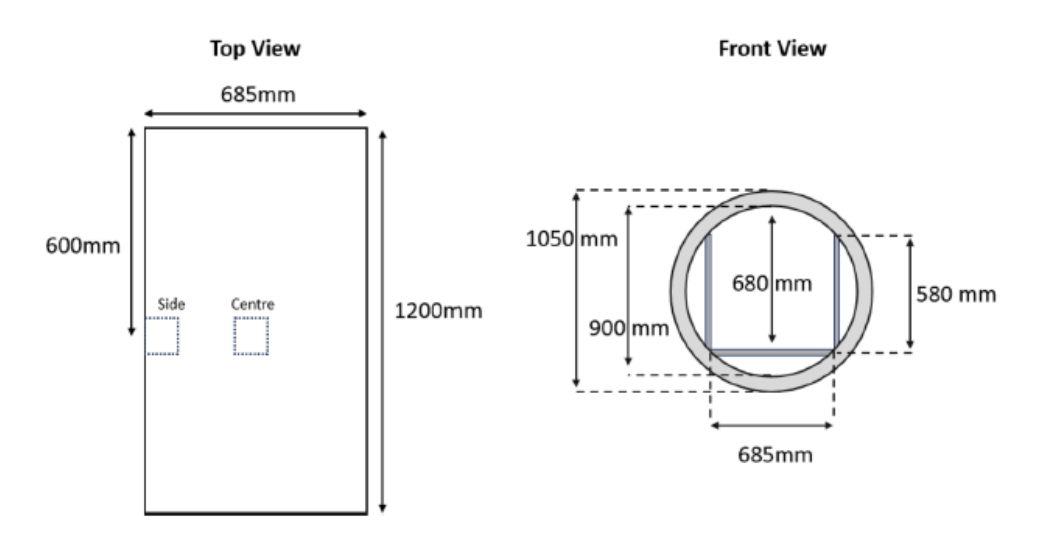


Figure 16: Dimensions of curvilinear tunnel setup (Sturdy and Johansson, 2025).

The study reveals that the curved geometry enhances the flow which resulted in longer flames, particularly for momentum dominated propane fires. However, for buoyancy dominated heptane pool fires, wall proximity decreases the HRR and limiting flame extensions. Their results exhibited that the curvature of the ceiling alters the momentum and buoyancy forces of the flame plume after impingement, enhancing the horizontal and vertical components of the flow. Unlike flat ceilings, where the flame spreads radially after impingement with predominantly horizontal momentum, the curved ceiling promotes additional vertical deflection and sustains longer flame extensions. In momentum-dominated fires, such as those generated by propane burners, the curved geometry caused unburnt fuel to travel further along the ceiling before complete combustion, leading to longer flame lengths than predicted by traditional flat-ceiling models. In buoyancydominated pool fires, the reduced air entrainment near the curved wall also influenced the heat release rate and subsequent flame extension. These findings highlight that conventional flame length models based on flat ceiling assumptions often underpredict or mischaracterize flame behaviour in curved geometries, necessitating model adaptations that account for combined buoyancy and momentum effects. This study emphasizes the need for more accurate fire safety design considerations for modern structures utilizing curved architectural forms (Sturdy and Johansson, 2025). This study focused on in-compartment fire behaviour and ceiling flame extension within curved ceiling configurations, whereas the present study investigates the external venting flame characteristics of curvilinear geometries.

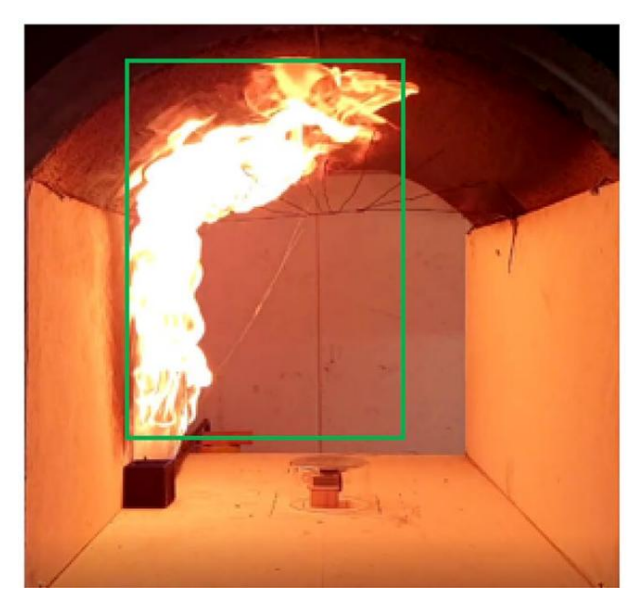


Figure 17: Reduced scale tests to investigate the flame extension under curved ceilings (Sturdy and Johansson, 2025).

2.5 Concluding remarks

In conclusion, the above reviewed literature highlights the profound influence of building characteristics, particularly façade geometry and opening configurations, on the development and behaviour of EVF. The presence of multiple openings in a building's facade can significantly impact the flame spread and EVF intensity. The size, location, and design of these openings can influence both the interior and exterior fire, increasing the risk of vertical and horizontal fire spread as these openings provide a pathway for flames and causing complex flow behavior both inside the fire compartment and on external facades. The literature review also revealed that numerous factors, including window opening designs and shapes such as circular, rectilinear, casement, triangular, and top-hung windows, can significantly affect EVF, leading to intricate flow behaviors. These findings underline the need for a deeper understanding of fire flow dynamics within curvilinear openings, which present a unique challenge due to their non-rectilinear or non-circular shape. This gap is particularly significant given the growing adoption of architecturally complex forms in modern construction, where curvature and sloping façades may alter plume attachment, entrainment, and radiation feedback mechanisms.

The literature review has shown only two main research methods are being used: numerical simulations and predominantly reduced scale experiments. The methodology of this study is therefore informed by cutting-edge research and uses both experimental and numerical approaches. However, several critical challenges remain unaddressed, for example scenarios where the opening for EVF is located on a sloping wall, the opening is not in the center of a roomwall or is not a flat window, or the building façade itself is not flat. This research work is informed

by the literature, exactly targeted at such cutting-edge problems under the general category 'curvilinear'. The methodology is also literature informed in obtaining case studies for validation. While these approaches have advanced understanding of fundamental EVF mechanisms, their applicability to large-scale, non-orthogonal geometries remains limited. The current research therefore aims to address this gap by systematically investigating the effects of façade curvature and opening geometry on EVF development through combined experimental and numerical methods.

Building upon the insights gained from this literature, the forthcoming sections will specifically concentrate on the fire flow behavior within curvilinear openings. This investigation aims to provide a comprehensive understanding of the complex fire dynamics and flow behaviors that arise within such unconventional opening geometries. By conducting numerical simulations and analysis, this research endeavors to shed light on the EVF development and its characteristics in curvilinear buildings.

3 FORCED DRAUGHT IMPACT ON EXTERNALLY VENTING FLAMES: AN EXPERIMENTAL AND NUMERICAL INVESTIGATION

3.1 Introduction

Factors such as fuel load, building height, compartment geometry, ventilation, external wind conditions, and the compartment opening dimensions plays very crucial roles in the development and spread of fire and smoke within and outside buildings (Drysdale, 2011; Quintiere, 2016). In a compartment fire scenario, following ignition, burning gases such as flames or hot unburnt combustion gases may exit through the compartment openings (through doors, windows, etc.) and burn outside when this excess fuel mixes with ambient air. Fire development and intensity both inside and outside the room of fire's origin may be significantly influenced by changes in compartment ventilation, horizontal and vertical openings, and size (Drysdale, 2011; Smolka et al., 2021; Madrzykowski, 2009).

As seen above, previous works have mainly focused on fire compartment and do not fully address how wind affects EVF development and its impact on the façade in varied ventilation conditions with respect to FD and NoFD (No wind) conditions. The present study focuses on a reduced-scale compartment with a facade wall on both sides. Openings of equal size are provided at the centre of both side walls of the compartment, and an external wind that is normal to the opening was considered. The aim of the present study was to further widen knowledge of EVF development using numerical and experimental techniques to investigate the influence of wind velocity, ventilation conditions and openings dimensions.

3.2 Experimental and Numerical Investigation

3.2.1 Experimental setup

In this study, utilization of experimental results from a previously conducted doctoral study of Jan Smolka, University of Ostrava, which have been employed as a foundation for the subsequent numerical simulations conducted using CFD (Smolka, 2022). It is noteworthy to highlight that permission was duly obtained from the respective researcher to employ their PhD experimental data in conjunction with the CFD simulations. Figure 18 illustrates the complete experimental setup built, including the smoke extractor's locations, the fire compartment and the two façade rigs at the inlet and outlet. The experimental compartment was built based on a 1:4 scale of the ISO 9705 room, having a length of 900 mm, width of 600 mm, and height of 600 mm and two façade rigs 600 mm width and 600 mm height installed at the inlet and outlet side. It was constructed of 50 mm thick fire-resistant vermiculite boards (THERMAX ECO) and facade rigs were made of

fiber cement boards. Both openings on inlet and outlet side were placed under hoods for smoke extraction with dimensions of 1000 mm x 1000 mm. The smoke extractor was connected to an industrial centrifugal blower extractor fan with a capacity of 2600 m³/h.

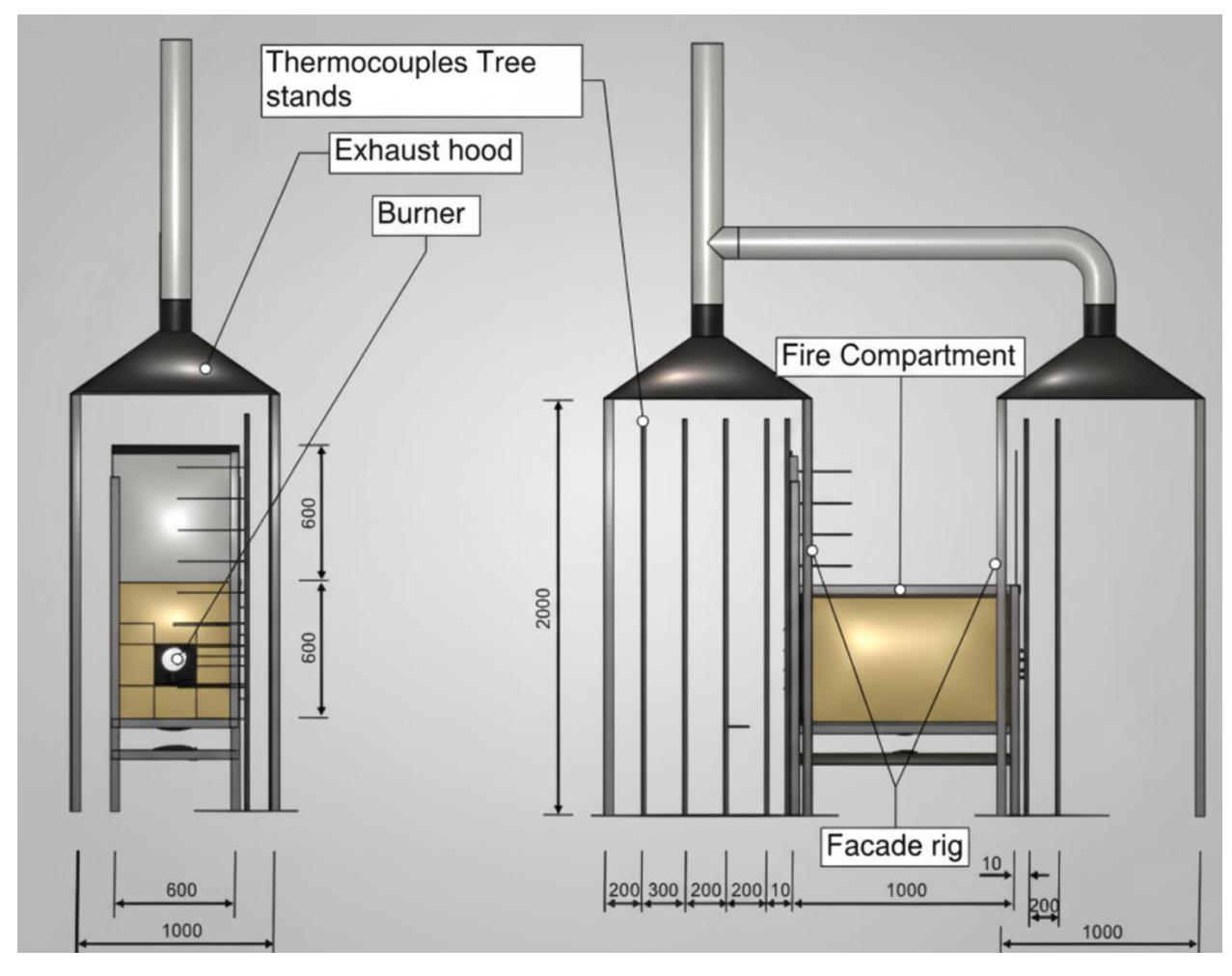


Figure 18: Front view of the experimental setup (dimensions in mm).

For the parametric study, it was decided that three sizes of opening dimensions, such as 200 mm x 200 mm, 300 mm x 300 mm, and 400 mm x 400 mm, which are located on opposite sides, would be investigated. The selection of the three opening sizes was based on a combination of literature evidence, experimental constraints, and practical representativeness of façade openings in real high-rise buildings. The chosen dimensions (200 mm x 200 mm, 300 mm x 300 mm, and 400 mm x 400 mm) were intended to capture a progressive variation in the ventilation factor, thereby enabling assessment of its influence on flame behaviour, external flame projection, and compartment temperature. These sizes represent typical ranges of window-to-wall openings used in scaled fire experiments and align with the scaling principles reported in previous studies. An external wind speed of 2.9 m/s was set normal at a distance of 2.5 m from the opening to simulate FD conditions for all three opening sizes. The fan was set to start when the fire fully evolved in the compartment, e.g., when the compartment temperature reaches 500°C or when EVF are visible;

whichever happens first, as this will ensure to investigate the characteristics and consequences of EVF on the façade extensively. Current work builds up on the previous experimental work of the authors on forced draught conditions in enclosure fire development (Smolka, 2022). In these previous experiments, an extensive range of different fan speeds, from 0 m/s (no wind) to 3.5 m/s at different horizontal fan distances from the opening (ranging from 1.5m to 4.5 m), were studied and critical conditions relevant to the study (with respect to the mass loss rate, heat release rate, temperature, uni- and bi-directional flow) were observed at a fan speeds of 2.6 m/s to 2.9 m/s. The positive pressure fan used in the experiment with an outer surface area of 0.0225 m² (150 mm × 150 mm). The fan was positioned at a fixed distance 2.5 m from the compartment opening to ensure a uniform and controlled flow distribution. It is acknowledged that, in real-world scenarios, wind effects are far more complex and can vary in both magnitude and direction due to external environmental factors such as building geometry, atmospheric turbulence, and local microclimatic conditions. However, in the present study, the use of a unidirectional positive pressure fan was adopted to isolate and systematically evaluate the influence of a controlled FD on EVF behaviour (Smolka, 2022) In each experiment, 500 g n-Heptane was used as the fire source, placed in a 200 mm x 200 mm steel pan made of 2 mm steel sheets and welded at the centre of the compartment. The medium-scale compartment-façade fire test was designed to investigate the feasibility of simulating full-scale physical phenomena in a reduced-scale experiment by preserving key nondimensional parameters. The Buckingham Pi theorem has been applied to scale down the fire power to be used in the medium scale experimental configuration, ensuring the preservation of the second group (Π_2) as specified in equation 3.1 (Quintiere, 2006). The Π_2 group is derived from the energy conservation equation, it requires that the model fire power is selected in conformity with the prototype as specified in equation 3.2. The length scales l_p and l_m correspond to the physical dimension of the prototype and model system respectively, with their ratio $\frac{l_m}{l_m}$ being $\frac{1}{4}$. The fire power measured during the test conducted in the compartment varied between 250 kW and 350 kW. Here, \dot{Q} denotes the heat release rate (HRR), while Q_m^* and Q_p^* represent the HRR, in kW for the model and the prototype respectively. The terms ρ_{∞} , C_{p} , T_{∞} and g are the density in kg/m³, specific heat in kJ/kg K, temperature in Kelvin under ambient conditions and g is the gravitational acceleration in m/s².

$$\Pi_2 = \frac{\dot{Q}}{\rho_{\infty} C_n T_{\infty} \sqrt{g(l)^{5/2}}} \tag{3.1}$$

$$\frac{Q_m^*}{\rho_\infty c_p T_\infty \sqrt{g} (l_m)^{5/2}} = \frac{Q_p^*}{\rho_\infty c_p T_\infty \sqrt{g} (l_p)^{5/2}} \Rightarrow Q_m^* = Q_p^* \left(\frac{l_m}{l_p}\right)^{5/2}$$
(3.2)

The HRR was calculated from the experimentally measured mass loss rate of the fuel and heat of combustion using the equation 3.3. where (\dot{m}'') is burning rate is given per unit area, (A_f) , is the burner area, (ΔH_c) , is the effective heat of combustion and (η) is the combustion efficiency. (Karlsson & Quintiere, 2000)

$$\dot{Q} = \dot{m}^{"} \times A_b \times \Delta H_c \times \eta \tag{3.3}$$

In this study, heptane was used as the fuel, with a combustion efficiency factor of 0.7, consistent with values adopted in previous experimental fire studies. The effective heat of combustion for heptane was taken as 44.6 MJ/kg. (Karlsson & Quintiere, 2000)

In Table 4, the geometrical dimensions of the reduced scale setup and the corresponding full-scale compartment are shown.

Table 4: Main parameters of the test setup and the corresponding full-scale experiment.

Main parameters of test setup	Reduced Scale	Full Scale	
Compartment length/width/height (mm)	900/600/600	3600/2400/2400	
Opening width/height (mm)	200/300/400	800/1200/1600	
Fire Power (kW)	250/350	8000/11200	

To measure the mass loss rate, which was further used for calculating HRR, a scale made from an Arduino, a 20 kg load cell sensor, and 24 bit Analog/Digital convertor HX711 were used. The scale was constructed from 3D-printed parts made of PET-G with adequate robustness and durability and calibrated with accuracy of 1gram. STL files are published on Thingiverse (Smolka, 2020). A total of 72 K-type thermocouples 1.5 mm were used for measurement of the temperature profile of compartment fire and EVF. In this work, thermocouples with the limits of error values of ± 1.1 °C or ± 0.4 % have been used (OMEGA, 2023). The measurement uncertainty was determined to be ± 1 °C or approximately ± 4 % of the measured value, whichever is greater. The schematic of measuring instruments is shown on Figure 19 which describes the locations of thermocouples located in the internal and external spaces of the experimental setup on twelve

thermocouple trees. Thermocouples were positioned horizontally extending outward from the side of the façade wall, to capture the gas temperature distribution adjacent to the façade. Because EVF may induce high fire plume velocities, which could cause displacement of thermocouples, one of the main design requirements for the measurement system was to ensure that the spatial position of the thermocouple tips remained unaltered during the tests. Prior to each fire test, the thermocouples were carefully positioned and aligned, and post-test inspection confirmed that the majority of the thermocouple tips remained in their intended positions.

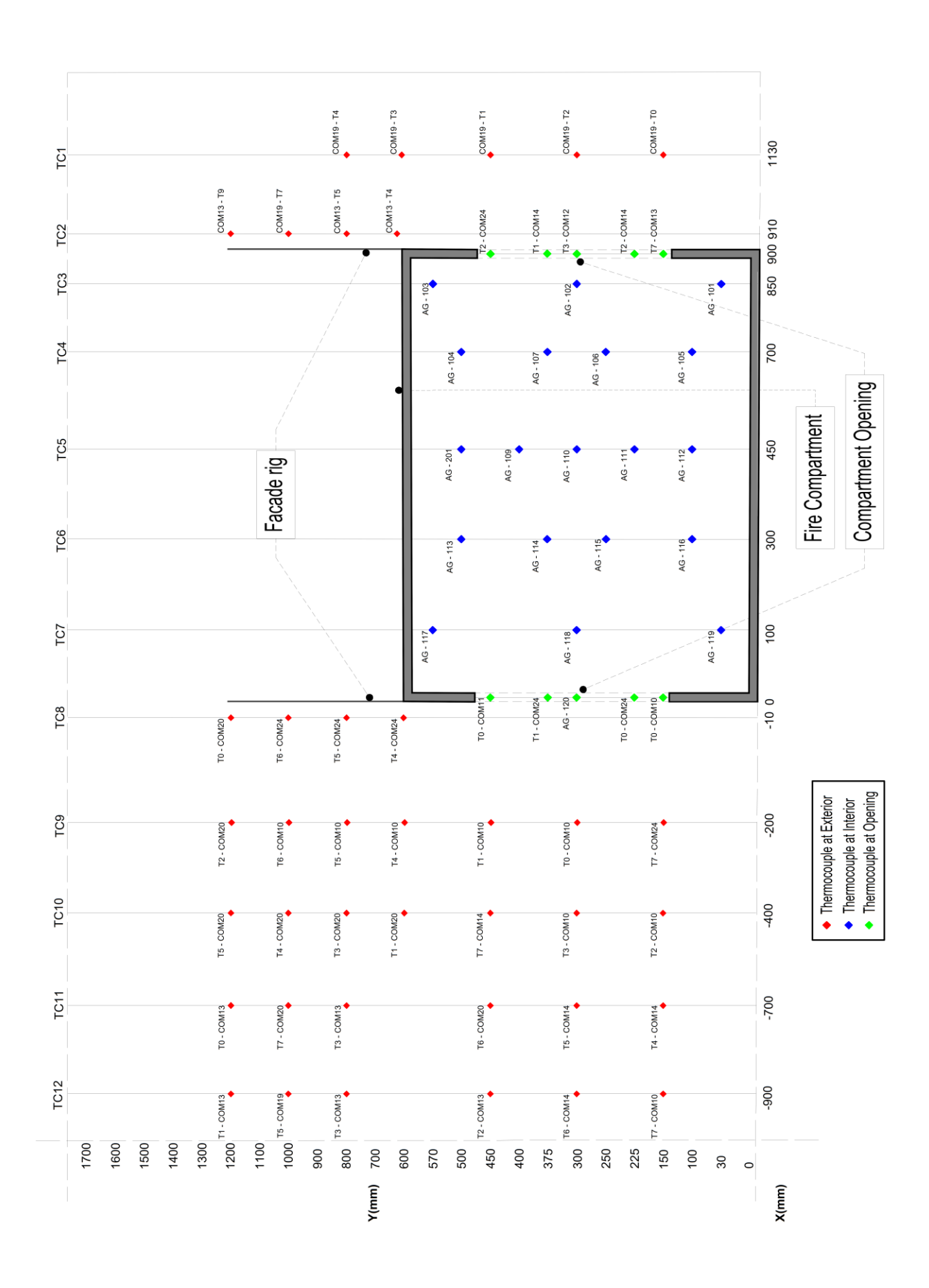


Figure 19: Thermocouples layout at the experimental configuration.

The airflow velocity and hot gas pressure difference inside the compartment were measured using a bi-directional velocity probe (BDVP). The probe was calibrated in a custom 3D-printed wind tunnel, as described and validated by Smolka et al. 36 and consistent with the original calibration methodology of McCaffrey & Heskestad (McCaffrey & Heskestad, 1976). This setup enables velocity measurements up to 4 m/s with a standard deviation of 1.2% and a turbulence intensity of 1% (Smolka et al., 2023). Prior to each fire test, the airflow field generated by the fan was evaluated in the absence of combustion to ensure stability and uniformity. The results showed a relatively consistent velocity profile, with variations within $\pm 5\%$ across the measurement grid demonstrating that the flow field was reasonably uniform in the region of interest. The fan used in the experiments was positioned 2.5 meters from the compartment opening, with the intention of creating a uniform forced draught condition at the plane of the compartment opening. The air velocity of 2.9 m/s refers to the average velocity measured at the centre of the compartment opening during pre-fire testing using a calibrated BDVP. The fan outlet itself had a circular crosssection with a diameter of 350 mm, and the airflow profile was reasonably uniform across the horizontal centreline of the opening due to the fan distance and axial alignment. The BDVP and thermocouple locations are described in the openings shown in Figure 20.

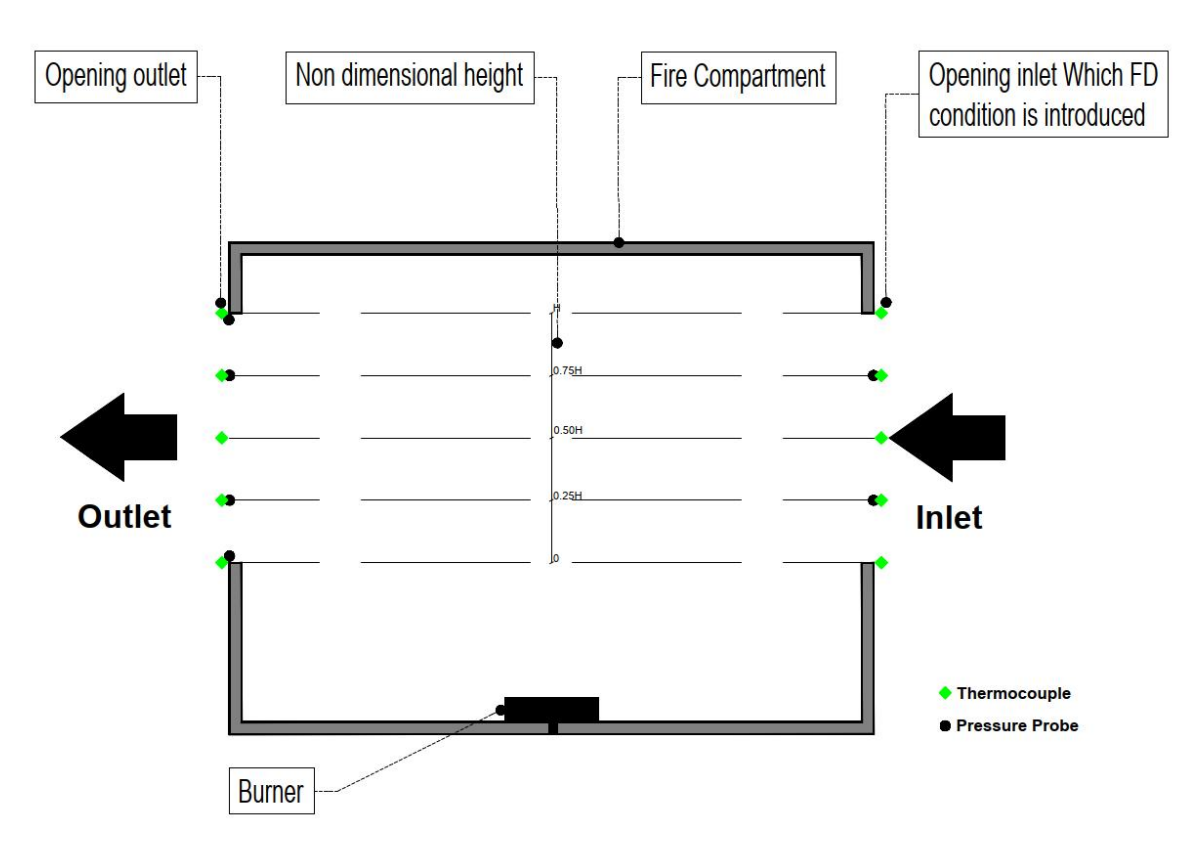


Figure 20: Thermocouples and BDVP location at the openings.

Table 5 describes the list of experiments, including wind speed, opening dimensions, and ventilation factors used for the experiments.

Table 5: Experimental test scenarios.

Test Cases	Opening dimensions		Ventilation Factor	Wind Speed	
1 est cuses	Width (m)	Height (m)	$(m^{5/2})$	(m/s)	
NoFD-20×20	0.20	0.20	0.0358	0.0	
FD-20×20	0.20	0.20		2.9	
NoFD-30×30	0.30	0.30	0.0986	0.0	
FD-30×30	0.30	0.30	0.07.00	2.9	
NoFD-40×40	0.40	0.40	0.2024	0.0	
FD-40×40	0.40	0.40	3.2021	2.9	

3.3 Numerical setup

To investigate the influence of FD conditions on the development of an EVF, the experimental test cases mentioned in Table 5 have been simulated using the Fire Dynamic Simulator (FDS, Version 6.7.9) (McGrattan et al., 2019). CFD in fire modelling involves the study of fluid systems that are either static or dynamically changing in time and space, focusing on the behavior of fireinduced flows, smoke, and heat transfer. In fire modelling, the physical characteristics of fluids in motion, such as smoke dispersion, heat transfer, and combustion processes, are typically described by fundamental mathematical equations (McGrattan et al., 2019). The algebraic equations are solved using dedicated numerical methods, enabling the accurate simulation of fire behavior, smoke movement, and their interactions with surrounding environments. The governing equations for turbulent flows are derived from the Navier-Stokes equations, which describe the conservation of mass, momentum, and energy in a fluid. FDS is a sophisticated, Fortran-based CFD code specifically designed for simulating fire dynamics and smoke propagation in both enclosed and open environments. The default combustion model in FDS adopts a mixing-limited, infinitely fast reaction approach for simplified chemical kinetics, utilizing three lumped species (oxidizer, fuel, and products) to represent the combustion process. A limitation of the default mixing-controlled reaction model is that it assumes fuel and oxygen always react regardless of the local temperature, reactant concentration or strain rate. For large-scale well-ventilated fires, this approximation is usually sufficient, however, if a fire is in an under-ventilated compartment where strain between the fuel and oxidizing streams is high, burning may not occur. FDS uses simple empirical rules which ignore strain to predict local extinction within a given grid cell based on resolved species concentration and the mean cell temperature. Thermal radiation is modelled using the Radiation Transport Equation (RTE), discretized via the Finite Volume Method (FVM) for participating media. Turbulence is captured through the Large Eddy Simulation (LES) framework, which resolves large-scale turbulent structures while employing sub grid-scale models to account for the effects of smaller, unresolved eddies. This combination of advanced modelling techniques enables FDS to deliver high-fidelity simulations of fire behavior and smoke dynamics (McGrattan et al., 2019).

The numerical model was designed to replicate the experimental configuration and dimensions. All solid surfaces, including walls and floors, are provided with boundary condition with the material properties corresponding to the experimental setup. Figure 21 shows the experimental along with the numerical setup. The soot yield, which represents the fraction of heptane fuel mass converted to smoke particulates, was set equal to 0.015 kg/kg and the corresponding CO yield was set equal to 0.006 kg/kg (Hamins et al., 2003). FDS incorporates a sub-model for wind that imposes mean flow velocities based on Monin–Obukhov similarity parameters. This method enables the modelling of velocity and temperature profiles as a function of height within the domain, considering aerodynamic roughness length, scaling potential temperature, and the Obukhov length (McGrattan et al., 2019), (Wegrzynski et al., 2018). However, the experimental setup in the current study uses a fan to establish the FD conditions, which is represented in FDS by modelling a vent with a constant velocity profile of 2.9 m/s.

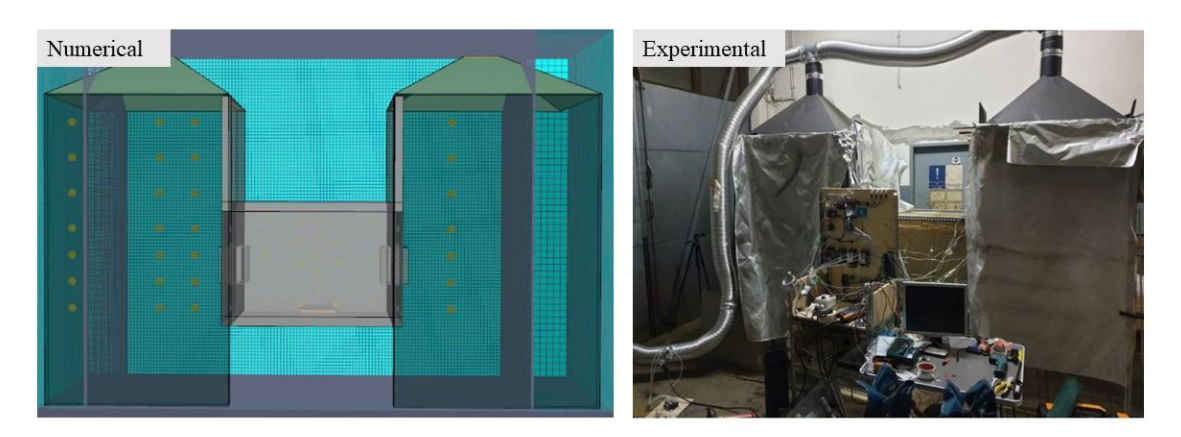


Figure 21: Numerical (left) and experimental (right) setup.

3.3.1 Computational Domain

The computational domain was selected to accurately represent the flow and thermal characteristics of the EVF flame. However, an increased domain was chosen for the FD condition in all cases, as the fan was placed at 2.5 m from the edge of the opening. The domain was extended

1 meter in the positive and negative X axis for the NoFD conditions from the edge of the respective openings on the opposite side of the compartment and 2.7 meters in the positive X axis for the FD due to the location of the fan. The increased domain dimensions considered are depicted in Figure 22 below.

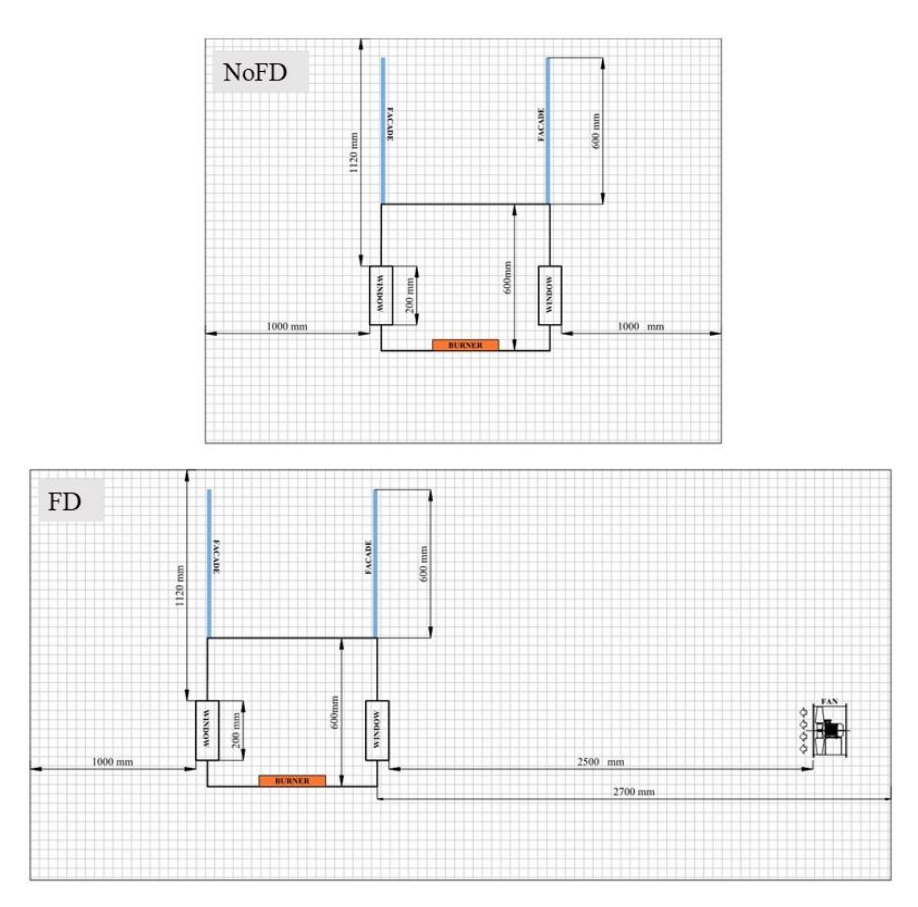


Figure 22: Computational domain and relevant dimensions of the model NoFD (left) and FD (right).

3.3.2 Grid independence

The non-dimensional expression D^*/dx is a measure of how well the flow field is resolved in the simulation of buoyant plumes. Where dx is the size of cells and D^* is the characteristic fire diameter (McGrattan et al., 2019). The D^*/dx ratio indicates the adequacy of the grid resolution. A higher D^*/dx would mean a better resolution for the simulation of fire, as FDS uses a structured mesh. A grid sensitivity analysis for three different D^*/dx values namely 4 (coarse mesh), 10 (moderate mesh), 16 (fine mesh) was conducted and results for the temporal evolution of temperature and velocity at the middle of the opening for case of FD-20×20 of FD condition is depicted in Figure 23. The D^*/dx ratio of 16 was found to be the most optimal with a corresponding cell size of 0.02 m. Further to this, to reduce the computational time for the simulation, an additional sensitivity analysis was performed with multiple mesh sizes. To capture the buoyant plume and fire flow field accurately, the inside of the compartment is provided with a 0.02 m mesh and the rest (both sides of the opening) with a 0.04 m mesh size. However, a coarse mesh was

initially performed as part of the mesh sensitivity study; however, it was observed that the flow field and flame structure were not adequately resolved under coarse grid conditions. Consequently, the simulation did not produce a physically representative fire scenario suitable for meaningful comparison. For this reason, only the moderate and fine mesh results are presented and discussed in the thesis. Figure 23 depicts temperature and velocity values at the opening's centre, showing that moderate mesh results are slightly higher with more fluctuations compared to the others. The steady curve of fine and multiple meshes led to the decision to use multiple mesh for simulation, providing a more comprehensive output while also reducing computational time. The total computational grid consisted of 498,432 cubic cells for NoFD conditions and 542,784 cubic cells for FD conditions.

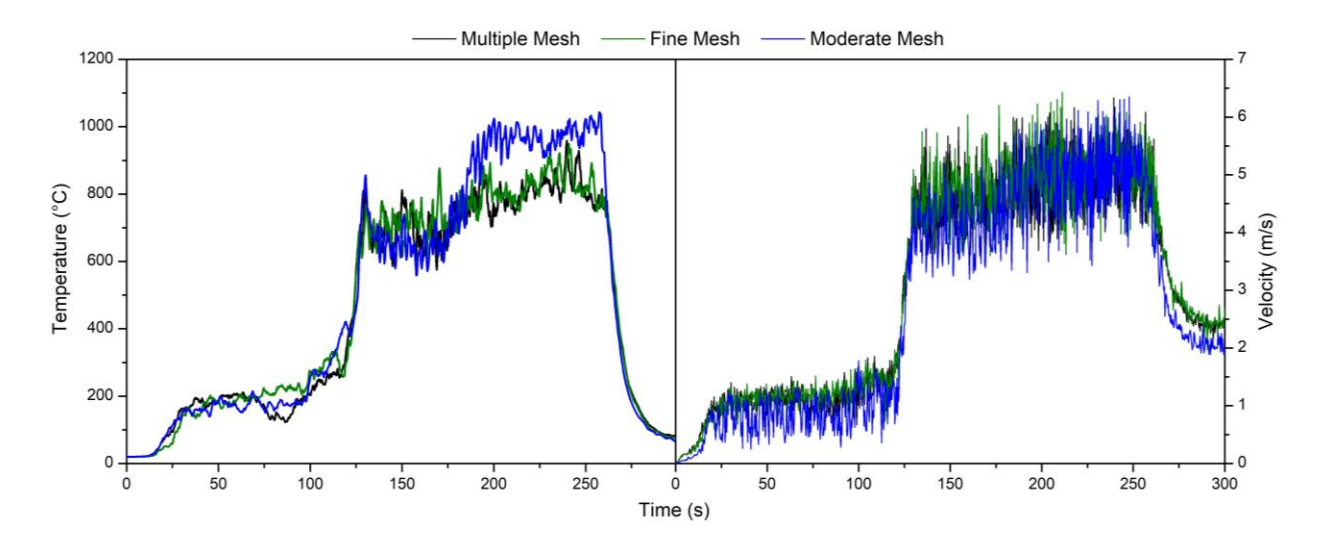


Figure 23: Grid sensitivity analysis for FD-20×20 through the temporal distribution of the temperature (a) and velocity (b) at centre of outlet opening for NoFD (left) and FD (right) conditions.

3.3.3 Turbulence model

A preliminary study of turbulence models including Large Eddy Simulations (LES), Very Large Eddy Simulations (VLES), and Simply Very Large Eddy Simulations (SVLES) was conducted for the case FD-20×20 to ensure proper modelling of flow turbulence. Figure 24 depicts the resulting temperature and velocity at the opening's centre, indicating that SVLES has a wider range with more fluctuations compared to LES and VLES. However, the current study uses Large Eddy Simulations (LES) to model flow turbulence with the Smagorinsky sub-grid scale model (Okaze et al., 2020). The Smagorinsky model's constant value, $C_s = 0.2$, and the CFL region of 0.8 and 1, along with a *Schmidt* and *Prandtl number* of 0.5 were used. Previous studies e.g. (Smagorinsky, 1963) have shown that the Smagorinsky model performs well in simulating wind flow.

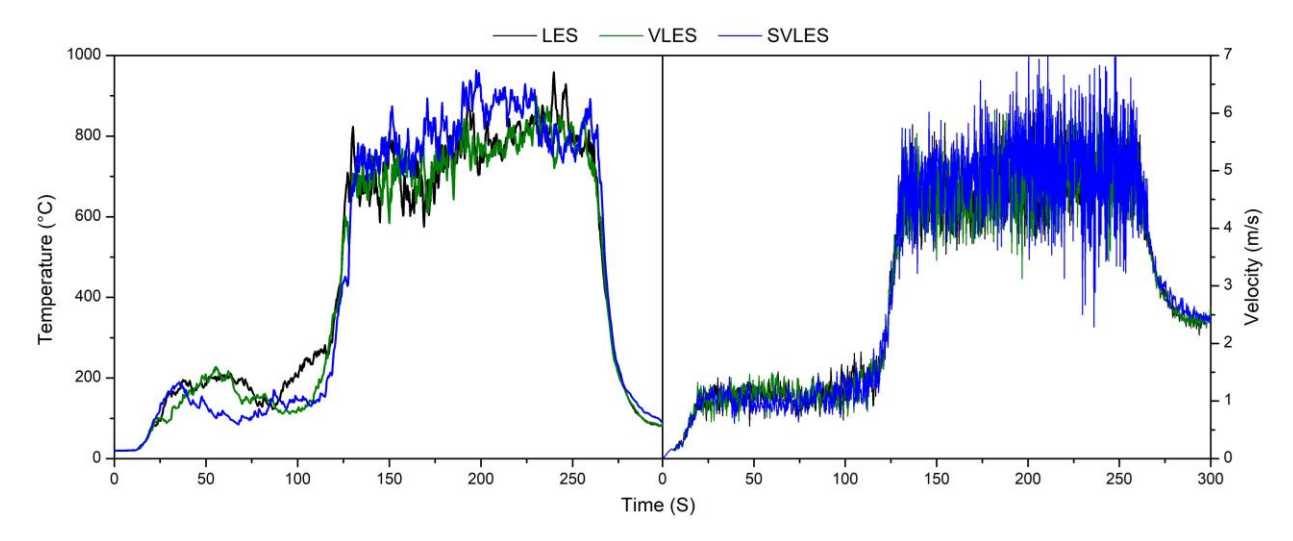


Figure 24: Temporal distribution for FD-20×20 of the temperature (a) and velocity (b) at centre of the outlet opening for different LES models for NoFD (left) and FD (right) conditions.

3.3.4 Validation of Numerical Simulation

To validate the numerical results, experimental data of FD 20×20 case was used to analyse the temporal evolution of velocity and temperature measurements at the opening's centre. The validation of these velocity and temperature measurements are considered as important to determine outward gas temperature and its velocity for the FDS validation. Figure 25 thus illustrates the outward gas velocity for the FD 20×20 case, where the vertical axis represents numerical results, and the horizontal axis represents experimental data. The error margins are represented by dotted lines, and the red diagonal dashed line indicates a perfect match between simulation and experimental data. The data show that 70% of the predictions fall within a $\pm30\%$ error margin, indicating good agreement. The R-squared value, also known as the coefficient of determination, is found to be 0.9, and the linear regression slope is approximately 1, suggesting a moderate-to-strong positive linear relationship, and the model is a good fit for the data.

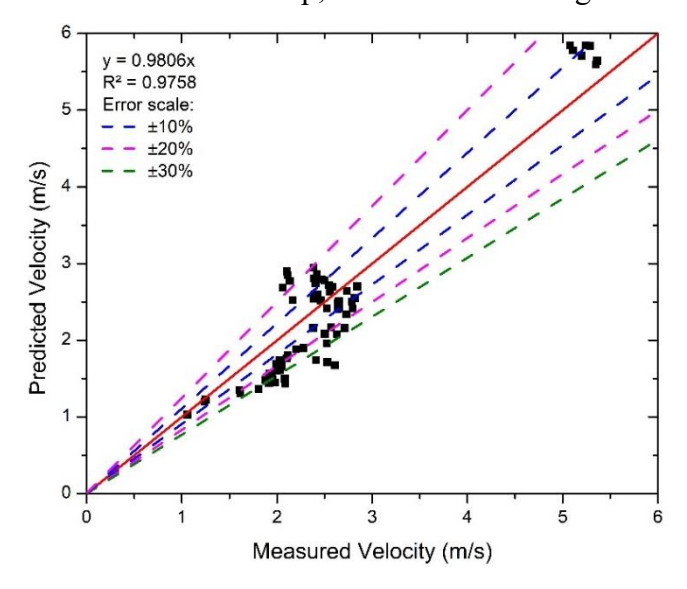


Figure 25: Validation based on predicted velocity at centre of outlet opening for NoFD 20×20.

Figure 26 depicts the validation case for temperature at the center of the opening. The validation also considered the temperature distribution at horizontal distances of 10 mm to 900 mm. The data in Figure 26 presents temporal temperature measurements obtained from both experimental observations and numerical simulations at the center of the outlet opening. In addition, temperatures measured by the thermocouple tree, positioned at horizontal distances of 10 mm to 900 mm with sensors located at different heights (as shown in Figure 15), were analyzed using a 20-second time-averaging window applied over the period from 310 to 330 seconds after ignition. This interval corresponds to the fully developed fire stage, during which flame behavior was stable and externally venting flames were consistently observed. For the current validation case, the focus is primarily on the outward-flowing gas temperature distribution. Additionally, the model considered the temperature distribution at the opening and façade for different opening sizes and compared these results with experimental results in sections 3.1 and 3.2, respectively. The data show that 70% of the predictions fall within a $\pm 30\%$ error margin, indicating good agreement. The R-squared value is found to be 0.98, and the linear regression slope is approximately 1, suggesting a moderate-to-strong positive linear relationship and a good fit for the data.

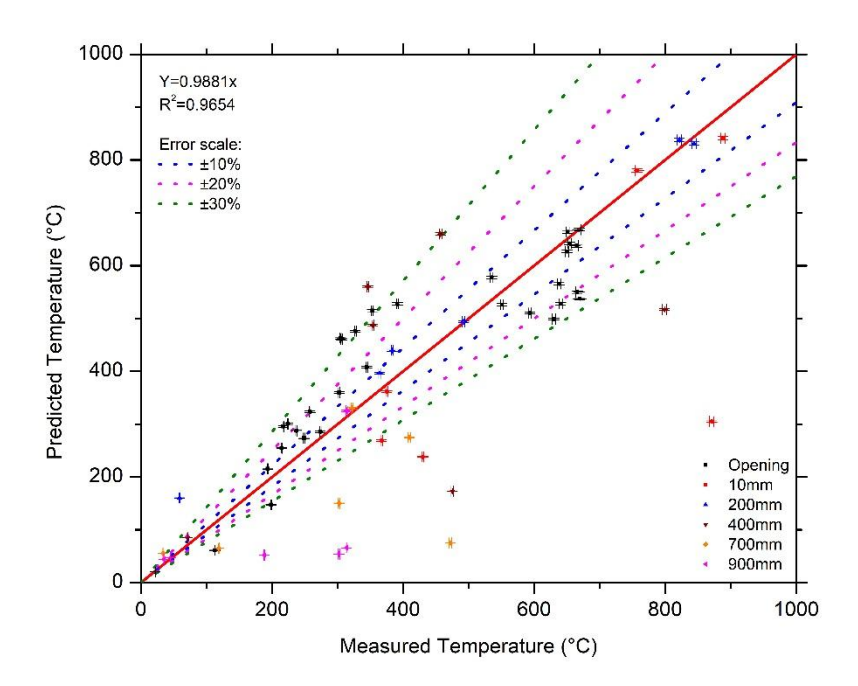


Figure 26: Validation based on predicted temperature at centre of outlet and temperature distribution at horizontal distances of 10 mm to 900 mm.

3.4 Result and Discussion

3.4.1 Effect of opening size on EVF thermal characteristics

Figure 20 depicts the placement of 5 thermocouples at equal intervals at the compartment openings for the various opening sizes. Figure 27 presents the temperature readings from five thermocouples positioned at varying heights along the compartment opening for the NoFD 20x20 experimental setup. For the NoFD cases, the experimental setup was fully symmetric, with identical opening dimensions and boundary conditions on both sides of the compartment. During testing, the EVF behavior and temperature measurements at both openings were observed to be consistent, to avoid redundancy and maintain clarity, figure 27 presents the temperature results from one representative opening. It was observed that the flame consistently spilled out of the opening around 310 seconds, coinciding with the time when the fuel was nearly fully consumed. Data collection ceased at approximately 350 seconds. The recorded data from the loggers were analyzed, and the selected data represents the time-averaged values for a 20-second period, spanning from 310 to 330 seconds, when the fire was at its peak and flames were visible outside. This approach was applied consistently across all experiments, where data were analysed, and the selected data represents the time-averaged values for a 20-second period. To assess the sensitivity of the 20-second averaging window, we performed an additional analysis using 10-second, 15second, and 30-second time-averaging intervals centred around the fully developed fire period (310–330 seconds). The variation in the average temperature values was found to be within $\pm 5\%$ for the 10- and 15-second windows. However, the 30-second average showed up to $\pm 10\%$ variation, as in some cases this interval fire extended into the decay phase where the mass burning rate dropped significantly. For consistency and reliability, we used the mean value over the 20second interval in all comparisons, rather than the midpoint value. This method ensured that transient fluctuations were smoothed out while still capturing the peak fire behavior in a stable phase. Also, to ensure consistency across all test cases, a 20-second time-averaging window (where flame consistently spilled out from the opening) was applied to thermocouple measurements, chosen to reflect the steady-state EVF condition, regardless of the exact burn duration.

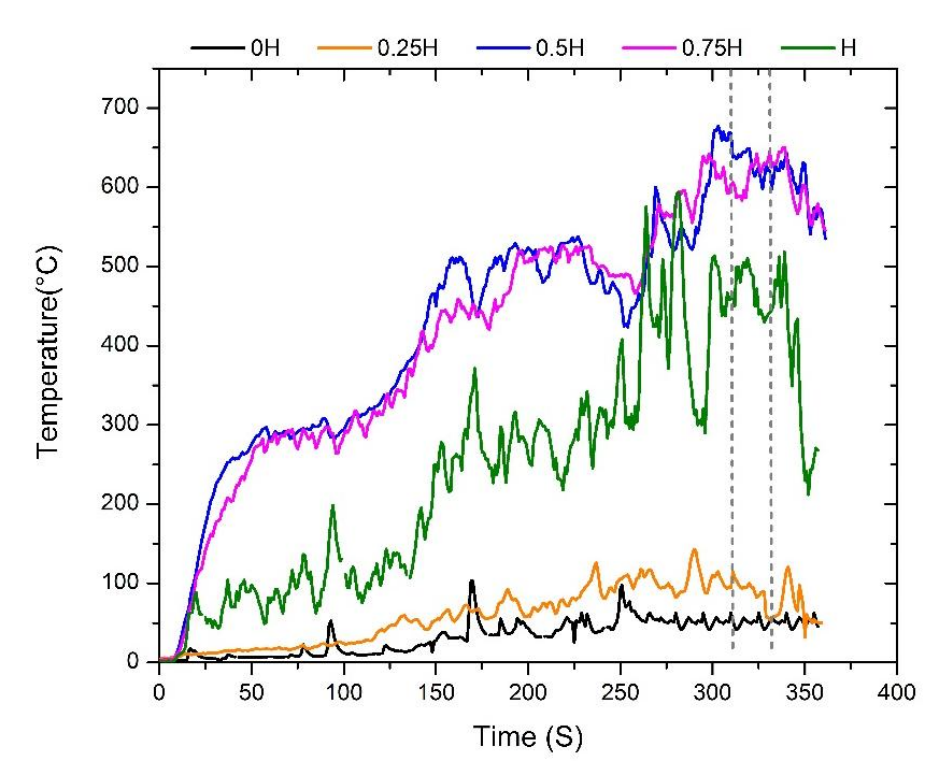


Figure 27: Temperature measurement at the opening for the case of NoFD 20×20.

Figure 28 depicts the experimental and numerical analysis (FDS) results for all the three different wall opening sizes, under NoFD and FD conditions. The term "non-dimensional height" refers to the relative placement of thermocouples along the opening height (H) of the compartment. For each opening size (20 cm, 30 cm, and 40 cm), thermocouples were placed at five discrete vertical positions: 0H, 0.25H, 0.5H, 0.75H, and H, where H corresponds to the full opening height. This approach enables consistent comparison of temperature distributions across different opening configurations by normalizing sensor locations relative to opening height.

For experiments under NoFD conditions, it can be observed that there is a decrease in temperature in the middle of both the wall openings with the increase in wall opening dimensions. Also, temperature values at the top of the compartment opening increases with the increase in the compartment opening dimension. This is mainly due to the change in the opening size, which influences the air entrainment and the exiting of EVF gases. For walls opening sizes 20 cm and 30 cm, (NoFD-20×20 and NoFD-30×30 cases) the FDS and experimental result are in good agreement. However, for the 40 cm wall opening (NoFD-40×40 case), there is a major difference in the FDS and experimental results, for the temperature at the bottom of the compartment opening. This is due to the evident bi-directional flow in and out of the compartment, with more fresh air entering the compartment from the lower part of the opening during the FDS simulation. Additionally, FDS uses a simplified chemistry approach for turbulent combustion. In FDS, the experimentally measured MLR was prescribed directly as an input parameter. While this approach ensures that the target MLR is accurately modelled, it also means that the combustion model accuracy is not adequately predicting experimentally measured MLR in under ventilated conditions. This behavior is consistent with the limitations of the simplified combustion treatment in FDS: although it reproduces the experimentally measured MLR, it does not fully resolve the fire and ventilation dynamics. Consequently, in the 40 × 40 opening case, this limitation can accentuate discrepancies between numerical predictions and experimental measurements. For the no-wind condition for all three opening sizes, bidirectional flow was observed, whereas in FD condition only unidirectional flow was observed in the experiment.

During the experiments under FD conditions, temperature profiles at compartment openings are higher compared to the NoFD conditions. It is noted that as compartment opening dimension increases, temperature in the center of the compartment opening decrease. For compartment openings 20 cm and 30 cm (FD-20×20 and FD-30×30 cases), it is noted that the temperature are almost identical, except the value for the thermocouple at the bottom. In contrast to NoFD conditions, it is observed that once the fire is fully evolved with forced draught, there is only unidirectional flow through the compartment opening instead of bi-directional flow. In the 20 cm and 30 cm FDS cases, it is observed that a uniform temperature profile is maintained through the entire opening. For 40 cm openings, flames are exiting mainly through the lower part of the opening, and thus there is an increased temperature in the lower part of the opening. This can be attributed to the fact that with forced draught wind resulting in more efficient airflow exchange. This further results in increased burning within the fire compartment pushing the flames outwards, also changing the fire dynamics within the fire compartment. For cases with 40 cm openings and FD conditions more flames will exit through the bottom of the opening as there is a larger opening

dimension. This behavior was observed specifically in the FD 40×40 case, where the forced draught induced by the fan significantly influenced the flow field at the compartment opening. Due to the increased vertical height of the opening, the incoming airflow from the fan primarily going through the upper portion, while the hot gases and flame were pushed downward, exiting through the lower part of the opening. The wind effect caused the flame to tilt downward. In contrast, for cases with smaller opening heights (e.g., 20 cm and 30 cm), the entire opening was generally filled with flame. Additionally, a notable discrepancy in temperature was observed at the lower part of the opening in the FD-40×40 case when comparing experimental and simulation results. This variation is primarily attributed to the turbulence model employed in numerical analysis. As the opening size increases and wind influence is introduced, turbulence becomes more pronounced, leading to greater modelling uncertainty. In addition, the influence of radiative heat flux on thermocouple readings can lead to higher measured temperatures in experiments. Although the FDS thermocouple model accounts for this effect to some extent, since the thermocouple (TC) model, temperature lags the true gas temperature depending mainly on bead size. During the experiments, sheathed thermocouples were used to mitigate direct radiative effects. The presence of multiple metal and air gaps in the thermocouple device construction may limit the model's ability to fully capture the complex radiative—convective balance. This limitation is particularly relevant for scenarios with strong flame impingement, such as the 40×40 opening case.

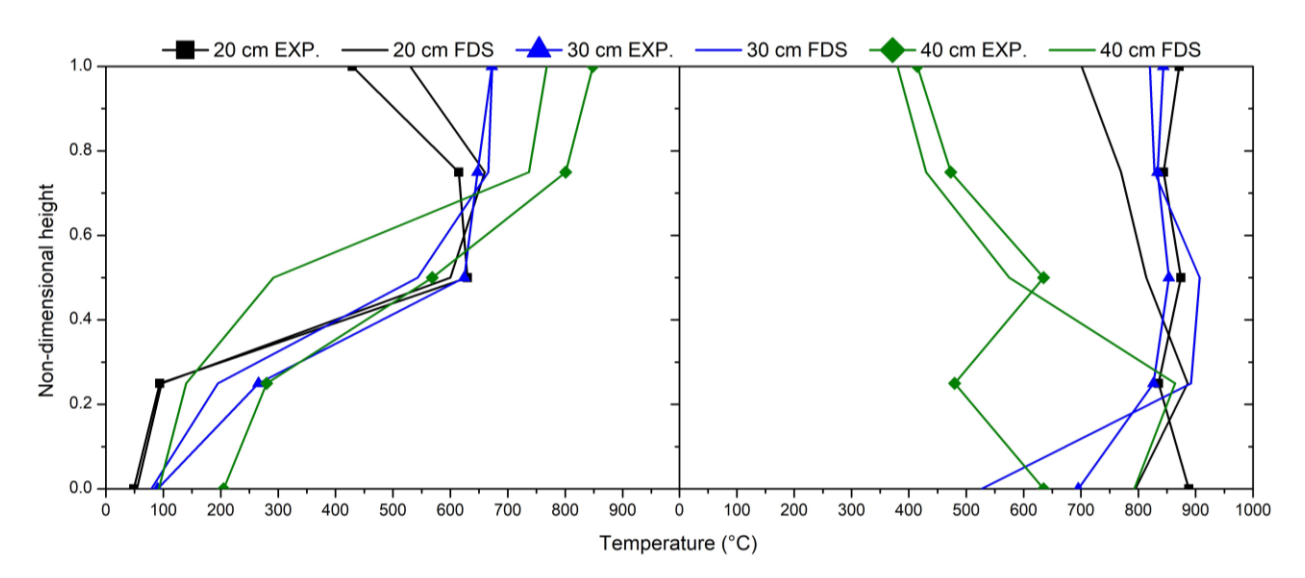


Figure 28: Non dimensional vertical distribution of the temperature profile at the outlet opening for NoFD (left) and FD (right) conditions.

To investigate the EVF temperature profile outside the compartment opening, a further analysis has been carried out considering horizontal distances of 10 mm, 200 mm, 400 mm, 700 mm, and 900 mm, normal to the compartment opening centre; and results are plotted in Figure 29. A total

of 35 thermocouples were positioned as depicted in Figure 19 to affect a temperature analysis of the EVF spilling out from the opening. However, only the data from the thermocouples which are located normal to the compartment opening centre line were considered for the analysis. The selected data is the time average for a period of 20 seconds, when the fire is at its peak; for all the experiments.

It was observed that the temperature at the centreline of the opening decreases with the increase in horizontal distance, in NoFD conditions, for all opening sizes. Furthermore, as the vertical distance from the opening increases, the EVF temperature is observed to be increasing as well. This agrees with results agreed with Asimakopoulou's (Asimakopoulou et al., 2016) that presented time averaged temperature contours at the centreline plane perpendicular to the façade of medium scale experiments demonstrating that the developing EVF temperatures gradually decrease with increasing height and projection from the facade. The EVF shape has been demonstrated to depend on both the fire load and the opening geometry resulting in the total volume of the EVF envelope to increase with increasing fire load and opening area.

Maximum temperature was measured at a distance of 10 mm in NoFD condition and in FD, the maximum temperature appears at 200 mm. The overall horizontal temperature profile for the FD conditions is much higher in consideration to the NoFD conditions. For the 20 cm and 30 cm cases, similar temperature profiles were identified; however, in 40 cm case, less overall temperature profile was observed. The numerical results exhibit good agreement with the experimental results. Under the NoFD conditions, there is an approximate 6% variance in values when compared to the outcomes of the numerical analysis. Similarly, in the FD conditions, there is an approximately 15% temperature differential, as shown in the Figure 29.

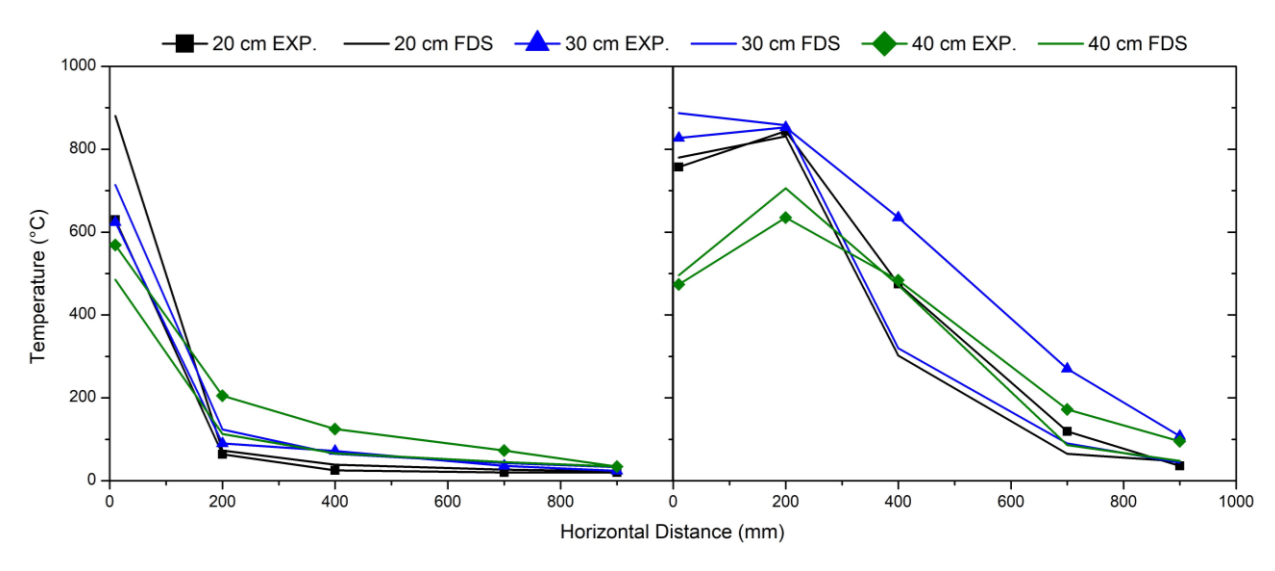


Figure 29: Temperature profile versus the horizontal distance at the center of the outlet opening for NoFD (left) and FD (right) conditions.

3.4.2 Effect of opening size on the façade

Thermocouples were positioned in the façade as depicted in the Figure 19. Figure 30 shows the temperature profile at the façade for NoFD and FD condition. The temperature for the 40 cm compartment opening (both FD-40×40 and NoFD-40×40) during numerical and experiment analysis in NoFD, is not in agreement. This is due to the turbulence modelling issue with numerical analysis. A similar observation is found in the 30 cm FD-30×30 case with FD condition. In NoFD conditions, 30 cm and 40 cm opening size (NoFD-30×30 and NoFD-40×40) was showing increased temperature when compared to 20 cm opening size (NoFD-20×20). In FD condition, for all opening sizes, the façade temperatures were observed to be less, when compared to the NoFD condition. This is due to the forced draught wind pushing the EVF gases outwards, and thus increasing the horizontal projection and there is a corresponding decrease in the flame height. The decreased flame height leads to a diminished radiative and convective thermal impact on the façade surfaces in FD conditions relative to NoFD conditions. This finding is consistent with the results reported by Ren et. al. who conducted small-scale compartment fire tests in a wind tunnel (Ren et al., 2018). Ren's study found that the maximum temperatures measured on the façade decreased with increasing wind velocity from 0 to 2.0 m/s. In NoFD conditions, an average temperature increase exceeding 30% was observed for the 20 cm case, while the temperature increased by 150% and 200% for the 30 cm and 40 cm NoFD cases, respectively. Numerical results of façade temperatures under NoFD conditions for 20 cm and 40 cm cases, are in good agreement with experimental results as there is 7% variance but this was increased to 10% when compared with experimental measurements of temperature under FD conditions.

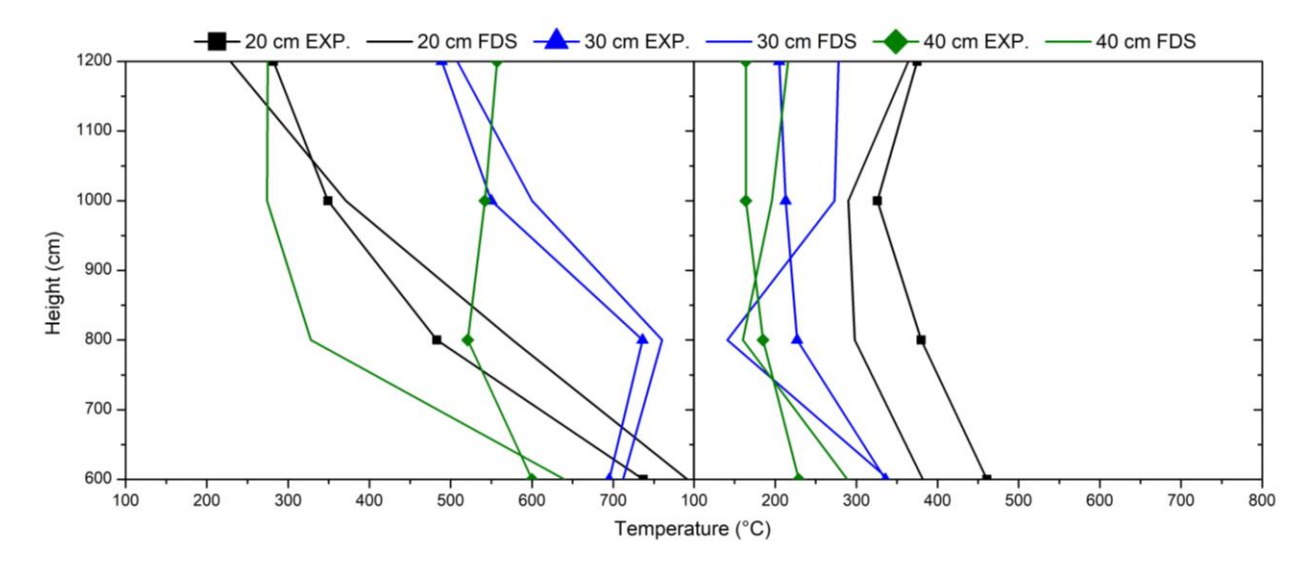


Figure 30: Vertical distribution of the temperature profile at the centreline of the outlet façade with fibre cement board for NoFD (left) and FD (right) conditions.

3.4.3 Developed thermal field

The evolution of the thermal field near the façade was analysed under both NoFD (no forced draught) and FD (forced draught) conditions for two different façade geometries (20 cm and 40 cm), as presented in Figure 31. The analysis focuses on representative time points that capture the fully developed fire stage, during which external flames were consistently visible and the wind flow, when applied, had reached a steady state. Instead of time-averaged 20 second slice files in Smokeview, instantaneous snapshots were chosen to present thermal field. This is because the overall profiles and values obtained from the averaged slice files are comparable to those from the instantaneous snapshots presented in figures 31 d and 32 d. The primary difference is that the averaged plots exhibit smoother contours with reduced turbulence, which is consistent with the expected effect of temporal averaging.

For the 20 cm façade geometry, temperature distributions are shown at 150 seconds. This time point was selected as it corresponds to the period when the fire had fully evolved, the fan was operating in the FD scenario, and the wind flow had stabilised. Similarly, for the 40 cm façade geometry, results are presented at 200 seconds, which also marks the fully developed fire stage with established external flaming and a steady wind field. These selections ensure comparability between cases in terms of fire development and ventilation state.

The thermal field shows significant differences between NoFD and FD conditions. Under FD conditions, temperatures near the compartment opening reached values between 700°C and 800°C. However, as the external plume rose, a rapid temperature decay was observed due to increased air entrainment and mixing. Inside the compartment, the forced ventilation disrupted thermal stratification, resulting in relatively uniform and much lower gas temperatures ranging from approximately 30°C to 100°C. This mixing effect is characteristic of wind-driven ventilation and limits the build-up of hot gas layers.

In contrast, NoFD conditions led to the formation of distinct thermal stratification within the compartment. Higher gas temperatures, in the range of 700°C to 900°C, were observed in the upper layer near the opening. The absence of wind allowed for a more vertically extended flame, which increased the thermal impact on the façade surface. These differences in flame behaviour under varying ventilation conditions are clearly reflected in the façade temperature distributions.

For the 40 cm façade, NoFD conditions resulted in maximum temperatures along the façade surface between 600°C and 750°C, indicating strong exposure. In comparison, the 20 cm façade under NoFD conditions exhibited lower façade surface temperatures, around 150°C to 200°C, suggesting a more confined heat plume and reduced external exposure. Under FD conditions, both

façade geometries experienced significantly reduced temperatures at the façade surface, highlighting the dampening effect of wind on vertical flame spread.

The results clearly indicate that forced draught plays a critical role in modifying fire plume behaviour and reducing thermal exposure to external surfaces. The wind appears to limit the vertical extent of the fire plume, thereby decreasing the thermal exposure to the façade surface. These results align with previous findings by Hu et al., Ren et al., and Zhao, which showed that the height at which elevated temperatures were measured on the façade decreased with increasing wind velocities (Hu et al., 2017; Ren et al., 2018; Zhao et al., 2024). The decreased flame height leads to diminished radiative and convective thermal impact on the façade in FD conditions compared to NoFD conditions.

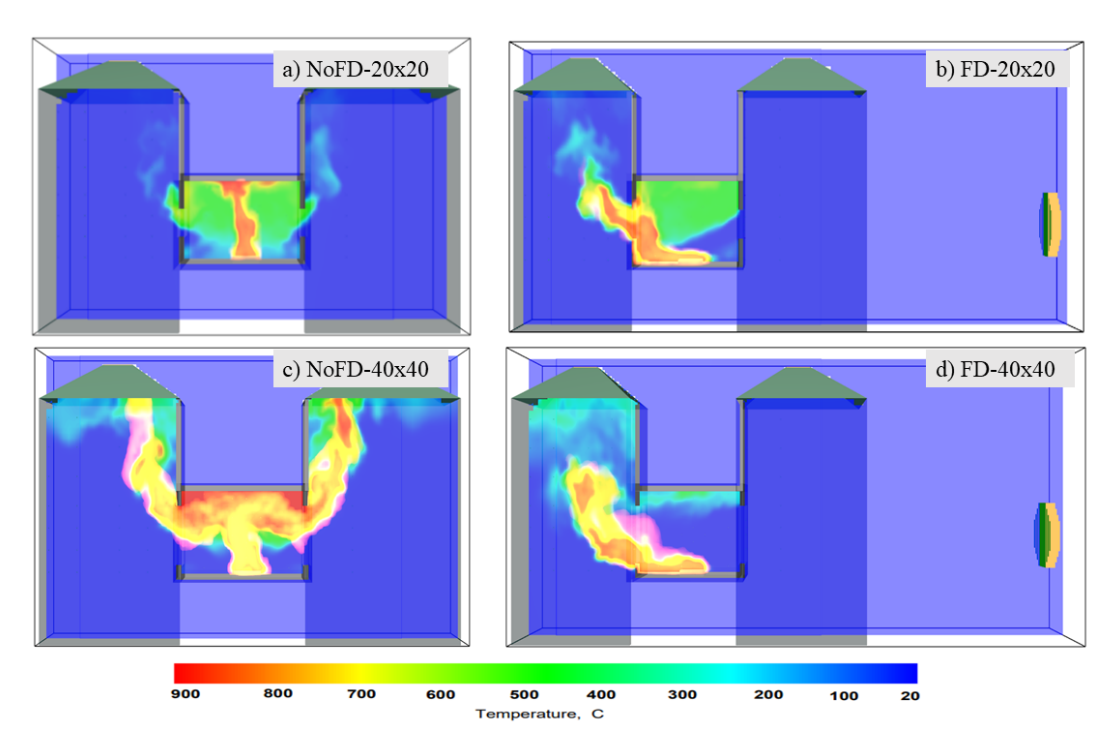


Figure 31: Spatial distribution of gaseous temperature 150 s and 200 s after fire initiation under NoFD (a) and (c) and FD (b) and (d) conditions; 20 cm (top) and 40 cm (bottom) opening size.

3.4.4 Effect of wind velocity on EVF development

Figure 32 (a) and (b) depicts predictions of gas mixture velocity and flame locations at 150 seconds after ignition for a 20 cm opening with NoFD and FD conditions (wind speed of 2.9 m/s for FD conditions) respectively. Similarly Figure 32 (c) and (d) depicts predictions of gas mixture velocity and flame location at 200s for 40 cm opening size in both NoFD and FD conditions. Times of 150s and 200s were chosen to ensure that the fire has fully evolved in the compartment, fan was switched on and wind flow was stabilized for both opening sizes.

Under NoFD conditions, as there are two openings in the opposing directions, cold air enters from both sides of the compartment opening resulting in the formation of two recirculation zones inside the compartment (from both sides). For all opening sizes, bidirectional flow is observed as fresh air enters through the bottom part of the opening and hot gases exits through the upper part of the opening. EVF is located closer to the adjacent façade, causing high heat transfer to the facades. As in the case of NoFD, the fire behavior is similar to a conventional compartment fire and air entrainment in the compartment varies primarily with the ventilation factor $A\sqrt{H}$, where A represents area of the opening and H represents height of the opening. Higher ventilation factor increases air entrainment rate and higher venting of fire gases exiting from the compartment. Additionally, this can also influence the gas mixture velocity and flame locations as represented in Figure 32 below.

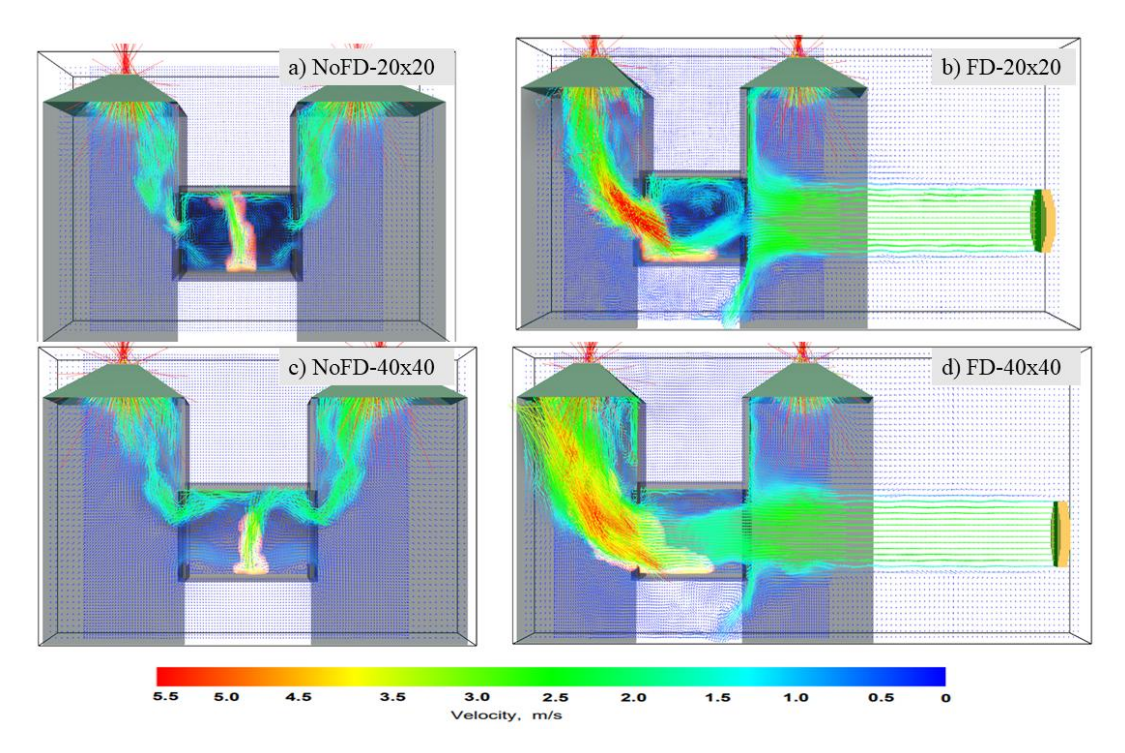


Figure 32: Gas mixture velocity and EVF 150 s and 200 s after fire initiation under NoFD (a) and (c) and FD (b) and (d) conditions; 20 cm (top) and 40 cm (bottom) opening size.

Under FD conditions, similar inflow of air from the bottom part of both openings formulates two recirculation zones, however, once the fan induces the presence of wind, the recirculation zones near the openings are no longer visible, and a single recirculation zone at the interior of the fire compartment is created. Only unidirectional flow can be observed for all three opening sizes, where hot gases including flame exits through the entire opening. Similar, observation was found in NoFD condition, as, in all three opening size cases observed a bi-directional flow in the experiment. However, in FD condition for all these three cases only uni-directional flow was observed.

Additionally, as the area of opening increases, e.g., as observed in the case of 40 cm opening size FD-40×40, it is observed that the flame exits through the bottom part and hot gases exits through

the upper part of the opening. A maximum velocity of 5.5 m/s was measured for the FD conditions due to the presence of wind speed and EVF flow velocities are relatively low in the NoFD condition for all the cases. The introduction of wind changes the in-compartment fire dynamics, flow behavior, pressure distribution, temperature, velocity and the flame locations. Also, Wind creates a positive pressure on the windward side and a negative pressure on the leeward side further aided by an increase in opening size resulted in a more efficient way of venting of hot gases (due to the higher ventilation factor) as EVFs are pushing outwards resulting in higher EVF projection. The results demonstrated that wind significantly impacts the fire dynamics within the compartment. These findings align with a previous study conducted by Beshir et al, which investigated the effect of external wind conditions on fire spread between two informal settlement dwellings spaced 1 meter apart (Beshir et al., 2023). They underscore the critical importance of considering wind effects when assessing the fire safety of buildings, particularly concerning fire separation distances in densely populated areas.

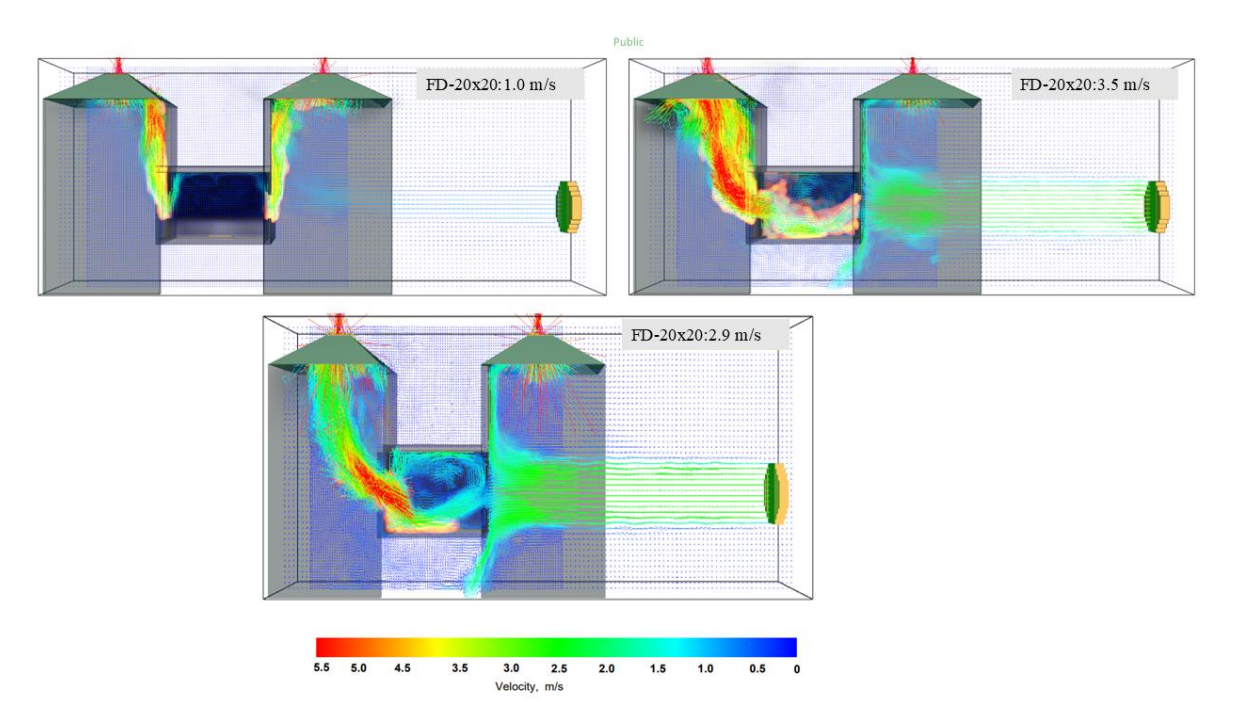


Figure 33: Gas mixture velocity and EVF at 200 s after fire initiation under FD condition with different wind velocities.

Figure 33 presents the velocity field and EVF characteristics for the FD-20×20 configuration under three different fan inlet velocities: 1.0 m/s, 2.9 m/s, and 3.5 m/s. The analysis demonstrates the significant influence of wind speed on flame trajectory, façade attachment, and flow symmetry. At 1.0 m/s, the flame behavior closely resembles that of the NoFD condition. Flames emerge symmetrically from both openings with a predominantly vertical projection, maintaining attachment to the façade surfaces. This condition results in increased thermal exposure to the

external wall, thereby promoting upward flame spread. As the inlet velocity increases to 2.9 m/s, the incoming airflow causes the flame to tilt toward the leeward opening, resulting in a more pronounced EVF with horizontal projection. At 3.5 m/s, the highest fan velocity condition, the forced draught dominates the flow behavior. The flame is strongly pushed out through a single opening and redirected with a fully tilted profile. EVF under this condition exhibits the longest horizontal projection with intense velocity among the three cases.

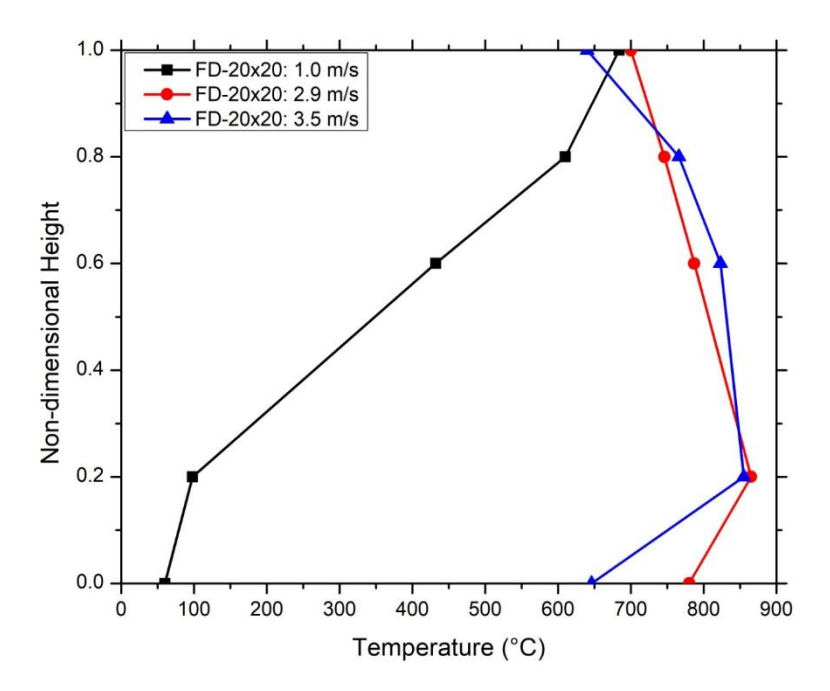


Figure 34: Non dimensional vertical distribution of the temperature at the outlet opening with different wind speed.

To evaluate the thermal impact at the compartment opening under different wind conditions with three velocities. Figure 34 presents the temperature distribution at the opening and the results demonstrate a strong correlation between wind velocity and temperature distribution. At 1.0 m/s, the temperatures are significantly lower, particularly at the lower portions of the opening. This is consistent with the observed bi-directional flow. In contrast, at 2.9 m/s and 3.5 m/s, the forced draught conditions dominate the flow field, pushing hot gases and flames directly toward the opening. The 3.5 m/s case shows a slightly broader distribution of high temperatures, indicating a more forceful redirection of the EVF outward.

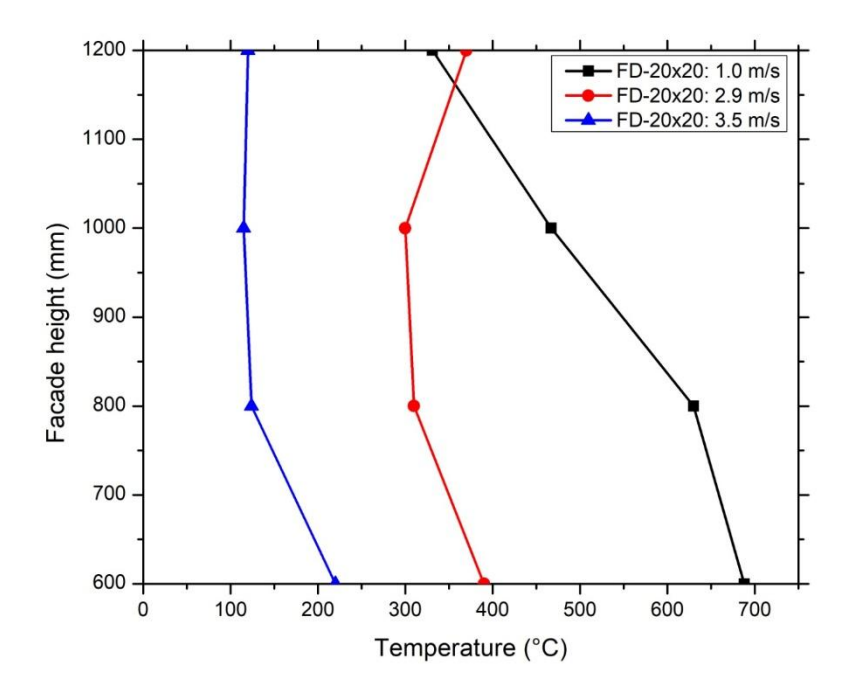


Figure 35: Vertical distribution of the temperature at the facade with different wind speed.

Figure 35 presents the thermal exposure to the façade. At 1.0 m/s, the façade experiences significantly higher temperatures, indicating strong flame attachment to the façade. This condition resembles the NoFD scenario, where the flame rises vertically and remains in contact with the building surface, resulting in higher thermal exposure and potential for upward fire spread. In contrast, for both the 2.9 m/s and 3.5 m/s cases, the temperatures at all measured heights are notably lower. This reduction is attributed to the increased horizontal projection of the externally venting flame (EVF), where the flame is tilted away from the façade due to the imposed wind.

3.4.5 Oxygen Concentration

Figure 36 depicts the spatial distribution of oxygen concentration inside the compartment at 150 s for 20 cm opening size (NoFD-20×40 and FD-20×20) and 200s for 40 cm opening size (NoFD-40×40 and FD-40×40) after fire initiation. A decreased oxygen concentration was observed during NoFD conditions compared to FD conditions. As stated previously in temperature field, when fire sustains with consumption of oxygen, oxygen concentration inside the upper part of the compartment decreases and temperature increases. This zone is termed the hot zone, whereas the entrainment of fresh air from the opening resulted in formation a cold zone similar to the temperature field, characterized by lower temperature and higher oxygen concentration.

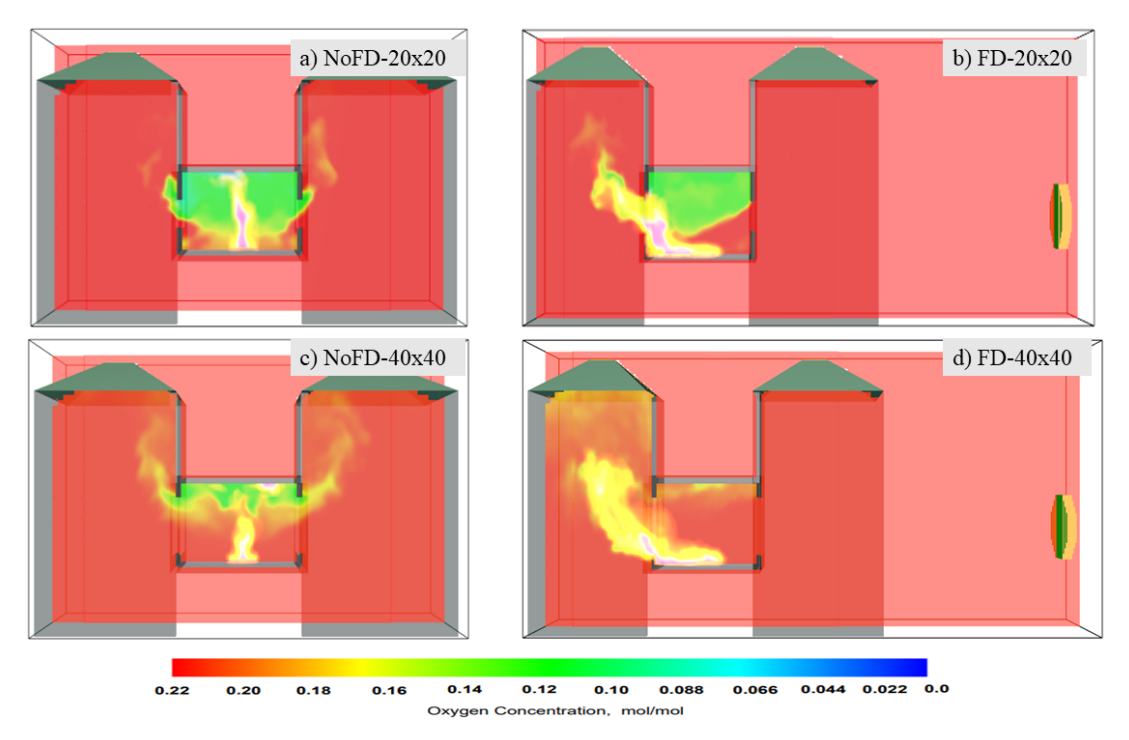


Figure 36: Spatial distribution of oxygen concentration 150 s and 200 s after fire initiation under NoFD (a) and (c) and FD (b) and (d) conditions; 20 cm (top) and 40 cm (bottom) opening size.

3.5 Conclusions

The present study focuses on the impact of ventilation conditions on the development of EVF development and impact on the façade in medium scale configurations. A numerical model was used and validated with the experimental results to investigate what is the effect of different wind velocities and opening sizes on the EVF development and impact on the façade of the outlet opening.

The effect of opening size on the EVF thermal characteristic and on the façade was experimentally and numerically investigated. As experimentally investigated, under FD conditions, the thermal impact on façade wall is reduced compared to NoFD conditions as the wind pushes EVF in the outward direction from the outlet opening and thus increasing EVF projection. This is an important aspect to consider when determining the fire separation distance between buildings for the fire and life safety design of structures. Notably, in NoFD conditions, an average temperature increase exceeding 30% was observed for the 20 cm case, while the temperature increased by 150% and 200% for the 30 cm and 40 cm NoFD cases, respectively. Also, the overall projection of the EVF for FD conditions is higher compared to NoFD as indicated by the maximum recorded experimental measurements. The maximum temperature observed at the top of the window lintel is 870°C for the FD 20×20 case and 430°C for the NoFD case. This is another critical aspect to consider when selecting façade materials, designing horizontal fire barriers, and implementing passive fire stopping measures in building design. Numerical results of NoFD conditions are in

good agreement with experimental results as there is 6% variance but this was increased to 15% when compared with experimental measurements of temperature under FD conditions. As indicated in both experimental and numerical work, results are in good agreement, and the numerical model can predict the phenomena of compartment fire development both inside and outside the compartment. This numerical model can be used with confidence as part of the performance-based design in building fire and life safety design.

It was revealed that opening size has significance influence on the development and temperature distribution of EVF under both NoFD and FD conditions, as increased opening resulted in different flow fields and reoutlining recirculation zones near the openings. For increased opening sizes, the vertical distribution of the temperature profile at the centreline of the outlet at the façade yielded increased gas temperatures. Under FD conditions, for all different sizes, the façade temperatures recorded were decreased compared to NoFD conditions. Numerical results of façade temperatures under NoFD conditions for 20 cm and 40 cm cases, are in good agreement with experimental results as there is 7% variance. This was increased to 10% when compared with experimental measurements of temperature under FD conditions. Stratification of the gas layer at the interior of the fire compartment was not observed during FD conditions as there was increased mixing of air due to the presence of wind, as also observed from the analysis of the gas mixture velocity profile for different opening sizes where a maximum of 5.5 m/s was calculated for the FD-40×40 case. This is supported by the decreased oxygen concentration observed during NoFD conditions compared to FD conditions due to the introduction of wind and this changes the in-compartment fire dynamics, flow behavior, temperature, velocity, and the flame locations.

Numerical modelling has predicted the temperature profile reasonably well when smaller compartment opening sizes are considered. However, when the opening size is increased, and the wind factor is introduced the model becomes more complex and the relevant error difference was in the range of 30% or more. Future research should prioritize investigating what is the impact of the different turbulence models.

Overall, this study highlights the critical importance of considering ventilation conditions in fire safety design and the necessity of precise modelling to predict fire behavior and its impact on building structures. The insights gained from this research can shape fire safety regulations and lead to the development of more effective fire protection strategies, ultimately enhancing the safety and resilience of building designs.

4 EFFECTS OF BUILDING FEATURES ON THE DEVELOPMENT OF EXTERNALLY VENTING FLAMES: EXPERIMENTAL AND NUMERICAL INVESTIGATION IN RECTILINEAR AND CURVED GEOMETRIES

4.1 Introduction

Exterior fire spread over building façades is predominantly influenced by their geometry, the combustibility of materials, and external weather conditions. The aim of the current work is to advance the state of the art by investigating the effects of building features on the development and characteristics of EVF. Although architectural geometry significantly alters fire behaviour, its specific influence on the development of EVF remains underexplored. In particular, the transition from traditional rectilinear forms to curvilinear designs introduces new fluid dynamic conditions that may impact the characteristics of EVF and the thermal exposure to façades. New engineering technologies and advanced manufacturing techniques have enabled the construction of novel façade systems, such as curved glass façades. Non-orthogonal, curvilinear, or "free form" geometries are increasingly used in building designs, posing significant challenges for fire safety engineering. The emphasis on aesthetics often leads to the incorporation of non-conventional building materials, which can aggravate and enhance fire spread in such constructions (White and Delichatsios, 2014). This chapter investigates the effect of compartment geometry, specifically rectilinear and curved geometries on EVF behaviour through a combination of medium-scale experiments and numerical simulations. The study provides new insights into how non-orthogonal designs may influence critical aspects of EVF behaviour, particularly with respect to temperature distribution and thermal exposure to the façade. While numerous studies have examined façade fires in orthogonal or rectilinear geometries, the influence of non-orthogonal geometries on EVF development has not been thoroughly investigated. The outcomes of this research aim to support a better understanding of fire dynamics in complex architectural forms and to provide evidencebased guidance for risk-informed design practices.

4.2 Experimental and Numerical Investigation

4.2.1 Experimental Setup

An experimental study was conducted in two different geometries; the experimental setup of compartments is depicted in Figure 37. Geometry 1 has a curvilinear shape with a length of 1.3 m, a width of 0.6 m, and a height of 0.75 m from floor level to the top. To keep a similar volume for comparative study, Geometry 2 has the same plan dimensions as that of Geometry 1, with rectilinear elevation, and is provided with a height of 0.80 m. To study the influence of ventilation condition on EVF development in these geometries, the compartment is provided with 2 equal sized openings on either side of the wall with a width of 0.25 m and height of 0.4 m to facilitate "Forced Draught" conditions (FD) and to simulate "No Forced Draught" condition (NoFD), the geometry is restricted to a single opening.



Figure 37: Experimental setup indoor (top) and outdoor (bottom).

4.2.2 Sensors and data acquisition system

The schematic of measuring instruments is shown in Figure 38, which describes the locations of thermocouples located in the internal and external locations of the experimental setup on thermocouple trees. A total of 26 K-type thermocouples of 1.5 mm diameter were used for measurement of the temperature profile of compartment fire and EVF. To measure the exterior temperature two thermocouple trees are located 0.15 m apart from the compartment and each Thermocouple tree provided with 5 thermocouples spaced 0.2m starting from mid height of the opening. Further to measure the interior compartment temperature 4 thermocouples located 0.5 m distance at a height 0.6m of the compartment. n-Heptane was used as the fuel for all the mediumscale experiments. The burner used had dimensions of 20 cm × 20 cm. In this work, thermocouples with a measuring range of -50°C to +1250°C and with the limits of error values of ±1.1°C or ±0.4% have been used (Omega, 2023). A water cooled, 25 mm diameter total heat flux sensor SBG01 was located at the 0.15 m above the opening height, i.e. at the centre line of the façade surface facing the EVF with a measuring range of 200 x 10³ W/m² with sensor technology of Gardon and Schmidt-Boelter used to measure the total heat flux (Hukseflux Thermal Sensors, n.d.). The fuel mass was continuously monitored using a load cell which is located below the fuel pan. In the present study, the curvilinear compartment being constructed from steel, has a higher thermal conductivity of 45.8 W/mK, in comparison to the rectilinear compartment, which is made of Monolux', a fire-resistant material with a low thermal conductivity of 0.15 W/mK. Monolux' s insulating properties develops conditions similar to fire-rated compartments owing to its interior heat retention characteristics.

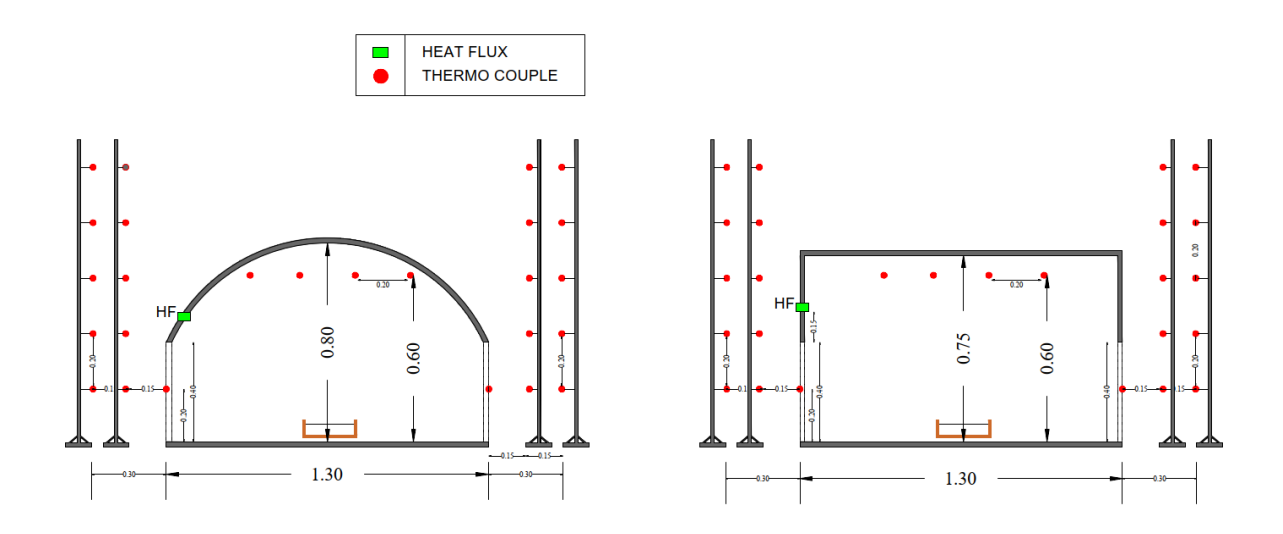


Figure 38: Schematic drawing of the experimental facility and sensor locations for curvilinear (left) and rectilinear (right).

4.2.3 Experimental Test Scenarios

A total of 16 experiments were conducted to analyse the effects of building features on the development of externally venting flames. Table 6 describes the list of experiments, ventilation condition, opening dimensions, fuel burner height location and ventilation factors used for the experiments.

• Ventilation condition: FD and NoFD

In accordance with EN 1991-1-2 (2002), two draught conditions were adopted—NoFD and FD) to examine the influence of ventilation configuration on compartment flow dynamics and externally venting flame development.

• Opening dimensions

Two opening sizes—25 × 20 cm and 25 × 40 cm—were selected to study the effect of the ventilation factor on compartment fire dynamics and external flame behaviour. The findings from the previous literatures indicate that window geometry, expressed through the ventilation factor, plays a critical role in determining the characteristics of compartment fires and the resulting façade flames. However, it is important to note that most previous investigations in the literature have been limited to cases with fully open windows positioned on the compartment's vertical façade. These dimensions correspond to ventilation factors (A \sqrt{H}) of 0.0223 m^{5/2} and 0.0632 m^{5/2}, respectively, which cover a realistic range for reduced-scale façade openings used in previous experimental studies. This systematic variation in opening size provides a controlled means to evaluate the transition between ventilation-limited and well-ventilated fire conditions under both FD and NoFD configurations.

• Fuel burner elevation

The fuel burner was positioned at two elevations—5 cm and 30 cm above the compartment floor—to assess the influence of fire source height on flow structure, heat release behavior, and façade flame development. In addition to varying opening size and ventilation conditions, the elevation of the fire source was considered as a key variable to better replicate realistic fire scenarios. In real building fires, the seat of the fire is often located at some height above the floor—such as sofa, bed, or hearth-level ignition sources—rather than directly on the floor surface. As previous studies in the literature fire source elevation significantly affects the internal flow field, smoke layer development, and façade flame behaviour (Kawagoe, 1958). When the burner is elevated from the compartment floor, the flow field and the resulting plume entrainment patterns are altered, leading to changes in the mixing layer development near the opening. This influences the critical heat

release rate for external flame ejection and the corresponding façade flame height (Merci & Beji, 2016). Accordingly, in the present work, the burner was elevated to 0.3 m from the floor level to represent a realistic fire source height equivalent to furniture-based ignition (such as sofa or hearth fires). This configuration ensured that the experiment captured the altered internal flow dynamics and heat transfer mechanisms relevant to real-scale compartment fires. The elevated configuration thus provided a more comprehensive understanding of how the vertical position of the fire source affects ventilation interaction, critical heat release rate, and externally venting flame characteristics for different opening sizes.

Table 6: Medium scale experimental test scenarios.

Case	Opening dimension W (cm) x H(cm)	Vent. Factor A√H (m ^{5/2})	Burner height measured from floor b_h (cm)	Comp. Geometry	Ventilation	Outdoor Experiment
1	25 x 40	0.0632	5			✓
2	25 x 20	0.0223	5	Cumvilinoor	NoFD	N/A
3	25 x 40	0.0632	30	Curvilinear Rectilinear		N/A
4	25 x 20	0.0223	30			N/A
5	25 x 40	0.0632	5			√
6	25 x 20	0.0223	5			N/A
7	25 x 40	0.0632	30			N/A
8	25 x 20	0.0223	30			N/A
9	25 x 40	0.0632	5			√
10	25 x 20	0.0223	5	Cumzilinaan	FD	N/A
11	25 x 40	0.0632	30	Curvilinear Rectilinear		N/A
12	25 x 20	0.0223	30			N/A
13	25 x 40	0.0632	5			√
14	25 x 20	0.0223	5			N/A
15	25 x 40	0.0632	30			N/A
16	25 x 20	0.0223	30			N/A

4.2.4 Repeatability Study

The repeatability of the experiments was assessed by performing three trials under identical conditions, focusing on temperature evolution and fuel mass loss over time, Table 7. n-Heptane was used as the fuel for all three experiments. The burner used had dimensions of 20 cm \times 20 cm, and the initial fuel mass was 650 g of n-Heptane. As shown in the temperature graph in Figure 39, the temperature profiles of all three experiments exhibit similar trends, with a relative difference of 16.13%. The profiles demonstrate consistent heating, peak temperatures, and cooling phases across the trials. Likewise, the mass loss graph highlights the uniformity of fuel consumption, with

a relative difference of 13.78% among the experiments. The closely aligned trends in both temperature and mass loss validate the repeatability and reliability of the experimental setup, providing a robust foundation for subsequent analyses.

T 11 7 C	c	1	1 • .1	. 1 .1
Table 7: Summary o	ot main operationa	I narameters usea	' in the renea	tahility tests
1 dote 1. Summing o	g main operationa	i parameters asea	in the repeat	icionity icons.

Test Case	Unit	Case 1 –	Case 2 –	Case 3 –
Test Case		Curvilinear FD	Curvilinear FD	Curvilinear FD
Height of Opening	m	0.4	0.4	0.4
Width of Opening	m	0.25	0.25	0.25
Amb. Temperature	°C	25.5	28	26.5
RH	%	45%	48%	46%
Duration	sec	780	802	810
Mass	kg	0.651	0.652	0.656
HRR	kW	147	150	151

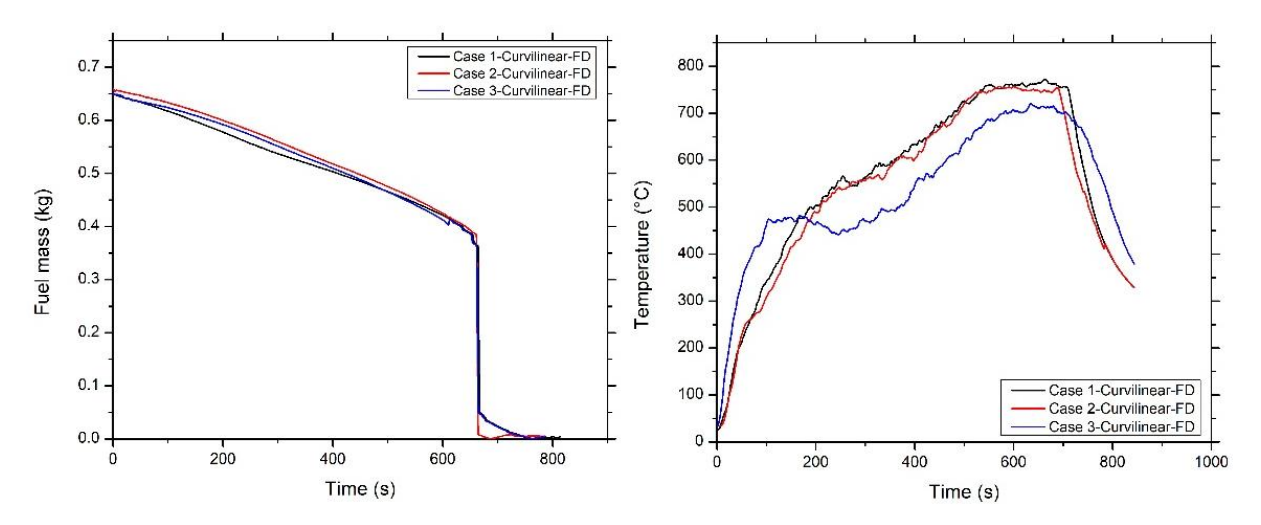


Figure 39: Fuel mass loss (left) and gas temperature inside the fire compartment (right) measurements obtained in the repeatability tests.

4.2.5 Numerical Simulation Details

Numerical simulation has become a crucial tool for investigating complex fire dynamics, offering the ability to understand detailed flow fields, thermal behaviour, and flame development beyond what can be captured through physical experiments alone. In the context of EVF, the influence of compartment geometry on fire behaviour introduces challenges that demand computational modelling.

The numerical simulations aim to replicate and extend the experimental findings by providing a deeper understanding of the flow structures, temperature fields, oxygen concentrations and EVF characteristics associated with different architectural forms.

A total of 8 experiments were conducted to analyse the effects of building features on the development of externally venting flames. Table 8 describes the list of experiments, ventilation condition, opening dimensions and ventilation factors used for the experiments.

Table 8: Medium scale experimental test scenarios considered for numerical simulations.

Test	Opening Dimension (in meter)	Ventilation Mode	Geometry	Fuel
Cases				
1	0.25 x 0.4 (Height)	No FD	Curvilinear	
2	0.25 x 0.4 (Height)		Rectilinear	
3	0.25 x 0.4 (Height)	FD	Curvilinear	
4	0.25 x 0.4 (Height)		Rectilinear	Heptane
5	0.25 x 0.2 (Height)	No FD	Curvilinear	
6	0.25 x 0.2 (Height)		Rectilinear	
7	0.25 x 0.2 (Height)	FD	Curvilinear	
8	0.25 x 0.2 (Height)		Rectilinear	

To investigate the influence of geometrical features, opening sizes and ventilation conditions on the development of an EVF, the experimental test cases mentioned in Table 8 have been simulated using the FDS, Version 6.7.9. The time step is dynamically adjusted to satisfy the CFL criterion. Turbulence is modelled using the Large Eddy Simulation (LES) approach for length scales smaller than those that are explicitly resolved on the numerical grid. The numerical simulations were performed using the default turbulence model in FDS, namely the Deardorff subgrid-scale (SGS) model, while the WALE model was applied near wall boundaries to improve resolution of shearlayer effects. An explanation of the various turbulence subgrid models available in FDS, along with their potential influence on in-compartment fire dynamics and externally venting flame (EVF) behaviour, has been included in Appendix B of the revised thesis. Thermal radiation is simulated using the finite volume methodology on the same grid as the flow solver. Conjugate heat transfer in solid bodies immersed in the computational domain are simulated by solving a 1-D heat transfer equation in the direction normal to the solid surface; a dedicated non-uniform mesh, independent of the CFD computational mesh, is used for the respective simulations. Multilayered wall assemblies can be simulated by utilizing detailed thermo-physical properties (e.g., density, thermal conductivity, specific heat) for each material. Solid reactions (e.g., pyrolysis) can be modelled by using appropriate chemical kinetics models. Predictions of the FDS code have been extensively validated (McGrattan et al., 2019).

Curvilinear geometries were all solid surfaces, including walls and floors, are provided with boundary condition with following material properties corresponding to steel, with 7850 kg/m3

density, 0.46 kJ/kgK specific heat, 45.8W/mK thermal conductivity, 0.02 m thickness, and emissivity of 0.95. However, rectilinear geometries are provided with a boundary condition with following material properties corresponding monolux fire resistant material with 750 kg/m³ density, 0.7 kJ/kgK specific heat, 0.15 W/mK thermal conductivity and emissivity of 0.8. The soot yield, which represents the fraction of heptane fuel mass converted to smoke particulates, is set equal to 0.015 kg/kg and the corresponding CO yield was set equal to 0.006 kg/kg (Hamins et al., 2003).

a. Computational domain

As previous studies have revealed (Zhang et al., 2010) the computational domain shall extend at least one hydraulic diameter for such studies. The calculated hydraulic diameter is 0.26 m. However, to capture the geometric and thermal characteristics of the flame more accurately, an increased domain dimension is considered (from the edge of the opening) as depicted in Figure 40 below. The domain was extended 1.0 meters in positive and negative X axis for FD Condition from edge of the respective openings on the opposite side of the compartment and 1.5 meters in positive Z axis for FD and NoFD Conditions.

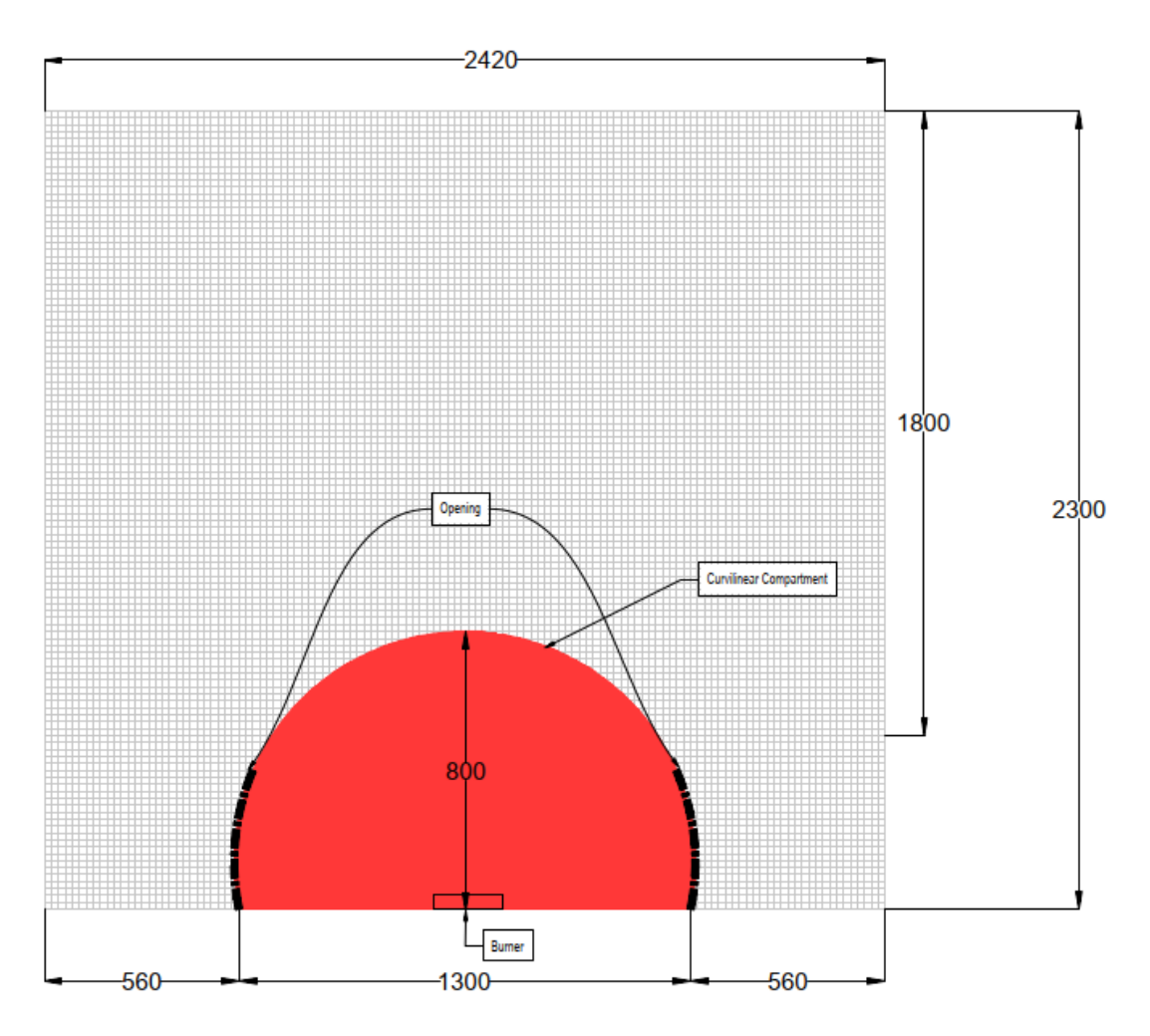


Figure 40: Schematic of Extended computational domain, dimensions in mm

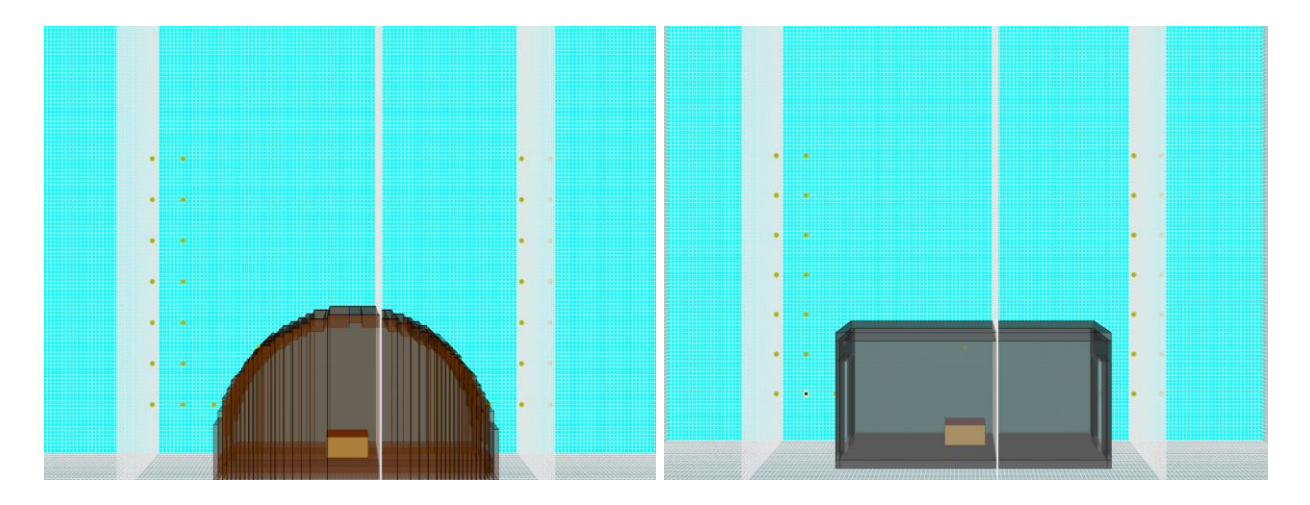


Figure 41: Extended Computational domain in FDS.

As previous studies have revealed (Zhang et al., 2010) the computational domain shall extend at least one hydraulic diameter for such studies. The calculated hydraulic diameter is 0.26 m.

b. Grid Sensitivity

The non-dimensional expression D^*/dx is a measure of how well the flow field is resolved in the simulation of buoyant plumes. Where dx is the size of cells and D^* is the characteristic fire diameter (D^*) (McGrattan et al., 2019). The D^*/dx ratio indicates the adequacy of the grid resolution. A higher D^*/dx would mean a better resolution for the simulation of fire, as FDS uses a structured mesh. The D^*/dx ratio of 16 for fine mesh was used with a corresponding cell size of 0.02 m. This will ensure adequate resolution of plume dynamics and other geometric characteristics of the model (McGrattan et al., 2019). The total computational grid consists of 765,325 cubic cells for the simulations. Aiming to investigate the effect of ventilation conditions and geometry on the development of EVF from the fire compartment, an experimental setup of curvilinear geometry and rectilinear geometry with FD ventilation condition for opening 0.2m x 0.4m opening size have been selected. A grid sensitivity analysis for three different D^*/dx values namely 4 (coarse mesh), 10 (moderate mesh), 16 (fine mesh) was conducted and results for the temporal evolution at the centreline of opening are depicted in Figure 42.

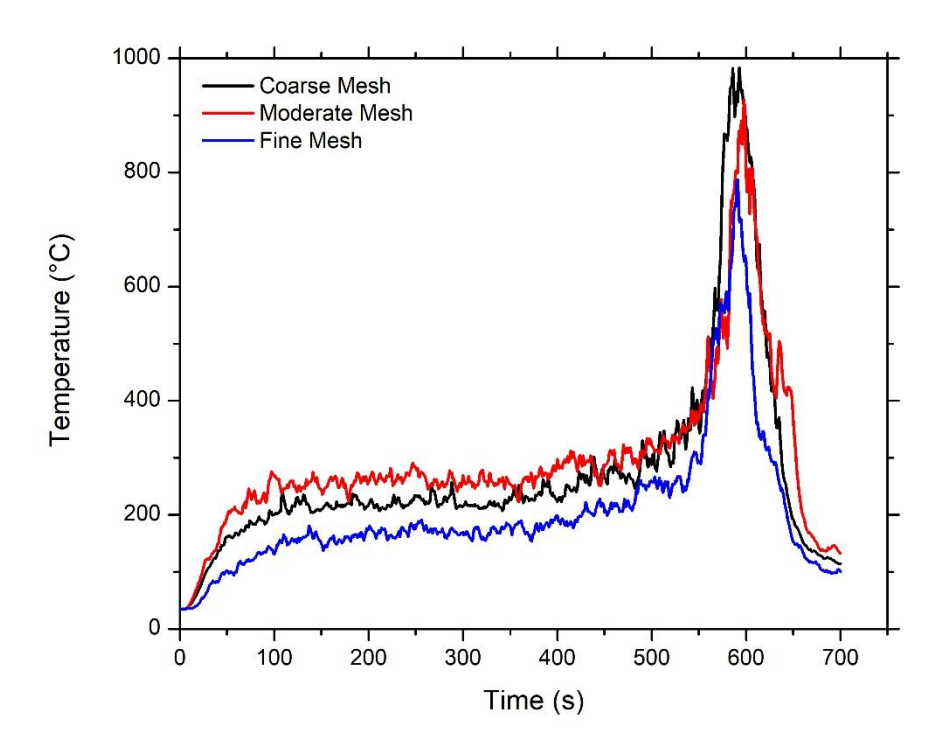


Figure 42: Temporal evolution of the temperature at the centreline of opening for the different meshes used.

c. Validation of computational models

To validate the numerical results, experimental data from the both geometry under both ventilation conditions FD and NoFD were used to analyse the temporal evolution of gas temperatures at the compartment interior and at the centre of the opening. This validation is essential to assess the accuracy of the FDS-predicted gas temperatures.

Figure 43 thus illustrates the outward gas temperature for the numerical case, where the vertical axis represents numerical results, and the horizontal axis represents experimental data. The error margins are represented by dotted lines, and the red diagonal dashed line indicates a perfect match between simulation and experimental data. The data show that 70% of the predictions fall within a $\pm 30\%$ error margin, indicating good agreement. The R-squared value, also known as the coefficient of determination, is found to be 0.83, and the linear regression slope is approximately 1, suggesting a moderate-to-strong positive linear relationship and a good fit for the data.

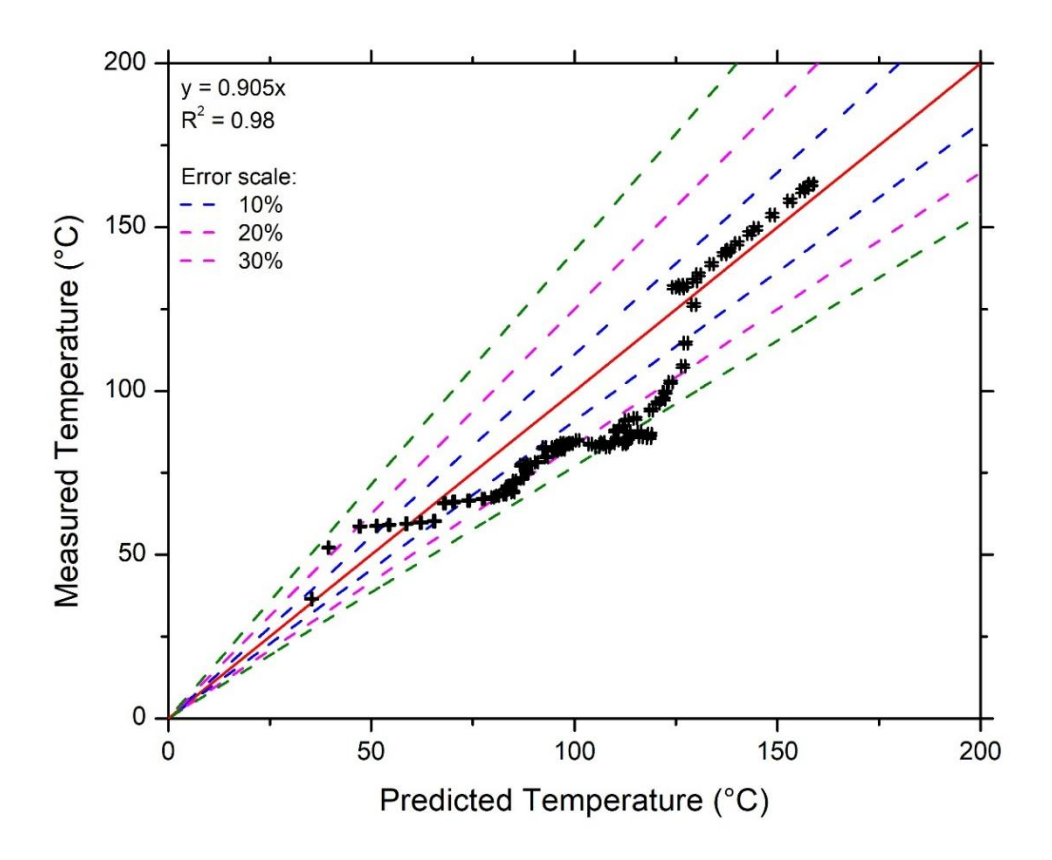
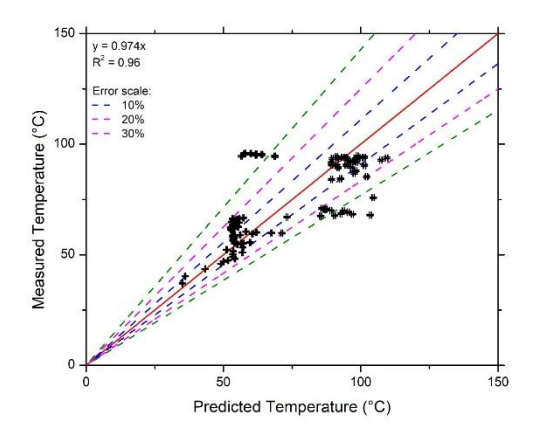


Figure 43: Validation based on predicted temperature at centre of the opening.

Figure 44 presents the comparison of predicted compartment gas temperatures and outward temperatures at the opening centre (right) under FD conditions. The vertical axis represents the numerical results, while the horizontal axis shows the corresponding experimental measurements. The red dashed diagonal line indicates perfect agreement, and the dotted lines represent $\pm 30\%$ error margins. Approximately 70% of the predicted values fall within these margins, demonstrating good agreement. The coefficient of determination (R²) is 0.97, with a regression slope close to 1, indicating a strong linear correlation and a reliable fit between numerical and experimental data. During the fire growth phase, the numerical predictions closely match the experimental data. However, as the fire becomes fully developed and EVF forms, followed by the decay phase, a noticeable deviation is observed, particularly in the form of overprediction by FDS. This discrepancy becomes more pronounced under NoFD conditions. Figure 45 illustrates the corresponding results for the NoFD case. A similar trend is observed: good agreement during the initial growth phase, but significant divergence during the fully developed fire and decay stages. This deviation is more substantial than in the FD condition. The R² value is approximately 0.80, and the regression slope indicates a larger disparity between the predicted and measured temperatures, especially in the NoFD conditions.



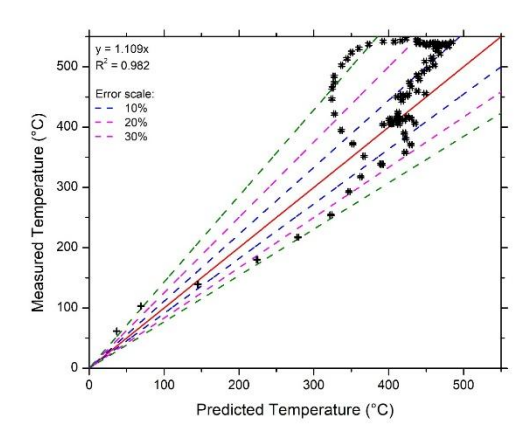
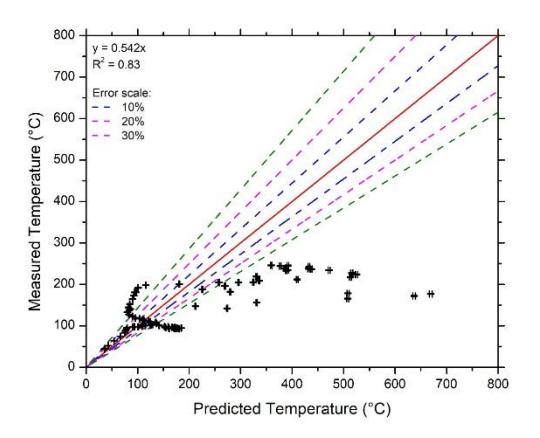


Figure 44: Validation based on the predicted temperature at the centre of the opening (left) and interior compartment temperature (right) under FD conditions.



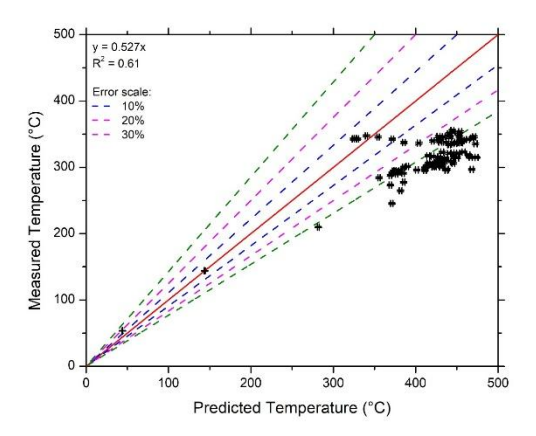


Figure 45: Validation based on the predicted temperature at the centre of the opening (left) and interior compartment temperature (right) under NoFD conditions.

4.3 Effect of material on compartment fire development

As outlined in the preceding section, the construction material of the compartment plays a critical role in fire compartment's thermal behaviour. In the current assessment, the curvilinear compartment being constructed from steel, has a higher thermal conductivity of 45.8 W/mK, in comparison to the rectilinear compartment, which is made of Monolux', a fire-resistant material with a low thermal conductivity of 0.15 W/mK. Monolux's insulating properties develops conditions similar to fire-rated compartments owing to its interior heat retention characteristics. In contradiction, Steel's high thermal conductivity leads to faster heat dissipation, resulting in reduced interior temperatures and impacting venting dynamics. The temperature profiles of both the interior and exterior of the compartments varies to a significant extent with respect to the two materials, independent of the compartment's geometrical features. In the Monolux compartment, the interior temperature peaked at approximately 750°C, owing to its low thermal conductivity, whereas Monolux demonstrated higher heat retention within the compartment, resulting in sustained high temperatures. Though the steel compartment exhibited a similar peak temperature, its high thermal conductivity resulted in rapid heat dissipation to the structure and subsequently a faster decline in interior temperature during the decay stage. The opening temperatures, aligned with the pattern, with the Monolux compartment opening temperature reaching approximately 160°C, while the steel compartment exhibited a lower temperature of 100°C due to higher heat dissipation. The EVF temperatures displayed corresponding pattern as well as in the appearance and duration of the flames. The Monolux compartment exhibited higher EVF temperatures and longer flame durations across various experimental scenarios, as presented in Table 8.

To further investigate the impact of material properties, a numerical study was conducted using FDS. Two simulation cases were performed under identical geometrical and experimental conditions, with only the material properties being varied. Case 1 utilized steel, while Case 2 employed Monolux, allowing for a comparative analysis of temperature profiles and EVF. This analysis was particularly important owing to the experimental condition that the rectilinear compartment was constructed from Monolux, whereas the curvilinear compartment was made of steel. A direct comparison of temperature characteristics between the two compartments was not apt due to the differences in material properties and thermal behaviour of the materials in use for the subject compartments. Figure 46 illustrates the differences in temperature profiles between the Monolux and steel compartments, demonstrating that compartment temperatures were higher in the Monolux case owing to its insulating properties. Beard et. al described the influence of boundary material properties on surface temperature using the equation presented in A.17 (Beard

et al., 1995). The temperature of the surface of the target object $T_{ve\ can}$ be calculated using the below Equation 4.1.

$$T_{ve} = T_a + U_{ve}(T - T_a) (4.1)$$

where U_{ve} is a function of both the geometry of the setup and the thermal characteristics of the surface material.

$$U_{ve} = \lambda_{ve} \left(1 - \left[\frac{D_1}{D_1 + D_2} \right]^{N_{\lambda}} \right) \tag{4.2}$$

The material-specific modifier λ_{ve}

$$\lambda_{ve} = exp(-\beta (K_{ve}\rho_{ve}C_{ve})^{\delta}) \tag{4.3}$$

 K_{ve} , ρ_{ve} , C_{ve} represents the thermal conductivity, density and specific heat of the tartet material and β and N_{λ} are empirically derived constants. $\left[\frac{D_1}{D_1+D_2}\right]^{N_{\lambda}}$ is the geometric correction factor. This equation illustrates that those materials with high thermal conductivity and thermal mass (e.g., steel) yield low values of U_{ve} , indicating a reduced surface temperature response to the gas-phase temperature. Conversely, materials like Monolux, with lower thermal conductivity and specific heat, result in higher U_{ve} values, allowing the surface to match the gas temperature at an accelerated rate. This material behavior has significant implications for flame spread, thermal feedback, and compartmental temperature evolution during fire scenarios. These results exhibit that temperature differences are critical when studying the compartment fire and EVF behavior where compartment is constructed with dissimilar materials.

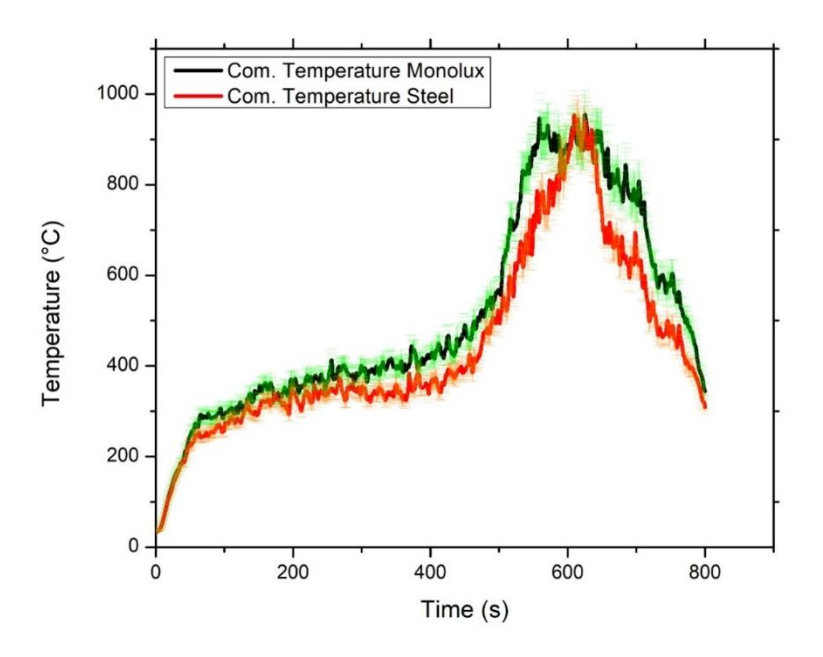


Figure 46: Interior temperature profiles of the curvilinear compartment constructed with steel and Monolux.

4.4 Experimental Investigation: Results and Discussion

4.4.1 Fuel mass loss

The burning rate of a compartment pool fire is influenced by several factors, including the ventilation openings, enclosure geometry, material properties of the bounding surfaces, radiation from these surfaces, fuel properties, surface area of the fuel and the thermal characteristics of the exposed rim above the fuel (White and Delichatsios, 2014; Hurley, 2016). Figure 47 below depicts the mass loss profiles differences between the curvilinear and rectilinear geometries. The enclosure geometry significantly influences the mass burning rate, as the hot smoke layer and the upper bounding surface radiate heat back toward the burning fuel, thereby increasing the burning rate (Karlsson, 2002). Rectilinear geometry exhibited comparatively rapid initial mass loss rate, understandably due to better airflow and heat distribution aided by its planar surfaces. This resulted in a higher rate of fuel consumption, as evident from the steeper decline in mass. Curvilinear geometry demonstrated a gradual mass loss, with combustion sustaining for a longer period compared to the rectilinear geometry. This is attributed to reduced air entrainment and heat feedback caused by the curved surfaces as uneven heat distribution in the ceiling resulted in fluctuating venting dynamics, affecting the combustion process leading to slower fuel consumption.

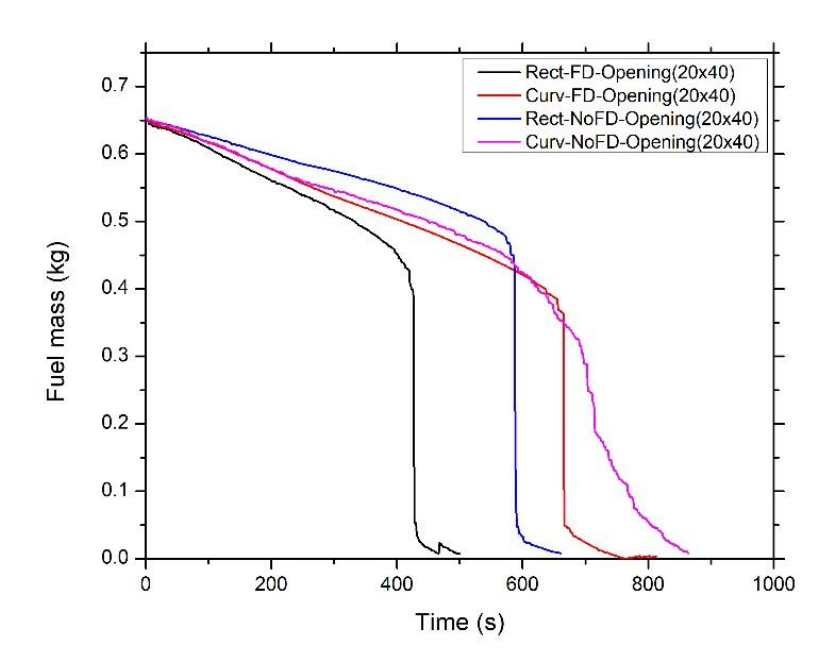


Figure 47: Fuel mass loss for curvilinear and rectilinear geometries.

In compartments with ventilation openings, the size, shape, and position of these openings are key parameters in fire behaviour. Kawagoe (1958) observed that the burning rate strongly depends on the ventilation factor $A\sqrt{H}$, and a proportional increase in the burning rate up to a certain threshold is observed with an increase in the ventilation factor. Kawagoe (1958) (Kawagoe, 1958). Similar patterns in burning rate were observed by Kawagoe for both geometries for FD as well as No FD conditions. The thermal properties of the bounding surfaces of the compartments, particularly their thermal inertia, plays an essential role in heat transfer. Materials with high thermal inertia conduct more heat into the material of construction, leading to lower hot gas temperatures and, consequently, a reduced burning rate. The rectilinear geometry being constructed of Monolux offers superior insulating properties and a lower thermal inertia, exhibited higher internal temperatures and slower cooling in the rectilinear compartment resulting in a faster combustion, understandably due to higher temperatures with an efficient burning condition. However, curvilinear compartment is made of Steel, and its high conductivity led to rapid heat dissipation from the surface, resulting in reduced internal temperatures and affecting venting behaviour and resulted in a slower, prolonged combustion in the curvilinear compartment.

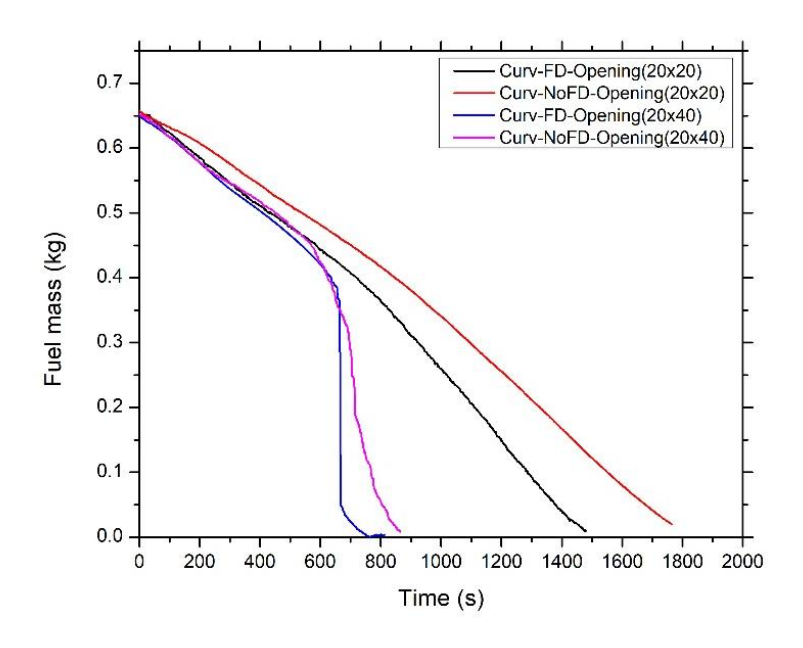


Figure 48: Fuel mass loss for curvilinear geometry with different opening size.

Figure 48 illustrates the impact of ventilation and opening size on the fuel consumption rate in a curvilinear compartment. The results revealed that the burning rate is significantly influenced by the size of the ventilation openings. Larger openings, such as the 20x40 configurations, facilitate a greater oxygen supply, leading to a higher combustion rate and faster fuel consumption compared to smaller openings (20 cm x 20 cm). This observation aligns with the findings of Kawagoe (1958), who demonstrated that the ventilation factor plays a critical role in determining the burning rate, with larger ventilation factors accelerating fuel depletion. The size of the opening primarily affects the duration of the fire event. For smaller openings (20 cm x 20cm), both FD) and NoFD conditions resulted in prolonged burning durations owing to reduced ventilation, which limited the oxygen flow to the pool fire. Specifically, for the 20 cm x 20 cm opening cases, the burning duration was approximately 1500 seconds under FD conditions and extended to 1700 seconds under NoFD conditions. Conversely, larger openings (20 cm x 40 cm) significantly reduced the burning duration aided by the increased opening size, facilitating greater oxygen availability. Under FD conditions, the burning process completed in approximately 800 seconds, while NoFD conditions resulted in a slightly longer duration of 864 seconds. In general, the NoFD condition exhibited a marginally slower burning rate compared to FD conditions, as the single opening limited the overall oxygen supply despite the increased opening size.

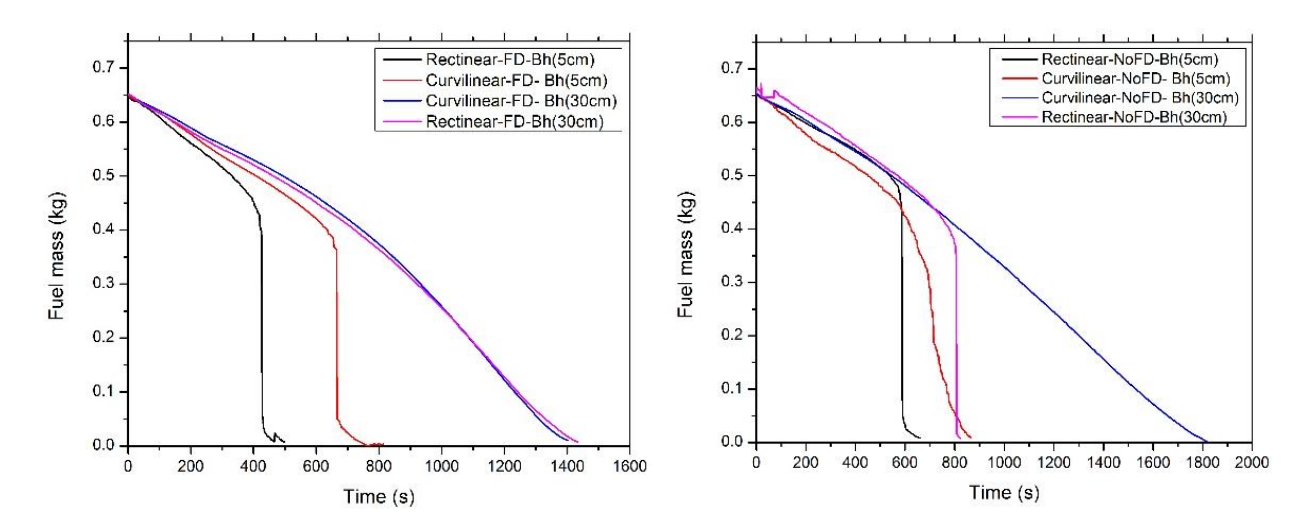


Figure 49: Fuel mass loss in compartments with varying fuel burner height locations under FD conditions (left) and NoFD conditions (right).

Figure 49 illustrates the effect of ventilation configuration, fuel pan or burner height, and compartment geometry on the fuel consumption rate in compartment fires. The flow field dynamics of the fire compartment is impacted by the height of the fuel pan from the compartment floor. Similarly, the interior thermal profile and affecting ventilation condition of both interior and exterior of the fire compartment is also influenced by the burner elevation. The rate of burning is significantly impacted by both burner height and compartment geometry under NoFD conditions. When the burner is located at 5 cm from the floor in the rectilinear compartment a higher fuel mass loss is observed, completing the burn in approximately 680 seconds, while the curvilinear compartment takes approximately 850 seconds for the full depletion of the fuel. At a burner height of 30 cm, the differences become more pronounced; the rectilinear geometry burns fuel in 800 seconds, while the curvilinear geometry takes significantly longer, approximately 1800 seconds. This suggests that the curvilinear geometry enhances heat feedback and the smoke filling time inside the compartment is greatly extended which restricts the oxygen supply, leading to prolonged burning durations under NoFD conditions. Under FD conditions the trends differ. For the burner located at 5 cm, the rectilinear geometry burns fuel much faster, completing in approximately 500 seconds, while the curvilinear geometry takes longer, about 850 seconds. At a burner height of 30 cm, both geometries exhibit similar trends, with burning durations of approximately 1400 seconds. This indicates that in FD conditions at elevated burner positions smoke filling time inside the compartment is greatly extended resulting in reduced fuel mass loss rate. FD conditions reduce the impact of geometry at higher burner positions, equalizing burning durations, but at lower burner heights, the rectilinear geometry still achieves faster combustion.

4.4.2 Air supply rate and Global Equivalence ratio

The air mass flow rate entering the compartment through the lower part of the opening (\dot{m}_a) can be estimated using Equation 4.4, as a function of the discharge coefficient (C_d), the density of ambient air (ρ_{amb}) and of the hot combustion products inside the compartment (ρ) and the opening width (W_v) and height (H_v); with the subscript v denoting the vent corresponding to the compartment opening (Makhviladze et al., 2006).

$$\dot{m}_{a} = \frac{2}{3} C_{d} \sqrt{2g\rho_{amb}(\rho_{amb} - \rho)} H_{v}^{\frac{2}{3}} W_{v}$$
 (4.4)

$$\dot{\mathbf{m}}_{\mathbf{a}} = 0.5 \, A_{\nu} \sqrt{H_{\nu}} \tag{4.5}$$

The calculated values, using the instantaneous temperature measurements at the opening and the interior of the compartment for various cases are depicted in the below graphs. The estimated values are compared to predictions using the empirical correlation, Equation 4.5.

Global equivalence ratio (GER) is the parameter used to differentiate the compartment fire ventilation condition which is under ventilated or well ventilated. GER is defined as the ratio of the fuel mass flux (m_f) to the oxygen mass flux entering the compartment (m_{o2}), divided by the fuel-to-oxygen stoichiometric ratio (r) in Equations 4.6 (Hurley, 2016; Quintiere, 2006).

$$GER = \frac{m_f}{rm_{o2}} \tag{4.6}$$

$$m_{o2} = \begin{cases} 0.5 \ Y_{o2,air} A_0 \sqrt{H_0} \ , natural \ ventilation \\ 0.23 \ \rho_{amb} V \ , mechanical \ ventilation. \end{cases}$$
(4.7)

The mass flow rate of the oxygen entering the compartment can be estimated using an empirical correlation Equation 4.7, where A_0 is the area of the opening and H_0 is the height of the opening (Hurley, 2016; Quintiere, 2006). When the value of GER exceeds unity, the fire is considered as fuel-controlled (well ventilated); when GER is less than one, the fire is considered as ventilation-controlled (under-ventilated).

Figure 50 graph depicts the incoming flow rate to the fire compartment (kg/s) as a function of time (s) for both rectilinear and curvilinear compartments under FD and NoFD conditions, with an opening size of 20 cm x 40 cm. The dashed green line represents the empirical equation, providing a reference for comparison. A good level of agreement is observed between the empirical equation and the simulated results for all the cases. The flow rates for both rectilinear and curvilinear geometries closely align with the predictions of the empirical model, particularly during the steady-state phase (beyond approximately 200 seconds). This indicates that the empirical equation effectively captures the flow dynamics for compartments with varying geometries and ventilation conditions.

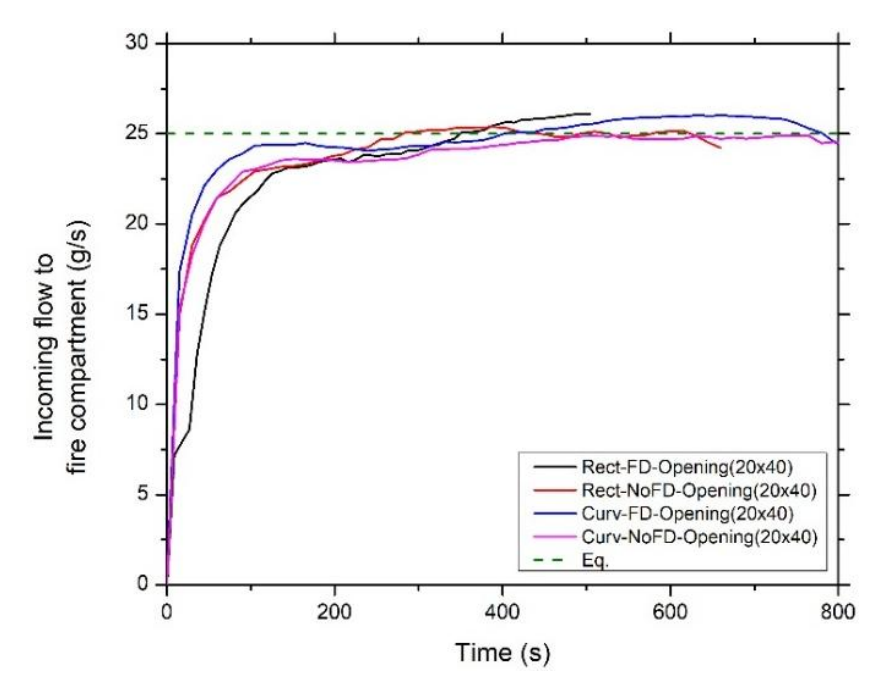


Figure 50: Temporal evolution of incoming flow to the fire compartment for rectilinear and curvilinear geometries.

Figure 51 depicts the incoming flow of air into a curvilinear fire compartment for two opening sizes (20 cm x 20 cm and 20 cm x 40 cm) under FD and NoFD conditions. The dashed green line and black line represents the empirical equation, providing a reference for comparison. A good level of agreement is observed between the empirical equation and the experimental results for all cases, regardless of the opening size or ventilation configuration. The result indicated that reducing the size of the opening decreases the air inflow rate to the compartment.

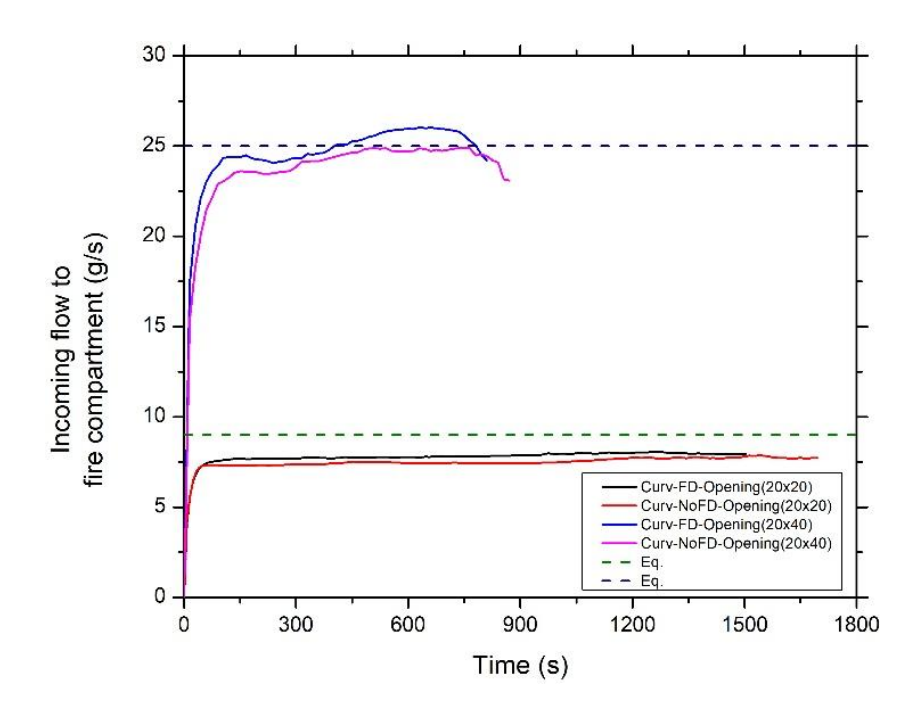


Figure 51: Temporal evolution of incoming flow to the fire compartment curvilinear geometries with different opening sizes.

Figure 52 illustrates the incoming flow rates into the fire compartment under FD (left) and NoFD (right) conditions for rectilinear and curvilinear geometries, comparing burner heights of 5 cm and 30 cm. A good agreement with the empirical equation is observed for most cases when the burner height is at 5 cm, regardless of geometry or ventilation configuration, indicating better airflow interaction at lower burner heights. However, at 30 cm, the flow rates are generally lower than the empirical predictions, except for the rectilinear geometry under FD conditions, where the flow aligns closely with or slightly exceeds the empirical value. The rectilinear geometry consistently exhibits higher flow rates compared to the curvilinear geometry, particularly at 30 cm. In contrast, the curvilinear geometry shows significant deviations from the empirical model to 30 cm, particularly under NoFD conditions, likely due to disrupted airflow patterns.

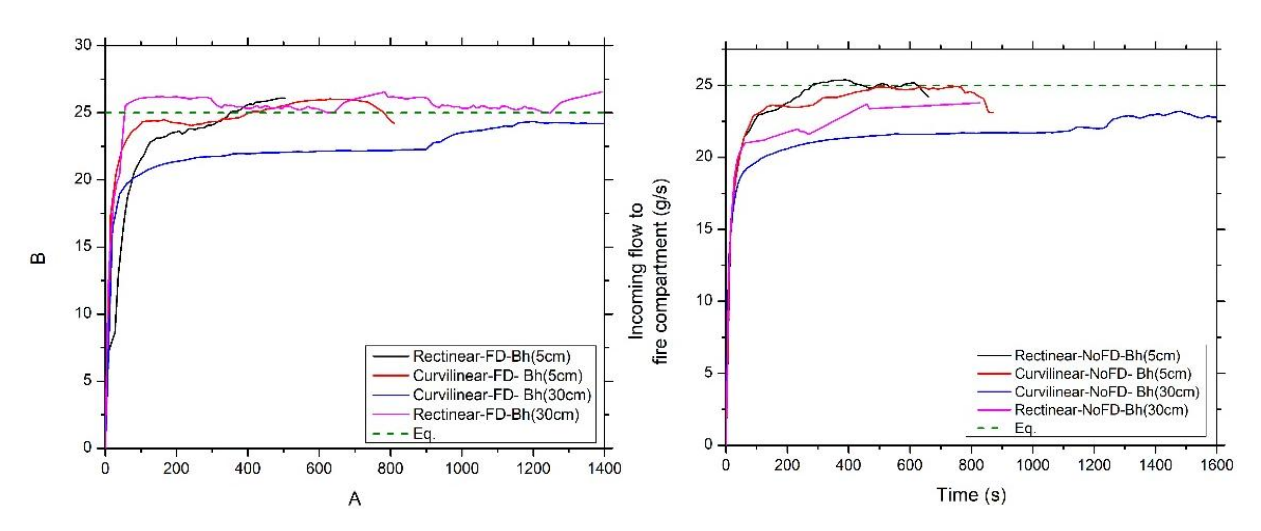


Figure 52: Temporal evolution of incoming flow to the fire compartment with different fuel burner height location for FD (left) and NoFD condition (right).

Temporal evolution of the calculated GER (Equation 4.6) for each test case is depicted in Figure 53. When the GER value exceeds unity (stoichiometric conditions), the fire is classified as "underventilated" (ventilation-controlled), whereas a GER value lower than 1.0 indicates a "well-ventilated" (fuel-controlled) fire. In all test cases, the GER value remains below 1.0 during the initial fire development stage, when the flames are primarily confined within the interior of the fire compartment. It was observed that when the GER value exceeds unity, external venting flames appeared from the compartment opening. This phenomenon was consistent with the GER trends depicted in the graph and occurred in the majority of test cases. However, for the curvilinear compartment with a 20 cm x 20 cm opening, well-ventilated fire conditions prevailed throughout the entire duration of the experiment, with no external flames observed. In most of the test cases investigated, the Intermittent Flame Ejection (IFE) stage occurred when the GER value ranged between 0.6 and 0.8, while Consistent External Flaming (CEF) conditions were observed when the GER value exceeded 1.

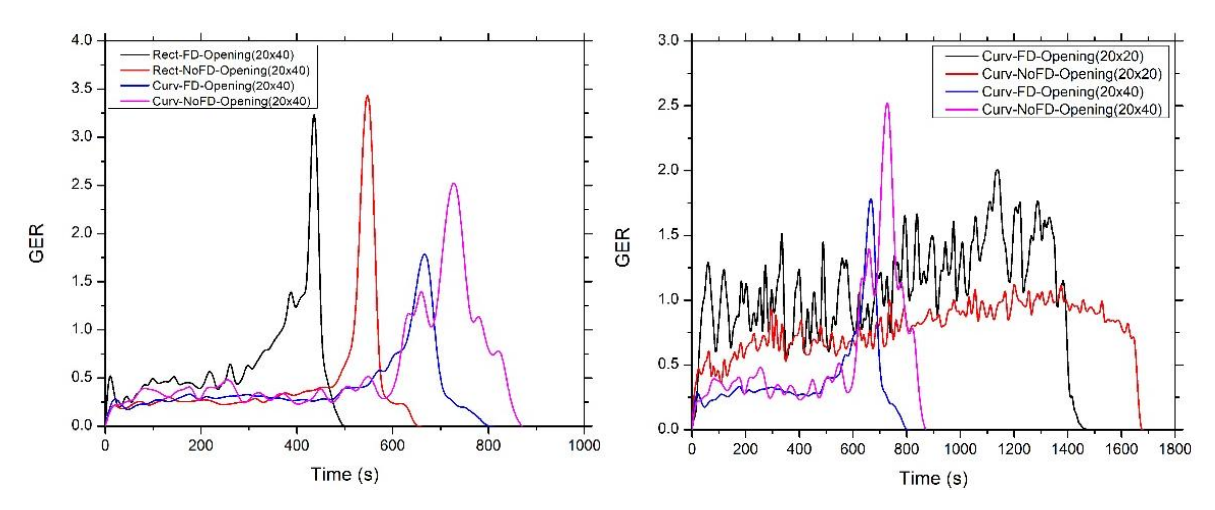


Figure 53: Calculated GER for curvilinear and rectilinear geometries (left) and for curvilinear geometries with different opening sizes (right).

4.4.3 Thermal characteristics

a. Interior Thermal Characteristics

Figure 38 depicts the placement of 4 thermocouples at a height of 0.6m from the compartment floor level with an equal spacing of 0.3m to measure the compartment temperature reading at the upper layer. Temporal evolution of upper layer gas temperature, an average of 4 thermocouples at the interior of the compartment is depicted in the figure below. Figure 54 illustrates the interior compartment temperature over time for rectilinear and curvilinear geometries under FD and NoFD ventilation configurations with opening sizes of 20x40 cm. The highest peak temperature of approximately 700°C is observed in both rectilinear and curvilinear geometry under FD conditions, while the rectilinear NoFD configuration reaches a lower peak of around 600°C and

for the curvilinear, lower peak temperature is at 550°C approximately. On the whole, consistent higher temperatures are produced in rectilinear geometries than curvilinear geometries, due to the material bounding surface and the attributing heat retention.

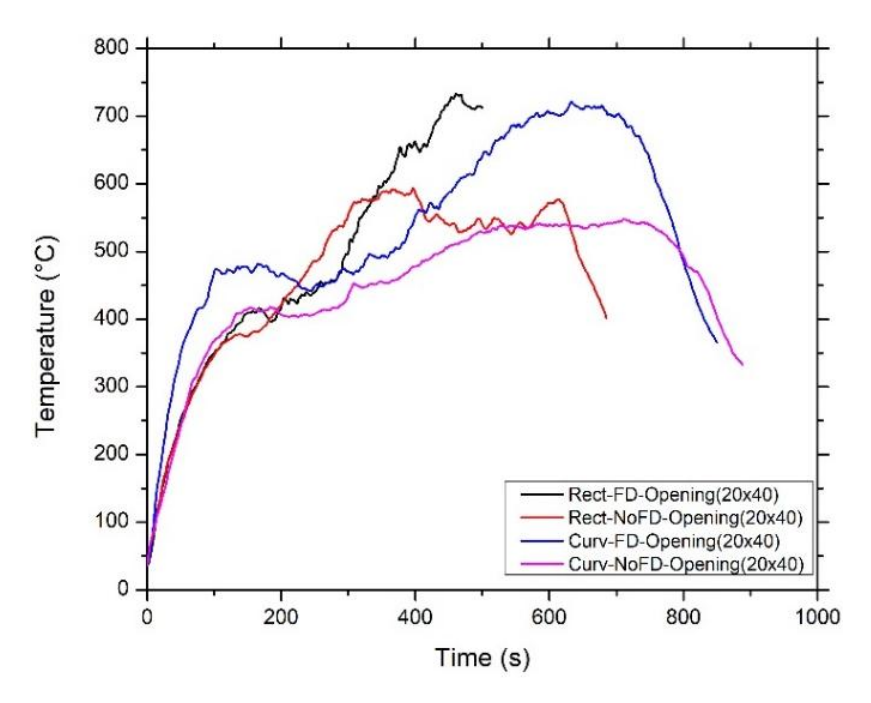


Figure 54: Temporal evolution of interior fire compartment temperature for rectilinear and curvilinear geometries.

Figure 55 depicts the temporal variation of interior compartment temperatures for a curvilinear geometry under FD and NoFD conditions, considering two different opening sizes: 20 cm x 20 cm and 20 cm x 40 cm. The temperature profiles indicate that larger openings (20 cm x 40 cm) consistently give rise to higher peak temperatures in comparison to smaller openings (20 cm x 20 cm), attributed to the increased oxygen supply. The highest peak temperature, approximately 700°C, is observed under FD conditions with a 20 cm x 40 cm opening, while for NoFD conditions with the same opening size, produces a peak temperature of around 500°C. In the case of the smaller 20 cm x 20 cm opening, the FD configuration produces relatively higher and steadier temperatures (around 300°C), due to restricted airflow that limits combustion intensity compared to the NoFD configuration for the same opening. Overall, larger openings and FD conditions in curvilinear compartments yield more pronounced temperature peaks, whereas smaller openings and NoFD conditions yield lower and steadier temperature profiles.

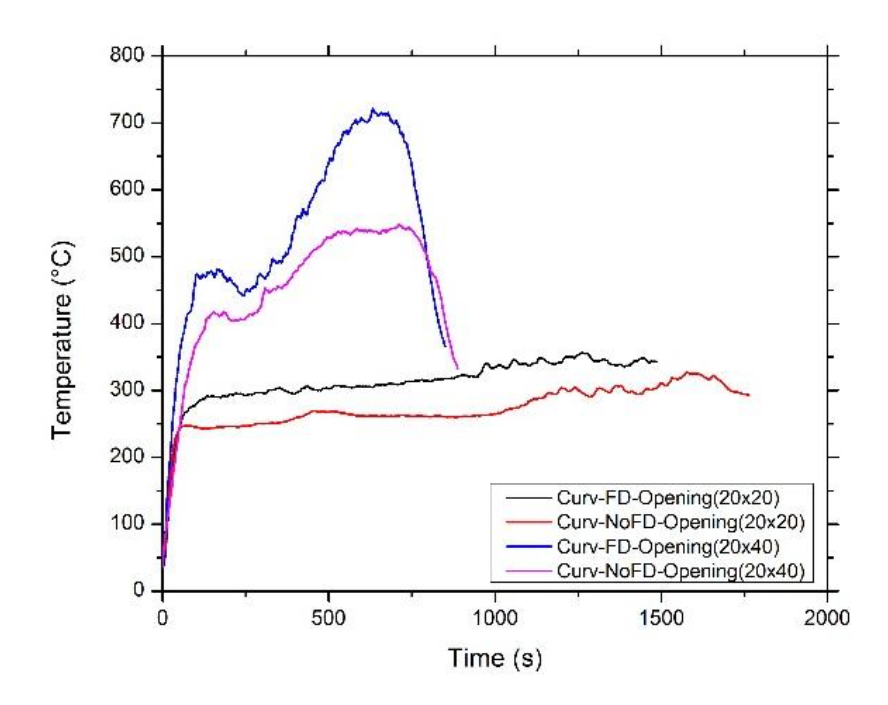


Figure 55: Temporal evolution of interior fire compartment temperature for curvilinear geometry with different opening sizes.

Figure 56 depicts the compartment temperature profiles for curvilinear and rectilinear geometries were analysed under FD conditions, with the fuel pan located at two heights: 5 cm and 30 cm above the compartment floor. As depicted in the graph, at a fuel pan height of 5 cm, both geometries exhibited a maximum peak temperature of approximately 700°C. In contrast, when the fuel pan was positioned at 30 cm, the maximum compartment temperature dropped to around 450°C for both geometries. This indicates a significant reduction in temperature, with a percentage difference of approximately 35.71% between the two fuel pan heights. The temperature trends also revealed that the profiles at the 30 cm height were remarkably similar for both geometries, with comparable peak temperatures, cooling rates, and burn durations, suggesting consistent combustion behaviour despite the geometric differences. However, at the 5 cm height, while the general temperature trends were aligned, the temperature rise, and decay patterns were slightly more distinct between the two geometries. These observations highlight the influence of fuel pan height on the compartment's thermal dynamics, as lower fuel pan positions result in greater heat accumulation and higher peak temperatures, likely due to closer proximity to the compartment floor and enhanced radiative feedback. The findings underline the complex interaction between fuel placement, geometry, and fire development, as captured in the graph.

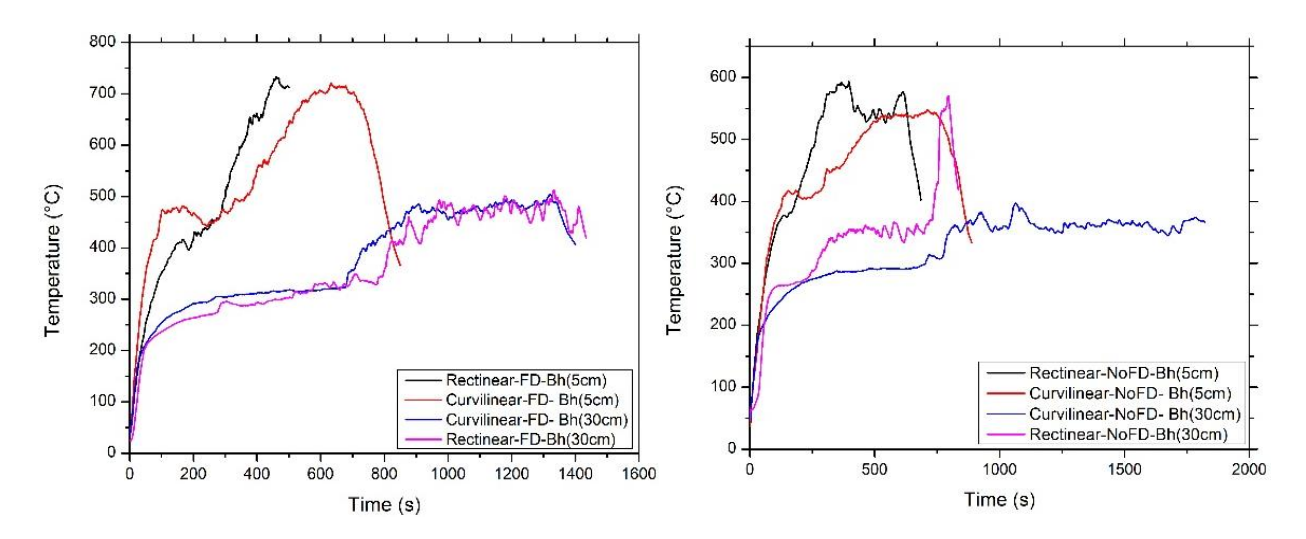


Figure 56: Temporal evolution of interior fire compartment temperature with varying fuel burner height location for FD (left) and NoFD condition (right).

The compartment temperature profiles under NoFD conditions were analysed for curvilinear and rectilinear geometries, with the fuel pan positioned at 5 cm and 30 cm above the compartment floor. Unlike FD conditions, the NoFD setup involved a single opening in the compartment, impacting the ventilation and fire behaviour. The graph reveals that at the 5 cm fuel pan height, the peak temperature for both geometries reached approximately 550°C, whereas at the 30 cm height, the peak temperature was significantly lower. For the curvilinear geometry at 30 cm, the maximum temperature was around 350°C. In the early stages of the fire, the temperature profile for the rectilinear geometry at 30 cm closely resembled that of the curvilinear geometry at the same height. However, during the fully developed stage, the rectilinear geometry at 30 cm exhibited a sudden increase in temperature, closely aligning with the trend observed at the 5 cm height. This sudden rise in temperature was accompanied by an increased burning rate, with flames emerging from the compartment opening. This behaviour indicates an increased GER, signifying that the compartment fire transitioned to a fuel-controlled regime and was well-ventilated.

b. Thermal characteristics at the compartment opening

Figure 38 illustrates the placement of thermocouples in the experimental setup. To measure the temperature at the centre of the opening, the thermocouple was positioned at a height of 0.2 m for a 0.4 m opening and at 0.1 m for a 0.2 m opening. Figure 57 depicts the temporal evolution of temperature at the centre of the compartment opening was analysed for both curvilinear and rectilinear geometries under FD and NoFD conditions. The graph shows that the NoFD condition generally resulted in higher temperatures compared to the FD condition for both geometries, with similar temperature profiles observed in each case. Under NoFD conditions, the rectilinear geometry exhibited a peak temperature of approximately 420°C, whereas the curvilinear geometry peaked at a significantly lower temperature of about 220°C. This highlights a considerable

difference in thermal behaviour between the two geometries in NoFD conditions. For FD conditions, the rectilinear geometry showed an overall higher temperature profile compared to the curvilinear geometry, reflecting differences in ventilation dynamics and flame interaction influenced by the geometric configuration.

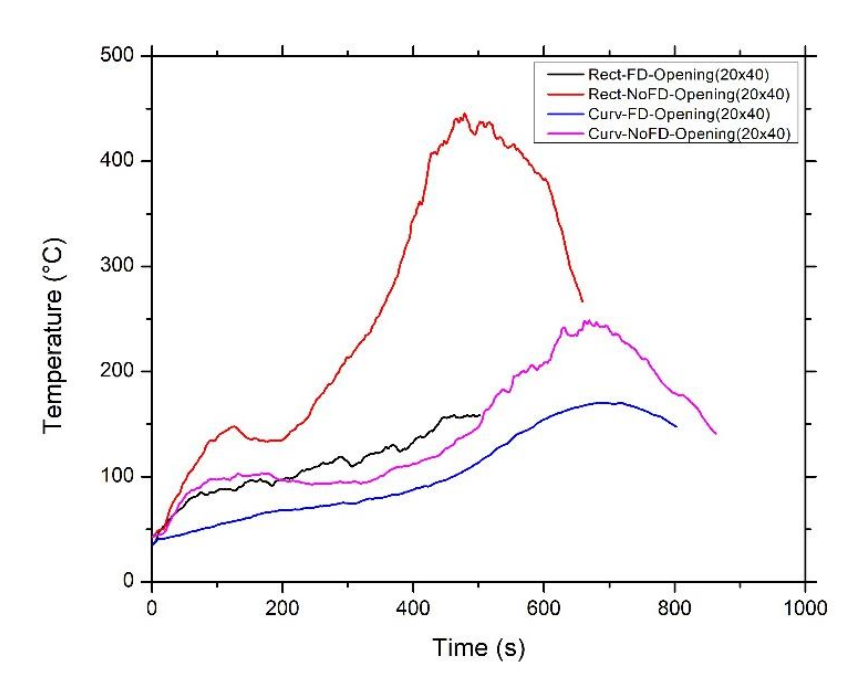


Figure 57: Temporal evolution of opening temperature for rectilinear and curvilinear geometries.

Figure 58 illustrates the temperature at the centre of the opening for curvilinear geometries under FD and NoFD conditions, with two opening sizes: 25 cm x 40 cm and 25 cm x 40 cm. The results highlight distinct temperature trends based on the opening size and ventilation conditions. For the larger opening (25 cm x 40 cm), higher temperatures were observed compared to the smaller opening (25 cm x 20 cm) under both FD and NoFD conditions. Specifically, the NoFD condition for the 25 cm x 40 cm opening exhibited the highest peak temperature, comparing the FD condition for the same opening size due to the restricted ventilation in the NoFD condition led to greater hot gases accumulating and exiting through the opening. For the smaller opening (25 cm x 20 cm), the temperature profiles under FD and NoFD conditions were nearly identical. In both opening sizes, the NoFD condition generally resulted in higher temperatures compared to the FD condition.

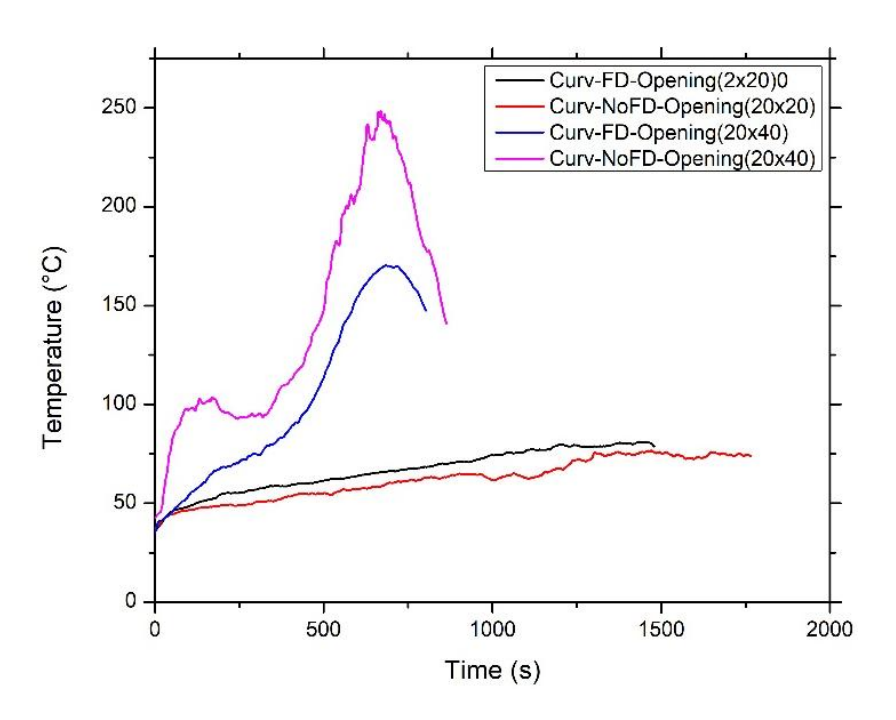


Figure 58: Temporal evolution of opening temperature for curvilinear geometry with different opening sizes.

Figure 59 (left) depicts the temperature at the centre of the compartment opening for rectilinear and curvilinear geometries under FD conditions, with the fuel burner positioned at 5 cm and 30 cm above the compartment floor. For the 5 cm above ground fuel burner height, the temperature at the opening is higher for both geometries compared it with 30cm, with the rectilinear geometry exhibiting slightly higher temperatures compared to the curvilinear geometry. The temperature profiles for both geometries show a similar trend. At the 30 cm height, the temperature profiles for both geometries also follow a similar pattern. However, the temperatures at the centre of the opening remain only slightly above ambient levels, suggesting that majority of the hot gases are flowing out through top part of the opening. This could be attributed to the reduced radiative feedback and altered flame dynamics caused by the higher burner position.

Figure 59 (right) depicts the temperature evolution at the centre of the compartment opening for rectilinear and curvilinear geometries under NoFD conditions, with the fuel burner positioned at 5 cm and 30 cm above the compartment floor. At the 5 cm burner location, the temperatures at the opening are higher for both geometries during the fully developed stage. The rectilinear geometry exhibits a peak temperature exceeding 400°C, while the curvilinear geometry reaches a maximum of approximately 220°C. At the 30 cm height, the temperature profiles for both geometries are initially similar and remain only slightly above ambient levels, indicating limited hot gases flowing out and majority going out through the top part of the opening during the early stages. However, as the fire reaches the fully developed stage, the rectilinear geometry exhibits a sharp increase in temperature at the opening, peaking at approximately 300°C. This spike corresponds

to an increased burning rate and the appearance of flames emerging from the opening, signifying a transition to a more intense combustion phase. In contrast, the curvilinear geometry maintains a consistent low-temperature profile throughout, indicating less intense burning.

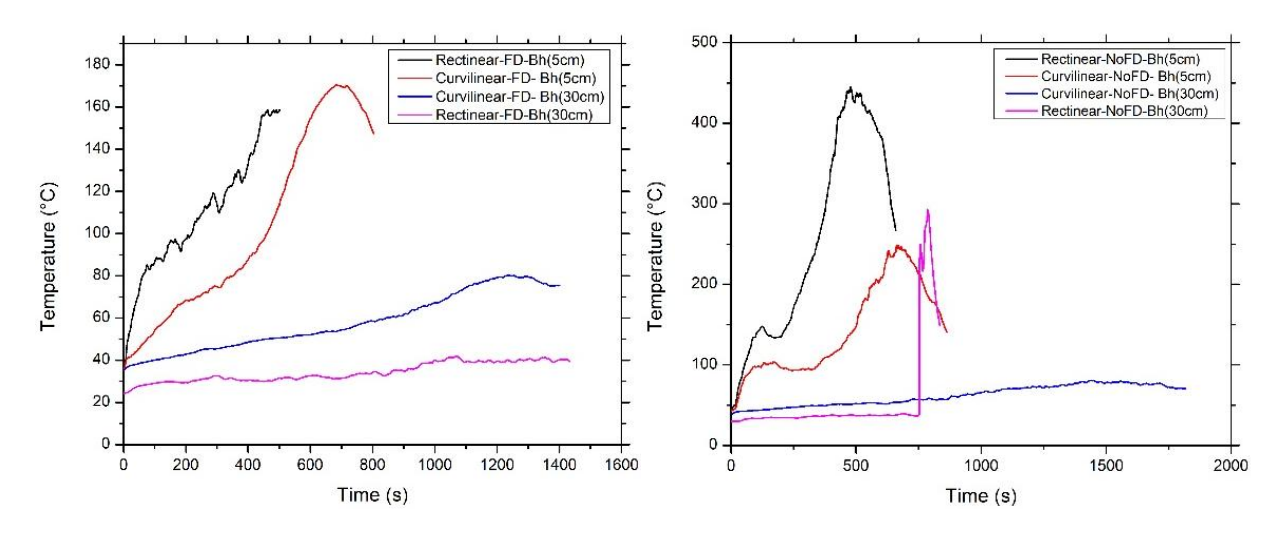


Figure 59: Temporal evolution of opening temperature with varying fuel burner height location for FD condition(left) and NoFD condition (right).

c. Thermal characteristics of the EVF

The time averaged temperature contour plots help in understanding the spatial distribution of the thermal field generated by EVF outside the fire compartment. The recorded data from the loggers were analysed, and the selected data represents the time-averaged values for a 50-second period, this period is chosen on the fact that when the fire was at its peak and flames started appearing outside. This approach was applied consistently across all experiments. Figure 38 depicts the thermocouple tree measurements that were conducted at two horizontal distances from the opening: 0.15 m and 0.3 m. Each thermocouple tree consisted of five thermocouples, with the first located at 0.2 m height (mid-height of the opening) and the remaining sensors spaced 0.2 m apart, covering heights of 0.2 m, 0.4 m, 0.6 m, 0.8 m, and 1.0 m. These measurements provide insight into EVF temperature characteristics with respect to height, and how they are influenced by compartment geometry and ventilation conditions. Figure 60 depicts the time-averaged temperature at the centre line plane perpendicular to the façade for the curvilinear and rectilinear geometries in FD and NoFD conditions.

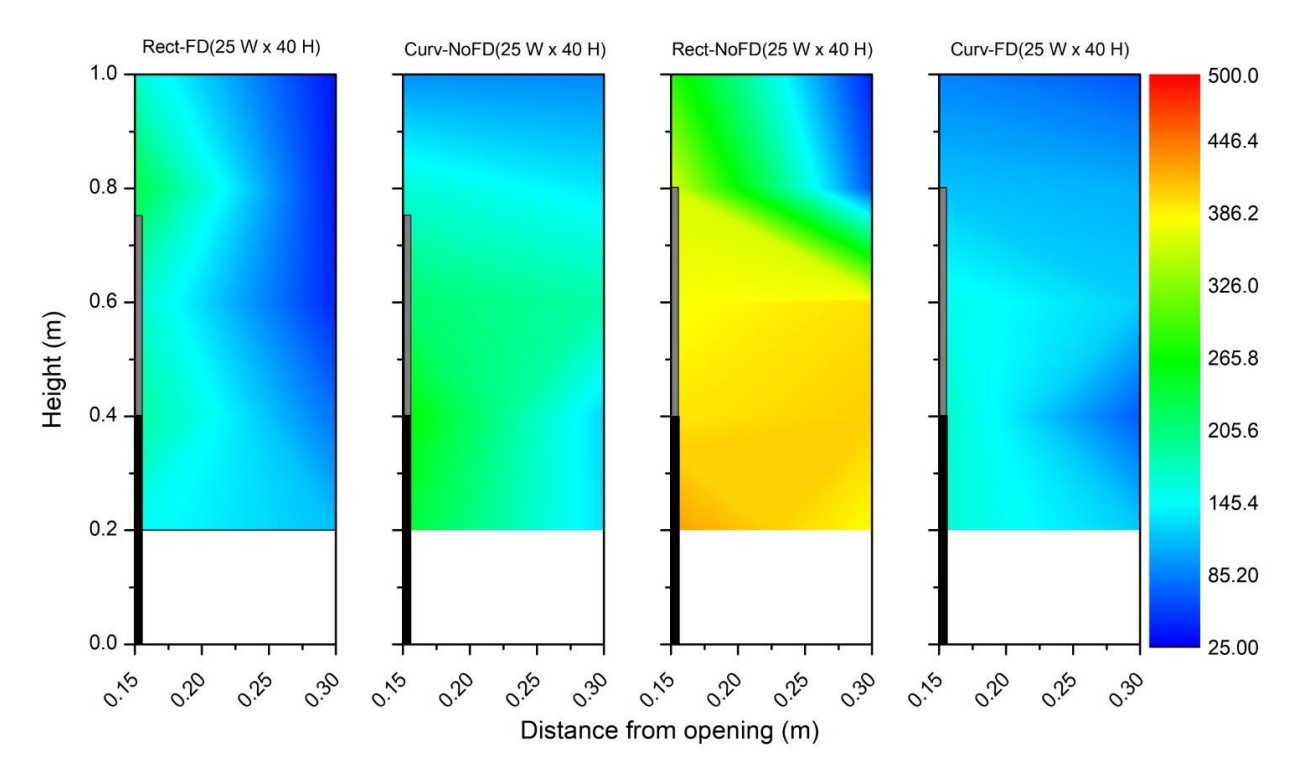


Figure 60: Time averaged EVF temperatures for curvilinear and rectilinear geometries in FD and NoFD conditions.

Peak temperatures are seen near the opening, in the NoFD conditions of rectilinear geometries, a large EVF envelope forms, while in the FD conditions of curvilinear geometries, a smaller EVF envelope develops. In general, curvilinear geometries form a lesser EVF envelope in comparison to the rectilinear geometries for both FD and NoFD conditions. The maximum gas temperature observed in the rectilinear NoFD conditions was in the range of 400°C to 450°C, and this can be observed at a horizontal distance of 0.3 m from the façade and EVF temperature gradually decreases with increasing height. This decrease in temperature is consistent in all four test cases, demonstrating a consistent vertical temperature gradient.

Figure 61 depicts comparison of gas temperature distributions in curvilinear geometries under FD and NoFD conditions for two different opening sizes: 25 cm x 20 cm and 25 cm x 40 cm. For the 25 cm x 20 cm opening, both FD and NoFD cases show relatively low temperatures, with peak values not exceeding 90°C. Slightly higher temperatures are observed in the NoFD condition, particularly at lower heights, suggesting minor differences in external heat flow due to limited venting through the smaller opening. In contrast, the 25 cm x 40 cm opening results show a noticeable increase in temperatures, especially under the NoFD condition. Peak values reach up to 240°C, indicating the development of a larger EVF envelope. The FD condition in the 25 cm x 40 cm case shows a comparatively smaller EVF envelope, with reduced peak temperatures and a more rapid temperature drop with height.

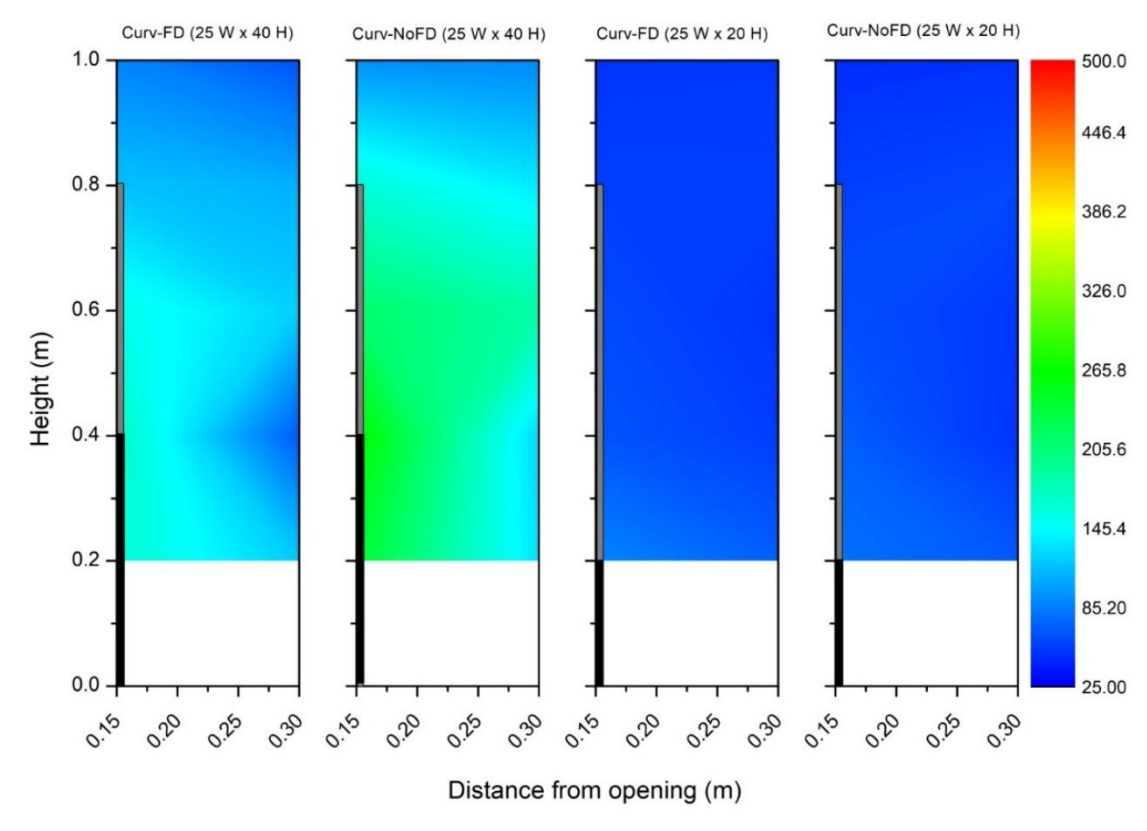


Figure 61: Time averaged EVF temperatures for curvilinear geometry with different opening sizes.

4.4.4 Heat flux at the façade surface

Figure 62 illustrates the heat flux measured at 0.1 m above the compartment opening for both curvilinear and rectilinear geometries. The temporal evolution of heat flux shows a similar profile for both geometries, with a notable divergence during the fully developed fire stage. During the fully developed fire stage, the rectilinear geometry exhibited a significantly higher peak heat flux of approximately 20 kW/m², while the curvilinear geometry showed a much lower peak, remaining below 5 kW/m². This substantial difference in heat flux is primarily attributed to the enclosure bounding surface materials of the two geometries. The rectilinear geometry, constructed with Monolux, a fire-resistant material, retains and radiates more heat to the façade. Conversely, the curvilinear geometry, made of steel, facilitates greater heat conduction through its surface, reducing the thermal impact on the façade and leading to a lower heat flux.

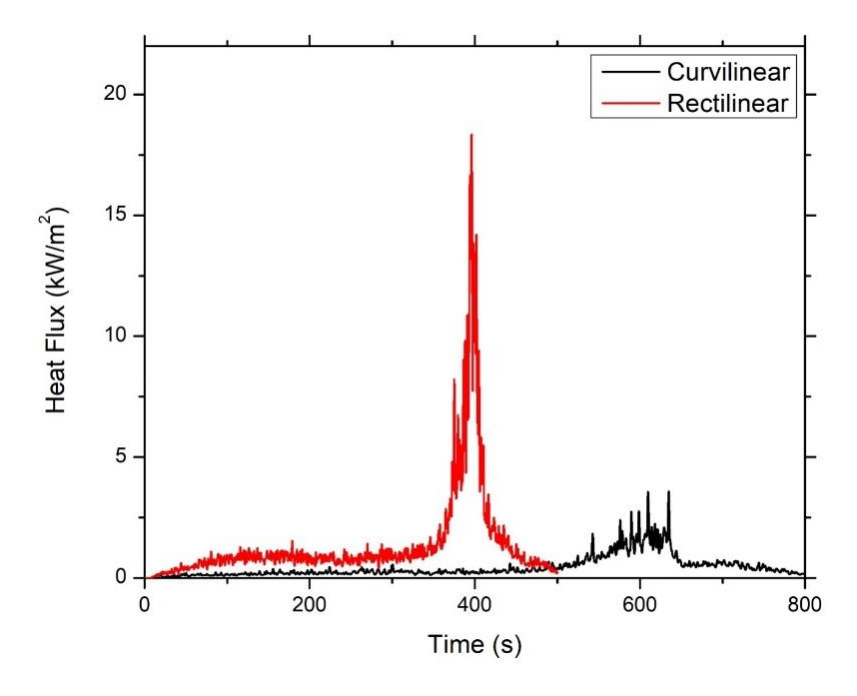


Figure 62: Temporal evolution of heat flux on the facade for rectilinear and curvilinear geometries.

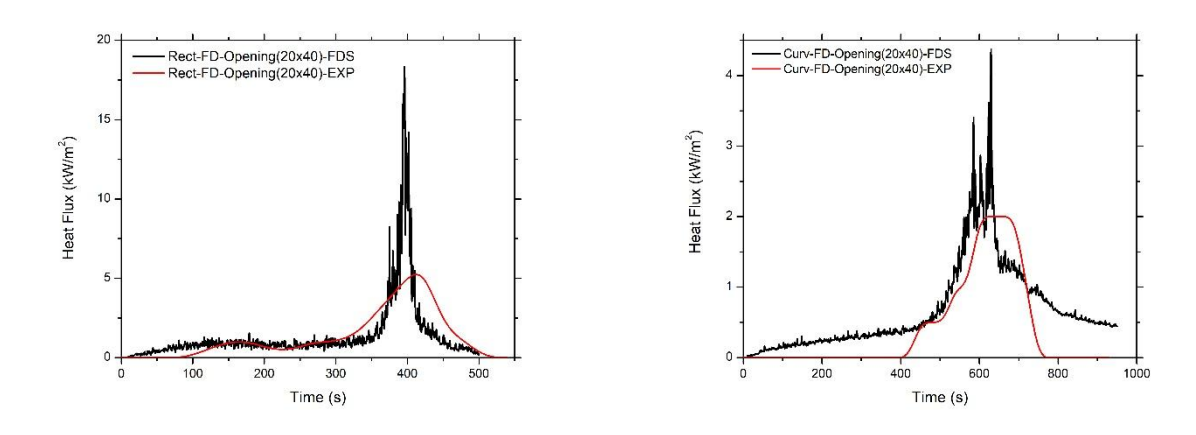


Figure 63: Temporal variation of façade heat flux: comparison between experiment and FDS for rectilinear (left) and curvilinear (right) geometries

Figure 63 (left) illustrates the temporal evolution of heat flux on the façade for the rectilinear compartment under FD conditions, comparing experimental and FDS predictions. The experimental data exhibit a gradual rise in façade heat flux, reaching a peak of approximately 4.5 kW/m² at around 400 s, followed by a smooth decay as the fire intensity subsided. In contrast, the FDS-predicted heat flux shows a much sharper increase, attaining a maximum value of nearly 17 kW/m² at approximately 400 s, almost twice the experimental peak. Despite this overprediction, the general trend and timing of peak occurrence are consistent, indicating that the model captured the main transient behaviour of heat transfer at the façade. The differences can

be attributed to the radiation model in FDS, as well as potential sensor response lag in the experimental setup. The façade heat flux for the curvilinear compartment under FD condition in Figure 63 (right) shows a temporal profile with the experiment peaking at approximately 2 kW/m² around 600 s, while FDS predicts a higher and sharper peak of about 4 kW/m² Although the timing of the peak is consistent, FDS overestimates the magnitude and exhibits stronger short-term fluctuations. The overall heat flux levels are notably lower than in the rectilinear case, indicating reduced flame attachment and radiative exposure due to the curved façade geometry and also due to the steel construction.

4.5 Comparison of Indoor versus Outdoor experiments

To understand the influence of geometry and environmental factors on fire dynamics, a series of experiments were conducted under FD conditions. The experiments compared the thermal and combustion behaviors of rectilinear and curvilinear geometries in both indoors (in lab) and outdoor settings, refer the figure 37. The outdoor experiments were carried out on the same day under similar environmental conditions to minimize variability, but wind played a significant role in influencing the results, particularly in the temperature profile.

Figure 64 (left) depicts the fuel mass loss; the mass loss rate was significantly higher in the outdoor experiments compared to the indoor setup for both geometries. Wind-induced ventilation outdoors enhanced the combustion process, resulting in faster fuel consumption. The rectilinear geometry exhibited a steeper mass loss rate compared to the curvilinear geometry in both conditions, attributed to its material's ability to retain heat and sustain combustion more effectively. The curvilinear geometry, made of steel, conducted heat away more efficiently, slowing down the burning rate. Figure 64 (right) depicts the incoming flow rates to the fire compartment, which showed good agreement with empirical equations under both indoor and outdoor conditions.

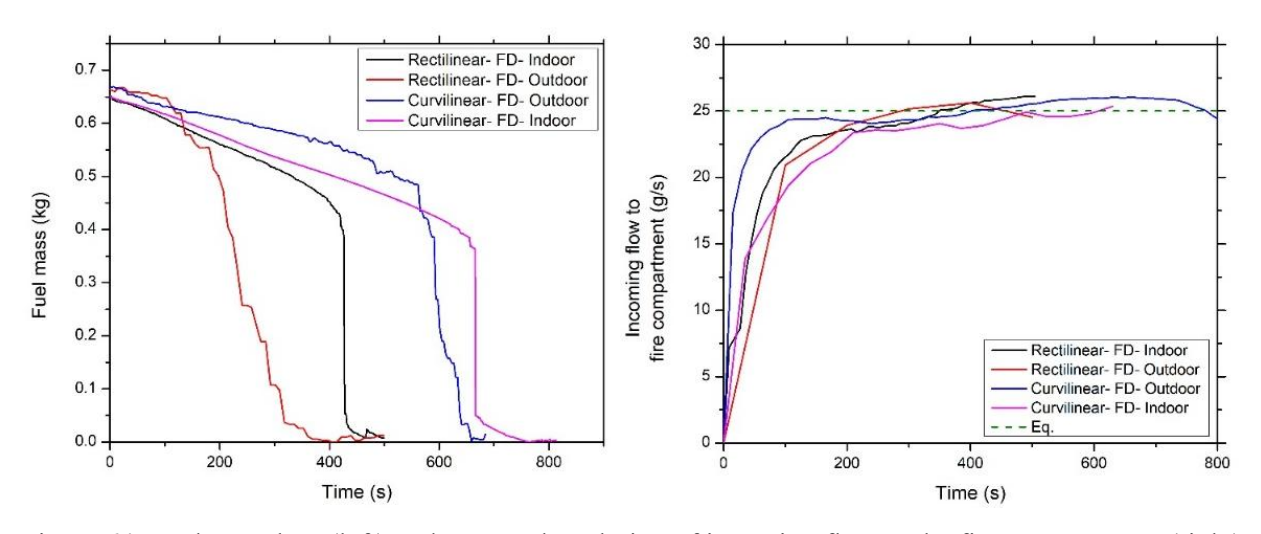


Figure 64: Fuel mass loss (left) and temporal evolution of incoming flow to the fire compartment (right) for rectilinear and curvilinear geometry.

Figure 65 (left) depicts the interior compartment temperature, the interior compartment temperatures exhibited similar trends and patterns for both rectilinear and curvilinear geometries in both indoor and outdoor setups. However, outdoor experiments showed slightly higher peak temperatures due to increased airflow and enhanced combustion intensity. Figure 65 (right) depicts the opening temperature, and at the opening, outdoor experiments showed a significant increase in temperature, for both the geometries, which reached its peak during the fully developed stage. This increase was mainly due to wind-driven ventilation and flame extension through the opening.

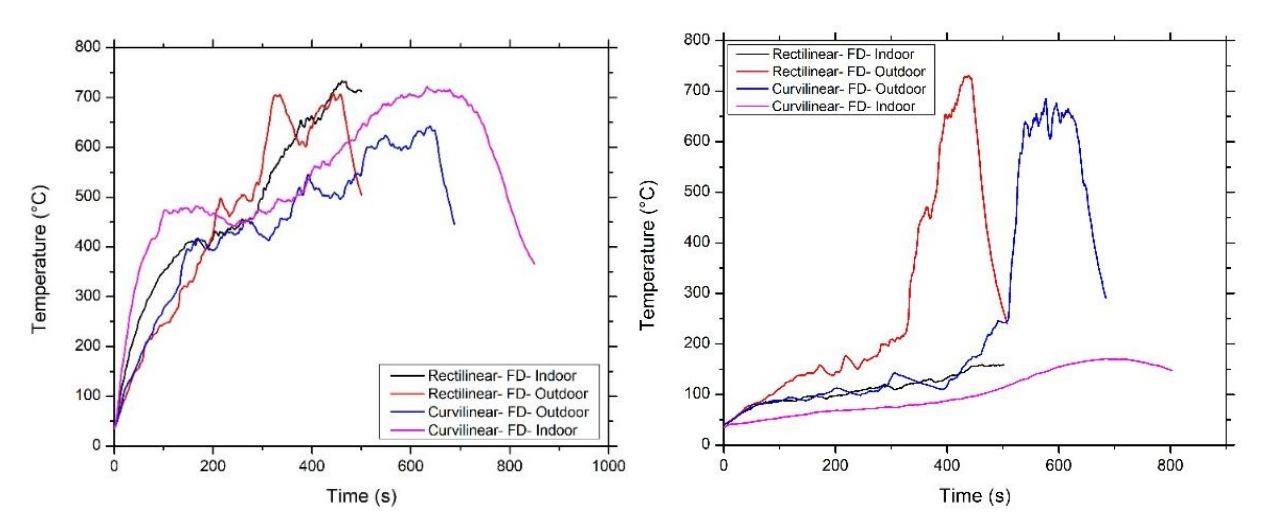


Figure 65: Temporal evolution of interior compartment temperature (left) and opening temperature (right) for rectilinear and curvilinear geometries.

4.6 Conclusions from experimental investigations

This study analysed the effects of building geometry on the smoke flow pattern and development of EVF through experimental and numerical analyses in rectilinear and curvilinear compartments. The key factors that influence fire dynamics, including fuel mass loss, air supply rate, GER, thermal characteristics, and external heat flux, were analysed under varying ventilation conditions of FD and NoFD. The findings provided significant insights on to smoke flow pattern and fire dynamics in both interior and exterior of the compartment in reference to the varying compartment geometry, ventilation, and bounding materials.

The results demonstrated that rectilinear compartments exhibited a comparatively rapid initial fuel mass loss rate and higher peak internal temperatures to curvilinear compartments. This is attributed to better airflow and heat retention due to the insulating properties of Monolux used in rectilinear compartment. Conversely, the curvilinear compartment exhibited slower fuel consumption due to enhanced heat dissipation aided by the material properties of steel, which the compartment is constructed of. Variations in opening sizes and ventilation conditions also have significantly influenced combustion dynamics. The larger openings in the compartments aided greater oxygen inflow, accelerated the fuel depletion and resulted in an increase in interior compartment temperatures. The GER analysis pointed out that external venting flames predominantly emerged when GER values exceeded unity, indicating under-ventilated fire conditions.

Although these findings provide significant insights, one limitation of this study is the use of different bounding materials (Monolux for rectilinear geometry and steel for curvilinear geometry), which may introduce material-dependent thermal effects that influence heat transfer and combustion rates. Future research should explore experiments with identical bounding materials to isolate the impact of geometry alone. Additionally, investigating other fire scenarios, such as varying fuel loads and multi-ventilation configurations, would further enhance our understanding of EVF behavior in complex compartment geometries.

4.7 Numerical investigation: Results and Discussion

The result and discussion section presents a comparative analysis of experimental and numerical results to investigate the effects of geometry, opening size, and ventilation conditions on compartment fire behavior and EVF. The analysis is structured mainly under the below subsections.

- 1. Effect of Geometry
- 2. Effect of Opening Size
- 3. Effect of Ventilation (FD and NoFD)

For each case, the comparison focuses on three critical parameters: (i) the temporal evolution of compartment interior temperature, (ii) the temporal evolution of opening centreline temperature, and (iii) the time-averaged externally venting flame (EVF) temperature. One of the objectives of these comparisons is to assess the accuracy of FDS predictions in replicating experimental measurements under varying physical configurations and ventilation conditions. The analysis highlights the influence of each parameter on fire development and EVF behaviour, as well as the level of agreement or deviation between numerical and experimental data. The influence of radiative heat flux on thermocouple readings can lead to higher measured temperatures in experiments. Although the FDS thermocouple model accounts for this effect to some extent, since the thermocouple (TC) model, temperature lags the true gas temperature depending mainly on bead size. During the experiments, sheathed thermocouples were used to mitigate direct radiative effects. The presence of multiple metal and air gaps in the thermocouple device construction may limit the model's ability to fully capture the complex radiative—convective balance.

4.7.1 Effect of geometry on fire development and EVF.

To investigate the influence of compartment geometry on fire development and externally venting flames, a comparative analysis was performed between rectilinear and curvilinear compartments using both experimental data and numerical simulations. Figure 66 illustrates the temporal evolution of interior gas temperature for curvilinear and rectilinear compartments, comparing FDS predictions with experimentally measured values.

a. Compartment gas temperature

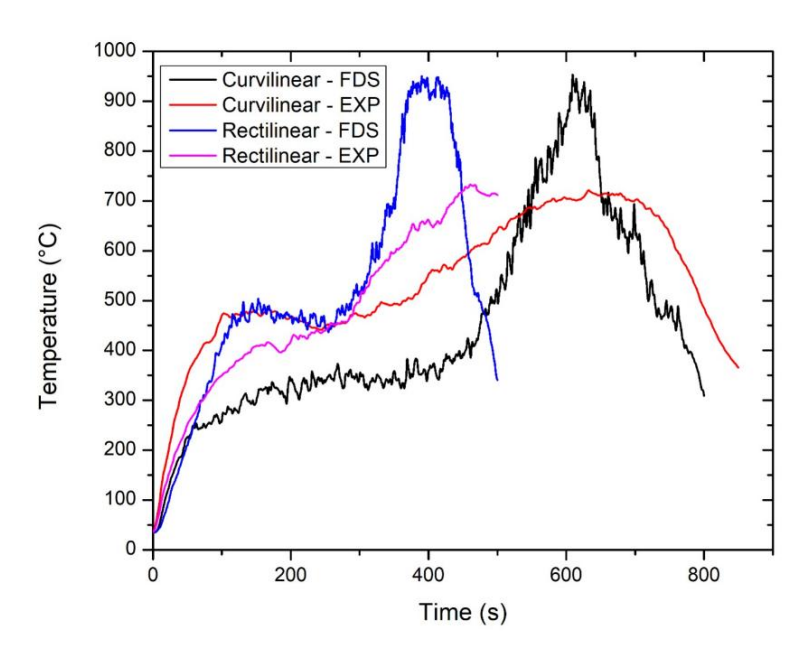


Figure 66: Interior temperature profiles for curvilinear and rectilinear compartments: experimental vs. FDS results.

In the early stages of fire development, during the growth stage (0–300 s), both geometries show a relatively consistent rise in temperature. However, definite differences in the temperature between geometries are evident. The experimental data for the rectilinear compartment exhibits a more rapid temperature rise compared to the curvilinear case (red line), reaching a peak of approximately 750°C. This is mainly attributed to the fact that rectilinear compartment is constructed of Monolux, and which has a lower thermal inertia due to the fire resistant insulating properties which resulted in heat accumulation within the rectilinear configuration, which promotes faster combustion and gas temperature rise. The curvilinear compartment, on the other hand, shows a comparatively moderate temperature increase during the same period, peaking approximately the same as rectilinear in the experimental test.

FDS predicted temperatures (black and blue lines for curvilinear and rectilinear, respectively) follow a similar trend in the growth phase but tend to under predict the temperature during this phase, however, in fully developed phase, where EVF form and during decay phase FDS overpredict the temperatures. Numerical results reach a peak of nearly 950°C for both curvilinear and rectilinear geometries, significantly higher than the experimental measurement. A key observation is that, in both geometries, the agreement between experimental and simulated results is stronger during the fire growth phase, while discrepancies become more pronounced during the fully developed and decay phases.

The FDS model over-predicts temperatures is mainly due to the FDS modelling uncertainties such as use of a prescribed MLR in FDS as this prevents pyrolysis and converts HRR to a reactant loss

via an assumed heat of combustion, which can maintain burning independent of oxygen availability. Further, FDS using the 1-D solid heat-transfer model in FDS, whereas in experiment experiences higher heat losses through the compartment wall and boundaries. Additionally, radiation modelling assumptions, including a fixed radiative fraction (~0.30–0.35 by default) and soot/emissivity settings, which may differ from the experiment. These points, together with the associated uncertainties documented in the FDS Validation Guide (compiled from prior research studies), are discussed explicitly in Section 4.2.5 (McGrattan *et al.*, 2023).

b. Opening temperature

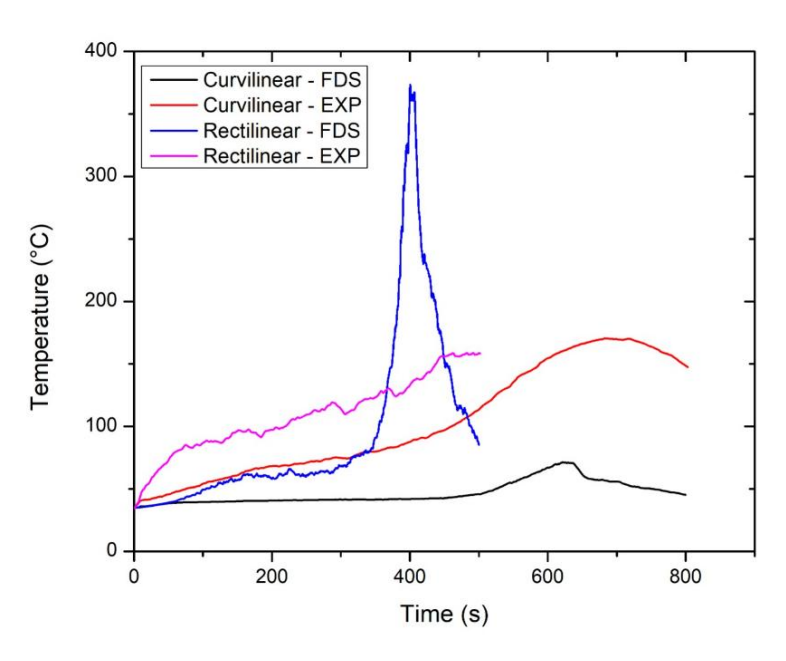


Figure 67: Temporal temperature profile at the centre of the opening for curvilinear and rectilinear compartments: experimental vs. FDS results.

The temporal temperature profiles at the centre of the compartment opening provides a distinct difference between the curvilinear and rectilinear geometries. In the rectilinear case, the FDS simulation predicts a sharp peak temperature of approximately 370°C, indicating a rapid outflow of hot gases and the onset of EVF. In contrast, the curvilinear geometry under FDS shows a much lower and broader peak of about 120°C, suggesting weaker EVF development and a more moderated flow of hot gases through the opening. The experimental data supports these observations, with the rectilinear configuration reaching a peak of around 180°C and the curvilinear case peaking at approximately 150°C, both occurring at a more gradual rate compared to the FDS results. Notably, FDS significantly overpredicts the opening temperature in the rectilinear case, exceeding the experimental measurement by more than 100°C at peak, while underpredicting in the curvilinear case.

c. EVF average temperature

To investigate the influence of geometry on EVF behaviour, time-averaged temperature contours were generated from both numerical simulations and experimental measurements over a 50-second interval during the fully developed fire stage, this time interval chosen when continuous outflow of hot gases and flames was observed. Figures 68 and 69 present the thermal field beyond the compartment opening for curvilinear and rectilinear geometries under FD conditions. The vertical axis represents height above the floor (with 0.4 m corresponding to the top of the opening), and the horizontal axis spans from 0.15 m to 0.30 m, representing the horizontal distance from the façade.

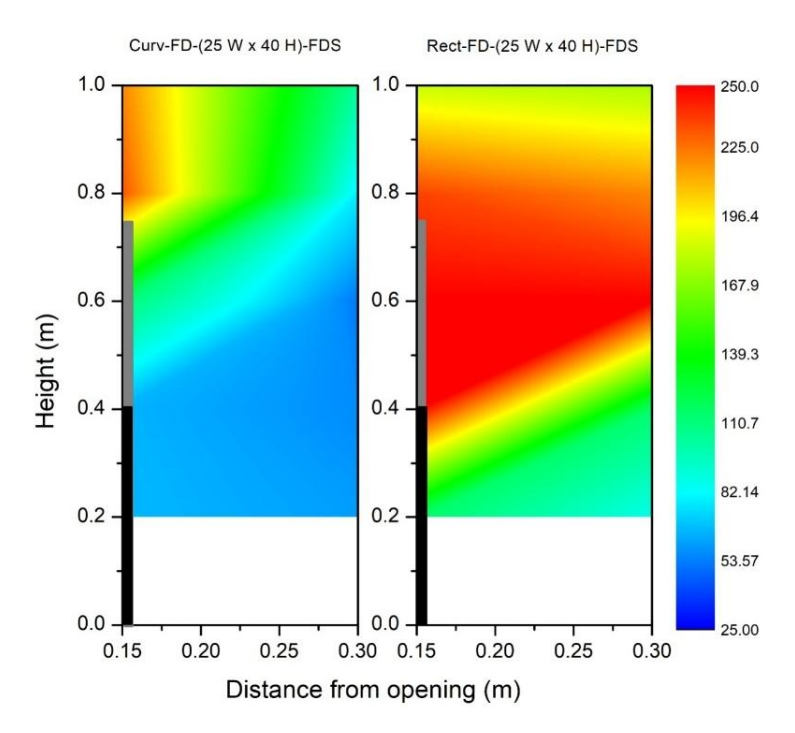


Figure 68: Time averaged EVF temperatures for curvilinear and rectilinear geometry from FDS.

Figure 68 depicts the FDS predicted results and reveal a more intense and vertically extended EVF temperature field in the rectilinear configuration, where temperatures exceed 250°C, particularly above the opening and between 0.15 m –0.25 m from the wall. This indicates a concentrated, high-momentum thermal plume originating from the rectangular opening. In comparison, the curvilinear compartment shows a broader, less intense temperature distribution, with values mostly below 170°C and a dominant range between 100°C –150°C, suggesting a more diffused outflow.

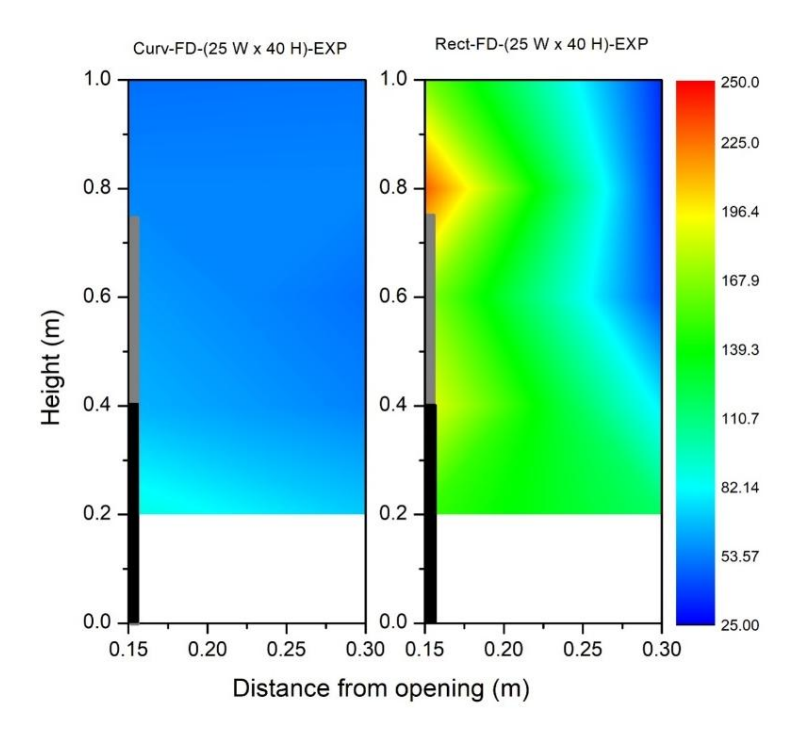


Figure 69: Time averaged EVF temperatures for curvilinear and rectilinear geometry from experiment.

The experimentally measured temperature contours in figure 69 follow a similar trend but with generally lower temperature magnitudes. The rectilinear experimental case shows elevated plume temperatures, reaching up to 200°C, located just above the opening height and within a narrow horizontal spread. Meanwhile, the curvilinear experimental data exhibit a mostly uniform and low temperature profile, rarely exceeding 100°C.

This comparison also reveals that FDS tends to overpredict EVF temperatures, particularly for the rectilinear compartment; however, it accurately captures the relative trend in venting severity between the two geometries. The rectilinear geometry, due to the bounding material surface, tends to retain heat within the compartment, leading to elevated gas temperature and a more thermally buoyant outflow. Additionally, the flat ceiling and sharp internal boundaries in the rectilinear setup promote the development of a high velocity, axially directed plume, resulting in a more intense and concentrated EVF. In contrast, the curvilinear compartment, constructed from steel, exhibits higher conductive heat losses through the enclosure surfaces, contributing to lower gas temperatures. Furthermore, the curved ceiling geometry facilitates the dispersion of thermal flow, redirecting and spreading the plume energy over a wider area. As a result, the EVF in the curvilinear case appears significantly less focused and thermally intense, this is consistent in both the experimental and simulated outcomes.

d. Temperature field

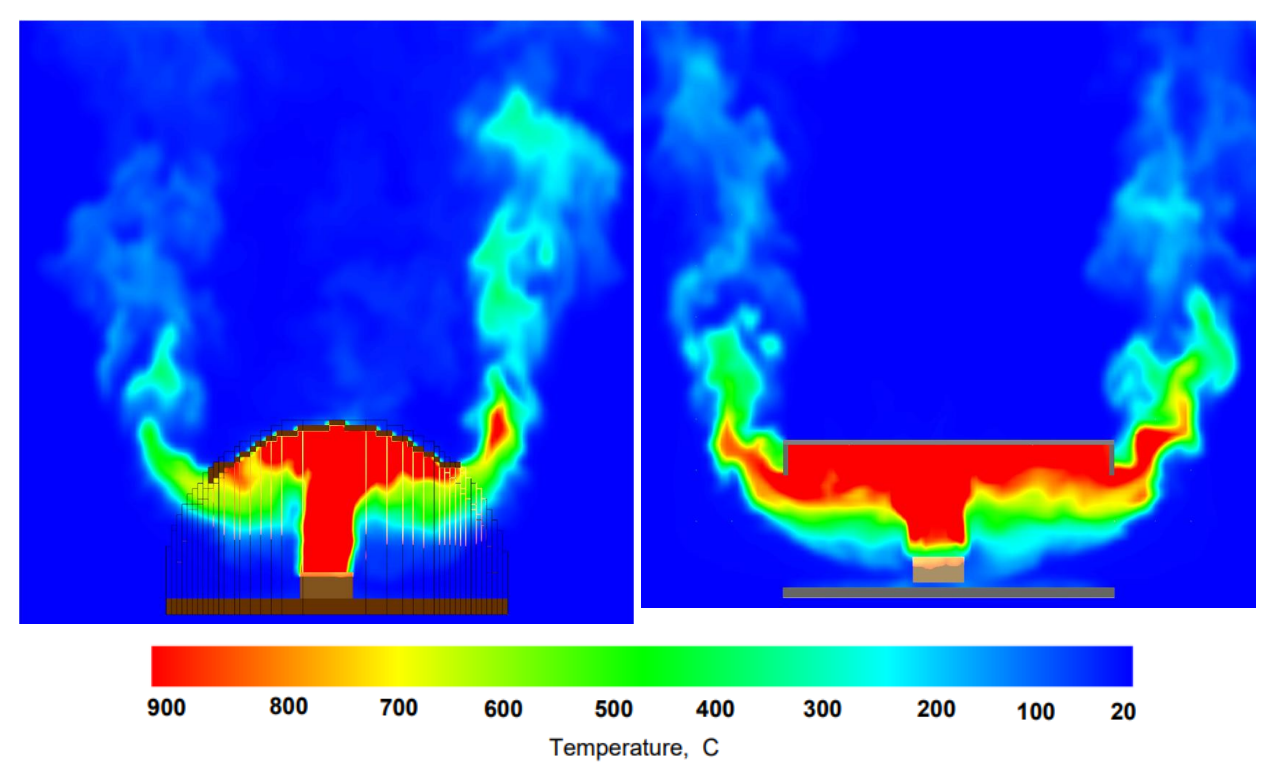


Figure 70: Spatial distribution of gaseous temperature 600 s and 400 s after fire initiation with curvilinear (left)and rectilinear (right) compartment under FD conditions.

Figures 70 present the temperature contours from FDS simulations for the curvilinear and rectilinear compartments under FD conditions, captured at 600 seconds and 400 seconds, respectively. These time frames correspond to the fully developed fire stage, during which EVF begin to emerge prominently from the compartment openings.

In the rectilinear geometry in figure 70 (right), a distinct horizontal hot gas layer is clearly visible, with temperatures in the upper region exceeding 800°C and reaching up to 900°C near the ceiling. The stratification is sharp, indicating minimal vertical mixing and well-defined layering of the thermal field. This thermal retention is attributed to the use of Monolux panels, which has high thermal inertia that effectively retain thermal energy within the compartment, limiting heat dissipation through the walls. As a result, the thermal plume remains confined and buoyantly exits through the opening in a strong, concentrated jet, characteristic of a vigorous EVF. Conversely, in the curvilinear geometry in figure 70 (left), the thermal distribution is more diffuse, with the hot gases following the curvature of the ceiling and exhibiting a smoother vertical gradient. Peak temperatures are lower, remaining below 700°C, and the hot layer appears less sharply defined compared to the rectilinear case. This behavior is primarily influenced by two factors: (1) the high thermal conductivity of steel, which promotes rapid heat dissipation through the compartment boundaries, and (2) the curved ceiling profile, which guides the flow along its surface and

discourages strong thermal stratification. The result is a more distributed outflow pattern with reduced buoyant energy at the vent opening.

This comparison highlights that compartment geometry and boundary material significantly affect the internal thermal structure and venting behaviour during the fully developed fire stage. While the rectilinear compartment promotes strong thermal accumulation and layering, leading to a sharp and focused EVF, the curvilinear configuration distributes heat more broadly, resulting in a more gradual transition from internal combustion to external venting.

e. EVF Gas mixture velocity

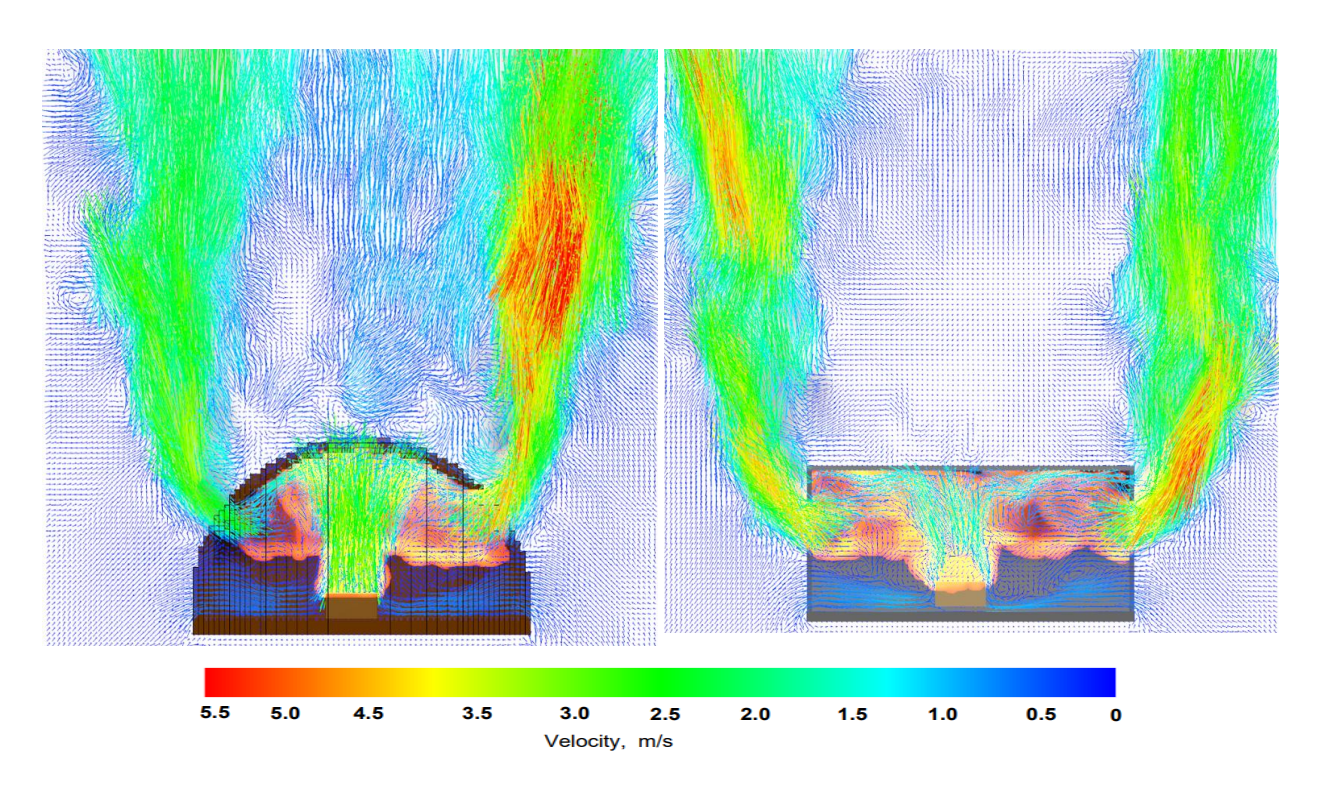


Figure 71: Gas mixture velocity and EVF 600 s and 400 s after fire initiation with curvilinear (left)and rectilinear (right) compartment under FD conditions.

Figures 71 depicts the velocity vector fields for the curvilinear and rectilinear compartments, respectively, under FD ventilation conditions during the fully developed fire stage in order to observe and understand the flow dynamics at the opening and in the external plume region, providing insights into the effect of geometry on EVF velocity, bidirectional flow behavior, and recirculation patterns.

In both geometries, the bidirectional nature of flow at the vent opening is evident. A high-velocity outflow of hot gases is observed in the upper region of the opening, while ambient air enters the compartment from the lower portion, forming an inflow jet. In the rectilinear case, the outflow velocity at the vent reaches approximately 4.5 m/s–5.0 m/s, with a relatively stable and vertically directed EVF plume. The inflow velocity near the base of the opening ranges between 1.0 m/s–

1.5 m/s, indicating strong buoyancy-driven exchange facilitated by the flat geometry and axial configuration of the compartment. In the curvilinear geometry, the outflow pattern is more dispersed and curved, with the main upward jet deflecting outward along the curvilinear ceiling before exiting. The EVF velocity also peaks at around 4.0 m/s-4.5 m/s, but the flow spreads laterally as it exits, leading to a wider and more deflected plume trajectory compared to the rectilinear case. The inflow at the lower part of the vent is somewhat weaker (~0.8 m/s–1.2 m/s) and less uniform, influenced by the asymmetrical redirection of gases within the compartment. A notable feature in the curvilinear compartment is the presence of multiple recirculation zones, particularly near the sidewalls and ceiling. These are formed as the curved surface promotes lateral gas movement and induces vortical flow structures. These recirculation cells enhance internal mixing, redistribute thermal energy, and somewhat reduce the momentum of the upward plume, contributing to the broader and less vertically focused EVF. Externally, the rectilinear plume remains narrow and rises vertically, maintaining its structure up to a considerable height due to the preserved momentum and minimal dispersion. Conversely, the curvilinear plume broadens significantly, with flow vectors showing lateral deflection and entrainment, reducing vertical reach but increasing horizontal spread.

f. Oxygen concentration

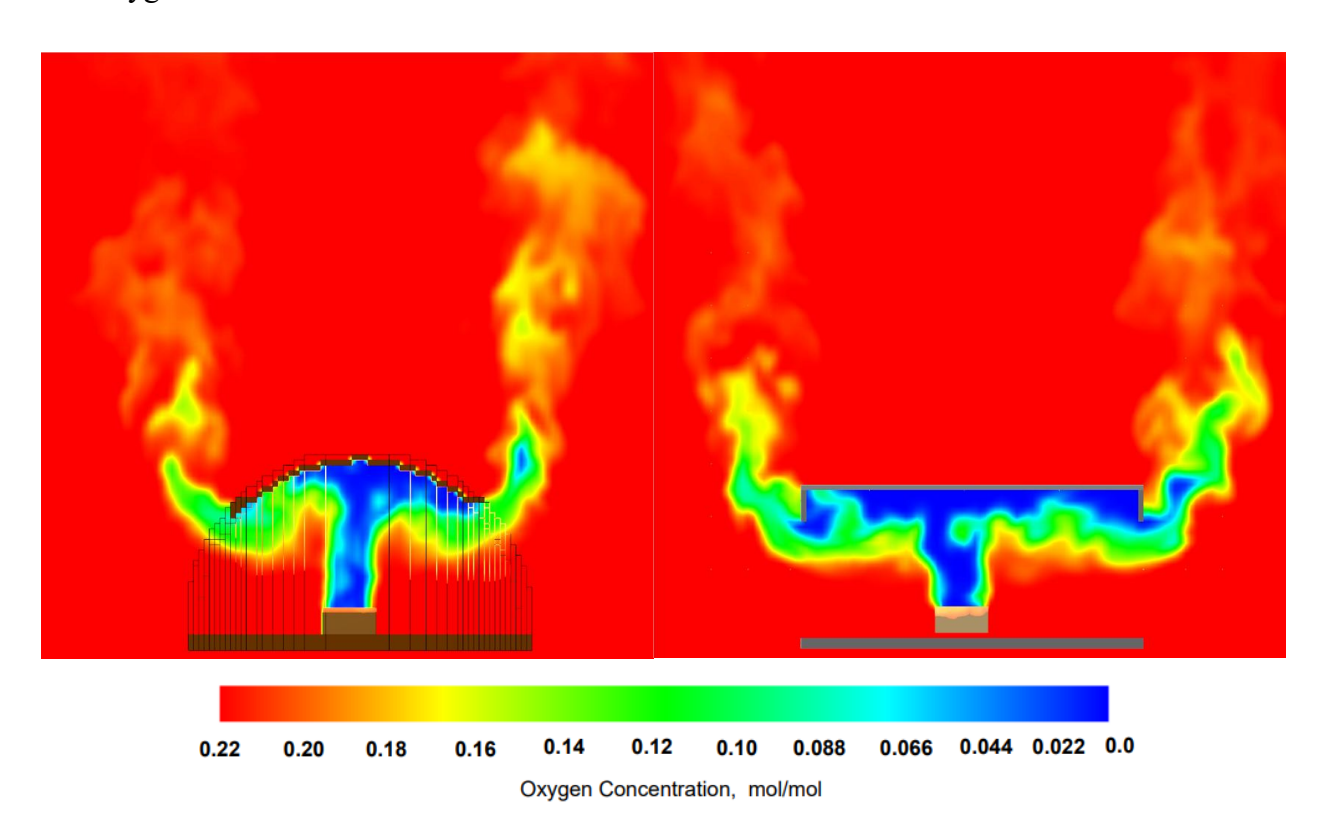


Figure 72: Spatial distribution of oxygen concentration 600 s and 400 s after fire initiation with curvilinear (left)and rectilinear (right) compartment under FD conditions.

Figures 72 illustrate the spatial distribution of oxygen concentration (X_{O2}) during the fully developed fire stage for the curvilinear (600 s) and rectilinear (400 s) compartments under FD conditions. In both cases, the core combustion zones are marked by severely oxygen-depleted regions ($X_{O2} < 0.05$ mol/mol), concentrated inside the compartment near the flame base and upper gas layer. In the rectilinear geometry, the oxygen-depleted zone aligns sharply with the hot gas layer, forming a well-defined stratification of hot and cold layers. The hot layer near the ceiling is rich in combustion products and depleted of oxygen, while the lower cold layer retains higher O₂ levels, consistent with fresh air inflow. In the curvilinear compartment, the oxygen-depleted region follows the arched ceiling, and the transition between high and low O₂ concentrations is more diffuse. This pattern mirrors the smeared hot gas layer observed in the temperature contours. The curved ceiling promotes lateral redirection and recirculation, enhancing gas mixing and disrupting the sharp layering typically seen in flat geometries. Additionally, the steel boundaries facilitate faster heat loss, weakening stratification and contributing to a more blended thermal and oxygen concentration profile.

4.7.2 Effect of Opening Size on Fire Development and Externally Venting Flames

This section investigates the influence of opening size on compartment fire dynamics and the development of EVF in both rectilinear and curvilinear geometries. As described in the Table 8, two opening configurations are considered for this study, a larger opening measuring 25 cm width \times 40 cm in height, which corresponding to a ventilation factor of 0.0632 and a smaller opening of 25 cm width \times 20 cm height, with a ventilation factor of 0.0223. By examining both experimental and numerical results, this analysis aims to elucidate how changes in ventilation factor affect heat accumulation within the fire compartment, gas venting characteristics, and the thermal behaviour of the plume emerging from the opening.

a. Interior gas temperature

The effect of opening size on the development of compartment interior gas temperature is shown in Figures 73 for curvilinear and rectilinear geometries, respectively. Both experimental measurements and FDS simulations results are compared for the larger opening ($25 \text{ cm} \times 40 \text{ cm}$) and the smaller opening ($25 \text{ cm} \times 20 \text{ cm}$) under FD conditions.

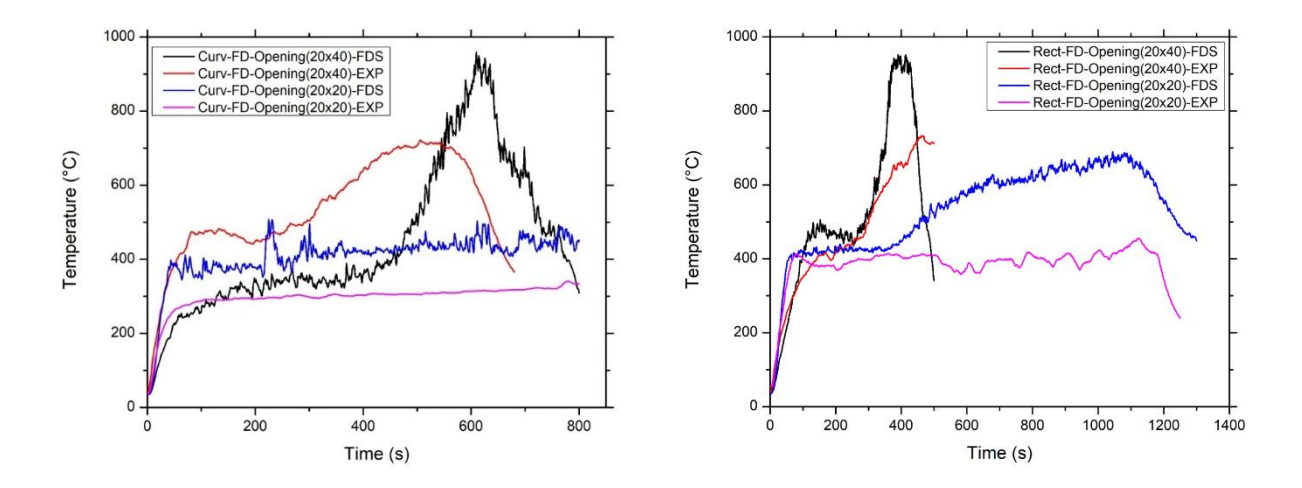


Figure 73: Interior temporal profiles of the curvilinear compartment (left) and rectilinear compartment (right) with different opening dimension for experiment and numerical analysis.

For the curvilinear compartment figure 73 (left), the interior gas temperature rises significantly faster and reaches higher peak values in the case of the larger opening (25 cm × 40 cm). The experimental peak temperature for this configuration is approximately 720°C, while the FDS prediction reaches around 900°C, indicating an overestimation of nearly 180°C. In both the experimental and numerical results, the larger opening clearly exhibits a well-defined growth phase, followed by a peak, and then a decay phase, reflecting the typical stages of a fully developed compartment fire. In contrast, for the smaller opening (25 cm × 20 cm), the temperature rise is notably slower and lower. The experimental peak is around 300°C and remains relatively steady throughout the fire duration, while the FDS prediction also stabilizes but at a higher level, around 400°C. In this case, no distinct peak or decay is observed; instead, the fire exhibits a prolonged growth phase followed by a steady-state temperature, indicating limited combustion due to restricted ventilation. The lower ventilation factor reduces oxygen supply, which in turn limits combustion efficiency and delays the onset of full fire development. Throughout the fire growth and steady phases, the larger opening supports greater air entrainment and a more vigorous combustion process, resulting in increased thermal energy generation and accumulation within the compartment. This trend is consistently reflected in both experimental measurements and FDS predictions.

In the rectilinear geometry figure 73 (right), the impact of opening size is even more pronounced. For the 25 cm × 40 cm opening, the experimental peak temperature reaches approximately 700°C, while the FDS predicted value exceeds 900° and again highlights the FDS tendency to overpredict temperatures during the fully developed and decay phases. With the reduced opening size (25 cm × 20 cm), both the experimental and numerical temperature curves show lower, delayed peaks and steady temperature throughout the experiment. The experimental value stabilizes around 400°C,

while the FDS result peaks at approximately 600°C. Although the general shape of the curves remains similar, the difference in magnitude emphasizes the impact of reduced ventilation in limiting fire growth and delaying the peak heat release rate. As observed in the curvilinear geometry, the rectilinear compartment with the larger opening exhibits all typical stages of compartment fire development. However, in the case of the smaller opening, no distinct peak or decay phase is evident; instead, the temperature remains relatively steady after a slower growth phase. This comparison clearly demonstrates that larger openings promote faster fire development, earlier peak temperatures, and higher heat retention due to increased oxygen availability and enhanced convective venting.

b. Opening temperature

The temperature at the centre of the compartment opening provides insight into the venting characteristics and the thermal intensity of the outflow. Figures 74 illustrate the temporal evolution of opening temperatures for both curvilinear and rectilinear compartments, with two opening sizes, $25 \text{ cm} \times 40 \text{ cm}$ and $25 \text{ cm} \times 20 \text{ cm}$ under FD conditions.

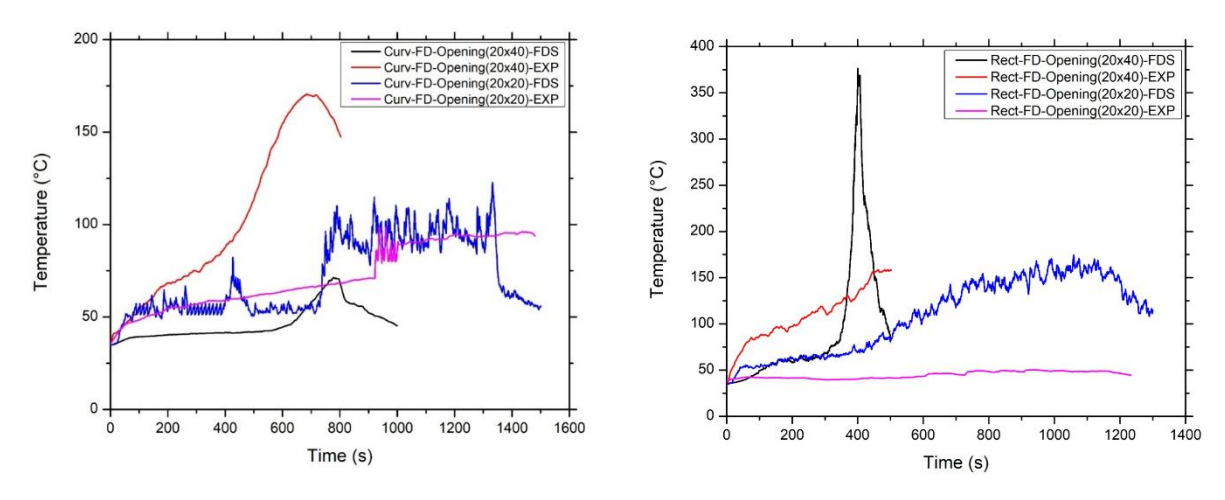


Figure 74: Opening temporal profiles the curvilinear compartment (left) and rectilinear compartment (right) with different opening dimension for experiment and numerical analysis.

In the curvilinear compartment (Figure 74 left), the larger opening (25 cm × 40 cm) results in a more pronounced increase in opening temperature. The experimental temperature gradually rises to a peak of approximately 160°C, while the FDS prediction significantly underestimates this, stabilizing around 60°C. This discrepancy may be due to FDS's underprediction of the convective heat transfer near the opening boundary, especially in curved geometries with complex flow dispersion. For the smaller opening (25 cm × 20 cm), both the FDS and experimental results show a relatively stable and lower temperature profile. The experimental curve stabilizes around 85°C, while the FDS predicted curve fluctuates around 75°C –90°C. The absence of a significant temperature rise in both datasets reflects the reduced thermal output and lower plume, forming

from the smaller ventilation factor and limited oxygen supply. In both opening sizes, the curved ceiling continues to play a role in dispersing the hot gases, reducing the direct thermal impact at the centre of the vent.

In the rectilinear compartment (Figure 74 right), a more distinct effect of opening size is observed on the opening temperature at the centre. For the larger opening (25 cm × 40 cm), the FDS simulation shows a sharp peak of nearly 370°C, while the experimental value peaks around 180°C, again showing a considerable overprediction by FDS during the fully developed phase. This intense venting behavior corresponds to stronger axial flame projection, as also seen in the interior temperature results. With the smaller opening (25 cm × 20 cm), both FDS and experimental temperatures are lower and relatively flat and exhibit similar trends. The FDS prediction peaks at approximately 180°C, while the experimental curve remains mostly steady around 100°C.

c. EVF average temperature

Figure 75 presents the time-averaged temperature distribution of EVF for the curvilinear compartment geometry under FD conditions. The analysis considers two opening sizes 25 cm × 40 cm and 25 cm × 20 cm and includes both experimental measurements and FDS predicted results. The vertical axis represents height above the floor, with 0.2 m corresponding to the centre of opening height, while the horizontal axis spans 0.15 m to 0.30 m from the façade. The time averaging was performed over a 50-second period during the fully developed fire stage, where sustained flame or hot gas venting from the opening was observed.

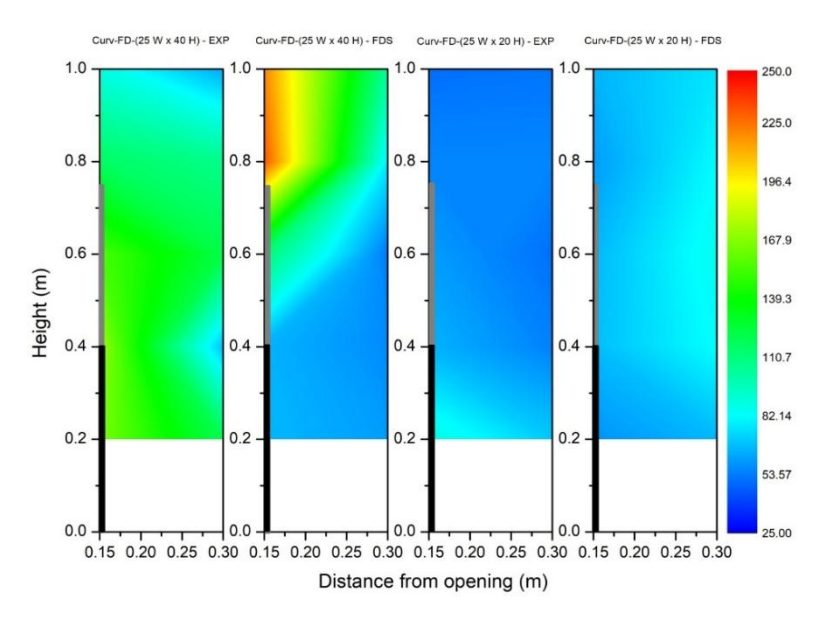


Figure 75: Time averaged EVF temperatures for curvilinear geometry with different opening dimension for both experiment and FDS.

For the larger opening (25 cm × 40 cm), a moderately developed EVF structure is observed. The experimental results show a broad thermal field extending above the opening, with maximum

temperatures approaching 150°C –160°C, concentrated in the upper part of the plume, above 0.6 m height. The plume exhibits a dispersed thermal profile, indicating a relatively lower momentum vent flow compared to the rectilinear configuration, which can be attributed to the curved ceiling geometry that redirects and diffuses the thermal outflow. The FDS simulation captures the general shape and extent of the plume but slightly overpredicts the peak temperature, showing values exceeding 200°C in the upper region. However, the plume appears less focused compared to the rectilinear case, consistent with the experimentally observed broader distribution. The curved surface likely contributes to more distributed convection and less axial velocity in the venting gases. For the smaller opening (25 cm × 20 cm), both experimental and FDS results indicate a significantly reduced EVF temperature field. In the experiment, temperatures remain below 100°C, with no concentrated high-temperature zone, suggesting minimal to nonexternal flaming or thermal plume behavior. The FDS prediction similarly shows a weak plume with temperatures mostly in the range of 80°C –110°C, distributed uniformly with no distinct thermal core.

Figure 76 depicts the time averaged EVF temperature for rectilinear geometry, for the larger opening (25 cm × 40 cm), both the experimental and numerical results reveal the presence of a strong and focused EVF. The FDS contour indicates peak temperatures exceeding 250°C, concentrated in the upper region of the plume, particularly above 0.6 m height and within 0.15 m -0.25 m from the façade. This sharp thermal gradient suggests a high-energy buoyant jet, driven by enhanced combustion and convective outflow through the large opening. In comparison, the experimental contour shows a more diffused thermal field, with maximum temperatures around 170-180°C and a broader vertical distribution. While both methods capture the presence of a strong EVF, FDS significantly overpredicts the peak temperatures. In contrast, for the smaller opening (25 cm × 20 cm), a substantial reduction in venting behavior is evident. The FDS prediction shows a moderately developed plume with peak temperatures limited to approximately 150°C –170°C, and a more vertically stretched distribution. The plume appears weaker and less focused, reflecting reduced heat release and slower gas flow due to the lower ventilation factor. The experimental result further confirms this trend, showing a lower thermal field with temperatures remaining mostly below 100°C and a dispersed contour with no clear plume core. The weak venting behavior is consistent with the observed reduction in fire growth and combustion intensity due to restricted oxygen supply.

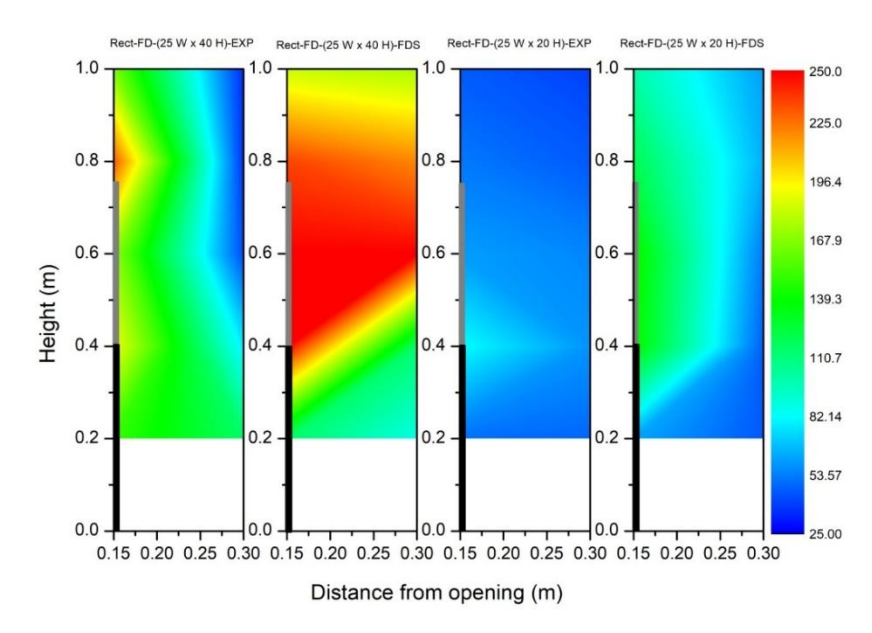


Figure 76: Time averaged EVF temperatures for rectilinear geometry with different opening dimension for both experiment and FDS.

The comparative analysis of EVF temperature distributions across rectilinear and curvilinear compartments demonstrates a clear dependence on opening size and geometry. In both configurations, the larger opening (25 cm × 40 cm) results in higher plume temperatures and a more developed EVF structure. The rectilinear geometry, due to its flat ceiling and enclosure bounding surface material is constructed of thermally insulating Monolux, promotes stronger and more focused thermal plumes, with FDS predicting peak temperatures exceeding 250°C, while experimental values reach up to 170°C –180°C. In contrast, the curvilinear geometry, constructed with steel and featuring a curved ceiling, yields a more diffused and weakened plume, with FDS-predicted peaks slightly over 200°C and experimental peaks around 150°C –160°C. This suggests that the curved surface promotes greater flow dispersion and conductive heat loss, thereby weakening the intensity of the EVF.

These results clearly demonstrate that opening size has a significant influence on the magnitude and structure of externally venting flames. Larger openings promote more intense combustion, stronger gas ejection, and higher external temperatures, whereas smaller openings restrict airflow and limit the development of a pronounced EVF. While FDS effectively captures the general trend, it consistently overestimates plume temperatures, particularly for the larger opening.

d. Temperature field

To evaluate the effect of opening height under FD ventilation, Figures 77 compare the temperature contours for curvilinear and rectilinear compartments with openings of 25 cm width \times 40 cm height and 25 cm width \times 20 cm height.

In the curvilinear geometry the compartment exhibits a well-mixed thermal field in the reduced opening configuration, with no clear stratification between hot and cold layers. The internal temperatures are substantially lower, averaging around 250°C –300 °C, and EVF behavior is weak to nearly absent, due to limited oxygen inflow and enhanced heat loss through the steel boundaries. The curvature of the ceiling further promotes recirculation, distributing heat uniformly but reducing the momentum needed for flame projection beyond the opening. In contrast, the rectilinear compartment (at 1050 s) still shows signs of thermal stratification even with the 20 cm high opening. The upper hot layer reaches temperatures of 550°C –600°C, but the thermal layer extends downward, descending close to floor level due to the restricted venting capacity. Although EVF is present, it is markedly weaker than in the 40 cm case, with less concentrated and shorter flame plumes as the lower opening limits the development of strong outflow jets. As previously discussed, the 40 cm high openings in both geometries promote stronger fire development and pronounced EVFs. However, reducing the opening height to 20 cm significantly alters the fire dynamics in the compartment, especially in terms of internal temperature distribution, ventilation efficiency, and EVF formation.

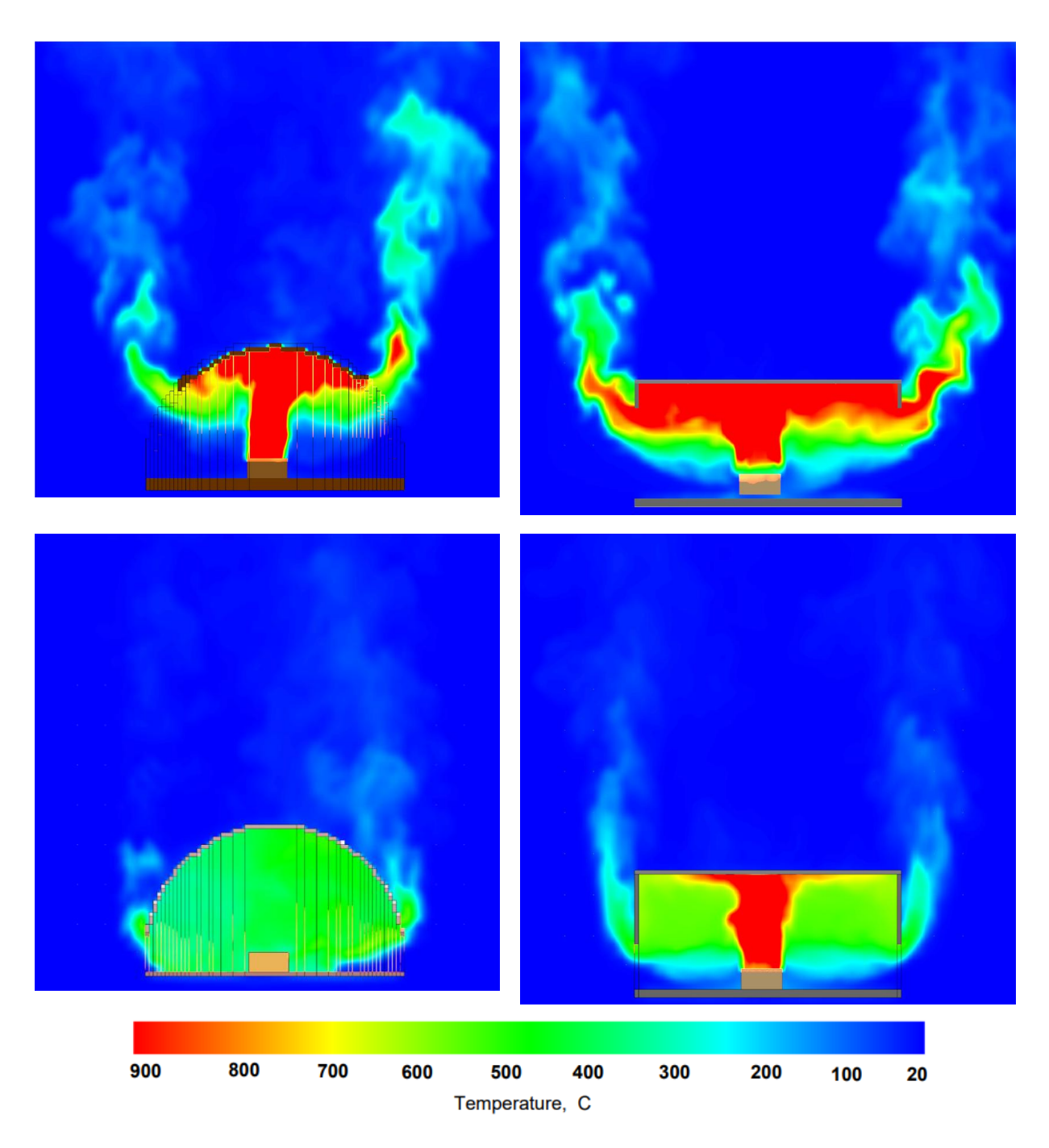


Figure 77: Spatial distribution of gaseous temperature 600 s & 1150s after fire initiation with 25W x 40H cm (top) and 25W x 20H cm (bottom) conditions for curvilinear (left) and 400 s and 1050s after fire for rectilinear (right).

e. EVF Gas mixture velocity.

Figure 78 depicts the EVF velocity vector fields for both curvilinear and rectilinear geometries under FD conditions, comparing the impact of a reduced opening height ($25 \text{ cm} \times 20 \text{ cm}$) to the standard opening ($25 \text{ cm} \times 40 \text{ cm}$).

In the curvilinear compartment with the 25 cm \times 20 cm opening, flow field exhibits strong internal recirculation beneath the arched ceiling, with reduced vent velocities around 2.5–3 m/s. The EVF

plume, once exiting, disperses laterally rather than projecting vertically, influenced by the curved geometry and lower buoyant thrust compared to the 40 cm opening case. Stratification is minimal, indicating a well-mixed layer throughout the compartment. Notably, the plume tends to follow the curvature of the façade, potentially increasing the risk of fire spread along the external surface in real-world scenarios involving curved architectural elements. Peak vent velocities are observed in the range of 2.5–3 m/s, significantly lower than the 4.5–5 m/s velocities seen in the larger opening configuration.

In contrast, the rectilinear compartment with a 25 cm × 20 cm opening, maintains a more stratified environment despite the smaller vent, with a distinct bi-directional flow pattern at the opening. Hot gases exit through the upper half of the vent at velocities reaching 4–4.5 m/s, while cool air enters from below, bi-directional flow is evident at the opening, with inflow at the bottom and outflow at the top, similar to the larger opening scenario but at reduced intensity. In summary, reducing the opening height reduces both EVF intensity and velocity across both geometries, though the effects are more pronounced in the curvilinear case due to enhanced internal mixing and the redirection of thermal flow by the arched ceiling. Rectilinear geometry retains a more axial and focused plume, even at smaller openings, while the curvilinear configuration produces broader, less intense EVF behavior driven by geometry-induced recirculation.

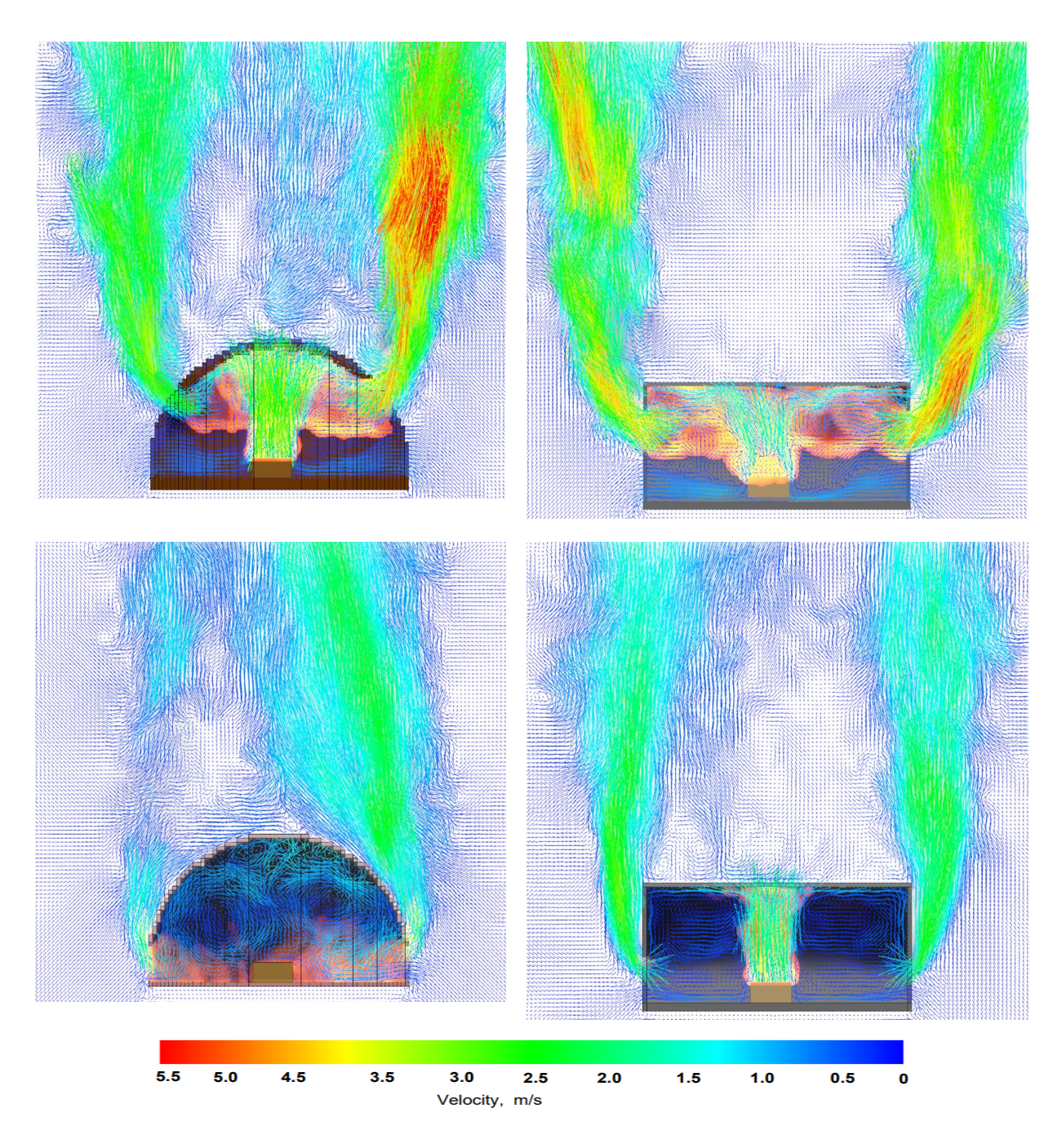


Figure 78: Gas mixture velocity and EVF 600 s & 1150s after fire initiation with 25W x 40H cm (top) and 25W x 20H cm (bottom) conditions for curvilinear (left) and 400 s & 1050s after fire for rectilinear (right).

f. Oxygen Concentration

The oxygen concentration fields for the four configurations in figure 79 clearly reflect the ventilation effects and geometrical influence on combustion dynamics. In the curvilinear geometry with the 40 cm high opening, a well-developed low-oxygen layer ($X_{O_2} < 0.05$) forms near the ceiling and exits through the opening, indicating an efficient flame spread and oxygen consumption. In contrast, the 20 cm high curvilinear case shows a much more uniform oxygen

profile, suggesting well-mixed conditions with minimal stratification and subdued externally venting flames.

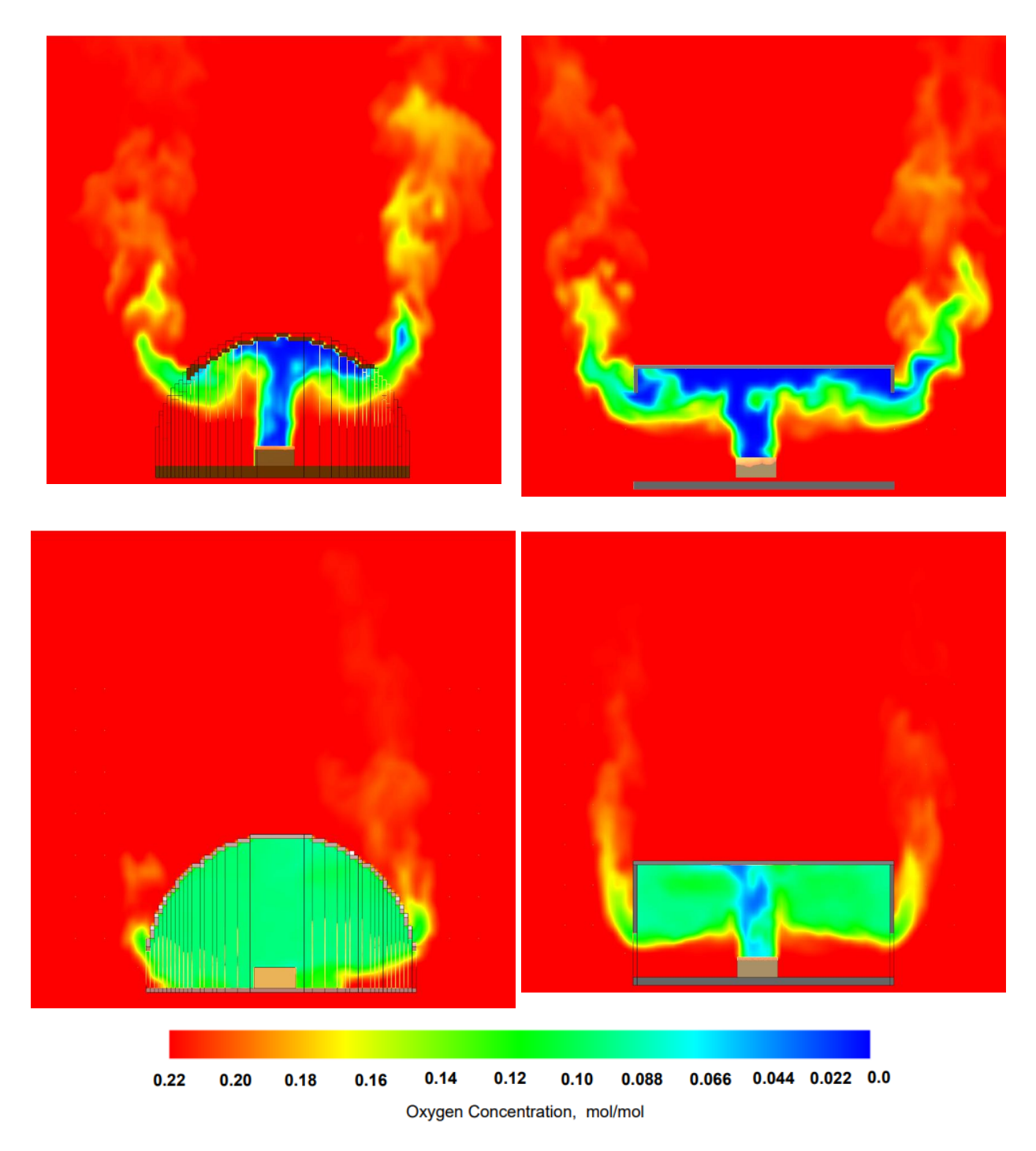


Figure 79: Spatial distribution of oxygen concentration 600 s & 1150s after fire initiation with 25W x 40H cm (top) and 25W x 20H cm (bottom) conditions for curvilinear (left) and 400 s & 1050s after fire for rectilinear (right).

In the rectilinear geometry, the 40 cm high opening promotes a strong low-oxygen hot layer near the ceiling ($X_{O_2} \sim 0.04$), while in the 20 cm high case, although stratification is still evident, the oxygen-depleted zone extends deeper, nearing floor level, reflecting a slow and ventilation-limited combustion environment. Overall, the 20 cm openings in both geometries show higher average

oxygen levels inside the compartment, consistent with the reduced fire growth and EVF observed previously.

4.7.3 Effect of ventilation conditions on fire development and EVF

This section investigates the influence of ventilation conditions on compartment fire dynamics and EVF behaviour by comparing two distinct conditions: FD and NoFD. In the FD condition, the compartment is provided with two symmetrically positioned openings of equal size on opposite walls, promoting cross-ventilation. In contrast, the NoFD condition consists of a single opening, thereby limiting ventilation. Results are presented for both curvilinear and rectilinear compartment geometries, using experimental measurements and numerical simulations. The objective is to understand how ventilation conditions influence combustion development, EVF, and the nature of externally venting flows under different architectural and boundary conditions.

a. Interior gas temperature

Figure 80 left presents the temporal evolution of interior gas temperature for the curvilinear compartment under two ventilation configurations FD and NoFD considering an opening size of 25 cm × 40 cm. The results include both numerical predicted and experimentally measured temperatures at the compartment centre.

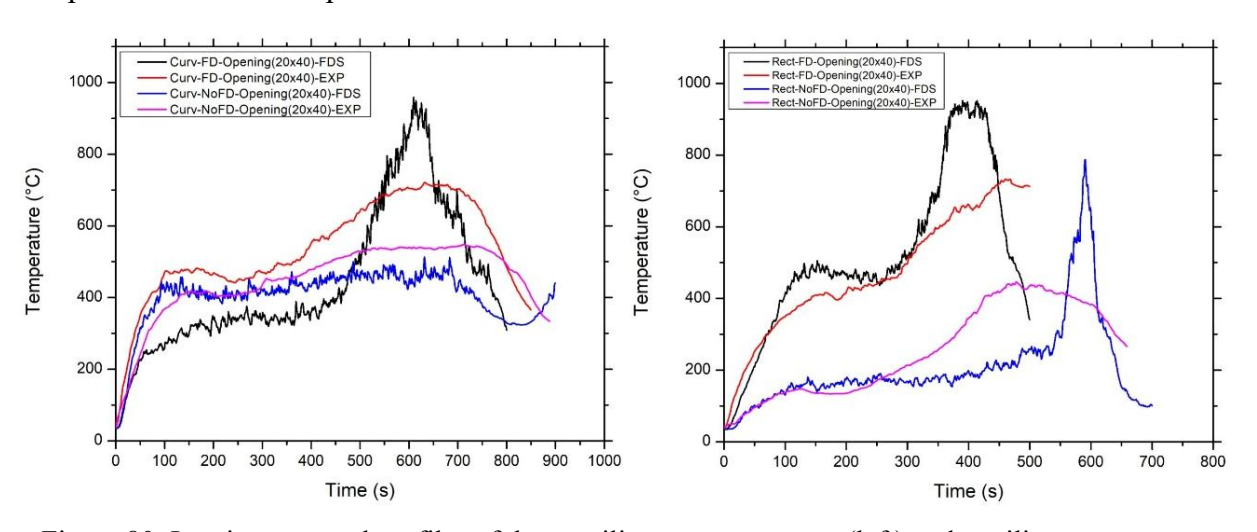


Figure 80: Interior temporal profiles of the curvilinear compartment (left) and rectilinear compartment (right) with different ventilation conditions for experiment and numerical analysis.

Curvilinear compartment, in the FD condition, where symmetric openings on both sides of the compartment enable cross-ventilation, the fire develops rapidly and reaches a distinct peak temperature. The experimental data show a sharp rise in gas temperature, reaching a peak of approximately 700°C, followed by a clear decay phase. Numerical predictions also captures this trend, peaking at around 900°C, indicating an overprediction of nearly 200°C. The FD condition demonstrates a full progression of fire development such as a growth, peak, and decay exhibit a

characteristic of well-ventilated compartment fires. The symmetrical vent arrangement promotes high air entrainment, enhanced combustion, and effective venting of combustion products, all of which contribute to a sharp thermal buildup followed by a clear decay once fuel is consumed. Under the NoFD condition, where only a single opening is provided, the fire exhibits a lower thermal profile. The experimental results show a slower temperature rise and a lower peak value of approximately 500°C, while the FDS result peaks slightly lower, at around 480°C. Compared to the FD condition, the absence of cross-ventilation in NoFD limits oxygen supply, which slows combustion kinetics, reduces peak heat release rate, and extends the duration of the steady-state burning period. In both FDS and experimental results, the NoFD condition lacks a distinct decay phase, and instead the temperature stabilizes at a relatively lower level before gradually declining. In the rectilinear compartment (Figure 80, right), under the FD condition, experimental

observations show a steady rise in temperature, peaking at around 700°C, while the FDS simulation significantly overpredicts the peak, reaching values close to 900-950°C. This sharp discrepancy of over 200°C is consistent with prior trends observed in rectilinear geometries, where FDS tends to overpredict during the peak phase, although it aligns well with experimental data during the growth stage. The FD configuration supports a complete fire development phase in a compartment, with clearly defined growth, peak, and decay phases in both experiment and simulation. The presence of openings on both sides enhances oxygen availability, promotes more efficient combustion, and facilitates rapid venting of combustion products which factors that collectively accelerate fire growth and intensify the thermal environment within the compartment. In contrast, under the NoFD conditions, where only a single opening is provided, the thermal profile is significantly altered. The experimental results show a slower temperature rise, reaching a peak of approximately 450°C, followed by a gradual decay. The FDS prediction exhibits a delayed but sharp peak of around 750°C, before rapidly declining. The difference between experiment and FDS at peak reaches nearly 300°C, though the overall trend remains like that observed under FD conditions. Unlike the FD case, the NoFD experimental data do not exhibit a clear decay phase; instead, a prolonged period of elevated temperature is observed. This behavior is typical of ventilation-limited fires, where combustion is governed by restricted oxygen availability rather than fuel supply. The reduced airflow slows the combustion rate and alters the internal fire dynamics, resulting in a more thermally stable but less intense fire.

The comparison of FD and NoFD conditions across both curvilinear and rectilinear compartments confirms the significant influence of ventilation configuration on compartment fire dynamics. FD conditions lead to faster, more intense combustion and rapid heat build-up, while NoFD conditions limit fire intensity and produce a more oxygen-constrained and stable thermal environment.

b. Opening temperature

Figure 81 (left) depicts the evolution of opening centerline temperatures for the curvilinear compartment under FD and NoFD conditions. The FD condition, with two symmetrically positioned openings, facilitates efficient venting and steady airflow through the compartment. As a result, both experimental and FDS opening temperatures remain relatively low and stable throughout the fire duration. The experimental curve peaks at approximately 170°C, while the FDS simulation underpredicts the value, stabilizing around 80–100°C. The low thermal outflow is consistent with the curved geometry's flow-dispersing behavior and the use of high-conductivity steel, which promotes heat loss through conduction, thereby reducing the amount of thermal energy escaping through the vent. In contrast, the NoFD condition, characterized by a single opening, shows a markedly different profile. Both experimental and FDS results exhibit higher peak temperatures, with the FDS curve reaching up to 600°C and the experimental curve peaking near 350°C. This increase in temperature at the opening is due to the accumulation of hot gases within the compartment, driven by restricted airflow and limited oxygen supply.

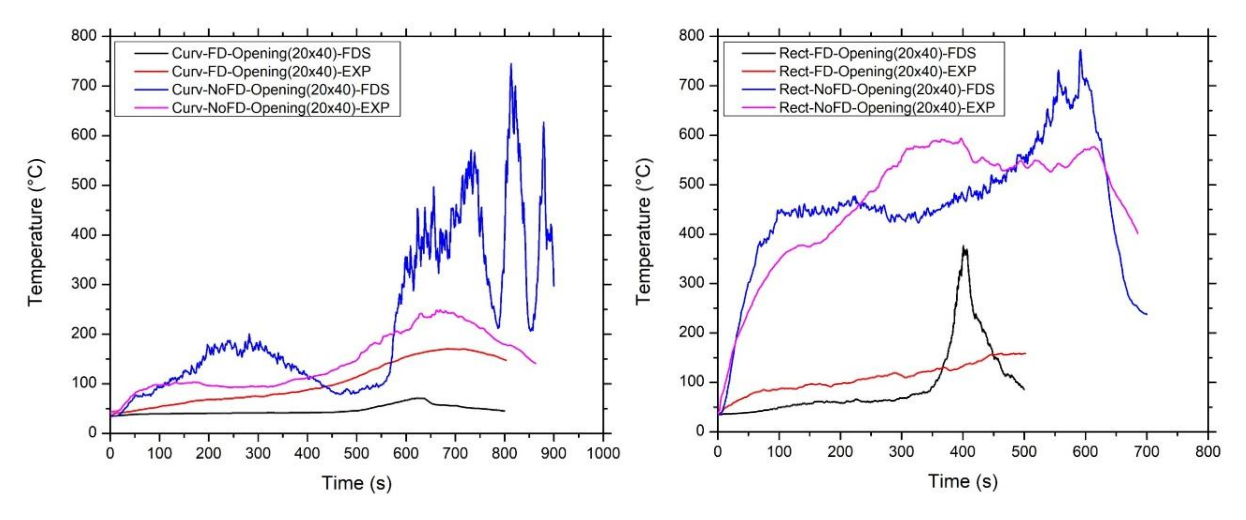


Figure 81: Opening temporal profiles of the curvilinear compartment with different ventilation conditions for experiment and numerical analysis.

For the rectilinear compartment (Figure 81 right), the difference between FD and NoFD conditions is even more pronounced. Under the FD condition, opening temperatures remain low in both datasets, with experimental values peaking around 120°C and FDS predictions stabilizing around 100°C. The symmetrical venting facilitates consistent gas exchange and cooling, while the Monolux insulation minimizes internal heat transfer to the vent area, resulting in a less thermally aggressive plume. In the NoFD condition, however, both experimental and FDS results indicate significantly elevated vent temperatures. The FDS prediction rises sharply to nearly 750°C, while the experimental curve peaks around 600°C, indicating strong thermal ejection from the single

opening. The rectilinear geometry promotes linear channeling of the plume, resulting in more focused and energetic venting when flow is restricted to one direction. Additionally, the insulation properties of Monolux reduce heat loss through the walls, causing more energy to be expelled through the vent, particularly in under-ventilated conditions.

The comparison of FD and NoFD conditions across curvilinear and rectilinear geometries shows a consistent trend where NoFD configurations produce significantly higher vent temperatures, while FD conditions limit thermal outflow due to enhanced ventilation and symmetrical airflow. In curvilinear compartments, the curved ceiling and steel walls promote flow dispersion and conductive cooling, reducing peak vent temperatures even under NoFD. In contrast, rectilinear compartments, especially under NoFD show a concentrated, high-temperature venting at the center of the opening. FDS generally captures the trends well but tends to overpredict peak vent temperatures, especially under NoFD conditions where unstable flow and high-pressure venting dominate.

c. EVF average temperature

Figure 82 presents the time-averaged temperature contours of externally venting gases for the curvilinear compartment geometry under FD and NoFD conditions, based on both experimental measurements and FDS simulations.

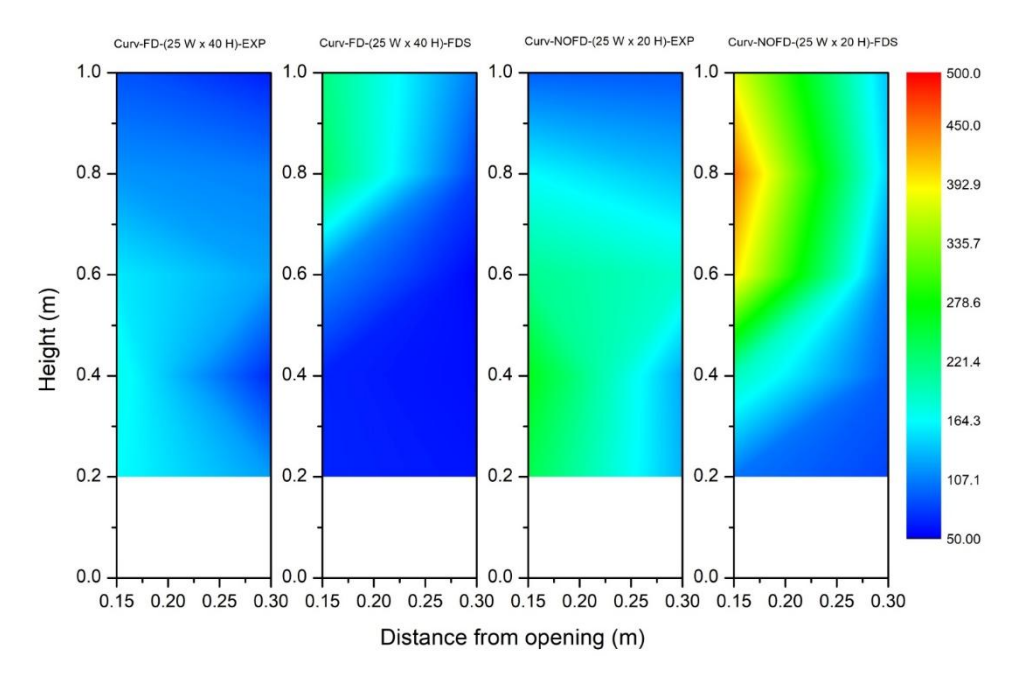


Figure 82: Time averaged EVF temperatures for curvilinear geometry with different ventilation condition for both experiment and FDS.

Under the FD condition, the experimental temperature contour shows a low-intensity venting profile, with temperatures generally below 130°C, and only a small region near the upper plume

reaching 150°C. The flow appears well-ventilated and dispersed, with minimal thermal accumulation above the opening. This is consistent with the curvilinear ceiling geometry, which spreads the internal flow due to the curved nature of the ceiling and reduces the upward momentum of the outflow. The FDS-predicted contour for the same also reflects this behavior, with temperatures ranging between 100°C –140°C, showing a slight upward thermal gradient but no focused high-temperature plume. In the NoFD condition, the temperature distribution undergoes a substantial change. The experimental results show a more concentrated and vertically extended thermal plume, with peak temperatures reaching in the range of 260°C –280°C, especially near the top center of the plume zone (above 0.7 m). This suggests increased thermal build-up and ejection of hot gases due to restricted ventilation and reduced airflow, leading to a ventilation-limited fire scenario. The FDS simulation shows a strong and focused plume, with maximum temperatures exceeding 450°C in the upper portion of the domain. A steep gradient is observed from the vent exit upwards and outward, suggesting high-velocity ejection of buoyant gases. This is a clear contrast to the FD scenario and shows that FDS significantly overpredicts the vent temperature under NoFD, particularly in curvilinear geometries.

Figure 83 presents the time-averaged temperature distribution of EVF for the rectilinear compartment under FD and NoFD conditions. Under the FD condition, the experimental contour shows a relatively cool and dispersed EVF structure, with most of the thermal field remaining below 160°C, and only minor regions approaching 180°C near the upper right portion of the opening. The outflow is weak and lacks concentrated buoyancy, consistent with efficient ventilation. The FDS-predicted contour shows slightly higher temperatures, reaching up to 220°C -230°C, particularly along the upper central above the opening. Nonetheless, both simulation and experiment agree that under FD, venting is minimal, and flame projection is weak. In contrast, the NoFD condition with only a single opening forms a higher thermal field. The experimental contour shows a well-defined EVF structure with temperatures exceeding 320°C, extending vertically from the opening and spreading outwards, consistent with a high-pressure, buoyancy-driven jet. The plume displays steep thermal gradients. The FDS simulation significantly overpredicts the EVF temperature, showing values exceeding 500°C over a wide area and forming an intense, vertically dominant plume. The simulation captures the general structure of the EVF but lacks the gradual gradient seen in the experimental result, indicating a possible underrepresentation of heat losses in under-ventilated scenarios. Across both geometries, FD conditions result in lowtemperature, well-dispersed EVFs due to effective cross-ventilation, with curvilinear geometry exhibiting broader dispersion and rectilinear geometry showing slightly more axial flow. Under NoFD conditions, higher and more concentrated EVFs are observed, particularly in the rectilinear case where the flat surfaces and insulating material promote focused, high-temperature outflow. FDS captures overall trends but tends to underpredict EVF temperatures under FD curvilinear geometry and overpredict under NoFD.

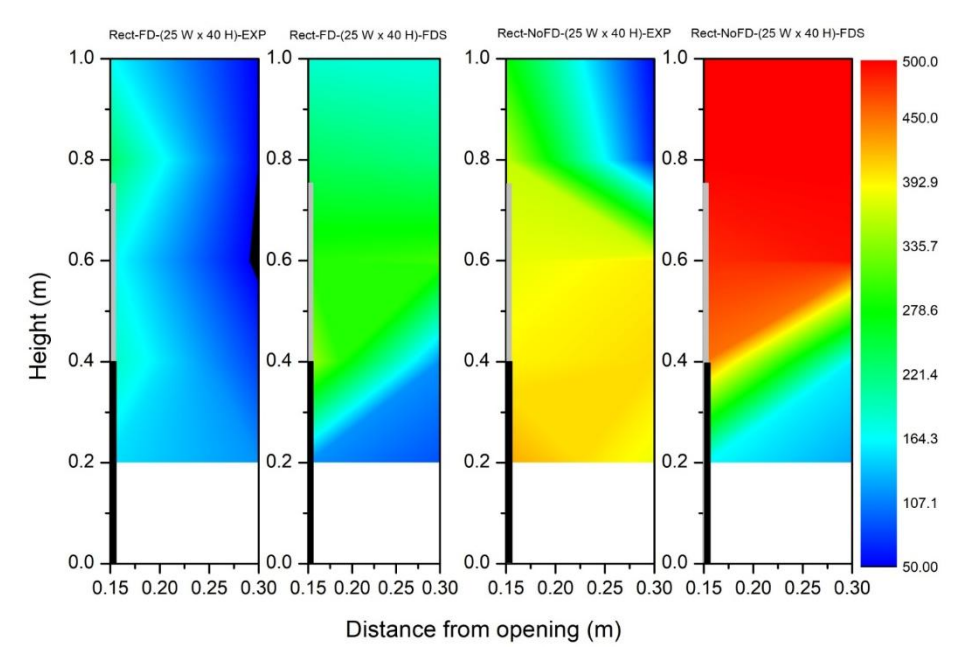


Figure 83: Time averaged EVF temperatures for rectilinear geometry with different ventilation condition for both experiment and FDS.

d. Temperature field

Figure 84 presents the temperature distribution during the fully developed fire stage for both rectilinear and curvilinear compartments under FD and NoFD ventilation conditions. The time frames selected (590 s for rectilinear NoFD and 810 s for curvilinear NoFD) correspond to the time when the fire is fully developed, and externally venting flames (EVF) are emerging from the enclosure opening.

The curvilinear geometry under NoFD shows a more dispersed and moderately rising EVF plume with a peak temperature in the range of 800°C –900°C. Interior temperatures are comparatively lower, and there is well mixed case and no stratification, the curved ceiling appears to encourage a more distributed thermal field. The plume, after exiting, follows the curvature of the façade, which may pose additional risk for vertical flame spread along the building envelope. In contrast, the NoFD condition for rectilinear geometry, a strong EVF plume is clearly observed projecting from the single opening, with peak external gas temperatures exceeding 850°C –900°C. Inside the compartment, the hot gas layer is thick and extends down close to the floor level, with interior gas temperatures exceeding 700°C. Under FD conditions, both geometries exhibit bi-directional vent flows with clearly separated inflow (bottom) and outflow (top) layers. The EVF is more symmetrical and less aggressive compared to NoFD cases, with peak external temperatures of

around 700°C -800°C, as seen in the rectilinear and curvilinear FD images. The rectilinear geometry retains a thicker hot layer with a more focused vertical plume, while the curvilinear geometry shows a broader, more laterally spread EVF pattern due to the ceiling-induced redirection of flow.

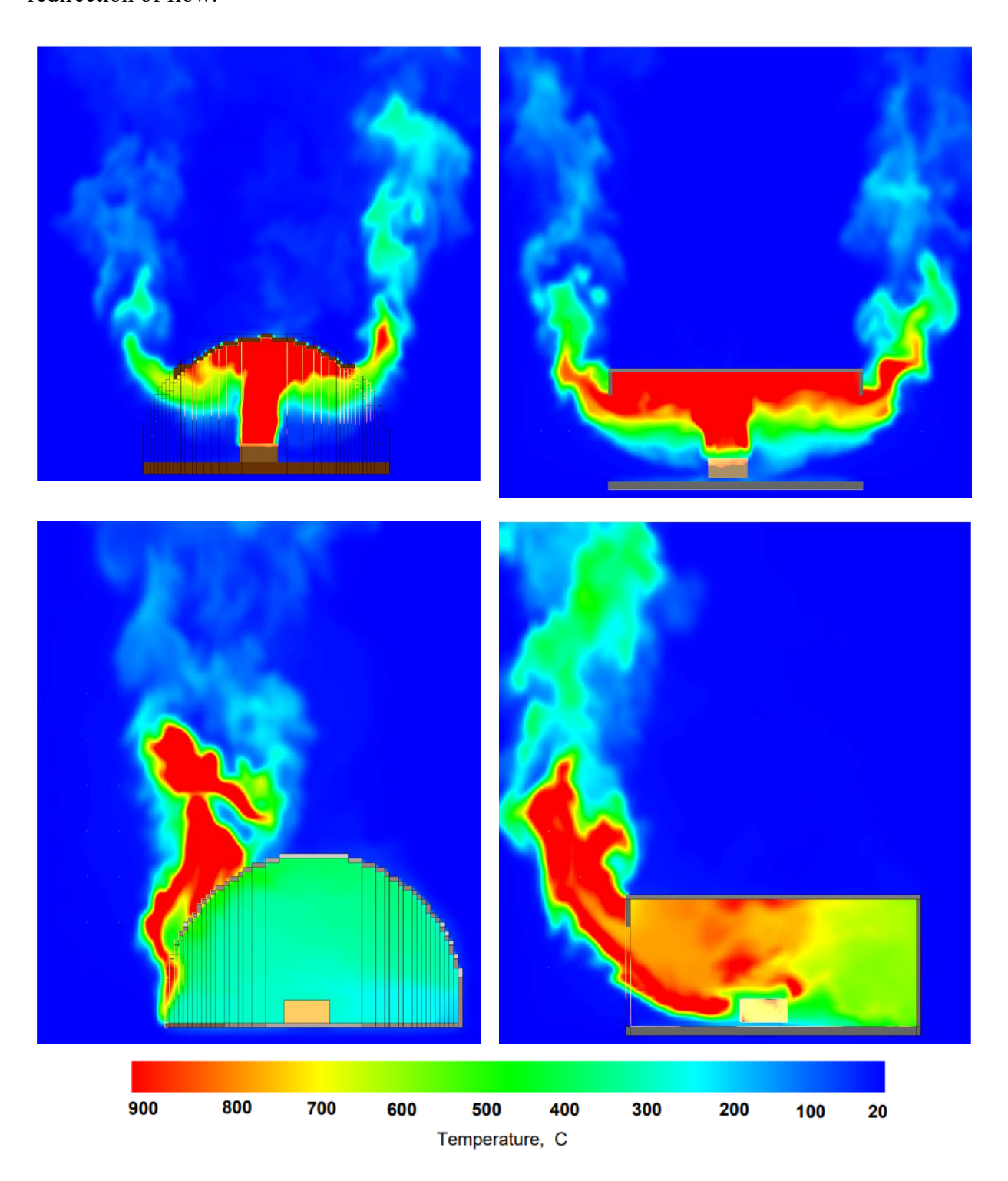


Figure 84: Spatial distribution of gaseous temperature 600 s & 810s after fire initiation with 25W x 40H cm (top) and 25W x 20H cm (bottom) conditions for curvilinear (left) and 400 s & 590s after fire for rectilinear (right).

In summary, NoFD conditions lead to stronger, unidirectional EVF jets driven, with higher compartment gas and plume temperatures. FD conditions, on the other hand, moderate fire behavior through increased oxygen availability and vent efficiency.

e. EVF gas mixture velocity

The comparison of mixture velocity under both FD and NoFD conditions for curvilinear and rectilinear geometries reveals the significant influence of ventilation condition on fire dynamics and EVF behaviour. In the curvilinear NoFD case, the EVF plume exhibits a relatively narrow and vertically rising stream, with peak mixture velocities reaching up to approximately 4.5 m/s near the opening. There is no inflow of air to the compartment and a large volume of hot gases are burning outside the compartment. This generates an intense plume that curves along the geometry once outside. In contrast, under FD conditions, the same geometry shows a more diffused plume, with a peak velocity in the range of 3.8 m/s –4.0 m/s and significant lateral dispersion. There is clear bidirectional flow in the FD condition, such as inflow of air from the bottom of the compartment opening and hot gases including flames ejecting through the top of the opening. For the rectilinear geometry, the NoFD condition shows a strong, sharply defined upward plume exiting the opening with higher peak velocities exceeding 5 m/s, indicating a pressure-driven outflow due to hot gas buildup. On the other hand, in FD condition, there is a well-formed bidirectional flow at the compartment and maximum velocity are in the range of 3 m/s - 4 m/s.

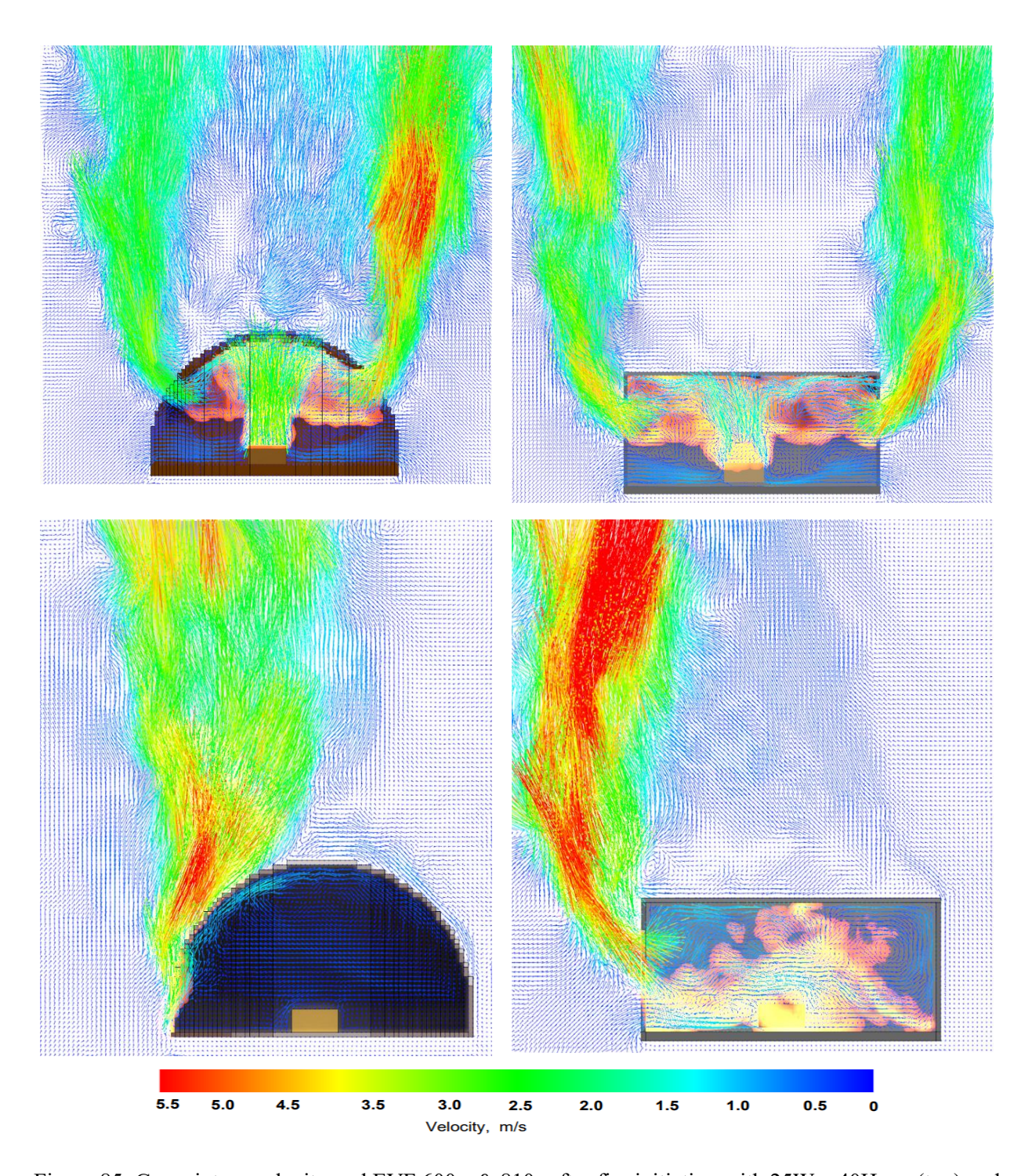


Figure 85: Gas mixture velocity and EVF 600 s & 810s after fire initiation with 25W x 40H cm (top) and 25W x 20H cm (bottom) conditions for curvilinear (left) and 400 s & 590s after fire for rectilinear (right).

NoFD conditions promote stronger, narrower, and more vertically extended EVF plumes due to accumulated pressure and thermal energy, especially in the rectilinear geometry. FD cases, although inducing more turbulence and mixing, lead to more dispersed and lower-velocity outflows. Curvilinear geometries under NoFD produce plumes that follow the curvature of the structure post-exit, potentially increasing flame spread risk along the façade, whereas rectilinear flows remain axially directed.

f. Oxygen concentrations

Figure 86 presents the oxygen concentration profiles for curvilinear and rectilinear compartments under both FD and NoFD conditions. In the curvilinear NoFD condition, oxygen levels inside the compartment drop close to zero ($X_{O_2} < 0.01 \text{ mol/mol}$), indicating oxygen-depleted combustion and confirming that sustained burning is occurring primarily outside the compartment. In contrast, the rectilinear NoFD condition, shows a slight but noticeable inflow of fresh air near the lower portion of the opening (X_{O_2} up to 0.10 mol/mol), suggesting a weak bi-directional flow that still allows some internal combustion to persist. Under FD conditions, both geometries display clear bi-directional exchange, with higher internal oxygen concentrations (X_{O_2} ranging from 0.05 to 0.15 mol/mol) enabling more strong internal burning and a well-established hot gas layer and cold layer. These differences underscore the critical influence of ventilation and geometry on combustion dynamics and oxygen replenishment within enclosures.

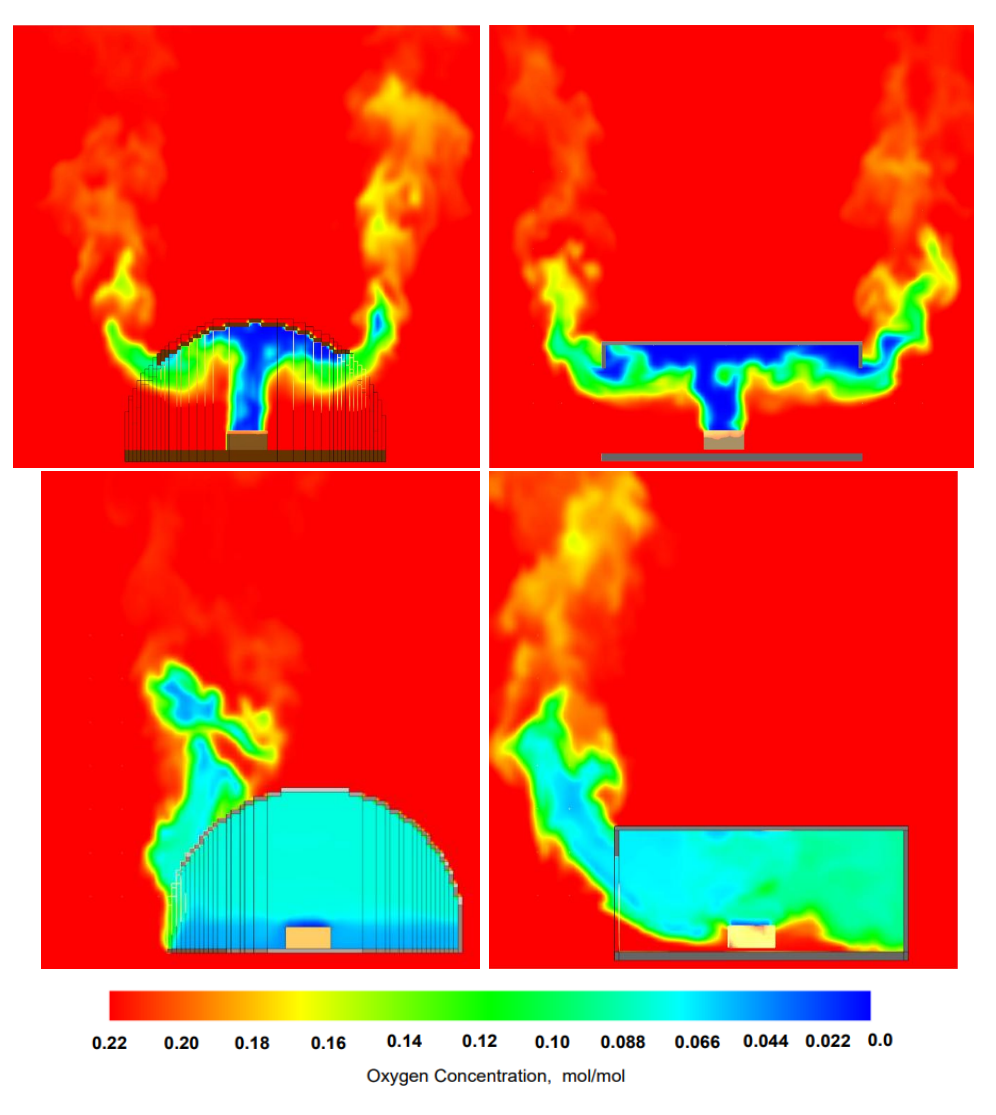


Figure 86: Spatial distribution of oxygen concentration 600 s & 810s after fire initiation with 25W x 40H cm (top) and 25W x 20H cm (bottom) conditions for curvilinear (left) and 400 s & 590s after fire for rectilinear (right).

4.7.4 Additional Analysis with Rectilinear and Curvilinear Geometry

Additional analysis has performed showing a simplified comparison between rectilinear and curvilinear with FD condition with respect to the velocity flow field, temperature field and oxygen concentration.

a. Velocity Flow field

For any fire in a compartment, during its growth phase, the plume developed will impinge on the ceiling and the hot gases including the flame spread out radially through the ceiling and flow out through the available opening(s). However, in compartments with curvilinear geometry smoke movement/flow can be a complex fire dynamic process due to the interaction of turbulence, combustion, radiation etc. with the geometry of the compartment. To study the differences in the smoke flow field both interior and exterior of the compartment with respect to the rectilinear geometry, experiments of rectilinear and curvilinear with FD conditions 25 cm x 40 cm opening sizes were analysed using CFD.

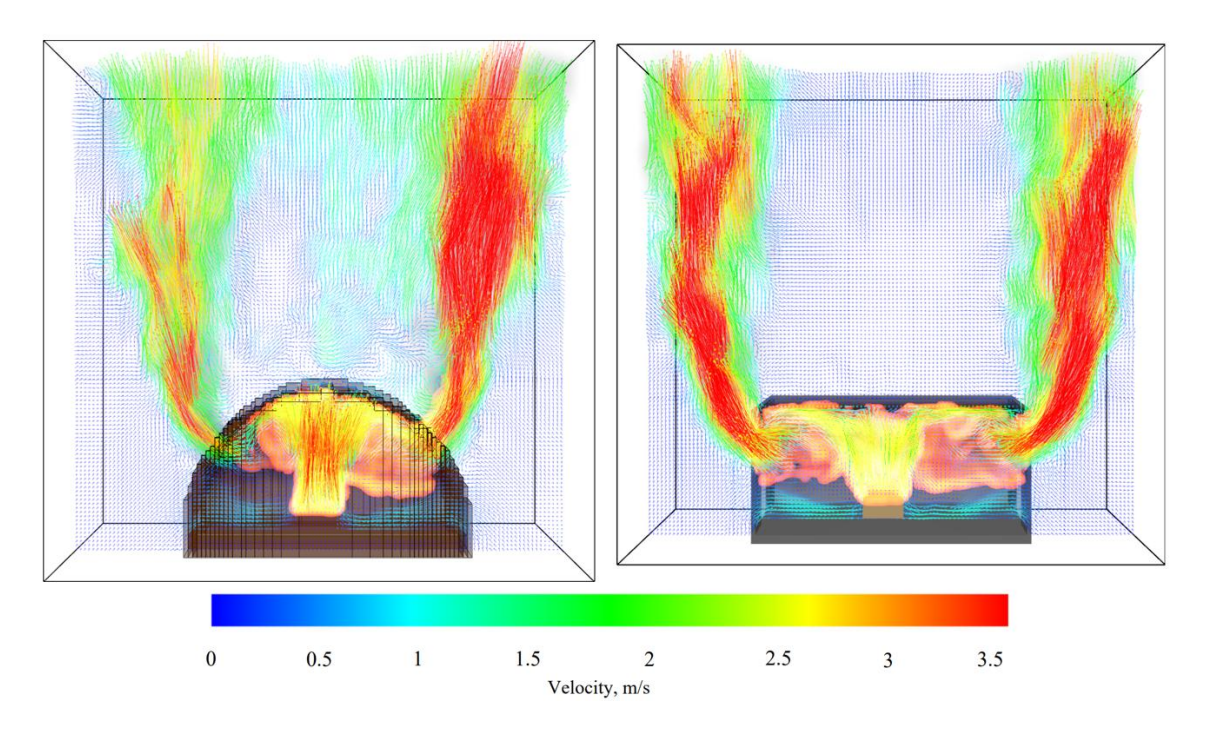


Figure 87: Gas mixture velocity 600 s after fire initiation for curvilinear (left) and 400s after fire initiation for rectilinear (right).

The maximum velocity recorded in the EVF is exceeding 3.5 m/s, this velocity primarily on the centre axis of the EVF throughout for the rectilinear case on both sides. In the curvilinear, a similar trend is observed; however, the velocity distribution is less pronounced compared to the rectilinear case. Further to this, it is noticed that due to the curvilinear geometry there are additional recirculation zones formed outside the compartment, next to the opening, pushing the plume

outward causing further projection of external plume. At the initial stage of EVF flow, an orderly laminar flow projects out from the opening and continues with a high velocity, outside the opening. External combustion exists as the EVF progresses outside the opening since the reaction is supported by the availability of air. Due to the compartment enclosure material, there is significant external flame from both sides of the opening emerging from the rectilinear geometry than curvilinear compartment. As the flow progresses further up, turbulence starts to develop and once the reaction is completed (this can be analysed through the oxygen concentration spatial distribution as seen in Figure 89) the laminar jet turns into a buoyancy driven flow.

b. Temperature field

The maximum temperature distribution is observed with rectilinear geometry, after 10 seconds of fire initiation, where a clear stratification of hot and cold layer inside the compartment and a transient increase in temperature with respect to height. Following this, an increase in the volume of hot upper layer and larger volume of unburned gas flows out in the exterior domain forming larger EVF and a stronger buoyant plume. It is important to note that as the plume further goes up, the EVF temperature decreases with respect to the height.

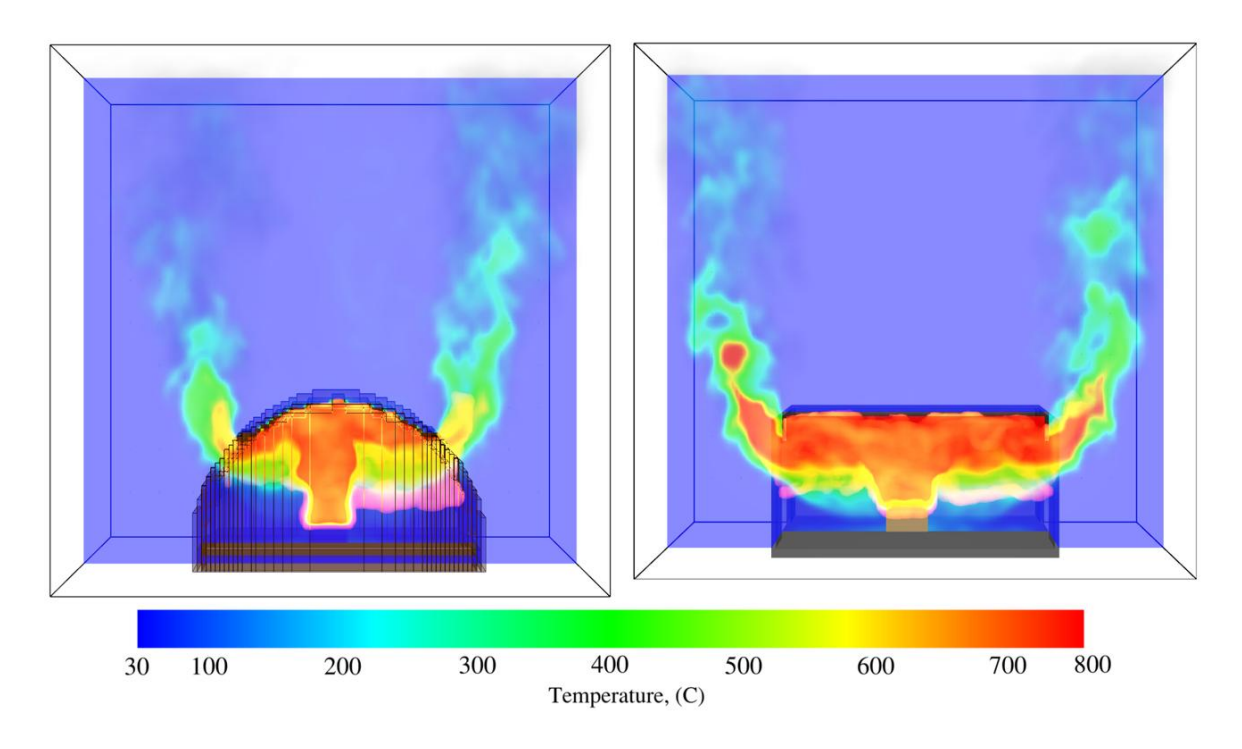


Figure 88: Spatial distribution of gaseous temperature 600 s after fire initiation for curvilinear (left) and 400 s after fire initiation for rectilinear (right).

c. Oxygen concentration field

Figure 89 depicts the spatial distribution of oxygen concentration inside the compartment 600 s after fire initiation for the curvilinear geometry and 400 s for the rectilinear geometry. A lesser concentration of oxygen is observed in rectilinear geometry compared to curvilinear geometry. As stated above, similar to the temperature field, there is a clear distinction of hot and cold zone in FD conditions which is attributed to the incoming flow of cold air from both openings.

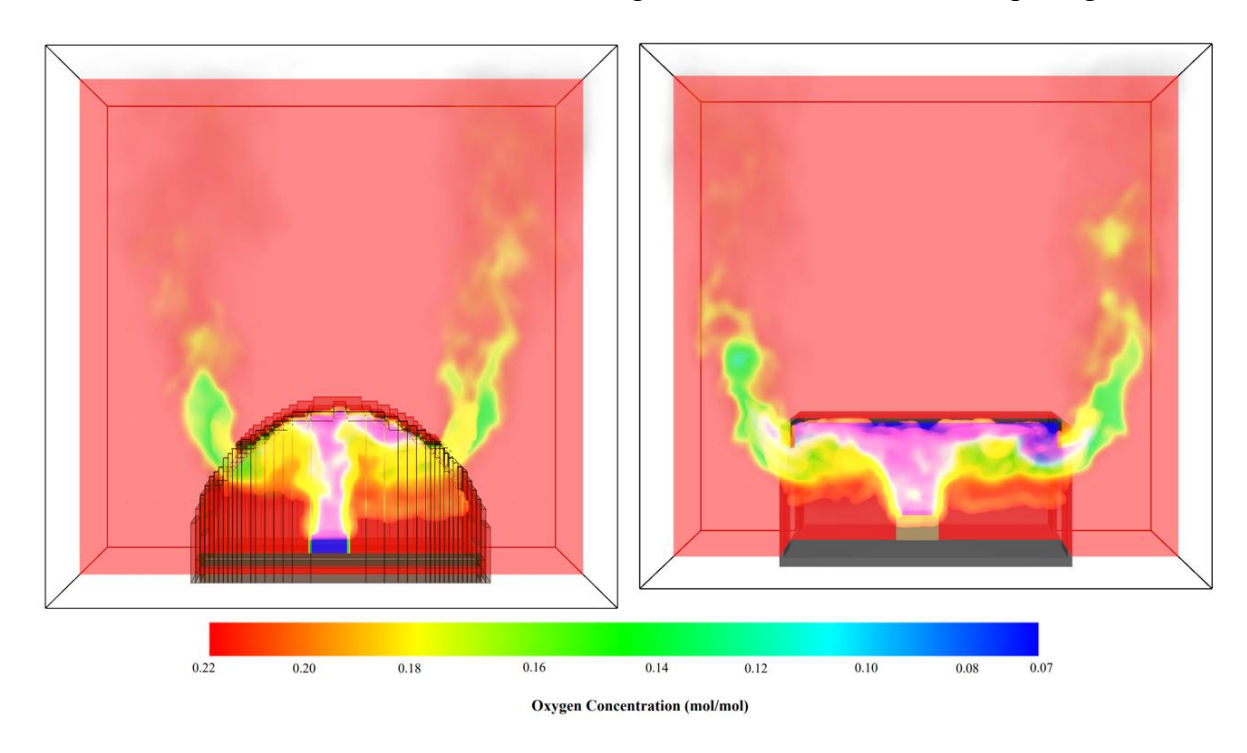


Figure 89: Oxygen concentration 600 s after fire initiation for curvilinear (left) and 400s after fire initiation for rectilinear (right).

Numerical simulations supported the experimental findings, illustrating distinct differences in velocity flow fields, temperature distribution, and oxygen concentration among the two geometries. The rectilinear geometry exhibited stronger plume buoyancy, leading to larger external flames and higher heat flux at the façade surface. In contrast, curvilinear geometries indicated recirculation zones near the ventilation openings, which altered the external flame projection dynamics. Additionally, the outdoor experiments indicated increased combustion and temperature differences due to wind-driven ventilation effects, which reaffirmed the influence of environmental conditions on fire behaviour.

4.8 Conclusion from Numerical investigations

A detailed numerical investigation into the effects of compartment geometry, ventilation configuration, and opening size on compartment fire development and externally venting flames (EVF), supported by validation against medium-scale fire experiments was done in this analysis. Comparative analyses were performed using curvilinear and rectilinear compartments under both FD and NoFD conditions, employing CFD software FDS for numerical modelling.

- Geometry significantly influences the internal temperature field and EVF behaviour. Rectilinear compartments were constructed using Monolux, exhibited higher peak temperatures (experimental: ~750°C; FDS: >900°C) and strong thermal stratification due to heat retention and axial flow behaviour. In contrast, curvilinear compartments, constructed from steel, experienced greater conductive losses and promoted flow recirculation, resulting in more diffused and lower-intensity EVFs (experimental: ~600°C –700°C; FDS: ~800°C) and minimal stratification.
- Larger openings (25 cm × 40 cm) facilitated faster fire growth and clearer peak and decay phases but resulted in lower EVF temperatures (experimental: up to ~180 °C; FDS: 200 °C–250 °C). In contrast, smaller openings (25 cm × 20 cm) introduced ventilation constraints, leading to significantly higher compartment temperatures (experimental: ~300 °C–400 °C; FDS ~ 500 °C). Regarding plume structure, smaller openings produced a stronger, more concentrated plume, particularly under NoFD conditions. Conversely, in the case of curvilinear geometry with larger openings, the plume was significantly weakened, indicating a greater influence of geometric and ventilation interactions on flame dynamics.
- FD conditions enabled bidirectional flow, supporting oxygen supply and enhancing internal combustion, whereas NoFD resulted in unidirectional high-pressure outflows with elevated EVF temperatures. In NoFD, curvilinear compartments saw oxygen depletion (XO₂ < 0.01 mol/mol) and combustion shifted outside the opening. In rectilinear NoFD cases, a minimal oxygen inflow was still observed (XO₂ ~0.10 mol/mol), enabling limited internal combustion. FDS captured these trends but consistently overpredicted peak temperatures, particularly in NoFD conditions.
- EVF Velocity and Flame Projection: EVF plumes in rectilinear NoFD cases reached velocity peaks exceeding 5 m/s, forming a larger laminar jet in greater length. Curvilinear NoFD plumes were lower in momentum (~2.5 m/s–3 m/s) and followed the building curvature, raising potential concerns about fire spread to the façades. FD conditions led to weaker, more laterally dispersed flows (velocities ~3 m/s–4 m/s) in both geometries.

5 EXTERNAL VENTING FLAMES FROM CURVILINEAR ENCLOSURES: A NUMERICAL AND EXPERIMENTAL INVESTIGATION ON THE EFFECTS OF VENTILATION

5.1 Introduction

Large-scale fire experiments play an important role in fire safety engineering, particularly in the development of fire strategies, code development and performance-based design approaches, as they offer critical insights into the behavior of fully developed compartment fires with realistic fuel loads. Unlike small-scale tests, large-scale experiments replicate real-world conditions, capturing the complex interactions of fire dynamics within actual building configurations and construction materials. In recent years, there has been a renewed focus on large-scale structural fire testing, driven by the need to better understand realistic fire behavior and structural performance beyond the limitations of standard testing methods. As highlighted by Bisby et al. (2013), many shortcomings in our understanding of structural response to real fires—especially those related to continuity, restraint, and membrane action—have only become apparent through such full-scale experimental investigations. (Bisby, 2013)

While several large-scale tests have been conducted in the past to study façade fire behavior and EVF, such as the BRE Cardington fire tests, Dalmarnock fire tests (Empis, 2010); EVF geometry under both FD and NoFD conditions (Klopovic and Turan, 2001), (Asimakopoulou, 2016) and the KRESNIK project (Bonner et al., 2021) etc. and these investigations have primarily focused on traditional rectilinear geometries. To address this gap, the present study includes a large-scale experimental investigation of EVF development in curvilinear compartments, offering new insights into how non-orthogonal architectural forms influence flame behavior, thermal exposure, and fire-induced flow characteristics.

5.2 Large Scale Experimental Setup

Aiming to investigate the fire behaviour of the EVF from a curvilinear enclosure a large-scale fire test was performed (Figure 90). Figure 91 presents a schematic drawing of the large-scale compartment. The curvilinear compartment was constructed with steel which has a 4 mm thickness and has a length of 3.5 m, a width of 4 m, and a height of 3 m from floor level to the top. The compartment is of circular section with a total diameter of 4m. However, a perforated floor is provided at a height of 1m from the ground.

To study the influence of ventilation condition on EVF development in these geometries, the compartment is provided with 2 equal sized openings on either side of the wall with a width of 1.1

m and height of 2 m to facilitate "Forced Draught" conditions (FD) and to simulate "No Forced Draught" condition (NoFD), the geometry is restricted to a single opening. Measuring devices are set up in the compartment and outside to measure temperature and heat flux on the façade walls of the geometries.



Figure 90: Indicative photos of fire test configuration and the experimental setup.

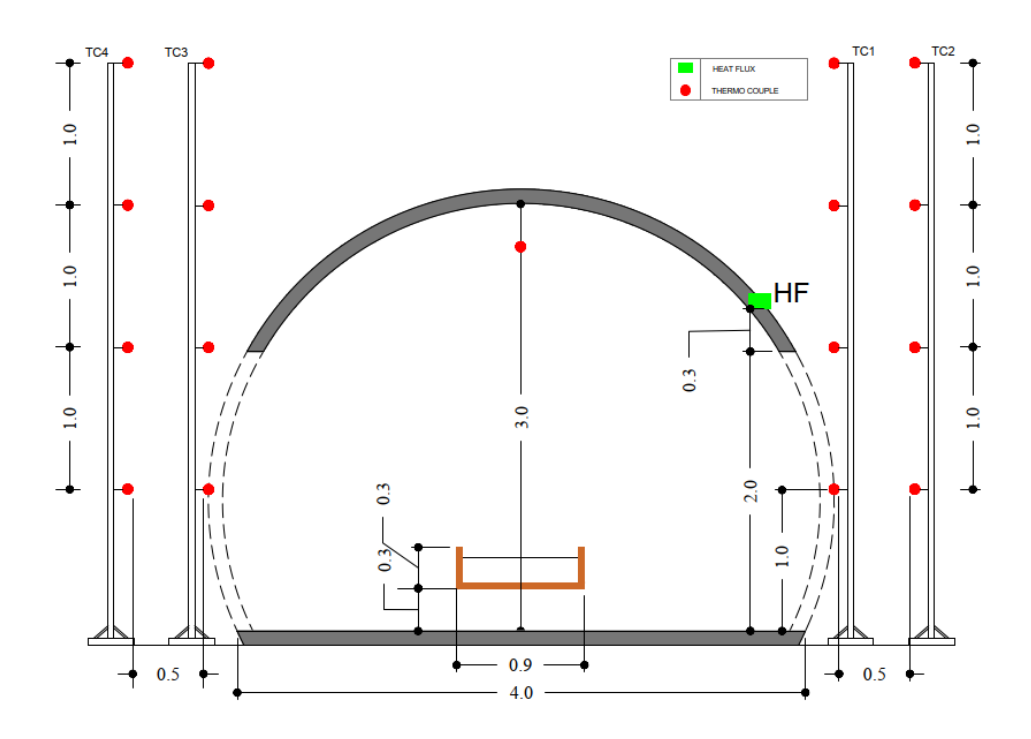


Figure 91: Schematic drawings of the large-scale test setup.

5.2.1 Measuring devices and Data acquisition

The thermal characteristics of EVF from the curvilinear enclosure were assessed through temperature and heat flux measurements. A total of eight K-type thermocouples, each with a

diameter of 1.5 mm, were positioned externally. The schematic layout of the device locations is illustrated in Figure 91. Two thermocouple trees were employed: the first was placed at the centreline of the opening with four thermocouples vertically aligned at 1-meter intervals, while the second was positioned 0.5 meters horizontally from the centreline, following the same vertical spacing. Additionally, an internal thermocouple was installed at the offset 0.8 m from the centre of the compartment, 2.7 meters above the floor, to measure the interior temperature of the compartment. During FD conditions, this thermocouple arrangement was replicated on both sides of the opening. Thermocouples with a measuring range of -50°C to +1250°C and with the limits of error values of ±1.1°C or ±0.4% have been used (Omega, 2023). A water cooled, 25 mm diameter total heat flux sensor SBG01 was located at the 0.3 m above the opening height, i.e. at the centre line of the curvilinear façade surface facing the EVF with a measuring range of 200 x 10³ W/m² with sensor technology of Gardon and Schmidt-Boelter used to measure the total heat flux with an error value of $\pm 2.2\%$ (Hukseflux Thermal Sensors, n.d.). The placement was determined based on guidance from previous research studies on EVF (e.g., (Lee, Delichatsios and Silcock, 2007); (Quintiere and Cleary, 1994); Oleszkiewicz, 1990 and (Ohmiya et al., 2000), which indicate that the region immediately above the opening is critical for capturing the dominant radiative and convective heat fluxes from the façade-impinging flame. In the present work, the heat flux gauge was positioned 0.3 m above the top edge of the opening, aligned normal to the façade surface. This distance was selected to ensure that the measurement captured the upper region of the externally venting flame, where peak incident heat flux is generally observed. Additionally, due to the curvilinear façade geometry, the heat flux distribution was expected to differ from rectilinear cases because of localized flame attachment and curvature-induced flow acceleration. Therefore, locating the gauge 0.3 m above the opening provided valuable information on how façade curvature modifies the thermal exposure zone and radiative feedback to the façade surface.

It is acknowledged that, although this setup captures the dominant flame—façade interaction region, portions of the far-field plume and lateral heat flux variations are not fully recorded. All thermocouples and the heat flux sensor were connected to data loggers for continuous recording. Furthermore, a thermal camera was positioned 6 meters away from the curvilinear structure, oriented toward the side of the test compartment, to monitor the thermal response of the exposed façade.



Figure 92: Indicative photos of fire test configuration and the experimental setup.

A stainless-steel rectangular pan measuring 900 mm \times 900 mm \times 300 mm was positioned at the centre of the compartment, elevated 300 mm above the floor, to contain 20 kg of liquid fuel. Diesel was selected as the fuel for the experiment. The fuel mass was continuously monitored using a load cell with a 200 kg capacity and a sensitivity of 2 mV/V, which was installed beneath the pan. Figure 93 below shows the fuel pan, and the load cell arrangement used in the experimental setup.



Figure 93: Fuel pan height located 0.3 m from the floor.



Figure 94: Indicative photos of fire test configuration and the experimental setup.

Table 9 outlines the test parameters and experimental scenarios considered in this study. A total of two large-scale fire experiments were conducted: one under FD conditions and the other under natural ventilation NoFD conditions, in which only one door remained open during the test.

Table 9: Full scale experimental test scenarios.

Test Case	Unit	Case 1 – FD-Curv	Case 2 – NoFD-Curv
Height of Opening	m	2	2
Width of Opening	m	1.1	1.1
Opening at Both sides	-	Yes	No
Amb. Temperature	С	25	34
RH	%	50%	51%
Duration	sec	1350	1240
Mass	kg	21.59	21.21

5.2.2 Simulation details.

FDS was used as the CFD tool for this numerical investigation. The use of curvilinear geometries in FDS had already been validated in the previous chapter through comparison with medium-scale experimental results. All curvilinear surfaces, including walls and floors, were modelled as solid boundaries with material properties representative of steel: a density of 7850 kg/m³, specific heat capacity of 0.46 kJ/kgK, thermal conductivity of 45.8 W/mK, thickness of 0.02 m, and surface emissivity of 0.95.

Diesel fuel was used as the fire source, with a soot yield of 0.03 kg/kg, heat of combustion of 43.4 mJ/kg and a carbon monoxide (CO) yield of 0.02 kg/kg, based on values reported by Tewarson et al. (2008). Diesel fuel combustion efficiency in a liquid pool fire varies depending on conditions, but studies report values ranging from 0.68 to 0.85 (Liang et al., 2006). The current analysis a combustion efficiency of 0.7 was used for the HRR calculation. The computational domain was appropriately extended to capture the full geometric and thermal characteristics of the externally venting flames (EVF). A fine mesh resolution was used, maintaining a D*/dx ratio of 16, which corresponds to a grid cell size of 0.05 m.

5.3 Result and Discussion

5.3.1 Fuel mass loss and HRR

Figure 95 depicts the fuel mass and HRR for the FD condition, both of which demonstrates a consistent combustion process facilitated by stable ventilation from both sides of the curvilinear compartment. The initial fuel load of approximately 21 kg decreases gradually and steadily throughout the 1300 second duration of the experiment, indicating effective and sustained fuel

consumption The HRR curve, derived from the fuel mass loss rate, exhibits periodic peaks reaching values of up to approximately 3500 kW. These recurring peaks are observed throughout the experiment and suggest transient intensification of combustion, likely influenced by localized turbulence and dynamic interactions between the flame front and the incoming air through the compartment openings.

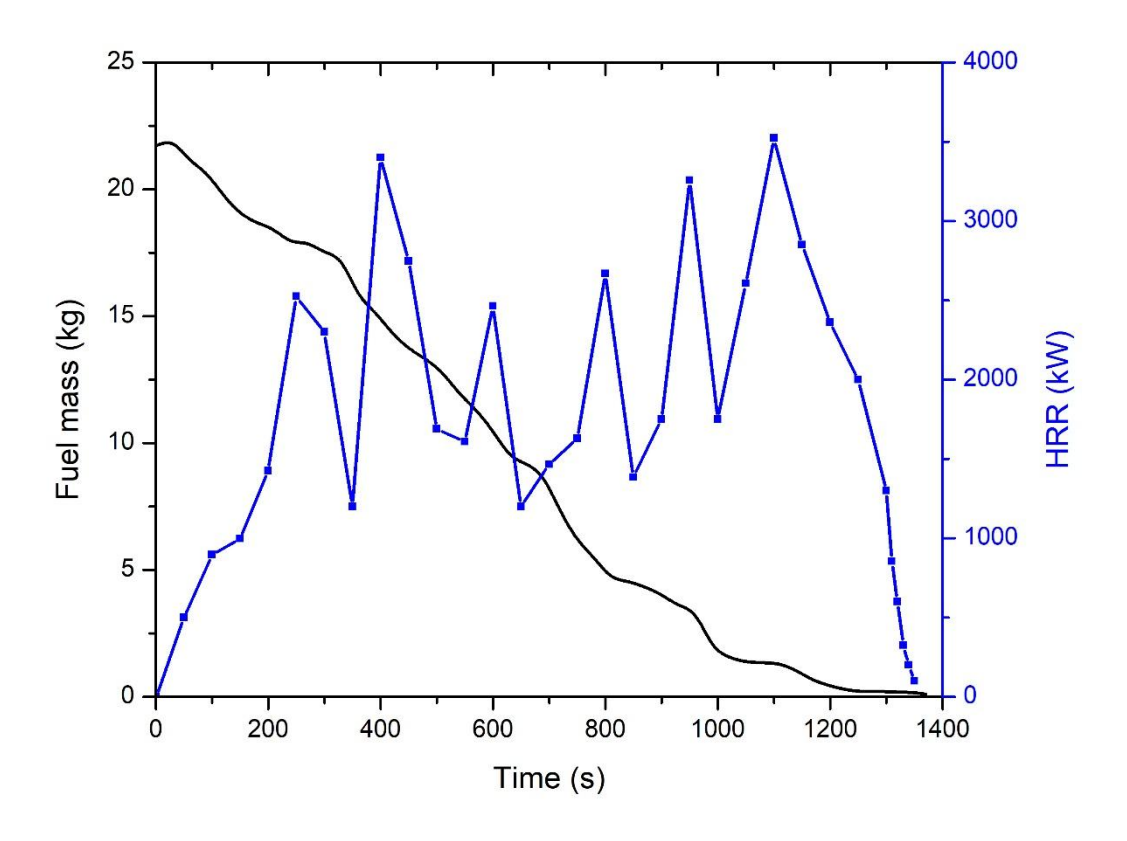


Figure 95: Fuel mass loss and measured heat release rate for FD condition.

Figure 96 presents the fuel mass and HRR curves for the NoFD condition. In contrast to the FD condition, the combustion process in the NoFD scenario shows a delay in the fire initiation and growth, with minimal fuel consumption observed during the first 300 seconds of the test. The initial fuel mass remains close to 21 kg for this duration, indicating limited ignition and sustained flaming, however, once combustion becomes fully established, a more rapid decrease in fuel mass is observed between 400–800 seconds, suggesting an onset of sustained burning. The HRR shows a slow growth in the HRR but a sharp peak HRR reaching approximately 5800 kW around 1200 seconds this is almost 30% higher than the peak in the FD case.

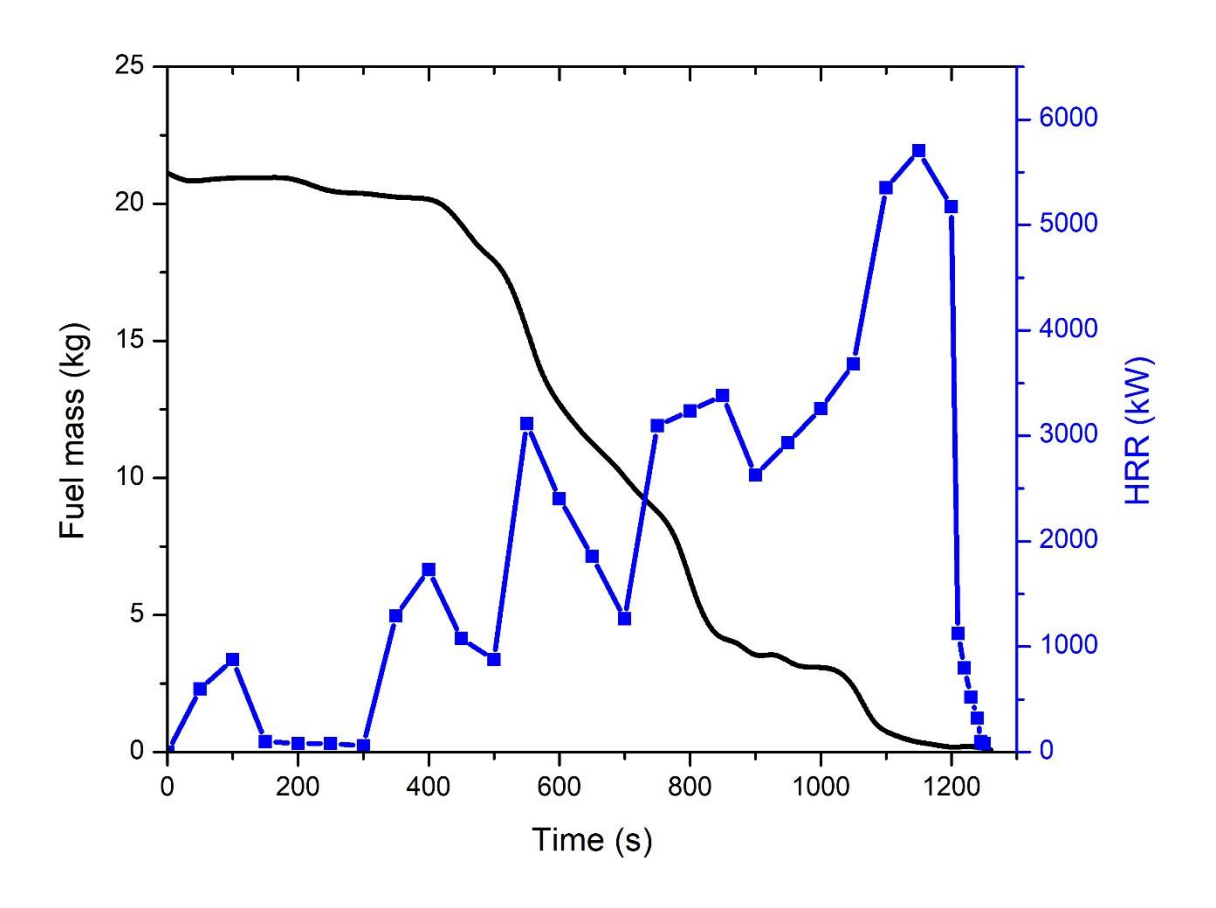


Figure 96: Fuel mass loss and measured heat release rate for NoFD condition.

5.3.2 Interior gas temperature.

The temporal evolution of the compartment gas temperature is presented in figure 97, depicting the fire development stages under both FD and NoFD conditions. The measurements were taken using a thermocouple placed at 2.7 m above the floor level and horizontally offset by 0.5 m from the center of the compartment. In both FD and NoFD experimental scenarios, the temperature profiles clearly exhibit the characteristic phases of fire growth, fully developed stage, and decay, except in the case of FD. The FD condition shows a rapid temperature rise, peaking around 450°C, and maintains elevated temperatures over an extended duration without a distinct decay phase. In contrast, the NoFD condition reaches approximately similar temperature that of FD condition, however, shows an earlier onset of decay. The numerical simulation for the FD condition shows a peak temperature of approximately 620°C, which is about 20–30% higher than the experimental value.

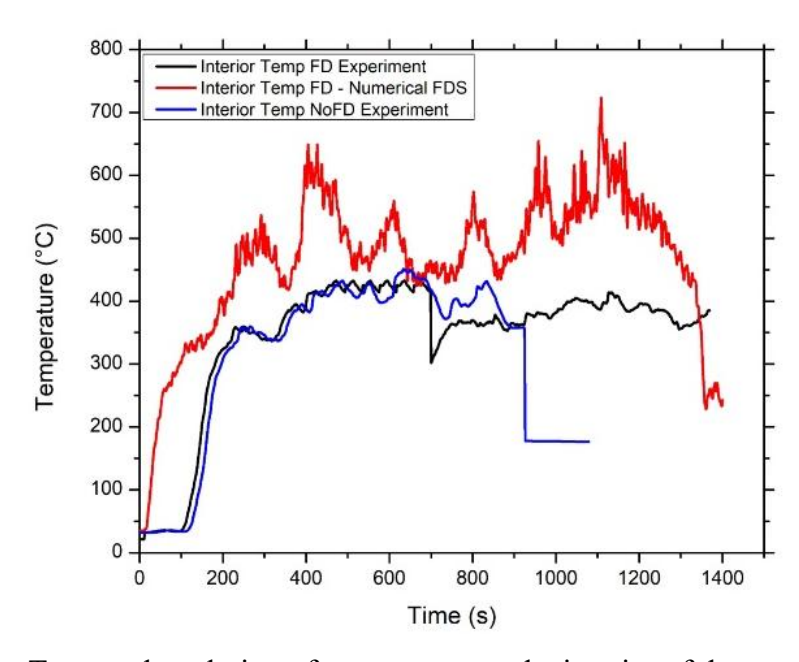


Figure 97: Temporal evolution of temperature at the interior of the compartment

5.3.3 Heat Flux

Figure 98 depicts the temporal evolution of heat flux to the façade wall, heat flux are located at the façade wall at a height 0.3 m from the opening. In the experimental results (Figure 98 left), the heat flux values for both the FD and NoFD conditions demonstrate a consistent trend, with the NoFD case exhibiting slightly higher peak values compared to the FD case. Specifically, the peak heat flux for the NoFD condition reaches approximately 18 kW/m², while the FD condition peaks around 16 kW/m². This increased thermal exposure in the NoFD condition can be attributed to the limited ventilation, which allows more combustion products to accumulate near the façade, enhancing radiative heat transfer. In contrast, the numerical simulations using FDS (Figure 98 right) significantly overpredict the heat flux values for both scenarios. The FD simulation shows heat flux values fluctuating up to 40 kW/m², whereas the NoFD simulation reaches extremely high values close to 80 kW/m². These elevated values may result from limitations in the radiation model or ambient boundary condition setup in the FDS. Overall, the NoFD condition consistently exhibits higher heat flux values in both experimental and simulation cases due to the reduced ventilation, which results in a longer residence time of hot gases near the façade. Both the radiation model and the ambient boundary-condition setup in FDS can contribute to this discrepancy. The large-scale experiments were conducted outdoors, so small drafts/crosswinds could influence the EVF temperatures outside the opening (dilution, plume deflection, enhanced convective cooling). In the FDS setup these effects were not accounted for.

For the current study, additional simulations were not considered with alternative radiation settings. However, the notable overprediction by FDS highlights the importance of careful

calibration and validation against experimental data when using CFD tools for heat flux assessment on building facades and this has been added to the Future work section.

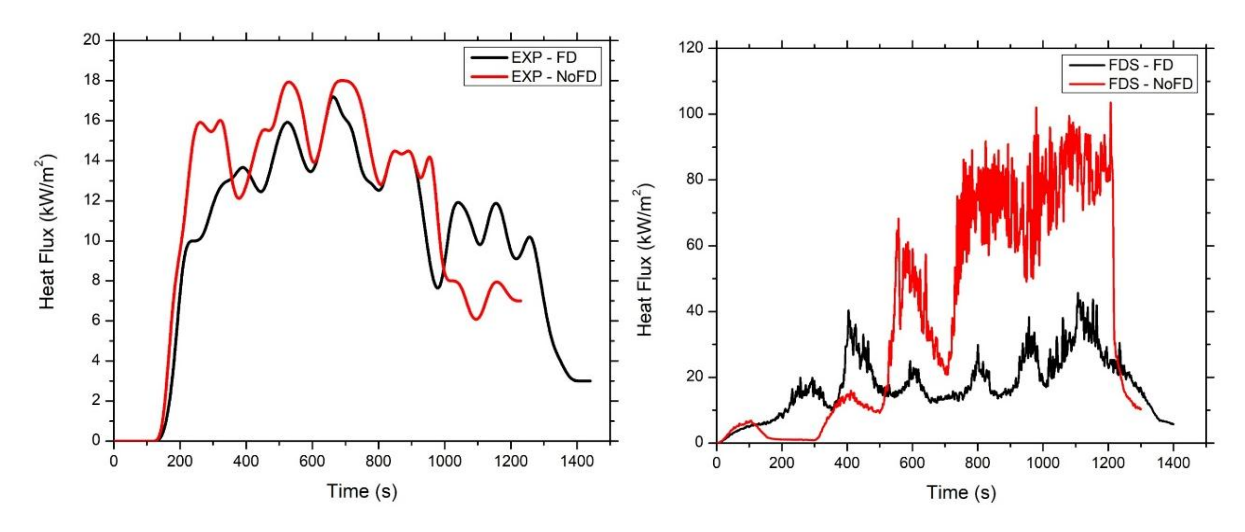


Figure 98: Temporal evolution of heat flux to the façade wall, at a height 0.3 m from the opening for experiment (left) and for FDS cases (right).

5.3.4 EVF temperature

To assess the EVF plume development from the curvilinear compartment, two thermocouple trees TC1 and TC2 were strategically positioned outside the opening as depicted in the Figure 91. TC1 was aligned centrally at the compartment opening, with four K-type thermocouples mounted at 1-meter intervals, beginning from 1.0 m at the centre the opening. TC2 was placed at a horizontal distance of 0.5 m from the opening centreline, mirroring the same vertical distribution of thermocouples. This setup enabled spatially resolved temperature measurements in the EVF plume.

The EVF temperature data were averaged over four temporal windows: 0–300 s, 300–600 s, 600–900 s, and 900–1200 s. A comparative analysis was conducted between the FD and No NoFD conditions. Furthermore, to characterize the EVF temperature envelope, Eurocode-based correlations were applied to estimate average EVF temperatures as a function of flame length and distance from the façade. This approach allowed the comparison of experimentally measured data with standardized design equations for thermal actions on external surfaces. The resulting data provide insight into the influence of ventilation conditions on façade thermal exposure, relevant for performance-based design applications in non-orthogonal geometries.

Figure 99 (left) presents the vertical temperature distribution measured at 300 seconds using Thermocouple Trees TC1 and TC2 for both FD and NoFD conditions. TC1 is aligned with the centerline of the compartment opening, while TC2 is positioned 0.5 m horizontally from the

center. During the initial 300 seconds of the experiment, the average heat release rate (HRR) was approximately 1100 kW for the FD case and 257 kW for the NoFD case. Despite the significantly lower HRR in the NoFD scenario, the external gas temperatures recorded are notably higher than those in the FD condition. At TC2, temperatures in the NoFD case peaked at around 130°C, compared to 70°C in the FD case. This is largely due to the ventilation condition, as in the NoFD condition, all combustion gases and smoke exit through a single opening, resulting in a concentrated, high-temperature plume that directly impacts the façade. In contrast, the FD condition, where openings on both sides promotes more balanced and distributed flow, reducing localized thermal exposure on either side.

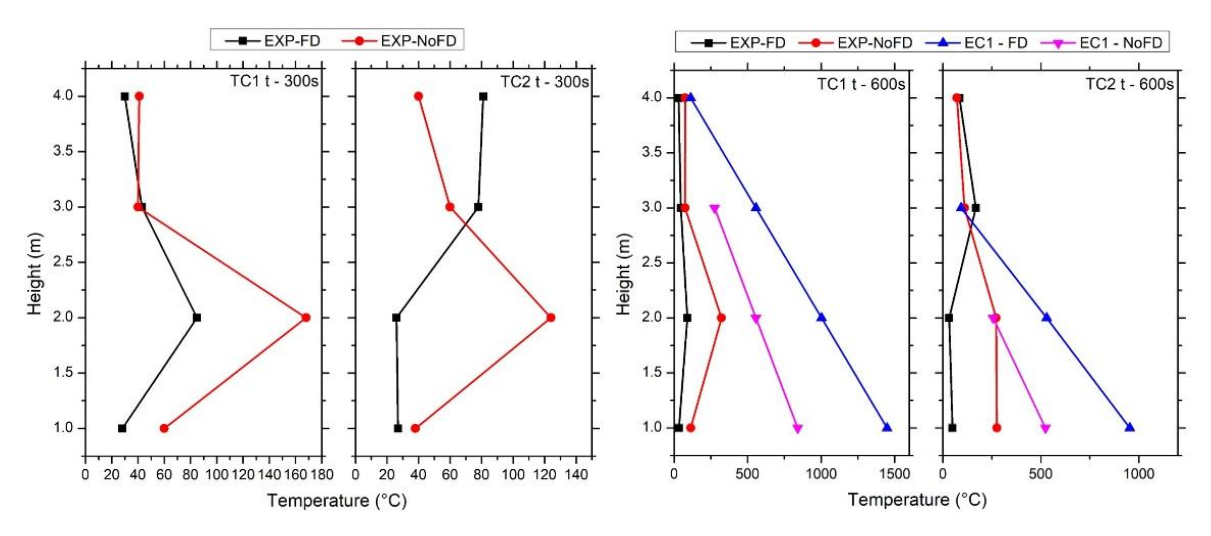


Figure 99: Time averaged EVF centreline temperature for experimental values FD and NoFD cases for 300 seconds (left) and 600 seconds (right).

Application of the Eurocode EC1 centerline flame temperature equation was assessed for both cases. However, the dimensionless parameter $\frac{L_x\sqrt{A_v}}{Q} < 1$ was found to be below the lower threshold of 1 in both scenarios, indicating the formula falls outside its valid range.

Figure 99 (right) depicts the vertical temperature profiles measured at 600 seconds at both TC1 and TC2 for the FD and NoFD conditions. During this interval (300–600 seconds), the HRR was 2185 kW for the FD condition and 1508 kW for the NoFD condition. In both thermocouple trees, experimental data show elevated temperatures at lower heights, with a gradual decrease in temperature observed toward the top. Notably, the NoFD case continues to display higher exterior façade temperatures due to the unidirectional flow of hot gases through the single opening, resulting in a concentrated plume impacting the same region of the façade. This behavior contrasts with the FD case, where bi-directional flow allows for more even plume dispersion and reduced peak surface exposure. EC1 centreline temperature predictions were also evaluated for both ventilation scenarios. For TC1, the EC1 equation under the NoFD condition becomes invalid at 4

m height, as the dimensionless applicability parameter $\frac{L_x\sqrt{A_v}}{Q}$ < 1 falls outside the specified range in EC1. Similarly, for TC2, the EC1 correlation is not valid at both 3 m and 4 m heights in the NoFD case and also becomes inapplicable at 4 m in the FD case. In general, EC1 predictions tend to overestimate the centreline temperatures at lower heights. However, as the vertical height increases, the predicted temperatures align more closely with the experimental values—until the equation becomes invalid at higher levels due to the applicability limits.

Average EVF temperate for 900 seconds measured by thermocouple trees TC1 and TC2 is presented in Figure 100 (left). The average HRR between 600 to 900 s was 1794 kW for the FD condition and 2500 kW for the NoFD condition. This higher HRR in the NoFD condition indicates the fire behavior due to restricted ventilation in the compartment, where all combustion gases exit through a single opening, resulting in greater thermal impact at the façade. For TC1, temperatures at 2 m reached approximately 250 °C for FD and 400 °C for NoFD, indicating a 37.5% increase in the latter. At 3 and 4m, both cases exhibited similar temperatures approximately in the range of 300 °C. For TC2, which is offset 0.5 m horizontally, the temperature of NoFD yields a more concentrated and vertically rising plume, producing higher façade exposure temperatures at all levels compared to the FD conditions. Eurocode EC1 predictions were also assessed for both conditions. For TC1, the EC1 equation was not applicable at 4 m height in the FD case, where it overpredicted the temperature significantly compared to the experiment. In the NoFD case, EC1 remained applicable across most heights but still demonstrated overpredictions, especially at lower heights. For TC2, the EC1 equation was not applicable at both 3 m and 4 m in the NoFD case, and also at 4 m in the FD scenario. Despite being within the applicable range at lower heights, EC1 consistently overestimated the temperatures, under NoFD conditions.

Figure 100 (right) depicts the EVF profile at 1200 seconds. The average HRR between 900–1200 seconds was 2725 kW for the FD and 3450 kW for the NoFD condition. EC1 was not applicable for FD conditions. For NoFD, EC1 was within its applicability limits, however over predicted the temperature.

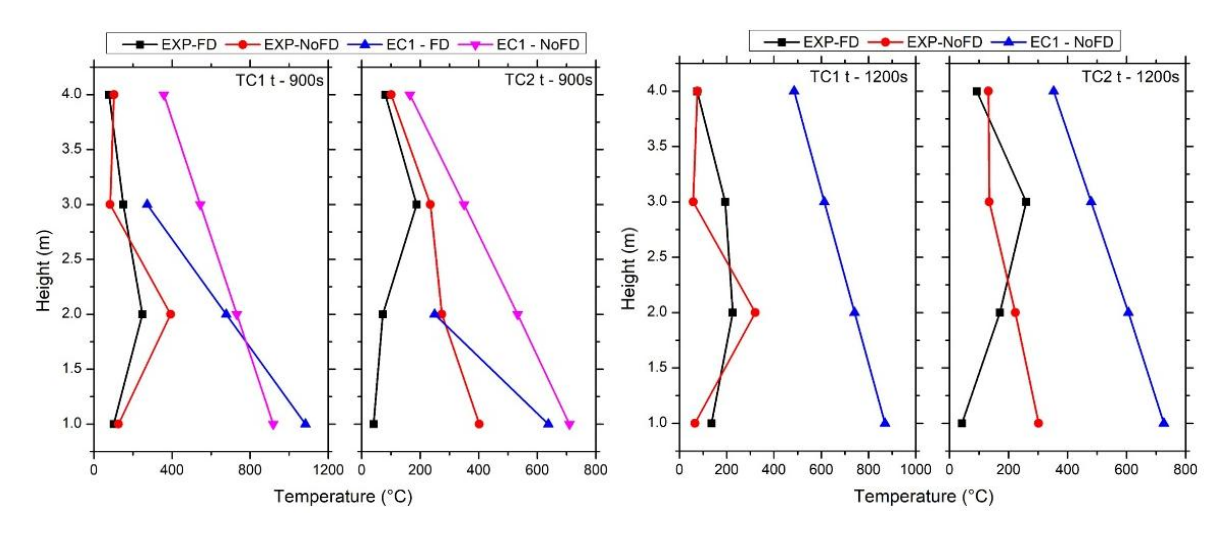


Figure 100: Time averaged EVF centreline temperature for experimental values compares with EC1 for FD and NoFD cases for 900 seconds (left) and 1200 seconds (right).

5.3.5 EVF Centreline temperature contours.

Figures 101 (left) and (right) depicts the comparison of EVF temperature fields at 300 seconds and 600 seconds under FD conditions, from both experimental measurements and FDS simulations. The results considering the average temperatures between 0–300 seconds and 300-600 seconds. At 300s, as the fire is still growing only, the maximum EVF temperatures were observed near the centreline of the plume, reaching approximately in the range of 80°C –100°C at a height of around 2.5 m and 0.1–0.2 m horizontal distance from the compartment opening. In contrast, the FDS-predicted plume exhibited substantially higher temperatures, with peak values approaching approximately 300°C in the same region. At 2 meters, the FDS simulation overpredicted centreline temperatures significantly, however, at 3 meter and 4 meters both results show in the same range. A similar trend is observed at 600 seconds, where the experimental plume exhibits slightly increased temperatures considering 300seconds, because fire in the compartment is increase in terms of HRR and hot gases are started exiting through the upper part of the opening. FDS also predicts even higher values approaching 470°C–490 °C in the same region.

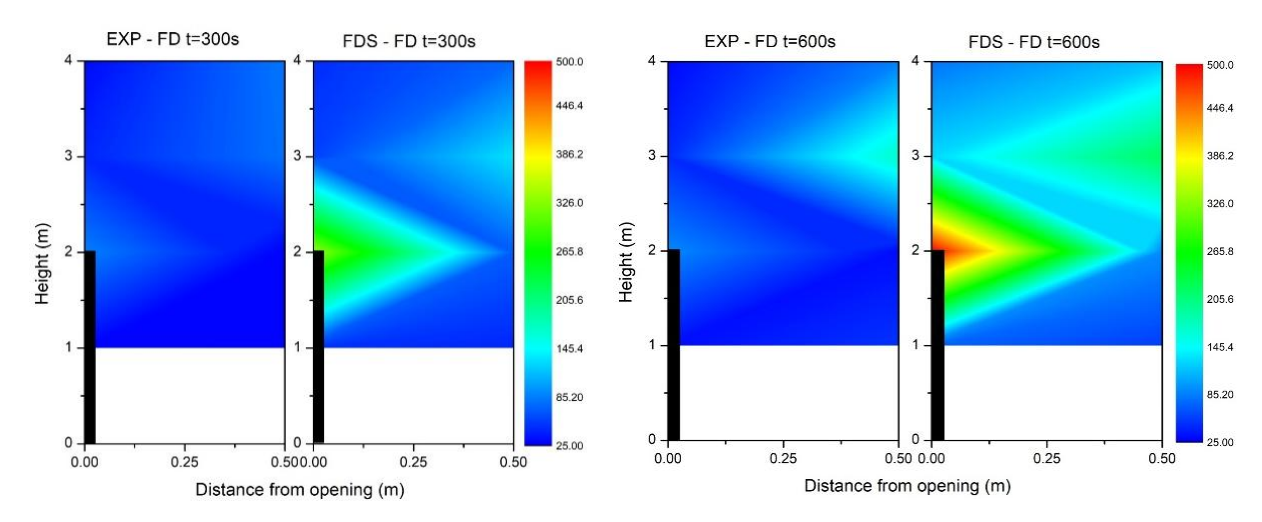


Figure 101: Time averaged EVF centreline temperature for experimental values FD case and numerical values (FDS) for 300 seconds (left) and 600 seconds (right).

Figures 102 (left) and (right) depicts the comparison of EVF temperature fields at 900 seconds and 1200 seconds under FD conditions with experiment and FDS results. At 900 seconds, the fire remains in a quasi-fully developed stage, with intensified combustion and increased gas flow toward the upper portion of the compartment opening. As a result, both the experimental and FDS depict elevated temperature distributions compared to earlier stages. The experimental field shows a smoother gradient, while the FDS results indicate a localized hot zone near the upper edge of the opening, with peak temperatures approaching 500°C indicating an overprediction relative to measured values. This discrepancy becomes more evident at 1200 seconds, where the fire reaches a fully developed phase with higher HRR. The temperature field further intensifies, with FDS again exhibiting concentrated hot zones near the opening that exceed experimental estimates.

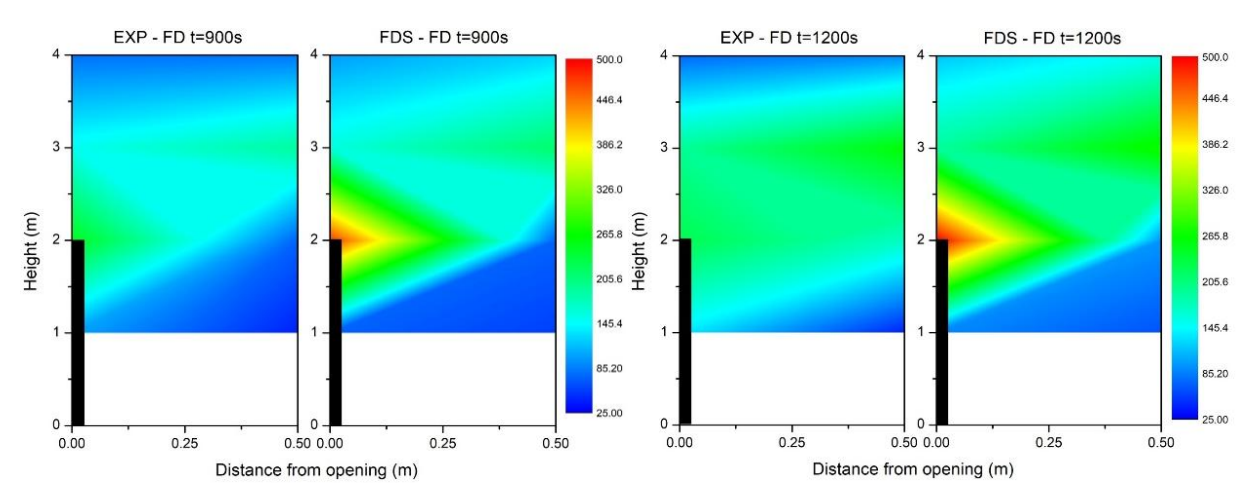


Figure 102: Time averaged EVF centreline temperature for experimental values FD case and numerical values (FDS) for 900 seconds (left) and 1200 seconds (right).

Figure 103 presents a comparison of EVF temperature fields at 1350 seconds under FD conditions based on both experimental and FDS results. At this stage, the fire appears to be transitioning toward the decay phase, as indicated by a slight reduction in HRR observed in earlier analyses. The experimental temperature distribution exhibits a more diffused and vertically extended thermal plume, with temperatures gradually decreasing from approximately 300°C near the opening to below 100°C at a height of 4 m. This trend reflects the typical cooling effect as the hot gases rise and entrain ambient air. In contrast, the FDS simulation shows a more localized high-temperature region near the upper edge of the opening, with peak values exceeding 400°C, suggesting an overprediction relative to the experimental data.

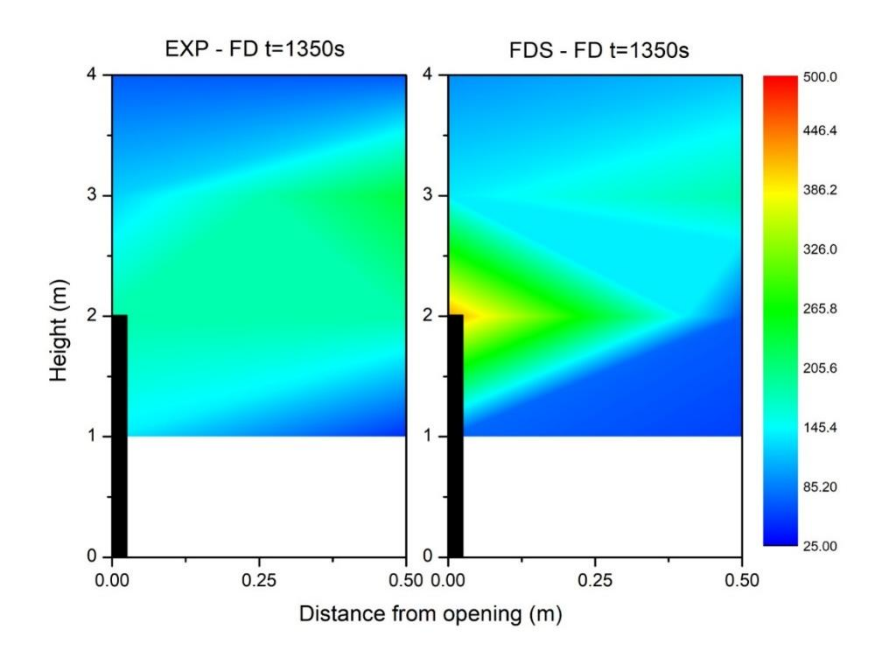


Figure 103: Time averaged EVF centreline temperature for experimental values FD case and numerical values (FDS) for 1350 seconds.

Figures 104 (left) and 104 (right) present the comparative temperature contours of EVF at 300 seconds and 600 seconds, respectively, under the NoFD condition from both experimental measurements and FDS simulations. At 300 s, the compartment is in the early growth phase, with minimal outflow observed from the opening. The EVF plume is yet to form and thermal stratification within the enclosure dominates the temperature field. The experimental data shows a relatively low and horizontally diffused thermal field, with temperatures gradually pointed upward, indicating a limited extent of flame projection. In contrast, FDS results reflect a slightly increased temperature gradient with a more localized thermal field around the upper edge of the opening. By 600 s, the compartment progresses further into the growth phase, with increased heat release and pronounced smoke and hot gas discharge through the single available opening. The experimental thermal field depicts an intensified and vertically extended EVF plume, with elevated temperatures distributed up to 2-3-meter height and temperature is seen to be consistent

for TC2 as well. However, FDS underpredicts the near-opening temperature region captured by Thermocouple Tree 1 (TC1), especially near 2 m height and at the centre of the opening. At greater vertical heights (above 3 m), the simulation tends to overestimate the temperature relative to experimental data. This overprediction becomes particularly evident in Thermocouple Tree 2 (TC2), positioned 0.5 m horizontally from the opening centreline, where FDS shows a broader and higher temperature profile than recorded in the experiment.

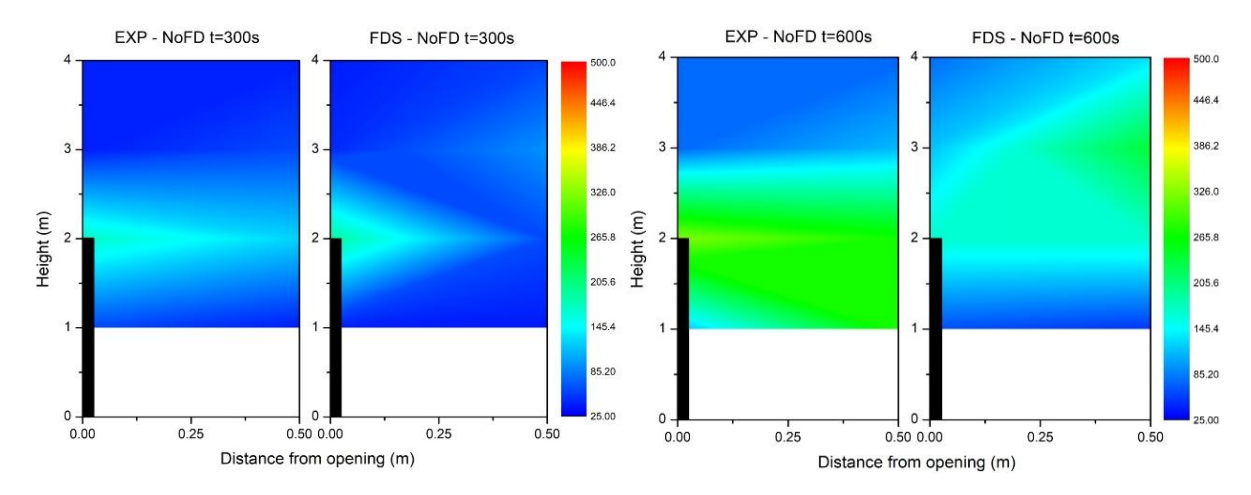


Figure 104: Time averaged EVF centreline temperature for experimental values NoFD case and numerical values (FDS) for 300 seconds (left) and 600 seconds (right).

Figures 105 (left) and (right) depicts the comparison of EVF temperature profiles at 900 s and 1200 s for the NoFD condition based on both experimental measurements and FDS simulations. At 900 seconds, the fire reaches its fully developed, corresponding to the higher HRR of 2500kW. In the experimental plot, the temperature distribution near the opening shows a higher temperature of 320 °C at the edge of the opening at 2 m height and gradually reducing with vertical height. The FDS simulation at the same times reveals a stronger and more buoyant thermal plume, with significantly higher predicted temperatures near the opening. For example, the FDS-predicted temperature at 2 m height for Thermocouple Tree 1 (TC1) exceeds 700 °C, while experimental values remain substantially lower. Although trends are broadly consistent across TC1 and TC2, FDS overprediction becomes slightly increased at higher elevations. At 1200 seconds, as the fire becomes fully developed, the plume becomes denser and stronger. The experimental data show that temperature at 2 m height near the opening peaks at approximately 320 °C, with a gradual decline observed at higher elevations. However, the FDS simulation predicts considerably higher temperatures, reaching nearly 700 °C at the same height and location showing an overprediction of the thermal buoyancy and plume strength. In general, a consistent decrease in temperature with increasing vertical height is observed, aligning with the typical behavior of EVFs dissipating temperature energy as they rise.

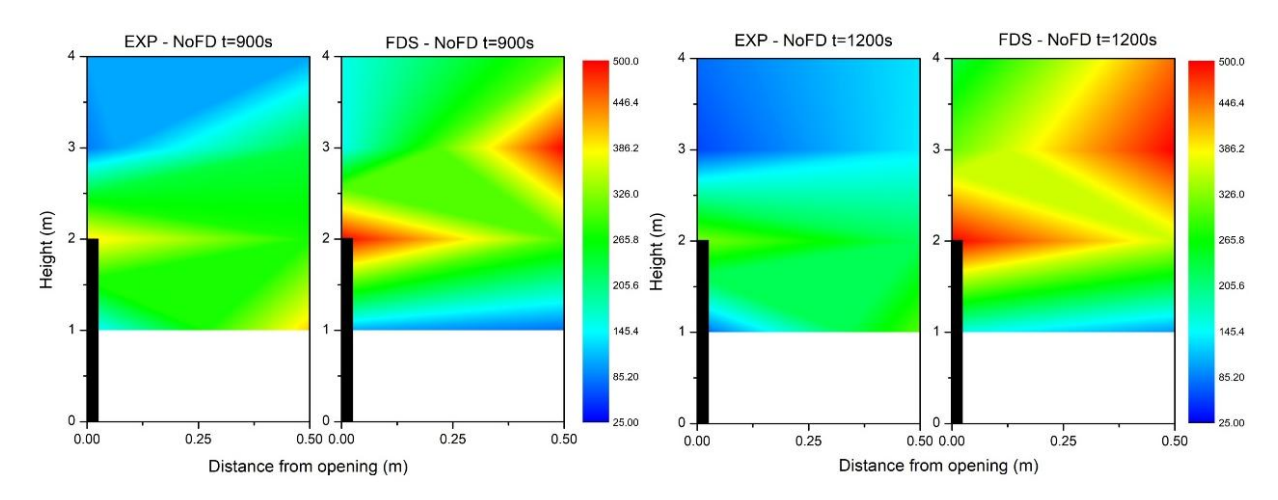


Figure 105: Time averaged EVF centreline temperature for experimental values NoFD case and numerical values (FDS) for 900 seconds (left) and 1200 seconds (right).

5.3.6 EVF Thermal Field

Figure 106 compares the FDS-predicted temperature fields for FD and NoFD conditions at 1100 seconds and 1150 seconds respectively. The time points selected based on the corresponding maximum HRR and prominent EVF development in each case. In the FD condition (1100 s), a clear thermal stratification is evident within the compartment, characterized by a distinct separation between the hot upper layer and cooler lower layer. The maximum gas temperature within the compartment reaches approximately 550°C–600 °C, indicating a well-ventilated, quasisteady fire behavior where hot gases are effectively exhausted through both side openings.

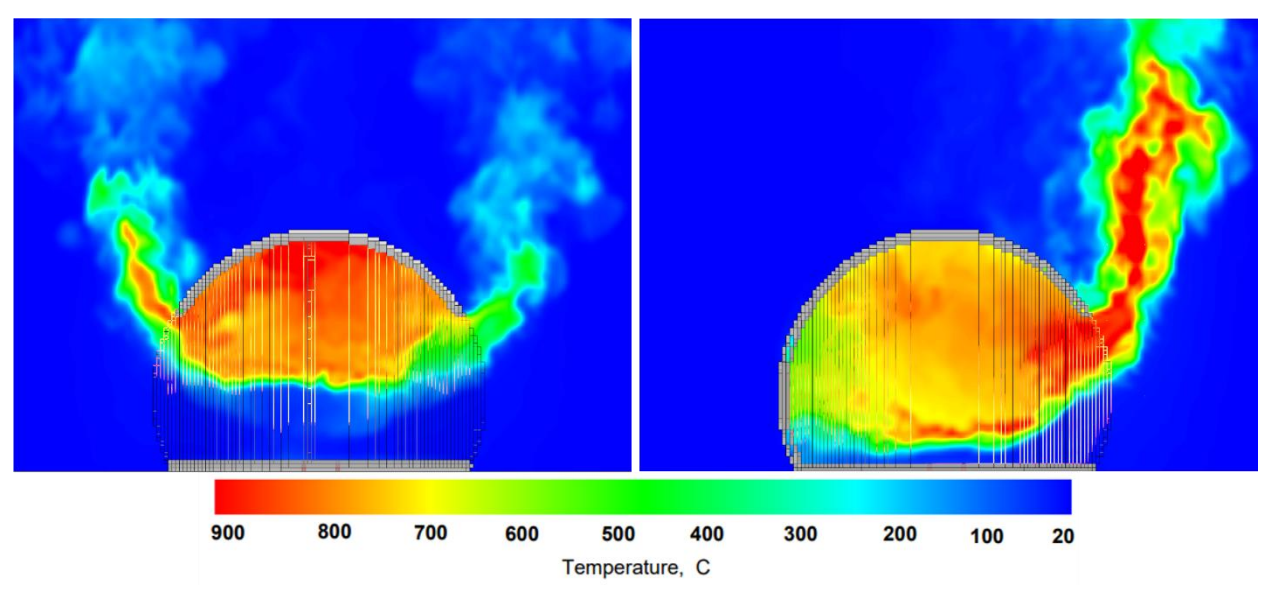


Figure 106: Spatial distribution of gaseous temperature 1100 s after fire initiation for FD case (left) and 1150s after fire initiation for NoFD case (right).

Conversely, in the NoFD condition at 1150 s, the temperature distribution reveals a nearly homogenous hot gas layer filling the entire compartment volume, with limited to no stratification. The maximum internal gas temperatures are observed around 800 °C, indicating a more intense

thermal environment due to the single opening present in the compartment. The single opening in NoFD restricts smoke and heat dissipation, resulting in heat accumulation and higher compartment temperatures. Furthermore, the EVF in the NoFD scenario is significantly stronger, with a continuous, buoyant flame plume extending vertically from the opening, exhibiting temperatures exceeding 900 °C. In contrast, the FD case shows a relatively weaker EVF with moderate plume. The enhanced flame visibility and higher external temperatures in NoFD highlights the critical role of ventilation in fire behavior and EVF exposure to the façade.

5.3.7 EVF gas mixture velocity flow field

Figure 107 depicts the velocity vector fields and flow behaviour of EVF for the FD and NoFD conditions, respectively. In the NoFD condition, the flow is distinctly unidirectional, with all hot gases exiting through a single opening. The plume velocity exceeds 8 m/s even at higher elevations, indicating strong thermal buoyancy and a high-momentum outflow. Conversely, in the FD condition, a characteristic bi-directional flow pattern is observed at both openings, as the fresh air enters from the lower part of the openings while hot gases exit through the upper region. This ventilation arrangement supports sustained combustion while preventing excessive pressure buildup within the compartment. The velocity of the gases exiting through each side of the opening in the FD case also approaches 5 m/s, but with more balanced and symmetrical behaviour compared to the NoFD condition. In both configurations, due to the curvilinear geometry of the compartment, localized recirculation zones are visible near the opening edges. These zones are likely induced by curvature-induced deflection of the flow and influence the stability and structure of the EVF.

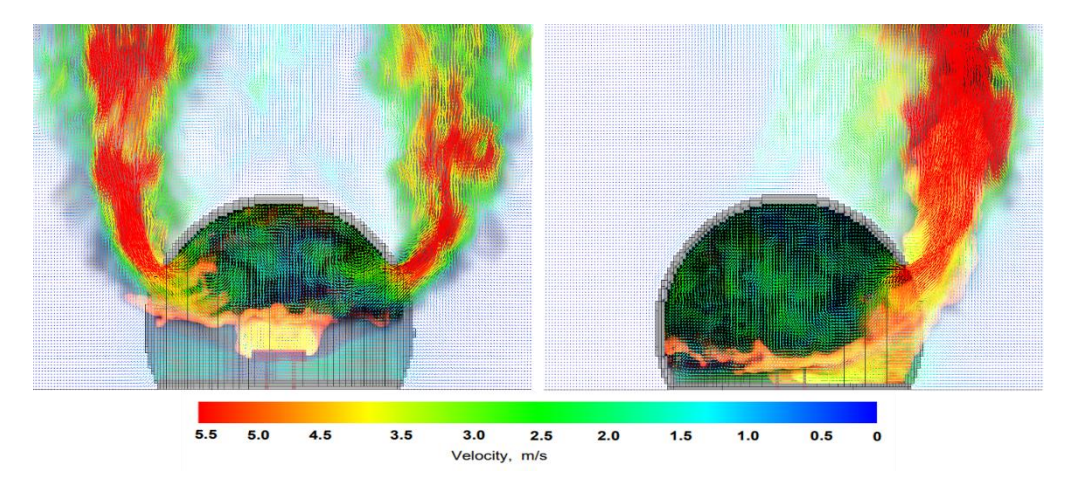


Figure 107: Gas mixture velocity 1100 s after fire initiation for FD case (left) and 1150s after fire initiation for NoFD case (right).

5.3.8 Oxygen Concentration

Figure 108 present the oxygen concentration fields within the curvilinear compartment under FD) and NoFD conditions at 1100 s and 1150 s, respectively. Under FD conditions, a clear stratification of oxygen is observed. The lower portion of the compartment near the openings maintains higher oxygen levels (0.14 mol/mol – 0.2 mol/mol), facilitating continued combustion, while the upper region is oxygen-depleted (below 0.05 mol/mol) due to the accumulation of combustion products. This stratification supports the bi-directional flow pattern where fresh air enters through the bottom and hot gases exit from the top openings on both sides. In contrast, the NoFD condition reveals a nearly complete depletion of oxygen across the compartment, especially near the upper region, where oxygen levels drop below 0.02 mol/mol. The entire compartment appears filled with combustion products, indicating a single opening-induced unidirectional flow that limits fresh air ingress. As a result, combustion becomes externally supported, and a more intense EVF is formed, as previously seen in the temperature field analysis.

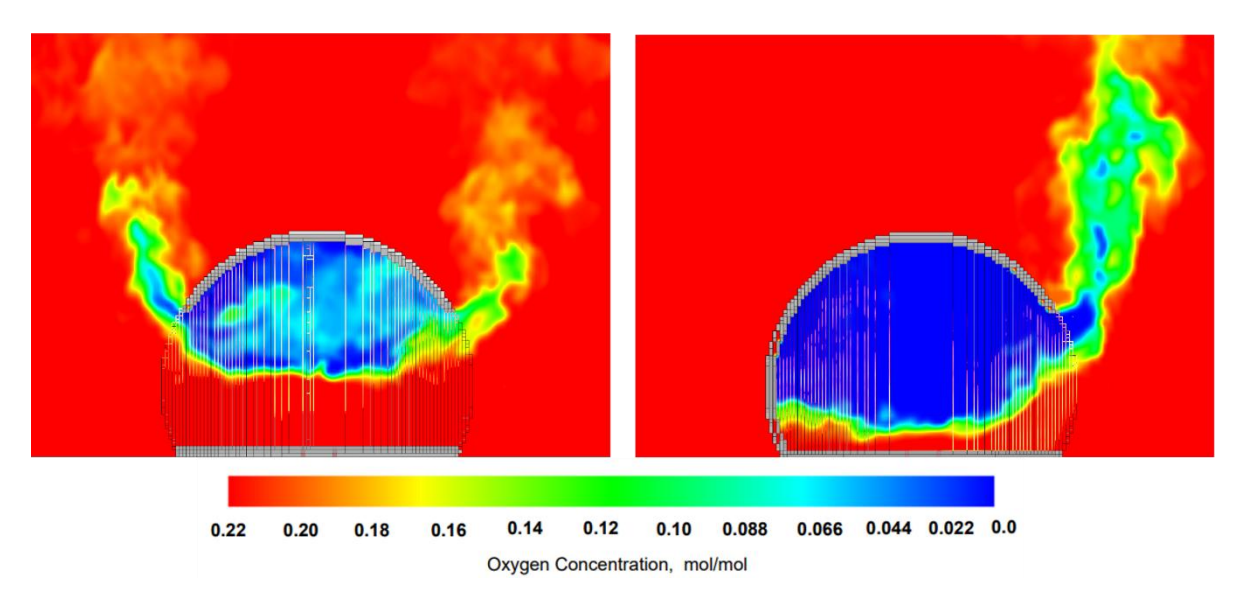


Figure 108: Oxygen Concentration 1100 s after fire initiation for FD case (left) and 1150s after fire initiation for NoFD case (right).

5.3.9 Conclusion

The comparative analysis of FD and NoFD conditions reveals significant differences in fire development, external flame behavior, and thermal impacts in curvilinear compartments in the large-scale experiments. The mass loss and corresponding heat release rate (HRR) were consistently higher in NoFD conditions due to limited ventilation, resulting in more intense combustion and accumulation of hot gases within the compartment. In contrast, FD conditions facilitated continuous air exchange, leading to more stable combustion and relatively lower HRR peaks.

Heat flux and temperature measures further confirmed this trend. Under NoFD conditions, higher experimental peak heat fluxes approximately 18 kW/m² were observed compared to FD, while FDS simulations significantly overpredicted values in both scenarios, reaching up to 80 kW/m² in NoFD, indicating an overstated depiction of radiative energy transfer. The EVF temperature field also showed absolute contrasts. In FD, stratification was evident, with bi-directional flow allowing fresh air inflow and hot gas outflow on both sides of the compartment, resulting in controlled EVF. NoFD conditions, however, led to unidirectional flow with extensive flame propagation outside the compartment and peak temperatures near the opening. Corresponding FDS simulations consistently overpredicted EVF temperatures, particularly at higher elevations and during fully developed fire stages.

Eurocode 1 (EC1) centerline temperature predictions were assessed for both configurations. Moreover, in many cases (e.g., at 3 m and 4 m heights or for higher HRRs), the EC1 equations were not valid due to exceeding their applicability limits, notably when the dimensionless parameter $\frac{L_x\sqrt{A_v}}{o}$ < 1 fell outside the recommended range.

In summary, this study underscores the influence of ventilation configuration on EVF behavior, highlighting the limitations of engineering design correlations like EC1 in complex geometries and the need for cautious interpretation of FDS results due to their tendency to overestimate thermal fields and heat fluxes. These insights are critical for fire safety design and performance-based engineering in non-orthogonal structures.

5.4 Parametric Study: Numerical Investigation of the Effect of Ventilation Conditions and Building Geometrical Features on the Development of Externally Venting Flames

Aiming to investigate the effect of ventilation conditions and fuel load on the development of an EVF from a curvilinear fire compartment, a set of relevant numerical test cases have been chosen using FDS. Both NoFD and FD conditions were investigated, and a parametric study has been conducting by varying the HRR using 1.5 MW, 2 MW, 3 MW and 4 MW fires to study the geometrical and thermal characteristics of EVF.

To bridge this knowledge gap, this parametric study aims at investigating following.

- 1. Assessment of EVF fire engineering design correlations as the previous studies suggesting that existing engineering design methodologies cannot describe with sufficient accuracy of the EVF.
- 2. The burning behaviour of liquid fuel pool fires in curvilinear geometries to help identify the influence of ventilation on EVF development and their impact on the façade.
- 3. To investigate the influence of building geometrical features by investigating the burning behaviour of liquid fuel pool fires in curvilinear and orthogonal geometries to help identify the key factors influencing EVF development and their impact on building façades.

5.4.1 Fire Engineering design correlation related to EVF

Significant amount of research has been conducted on EVF geometrical and thermal characteristics initially by Yokoi (Yokoi, 1960) followed by Webster and Seigel (Seigel, 1969) Based on the above studies Thomas and Law re-examined the experimental data and developed a correlation for EVF height (Thomas and Law, 1972). Further, Law developed a design methodology to assess fire safety of external structural elements based on EVF characteristics, which has been adopted in Eurocode 1 (EC1) (EN 1991-1-2, 2002) considering two distinct ventilation modes, namely No Forced Draught (NoFD) and Forced Draught (FD) (Law and O'Brien, 1989). If the fire compartment has openings on opposite sides or if additional air is being supplied using other sources, EC1 calculations shall be based on the FD condition and otherwise with the NoFD ventilation condition (EN 1991-1-2, 2002). Later, Klopovic and Turan studied the effect of ventilation and wind on EVF and its impact on the heat flux at the façade wall focusing on window breakage and suggested the risk of secondary fires (Klopovic and Turan, 2001). Asimakopoulou et al. investigated various design correlations and concluded that many of them were non-conservative and highlighted the need to improve EVF design methodologies

(Asimakopoulou et al., 2017). Most widely used correlations to estimate EVF thermal and geometrical characteristics are presented in Table 10.

 $Table\ 10: Empirical\ correlations\ for\ EVF\ shape\ and\ centerline\ temperature.$

EVF	Empirical correlations	NoFD	FD	Reference
Height	$L_{L} = \max \left[0; h_{eq} \left[2.37 \left[\frac{Q}{A_{v} \rho_{g} (h_{eq} g)^{\frac{1}{2}}} \right]^{\frac{2}{3}} - 1 \right] \right]$	√		(EN 1991-1-2, 2002)
	$L_{L} = \left[1.366 \left(\frac{1}{u} \right)^{0.43} \frac{Q}{A_{\nu}^{\frac{1}{2}}} \right] - h_{eq}$		✓	(EN 1991-1-2, 2002)
	$L_L = D_v \left[-1.02 + 0.23 \frac{Q^{\frac{2}{3}}}{D_v} \right]$	√		(Heskestaad , 1983)
Projection	$L_H = \frac{h_{eq}}{3} \text{ if } h_{eq} \le 1.25 w_t$ $L_H = 0.3 h_{eq} \left(\frac{h_{eq}}{w_t}\right)^{0.54} \text{ if } h_{eq} > 1.25 w_t \text{ and window distance} > 4 w_t$ $L_H = 0.454 h_{eq} \left(\frac{h_{eq}}{2w_t}\right)^{0.54} \text{ in any other cases}$	√		(EN 1991-1- 2, 2002)
	$L_H = 0.605 \left(\frac{u^2}{h_{eq}}\right)^{0.22} \left(L_L + h_{eq}\right)$		✓	(EN 1991-1- 2, 2002)
	$0.13L_L$	√		(Yokoi, 1960)
Width	w_t	√		(EN 1991-1- 2, 2002)
	$w_t + L_H$		√	(EN 1991-1- 2, 2002)
	$0.13L_L$	√		(EN 1991-1- 2, 2002)
Cent. Temp.	$T_Z = (T_w - T_o) \left\{ 1 - \left[0.4725 \left(\frac{L_x W_t}{Q} \right) \right] \right\} + T_o \text{ where } \frac{L_x w_t}{Q} < 1$	√		(EN 1991-1- 2, 2002)
	$T_z = (T_w - T_o) \left\{ 1 - \left[0.3325 \left(\frac{L_x \sqrt{A_v}}{Q} \right) \right] \right\} + T_o \text{ where } \frac{L_x \sqrt{A_v}}{Q} < 1$		√	(EN 1991-1- 2, 2002)
	$T_Z = \left\{ \left[1 - 0.0027 \left(\frac{lw}{\dot{m}} \right) \right] \left[T_o - T_a \right] \right\} + T_a$	√		(Law, 1978)
	$T_{Z} = \left\{ \left[1 - 0.019 A_{w}^{\frac{1}{2}} \left(\frac{l}{\dot{m}} \right) \right] [T_{o} - T_{a}] \right\} + T_{a}$		√	(Law, 1978)

5.4.2 Numerical simulation

a. Description of the geometry

The numerical simulations for the present study were conducted using FDS version 6.7.6. The study was conducted in two different geometries constructed with steel, the schematic views of which are depicted in Figure 109. Geometry 1 has a curvilinear shape with a length of 4.4 m, a width of 4 m, and a height of 3 m from floor level to the top. To keep a similar volume for the comparative study, geometry 2 has the same plan dimensions as that of geometry 1, with rectilinear elevation, and is provided with a height of 2.7 m. To study the influence of ventilation condition on EVF development in these geometries, the compartment is provided with 2 equal sized openings on either side of the wall with a width of 1.1 m and height of 2 m to facilitate FD conditions and to simulate NoFD condition, the geometry is restricted to a single opening. Measuring devices are set up in the numerical model to measure temperature and heat flux on the façade walls of the geometries. A parametric study has been conducted with varying HRR of 1.5 MW, 2 MW, 3 MW and 4 MW and with two ventilation conditions in both curvilinear and rectilinear geometries. A burner with size 0.9 m x 0.9 m x 0.15 m was positioned at the geometrical centre of the compartment, and a total of 16 different simulation cases were considered to investigate the EVF thermal and geometrical characteristics for comparison. Numerical results are compared to available empirical correlations.

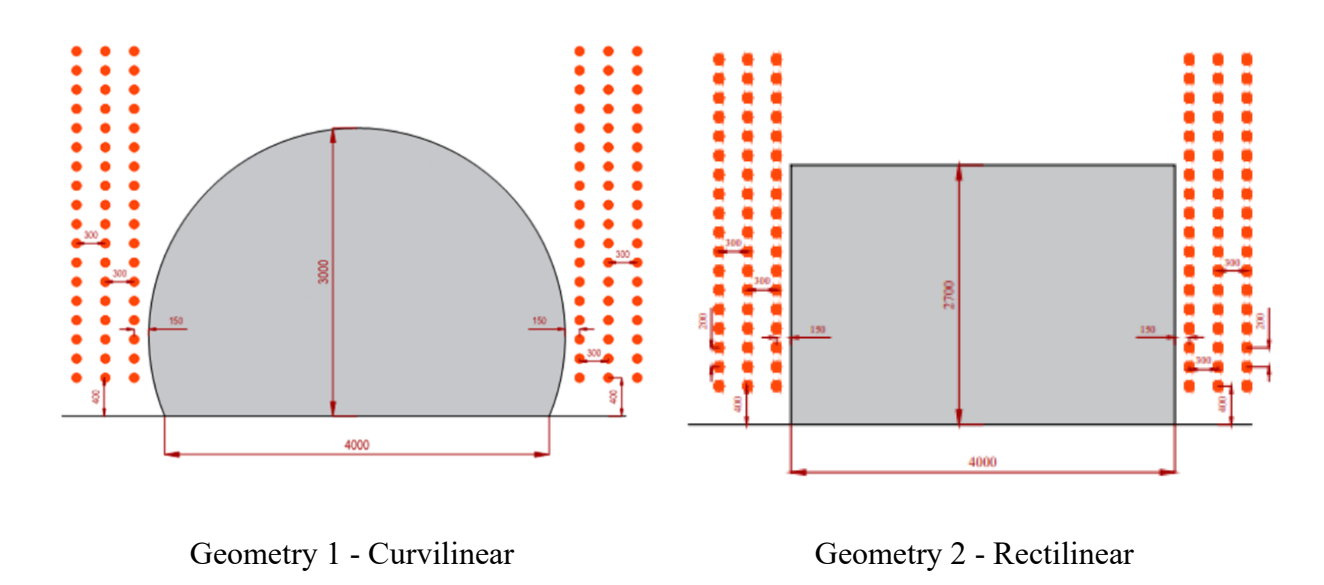


Figure 109: Geometry and location of measuring devices, all dimensions are in mm.

The fire compartments comprised of two equal sized openings on either side of the wall with a 1.1 m width and 2 m height. To replicate NoFD and FD conditions, two ventilations modes were simulated. Fig. 103 (right) is a top view the fire compartment with two equal sized openings on opposite walls of the compartment which will facilitate FD conditions, namely Door 1 and Door 2. All solid surfaces, including walls and floors, are provided with boundary condition with following material properties corresponding to steel, e.g., 7850 kg/m³ density, 0.46 kJ/(kg K) specific heat, 0.02 m thickness, and emissivity of 0.95. The soot yield, which represents the fraction of heptane fuel mass converted to smoke particulates, is set equal to 0.015 kg/kg and the corresponding CO yield was set equal to 0.006 kg/kg (Hamins et al., 2003).

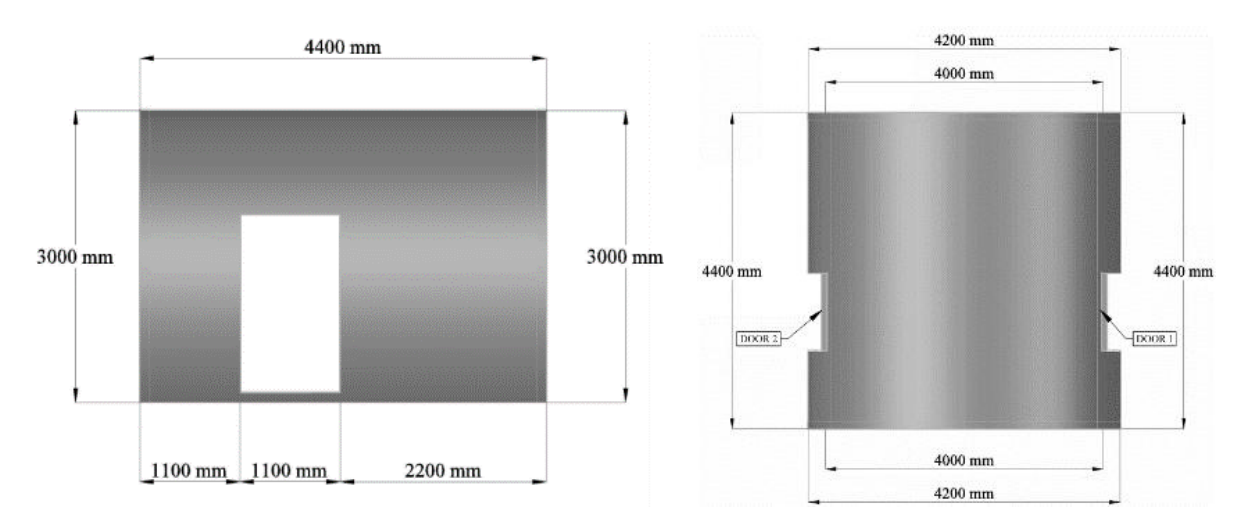


Figure 110: Openings of the fire compartment front (left) and top (right) view.

b. Computational domain

The computational domain has extended a minimum of at least one hydraulic diameter (Zhang et al., 2010). The calculated hydraulic diameter is 1.4 m. However, to capture the geometric and thermal characteristics of the flame more accurately, an increased domain dimension is considered (from the edge of the opening) as depicted in the Fig. 104. The domain was extended 2.5 meters in positive and negative X axis for FD Condition from edge of the respective openings on the opposite side of the compartment and 2.5 meters in positive for NoFD, 1.5 meter in positive and negative Y Axis for FD and NoFD and 5 meters in positive Z Axis for FD and NoFD Conditions.

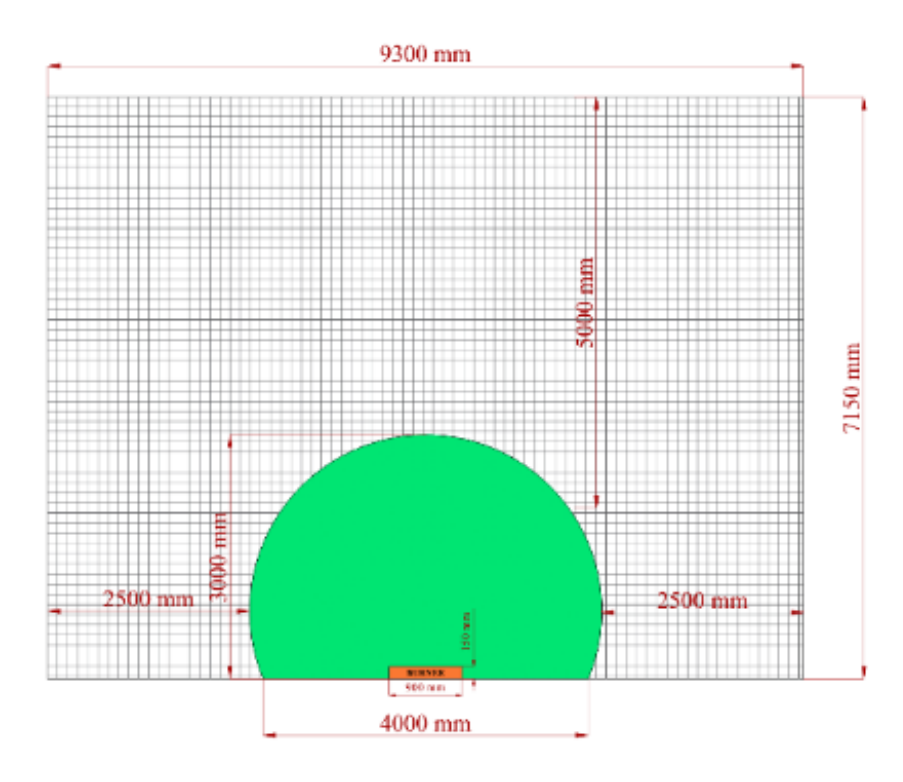


Figure 111: Extended computational domain used in this study.

c. Grid Sensitivity

The non-dimensional expression D^*/dx is a measure of how well the flow field is resolved in the simulation of buoyant plumes. Where dx is the size of cells and D^* is the characteristic fire diameter (K. McGrattan et.al, 2019). The D^*/dx ratio indicates the adequacy of the grid resolution. A higher D^*/dx would mean a better resolution for the simulation of fire, as FDS uses a structured mesh. A grid sensitivity analysis for three different D^*/dx values namely 4 (coarse mesh), 10 (moderate mesh), 16 (fine mesh) was conducted and results for the temporal evolution at 1.8 m height at the centreline of Door 1 are depicted in Figure 112. The D^*/dx ratio of 16 was found to be the most optimal with a corresponding cell size of 0.07 m. These values enable adequate resolution of plume dynamics and other geometric characteristics of the model (McGrattan et al., 2022). The total computational grid consists of 716,958 cubic cells for NoFD and 963,186 cubic cells for FD conditions. The numerical investigation for both models assumed ambient conditions and an ambient temperature of 40°C.

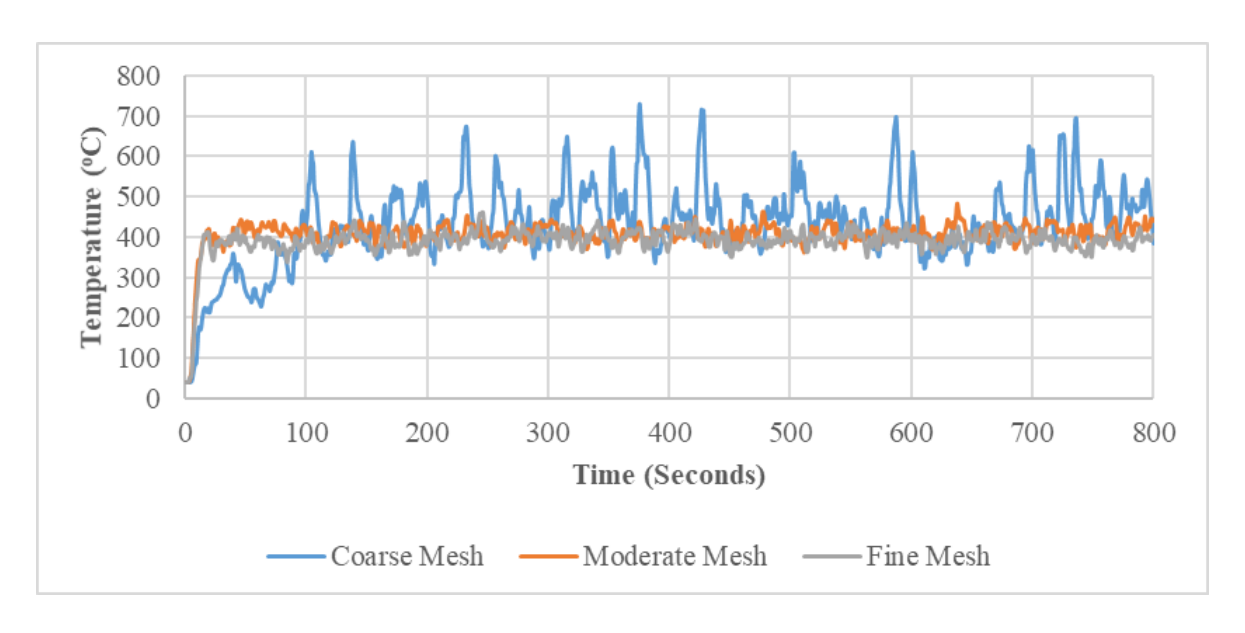


Figure 112: Temporal evolution of the temperature at the centerline of Door 1 of Geometry 2, 1.8 m height from the ground for the different meshes used.

5.4.3 Examined test cases

Aiming to investigate the effect of ventilation conditions and fuel load on the development of an EVF from a curvilinear fire compartment, a set of relevant numerical test cases have been chosen. As indicated in Table 11, both NoFD and FD conditions were investigated and a parametric study has been conducting by varying the HRR using 1.5 MW, 2 MW, 3 MW and 4 MW fires. in the Table 11.

Table 11: Examined test cases.

Case	Geometry-1	Geometry-2	Ventilation	Door 1	Door 2	HRR
NoFD-1.5-G2		✓		✓	N/A	1.5 MW
NoFD-2.0-G2		✓		✓	N/A	2.0 MW
NoFD-3.0-G2		✓		✓	N/A	3.0 MW
NoFD-4.0-G2		✓	NoFD	✓	N/A	4.0 MW
NoFD-1.5-G1	✓		NOLD	✓	N/A	1.5 MW
NoFD-2.0-G1	✓			√	N/A	2.0 MW
NoFD-3.0-G1	✓			√	N/A	3.0 MW
NoFD-4.0-G1	✓			√	N/A	4.0 MW
FD-1.5-G2		✓		✓	✓	1.5 MW
FD-2.0-G2		✓		√	✓	2.0 MW
FD-3.0-G2		✓		√	✓	3.0 MW
FD-4.0-G2		✓	FD	√	✓	4.0 MW
FD-1.5-G1	✓		ΓD	✓	✓	1.5 MW
FD-2.0-G1	✓			✓	✓	2.0 MW
FD-3.0-G1	✓			✓	✓	3.0 MW
FD-4.0-G1	✓			✓	✓	4.0 MW

5.5 Result and discussion

5.5.1 Effect of ventilation condition on EVF development

a. Velocity Flow field

For any fire in a compartment, during its growth phase, the plume developed will impinge on the ceiling and the hot gases including the flame spread out radially through the ceiling and flow out through the available opening(s). However, in compartments with curvilinear geometry smoke movement/flow can be a complex fire dynamic process due to the interaction of turbulence, combustion, radiation etc. with the geometry of the compartment (Feng et al., 2017). Similar studies have been conducted in the past with semi cylindrical ceiling in geometries like tunnels, atriums, etc. to understand the smoke flow movement. Kaihua et al studied the smoke flow movement in a curvilinear tunnel with various curvatures and revealed that due to the bending wall effect in curved tunnels, the smoke movement is impacted which results in the inconsistency of temperature profile (Kaihua et al., 2021).

In this study, ceiling is of curvilinear shape and the fire is seated at the centre of the compartment with a constant heat release rate of 1.5 MW, 2 MW and 4 MW, as shown in Figure 113. As in the case of a rectangular compartment fire, the mass flow entrainment through the bottom half of the opening causes a recirculation zone inside the compartment. However, in the case of FD conditions, a more rigorous and intense mixing of cold air from both side of the compartment opening occurs and results in the formation of two recirculation zones inside the compartment (from both sides) ensuing a more turbulent flow which owes to the higher velocity and high Reynolds number of the incoming flow.

Under NoFD conditions, the plume including the flame can be seen tilting sideways (X direction as seen in Figure 113, top right) due to the incoming flow of air. However, in the FD conditions the incoming flow from both sides induces a backward tilt of the flame (Y direction as seen in Figure 113, bottom right). Under NoFD condition a circular flow pattern is visible inside the compartment which is due to the curvilinear ceiling shape and as the incoming flow is from one side.

The maximum velocity recorded in the EVF is 9.5 m/s under NoFD condition. Further to this, it is noticed that due to the curvilinear geometry there are additional recirculation zones formed outside the compartment, next to the opening, pushing the plume outward causing further projection of external plume. At the initial stage of EVF flow, an orderly laminar flow projects out from the opening and continues with a high velocity, outside the opening. External combustion

exists as the EVF progresses outside the opening since the reaction is supported by the availability of air. As the flow progresses further up, turbulence starts to develop and once the reaction is completed (this can be analysed through the oxygen concentration spatial distribution as seen in Figure 115) the laminar jet turns to a buoyancy driven flow.

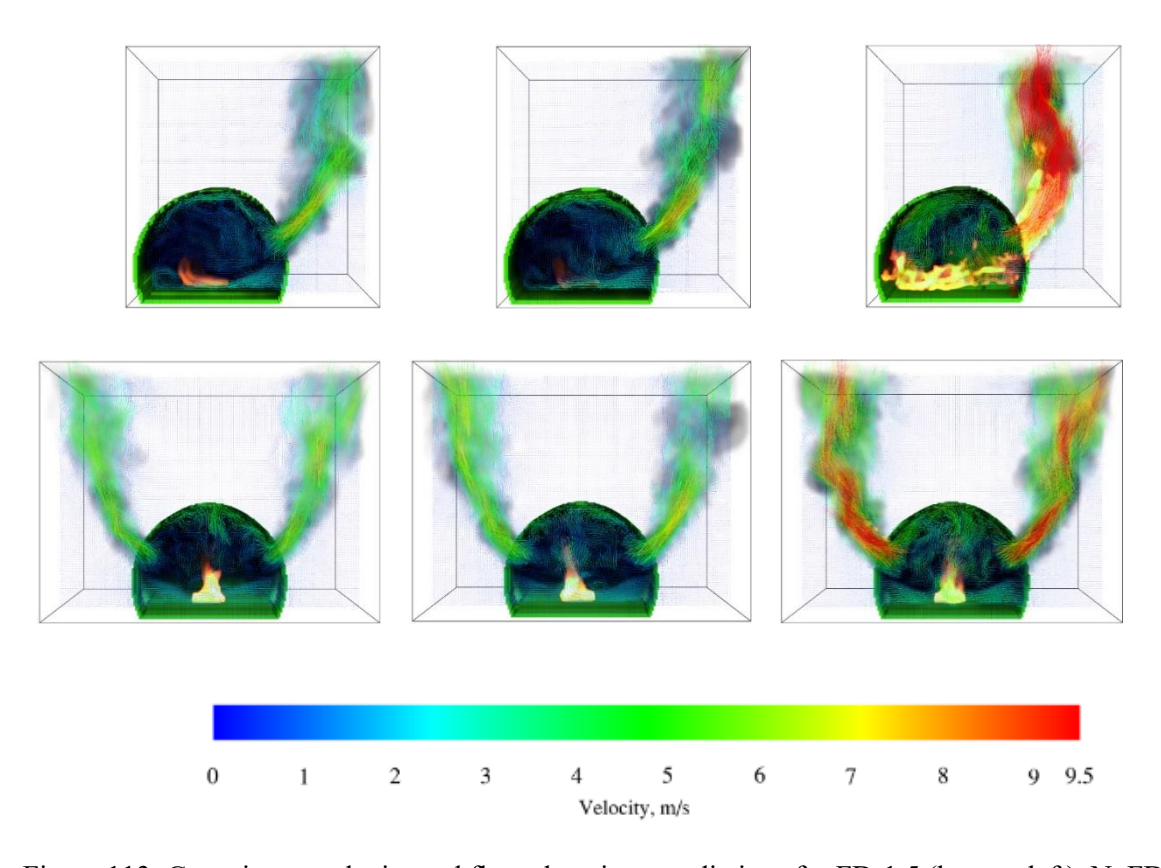


Figure 113: Gas mixture velocity and flame locations predictions for FD-1.5 (bottom left), NoFD-1.5 (top left) FD-2.0 (top middle), NoFD-2.0(bottom middle), FD-4.0 (top right) and NoFD-4.0 (top right) 500 s after fire initiation.

b. Temperature field

Maximum temperatures were observed at the centreline of the opening approximately at a height of 1.8 m from the floor level and EVF temperature gradually decreased with increasing height and distance from the opening. The temperature increases with respect to height at the interior of the compartment and higher temperature values exist in the ceiling due to the upward flow movement and an increased temperature in the range of 790° C is observed for the cases of higher HRR (4 MW).

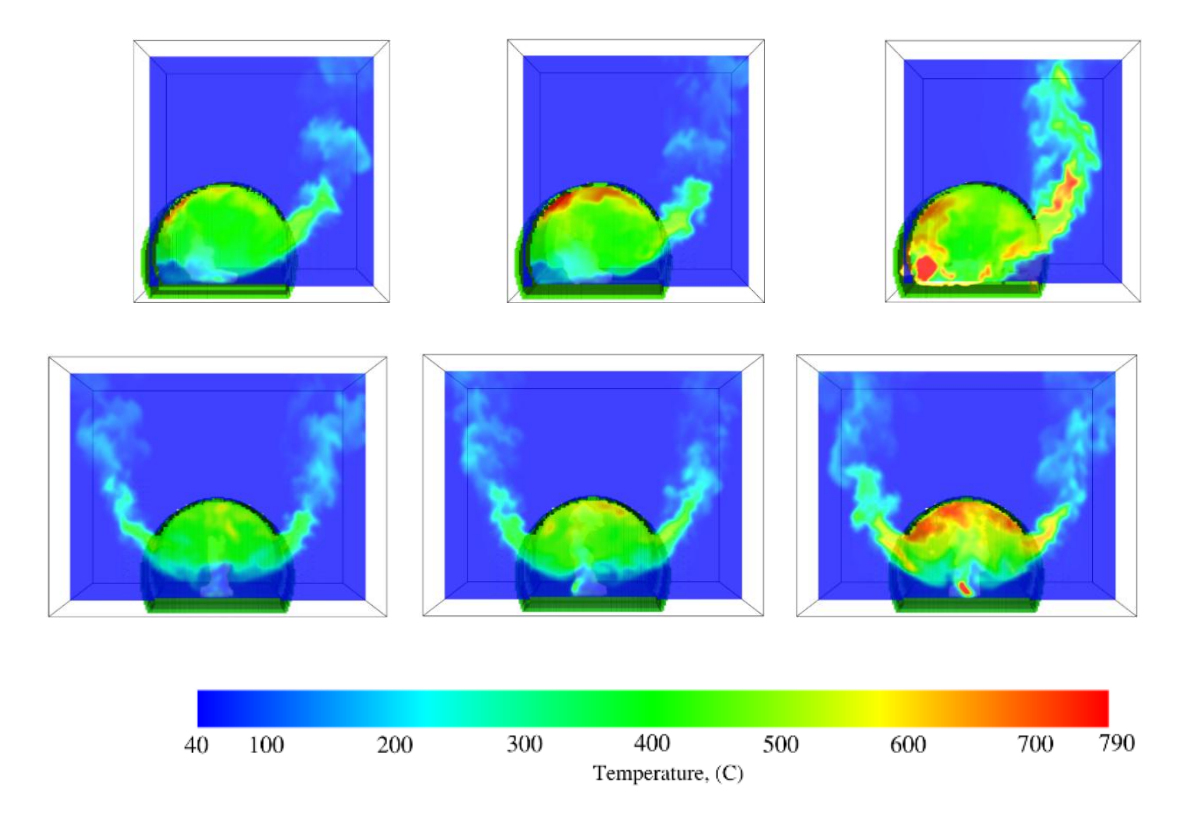


Figure 114: Spatial distribution of gaseous temperature 500 s after fire initiation for FD-1.5MW (bottom left), No FD-1.5MW (top left) FD-2.0 MW (bottom middle), NoFD-2.0 MW (top middle) and FD-4.0 MW (bottom right), NoFD-4.0MW (top right).

The maximum temperature distribution is observed under NoFD conditions with 4 MW fire (Figure 114, top right), after 10 seconds of fire initiation, where a clear stratification of hot and cold layer inside the compartment and a transient increase in temperature with respect to height. Following this, an increase in the volume of hot upper layer and larger volume of unburned gas flows out in the exterior domain forming larger EVF and a stronger buoyant plume. It is important to note that as the plume further goes up, the EVF temperature decreases with respect to the height. At 500 s after the fire initiation, a clear division of hot and cold layer can be seen at the interior of the compartment for the case of FD condition whereas the separation of hot and cold layer are no longer visible in NoFD where a well-mixed layers of hot gases is sustained. Under NoFD conditions higher temperature ranges are observed.

c. Oxygen Concentration

Figure 115 depicts the spatial distribution of oxygen concentration inside the compartment 500 s after fire initiation. A lesser concentration of oxygen is observed during NoFD conditions compared to FD conditions. As stated above, like the temperature field, there is a clear distinction of hot and cold zone in FD conditions which is attributed to the incoming flow of cold air from both openings.

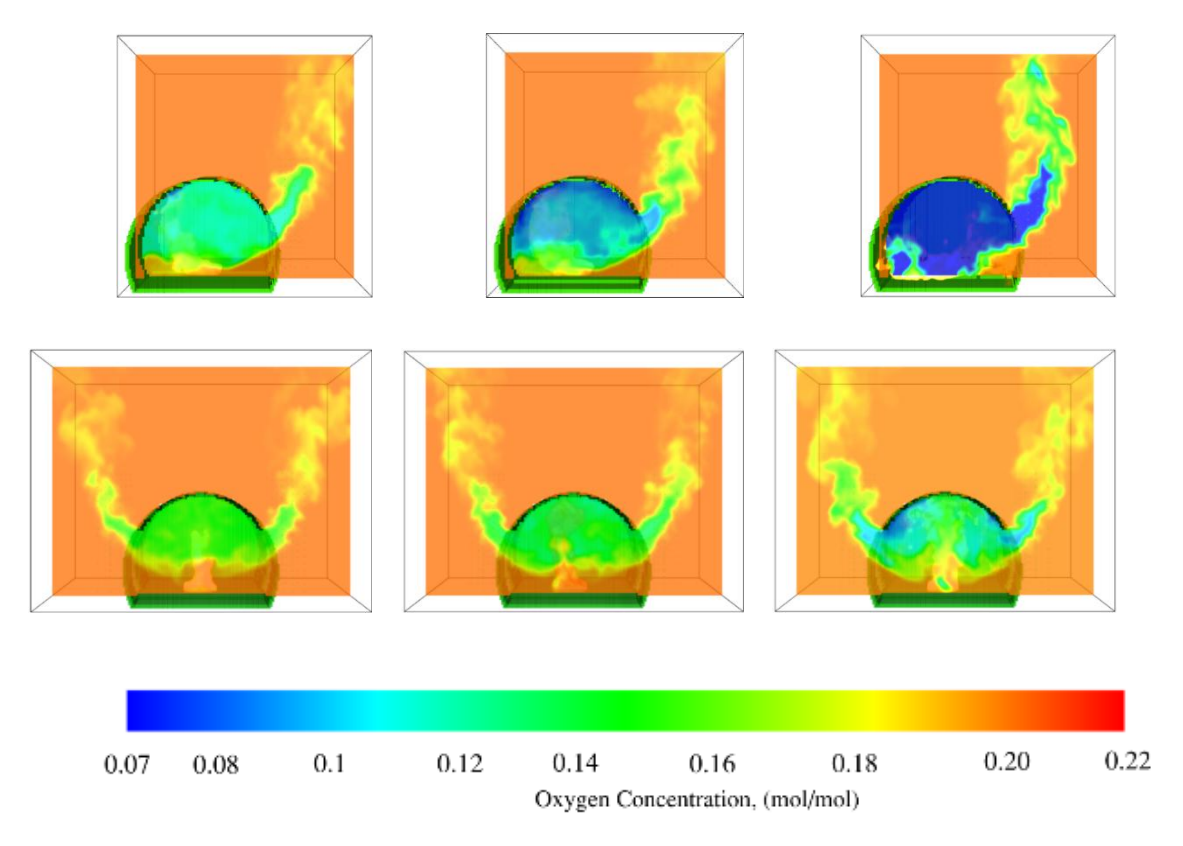


Figure 115: Spatial distribution of oxygen concentration 500 s after fire initiation for FD-1.5MW (bottom left), No FD-1.5MW (top left) FD-2.0 MW (bottom middle), NoFD-2.0MW(top middle) and FD-4.0 MW (bottom right), NoFD-4.0MW (top right).

5.5.2 Effect of building geometrical features

To investigate the influence of building geometrical features by investigating the burning behaviour of liquid fuel pool fires in curvilinear and orthogonal geometries to help identify the key factors influencing EVF development and their impact on building façades.

a. Velocity field

The velocity flow field is differed in all cases, owing primarily to the difference in the flow field at the interior of the fire compartment. As an example, the relevant flow field for the most increased HRR NoFD-4.0-G2, FD-4.0-G2, NoFD-4.0-G1 and FD-4.0-G1 cases are depicted in Figure 116. In compartments with curvilinear geometry under both FD and NoFD conditions smoke movement can be a complex fire dynamic process due to the interaction of turbulence, combustion, and radiation with the geometry of the compartment (Feng et al., 2017). A clear circulation zone is evident in all NoFD cases, but for the curvilinear compartment, NoFD-4.0-G1, the flow is closely attached to the solid curved boundaries of the compartment when compared with the rectilinear walls and velocity field is more intense with peak velocities at a range of 8.5 m/s. Under FD conditions, a more rigorous and intense mixing of cold air from both side of the compartment openings occurs and results in the formation of two recirculation zones inside both

rectilinear and curvilinear compartments ensuing a more turbulent flow which owes to the higher velocity and high Reynolds number of the incoming flow; in the FD-4.0-G2 case, EVF velocities are higher.

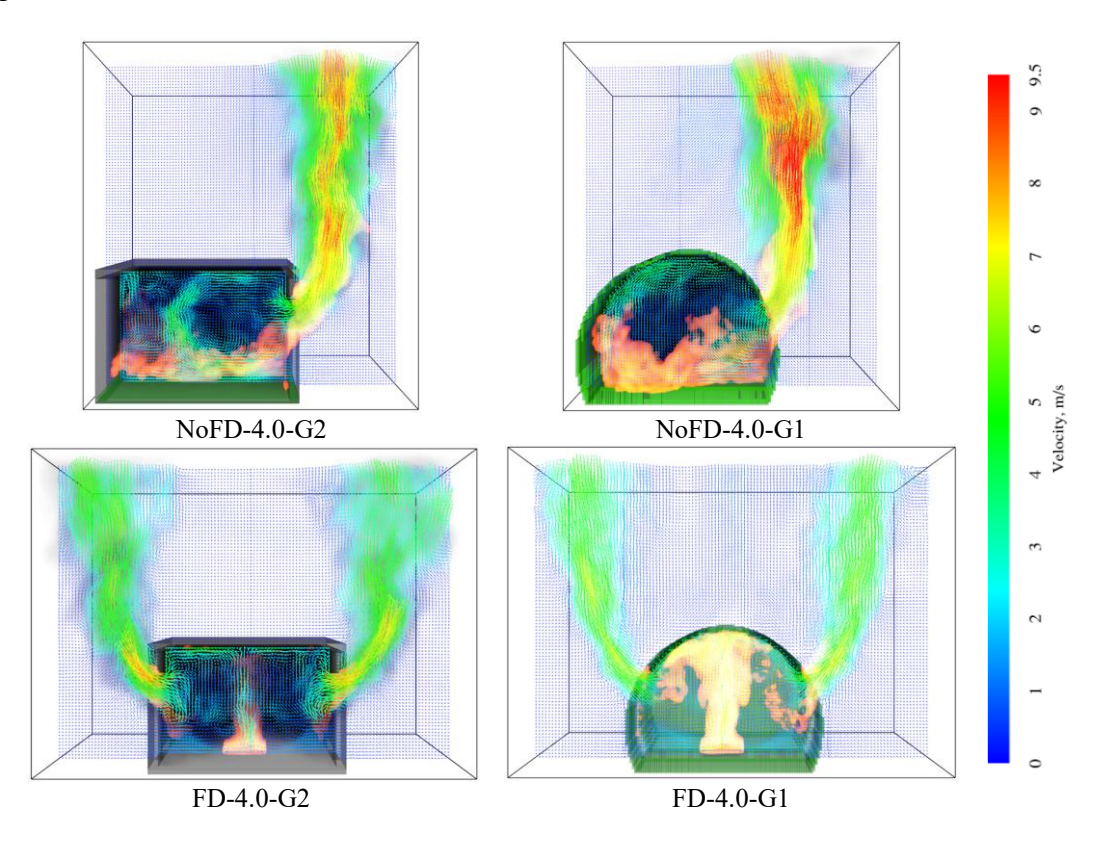


Figure 116: Gas mixture velocity 500 s after fire initiation for NoFD (top) and FD (bottom) conditions for both rectilinear (left) and curvilinear (right) 4 MW cases.

b. Temperature field

The maximum temperature distribution is observed for case NoFD-4.0-G1, after 10 seconds of fire initiation, where a clear stratification of hot and cold layer inside the compartment and a transient increase in temperature with respect to height. Following this, an increase in the volume of hot upper layer and larger volume of unburned gas flows out in the exterior domain forming larger EVF and a stronger buoyant plume. It is important to note that as the plume further goes up, the EVF temperature decreases with respect to the height. At 500 s after the fire initiation, a clear division of hot and cold layer can be seen at the interior of the compartment for the case of FD condition whereas the separation of hot and cold layer is no longer visible in NoFD where a well-mixed layers of hot gases is sustained. Under NoFD conditions higher temperature ranges are observed.

To investigate the effect compartment geometry on the EVF development the spatial distribution of the gaseous temperature is also investigated for both rectilinear (Geometry 2) and curvilinear (Geometry 1) geometries. The relevant temperature field for the most increased HRR NoFD-4.0-

G2, FD-4.0-G2, NoFD-4.0-G1 and FD-4.0-G1 cases are depicted in Figure 117. As can be observed, under FD conditions the hot gas layer reached a steady state condition after the first 60 s of the simulation as the hot combustion gases aggregated at the ceiling and the hot gas layer gradually descended resulting in cold air area shrinkage; this process was faster for the rectilinear cases. EVF shaping was fluctuating but in general, EVF plume sizes were increased in curvilinear geometries for all HRRs.

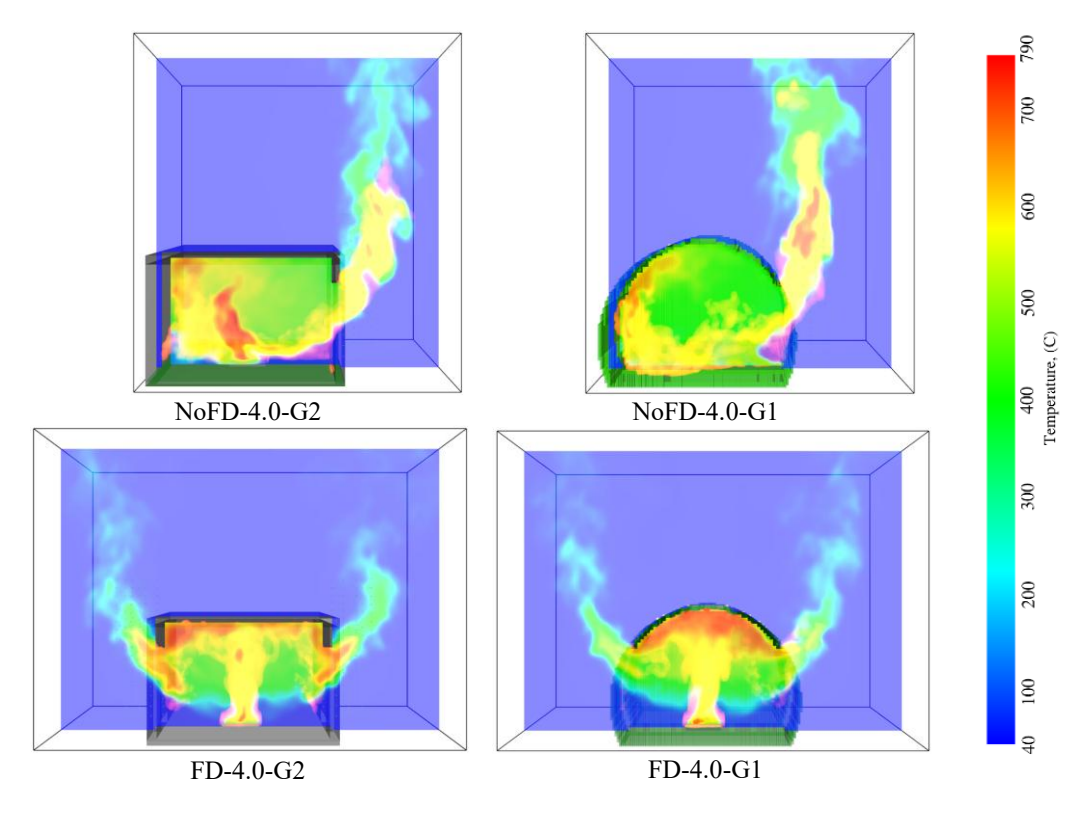


Figure 117: Spatial distribution of gaseous temperature 500 s after fire initiation NoFD (top) and FD (bottom) conditions for both rectilinear (left) and curvilinear (right) 4 MW cases.

c. Oxygen concentration field

Figure 118 depicts the spatial distribution of oxygen concentration inside the rectilinear and curvilinear compartments of the NoFD-4.0-G2, FD-4.0-G2, NoFD-4.0-G1 and FD-4.0-G1 cases 500 s after fire initiation. A lesser concentration of oxygen is observed during NoFD conditions compared to FD conditions. As stated above, like the temperature field, there is a clear distinction of hot and cold zone in FD conditions which is attributed to the incoming flow of cold air from both openings. Under NoFD cases the oxygen deficient areas at the interior of the compartment are more increased thus resulting in larger volume of hot combustion products exiting the fire compartment that ignite and form an EVF when in contact with fresh air. This behaviour is more intense in curvilinear geometries resulting in even bigger volume of EVF.

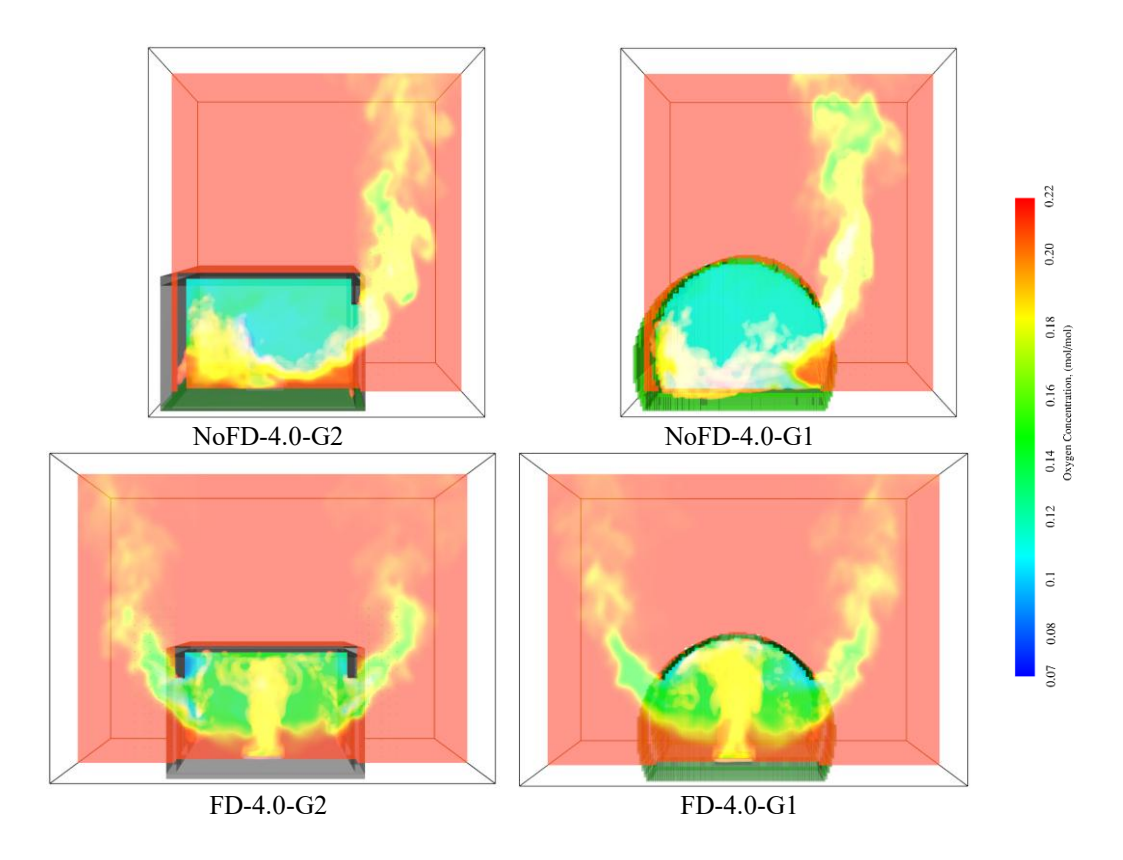


Figure 118: Oxygen concentration 500 s after fire initiation NoFD (top) and FD (bottom) conditions for both rectilinear (left) and curvilinear (right) 4 MW cases.

5.5.3 EVF geometric characteristics

To quantify the geometric characteristics of the EVF envelope, a digital image processing tool using MATLAB code has been developed, and in all cases aiming to determine the geometric characteristics of the EVF envelope. Each image frame was cropped, aligned, and assigned proper world coordinates. A modified version of the methodologies proposed by Vipin (Vipin, 2012) was used. Each frame was converted into a binary image using a set of rules, employing appropriate threshold limits for red, green, and blue colour levels and luminosity, based on the prevailing lighting conditions in each test case. The threshold limits were acquired through an extended statistical analysis of the various flame regions in each stage of the flame cycle. The EVF envelope dimensions were determined by calculating the average flame probability (intermittency). All images were processed and the results of a 4 MW fire for both FD and NoFD conditions. The calculated spatial distribution of flame envelope probability, expressed via the flame intermittency, is illustrated in Figure 119. Mean flame height for these cases has been determined, which demonstrates that geometrical features, ventilation, and heat release rate having an influence on the development and geometric characteristics of EVF.

For the NoFD cases it is depicted that the overall EVF volume generally increases with increasing heat release rate. The relevant EVF envelope tends to assume an elliptical shape, which is

compatible to the EVF shapes proposed in widely used engineering design methodologies (Asimakopoulou et al., 2017). The EVF shape in low fire loads and under FD conditions, is significantly limited. The flame intermittency contours represent time-averaged data, considered from the ignition of the fire until its complete duration. This approach provides an averaged representation of flame fluctuations over the entire fire period, enabling a consistent comparison of flame width and height trends.

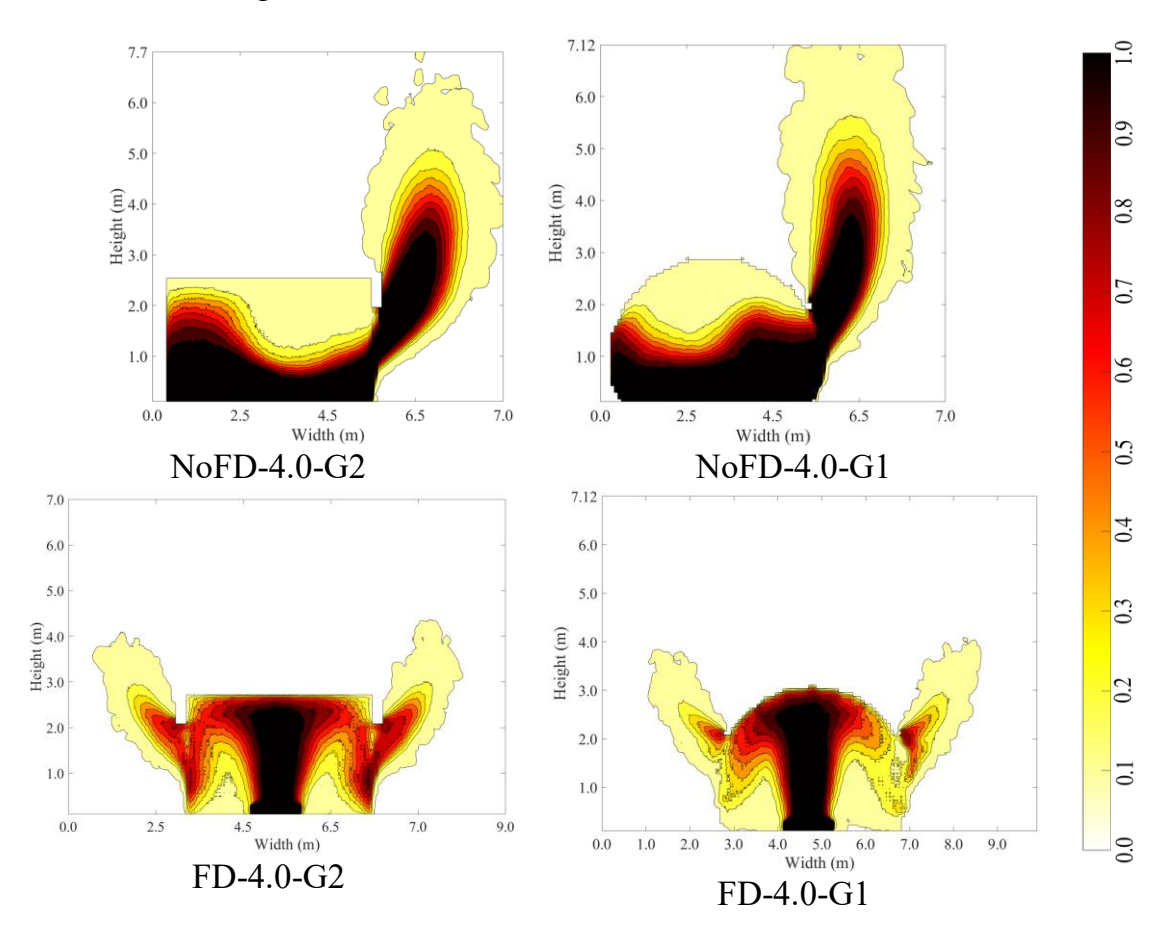


Figure 119: Side view of the flame intermittency contours for NoFD (top) and FD (bottom) conditions for both rectilinear (left) and curvilinear (right) 4 MW cases.

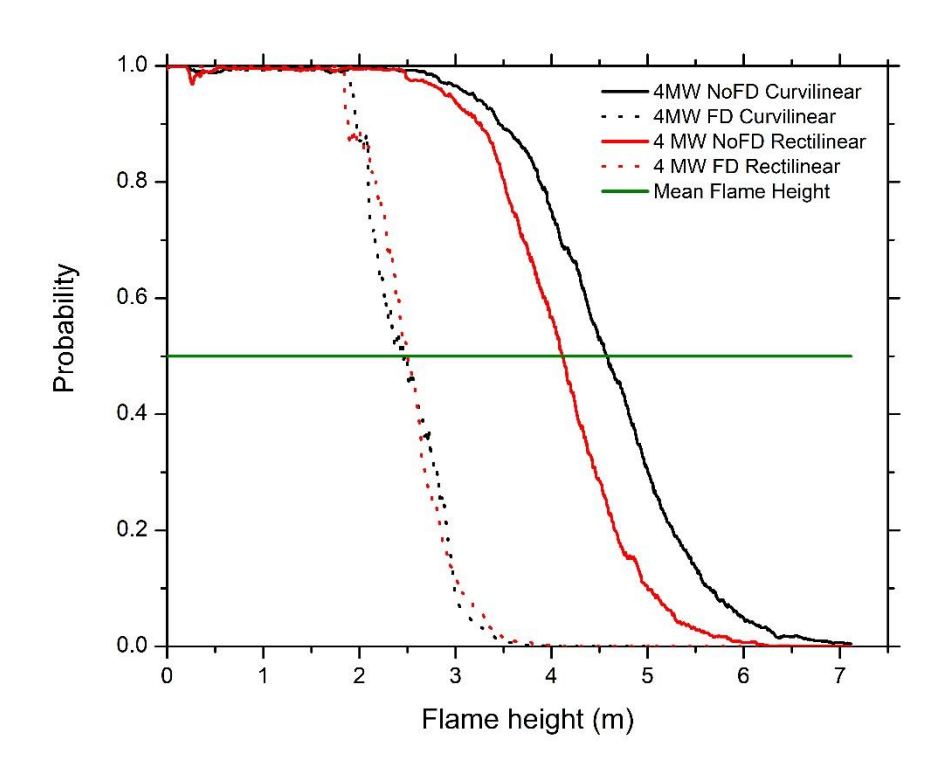


Figure 120: Mean flame height NoFD and FD 4 MW.

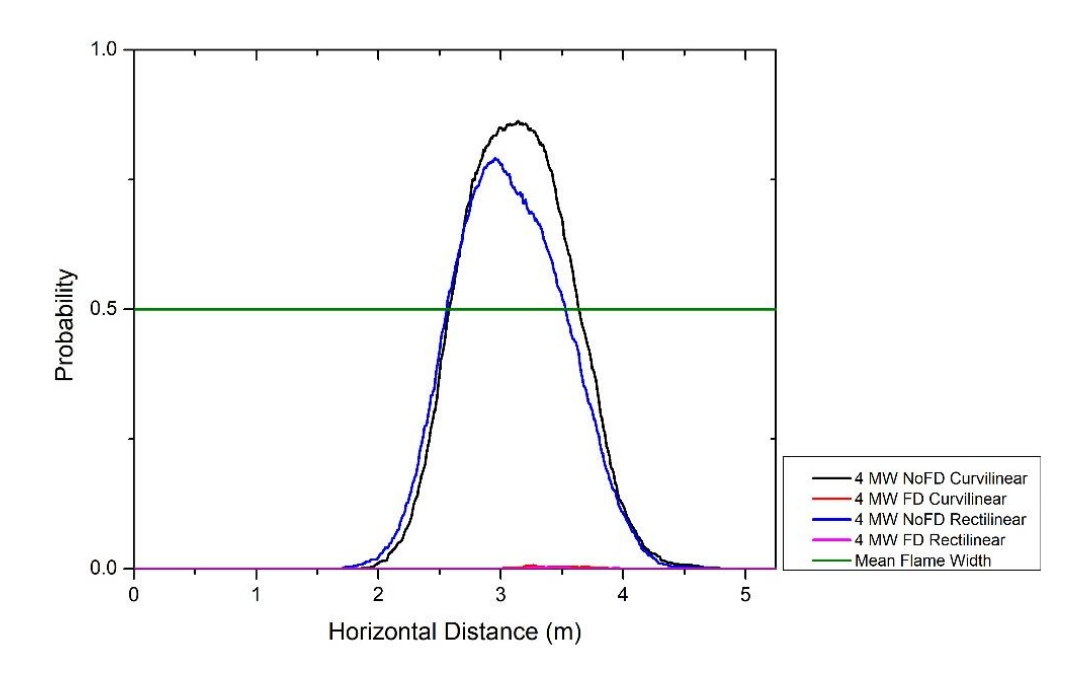


Figure 121: Mean flame width for NoFD and FD 4 MW.

5.5.4 Validation of Numerical Result with Engineering Correlation

Table 12 below depicts the calculated values based on the correlations as illustrated in Table 10. Note that the calculation methodologies for FD conditions are based on a wind speed of 0.1 m/s. EVF centreline temperature is calculated with an axis length from window, L_x equal to 1.5 m and

this applicable to all cases. Under FD conditions with higher HRR values (2 MW and 4 MW) EC1 design methodology falls beyond the range of applicability for the calculation of centreline temperature. This is mainly because centre line temperature equation specified in EC1 for FD condition is not in the range of applicability, $\frac{L_X\sqrt{A_V}}{Q} < 1$ for HRR of 1.5 MW,2 MW, 3 MW and 4 MW, as the calculated value is more than 1. The EVF flame height for No FD Conditions showed varying values for different HRR. For NoFD condition with 1.5 MW EC1 values agreed with numerical results whereas in 2 MW, EVF was showing fluctuating/pulsating results in the numerical simulations. While considering the mean flame height, an approximate value of 1 m is observed, and this is consistent in correspondence to the EC1 value of 0.81 m. However, the maximum flame height is in the range of 3 m for this case. For 4 MW, EC1 value of 2.9 m was an underprediction compared to the consistent flame height of 6 m appeared on FDS.

Under FD conditions, in all three cases, EC1 values overestimated the numerical results. Under 4 MW numerical cases, the flame height which appeared on both sides of the opening corresponded to 3 m compared to an EC1 value of 5 m. Comparing numerical results with Heskestad correlation, it can be generally seen that Heskestad values were also on the increased side compared to the FDS results, except in NoFD with 4 MW fire where the values are found to be in good agreement. The analysis of EVF Width in NoFD indicates that 1.5 MW and 2 MW shows good agreement between FDS values and EC1 which corresponds to the actual door width of 1.1m. However, the 4 MW fire shows an increased flame width. In FD condition EC1 values were on an increased side compared to the FDS results. Finally, the EVF Projection analysis demonstrates that for all cases, including FD and NoFD ventilation conditions, FDS predicts higher values than the engineering correlations of EC1 and Yokoi.

Table 12: EVF geometrical characteristics according to empirical correlations.

Cases	Height (m)		Projection (m)		Width (m)	C. Temperature (K)	C. Temperature (K)
	EC1	Heskestad	EC1	Yokoi	EC1	EC1	FDS
NoFD-1.5MW	0.32	3.16	0.86	0.04	1.1	593.8	515
NoFD-2.0MW	0.81	3.68	0.86	0.10	1.1	714.8	540
NoFD-3.0MW	1.68	4.53	0.86	0.21	1.1	899.3	805
NoFD-4.0MW	2.91	5.22	0.86	0.37	1.1	986.1	900
FD-1.5MW	0.62	1.02	0.50	0.08	2.39	NR	543
FD-2.0MW	1.50	1.40	0.66	0.20	2.46	NR	553
FD-3.0MW	3.25	2.04	0.99	0.42	2.59	NR	635
FD-4.0MW	5.00	2.56	1.32	0.65	2.72	NR	663

^{*}NR – Not in Range.

a. EVF Temperature analysis

The gas mixture temperature formed outside the compartment was measured during the fully developed phase of the fire, the vertical distribution of the temperatures of the final 100 s of the simulations are shown on Figure 122. The total simulation run time for both ventilation mode cases was 900 s, which was chosen to ensure the fire has fully evolved in the compartment and reached relatively steady state. A comparative analysis is only possible for FD conditions for 1.5 MW fire, which indicates that the EC1 methodology and numerical results have similar patterns. The EC1 design methodology results at lower heights have increased values that gradually decrease as the height increases. It is important to note that comparison is not possible for other FD cases with higher HRR (2 MW and 4 MW) as the EC1 design methodology falls beyond the range of applicability of the engineering correlation for centreline temperature. However, under NoFD condition all three cases were compared which indicates that EC1 values predict an increased temperature when compared to the numerical results as depicted in Figure 122 (right). This necessitates further validation using experimental analysis.

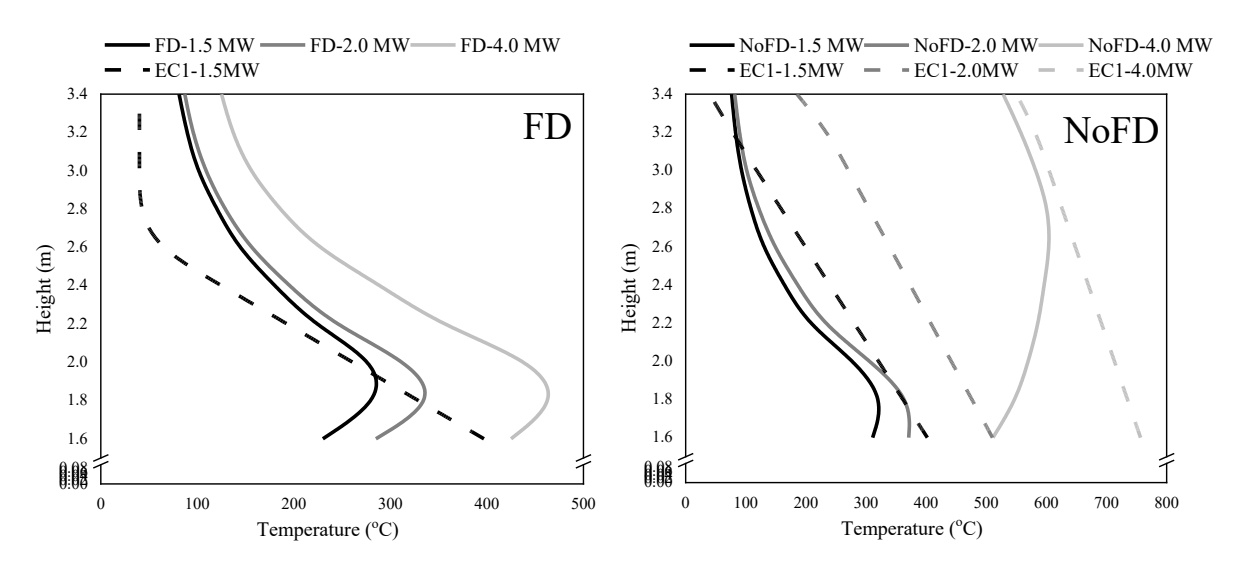


Figure 122: Vertical distribution of averaged temperature at the exterior of the fire compartment; effect of ventilation conditions FD (left) and NoFD (right).

Figure 123 shows the vertical distribution of the averaged centreline temperature at the exterior of the fire compartment for NoFD conditions for the rectilinear and curvilinear cases as calculated with EC1 and relevant predictions. EC1 methodology tends to over predict centreline temperatures for all rectilinear NoFD cases. At the region at the proximity of the opening a larger discrepancy is observed as EC1 results are twice the value of the numerical data. For lower HRR there is better agreement for the NoFD cases in rectilinear geometries especially in higher heights. This is not the case for NoFD conditions in curvilinear geometries, Figure 124, as in some cases, (1.5 MW, 2 MW, 3MW and 4 MW), EC1 underpredicts values compared to predictions.

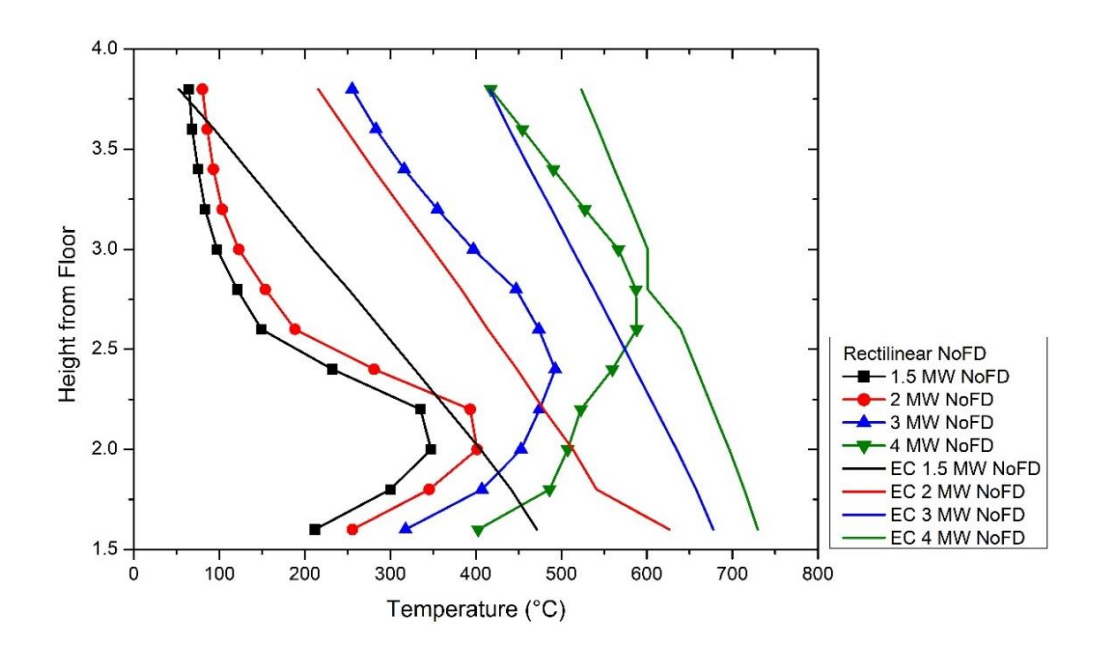


Figure 123: Vertical distribution of the averaged centerline temperature at the exterior of the fire compartment for NoFD conditions for the rectilinear cases.

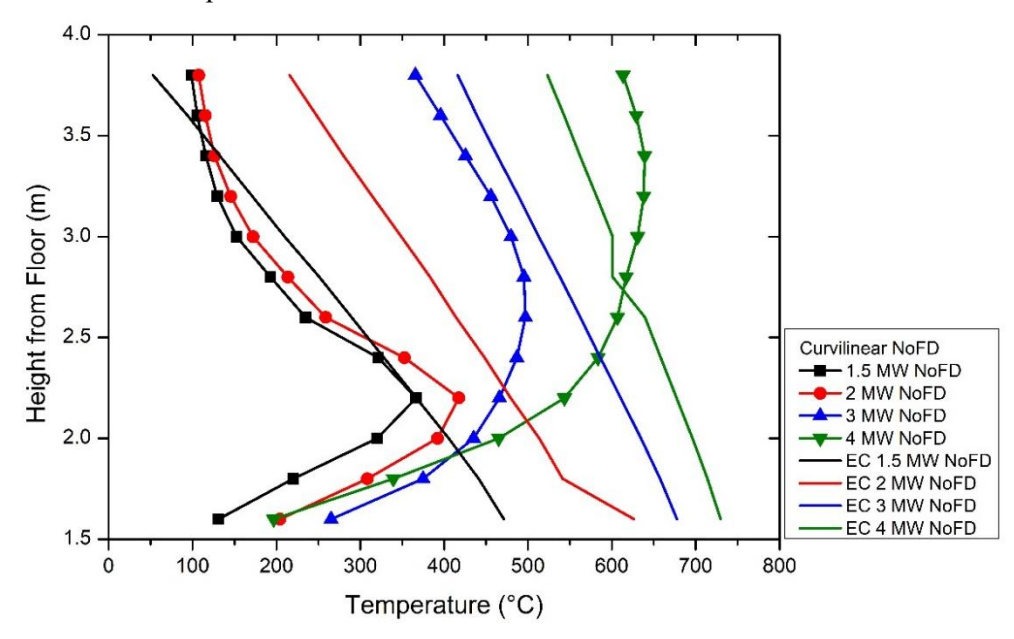


Figure 124: Vertical distribution of the averaged centerline temperature at the exterior of the fire compartment for NoFD conditions for the curvilinear cases

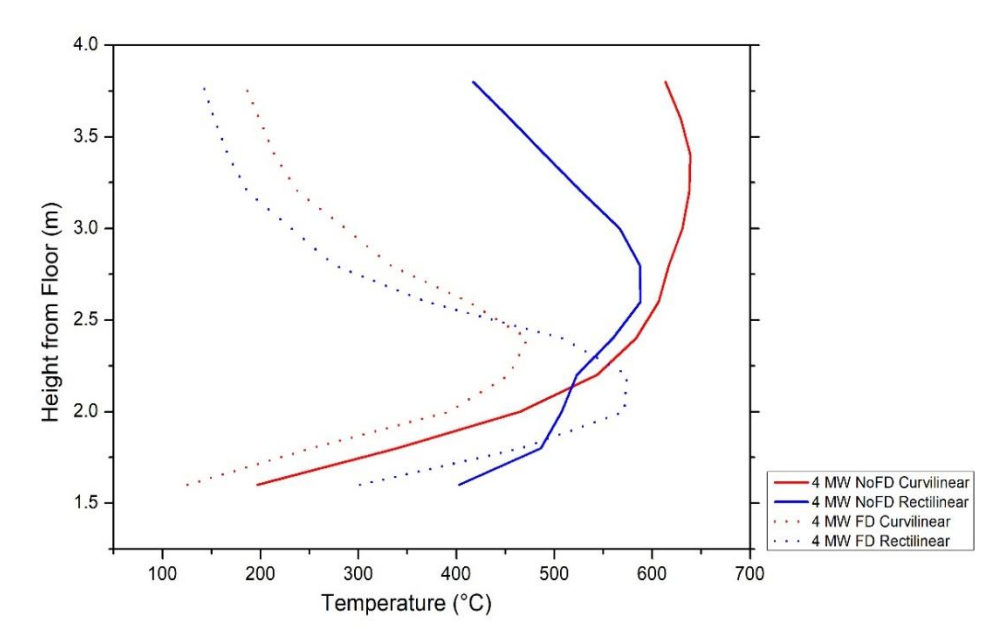


Figure 125: Vertical distribution of temperature at the exterior of the fire compartment for NoFD and FD conditions for the 4 MW rectilinear and curvilinear cases.

In general, more increased temperature profiles are observed and it is obvious that the inability of EC1 to predict centerline temperatures at curvilinear geometries may pose increase risks. This is also depicted in the relevant heat fluxes 10 cm above the height of the opening were, Figure 126, is it observed that for the curvilinear geometries there is an increase in the range of 25% in the average heat flux values. Under FD conditions, heat fluxes are decreased, and curvilinear geometries are exposed to less heat.

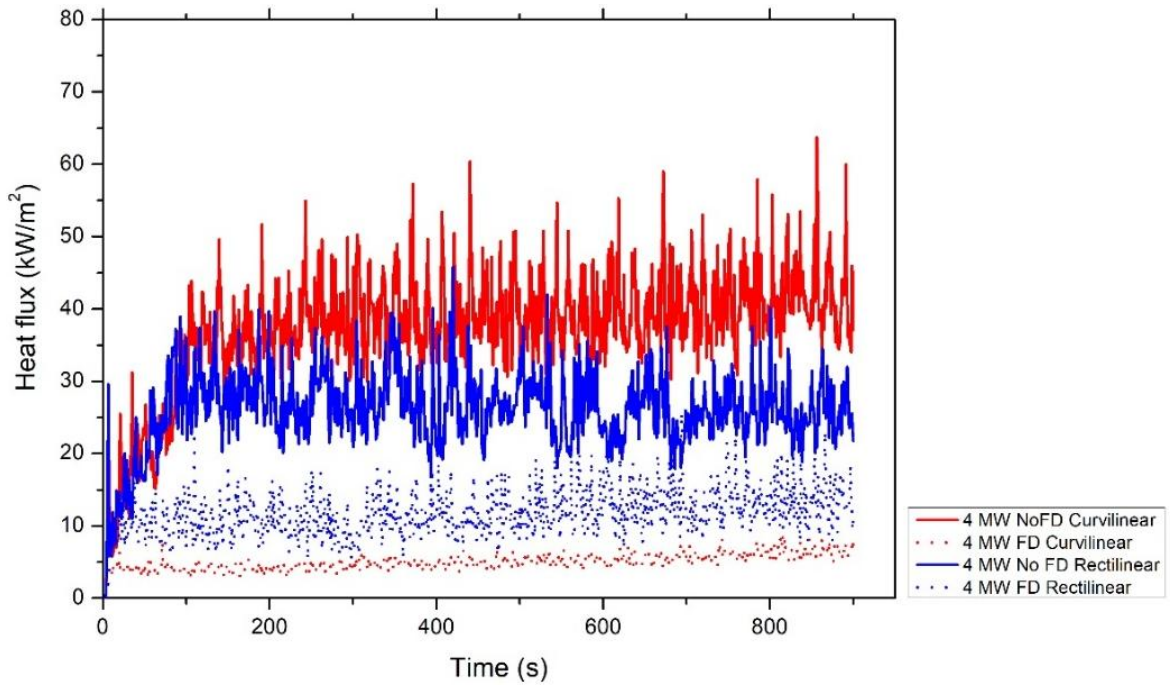


Figure 126: Heat flux at the facade for NoFD and FD conditions for the 4 MW rectilinear and curvilinear cases.

5.6 Conclusion

A wide range of numerical simulations and relevant analysis was performed, and results indicate that geometrical features, e.g., multiple openings and curvilinear features, of the building have an influential role in the development of EVF. Regarding empirical correlations effectiveness to be used in curvilinear geometries, key finding include:

- Predictions using the empirical correlations for the estimation of the EVF heigh (L_L) and width (w_f) were compared against the available empirical correlations. EC1 methodology for the estimation of L_L for NoFD conditions were found to yield decreased EVF height for both rectilinear and curvilinear geometries compared to numerical data. For FD conditions both EC1 and Heskestad methodology seem to over-estimate EVF height compared to current predictions.
- Values of EVF width (*w_f*) were found to strongly depend on both excess heat release rate from the compartment fire. Under NoFD conditions EC1 methodology shows a strong disagreement with numerical values as it underpredicts EVF width. Under FD conditions, for all geometries, EC1 methodology overestimates width compared to predictions.
- EC1 methodology tends to over predict centreline temperatures for all rectilinear NoFD
 cases. This is not the case for NoFD conditions in curvilinear geometries as in most of the
 cases EC1 underpredicts values compared to predictions.
- The parametric study presented in Section 5.4 was conducted using a constant HRR. During the FD condition, the predicted heat flux was within the range of less than 10 kW/m², whereas under the No-FD condition it remained below 40 kW/m². However, the geometric dimensions of the model used in this analysis differed from those in the experimental test in the section 5.3.3; therefore, a direct comparison was not feasible. The predicted heat flux values still exceeded those obtained in the 4 MW parametric case, primarily because the geometric dimensions in the current study were smaller than those used in the 4 MW case. Additional research should focus on the façade heat flux, given the considerable discrepancies observed between the curvilinear and rectilinear geometries.

The obtained extensive set of numerical data, derived for the interior and exterior of the fire compartment will be further validated with experimental results in curvilinear geometries. Emphasis will be given in evaluating the accuracy of available empirical correlations and methodologies used for the calculation of EVF envelope, centreline temperatures and heat flux on the façade.

6 CONCLUSION & FUTURE WORKS

6.1 Conclusion

This thesis investigated the development and behavior of EVF under varying ventilation conditions and geometrical configurations, with particular emphasis on non-orthogonal, curvilinear buildings. Motivated by the critical gaps identified in the literature regarding fire dynamics in complex geometries, a comprehensive research framework was developed combining both medium- and large-scale experimental investigations with extensive numerical investigations. The major findings and contributions of this thesis are summarized below.

- The literature review established that there exists a profound influence of building characteristics, particularly façade geometry and opening configurations, on the development and behavior of EVF. The size, location, and design of these openings can influence both the interior and exterior fire, increasing the risk of vertical and horizontal fire spread as these openings provide a pathway for flames and causing complex flow behavior both inside the fire compartment and on external facades. The literature review also revealed that numerous factors, including window opening designs and shapes such as circular, rectilinear, casement, triangular, and top-hung windows, can significantly affect EVF, leading to intricate flow behaviors. It highlighted a substantial research gap in understanding fire dynamics with respect to non-orthogonal structure, and also underscoring the need for systematic studies focused on curvilinear geometries.
- The experimental and numerical investigation of FD influence on EVF behavior in rectilinear medium scale configurations demonstrated that FD ventilation significantly alters flame behavior, leading to reduced façade thermal loads and increased EVF projection compared to NoFD conditions. It was revealed that opening size has significant influence on the development and temperature distribution of EVF, as increased opening resulted in different flow fields and an additional recirculation zone formed near the openings. The validated numerical models provided a reliable predictive tool when smaller compartment opening sizes are considered. Numerical results of NoFD conditions are in good agreement with experimental results as there is 6% variance but this was increased to 15% when compared with experimental measurements of temperature under FD conditions. However, when the opening size is increased, and the wind factor is introduced the model becomes more complex and the relevant error difference was in the range of 30% or more. This study also highlights the critical importance of considering ventilation conditions in fire safety design and the necessity of precise modelling to predict fire

- behavior and its impact on building structures. The insights gained from this research might help in shaping fire safety regulations for more effective fire protection strategies, ultimately enhancing the safety and resilience of building designs.
- A comparative study between rectilinear and curvilinear compartments at medium scale experiments revealed that compartment geometry exerts a strong influence on internal fire dynamics and EVF characteristics. The findings provided significant insights into smoke flow pattern and fire dynamics in both interior and exterior of the compartment in reference to the varying compartment geometry, ventilation, and bounding materials. Rectilinear compartments exhibited higher peak internal temperatures, stronger plume buoyancy, and more intense EVF development compared to curvilinear compartments, primarily due to differences in material thermal properties. The highest peak temperature of approximately 700°C is observed in both rectilinear and curvilinear geometry under FD conditions, while the rectilinear NoFD configuration reaches a lower peak of around 600°C and for the curvilinear, lower peak temperature is at approximately 550°C. Overall, consistent higher temperatures are produced in rectilinear geometries than curvilinear geometries, due to the material bounding surface and the attributing heat retention. Curvilinear compartments, constructed from steel, demonstrated greater conductive heat losses and enhanced recirculation near openings, resulting in lower intensity but more laterally dispersed EVFs. Variations in opening sizes, fuel location and ventilation conditions also have significantly influenced combustion dynamics. The fuel pan location at elevated height resulted in the maximum compartment temperature dropped to around 450°C for both geometries. This indicates a significant reduction in temperature, with a percentage difference of approximately 35.7% between the two fuel pan heights. The GER analysis pointed out that external venting flames predominantly emerged when GER values exceeded unity, indicating under-ventilated fire conditions for the case of lower opening sizes. An underventilated fire is not very sensitive to the inner boundary surface temperature, only to the area of ventilation and its location.
- Additionally, the outdoor large-scale experiments indicated increased combustion and temperature differences due to wind-driven ventilation effects, which reaffirmed the influence of environmental conditions on fire behavior.
- A detailed large-scale numerical investigation into the effects of compartment geometry, ventilation configuration, and opening size on compartment fire development and EVF, supported by validation against medium-scale fire experiments was done in this analysis.
 The numerical investigations deepened the understanding of velocity flow fields affect

with respect to the geometrical differences, ventilation configuration, and opening size and further on compartment fire behavior and EVF formation. It was shown that larger openings (25 cm × 40 cm) promoted faster fire growth and clearer peak and decay phases but resulted in lower EVF temperatures (experimental: up to ~180 °C; FDS: 200 °C–250 °C). In contrast, smaller openings (25 cm × 20 cm) introduced ventilation constraints, leading to significantly higher compartment temperatures (experimental: ~300 °C–400 °C; FDS ~ 500 °C). FD conditions enabled bidirectional flow, supporting oxygen supply and enhancing internal combustion, whereas NoFD resulted in unidirectional high-pressure outflows with elevated EVF temperatures. EVF plumes in rectilinear NoFD cases reached velocity peaks exceeding 5 m/s, forming a larger laminar jet in greater length. Curvilinear NoFD plumes were lower in momentum (~2.5 m/s–3 m/s) and followed the building curvature, raising potential concerns about fire spread to the façades. FD conditions led to weaker, more laterally dispersed flows (velocities ~3 m/s–4 m/s) in both geometries. FDS captured the EVF trend in both geometries with respect to the EVF temperature but consistently overpredicted peak temperatures, particularly in NoFD conditions.

- The comparative analysis of FD and NoFD conditions reveals significant differences in fire development, external flame behavior, and thermal impacts in curvilinear compartments in the large-scale experiments. Large-scale experiments focused on curvilinear enclosures reaffirmed these findings, illustrating the pronounced impact of ventilation on fire growth, temperature, and EVF behavior. Under NoFD conditions, intense combustion, unidirectional hot gas flows, and extensive external flame propagation were observed. FD ventilation introduced bidirectional flow dynamics, stabilizing combustion and moderating thermal impacts. However, numerical simulations using FDS tended to overpredict peak heat fluxes and temperatures, highlighting the need for careful interpretation when using CFD models for performance-based design in non-orthogonal geometries.
- The final stage of the research evaluated the applicability of empirical fire engineering design correlations, particularly those of Eurocode 1 (EC1) and Heskestad, in predicting EVF parameters in both rectilinear and curvilinear compartments. Predictions using the empirical correlations for the estimation of the EVF heigh (L_L) and width (w_f) were compared against the available empirical correlations. EC1 methodology for the estimation of L_L for NoFD conditions were found to yield decreased EVF height for both rectilinear and curvilinear geometries compared to numerical data. For FD conditions both EC1 and Heskestad methodology seem to over-estimate EVF height compared to current

predictions. Values of EVF width (w_f) were found to strongly depend on both excess heat release rate from the compartment fire. Under NoFD conditions EC1 methodology shows a strong disagreement with numerical values as it underpredicts EVF width. Under FD conditions, for all geometries, EC1 methodology overestimates width compared to predictions. EC1 methodology tends to over predict centreline temperatures for all rectilinear NoFD cases. This is not the case for NoFD conditions in curvilinear geometries as in most of the cases EC1 underpredicts values compared to predictions. Moreover, in many cases, the EC1 equations were not valid due to exceeding their applicability limits, notably when the dimensionless parameter $(L_x\sqrt(A_v))/Q<1$ fell outside the recommended range. These findings emphasize the limitations of applying conventional empirical models developed for rectilinear geometries to complex, non-orthogonal building forms.

In summary, this research presents several significant contributions to the understanding of EVF in modern architectural contexts. Through a comprehensive experimental investigation which includes both medium and large scale and validated numerical simulations, it systematically compares the development of EVF between rectilinear and curvilinear geometries. The findings clearly demonstrate that geometric configuration plays a pivotal role in influencing the behavior of EVF, affecting flame trajectory, plume dynamics, and thermal exposure patterns. By studying both traditional rectilinear forms and emerging curvilinear designs, this work provides a strong database that improves the state of knowledge in fire dynamics related to façade openings.

A major contribution of this study lies in highlighting the critical influence of ventilation conditions and opening size on EVF characteristics, particularly within non-orthogonal geometries. It was observed that changes in ventilation conditions (FD, NoFD, wind etc.) can lead to marked differences in EVF, temperature profiles, and thermal impact on the façade surface. These results underline the importance of moving beyond conventional norms when assessing fire risk in complex building forms. The research shows that in curvilinear geometries, flow patterns become more intricate, leading to variations in compartment fire dynamics and the nature of EVF compared to their rectilinear counterparts.

In addition, this study critically evaluates the applicability of existing empirical correlations developed predominantly for rectilinear or simple façade geometries. While traditional correlations have been used in the fire engineering community, however, their application to non-orthogonal geometries appears limited. Hence, discrepancies may lead to underestimation or overestimation of façade fire risks if not properly accounted for in design assessments. The

findings thus call for the refinement of empirical models or the development of new design methodologies that are applicable to complex geometries.

The development and validation of detailed numerical models constitute another major contribution to this work. Using the FDS, numerical models were validated against experimental results to ensure that key fire dynamics phenomena were accurately captured. These models provide a practical resource for fire safety engineers aiming to adopt performance-based design methods for complex architectural projects to predict EVF behavior, evaluate potential impacts on façades and adjacent structures, and design targeted mitigation strategies based on realistic scenarios.

The findings of this research significantly contribute to improved fire risk assessment, particularly for buildings with complex geometries. By providing validated experimental data and numerical models, the study enhances the understanding of how architectural features influence EVF behaviour. This improved insight enables more accurate evaluation of façade exposure risks, supporting more reliable performance-based fire safety designs. Furthermore, the research outcomes offer a scientific basis that could potentially inform future fire safety design practices and guidelines.

6.2 Limitations

Nonetheless, some limitations of this research must be acknowledged. The use of different construction materials (Monolux and steel) introduced material effects that could influence combustion dynamics and heat transfer rates. Additionally, while numerical models achieved good agreement in most cases, discrepancies in predicting peak temperatures and heat fluxes under ventilation conditions suggest the need for further model refinement and careful consideration in fire safety engineering design using performance-based approaches.

6.3 Recommendation for Future Works

Future research should aim to conduct additional experiments using similar construction materials across different geometries to avoid material-dependency. In the current study, although efforts were made to control variables, differences in thermal conductivity, specific heat capacity, and surface emissivity between construction materials of compartments could have influenced heat transfer processes and combustion rates. By maintaining consistent material properties across experiments, future studies can more accurately attribute observed variations in EVF characteristics, thereby strengthening the reliability of the findings for the further understanding

of dynamics in the non-orthogonal geometries and its further application in fire risk assessment and performance-based fire safety design.

Investigating a wider range of fuel loads and incorporating multi-vent configurations is essential for a deeper understanding of EVF behaviour in complex compartment geometries. The current FDS model can be used to simulate multi-opening scenarios. The existing domain setup, boundary conditions, and grid resolution are sufficiently flexible to accommodate additional openings. This will allow future studies to investigate the influence of multiple openings on EVF behaviour using the same validated modelling framework. Varying the fuel load would allow for the exploration of different fire growth rates, heat release rates, and combustion efficiencies, all of which can significantly influence the characteristics of the EVF. In the present work, large-scale experiments were conducted using a 20 kg fuel load; however, repeating similar experiments with a higher fuel mass, approximately 50 kg, would provide valuable insights into the behaviour of EVF under more severe fire conditions. Additionally, the introduction of multiple openings and aspect ratio of the opening would generate more complex ventilation-driven flow patterns, altering the EVF shape, velocity fields, and external heat fluxes. Since multiple openings are common in real-world building designs, considering such scenarios would lead to a more comprehensive and realistic understanding of EVF development under practical architectural conditions.

Finally, future work should also focus on developing more predictive models or adjusted empirical correlations specifically tailored to curvilinear and non-orthogonal enclosures. Current engineering design correlations for EVF are predominantly derived from studies involving rectilinear geometries, limiting their applicability to modern architectural forms featuring curvature or other complex geometries. It is suggested that future correlations can incorporate a set of non-dimensional parameters representing both ventilation and geometric characteristics. The influence of ventilation can be captured using parameters such as the heat release rate (Q) and the ventilation factor $(A_o\sqrt{h_o})$, which account for the combined effect of opening area and height. For the geometric contribution, parameters such as the curvature ratio (H/R)—where R denotes the radius of curvature of the enclosure surface, H represents a characteristic vertical length scale — usually taken as the height of the opening or the compartment height (depending on what geometric feature the correlation is normalized against) and a non-orthogonality angle (α) between the wall plane and the opening can be used to quantify deviation from rectilinear geometry. In developing such correlations, it is important to note that while the opening width and height remain constant in rectilinear configurations, this may not hold true for other geometrical forms. For circular openings, both the width and height can vary continuously with the curvature. In contrast, for curvilinear openings—whether convex or concave—the width generally remains unchanged, but the effective height relative to the wall surface may vary depending on the local radius of curvature. Hence, careful consideration and consistent definition of the opening parameters are essential to ensure that the influence of geometry on ventilation characteristics is correctly captured. Rather than developing correlations for a fixed opening size, the proposed form of the correlations would therefore treat the geometric parameters $(H/R, \alpha)$ as correction factors applied to conventional rectilinear correlations (e.g., Heskestad or EC1-based formulations). This concept could also be considered as a recommendation for future work. Such an approach ensures that the resulting model remains physically scalable and valid across a range of opening configurations.

Through the combined experimental, numerical, and analytical work, this thesis advances the understanding of fire dynamics and EVF characteristics in modern, architecturally complex building forms, contributing valuable knowledge to the field of fire safety engineering, in performance-based design, Risk assessment etc.

7 REFERENCES

- Abu-Zidan, Y. et al., (2022) Effect of wind speed and direction on facade fire spread in an isolated rectangular building, Fire Safety Journal. 129. 103570. https://doi.org/10.1016/j.firesaf.2022.103570
- Asimakopoulou, E. K., (2016). Development and assessment of experimental and numerical tools for characterization of externally venting flames and evaluation of their effect on building facades (Doctoral dissertation) National Technical University of Athens.
- Asimakopoulou, E. K., Chotzoglou, K., Kolaitis, D. I., & Founti, M. A. (2016). Characteristics of externally venting flames and their effect on the façade: a detailed experimental study. *Fire technology*, *52*, 2043-2069.
- Asimakopoulou, E. K., Dionysios, I. K., and Founti, M. A. (2016) Geometrical characteristics of externally venting flames: Assessment of fire engineering design correlations using medium-scale compartment-façade fire tests. Journal of Loss Prevention in the Process Industries. 44. 780-790. https://doi.org/10.1016/j.jlp.2016.09.006
- Asimakopoulou, E., Chotzoglou, K., Kolaitis, D., Zhang, J. and Delichatsios, M. (2019)

 Numerical investigation of externally venting flame characteristics in a corridor-façade configuration. Fire Safety Journal. 110. 102912.

 https://doi.org/10.1016/j.firesaf.2019.102912
- Asimakopoulou, E.K., Kolaitis, D.I. and Founti, M.A. (2017) Assessment of fire engineering design correlations used to describe the geometry and thermal characteristics of Externally Venting Flames. Fire Technology. 53(2).709-739. https://doi.org/10.1007/s10694-016-0594-2
- Asimakopoulou, E.K., Kolaitis, D.I. and Founti, M.A. (2020). Performance of a ventilated-façade system under fire conditions: An experimental investigation. Fire and Materials. 44 (6). 776-792. https://doi.org/10.1002/fam.2863
- BBC. (2016) Dubai hotel fire: The Address Downtown hotel engulfed in flames, BBC News Middle East. Available at: https://www.bbc.com/news/av/world-middle-east-35208484 (Accessed 21 June 2022).

- BBC. (2017) Dubai's Torch Tower catches fire for second time in two years. BBC News Middle East. Available at: https://www.bbc.com/news/world-middle-east-40822269 (Accessed 21 June 2022).
- Beard, A. N., Drysdale, D. D., & Bishop, S. R. (1995). A non-linear model of major fire spread in a tunnel. *Fire Safety Journal*, 24(4), 333-357.
- Beshir M, Mohamed M, Kouritem SA, Lemmertz CK, Centeno FR, Rush D. (2023) Investigating numerically the effect of wind on fire spread between two informal settlement dwellings. Fire Technol. 1-36. https://doi.org/10.1007/s10694-023-01374-y
- Bisby L., Gales J., Maluk C. (2013) "A contemporary review of large-scale non-standard structural fire testing", Fire Science Reviews, 2:1, 1-27.
- Bonner, M. and Rein, G. (2020). List of Facade Fires 1990 2020. [online] Zenodo. Available at: https://zenodo.org/record/3743863#.Y1oXKHZBwdU [Accessed 27 Oct. 2022].
- Bonner, M., Wegrzynski, W., Papis, B.K. and Rein, G. (2020). Kresnik: A top-down, statistical approach to understand the fire performance of building facades using standard test data. Building and Environment. Elsevier. 169. 106540. https://doi.org/10.1016/j.buildenv.2019.106540
- Bullen, M.L. and Thomas, P.H. (1979). Compartment fires with non-cellulosic fuels. In Symposium (International) on Combustion. Elsevier. 17 (1). 1139-1148. https://doi.org/10.1016/S0082-0784(79)80108-3
- Chen, H. X., Liu, N. A. and Chow, W. K. (2011) Wind tunnel tests on compartment fires with crossflow ventilation. Journal of wind engineering and industrial aerodynamics. 99 (10). 1025-1035. https://doi.org/10.1016/j.jweia.2011.07.006
- Drysdale, D. (2011) An introduction to fire dynamics, 3rd. Ed. John Wiley & sons. https://doi.org/ https://doi.org/10.1002/9781119975465
- Empis, C.A. (2010) Analysis of the compartment fire parameters influencing the heat flux incident on the structural façade. Ph.D. Thesis. University of Edinburgh, U.K. Available at: https://era.ed.ac.uk/handle/1842/4188 [Accessed 27 Oct. 2022]

- EN 1991-1-2. (2002). Euro code 1: Actions on Structures, Part 1-2 General Actions Actions on Structures Exposed to Fire, European Committee for Standardization, Brussels, Belgium.
- Fahd, J. (2017) Fire Investigation Report of Findings. Cohoe: Homeland Security and Emergency Services. Available at: https://www.edgewood.edu/docs/default-source/aboutdocs/2018-security-and-fire-safety-report.pdf [Accessed 27 Oct., 2022]
- Fang, X., Tang, F., & Ren, F. (2024). Flame Extension Length Beneath an Inclined Eave Induced By Facade Fire Plume. *Fire Technology*, 1-18.
- Feng, W., Mingnian, W., Ricky, C. and Yu., W. (2017) Numerical study on fire smoke movement and control in curved road tunnels. Tunnelling and Underground Space Technology. 67. 1-7. https://doi.org/10.1016/j.tust.2017.04.015
- Gao, W. et. al. (2016) Fire spill plume from a compartment with dual symmetric openings under cross wind. Combustion and Flame. 167. 409-421. https://doi.org/10.1016/j.combustflame.2016.01.011
- Guoxiang Z. (2017) Numerical study on under-ventilated enclosure fires and fire spread on building façades. PhD Thesis, University of Ghent, Belgium. ISBN 978-94-6355-079-6. Accessed June 10, 2024.
- Hamins, A. Maranghides and G. Mulholland. (2003) The Global Combustion Behavior of 1 MW to 3 MW Hydrocarbon Spray Fires Burning in an Open Environment, Building and Fire Research Laboratory. National Institute of Standards and Technology (NIST). USA. Available at: https://nvlpubs.nist.gov/nistpubs/Legacy/IR/nistir7013.pdf [Accessed Oct. 26, 2022]
- Hanna, J., Fantz, A. and Shoichet, C. E. (2015) Fire engulfs downtown Dubai's high-rise Address hotel. CNN. Available at: https://edition.cnn.com/2015/12/31/middleeast/dubai-address-hotel-fire/index.html (Accessed 21 June 2022)
- Hansen, S. et. al. (2016) The Large Fire in Lærdal, January 2014: How did the Fire Spread and what Restricted the Fire Damage?, in: R. H. Gabrielsen and S. Lacasse (eds.), Fagtrykk Trondheim AS, Norway. pp. 99-112.

- Hardy, J. and Mendick, R. (2019) Grenfell Tower report section by section: the 1,000 pages of damning criticism on failures that compounded tragedy. The Telegraph. Available at: https://www.telegraph.co.uk/news/2019/10/28/grenfell-tower-report-section-section-1000-pages-damning-criticism/ (Accessed 21 June, 2022).
- Heskestad, G. (1983) Virtual origins of fire plume. Fire Safety Journal. 5 (2). 109–114.
- Hirschler, M.M. (2020). Façade requirements in the 2021 edition of the US International Building Code. Fire and Materials. 45 (5). 586-597. https://doi.org/10.1002/fam.2803
- Hu, L. et. al. (2019) Façade flame height and horizontal extending distance from opening of compartment fire with external sideward wind. Proceedings of the Combustion Institute. 37. 3859-3867. https://doi.org/10.1016/j.proci.2018.06.201
- Hu, L., et al. (2017) Facade flame height ejected from an opening of fire compartment under external wind. Fire Safety Journal. 92. 151-158. https://doi.org/10.1016/j.firesaf.2017.06.008
- Hu, L., Milke, J.A., and Merci, B. (2017) Special Issue on Fire Safety of High-Rise Buildings. Fire Technology. 53(1). 1-3. https://doi.org/10.1007/s10694-016-0638-7
- Huang, H. et al. (2009) Experimental study of fire growth in a reduced-scale compartment under different approaching external wind conditions. Fire Safety Journal. 44 (3). 311-321. https://doi.org/10.1016/j.firesaf.2008.07.005
- Hurley, M. J. (2016) SFPE Handbook of fire protection engineering. 5th Ed. Society of Fire Protection Engineers. Massachusetts, U.S.A. https://doi.org/10.1007/978-1-4939-2565-0
- J Hackett, J., (2018) Building a Safer Future: Independent Review of Building Regulation and Fire Safety. London, United Kingdom: Ministry of Housing, Communities and Local Government.
- Li. J. M. Yin, C.C., Hu, C., Li, Y.F., Xu, P. (2013) Computational study of wind effect on window flame spread across the exterior wall of high-rise building. Applied Mechanics and Materials. Trans Tech Publications Ltd. 438-439 and 1898-1902. https://doi.org/10.4028/www.scientific.net/AMM.

- Ji, J. et al. (2015) Ambient wind effect on combustion characteristics in compartment with simultaneous door and window opened, Energy and buildings. 105. 217-225. https://doi.org/10.1016/j.enbuild.2015.07.046
- Kaihua, L., Kaihua, X., Congling, S., Manjiang, Y., Jie, W. and Yanming, D. (2021) Investigation on the tunnel curvature effect upon the ceiling temperature of tunnel fires: a numerical simulation. Fire technology. 57. 2839-2858. https://doi.org/10.1007/s10694-021-01183-1
- Karlsson, B. and Quintiere, J.G. (2000) Enclosure Fire Dynamics. Boca Raton: CRC Press.
- Kawagoe K. (1958) "Fire behavior in rooms", Report No.27, Tokyo: Building Research Institute, Ministry of Construction.
- Klopovic, S. and Turan, Ö.F. (2001) 'A comprehensive study of externally venting flames Part I: External plume characteristics for through-draught and no-through-draught ventilation conditions and repeatability', *Fire Safety Journal*, 36(2), pp. 99–133.
- Klopovic, S. and Turan, Ö.F. (2001). A comprehensive study of externally venting flames Part II: Plume envelope and centre-line temperature comparisons, secondary fires, wind effects and smoke management system. Fire Safety Journal. 36(2). 135-172. https://doi.org/10.1016/S0379-7112(00)00041-2
- Kolaitis, D., Asimakopoulou, E. and Founti, M. (2017) Fire behaviour of gypsum plasterboard wall assemblies: CFD simulation of a full-scale residential building. Case Studies in Fire Safety. 7. 23-35. https://doi.org/10.1016/j.csfs.2016.11.001
- Law, M. (1978). Fire safety of external building elements The design approach. Engineering Journal. Second Quarter. American Institute of Steel Construction. U.S.A. 59-74.
- Law, M. and O'Brien, T. (1989). Fire safety of bare external structural steel, The Steel Construction Institute. SCI Publication. U.K.
- Lee, Y.-P., Delichatsios, M.A. and Silcock, G.W.H. (2007) Heat fluxes and flame heights in façades from fires in enclosures of varying geometry. Proceedings of the Combustion Institute. 31(2). 2521–2528. https://doi.org/10.1016/j.proci.2006.08.033

- Li, M., Gao, Z., Li, K. and Sun, J. (2017) Wind effects on flame projection probability from a compartment with opposing openings. Fire Safeety Journal. 91. 414-421. https://doi.org/10.1016/j.firesaf.2017.04.037
- Liang, Y., Huo, R., Zhang, J.Y. and Zhang, H.-P. (2006) 'Characteristics of heat release rate of diesel oil pool fire', *Ranshao Kexue Yu Jishu (Journal of Combustion Science and Technology)*, **12**(2), pp. 164–168.
- Lönnermark, A. and Haukur, I. (2007) The Effect of Cross-sectional Area and Air Velocity on the Conditions in a Tunnel during a Fire. Fire Technology. SP Report, SP Technical Research Institute of Sweden. Available at: https://www.diva-portal.org/smash/get/diva2:962400/FULLTEXT01.pdf [Accessed 12 June 2022]
- Lu, K., Hu, L., Delichatsios, M., Tang, F., Qiu, Z. and He, L., (2015) Merging behavior of facade flames ejected from two windows of an under-ventilated compartment fire. Proceedings of the combustion institute. 35(3). 2615-2622. https://doi.org/10.1016/j.proci.2014.05.083
- Lu, K.H., Hu, L.H., Tang, F., He, L.H., Zhang, X.C. and Qiu, Z.W. (2014) Experimental investigation on window ejected facade flame heights with different constraint side wall lengths and global correlation. International Journal of Heat and Mass Transfer. 78. 17-24. https://doi.org/10.1016/j.ijheatmasstransfer.2014.06.060
- Li, M., Gao, Z., Ji, J., & Wan, H. (2021) External Wind Effect on Flame Behavior Inside and Outside a Compartment with Opposing Openings. Fire Technology. 57. 1987-2006. https://doi.org/10.1007/s10694-021-01104-2.
- Madrzykowski, D., and Kerber, S., (2009) Fire Fighting Tactics Under Wind Driven Fire Conditions: 7-Story Building Experiments. Technical Note (NIST TN), National Institute of Standards and Technology. Gaithersburg, MD. Available at: https://tsapps.nist.gov/publication/get_pdf.cfm?pub_id=902177 (Accessed 21 June 2022).
- Makhviladze G.M., Shamshin A.V., Yakush S.E., Zykov A.P. (2006) "Experimental and numerical study of transient compartment fires", Combustion Explosion and Shock Waves, 42, 723-730.

- McAllister, S. and Finney, M. (2016) The effect of wind on burning rate of wood cribs, Fire Technology. 52. 1035-1050. https://doi.org/10.1007/s10694-015-0536-4
- McCaffrey BJ, Heskestad G. (1976) A robust bidirectional low-velocity probe for flame and fire application. Combust Flame. 26(1):125–127. https://doi.org/10.1016/0010-2180(76)90062-6
- McGrattan, K. et al. (2019) Fire dynamics simulator user's guide, NIST Spec. Publ. 6. 2019. Available at: https://pages.nist.gov/fds-smv/manuals.html [Accessed Oct. 22, 2022]
- McGrattan, K., Hostikka, S., Floyd, J., McDermott, R., Vanella, M., Weinschenk, C. & Peacock,
 R. (2023) Fire Dynamics Simulator Technical Reference Guide: Volume 3 Validation.
 NIST Special Publication 1018-3, Sixth Edition. National Institute of Standards and
 Technology, Gaithersburg, MD. Available at: https://doi.org/10.6028/NIST.SP.1018-3
- Merci B, Beji T. (2016) Fluid mechanics aspects of fire and smoke dynamics in enclosures [M]. CRC Press.
- Ohmiya, Y., Hori, Y., Safimori, K. and Wakamatsu, T. (2000). Predictive method for properties of flame ejected from an opening incorporating excess fuel. Fire Safety Science. 4. 375-386.
- Ohmiya, Y., Yusa, S., Suzuki, J-I., Koshikawa, K. and Delichatsios, M.A. (2003)

 Aerothermodynamics of fully involved enclosure fires having external flames. In:

 Proceedings of the 4th International Seminar on Fire and Explosion Hazards, pp. 121–129.
- Okaze, T. et al. (2020) Benchmark test of flow field around a 1:1:2 shaped building model using LES: influences of various calculation conditions on simulation result. AIJ Journal of Technology and Design. 26 (62). 179–184. https://doi.org/10.3130/aijt.26.179
- Oleszkiewicz, I. (1990). Fire exposure to exterior walls and flame spread on combustible cladding. Fire Technology. 26(4). 357-375. https://doi.org/10.1007/BF01293079
- Oleszkiewicz, I. (1991). Vertical separation of windows using spandrel walls and horizontal projections. Fire technology. 27(4). 334-340. https://doi.org/10.1007/BF01039884
- Omega. (2023) Wire Colour Codes and Limits of Error. Omega Engineering Inc. Available at: https://in.omega.com/techref/colorcodes.html. (Accessed April 03, 2023)

- Pan, R., Zhu, G., Liang, Z., Zhang, G., Liu, H., & Zhou, X. (2020). Experimental study on the fire shape and maximum temperature beneath ceiling centerline in utility tunnel under the effect of curved sidewall. *Tunnelling and Underground Space Technology*, 99, 103304.
- Pan, R., Zhu, G., Xu, G., & Liu, X. (2022). Experimental and theoretical analysis on extension flame length of buoyancy-induced fire plume beneath the curved ceiling. *Tunnelling and Underground Space Technology*, 122, 104365.
- Quintiere, J. G. (2006) Fundamentals of fire phenomena. John Wiley. West Sussex, U.K. https://doi.org/10.1002/0470091150
- Quintiere, J.G. and Cleary, T.G. (1994). Heat flux from flames to vertical surfaces. *Fire Technology*, 30(2), pp.209–231.
- Quintiere, J. G. (2016) Principles of fire behavior. 2nd. Ed. CRC Press.
- Ren F., Hu L, Sun X, Hu K. (2018) An experimental study on the vertical temperature profile of façade fire plume ejected from a compartment with an opening subjected to external wind normal to the façade. Int J Therm Sci. 130:94-99. https://doi.org/10.1016/j.ijthermalsci.2018.04.008
- Seigel, L.G. (1969). The projection of flames from burning buildings. Fire Technology, 5, 43-51. https://doi.org/10.1007/BF02591612
- Smagorinsky, J. (1963) General circulation experiments with the primitive equations: I, The basic experiment. Monthly Weather Review. 91 (3). 99–164. https://doi.org/10.1175/1520-0493(1963)091<0099:GCEWTP>2.3.CO;2
- Smolka J, (2022) The effect of forced draught on the externally venting flame parameters of enclosure fire" PhD Thesis, Technical University of Ostrava, Czech Republic.
- Smolka J, Kempná K, Kučera P, Kempný K, Asimakopoulou E, Danihelka P. (2023) Setup of a 3D printed wind tunnel: application for calibrating bi-directional velocity probes used in fire engineering applications. HardwareX 15. https://doi.org/10.1016/j.ohx.2023.e00440
- Smolka, J. (2020) Scale base for load cell by Majaczech, Thingiverse. Available on: https://www.thingiverse.com/thing:4330707 (Accessed July 26, 2022).

- Smolka, J. et. al. (2021). Wind Driven (Forced Draught) Impact On Enclosure Fires.

 Applications of Structural Fire Engineering, 9-11 June 2021, Ljubljana, Slovenia.
- Sturdy, M., & Johansson, N. (2025). Flame Extensions Under a Curved Ceiling. *Fire Technology*, 1-18.
- Sun, X., Hu, L., Yang, Y., Ren, F. and Fang, X., (2020) Evolutions of gas temperature inside fire compartment and external facade flame height with a casement window. Journal of hazardous materials. 381. 120913. https://doi.org/10.1016/j.jhazmat.2019.120913
- Sun, X., Tang, F., Lu, K., Ren, F., Shi, C., Merci, B. and Hu, L., (2023) Fundamentals of window-ejected fire plumes from under-ventilated compartment fires: Recent progresses and perspectives. Progress in Energy and Combustion Science. 94. 101039. https://doi.org/10.1016/j.pecs.2022.101039
- Thomas, P.H., & Law, M. (1972). The projection of flames from burning buildings. Fire Safety Science. 921. 1-1.
- User Manual SBG Series Water-cooled heat flux sensors Hukseflux Thermal Sensors. (n.d.).

 Available at: https://huksefluxjapan.com/manage/wp-content/uploads/2023/07/SBG_series_manual_v2301.pdf [Accessed 12 Mar. 2025].
- Vipin, V. (2012) Image processing-based forest detection. International Journal of Emerging Technology and Advanced Engineering. 2 (2). 87-95.
- Warrier A., Khan K., Nasriani H.R., Ndlovu S., Chamchine A., Graham T.L., Asimakopoulou E., (2022) Numerical investigation of the effect of ventilation conditions of Externally Venting Flames on curvilinear geometries", 10th International Seminar on Fire and Explosion Hazards, Oslo, Norway.
- Webster, C.T., Raftery, M.M. and Smith, P.G. (1961) *The burning of fires in rooms Part III*. Fire Research Note No. 474. Joint Fire Research Organization, Borehamwood, U.K.
- Webster, C.T. and Smith, P.G. (1964) The burning of well-ventilated compartment fires Part IV: Brick compartment, 2.4 m (8 ft) cube. Fire Research Note No. 578. Joint Fire Research Organization, Borehamwood, U.K.

- Węgrzyński W, Lipecki T, Krajewski G. (2018) Wind and fire coupled modeling—Part II: Good practice guidelines. Fire Technol. 54(5):1443-1485. https://doi.org/10.1007/s10694-018-0749-4
- White, N. and Delichatsios, M. (2015). Fire hazards of exterior wall assemblies containing combustible components. 1st. Ed. Springer New York. https://doi.org/10.1007/978-1-4939-2898-9
- Yanagisawa, A., Goto, D., Ohmiya, Y., Delichatsios, M.A., Lee, Y. and Wakatsuki, K.A.O.R.U. (2008) Effect of a facing wall on facade flames. In Fire Safety Science_Proceedings of the Ninth International Symposium, IAFSS. 801-811.
- Yokoi, S. (1960). Study on the prevention of fire-spread caused by hot upward current. BRI Report, 34.
- Yung, D. & Oleszkiewicz, I. (1988) *Fire spread via exterior walls of buildings*. Proceedings of the Fourth Conference on Building Science and Technology, Toronto, Ontario, 18–19 February 1988, pp. 1–12. National Research Council of Canada, Institute for Research in Construction.
- Zhang, X., Yang, Y., Sun, X., Ren, F., Fang, X. and Hu, L., (2022) A reduced-scale experimental investigation of facade flame behavior ejected from a top-hung window of fire compartment. Proceedings of the Combustion Institute. https://doi.org/10.1016/j.proci.2022.07.210
- Zhang, X., Zhang, Z., Zhang, Z., Xu, W., Luo, Q., Tao, H. and Li, X., (2020) Experimental investigation of compartment fires with circular opening: From the aspects of internal temperature and facade flame. Combustion and Flame. 213.107-116. https://doi.org/10.1016/j.combustflame.2019.11.027
- Zhang, X., Yang, M., Wang J., and He, Y (2010) Effects of computational domain on numerical simulation of building fires, Journal of Fire Protection Engineering. 20. 225-250. https://doi.org/10.1177/1042391510367349
- Zhang, Z., Zhang, X., Chen, L., Zhou, G., Tao, H., Zhou, L. and Yang, H., (2023) Effect of vertical facing wall on facade flame height of under-ventilated compartment fire with triangular opening. Thermal Science and Engineering Progress. 38. 101667. https://doi.org/10.1016/j.tsep.2023.101667

APPENDIX A: INFLUENCE OF TURBULENCE MODELLING IN FDS ON FORCED DRAUGHT CONDITIONS AND EVF IN COMPARTMENT FIRES

A.1 Introduction

The historical development of fire modelling has evolved to address the challenges posed by enclosure fires, exemplified by disasters such as the Kings Cross Fire (1987) and the World Trade Center collapse (2001). Early fire studies relied heavily on experimental techniques and theoretical approaches to understand fire dynamics, focusing on interactions involving fluid dynamics, thermodynamics, combustion, and radiation. While experiments provided valuable insights, their high costs and limited scalability highlighted the need for alternative methodologies. This led to the rise of computational models, initially categorized as stochastic models for probabilistic fire event analysis and deterministic models based on physics and chemistry. The most prominent deterministic models, known as zone models, simplified compartment fire analysis by dividing enclosures into two layers: hot gases and ambient air; enabling practical predictions of fire behaviour (Karlsson, 2000).

Advancements in computational power and the understanding of fire physics spurred the development of field models, also known as CFD-based fire models, as an alternative to zone models. These models divide the computational domain into a three-dimensional grid and solve time-dependent, nonlinear partial differential equations governing mass, momentum, and energy conservation. By offering greater spatial resolution and the ability to simulate complex geometries, field models overcome the limitations of empirical correlations and provide more precise predictions of fire behaviour. The transition to CFD-based fire modelling has been instrumental in enabling flexible, detailed simulations for diverse fire scenarios, advancing fire safety research and engineering practices (Karlsson, 2000).

CFD in fire modelling involves the study of fluid systems that are either static or dynamically changing in time and space, focusing on the behaviour of fire-induced flows, smoke, and heat transfer. The fluid dynamics calculations are performed using numerical methods implemented on high-speed digital computers, aligning with the computational nature of the process. In fire modelling, the physical characteristics of fluids in motion, such as smoke dispersion, heat transfer, and combustion processes, are typically described by fundamental mathematical equations. These equations, often in partial differential form, govern key phenomena such as airflow, temperature distribution, and chemical reactions. To solve these equations, they are transformed into discrete forms using advanced computational techniques and implemented through high-level

programming languages. These formulations are then executed using custom in-house programs or commercial CFD software designed for fire modelling (McGrattan et al., 2019). The resulting algebraic equations are solved using dedicated numerical methods, enabling the accurate simulation of fire behaviour, smoke movement, and their interactions with surrounding environments. This approach provides valuable insights into fire dynamics, supporting the development of fire safety strategies and systems.

A.2 Turbulence Modelling

Turbulence is a complex, chaotic, and three-dimensional phenomenon characterized by the irregular and stochastic motion of fluid particles. It occurs in many engineering and natural systems, including fire modelling, atmospheric flows, and industrial processes. The governing equations for turbulent flows are derived from the Navier-Stokes equations, which describe the conservation of mass, momentum, and energy in a fluid:

1. Continuity Equation (Mass Conservation):

$$\frac{\partial \rho}{\partial t} + \nabla \cdot (\rho u) = 0 \tag{A1}$$

2. Momentum Equation:

$$\rho\left(\frac{\partial u}{\partial t} + u \cdot \nabla u\right) = -\nabla p + \mu \nabla_u^2 + f$$
 A2

3. Energy Equation:

$$\frac{\partial}{\partial t}(\rho e) + \nabla \cdot (\rho e u) = -\nabla \cdot q + \Phi$$
 A3

where u is velocity, ρ is density, p is pressure, μ is dynamic viscosity, f represents external forces, e is specific energy, q is heat flux, and Φ is the viscous dissipation term.

In turbulent flows, these equations exhibit a wide range of spatial and temporal scales, making direct numerical simulation (DNS) computationally expensive for practical applications. (McGrattan et al., 2019)

A.2.1 Turbulence Modelling Approaches

• Reynolds-Averaged Navier-Stokes (RANS):

RANS models decompose flow variables into mean and fluctuating components (Reynolds decomposition):

$$u = \bar{u} + u'$$
 A4

Substituting this into the Navier-Stokes equations introduces the Reynolds stress tensor, $-\rho \overline{u'u'}$ which represents the effects of turbulence and requires closure through turbulence models like $k - \epsilon$, $k - \omega$, or Reynolds Stress Models (RSM). (McGrattan et al., 2019)

Large Eddy Simulation (LES):

LES resolves larger turbulent scales directly and models the smaller scales using sub grid-scale (SGS) models. Filtering the Navier-Stokes equations yields the SGS stress tensor, which is modelled using approaches like the Smagorinsky model. (McGrattan et al., 2019)

Direct Numerical Simulation (DNS):

DNS resolves all turbulence scales without modelling, solving the full Navier-Stokes equations. It is accurate but computationally prohibitive for high-Reynolds-number flows.

Turbulence modelling is crucial in predicting flow behaviours where turbulence significantly influences mixing, heat transfer, and momentum transport. Each approach balances accuracy and computational cost, with the choice depending on the specific application and available resources. (McGrattan et al., 2019)

A.3 Fire Dynamic Simulator (FDS)

The Fire Dynamics Simulator (FDS) is a sophisticated, Fortran-based Computational Fluid Dynamics (CFD) code specifically designed for simulating fire dynamics and smoke propagation in both enclosed and open environments. FDS numerically solves a specialized form of the Navier-Stokes equations tailored for low-Mach number (Ma < 0.3), thermally-driven flows, with a primary focus on modelling heat transfer and smoke movement resulting from fires.

The combustion model (Default) in FDS adopts a mixing-limited, infinitely fast reaction approach for simplified chemical kinetics, utilizing three lumped species—oxidizer, fuel, and products—to represent the combustion process. Thermal radiation is modelled using the Radiation Transport Equation (RTE), discretized via the Finite Volume Method (FVM) for participating media. Turbulence is captured through the Large Eddy Simulation (LES) framework, which resolves large-scale turbulent structures while employing sub grid-scale models to account for the effects of smaller, unresolved eddies. This combination of advanced modelling techniques enables FDS to deliver high-fidelity simulations of fire behaviour and smoke dynamics (McGrattan et al., 2019).

A.3.1 Turbulence models in FDS

In the Fire Dynamics Simulator (FDS) version 6.1, turbulence is primarily modelled using the Large Eddy Simulation (LES) framework, which resolves the larger, energy-containing turbulent structures while modelling the effects of smaller, sub grid-scale models. Additionally, FDS offers alternative modelling approaches to reduce computational cost, including Very Large Eddy Simulation (VLES) and Simple Very Large Eddy Simulation (SVLES).

These approaches relax some of the computational constraints associated with LES and Direct Numerical Simulation (DNS). Specifically, VLES and SVLES reduce the strict dependence on the Courant–Friedrichs–Lewy (CFL) condition, which imposes stringent time-step limitations in DNS and LES. By simplifying the resolution of turbulent structures and leveraging less restrictive time-stepping criteria, these methods enable faster computations while retaining sufficient accuracy for many practical fire modelling applications (McGrattan et al., 2019).

A.3.2 Models for the Turbulent Viscosity (SGS Models)

In FDS, the gradient diffusion approach is utilized as the turbulence model to close the sub grid-scale (SGS) momentum and scalar flux terms. This requires modelling the turbulent transport coefficients, specifically the turbulent (eddy) viscosity and the turbulent (eddy) diffusivity.

The turbulent diffusivity is determined using a constant turbulent Schmidt number (for mass diffusivity) or turbulent Prandtl number (for thermal diffusivity). Consequently, the turbulent viscosity emerges as the key transport coefficient for accurately modelling turbulence effects. There are several different SGS model options in FDS discussed below:

• Constant Coefficient Smagorinsky model

The eddy viscosity can be modelled as follows:

$$u_t = \rho(C_s \Delta)^2 |S|$$
 A5

$$|s| = \left(2s_{ij}s_{ij} - \frac{2}{3}(\nabla \cdot u)^2\right)^{\frac{1}{2}}$$
 A6

Where $C_s = 0.2$ is a constant and $\Delta = (\delta_x \quad \delta_y \quad \delta_z)^{\frac{1}{3}}$ is the filter width. The value of the Smagorinsky constant, $C_s = 0.2$, is derived from Lilly's theoretical analysis (Lilly, 1967), which assumes a balance between turbulence production and dissipation. This value is specifically applicable to a spectral cutoff filter, as implicit filtering used in energy-conserving numerical schemes more closely approximates a spectral cutoff filter than a box filter.

• Dynamic Smagorinsky model

For the dynamic Smagorinsky model (Germano, 1991), (Moin, 1991), the coefficient C_s in Smagorinsky model equation above is no longer taken as a constant, but rather computed based on the local flow conditions.

Deardorff's Model

FDS uses a variation of Deardorff's model (Deardorff, 1980).

$$u_t = \rho c_v \Delta \sqrt{k_{sqs}}$$
 A7

$$k_{sgn} = \frac{1}{2} ((\bar{u} - \dot{\bar{u}})^2 + (\bar{v} - \dot{\bar{v}})^2 + (\bar{w} - \dot{\bar{w}})^2)$$
 A8

Where \bar{u} is the average value of u at the grid cell center (representing the LES filtered velocity at the length scale Δ) and $\dot{\bar{u}}$ is the weighted average of u over the adjacent cells (representing a test-filtered field at the length scale 2Δ):

$$\bar{u} = \frac{u_{ijk} + u_{i-1,jk}}{2}$$
 A9

$$\dot{\bar{u}}_{ijk} = \frac{\pi_{ijk}}{2} + \frac{\bar{u}_{i-1,jk} + \bar{u}_{i+1,jk}}{4}$$
 A10

The terms \dot{v} and \dot{w} are defined similarly. The model constant is set to the literature value $C_{v=}0.1$ (Pope., 2000).

• Vreman's Model

Verman's eddy viscosity model (Vreman, 2004) is given by

$$\mu_t = \rho c \sqrt{\frac{B\beta}{\alpha_{ij}\alpha_{ij}}}$$
 A11

Where,

$$B_{\beta} = \beta_{11}\beta_{22} - \beta_{12}^2 + \beta_{11}\beta_{33} - \beta_{13}^2 + \beta_{13}^2 + \beta_{22}\beta_{33} - \beta_{23}^2$$
 A12

$$\beta_{ij} = \Delta_m^2 \alpha_{m_i} \alpha_{mj}$$
 A13

$$\alpha_{ij} = \frac{\partial u_j}{\partial x_i}$$
 A14

The model considers a possible anisotropy in the filter width in direction m, contraction on m. The basic idea behind Vreman's model is to expand the velocity field in a Taylor series and to test filter this field analytically, thus avoiding the expensive explicit test filtering operations necessary

in the dynamic model. Therefore, this model is inexpensive. Unlike constant coefficient Smagorinsky, however, Vreman's model is convergent, making it applicable to highly resolved LES calculations.

A.4 Turbulence model and forced draught impact on EVF

As discussed in Chapter 3, "Forced Draught Impact on Externally Venting Flames: An Experimental and Numerical Investigation," it was observed that numerical predictions of temperature profiles were reasonably accurate when smaller compartment openings were used. However, as the opening size increased and external wind effects were introduced, the simulation complexity increased, resulting in significant deviations often exceeding 30% between numerical and experimental results. These discrepancies highlight the limitations of the default turbulence model in accurately capturing the complex flow dynamics under enhanced ventilation conditions.

The numerical simulations were conducted using the default turbulence model settings in FDS. However, during the journal submission process, reviewer feedback considered evaluating the influence of different turbulence sub-models to improve the accuracy of the predictions. This critical observation prompted the extended analysis presented in this appendix.

Given these findings, it was deemed essential to investigate the influence of different turbulence sub-models on the accuracy of numerical predictions. For this purpose, the FD-40x40 test case was selected for comparative analysis using the following turbulence sub-models:

Test case

Turbulence sub models

Deardorff's Model

Dynamic Smagorinsky model.

Vreman's Model.

Constant Coefficient Smagorinsky model.

Table 13: Turbulence model test scenarios.

A.4.1 Temperature at the opening with different turbulence models

Figure 127 depicts the relationship between non-dimensional height and temperature at the compartment opening with different turbulence models. The data corresponds to five thermocouples placed at discrete vertical positions: 0H, 0.2H, 0.5H, 0.75H, and H, where H represents the full height of the opening (40 cm) in the FD 40x40 experimental configuration. The thermocouple layout is shown in Figure 20 for reference. Consistent with the methodology

presented in Chapter 3, the temperature values represent a 20-second time-averaged period during peak fire conditions for all turbulence model cases under consideration.

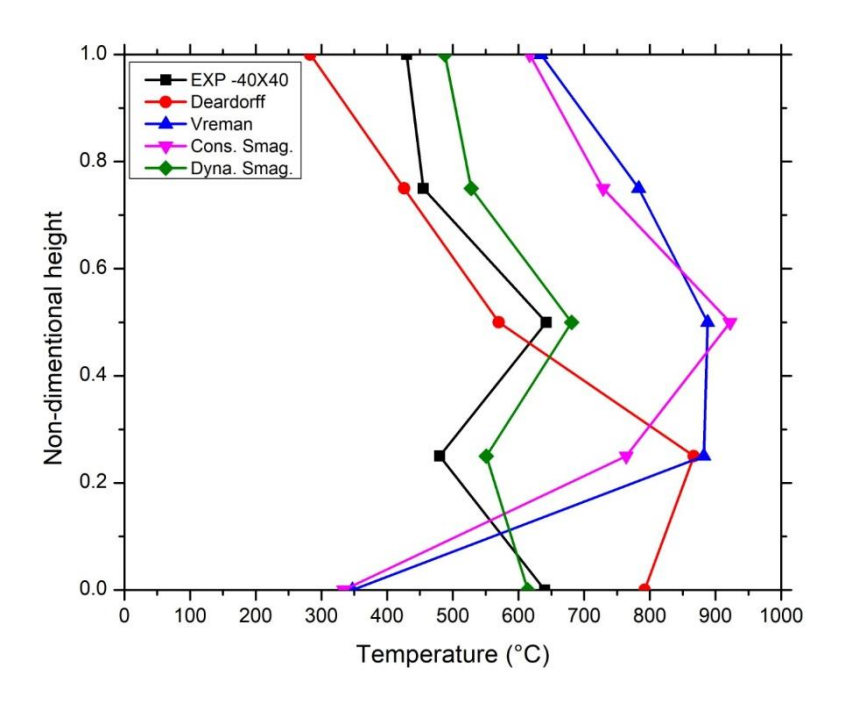


Figure 127: Non dimensional vertical distribution of the temperature profile at the outlet opening with turbulence models.

Figure 127 illustrates the non-dimensional height versus temperature profile for the FD-40x40 test case, comparing experimental data with FDS simulations using four different turbulence submodels: Deardorff, Vreman, Constant Smagorinsky, and Dynamic Smagorinsky. The non-dimensional height represents five thermocouple locations distributed along the opening height (H = 0.4 m). The FDS default model (Deardorff) showed significant deviations from the experimental temperature profile, particularly at the bottom and mid height levels with an error margin exceeding 40%. Both the Vreman and Constant Smagorinsky models also demonstrated noticeable overpredictions, especially at higher elevations. In contrast, the Dynamic Smagorinsky model yielded temperature predictions that closely followed the experimental trend across most of the thermocouple heights. Although it exhibited a slight overestimation, the temperature deviation remained within a 10% margin, indicating a good level of agreement with experimental result and in capturing the outward flow and stratification dynamics within the compartment and at the compartment opening. This comparison highlights the critical influence of turbulence model selection on compartment fire scenario under forced draught conditions with large openings.

A.4.2 Temperature at the Façade with different turbulence model

Thermocouples were positioned in the façade as depicted in the Figure 19. Figure 128 presents the facade temperature distribution along vertical heights ranging from 600 mm to 1200 mm for the FD-40x40 test case.

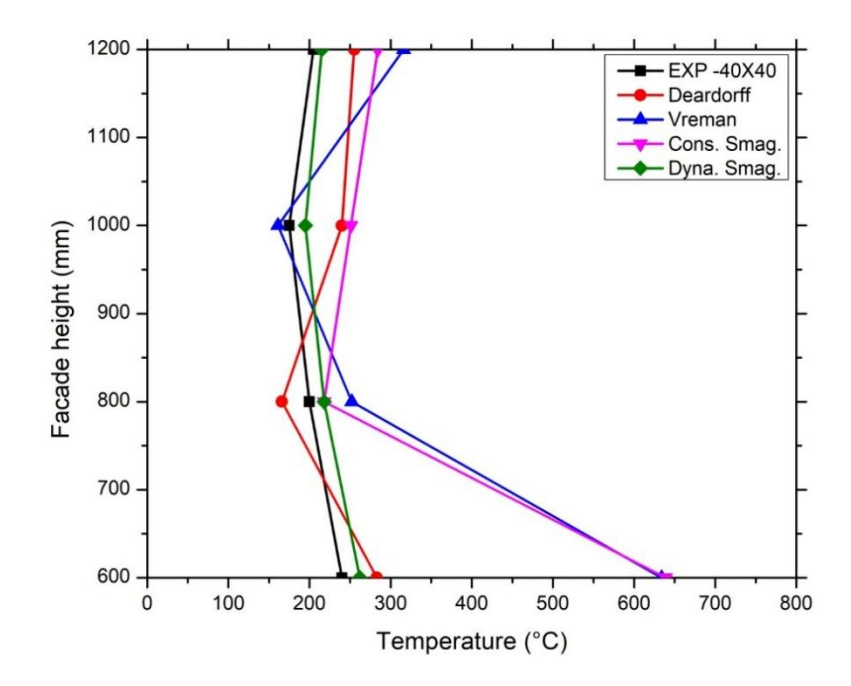


Figure 128: Vertical distribution of the temperature profile at the centerline of the outlet façade with different turbulence models.

The comparison includes experimental measurements and simulation results obtained from FDS using four different turbulence sub-models. Among the simulation models, the Deardorff and Dynamic Smagorinsky sub-models show reasonable alignment with the experimental trend. The Constant Smagorinsky and Vreman models, however, tend to significantly overpredict temperatures, with the Vreman model showing values exceeding 600 °C—more than double the experimental peak. Overall, the Dynamic Smagorinsky model maintain the good alignment with the experimental results and shows the best physical representation and maintaining error margins in less than 10% of the experimental values.

A.4.3 EVF flow and velocity field with different turbulence models

Figure 129 depicts the gas mixture velocity field for four different turbulence sub-models (Vreman, Deardorff, Dynamic Smagorinsky, and Constant Smagorinsky) at 200 seconds, as this selected timeline corresponding to the fully developed fire stage, as evidenced by peak HRR from the experiment and visible external flames in the experimental observations. The Dynamic Smagorinsky model captures EVF profile in a more realistic turbulence dissipation, resulting in a more diffused and slightly tilted EVF profile. Comparatively, while Vreman and Constant

Smagorinsky also predict high-velocity outflows, they display less physical entrainment behavior and also models tend to overpredict the extent and velocity of the external plume. Overall, both Deardorff and Dynamic Smagorinsky models offer reliable predictions of EVF behavior. However, the Dynamic Smagorinsky model shows slightly better agreement with the experimental temperature and velocity distributions due to its adaptive treatment of local turbulence scales, making it a good choice for simulating forced draught fire scenarios.

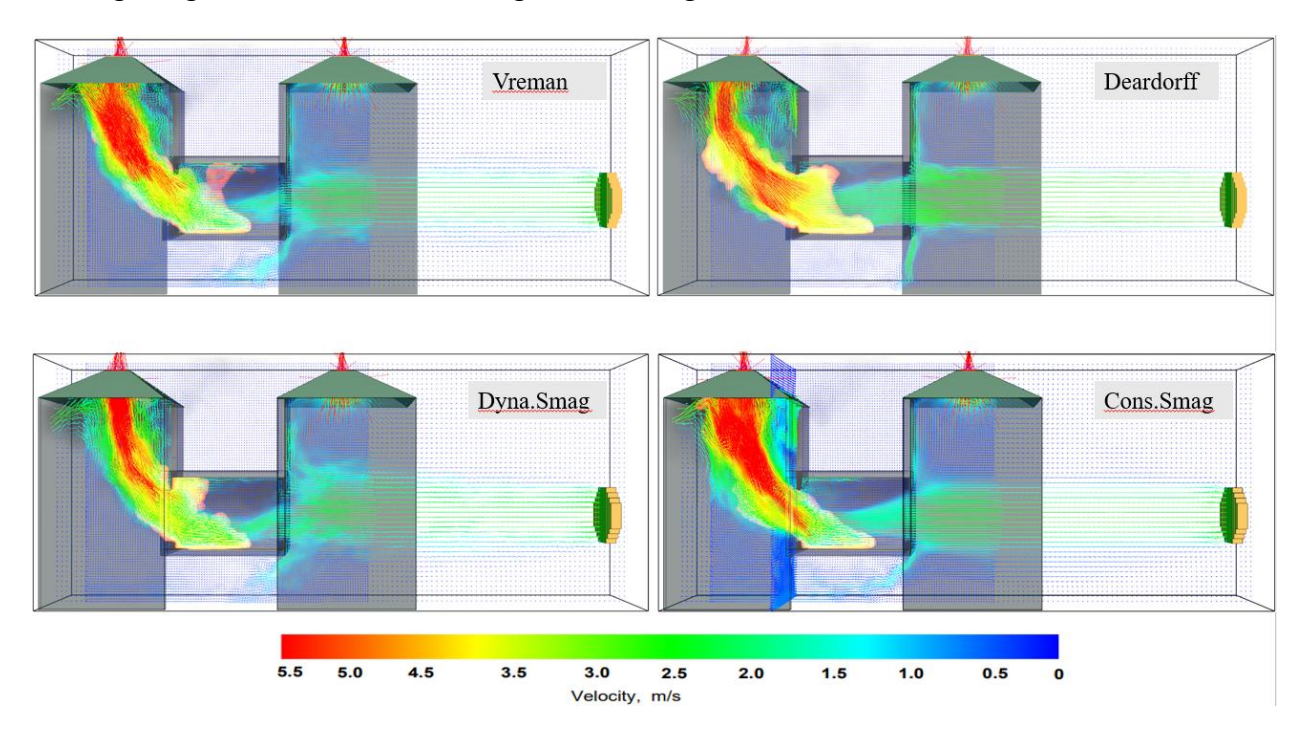


Figure 129: Gas mixture velocity and EVF at 200 s after fire initiation under FD conditions for 40 cm opening size with different turbulence models.

A.5 Conclusion

This appendix presented a comparative study of different turbulence sub-models in predicting EVF behavior under FD conditions, based on the findings of Chapter 3. While Chapter 3 used the default Deardorff model in FDS, and the results were not in good agreement with the experimental result, and this prompted further investigation into alternative turbulence models to improve simulation accuracy. The results indicate that while all models capture the general EVF trends, the Dynamic Smagorinsky model provided the closest agreement with experimental data in terms of temperature distribution and EVF shape, with less than 10% error. In contrast, other models like Vreman and Constant Smagorinsky significantly overpredicted temperature profiles, especially at the façade and opening regions.

This study highlights the importance of turbulence model selection, particularly in scenarios involving complex wind and opening interactions, and supports the use of dynamic models for improved predictive accuracy in future fire safety simulations.

Appendix A: References

- Karlsson, B., & Quintiere, J. (1999). Enclosure fire dynamics. CRC press.
- McGrattan, K. et al. (2019) Fire dynamics simulator user's guide, NIST Spec. Publ. 6. 2019. Available at: https://pages.nist.gov/fds-smv/manuals.html [Accessed Oct. 22, 2022]
- McGrattan, K. B., Klein, B., Hostikka, S., & Floyd, J. (2008). Fire Dynamics Simulator Technical User's Guide. Technical Report NISTIR Special Publication, 1018-5, National Institute of Standards and Technology, Gaithersburg, Maryland.
- Deardorff, J. (1980). Stratocumulus-capped mixed layers derived from a three-dimensional model. 11-29.
- Germano, M. (1991). A Dynamic Subgrid-Scale Eddy Viscosity. Physics of Fluids, 29.
- Lilly, D. (1967). The representation of small-scale turbulence in numerical simulation experiments. In Proceedings of the IBM Scientific Computing Symposium on Environmental Sciences, 29-179.
- Moin, P. (1991). A dynamic subgrid-scale model for compressible turbulence and scalar transport. Physics of Fluids, 29.
- Pope., S. B. (2000). Turbulent Flows. Cambridge University Press, 11-179.
- Vreman, B. (2004). An eddy-viscosity subgrid-scale model for turbulent shear flow. Physics of Fluids, 30.

APPENDIX B: Fire Incident Register

			Fire Incidents around the Globe											
Item No.	Date of Incident	Year	Facility/ Building Details	Country	Occupany Classification where Fire Originated	Time of the Day	Major Fire (Buildings > 23 m - highrise) or Minor Fire (<23 m)	Building Geometry	Description of the Fire Incident	Picture	Death/ Injury	No of Floor Affected	Source of Information	Additional Notes/ Remarks
1	1/10/1990	Y 1990	393 Kennedy St, Winnipeg	Canada	Apartment-Residential	Night	Greater that 23 m	Rectilinear	8 storey apartment building with 75 units, with covered and opensided car park at ground floor with space for 54 cars. Car park. Not spinklered and No fire detection system provided. EIFS was applied to the exterior wall. 5.00 am fire started in the ground floor cap park. — Fire quickly spread to 25 cars parked there at the time. EIFS on the exterior wall was ginted and top of the 4 storey except for a narrow strip on the east facade where fire spread to the top of the 71h storey and on the north facade where the fire spread to the top of the 71h storey and on the north facade where the fire spread to the top of the 71h storey and on the north facade where the fire spread to the top of the 71h storey and on the north facade where the fire spread to the top of the 71h storey and on the north facade where the fire spread to the top of the building.		No Injuries & Death	4	N. White & M. Delichatsios, 'Fire Hazards of Exterior Wall Assemblies Containing Combustible Components: Final Report' (2014)	Oleszkiewicz, I. (1990) "Fire performance of external insulation system : afer the fire at 393 Kennedy Street, Winnipeg, Manitoba, January 10, 1990"
2	4/5/1991	Y 1991	Knowsley Heights, Liverpool	u.ĸ	Apartment-Residential	Night	Greater that 23 m	Rectilinear	11 Floor Apartment. Rain screen cladding installed with 90 mm air gap, behind and rubberished paint coating over the external surface of the concrete wall behind. Fire started outside the building-> at rubbished compount -> Deliberate fire. (Around very early morning) Fire spread vertically through 90 mm air cavity. Extensive damage to the external part of the building. No internal fire spread.		No Injuries & Death	Extensive damage to the walls and windows of exterio part of the building. No fire spread to the interior of the building.	N. White & M. Delichatsios, 'Fire Hazards of Exterior Wall Assemblies Containing Combustible Components: Final Report' (2014) http://www.fiverpoolecho.co.uk/news/liv erpool-news/should-knowsley-heights- blaze-been-13271446	https://en.wikipedia.org/wiki/ Knowsley_Heights_fire#-:te xt=The%20fire%20spread% 20to%20all,was%20injured %20in%20the%20fire. https://www.liverpodecho.co uk/news/liverpod- news/miracle-knowsley- heights-how-residents- 15333465
3	1/1/1991	Y 1991	Mercantile Credit Building, Basingstoke	U.K	Business	Night	Greater that 23 m	Non Orthogonal	12 Storey Building. The columns had board fire protection and the composite floor beams had sprayapiled protection. The underside of the composite floor was not fire protected. The structure was designed to have 90 minutes fire resistance. The fire started on the eighth floor and spread rapidly to the ninth and then the tenth floor as the glazing failed. Glass curtain wall failure. Sprinkler sytem not provided.		Injury - No Death	3	http://doortofreedom.uk/wp- content/uploads/2017/06/Potential-risk- of-fire-spread-1999-evidence.pdf	https://www.911research.wt c7.net/~nin11evil911researc h/mirrors/guardian2/fire/SCI. htm
4	9/1/1994	Y 1994	Sun Valley Poultry Factory, Hereford	U.K	Industrial	Day	Less than 23 m	Rectilinear	Faulty defrosting machine caused a fire that quickly spread to other contents the structure of the building. Fire spread through the combustible core sandwich panels leading too large volumes of smoke delamination and internal structural cotlapse of panels. 2 fire fighters became trapped in the collapsing building and died.		Death	1	http://www.brandfolkene.dk/cm- webpic/pp_isoleringengelsk.pdf	https://www.ife.org.uk/Firefig hter-Safety-Incidents/sun- valley-1993/34014
5	4/11/1996	Y 1996	Dusseldorf Airport	Germany	Assembly	Day	Less than 23 m	Curvilinear	Fire broke out inside the passenger terminal of Düsseldorf Airport, Germany. Cause of fire due to welding work done to an expansion joint on the elevated access road of Terminal. 17 people killed by fire and 62 were injured. 17 people killed by fire and 62 were injured. Presence of combustible insulation (Use of polystyrene insulation) used in the void above the ceiling on the first level - ignited due to welding. Sprinkler system were missing in the fire area. Dry stand pipe - not connected with municipal water supply. No smoke detection system in void area.	fast Squide Scouter	Death		http://www.brandfolkene.dk/cm-webpic/pp_isoleringengelsk.pdf	https://web.archive.org/web/ 20111112000049/http://www. infpa.org/assesfiles/pdf/dus seldorf.pdf Image - http://www.ceramicsteelallian ce.com.sg/fire_safety_of_pa nel.php

This is a last of high-rise building fires where the fire spread in some way via the facade of the building. The data was found through searching Google for news reports and the fire safety Restaure. It is therefore likely to be biased towards high-profile events, and may have missed some smaller fires.

			Fire Incidents around the Globe											
Item No.	Date of Incident	Year	Facility/ Building Details	Country	Occupany Classification where Fire Originated	Time of the Day	Major Fire (Buildings > 23 m - highrise) or Minor Fire (<23 m)	Building Geometry	Description of the Fire Incident	Plicture	Death/ Injury	No of Floor Affected	Source of Information	Additional Notes/ Remarks
5	10/28/1996	Y 1996	Motomachi Apartments, Hiroshima	Japan	Apartment-Residential	Day	Greater that 23 m	Non Orthogonal	20 storey apartment building. Fire started on 9th floor vertically propagated along acrylic bindfold, PMMA boards of balcony, to the 20th floor (top floor). The fire development was due to a combination of the PMMA plus additional combustibles located on the balconies. The fire caused total or partial damage to 27 apartments.	11F 10F	Injury - No Death	12	N. White & M. Delichatsios, 'Fire Hazards of Exterior Wall Assemblies Containing Combustible Components: Final Report (2014), http://www.lafs.org/publications/ac/st/4/217/view/laofst_4-217.pdf	Intop://firesafreycomes.com/publications/fas/fb 64/hones/fas/fb 64/hones/fas/fb 7896/2021 1999 Times after policiations/self/st/217 1999 Times after policiations/self/st/217 1999/2021 1999/2021 1999/2021 1999/2021 1999/2021
7	9/30/1997	Y 1997	Eldorado Hotel, Reno	USA	Hotel-Residential	Night	Greater that 23 m		Large fire occurred on the façade of Eldorado Hotel due to an electrical fault on the external wall. Flame reached up to 50m above 2nd floor. Façade material was believed to be hard cost polyurethane over EPS. The building was sprinkler protected but no internal sprinkler are reported to have activated.	Fire erupts at hotel	Information Not Available	No Information Available.	N. White & M. Delichatsios, Fire Hazards of Exterior Wall Assemblies Containing Combustible Components: Final Report (2014) http://www.geocities.ws/mstudyvin/new s4.html	https://apnews.com/article/2f 08b728df6a60316332bf9e65 ecs46d, Accessed on 0306/2021 https://apnews.com/article/d d2ef61611fd3ff74766d08841 5dadf6, Accessed on 003/66/2021
8	6/20/1998	Y 1998	Palace Station Hotel and Casino, Las Vegas	USA	Hotel-Residential	Day	Greater that 23 m		20 Storey hotel and Casino Building. Fire started on the external façade at the top of building. Fire was confined to the outside of the building at the 20th floor and roof. An external decorative façade was the only object that burned. Polyurethane foem and urethane coated EPS was used. The fire was believed to have been caused by a lightning circuit on the outside of the facade.		No Injuries & Death	2	N. White & M. Delichatsios, 'Fire Hazards of Exterior Wall Assemblies Containing Combustible Components: Final Report' (2014)	https://news3iv.com/features //ideo-vaulit/video-vaulit- summer-storm-leads-to-near- disaster-at-place-station, Accessed on 03/06/2021
9	6/11/1999	Y 1999	Garnock Court, Irvine, Scotland	u.ĸ	Apartment-Residential		Greater that 23 m	Rectilinear	14 storey apartment tower. Fire started in a room on the 5th floor. The fire burnt out through the window and with approximately 10 minutes had spread vertically up 7 floors to the top of the building. Spread via external cladding.		Death	7	N. White & M. Delichatsios, 'Fire Hazards of Exterior Wall Assemblies Containing Combustible Components: Final Report' (2014) http://www.bbc.co.uk/news/uk-scotland-40406057 http://news.bbc.co.uk/1/hi/uk/366856.st m http://news.bbc.co.uk/scotland-hews/local-news/long-serving-troon-fireman-bids-10597705	https://www.bbc.com/news/ uk-scotland-40406057, Accessed on 03/06/2021
10	6/2/2002	Y 2002	Tip Top Bakery, Fairfield	Australia	Industrial	Day	Less than 23 m	Rectilinear	Single level large factory with a floor area of 10,000 m2. The walls and in some areas the roof were constructed to polysyerse insulated sandwich panel. Building was not sprinkler prtected but was provided with thermal fire detection system. Cause of the fire was failure of a gas fired heating system resulting in ignition of polenta flour.		Injury - No Death	1	N. White & M. Delichatsios, 'Fire Hazards of Exterior Wall Assemblies Containing Combustible Components: Final Report' (2014)	http://www.ecohousing.com/ wp- content/ploads/pdf/Tiptop% 20bakery%20fire.pdf. Accessed on 03/06/2021

Saudi Aramco: Company General Use

			Fire Incidents around the Globe											
Item No.	Date of Incident	Year	Facility/Building Details	Country	Occupany Classification where Fire Originated	Time of the Day	Major Fire (Buildings > 23 m - highrise) or Minor Fire (<23 m)	Building Geometry	Description of the Fire Incident	Picture	Death/ Injury	No of Floor Affected	Source of Information	Additional Notes/ Remarks
11	7/29/2003	Y 2003	Telstar House, London	u.ĸ	Business	Night	Greater that 23 m	Rectilinear	13 Storey Steel framed Concrete office building. Ground floor entrance lobby and upper floors are built above an open parking area. There is also a 2 storey retailfiving unit used as a public houst rivestaurant built adjacent to the ground floor entrance lobby. No sprinkler system in the building. Automatic fire detection system installed throughout the building. Fire was bronken due to faulty electricals in 7th floor. fre was eventually consumed whole of the 7th to 10 th floor.	and the second s	Injury - No Death	4	BRE Report	https://www.highrisefirefighti ng.co.uk/cstelstar.html, accessed on 30/05/2021
12	10/17/2004	Y 2004	Parque Central Complex, Caracas	Venezuela	Business	Day	Greater that 23 m	Curvilinear	Building is 225 meter tall has 56 stories. Parque Central Complex is a housing, commercial and cultural development in the city of caracas, Venezuela. A huge fire broke out in the building and more than sixteen floors (34th to 50th floor)were affected. Cause of the fire is unknown. Automatic sprinker system and standpipe system were non operational.		Injury - No Death	17	http://news.bbc.co.uk/1/hi/world/americ as/3751790.stm	https://en.wikipedia.org/wiki/ Parque_Central_Complex, accessed on 300/5/2021 http://en.people.cn/200410/1 8/print20041018_160544.ht ml, accessed on 30/05/2021
13	2/12/2005	Y 2005	Windsor Tower Fire, Madrid	Spain	Business	Day	Greater that 23 m	Non Orthogonal	Office building in the financial center of Madrid, Spain. 106 meter high, Total 32 floors of which 29 were above ground and 3 below. Curtain Wall - plazing façade. Building is not protected with Sprinkler system. Fire Originated on 21st floor of the building due to electrical fault and fire spread quickly through out the entire building. From 2nd floor and above.		Ispary - Ho Death	30	http://www.mace.manchester.ac.uk/project/research/structures/strucfre/CaseStudy/Historic-Fires/Building-Fires/default.	https://materialsforinteriorsin d54862016.files wordpress.c om/2016/08/Q-case- studies_historical-fires_ windsor-tower-fire.pdf, Accessed on 30/05/2021 https://en.wikipedia.org/wiki/ Windsor_Tower_(Madrid), Accessed on 30/05/2021 http://news.bbc.co.uk/2/hi/eu rope/4261315.stm, Accessed on 30/05/2021 lmage - http://www.911myths.com/ht m/madrid_windsor_tower.ht mi/madrid_windsor_tower.ht ml, Accessed on 30/05/2021
14	4/21/2005	Y 2005	Treskowstrasse Pankow Flats, Berlin	Germany	Apartment-Residential	Night	Greater that 23 m	Rectilinear	7 Storey apartment building. Fire started in a second floor apartment with flames from a window igniting the EIFS fagade. Fire and smoke spread into rooms above the starting floor. The fagade consisted of 80 mm flameretarded expanded polystyrene (EPS) with mesh and render and mounted on 25 mitokic chipboard, which was the formwork left in place when the concrete walls here built. In 2004 a 500 mm thick fire barrier (mineral fibre) was added to the second and fourth levels		Death	7	N. White & M. Delichatsios, "Fire Hazards of Exterior Wall Assemblies Containing Combustible Components: Final Report (2014): http://www.brandfokene.k/cm-weebpic/pp_isolering_engelsk.pdf http://www.homefiremodel.bam.delen/homefiremodel/fires_in_homes/index.htm	http://theriverofilife.com/2018 /04/25/grenfell-tower-why-in- 1995-did-the-bba-see-no- additional-hazari-in-using- combustible-render-rather- than-non-combustible/ Accessed on 030/06/2021 http://www.brandfolkene.dk/ cm- webpic/pp_isolering_engels k.pdf, Accessed on 03/06/2021

			Fire Incidents around the Globe											
Item No.	Date of Incident	Year	Facility/Building Details	Country	Occupany Classification where Fire Originated	Time of the Day	Major Fire (Buildings > 23 m - highrise) or Minor Fire (<23 m)	Building Geometry	Description of the Fire Incident	Picture	Death/ Injury	No of Floor Affected	Source of Information	Additional Notes/ Remarks
15	9/23/2007	Y 2007	Water Club Tower, Borgata Casino Hotel, Atlantic City	USA	Hotel-Residential	Day	Greater that 23 m	Rectilinear	42 Storey hotel / casino Building. The fire occurred while the building was nearing completion. The aluminium composite panels were used as a decorative finish on a structural frame set approximately 2 m distant from a concrete sheer wall that prevented major fire extension into the building. The fire started on the 3rd floor within the building. The fuel was rapidly consumed with around 10 to 15 min.		No Injuries & Death	39	N. White & M. Delichatsios, 'Fire Hazards of Exterior Wall Assemblies Containing Combustible Components: Final Report' (2014) http://www.fireengineering.com/articles/ 2010/05/modern-building-materials-are- factors-in-atlantic-city-fires.html	https://www.fireengineering. com/firefighting/modern- building-materials-are- factors-in-atlantio-city- firest#gref, Accessed on 03/06/2021
16	1/25/2008	Y 2008	MGM Monte Carlo Hotel, Las Vegas	USA	Hotel-Residential	Day	Greater that 23 m	Non-Dirthogonal	32 story Hotel and Casino building. The fire started on the upper levels of the hotel tower due to welding. The fire spread mainly laterally with some downward spread. Exterior windows broke but the activation of 17 internal sprinklers halted any interior fire spread.	i Coa	Injury - No Death	4	N. White & M. Delichatsios, 'Fire Hazards of Exterior Wall Assemblies Containing Combustible Components: Final Report' (2014) https://www.reuters.com/article/us-casino-fire/fire-strikes-las-vegas-hotel-casino-idUSN2535785320080126	http://www.chinadaily.com.c n/world/2008- 01/26/content_6422804.htm, Accessed on 03/06/2021
17	5/9/2008	Y 2008	De Punt Shipyard, De Punt	Netherlands	Indianal	Day	Less than 23 m	Reclinear	The shipyard was constructed of insulated sandwich panels with a core of combustible polyurethane insulation that, during the first minutes, was the main fuel for the fre. Believed to be accidental ignition, fire starting within the meter cupboard within the rear storeroom/workshop.	***************************************	Death	NA	http://www.brandfolkene.dk/cm-webpic/pp_isoleringengelsk.pdf	https://www.ife.org.uk/Incide nls-of-interest/2008-de- punt/38820, Accessed on 30/05/2021
18	2/9/2009	Y 2009	CCTV Tower, Beijing	China	Hotel Residental	Night	Greater that 23 m	Non-Orthogonal	44 storey building nearing completion of construction. he center would have included a television studio with seating for 1,500 audience members, recording studios, digital cinemas, news release facilities, and a 241-room five-star hotel to be operated by Mandarin Oriental. The total height of the 44-floor building was 159m. The upper portion of the China Central Television headquarters (CCTV) facade was ignited by lilegal firevorks. The fire spread to involve the majority of the facade over the entire height of building, which is believed to have included polystyrene insulation.		Death	44	N. White & M. Delichatsics, Fire Hazards of Exterior Wall Assemblies Containing or ombustible Components: Final Report (2014); http://www.brandfokene.dk/cm- webpic/pp_is-dering_engdsk.pdf	https://en.wikipedia.org/wiki/ Beijing_Television_Cultural_ Center_fire, Accessed on 03/06/2021

		ı	Fire Incidents around the Globe											
Item No.	Date of Incident	Year	Facility/Building Details	Country	Occupany Classification where Fire Originated	Time of the Day	Major Fire (Buildings > 23 m - highrise) or Minor Fire (<23 m)	Building Geometry	Description of the Fire Incident	Picture	Death/ Injury	No of Floor Affected	Source of Information	Additional Notes/ Remarks
19	7/3/2009	Y 2009	Lakanal House, London	u.ĸ	Apprinced Residuellal	Day	Greater that 23 m	Recilinear	14 storey building. It contains 96 flats and of total 41.91 meter high. Fire broke out of one of the flats in the 9th floor. Cause of fire - Electrical fault in a television set. Use of combustible cladding in the façade - fire spread to the adjacent stories.		Death	7	https://www.theguardian.com/uk- news/2017/feb/24/southwark-council- admits-safety-falings-tower-block- lakanal-house-blaze http://www.ndependent.co.uk/voices/gr enfell-tower-lakanal-house-why-we- need-an-inquest-a7808536.html	https://en.wikipedia.org/wiki/ Lakanal_House_fireft:=text= The%2Sourcef%20fe%20fe e%20fe_erected%20or%20 he%20fe_erected%20or%20 he%20seerath%20fex; Accessed on 30/05/2021 https://www.despingbuildings.co.uk/wikil_lakanal_House_fire_Accessed on 30/05/2021
20	8/15/2009	Y 2009	Kozepszer Street Flats, Miskolc	Hungery	Apartment Residential	Night	Greater that 23 m	Recilinear	11 shorey building againment building. First stated in a fill floor resolvent less that the security of reventical five resolvent less than the first of the first sharp saiding. Security of the fill of the first sharp saiding, and the fill of the		Death	6	N. White & M. Delichatsios, 'Fire Hazards of Exterior Wall Assemblies Containing Combustible Components: Final Report (2014); http://www.brandfolkene.dk/cm- webpic/pp_isolering_engelsk.pdf	https://lacoitulstrazii.files.wor dpress.com/2012/10/effua- combustible-facades.pdf, Accessed on 03/06/2021
21	7/8/2010	Y2010	Al Kuwait Tower, Sharjah	UAE	Apartners & Residential	Day	Greater that 23 m	Curvlinear	14 Storey building. Cause of fire is unknown, started at first or second floor of the building. Top floors of buildings were completely damaged, while the mezzanine and the ground floor were intact. Outer façade of building is made of fiber glass.		Injury - No Doubh	12	https://www.thenationalnews.com/uae/h undreds-relocated-after-huge-tower- block-fire1-487907, Accessed on 30/05/2021 https://gulfnews.com/uae/fate-d-al- kuwalt-tower-in-sharjah-uncertain- 1.700550, Accessed on 30/05/2021	https://www.daijiworld.com/n ews/newsDisplay/newsID=8 0695, Accessed on 30/05/2021
22	9/1/2010	Y 2010	Wooshin Golden Suites, Busan	South Korea	Agartiment Residential	Day	Greater that 23 m	Rectinear	38 story building above ground and 4 Stories underground, which is supported to the story of the		Injury - No Death	35	N. White & M. Delichatsics, 'Fire Hazards of Exterior Wall Assemblies Containing Combustible Components: Final Report' (2014) Intri/loco Lus- fire.com/eng/ffsar'?p=1761	https://en.wikipedia.org/wiki/ Wooshin_Gdden_Suites_fir e, Accessed on 03/09/2021

			Fire Incidents around the Globe											
Item No.	Date of Incident	Year	Facility/Building Details	Country	Occupany Classification where Fire Originated	Time of the Day	Major Fire (Buildings > 23 m - highrise) or Minor Fire (<23 m)	Building Geometry	Description of the Fire Incident	Picture	Death/ Injury	No of Floor Affected	Source of Information	Additional Notes/ Remarks
23	11/14/2010	Y 2010	4 Rue du Lac Flats, Dijon Sonacotra building	France	Apartment Residential	Night	Greater that 23 m	Reclinear	9 story residential halding. The fire stated in an externed gardings container all the base of the basic registry resulting years where their fire spread on the flaguest. The state of the spread of the stated in the spread on the flaguest. The stated is the stated in the state of the stated in the state of the states. The state of the states in the state of the st		Death	No Information Available.	N. White & M. Delichatsios, 'Fire Hazards of Exterior Wall Assemblies Containing Combustible Components: Final Report (2014). http://www.brandfolkene.di/cm-webpic/pp_isolening_nendsk.pdf http://www.bbc.co.uk/news/world- europe-11752303	time lines to commenciant areas.
24	11/15/2010	Y 2010	Residential Flats, Shanghai	China	Apartment Presidential	Day	Greater that 23 m		28 Storey high rise apartment building fire. Cause of fire: - spark from weldin gwork done on the building 10th floor. Fire started with construction material and spread through out the building> polyurathane foam insulation used in the building used in the facade.		Death	28	D. Barboza, 'Workers Detained as Toll Hits 53 in Shanghaf Fire', New York Times (2010) http://www.chinadaily.com.cn/china/201 0-11/15/content_11552718.htm	https://en.wikipedia.org/wiki/ 2010 Shanghai fire,
25	2/3/2011	Y 2011	Royal Wanxin Hotel, Shenyang	China	Hotel-Residential	Night	Greater that 23 m		38 storey Building, Royal Warxin Hotel, Shenyang is 267 meter tall building. Fire started in Tower B, in an apartment building in the 2 building dyarsty warxin complex in Shenyang. Fire spread quickly to Tower A 219 m tall building that hous a 5 star hotel. Fire was caused by Fire Works that ignited material on the exterior of the building.		Injury - No Death	No Information Available.	J. Dean, 'Fireworks Spark High-Rise Blaze in China', Wall Street Journal (2011) https://www.flickr.com/photos/niqodems s/5413468164/sizes/l/in/photostream/	https://www.wsj.com/articles //SB10001424052748703437 3045761211058201974. Accessed on 31/05/2021 https://www.flickr.com/photo schipdomus/512886045/si zes/fliri/photostream/, Accessed on 31/05/2021 https://en.wikipedia.org/wiki/ Royal_Wanxin_International_ Tower, Accessed on 31/05/2021
26	1/18/2012	Y 2012	Al Baker Tower, Sharjah	UAE	Apartment-Residential	Night	Greater that 23 m	Rectilinear	29 storey Building. Fire was caused by lit cigrette that was thrown off the balcony from an upper floor and landed in the balcony on the first floor. Building exterior was made of combustible material and weather and wind speed were major factors that caused the fire to spread quickly to other floors in the building. Out of total of 125 apartments 51 were completely gutted in addition to this 14 cars caught by fire.		No Injuries & Death	No Information Available.	M. Al Serkal, "Tossed, lighted cigarette caused fire in Al Baker tower", Gulf News (2012) http://gulfinews.com/news/uae/emergen cies/major-fire-incidents-in-uae-1.1965921	konline.com/article-16634- sharjah-al-baker-tower-fire-

			Fire Incidents around the Globe											
Iten No	Date of Incident	Year	Facility/ Building Details	Country	Occupany Classification where Fire Originated	Time of the Day	Major Fire (Buildings > 23 m - highrise) or Minor Fire (<23 m)	Building Geometry	Description of the Fire Incident	Picture	Death/ Injury	No of Floor Affected	Source of Information	Additional Notes/ Remarks
27	4/28/2012	Y 2012	Al Tayer Tower, Sharjah	UAE	Apartment-Residential	Day	Greater that 23 m	Curvilinear	40 storey residential building. 36 residential floors and 6 parking storeys. The exterior of the building was clad with metal composite panels consisting of aluminum with a polyethylene collection. Fire started on a balcony on the first floor. Fire started on a balcony on the first floor which contained cardboxed boxes and plastics. This resulted in vertical fire spread on the metal composite cladding to the box of the building. 46 whiches parked near the building due to building falling debris. No deaths or injuries reported.		No Injuries & Death	33	N. White & M. Delichatsics, "Fire Hazards of Exterior Wall Assemblies Containing Combustible Components: Final Report (2014) http://gulfnews.com/news/uae/emergen cies/timeline-of-uae-tower-fires- 1.1700696	https://www.emirates247.co m/news/emirates/tenants- allowed-back-in-to-view-fire- damage-2012-04-29- 1.456180, Accessed on 03/06/2021
28	5/14/2012	Y 2012	Mermoz Tower, Roubaix	France	Apartment-Residential	Day	Greater that 23 m	Curvilnear	18 storey Residential building. The fire started on a second floor balcory. The spread of the fire appeared to be enhanced by the profile created by the balconies and the fire also spread into the building. The first storey was covered with "formo-phenolic" decorative boards while the rest of the building was clad with 3 mm thick polyettlylene core sandwiched between two 0.5 mm thick aluminium sheets. Vertical ul shaped channel profile created by the balconies, with flames mowing indout for the balconies, with flames moving in the fire spread upwards. Thre fire resulted in one fatality and six injuries.		Death	17	N. White & M. Delichatsios, Fire Hazards of Exterior Wall Assemblies Containing Combustible Components: Final Report (2014) https://witter.com/sie2016dublin/status/ 687990749661626368	https://www.nfpa.org/- /media/Files/News-and- Research/Resources/Resear ch-Foundation/Current- projects/Filed- projects/FacadeSeminar201 5.asth/2la=m8has+1A9A50 F3289A89E55D42C1151BF 672CF515047BC, Accesed on 03/06/2021
29	7/17/2012	Y 2012	Polat Tower, Istanbul	Turkey	Apartment-Residential		Greater that 23 m	Rectilinear	Building is 42 stories and located on a central business district of istanbul. Building is 152 m high and houses over 400 luxury apartments. Also, includes shops and offices. Cause of fire may be faulty air condition. Fire spread through building exterior insulation (glazing used) and No major damages in the interior. Building is protected with automatic fire extinguishing system.		No Injuries & Death	No Information Available.	Fire Tears Through Istanbul Tower Block, Sky News	https://www.dailymail.co.uk/ news/article-2174853/Polat- Tower-Firefighters-huge- blaze-engulfed-150m- lstanbuls-skyscraper.html, Accessed on 31/05/2021 https://www.bbc.com/news/ world-europe-18867266, Accessed on 31/05/2021
30	10/6/2012	Y 2012	Saif Belhasa Building, Dubai	UAE	Apartment-Residential	Day	Greater that 23 m	Rectilinear	13 screy residential building with 156 apartments and lower level car parking The building was clad with metal composite panels consisting of aluminum with a polyethylene core. Fire started on the fourthe floor. The fire rapidly spread to reach the top of the building.		Injury - No Death	9	N. White & M. Delichatsios, 'Fire Hazards of Exterior Wall Assemblies Containing Combustible Components: Final Report (2014) http://guffnews.com/news/uae/emergen cies/fire-breaks-out-in-tecom-building- 1.1085705	

			Fire Incidents around the Globe											
Item No.	Date of Incident	Year	Facility/Building Details	Country	Occupany Classification where Fire Originated	Time of the Day	Major Fire (Buildings > 23 m - highrise) or Minor Fire (<23 m)	Building Geometry	Description of the Fire Incident	Picture	Death/ Injury	No of Floor Affected	Source of Information	Additional Notes/ Remarks
31	11/18/2012	Y 2012	Tarnweel Tower, Dubai	UAE	Agardnerit Residential	Night	Greater that 23 m	Recilinear	34 storey mixed use and residential building in Dubai. The building was clad with metal composite panels consisting of aluminium with a polyethylene core. The metal composit panel was also used as a decorative feature on the roof top. Fire started at the roof level, possibly near air conditioning equipment. The fire then spread down the exterior of the building. This is partially due to motten flaming debris from the cladding falling onto lower balconies and igniting the facade at lower levels. No fatalities were identified.		No Injuries & Death	No Information Available.	N. White & M. Delichatsios, Fire Hazards of Exterior Wall Assemblies Containing Combustible Components: Final Report (2014) http://www.khaleejtimes.com/nation/cri me/BOC-excusted-from-burning- tamweel-lower http://www.arabianbusiness.com/claddi ng-issue-causes-further-headache-for- fire-hit-tamweel-tower-648455.html	https://www.khaleejtimes.co m/nation/crime/600- evacuated-from-burning- tarmweel-tower, Accessed on 03/06/2021
32	4/3/2013	Y 2013	Grozny-City Towers, Chechnya	Russia	Hotel Residential	Day	Greater that 23 m	Recilinear	40 storey building. 145 m in height. Construction had just completed in this unoccupied, high rise building, lighting stributed to a short circuit in an air conditioner on upper floors. Fire spread to enguilf the fagade from ground level to the roof. Fagade materials believed to be metal composite panels, but actual details not reported. The fire system for the building has not been commissioned and there appeared to be no water supply to sprinklers or hydrants.		No Injuries & Death	40	N. White & M. Delichatsios, Fire Hazards of Exterior Wall Assemblies Containing Combustible Components: Final Report (2014) http://www.businessinsider.com/grozny. city-skyscraper-on-fire-2013-47/R=T	
33	4/22/2013	Y2013	Al Hafeet Tower 2, Sharjah	UAE	Apartment-Residential	Day	Greater that 23 m	Rectilinear	20 Storey Building. Fire started at 2 pm at Al hafeet Tower 2 from one of the apratment in the 7 th storey. 10 floors at the rear of the building were gutted by the fire. Combustible façade - increase the risk of fire spread. Fire alarm system was not working - under maintenance.	THE COLUMN TO TH	Injury - No Death	10	https://www.emirates247.com/news/em rates/sharjah-al-hafed-tower-fire-three- arrested-2013-04-23-1.503726	https://www.thenationalnews.com/uae/dozens-of-families-flee-as-sharpi-fire-guts-20-storey-tower-1.354963, Accessed on 01/06/2021 https://www.emirates247.com/news/emirates/sharjah-al-hafeet-tower-fire-three-arrested-2013-04-23-1.503726, Accessed on 01/06/2021 https://gulfnews.com/uae/two-women-arrested-for-causing-sharjah-building-fire-1.1174326, Accessed on 01/06/2021
34	9/21/2014	Y 2014	Krasnoyarsk Apartments, Krasnoyarsk	Russia	Apartment-Residential	Night	Greater that 23 m	Non Orthogonal	25 Storey Building. Fire started around 1 pm in one of the25 storey apartment building lower floor but spread rapidly through the entire 120 apartment complex. Cause of the fire is unknown / Information not available. Use of combustible cladding resulted in increased fire spread along the exterior of the building.	T HANDE TO THE PARTY OF THE PAR	No Injuries & Death	25	http://siberiantimes.com/other/others/ne ws/shocking-blaze-rips-through-25-floor apartment-block-in-krasnoyarsk/	http://siberiantimes.com/othe r/others/news/shocking- bizze-fips-tirrough-25-floor- apar timent-block-in- krasnoyarsk/, Accessed or 0.106/2021 https://ifipmag.mdmpublishin g.com/cladding-blamed- siberian-fire-destroyed- apartment-omplex/, Accessed on 01/06/2021

			Fire Incidents around the Globe											
Iten No	Date of Incident	Year	Facility/ Building Details	Country	Occupany Classification where Fire Originated	Time of the Day	Major Fire (Buildings > 23 m - highrise) or Minor Fire (<23 m)	Building Geometry	Description of the Fire Incident	Picture	Death/ Injury	No of Floor Affected	Source of Information	Additional Notes/ Remarks
35	11/25/2014	Y 2014	Lacrosse Building, Melbourne	Australia	Apartment-Residential	Night	Greater that 23 m	Non Orthogonal	Lacrosse Building is a twenty three (23) storey mixed -use building which includes fifteen levels of apartments with an effective building height of 83. metres. Levels six to twenty-one were affected by fire and many more were affected by water damage. There are approximately fifteen apartments per level. cause of the fire was cigerate left to burn in a plastic food contained in the balcony believed to be on the apartment 805. The fire spread vertically, spreading downwards to apartment 605 and upwards and affected all apartments above designated as apartment No. 5 on each level, up to apartment 2105. It was observed that on some apartment balconies large amount of household items were being stored, creating a higher fire load.	R 2 B	No Injuries & Death	10	http://www.melbourne.vic.gov.au/sitecol ectiondocuments/mbs-report-lacrosse-fire.pdf http://www.theage.com.au/victoria/disciplinary-action-for-lacrosse-tower-building-surveyor-20160323-gnpkkt.html	apartment-owners-win-5.7- million-cladding-fire- damages/10857060, Accessed on 01/06/2021 https://www.theage.com.au/ politics/victoria/docklands- owners-sue-for-24m-over- fire-as-date-10-fix-cladding- looms-20180909- p502pc.html, Accesssed on 01/06/2021
36	2/21/2015	Y 2015	Torch Tower, Dubai	UAE	Apartment-Residential	Night	Greater that 23 m	Non Orthogonal	Torch Tower is a residential skyscraper in Dubai. It is 336.8 m tall with 79 floors above ground. (Total 68 store) Fire started with a grill located on one of the building balconies possibly on the 50th floor. External cladding was charred from 50th floor to the top of the floor, Fire has reached 70th floor and debris falling from great height.		Injury - No Death	60	J. Ensor, 'Fire rips through 79-story Dubai Marina Torch', The Telegraph (2015) https://witter.com/conflicts/status/5689 15259926088194	https://www.bbc.com/news/ world-middle-east- 31562099, Accessed on 01/06/2021 https://gulfnews.com/use/ma ssive-fire-erupts-at-forch- tower-in-duba-marina- 1.1460107, Accessed on 01/06/2021 https://en.wikipedia.org/wiki/ The_Marina_Torch, Accessed on 01/06/2021 https://www.theguardian.co m/world/2015/feb/21/fire- dubal-skystagulon, Accessed on 01/06/2021
37	5/19/2015	Y 2015	Residential Flats, Baku	Azerbeijan	Apartment-Residential	Day	Greater that 23 m	Rectilinear	16 level residential building in Azarbaijan. The official death toll was 15 and 63 people were injured. Flammable styrofoam may have used on the exterior façade (exact material unknown). Fire may have started from first floor and in few minutes covered the entire high rise.		Death	16	http://www.miragenews.com/building- fire-kilis-16-injures-at-least-50-in- azerbajjan/ https://en.trend.az/azerbajjan/society/23 96371.html	https://www.ife.org.uk/Incide nts-of-Interest-1/2015-baku- azerbaijan-15-deaths/37306, Accessed on 1016/2021 https://en.wikipedia.org/wiki/ 2015_Baku_residence_buildi ng_free_Accessed on 01/06/2021 https://www.azernews.az/nat ion/82248.html, Accessed on 01/06/2021
38	10/1/2015	Y 2015	Al Nasser Tower, Sharjah	UAE	Apartment-Residential	Day	Greater that 23 m	Curvilinear	32 Storey building which consist of 26 resideential floor and 6 levels of car parking. No casualities were reported, but 40 people had to be treated for smoke inhalation. Initial report suggest that the fire started on the 3rd storey and moved up. Cause of the fire (No information available) Around 40 apartments affected by the fire and 7 vehicles parked below were damaged from the falling debris. Fire alarm system was not activated in the building during the fire.		Injury - No Death	26	A. Husain, Major Fire in Sharjah Residential Tower'. The Pawprint (2015 https://www.khalegitimes.com/sharjan- apartments-face-inspecion-after- massive-fire	https://www.khalegitimes.co m/sharjah-apartments-face- inspecion-after-massive-fire, Accessed on 01/06/2021 https://thepsoprintdas.com/ 2015/10/8/major-fire-in- sharjah-residental-tower/, Accessed on 01/06/2021

			Fire Incidents around the Globe											
iten No	Date of Incident	Year	Facility/Building Details	Country	Occupany Classification where Fire Originated	Time of the Day	Major Fire (Buildings > 23 m - highrise) or Minor Fire (<23 m)	Building Geometry	Description of the Fire Incident	Picture	Death/ Injury	No of Floor Affected	Source of Information	Additional Notes/ Remarks
39	12/31/2015	Y 2015	Address Hotel, Dubai	UAE	Hotel-Residential	Night	Greater that 23 m	Curvilinear	Address Downtown Dubai is a 63 Storey 302 meter tall hotel and residential building. Fire was caused by an electrical short circuit by electrical wires of the spotlight used to illuminate the building between 14th and 15th floor. Alarm did not sound immediately as the fire had stated on the outside of the building. Moments after the fire broke out, much of the building was engulted in flame fanned by strong winds and burning debris poured down or to the street below. Fire had rawaged circa 40 floors of the 63 storey building.		Injury - No Death	40	I. Johnston, S. Osborne, 'Dubai skyscraper Address Hotel engulfed in huge fire', The Independent (2015) https://www.thenational.ae/undelectrica fault-caused-the-address-downtown- dubai-hotel-fire-1.201694	Intips://en.wikipedia.org/wiki/ Address_Downtown, Accessed on 01/06/2021 https://www.thenationalnewscom/uaeelectrical-fauli- caused-tine-address- downtown-dubai-hotel-fire- 1.201694, Accessed on 01/06/2021 https://gulfnews.com/uae/cri meishort-circuit-caused- address-hotel-fire-say-dubai- police-1.1657190, Accessed on 01/06/2021 https://www.independent.co. uk/news/worl/dimiddle- ess/dubai-sykeraper-hotel- engulfied-huge-fire- 6702358 html. Accessed 1
40	3/28/2016	Y 2016	Ajman One Complex, Ajman	UAE	Apartment-Residential	Night	Greater that 23 m	Rectilinear	26 Storey tower - Residential apartment building> Total cluster of 12 towers. Fire was started on Tower 8, may have cuased by coal used for shisha smoking thrown on a construction waste pile near the tower. It spread to Tower 6 due to strong wind and also use of combustible cladding material. The affected tower had 26 stories and 3 storey car parking.		Injury - No Death	26	http://www.bbc.co.uk/news/world-middle-east-35913988 http://www.arabianbusiness.com/fire-hi-ajman-one-towers-be-repaired-by-summer633063.html	https://gulfnews.com/uae/shi sha-coal-sparked-ajman-one- fre-1.1810468, Accessed on 01/06/2021 https://www.hindustantimes. com/world/uae-fanned-by- strong-wind-fire-engulfs- styporaper-in-pinanylstoy- CWP-938kdrVgHKOkhhJtaK N.html. Accessed on 01/06/2021 https://www.khaleejtimes.co m/500-residents-homeless- as-fire-guits-two-ajman- towers. Accessed on 01/06/2021
41	7/20/2016	Y 2016	Al Sulafa Tower, Dubai	UAE	Apartment-Residential	Day	Greater that 23 m	Rectilinear	76 storey building. Sulafa Tover is a 76 storey high rise building with a height of 288m. A discarded eigerette butt may have caused the fire possibly on 36th storey. The fire has anyulled more than 30 storey due to comb		Ispary - No Death	30	http://www.bbc.co.uk/news/world- middle-aast-36846521 http://www.dailymail.co.uk/news/article- 3699272/Fire-breaks-luxury-75-storey- tower-Dubai.html	Sulafa Tower, Accessed on 01/06/2021 https://www.thenationalnews.com/uae/sulafa-tower-residents-spend-right-induba-hotel-flowing-1.167073, Accessed on 01/06/2021 https://www.dailymail.co.uk/news/article-3699272/Fire-breaks-Luxuy-75-storey-tower-Duak-Imit, Accessed on 02/06/2021 https://www.bbc.com/news/world-middle-east-36848521, Accessed on 02/06/2021

			Fire Incidents around the Globe											
Item No.	Date of Incident	Year	Facility/Building Details	Country	Occupany Classification where Fire Originated	Time of the Day	Major Fire (Buildings > 23 m - highrise) or Minor Fire (<23 m)	Building Geometry	Description of the Fire Incident	Picture	Death/ Injury	No of Floor Affected	Source of Information	Additional Notes/ Remarks
42	8/19/2016	Y 2016	Sheperds Court, London	u.ĸ	Apartment-Residential	Night	Greater that 23 m	Rectilinear	18 Storey Apartment residential building. Indest tumble dryer is believed to have caused the fire. Fire started on the 7th floor and quickly spread up the side of the building. Building façade panel comprised of 17-23 mm plywood board covered by polysyrene foam, 1 mm steel sheet and decorative white paint. When exposed to high flames, Polystyrene foam metted away, causing the metal sheet to fall and exposing the foam and wood to the flames. Fire affected 5 floors of the 18 storey building.		Ispay - No Death	5	https://www.theguardian.com/uk- news/2016/aug/19/fire-crews-tackle- blaze-at-shepherds-bush-towe-block- london https://www.insidehousing.co.uk/insigh/ i/insight/a-stark-warning-the-shepherds bush-tower-block-fire-50566 http://www.london- fire.gov.uk/news/LatestNewsReleases, nvestigation-concludes-dryer-to-blame- shepherds-bush.asp	uk-england-london- 37203933, Accessed on 02/06/2021
43	11/9/2016	Y 2016	Neo Soho Project, Jakarta	Indonesia	Apartment-Residential	Night	Greater that 23 m	Curvilinear	45 storie building with 200+ meter height. 45 storie building with 200+ meter height. Fire has spread externally by means of flammable cladding on the exterior of the building. Fire spread up the outside of the building. Fire spread up the outside of the building. Report indicate that fire rapidly spread and burned most of the flors of the neo soho apartment and some stories of the shopping mall. Source of the fire from the area of scho@podomore city apartment, buildign on the top of the Neo soho shopping mall. Shopping mall o-Durvilinear Geometry. Apartment on top - Rectilinear in geometry.		No Injuries & Death	No Information Available.	http://apfmag.mdmpublishing.com/a- perspective-on-high-rise-building-fires- involving-the-facade/ http://www.thejakartapost.com/news/2/ 16/11/09/neo-soho-in-west-jakarta-on- fire.html	https://apfmag.mdmpublishin g.com/jakarta-high-rise-fire- adds-to-the-current- flammable-cladding-debate/, Accessed on 02/06/2021 https://en.wikipedia.org/wiki/ List_of_tallest_buildings_in_ Jakarta_Accessed on 02/06/2021 https://en.brillo.net/news/vid
44	12/1/2016	Y 2016	Al Bandary Tower B, Sharjah	UAE	Apartment-Residential	Day	Greater that 23 m	Rectilinear	23 storey Building Al Banary is 23 storey Twin towers. Fire started inside an apartment on the 13th floor of Al Bandary Tower B and quickly spread to upwards. Aluminum composite panel façade. Flaming debris were seen falling from the building. Cause of the fire unknown.		No Injuries & Death	9	https://gulfnews.com/uae/sharjah-fire- tenants-move-into-tower-a-1.1938866	https://gulfnews.com/use/sh arjah-fire-tenants-move-into- tower-a-1.1938866, Accessed on 02/06/2021 https://gulfnews.com/use/fa milies-hit-by-sharjah-tower- fire-to-get-alternative- accommodation-1.1938528, Accessed on 02/06/2021 http://abroadnewstoday.blog spot.com/2016/1/2/fire-eruptsi- n-sharjah-bulding- blaze.html, Accessed on 02/06/2021
45	12/13/2016	Y 2016	Oceana Adriatic Building, Dubai	UAE	Apartment-Residential	Night	Greater that 23 m	Rectilinear	15 Story Building. Fire may have started in a coffe machine in a pentinous apartment, triggered by an electrical fault. The spread of the fire was aided by flammable exterior cladding. A section of middle and upper floors of the building were damaged by fire.		No Irgunes & Death	No Information Available.	http://www.khaleejtimes.com/nation/du ai/update-fire-put-out-at-dubais-palm- jumeirah-building http://www.dailystar.co.uk/news/latest- news/56973/Dubai-hote-fire-Palm- Oceania-Residences-Gulf-news-tourist destination	.com/uae/residents-return-to- palm-jumeirah-building-two- years-after-fire-1.778769, Accessed on 02/06/2021

			Fire Incidents around the Globe											
Item No.	Date of Incident	Year	Facility/Building Details	Country	Occupany Classification where Fire Originated	Time of the Day	Major Fire (Buildings > 23 m - highrise) or Minor Fire (<23 m)	Building Geometry	Description of the Fire Incident	Picture	Death/ Injury	No of Floor Affected	Source of Information	Additional Notes/ Remarks
45	5/3/2016	Y2016	Longsheng Building, Nanjing	China	Business	Day	Greater that 23 m	Non Orthogonal	28 Storey high rise building. Predominantly Office Occuapancy. Source andlocation of fire not known - However, 6th floor central air conditioning system as one suspected cause of fire. There were no casualities.		No Injuries & Death	No Information Available.	https://www.mirror.co.uk/news/world- news/nanjing-building-fire-terror- skyscraper-7885245	https://www.mirror.co.uk/ne ws/world-news/hanjing- bulding-fire-terror- skyscraper-7885245. Accessed on 02/06/2021. https://www.rt.com/viral/341 638-towering-inferno-bulding- nanjing/. Accessed on 02/06/2021. https://www.dailymail.co.uk/ news/article-3570678/Huge- fire-rips-office-bulding- forcing-hudreds-workers- flee-lives-China.html, Accessed on 02/06/2021
47	3/2/2017	Y 2017	Address Residences Fountain Views, Dubai	UAE	Apartment-Residential	Night	Greater that 23 m	Curvilinear	cica 60-75 storie high rise building. Fire started in a parking level of the 72 storey fountain view building under construction. Cause and damages - no information available.		hjury - No Death	No Information Available.	"Fire engulfs 72-storey skyscraper in downtown Dubar", The Telegraph (2017) http://www.emirates247.com/news/emirates/three-rescued-from-downtown-fire-dubal-civil-defence-reports-no-injuries-2017-04-02-1.650664	https://www.emirates247.co
48	6/14/2017	Y 2017	Grenfell Tower, London	U.K	Apartment-Residential	Night	Greater that 23 m	Rectilinear	24 Storey tower, A total of 37.3 meter tall building contained 120 one and two bedroom flats. Fire started at 4th floor apartment from a fridge freezer. Fire began to pentrate through the window(EVF) and setting the surrounding cladding panels on fire.		Death	24	B. Malkin, H. Siddique, 'What we know so far about the London tower block fire', The Guardian (2017) https://www.thesottishsun.co.uk/news.1145280/london-fire-live-latest-updates-af-firefighter-stackle-tuge-blazes-af-grenfell-tower-in-ladbroke-grover intp://metro.co.uk/2017/06/14/wilniesse s-describe-the-horror-of-grenfell-tower-fire-6706961/	/ https://en.wikipedia.org/wiki/ Grenfell_Tower_fire, Accessed on 02/06/2021
49	8/4/2017	Y 2017	Torch Tower, Dubai	UAE	Apartment-Residential	Night	Greater that 23 m	Non Orthogonal	Torch Tower is a residential skyscraper in Dubai. Bis storie high rise building. fire engulfed 30 to 40 residences. falling debris. 64 floors were affected by fire. Cause of fire - no information available. Fire erupted on the 26th floor and raged upward.		Vykry - Mo Death	64/87	https://www.theguardian.com/world/2017/aug/03/flames-engulf-86-storey-residential-tower-i-dubai-laber-i-residential-tower-i-dubai-laber-i-flames.com/news/lae/emergen cles/video-forch-tow-flames-dubai-marina-put-out-38-flats-damaged-1.2068756	https://www.theguardian.co m/world/2017/aug/03/flames- engulf-86-story-residential- tower-in-dubal, Accessed on 02/06/2021 https://gulfnews.com/uselvid eo-torch-tower-fire-at-dubal- marins-put-out-38-flats- damaged-1.208766, Accessed on 02/06/2021

	Fire Incidents around the Globe													
Item No.	Date of Incident	Year	Facility/ Building Details	Country	Occupany Classification where Fire Originated	Time of the Day	Major Fire (Buildings > 23 m - highrise) or Minor Fire (<23 m)	Building Geometry	Description of the Fire Incident	Picture	Death/ Injury	No of Floor Affected	Source of Information	Additional Notes/ Remarks
50	2/1/2018	Y 2018	Yuansheng International, Zhengzhou	China	Business	Day	Greater that 23 m	Rectilinear	20 storey Office building in Zhen gzhou. No casualities have been reported. According to Officials - Fire was initial seen on the buildings thermal insulation layer. Fire raged over an area of 2000 sq. meter. Comubustible exterior façade contributed to the spread of fire. Cause of fire unknown.		tişay - No Death	20	http://www.ibtimes.com/massive-fire- engulfs-office-building-chinas- zhengzhu-video-Z648256; https://www.reuters.com/article/us- china-fire/no-casualities-found-atter- blaze-rages-through-china-office- building-idUSKBN1FL4CP	http://www.ninhuanet.com/en glish/2018- 02/01/6_3894/2967 htm, Accessed on 02/06/2021 https://www.stratistimes.co m/asia/se-asia/fre-engulfs-office-building-in-central- china, Accessed on 02/06/2021 https://www.iblimes.com/ma ssive-fire-engulfs-office- building-chinas-zhengzhou- video-2848/259, Accessed on 02/06/2021
51	4/5/2018	Y 2018	Taksim Ilk Yardim Hospital, Istanbul	Turkey	Health Care	Day	Greater that 23 m	Curvilinear	14 Floor Hospital building in Istanbul. Highly flammable exterior cladding - as the reason behind the rapdi fire spread of the hospital fire. Fire seems to have broken out either rubbish bin outside of the building or one of the top floors in an airconditioning unit. Source unknown.		Information Not Available	14	https://www.middleeasteye.net/news/is anbus-granfell-hospital-fire-brings-city- safety-stark-relief	

			Fire Incidents around the Globe											
item No.	Date of Incident	Year	Facility/ Building Details	Country	Occupany Classification where Fire Originated	Time of the Day	Major Fire (Buildings > 23 m - highrise) or Minor Fire (<23 m)	Building Geometry	Description of the Fire Incident	Picture	Death/ Injury	No of Floor Affected	Source of Information	Additional Notes/ Remarks
52	5/15/2018	Y 2018	Zen Tower, Dubai	UAE	Apartment-Residential	Day	Greater that 23 m	Curvilinear	15 Storey Residential Building which has 74 apartments. An electrical short circuit and discarded smoking material were both suspected in a fire that started with outdoor furniture on a balcony of the first floor of the residential tower and spread to the exterior of the 15 storey building.		No Injuries & Death	15	https://www.khaleejtimes.com/nation/d.bai/15-floors-gutted-in-Dubai-Marina-fire	https://gulfnews.com/uae/rep ort-zen-tower-fire-started-on- balcomy-1.2288f0, Accessed on 02/06/2021 https://www.nfpa.org/News- and-Research/Publications- and-media/NFJ-Aune- 2020/Features/Gerfell, Accessed on 02/06/2021
53	3/14/2019	Y 2019	Kaifeng Apartments, Kaifeng	China	Apartment-Residential	Night	Greater that 23 m	Rectilinear	Fire broke out on the exterior of the highrise tower, winds reportedly helped it spread from the second floor to the 17th floor in less than 2 minutes. Cause of the fire unknown.	10 man 10 mm	Information Not Available	15	https://news.cgtn.com/news/3d3d674d/ 041444e33457a6333566d54/index.html	https://www.nfpa.org/News- and-Research/Publications- and-media/Pub-Ju- Journal/2020/May-June- 2020/Features/Grenfell, Accessed on 02/06/2021
54	5/27/2019	Y 2019	Golden Eagle Shopping Mall, Nanjing	China	Apartment-Residential	Night	Greater that 23 m	Non Orthogonal	Fire engulfed the 9th floor of the golden eagle shoping center. Fire started near a hotel under renovation on the block's 9th floor. Cause of the fire unknown.		Information Not Available	No Information Available.	http://shanghai.ist/2019/05/27/watch- massive-fire-breaks-out-at-nanjing- shopping-mall/#.XOw7Qfvhbsc.twitter	http://www.chinadaily.com.c n/a/201905/25/W55ce816f5 a3104842260bd05.html Accessed on 02/06/2021 https://www.youtube.com/wa tch?v=GYV/yaqV3wg. Accessed on 02/06/2021
55	5/29/2019	Y 2019	Commercial Building, Luoyang	China	Business	Day	Greater that 23 m	Curvilinear	Fire broke out in an office building in the Luoyang city. No casualities reported. Fire spread from the 3rd floor to the top of the roof, damaging exterior building.		Information Not Available	No Information Available.	http://news.sina.com.cn/o/2019-05- 29/doc-lhvhiqay/2320153.shtml;	http://news.sina.com.cn/o/20 19-05-29/doc- ihvhiqay/2320153.shtml; Accessed on 03/06/2021

	Fire Incidents around the Globe													
Item No.	Date of Incident	Year	Facility/Building Details	Country	Occupany Classification where Fire Originated	Time of the Day	Major Fire (Buildings > 23 m - highrise) or Minor Fire (<23 m)	Building Geometry	Description of the Fire Incident	Picture	Death/ Injury	No of Floor Affected	Source of Information	Additional Notes/ Remarks
56	8/14/2019	Y 2019	Residential Flats, Warsaw	Poland	Apartment-Residential	Night	Greater that 23 m	Rectilinear	10 storey Building. Discarded smoking materials were suspected in starting a garbage fire that ignited the façade of 10 storey residential building burning from ground level to the roof.		Information Not Available	No Information Available.	https://kvn24.pl/kvnwarszawa/najnowsze /spalona-elewacja-zniszczone-okna-od- parteru-az-po-sam-dach-297220	https://www.nfpa.org/News- and-Research/Publications- and-media/NFPA. Journal/2020/May-June- 2020/Features/Grenfel, Accessed on 30/36/2021 https://tvn24.pi/tvnwarszawa/najnowsze/spalora- elwadja-znizczone-okna- od-parteru-az-po-sam-dach- 652/130, Accessed on 03/06/2021
57	11/16/2019	Y 2019	The Cube Student Housing, Bolton	u.ĸ	Apartment-Residential	Night	Less than 23 m	Rectilinear	6 Storey building. Fire destroyed the 6 storey apartement block that housed 200 university students. High pressure laminate used as façade material. The fire may have been caused by a discarded cigerette.		Injury - No Death	6	https://www.ft.com/content/bb1e05b4- 0896-11ea-b2d6-9bf4d1957a67	https://www.bbc.com/news/ uk-england-manchester- 50438177, Accessed on 03/06/2021 https://www.freco.uk/what- has-the-botton-student- accommodation-fire-taught- us/, Accessed on 03/06/2021 https://www.thebottonnews.c o.uk/news/18617548.botton- cube-fire-cause-devastating- blaze-revealed/, Accessed on 03/06/2021
58	5/5/2020	Y 2020	ABBCO Tower, Sharjah	UAE	Apartment-Residential	Night	Greater that 23 m	Curvilinear	49 Storey Residential Building. 12 People were injured. Cause of the five was carelessly tossed oigerete but that was discarded in the corndor of the first floor. ACP used as cladding material.		Injury - No Death	48	https://www.bbc.com/news/world-middle-east-5255429, Accessed on 03/06/2021 https://www.daijiworld.com/news/news Display.aspx/news1D=706637, Accessed on 03/06/2021	
59	7/27/2020		Business Center, Ankara	Turkey	Business	Day	Greater that 23 m	Rectilinear	No Information Available.		Information Not Available	No Information Available.	https://www.dailysabah.com/turkey/fire- breaks-out-in-business-center-in-turkish capital-ankara/news, Accessed on 030/06/2021	

	Fire Incidents around the Globe													
Item No.	Date of Incident	Year	Facility/ Building Details	Country	Occupany Classification where Fire Originated	Time of the Day	Major Fire (Buildings > 23 m - highrise) or Minor Fire (<23 m)	Building Geometry	Description of the Fire Incident	Picture	Death/ Injury	No of Floor Affected	Source of Information	Additional Notes/ Remarks
60	8/27/2020	Y 2020	Madrid Tower Block	Spain	Apartment-Residential	Day	Greater that 23 m	Rectilinear	No Information Available.		Information Not Available	5	https://www.madridmetropolitan.com/bl aze-rips-through-madrid-tower-block/, Accessed on 30/66/2021 https://www.bbc.com/news/av/world- europs-53961937, Accessed on 03/06/2021	
61	10/8/2020	Y 2020	Apartment Block Ulsan	South Korea	Apartment-Residential	Night	Greater that 23 m	Non Orthogonal	33 Storey residential building. Cause of the fire is being investigated, the initial report says the fire may have started between 8th and 12 th floor. Strong winds helped the fire to spread and damage the entire building.		Injury - No Death	33	https://www.bbc.com/news/world-asia- 54470378, Accessed on 03/06/2021 https://www.dw.com/en/south-korea- massive-fire-oglifs-high-rise-block-in- ulsan/a-55211286, Accessed on 03/06/2021	
62	3/9/2021	Y 2021	Apartment Building, Shijiazhuang	China	Apartment-Residential	Day	Greater that 23 m	Curvilinear	26 storey tower - Residential apartment building. Fire may have started firm the first floor and spread rapidly through the insulation material on the external façade. No casualities were reported.		Information Not Available	No Information Available.	https://news.cgtn.com/news/2021-03-09/High-rise-building-catches-fire-in-north-China-YurhhCq3XWindex.html, Accessed on 03/06/2021 https://www.thestar.com.my/aseanplus/aseanplus-news/2021/03/11/huge-fire-engulfs-26-storey-building-in-shijiazhuang, Accessed on 03/06/2021	

APPENDIX C: FDS Input File

Large scale fire test FD:

large_scale_fire_test_FD_mesh_div.fds

&HEAD CHID='large_scale_fire_test_FD_mesh_div'/ &TIME T_END=1400.0/ &DUMP DT_RESTART=300.0, DT_SL3D=0.25/ &MISC TMPA=35.0/

&MESH ID='MESH-01', IJK=28.30.120, XB=-1.8,-0.4,-1.55,-0.05.0.0.6.0/ &MESH ID='MESH-02', IJK=28,25,120, XB=-1.8,-0.4,-0.05,1.2,0.0,6.0/ &MESH ID='MESH-03', IJK=28,22,120, XB=-1.8,-0.4,1.2,2.3,0.0,6.0/ &MESH ID='MESH-04', IJK=28,26,120, XB=-1.8,-0.4,2.3,3.6,0.0,6.0/ &MESH ID='MESH-05', IJK=28,21,120, XB=-1.8,-0.4,3.6,4.65,0.0,6.0/ &MESH ID='MESH-06', IJK=31,30,120, XB=-0.4,1.15,-1.55,-0.05,0.0,6.0/ &MESH ID='MESH-07', IJK=31,25,120, XB=-0.4,1.15,-0.05,1.2,0.0,6.0/ &MESH ID='MESH-08', IJK=31,22,120, XB=-0.4,1.15,1.2,2.3,0.0,6.0/ &MESH ID='MESH-09', IJK=31,26,120, XB=-0.4,1.15,2.3,3.6,0.0,6.0/ &MESH ID='MESH-10', IJK=31,21,120, XB=-0.4,1.15,3.6,4.65,0.0,6.0/ &MESH ID='MESH-11', IJK=43,30,120, XB=1.15,3.3,-1.55,-0.05,0.0,6.0/ &MESH ID='MESH-12', IJK=43,25,120, XB=1.15,3.3,-0.05,1.2,0.0,6.0/ &MESH ID='MESH-13', IJK=43,22,120, XB=1.15,3.3,1.2,2.3,0.0,6.0/ &MESH ID='MESH-14', IJK=43,26,120, XB=1.15,3.3,2.3,3.6,0.0,6.0/ &MESH ID='MESH-15', IJK=43.21.120, XB=1.15.3.3.3.6.4.65.0.0.6.0/ &MESH ID='MESH-16', IJK=34,30,120, XB=3.3,5.0,-1.55,-0.05,0.0,6.0/ &MESH ID='MESH-17', IJK=34,25,120, XB=3.3,5.0,-0.05,1.2,0.0,6.0/ &MESH ID='MESH-18', IJK=34,22,120, XB=3.3,5.0,1.2,2.3,0.0,6.0/ &MESH ID='MESH-19', IJK=34,26,120, XB=3.3,5.0,2.3,3.6,0.0,6.0/ &MESH ID='MESH-20', IJK=34,21,120, XB=3.3,5.0,3.6,4.65,0.0,6.0/ &MESH ID='MESH-21', IJK=28,30,120, XB=5.0,6.4,-1.55,-0.05,0.0,6.0/ &MESH ID='MESH-22', IJK=28,25,120, XB=5.0,6.4,-0.05,1.2,0.0,6.0/ &MESH ID='MESH-23', IJK=28,22,120, XB=5.0,6.4,1.2,2.3,0.0,6.0/ &MESH ID='MESH-24', IJK=28,26,120, XB=5.0,6.4,2.3,3.6,0.0,6.0/ &MESH ID='MESH-25', IJK=28,21,120, XB=5.0,6.4,3.6,4.65,0.0,6.0/

&REAC ID='FDS6 N-HEPTANE',

FYI='FDS6 Predefined', FUEL='N-HEPTANE', CO_YIELD=0.02, SOOT_YIELD=0.03, HEAT_OF_COMBUSTION=4.3E+4, RADIATIVE_FRACTION=0.3/

&DEVC ID='1', QUANTITY='THERMOCOUPLE', XYZ=0.15,0.65,1.0/ &DEVC ID='2', QUANTITY='THERMOCOUPLE', XYZ=0.15,0.65,2.0/ &DEVC ID='3', QUANTITY='THERMOCOUPLE', XYZ=0.15,0.65,3.0/ &DEVC ID='4', QUANTITY='THERMOCOUPLE', XYZ=0.15,0.65,4.0/ &DEVC ID='5', QUANTITY='THERMOCOUPLE', XYZ=4.4,0.65,1.0/ &DEVC ID='6', QUANTITY='THERMOCOUPLE', XYZ=4.4,0.65,2.0/ &DEVC ID='7', QUANTITY='THERMOCOUPLE', XYZ=4.4,0.65,3.0/ &DEVC ID='8', QUANTITY='THERMOCOUPLE', XYZ=4.4,0.65,4.0/ &DEVC ID='9', QUANTITY='THERMOCOUPLE', XYZ=4.9,0.65,1.0/

```
&DEVC ID='10', QUANTITY='THERMOCOUPLE', XYZ=4.9,0.65,2.0/
&DEVC ID='11', QUANTITY='THERMOCOUPLE', XYZ=4.9,0.65,3.0/
&DEVC ID='12', QUANTITY='THERMOCOUPLE', XYZ=4.9,0.65,4.0/
&DEVC ID='inside_mid_top', QUANTITY='THERMOCOUPLE', XYZ=2.25,1.75,3.0/
&DEVC ID='heat_flux_inside', QUANTITY='GAUGE HEAT FLUX', XYZ=4.05,1.75,2.0, IOR=-
3/
&DEVC ID='heat_flux_door', QUANTITY='GAUGE HEAT FLUX', XYZ=4.1,0.65,2.0, IOR=-3/
&MATL ID='STEEL'.
  FYI='Drysdale, Intro to Fire Dynamics - ATF NIST Multi-Floor Validation',
  SPECIFIC HEAT=0.46,
  CONDUCTIVITY=45.8,
  DENSITY=7850.0,
  EMISSIVITY=0.95/
&SURF ID='Fire',
  COLOR='RED',
  HRRPUA=4349.270483,
  RAMP Q='Fire RAMP Q',
  TMP_FRONT=300.0/
&RAMP ID='Fire_RAMP_Q', T=1.0, F=0.0/
&RAMP ID='Fire_RAMP_Q', T=50.0, F=0.141928/
&RAMP ID='Fire_RAMP_Q', T=100.0, F=0.254335/
&RAMP ID='Fire_RAMP_Q', T=150.0, F=0.283237/
&RAMP ID='Fire_RAMP_Q', T=200.0, F=0.404624/
&RAMP ID='Fire_RAMP_Q', T=250.0, F=0.716763/
&RAMP ID='Fire_RAMP_Q', T=300.0, F=0.653179/
&RAMP ID='Fire_RAMP_Q', T=350.0, F=0.34104/
&RAMP ID='Fire_RAMP_Q', T=400.0, F=0.965318/
&RAMP ID='Fire_RAMP_Q', T=450.0, F=0.780347/
&RAMP ID='Fire_RAMP_Q', T=500.0, F=0.479769/
&RAMP ID='Fire_RAMP_Q', T=550.0, F=0.456647/
&RAMP ID='Fire_RAMP_Q', T=600.0, F=0.699422/
&RAMP ID='Fire_RAMP_Q', T=650.0, F=0.34104/
&RAMP ID='Fire_RAMP_Q', T=700.0, F=0.416185/
&RAMP ID='Fire_RAMP_Q', T=750.0, F=0.462428/
&RAMP ID='Fire RAMP O', T=800.0, F=0.757225/
&RAMP ID='Fire_RAMP_Q', T=850.0, F=0.393064/
&RAMP ID='Fire_RAMP_Q', T=900.0, F=0.49711/
&RAMP ID='Fire_RAMP_Q', T=950.0, F=0.924855/
&RAMP ID='Fire_RAMP_Q', T=1000.0, F=0.49711/
&RAMP ID='Fire_RAMP_Q', T=1050.0, F=0.739884/
&RAMP ID='Fire_RAMP_Q', T=1100.0, F=1.0/
&RAMP ID='Fire_RAMP_Q', T=1150.0, F=0.809249/
&RAMP ID='Fire_RAMP_Q', T=1200.0, F=0.67052/
&RAMP ID='Fire_RAMP_Q', T=1250.0, F=0.567713/
&RAMP ID='Fire RAMP Q', T=1300.0, F=0.369013/
&RAMP ID='Fire_RAMP_Q', T=1310.0, F=0.242981/
&RAMP ID='Fire_RAMP_Q', T=1320.0, F=0.170314/
&RAMP ID='Fire_RAMP_Q', T=1330.0, F=0.092253/
&RAMP ID='Fire_RAMP_Q', T=1340.0, F=0.056771/
```

&RAMP ID='Fire_RAMP_Q', T=1350.0, F=0.028669/

```
&SURF ID='steel',
  RGB=146,202,166,
  TMP INNER=35.0,
  MATL_ID(1,1)='STEEL',
  MATL MASS FRACTION(1,1)=1.0,
  THICKNESS(1)=4.0E-3/
&OBST ID='FD.stl', XB=0.05,0.1,0.05,0.1,0.6,1.4, RGB=153,153,153,
TRANSPARENCY=0.392157, THICKEN=.TRUE., SURF_ID='steel'/
&OBST ID='FD.stl', XB=0.05,0.1,1.290634E-15,0.05,0.7,1.3, RGB=153,153,153,
TRANSPARENCY=0.392157, THICKEN=.TRUE., SURF_ID='steel'/
&OBST ID='FD.stl', XB=0.05,0.1,0.1,0.15,0.8,1.25, RGB=153,153,153,
TRANSPARENCY=0.392157, THICKEN=.TRUE., SURF_ID='steel'/
&OBST ID='FD.stl', XB=0.1,0.15,0.05,0.1,0.4,0.6, RGB=153,153,153,
TRANSPARENCY=0.392157, THICKEN=.TRUE., SURF_ID='steel'/
&OBST ID='FD.stl', XB=0.1,0.15,1.290634E-15,0.05,0.45,1.55, RGB=153,153,153,
TRANSPARENCY=0.392157, THICKEN=.TRUE., SURF_ID='steel'/
&OBST ID='FD.stl', XB=0.1,0.15,0.1,0.15,0.5,1.5, RGB=153,153,153,
TRANSPARENCY=0.392157, THICKEN=.TRUE., SURF ID='steel'/
&OBST ID='FD.stl', XB=0.1,0.15,0.05,0.1,1.4,1.6, RGB=153,153,153,
TRANSPARENCY=0.392157, THICKEN=.TRUE., SURF_ID='steel'/
&OBST ID='FD.stl', XB=0.15,0.2,0.05,0.1,0.25,0.4, RGB=153,153,153,
TRANSPARENCY=0.392157, THICKEN=.TRUE., SURF_ID='steel'/
&OBST ID='FD.stl', XB=0.15,0.2,1.290634E-15,0.05,0.3,1.75, RGB=153,153,153,
TRANSPARENCY=0.392157, THICKEN=.TRUE., SURF_ID='steel'/
&OBST ID='FD.stl', XB=0.15,0.2,0.1,0.15,0.35,1.7, RGB=153,153,153,
TRANSPARENCY=0.392157, THICKEN=.TRUE., SURF_ID='steel'/
&OBST ID='FD.stl', XB=0.15,0.2,0.05,0.1,1.6,1.75, RGB=153,153,153,
TRANSPARENCY=0.392157, THICKEN=.TRUE., SURF_ID='steel'/
&OBST ID='FD.stl', XB=0.2,0.25,0.05,0.1,0.1,0.25, RGB=153,153,153,
TRANSPARENCY=0.392157, THICKEN=.TRUE., SURF_ID='steel'/
&OBST ID='FD.stl', XB=0.2,0.25,1.290634E-15,0.05,0.15,1.85, RGB=153,153,153,
TRANSPARENCY=0.392157, THICKEN=.TRUE., SURF ID='steel'/
&OBST ID='FD.stl', XB=0.2,0.25,0.1,0.15,0.2,1.8, RGB=153,153,153,
TRANSPARENCY=0.392157, THICKEN=.TRUE., SURF_ID='steel'/
&OBST ID='FD.stl', XB=0.2,0.25,0.05,0.1,1.75,1.9, RGB=153,153,153,
TRANSPARENCY=0.392157, THICKEN=.TRUE., SURF_ID='steel'/
&OBST ID='FD.stl', XB=0.25,0.3,0.1,0.15,0.0,1.9, RGB=153,153,153,
TRANSPARENCY=0.392157, THICKEN=.TRUE., SURF_ID='steel'/
&OBST ID='FD.stl', XB=0.25,0.3,1.290634E-15,0.05,0.0,1.95, RGB=153,153,153,
TRANSPARENCY=0.392157, THICKEN=.TRUE., SURF_ID='steel'/
&OBST ID='FD.stl', XB=0.25,0.3,0.05,0.1,1.9,2.0, RGB=153,153,153,
TRANSPARENCY=0.392157, THICKEN=.TRUE., SURF_ID='steel'/
&OBST ID='FD.stl', XB=0.25,1.15,0.05,0.1,0.0,0.1, RGB=153,153,153,
TRANSPARENCY=0.392157, THICKEN=.TRUE., SURF_ID='steel'/
&OBST ID='FD.stl', XB=0.25,1.15,0.15,1.2,0.0,0.15, RGB=153,153,153,
TRANSPARENCY=0.392157, THICKEN=.TRUE., SURF ID='steel'/
&OBST ID='FD.stl', XB=0.3,0.35,0.1,0.15,0.0,2.05, RGB=153,153,153,
TRANSPARENCY=0.392157, THICKEN=.TRUE., SURF_ID='steel'/
&OBST ID='FD.stl', XB=0.3,0.35,1.290634E-15,0.05,0.0,2.1, RGB=153,153,153,
TRANSPARENCY=0.392157, THICKEN=.TRUE., SURF_ID='steel'/
```

```
&OBST ID='FD.stl', XB=0.3,0.35,0.05,0.1,2.0,2.1, RGB=153,153,153,
TRANSPARENCY=0.392157, THICKEN=.TRUE., SURF_ID='steel'/
&OBST ID='FD.stl', XB=0.35,0.4,1.290634E-15,0.05,0.0,2.15, RGB=153,153,153,
TRANSPARENCY=0.392157, THICKEN=.TRUE., SURF_ID='steel'/
&OBST ID='FD.stl', XB=0.35,0.4,0.1,0.15,0.0,2.15, RGB=153,153,153,
TRANSPARENCY=0.392157, THICKEN=.TRUE., SURF_ID='steel'/
&OBST ID='FD.stl', XB=0.35,0.4,0.15,1.2,2.05,2.15, RGB=153,153,153,
TRANSPARENCY=0.392157, THICKEN=.TRUE., SURF_ID='steel'/
&OBST ID='FD.stl', XB=0.35,0.4,0.05,0.1,2.1,2.15, RGB=153,153,153,
TRANSPARENCY=0.392157, THICKEN=.TRUE., SURF_ID='steel'/
&OBST ID='FD.stl', XB=0.4,0.45,0.1,0.15,0.0,2.1, RGB=153,153,153,
TRANSPARENCY=0.392157, THICKEN=.TRUE., SURF_ID='steel'/
&OBST ID='FD.stl', XB=0.4,0.45,1.290634E-15,0.05,0.0,2.25, RGB=153,153,153,
TRANSPARENCY=0.392157, THICKEN=.TRUE., SURF_ID='steel'/
&OBST ID='FD.stl', XB=0.4,0.45,0.15,1.2,2.05,2.1, RGB=153,153,153,
TRANSPARENCY=0.392157, THICKEN=.TRUE., SURF_ID='steel'/
&OBST ID='FD.stl', XB=0.4,0.45,0.05,0.1,2.1,2.25, RGB=153,153,153,
TRANSPARENCY=0.392157, THICKEN=.TRUE., SURF_ID='steel'/
&OBST ID='FD.stl', XB=0.4,0.45,0.1,1.2,2.15,2.25, RGB=153,153,153,
TRANSPARENCY=0.392157, THICKEN=.TRUE., SURF_ID='steel'/
&OBST ID='FD.stl', XB=0.45,0.5,1.290634E-15,0.05,0.0,2.3, RGB=153,153,153,
TRANSPARENCY=0.392157, THICKEN=.TRUE., SURF_ID='steel'/
&OBST ID='FD.stl', XB=0.45,0.5,0.1,0.15,0.0,2.3, RGB=153,153,153,
TRANSPARENCY=0.392157, THICKEN=.TRUE., SURF_ID='steel'/
&OBST ID='FD.stl', XB=0.45,0.5,0.15,1.2,2.1,2.3, RGB=153,153,153,
TRANSPARENCY=0.392157, THICKEN=.TRUE., SURF_ID='steel'/
&OBST ID='FD.stl', XB=0.45,0.5,0.05,0.1,2.15,2.3, RGB=153,153,153,
TRANSPARENCY=0.392157, THICKEN=.TRUE., SURF_ID='steel'/
&OBST ID='FD.stl', XB=0.5,0.55,0.1,0.15,0.0,2.2, RGB=153,153,153,
TRANSPARENCY=0.392157, THICKEN=.TRUE., SURF_ID='steel'/
&OBST ID='FD.stl', XB=0.5,0.55,1.290634E-15,0.05,0.0,2.35, RGB=153,153,153,
TRANSPARENCY=0.392157, THICKEN=.TRUE., SURF_ID='steel'/
&OBST ID='FD.stl', XB=0.5,0.55,0.15,1.2,2.15,2.4, RGB=153,153,153,
TRANSPARENCY=0.392157, THICKEN=.TRUE., SURF_ID='steel'/
&OBST ID='FD.stl', XB=0.5,0.55,0.05,0.15,2.25,2.4, RGB=153,153,153,
TRANSPARENCY=0.392157, THICKEN=.TRUE., SURF_ID='steel'/
&OBST ID='FD.stl', XB=0.55,0.6,0.1,0.15,0.0,2.25, RGB=153,153,153,
TRANSPARENCY=0.392157, THICKEN=.TRUE., SURF_ID='steel'/
&OBST ID='FD.stl', XB=0.55,0.6,1.290634E-15,0.05,0.0,2.45, RGB=153,153,153,
TRANSPARENCY=0.392157, THICKEN=.TRUE., SURF_ID='steel'/
&OBST ID='FD.stl', XB=0.55,0.6,0.15,1.2,2.2,2.45, RGB=153,153,153,
TRANSPARENCY=0.392157, THICKEN=.TRUE., SURF_ID='steel'/
&OBST ID='FD.stl', XB=0.55,0.6,0.05,0.15,2.3,2.45, RGB=153,153,153,
TRANSPARENCY=0.392157, THICKEN=.TRUE., SURF_ID='steel'/
&OBST ID='FD.stl', XB=0.6,0.65,0.1,0.15,0.0,2.35, RGB=153,153,153,
TRANSPARENCY=0.392157, THICKEN=.TRUE., SURF_ID='steel'/
&OBST ID='FD.stl', XB=0.6,0.65,1.290634E-15,0.05,0.0,2.5, RGB=153,153,153,
TRANSPARENCY=0.392157, THICKEN=.TRUE., SURF_ID='steel'/
&OBST ID='FD.stl', XB=0.6,0.65,0.15,1.2,2.3,2.5, RGB=153,153,153,
TRANSPARENCY=0.392157, THICKEN=.TRUE., SURF_ID='steel'/
&OBST ID='FD.stl', XB=0.6,0.65,0.05,0.15,2.4,2.5, RGB=153,153,153,
TRANSPARENCY=0.392157, THICKEN=.TRUE., SURF_ID='steel'/
```

```
&OBST ID='FD.stl', XB=0.65,0.7,0.1,0.15,0.0,2.4, RGB=153,153,153,
TRANSPARENCY=0.392157, THICKEN=.TRUE., SURF_ID='steel'/
&OBST ID='FD.stl', XB=0.65,0.7,1.290634E-15,0.05,0.0,2.55, RGB=153,153,153,
TRANSPARENCY=0.392157, THICKEN=.TRUE., SURF_ID='steel'/
&OBST ID='FD.stl', XB=0.65,0.7,0.15,1.2,2.35,2.55, RGB=153,153,153,
TRANSPARENCY=0.392157, THICKEN=.TRUE., SURF_ID='steel'/
&OBST ID='FD.stl', XB=0.65,0.7,0.05,0.15,2.45,2.55, RGB=153,153,153,
TRANSPARENCY=0.392157, THICKEN=.TRUE., SURF_ID='steel'/
&OBST ID='FD.stl', XB=0.7,0.75,0.1,0.15,0.0,2.45, RGB=153,153,153,
TRANSPARENCY=0.392157, THICKEN=.TRUE., SURF_ID='steel'/
&OBST ID='FD.stl', XB=0.7,0.75,1.290634E-15,0.05,0.0,2.6, RGB=153,153,153,
TRANSPARENCY=0.392157, THICKEN=.TRUE., SURF_ID='steel'/
&OBST ID='FD.stl', XB=0.7,0.75,0.15,1.2,2.4,2.6, RGB=153,153,153,
TRANSPARENCY=0.392157, THICKEN=.TRUE., SURF_ID='steel'/
&OBST ID='FD.stl', XB=0.7,0.75,0.05,0.15,2.5,2.6, RGB=153,153,153,
TRANSPARENCY=0.392157, THICKEN=.TRUE., SURF_ID='steel'/
&OBST ID='FD.stl', XB=0.75,0.8,0.1,0.15,0.0,2.5, RGB=153,153,153,
TRANSPARENCY=0.392157, THICKEN=.TRUE., SURF_ID='steel'/
&OBST ID='FD.stl', XB=0.75,0.8,1.290634E-15,0.05,0.0,2.65, RGB=153,153,153,
TRANSPARENCY=0.392157, THICKEN=.TRUE., SURF_ID='steel'/
&OBST ID='FD.stl', XB=0.75,0.8,0.15,1.2,2.45,2.65, RGB=153,153,153,
TRANSPARENCY=0.392157, THICKEN=.TRUE., SURF_ID='steel'/
&OBST ID='FD.stl', XB=0.75,0.8,0.05,0.15,2.55,2.65, RGB=153,153,153,
TRANSPARENCY=0.392157, THICKEN=.TRUE., SURF_ID='steel'/
&OBST ID='FD.stl', XB=0.8,0.85,0.1,0.15,0.0,2.55, RGB=153,153,153,
TRANSPARENCY=0.392157, THICKEN=.TRUE., SURF_ID='steel'/
&OBST ID='FD.stl', XB=0.8,0.85,1.290634E-15,0.05,0.0,2.7, RGB=153,153,153,
TRANSPARENCY=0.392157, THICKEN=.TRUE., SURF_ID='steel'/
&OBST ID='FD.stl', XB=0.8,0.85,0.15,1.2,2.5,2.7, RGB=153,153,153,
TRANSPARENCY=0.392157, THICKEN=.TRUE., SURF_ID='steel'/
&OBST ID='FD.stl', XB=0.8,0.85,0.05,0.15,2.6,2.7, RGB=153,153,153,
TRANSPARENCY=0.392157, THICKEN=.TRUE., SURF_ID='steel'/
&OBST ID='FD.stl', XB=0.85,0.9,0.1,0.15,0.0,2.6, RGB=153,153,153,
TRANSPARENCY=0.392157, THICKEN=.TRUE., SURF_ID='steel'/
&OBST ID='FD.stl', XB=0.85,0.9,0.15,1.2,2.55,2.75, RGB=153,153,153,
TRANSPARENCY=0.392157, THICKEN=.TRUE., SURF_ID='steel'/
&OBST ID='FD.stl', XB=0.85,0.9,0.05,0.15,2.65,2.75, RGB=153,153,153,
TRANSPARENCY=0.392157, THICKEN=.TRUE., SURF_ID='steel'/
&OBST ID='FD.stl', XB=0.85,0.95,1.290634E-15,0.05,0.0,2.75, RGB=153,153,153,
TRANSPARENCY=0.392157, THICKEN=.TRUE., SURF_ID='steel'/
&OBST ID='FD.stl', XB=0.9,0.95,0.1,0.15,0.0,2.65, RGB=153,153,153,
TRANSPARENCY=0.392157, THICKEN=.TRUE., SURF_ID='steel'/
&OBST ID='FD.stl', XB=0.9,0.95,0.15,1.2,2.6,2.75, RGB=153,153,153,
TRANSPARENCY=0.392157, THICKEN=.TRUE., SURF_ID='steel'/
&OBST ID='FD.stl', XB=0.9,0.95,0.05,0.15,2.7,2.75, RGB=153,153,153,
TRANSPARENCY=0.392157, THICKEN=.TRUE., SURF_ID='steel'/
&OBST ID='FD.stl', XB=0.95,1.0,1.290634E-15,0.05,0.0,2.8, RGB=153,153,153,
TRANSPARENCY=0.392157, THICKEN=.TRUE., SURF_ID='steel'/
&OBST ID='FD.stl', XB=0.95,1.0,0.15,1.2,2.65,2.8, RGB=153,153,153,
TRANSPARENCY=0.392157, THICKEN=.TRUE., SURF_ID='steel'/
&OBST ID='FD.stl', XB=0.95,1.0,0.05,0.15,2.75,2.8, RGB=153,153,153,
TRANSPARENCY=0.392157, THICKEN=.TRUE., SURF_ID='steel'/
```

```
&OBST ID='FD.stl', XB=0.95,1.05,0.1,0.15,0.0,2.7, RGB=153,153,153,
TRANSPARENCY=0.392157, THICKEN=.TRUE., SURF_ID='steel'/
&OBST ID='FD.stl', XB=1.0,1.05,0.15,1.2,2.65,2.85, RGB=153,153,153,
TRANSPARENCY=0.392157, THICKEN=.TRUE., SURF_ID='steel'/
&OBST ID='FD.stl', XB=1.0,1.05,0.05,0.15,2.75,2.85, RGB=153,153,153,
TRANSPARENCY=0.392157, THICKEN=.TRUE., SURF_ID='steel'/
&OBST ID='FD.stl', XB=1.0,1.1,1.290634E-15,0.05,0.0,2.85, RGB=153,153,153,
TRANSPARENCY=0.392157, THICKEN=.TRUE., SURF_ID='steel'/
&OBST ID='FD.stl', XB=1.05,1.1,0.1,0.15,0.0,2.75, RGB=153,153,153,
TRANSPARENCY=0.392157, THICKEN=.TRUE., SURF_ID='steel'/
&OBST ID='FD.stl', XB=1.05,1.1,0.15,1.2,2.7,2.85, RGB=153,153,153,
TRANSPARENCY=0.392157, THICKEN=.TRUE., SURF_ID='steel'/
&OBST ID='FD.stl', XB=1.05,1.1,0.05,0.15,2.8,2.85, RGB=153,153,153,
TRANSPARENCY=0.392157, THICKEN=.TRUE., SURF_ID='steel'/
&OBST ID='FD.stl', XB=1.1,1.15,0.1,0.15,0.0,2.8, RGB=153,153,153,
TRANSPARENCY=0.392157, THICKEN=.TRUE., SURF_ID='steel'/
&OBST ID='FD.stl', XB=1.1,1.15,1.290634E-15,0.05,0.0,2.9, RGB=153,153,153,
TRANSPARENCY=0.392157, THICKEN=.TRUE., SURF_ID='steel'/
&OBST ID='FD.stl', XB=1.1,1.15,0.15,1.2,2.75,2.9, RGB=153,153,153,
TRANSPARENCY=0.392157, THICKEN=.TRUE., SURF_ID='steel'/
&OBST ID='FD.stl', XB=1.1,1.15,0.05,0.15,2.85,2.9, RGB=153,153,153,
TRANSPARENCY=0.392157, THICKEN=.TRUE., SURF_ID='steel'/
&OBST ID='FD.stl', XB=0.05,0.1,1.25,2.3,0.6,1.4, RGB=153,153,153,
TRANSPARENCY=0.392157, THICKEN=.TRUE., SURF_ID='steel'/
&OBST ID='FD.stl', XB=0.05,0.1,1.2,1.25,0.75,1.3, RGB=153,153,153,
TRANSPARENCY=0.392157, THICKEN=.TRUE., SURF_ID='steel'/
&OBST ID='FD.stl', XB=0.1,0.15,1.25,2.3,0.4,0.6, RGB=153,153,153,
TRANSPARENCY=0.392157, THICKEN=.TRUE., SURF_ID='steel'/
&OBST ID='FD.stl', XB=0.1,0.15,1.2,1.25,0.45,1.55, RGB=153,153,153,
TRANSPARENCY=0.392157, THICKEN=.TRUE., SURF_ID='steel'/
&OBST ID='FD.stl', XB=0.1,0.15,1.25,2.3,1.4,1.6, RGB=153,153,153,
TRANSPARENCY=0.392157, THICKEN=.TRUE., SURF_ID='steel'/
&OBST ID='FD.stl', XB=0.15,0.2,1.25,2.3,0.25,0.4, RGB=153,153,153,
TRANSPARENCY=0.392157, THICKEN=.TRUE., SURF_ID='steel'/
&OBST ID='FD.stl', XB=0.15,0.2,1.2,1.25,0.3,0.8, RGB=153,153,153,
TRANSPARENCY=0.392157, THICKEN=.TRUE., SURF_ID='steel'/
&OBST ID='FD.stl', XB=0.15,0.2,1.25,2.3,0.6,1.4, RGB=153,153,153,
TRANSPARENCY=0.392157, THICKEN=.TRUE., SURF_ID='steel'/
&OBST ID='FD.stl', XB=0.15,0.2,1.2,1.25,1.25,1.75, RGB=153,153,153,
TRANSPARENCY=0.392157, THICKEN=.TRUE., SURF_ID='steel'/
&OBST ID='FD.stl', XB=0.15,0.2,1.25,2.3,1.6,1.75, RGB=153,153,153,
TRANSPARENCY=0.392157, THICKEN=.TRUE., SURF_ID='steel'/
&OBST ID='FD.stl', XB=0.2,0.25,1.25,2.3,0.1,0.25, RGB=153,153,153,
TRANSPARENCY=0.392157, THICKEN=.TRUE., SURF_ID='steel'/
&OBST ID='FD.stl', XB=0.2,0.25,1.2,1.25,0.1,0.5, RGB=153,153,153,
TRANSPARENCY=0.392157, THICKEN=.TRUE., SURF_ID='steel'/
&OBST ID='FD.stl', XB=0.2,0.25,1.25,2.3,0.4,0.6, RGB=153,153,153,
TRANSPARENCY=0.392157, THICKEN=.TRUE., SURF_ID='steel'/
&OBST ID='FD.stl', XB=0.2,0.25,1.25,2.3,1.4,1.6, RGB=153,153,153,
TRANSPARENCY=0.392157, THICKEN=.TRUE., SURF_ID='steel'/
&OBST ID='FD.stl', XB=0.2,0.25,1.2,1.25,1.45,1.85, RGB=153,153,153,
TRANSPARENCY=0.392157, THICKEN=.TRUE., SURF_ID='steel'/
```

&OBST ID='FD.stl', XB=0.2,0.25,1.25,2.3,1.75,1.9, RGB=153,153,153, TRANSPARENCY=0.392157, THICKEN=.TRUE., SURF_ID='steel'/ &OBST ID='FD.stl', XB=0.25,0.3,2.2,2.3,0.0,0.1, RGB=153,153,153, TRANSPARENCY=0.392157, THICKEN=.TRUE., SURF_ID='steel'/ &OBST ID='FD.stl', XB=0.25,0.3,1.2,1.25,0.15,0.35, RGB=153,153,153, TRANSPARENCY=0.392157, THICKEN=.TRUE., SURF_ID='steel'/ &OBST ID='FD.stl', XB=0.25,0.3,1.25,2.3,0.25,0.4, RGB=153,153,153, TRANSPARENCY=0.392157, THICKEN=.TRUE., SURF_ID='steel'/ &OBST ID='FD.stl', XB=0.25,0.3,1.25,2.3,1.6,1.75, RGB=153,153,153, TRANSPARENCY=0.392157, THICKEN=.TRUE., SURF_ID='steel'/ &OBST ID='FD.stl', XB=0.25,0.3,1.2,1.25,1.65,1.95, RGB=153,153,153, TRANSPARENCY=0.392157, THICKEN=.TRUE., SURF_ID='steel'/ &OBST ID='FD.stl', XB=0.25,0.3,1.25,2.3,1.9,2.0, RGB=153,153,153, TRANSPARENCY=0.392157, THICKEN=.TRUE., SURF_ID='steel'/ &OBST ID='FD.stl', XB=0.25,0.35,1.2,2.2,0.0,0.1, RGB=153,153,153, TRANSPARENCY=0.392157, THICKEN=.TRUE., SURF_ID='steel'/ &OBST ID='FD.stl', XB=0.3,0.35,1.2,1.25,0.15,0.2, RGB=153,153,153, TRANSPARENCY=0.392157, THICKEN=.TRUE., SURF_ID='steel'/ &OBST ID='FD.stl', XB=0.3,0.35,1.25,2.3,0.15,0.25, RGB=153,153,153, TRANSPARENCY=0.392157, THICKEN=.TRUE., SURF_ID='steel'/ &OBST ID='FD.stl', XB=0.3,0.35,1.25,2.3,1.75,1.85, RGB=153,153,153, TRANSPARENCY=0.392157, THICKEN=.TRUE., SURF_ID='steel'/ &OBST ID='FD.stl', XB=0.3,0.35,1.2,1.25,1.8,2.1, RGB=153,153,153, TRANSPARENCY=0.392157, THICKEN=.TRUE., SURF_ID='steel'/ &OBST ID='FD.stl', XB=0.3,0.35,1.25,2.3,2.0,2.1, RGB=153,153,153, TRANSPARENCY=0.392157, THICKEN=.TRUE., SURF_ID='steel'/ &OBST ID='FD.stl', XB=0.3,1.15,2.2,2.3,0.0,0.05, RGB=153,153,153, TRANSPARENCY=0.392157, THICKEN=.TRUE., SURF_ID='steel'/ &OBST ID='FD.stl', XB=0.35,0.4,1.25,2.3,1.85,1.95, RGB=153,153,153, TRANSPARENCY=0.392157, THICKEN=.TRUE., SURF_ID='steel'/ &OBST ID='FD.stl', XB=0.35,0.4,1.2,1.25,1.9,2.05, RGB=153,153,153, TRANSPARENCY=0.392157, THICKEN=.TRUE., SURF_ID='steel'/ &OBST ID='FD.stl', XB=0.35,0.4,1.2,2.3,2.1,2.15, RGB=153,153,153, TRANSPARENCY=0.392157, THICKEN=.TRUE., SURF_ID='steel'/ &OBST ID='FD.stl', XB=0.35,1.15,1.2,2.2,0.0,0.15, RGB=153,153,153, TRANSPARENCY=0.392157, THICKEN=.TRUE., SURF_ID='steel'/ &OBST ID='FD.stl', XB=0.35,1.15,2.2,2.3,0.1,0.15, RGB=153,153,153, TRANSPARENCY=0.392157, THICKEN=.TRUE., SURF_ID='steel'/ &OBST ID='FD.stl', XB=0.4,0.45,1.25,2.3,1.95,2.05, RGB=153,153,153, TRANSPARENCY=0.392157, THICKEN=.TRUE., SURF_ID='steel'/ &OBST ID='FD.stl', XB=0.4,0.45,1.2,1.25,2.0,2.05, RGB=153,153,153, TRANSPARENCY=0.392157, THICKEN=.TRUE., SURF_ID='steel'/ &OBST ID='FD.stl', XB=0.4,0.45,1.2,2.3,2.15,2.25, RGB=153,153,153, TRANSPARENCY=0.392157, THICKEN=.TRUE., SURF_ID='steel'/ &OBST ID='FD.stl', XB=0.45,0.5,1.2,2.3,2.05,2.3, RGB=153,153,153, TRANSPARENCY=0.392157, THICKEN=.TRUE., SURF_ID='steel'/ &OBST ID='FD.stl', XB=0.5,0.55,1.2,2.3,2.15,2.4, RGB=153,153,153, TRANSPARENCY=0.392157, THICKEN=.TRUE., SURF_ID='steel'/ &OBST ID='FD.stl', XB=0.55,0.6,1.2,2.3,2.2,2.45, RGB=153,153,153, TRANSPARENCY=0.392157, THICKEN=.TRUE., SURF_ID='steel'/ &OBST ID='FD.stl', XB=0.6,0.65,1.2,2.3,2.3,2.5, RGB=153,153,153, TRANSPARENCY=0.392157, THICKEN=.TRUE., SURF_ID='steel'/

&OBST ID='FD.stl', XB=0.65,0.7,1.2,2.3,2.35,2.55, RGB=153,153,153, TRANSPARENCY=0.392157, THICKEN=.TRUE., SURF_ID='steel'/ &OBST ID='FD.stl', XB=0.7,0.75,1.2,2.3,2.4,2.6, RGB=153,153,153, TRANSPARENCY=0.392157, THICKEN=.TRUE., SURF_ID='steel'/ &OBST ID='FD.stl', XB=0.75,0.8,1.2,2.3,2.45,2.65, RGB=153,153,153, TRANSPARENCY=0.392157, THICKEN=.TRUE., SURF_ID='steel'/ &OBST ID='FD.stl', XB=0.8,0.85,1.2,2.3,2.5,2.7, RGB=153,153,153, TRANSPARENCY=0.392157, THICKEN=.TRUE., SURF_ID='steel'/ &OBST ID='FD.stl', XB=0.85,0.9,1.2,2.3,2.55,2.75, RGB=153,153,153, TRANSPARENCY=0.392157, THICKEN=.TRUE., SURF_ID='steel'/ &OBST ID='FD.stl', XB=0.9,0.95,1.2,2.3,2.6,2.75, RGB=153,153,153, TRANSPARENCY=0.392157, THICKEN=.TRUE., SURF_ID='steel'/ &OBST ID='FD.stl', XB=0.95,1.0,1.2,2.3,2.65,2.8, RGB=153,153,153, TRANSPARENCY=0.392157, THICKEN=.TRUE., SURF_ID='steel'/ &OBST ID='FD.stl', XB=1.0,1.05,1.2,2.3,2.65,2.85, RGB=153,153,153, TRANSPARENCY=0.392157, THICKEN=.TRUE., SURF_ID='steel'/ &OBST ID='FD.stl', XB=1.05,1.1,1.2,2.3,2.7,2.85, RGB=153,153,153, TRANSPARENCY=0.392157, THICKEN=.TRUE., SURF_ID='steel'/ &OBST ID='FD.stl', XB=1.1,1.15,1.2,2.3,2.75,2.9, RGB=153,153,153, TRANSPARENCY=0.392157, THICKEN=.TRUE., SURF_ID='steel'/ &OBST ID='FD.stl', XB=0.05,0.1,2.3,3.45,0.6,1.4, RGB=153,153,153, TRANSPARENCY=0.392157, THICKEN=.TRUE., SURF_ID='steel'/ &OBST ID='FD.stl', XB=0.05,0.1,3.45,3.5,0.8,1.25, RGB=153,153,153, TRANSPARENCY=0.392157, THICKEN=.TRUE., SURF_ID='steel'/ &OBST ID='FD.stl', XB=0.1,0.15,2.8,3.45,0.35,0.6, RGB=153,153,153, TRANSPARENCY=0.392157, THICKEN=.TRUE., SURF_ID='steel'/ &OBST ID='FD.stl', XB=0.1,0.15,2.3,2.8,0.4,0.6, RGB=153,153,153, TRANSPARENCY=0.392157, THICKEN=.TRUE., SURF_ID='steel'/ &OBST ID='FD.stl', XB=0.1,0.15,3.45,3.5,0.5,1.5, RGB=153,153,153, TRANSPARENCY=0.392157, THICKEN=.TRUE., SURF_ID='steel'/ &OBST ID='FD.stl', XB=0.1,0.15,2.3,3.45,1.4,1.6, RGB=153,153,153, TRANSPARENCY=0.392157, THICKEN=.TRUE., SURF_ID='steel'/ &OBST ID='FD.stl', XB=0.15,0.2,2.8,3.45,0.25,0.35, RGB=153,153,153, TRANSPARENCY=0.392157, THICKEN=.TRUE., SURF_ID='steel'/ &OBST ID='FD.stl', XB=0.15,0.2,2.3,2.8,0.25,0.4, RGB=153,153,153, TRANSPARENCY=0.392157, THICKEN=.TRUE., SURF_ID='steel'/ &OBST ID='FD.stl', XB=0.15,0.2,3.45,3.5,0.35,1.7, RGB=153,153,153, TRANSPARENCY=0.392157, THICKEN=.TRUE., SURF_ID='steel'/ &OBST ID='FD.stl', XB=0.15,0.2,2.3,3.35,0.6,1.4, RGB=153,153,153, TRANSPARENCY=0.392157, THICKEN=.TRUE., SURF_ID='steel'/ &OBST ID='FD.stl', XB=0.15,0.2,3.35,3.4,0.8,1.25, RGB=153,153,153, TRANSPARENCY=0.392157, THICKEN=.TRUE., SURF_ID='steel'/ &OBST ID='FD.stl', XB=0.15,0.2,2.3,3.45,1.6,1.75, RGB=153,153,153, TRANSPARENCY=0.392157, THICKEN=.TRUE., SURF_ID='steel'/ &OBST ID='FD.stl', XB=0.2,0.25,2.3,3.45,0.1,0.25, RGB=153,153,153, TRANSPARENCY=0.392157, THICKEN=.TRUE., SURF_ID='steel'/ &OBST ID='FD.stl', XB=0.2,0.25,3.45,3.5,0.2,1.8, RGB=153,153,153, TRANSPARENCY=0.392157, THICKEN=.TRUE., SURF_ID='steel'/ &OBST ID='FD.stl', XB=0.2,0.25,2.3,3.35,0.4,0.6, RGB=153,153,153, TRANSPARENCY=0.392157, THICKEN=.TRUE., SURF_ID='steel'/ &OBST ID='FD.stl', XB=0.2,0.25,3.35,3.4,0.5,1.45, RGB=153,153,153, TRANSPARENCY=0.392157, THICKEN=.TRUE., SURF_ID='steel'/

TRANSPARENCY=0.392157, THICKEN=.TRUE., SURF_ID='steel'/ &OBST ID='FD.stl', XB=0.2,0.25,2.3,3.45,1.75,1.9, RGB=153,153,153, TRANSPARENCY=0.392157, THICKEN=.TRUE., SURF_ID='steel'/ &OBST ID='FD.stl', XB=0.25,0.3,2.3,2.95,0.0,0.1, RGB=153,153,153, TRANSPARENCY=0.392157, THICKEN=.TRUE., SURF_ID='steel'/ &OBST ID='FD.stl', XB=0.25,0.3,2.95,3.45,0.05,0.1, RGB=153,153,153, TRANSPARENCY=0.392157, THICKEN=.TRUE., SURF_ID='steel'/ &OBST ID='FD.stl', XB=0.25,0.3,3.45,3.5,0.1,1.9, RGB=153,153,153, TRANSPARENCY=0.392157, THICKEN=.TRUE., SURF_ID='steel'/ &OBST ID='FD.stl', XB=0.25,0.3,2.3,3.35,0.25,0.4, RGB=153,153,153, TRANSPARENCY=0.392157, THICKEN=.TRUE., SURF_ID='steel'/ &OBST ID='FD.stl', XB=0.25,0.3,3.35,3.4,0.35,1.65, RGB=153,153,153, TRANSPARENCY=0.392157, THICKEN=.TRUE., SURF_ID='steel'/ &OBST ID='FD.stl', XB=0.25,0.3,2.3,3.35,1.6,1.75, RGB=153,153,153, TRANSPARENCY=0.392157, THICKEN=.TRUE., SURF_ID='steel'/ &OBST ID='FD.stl', XB=0.25,0.3,2.3,3.45,1.9,2.0, RGB=153,153,153, TRANSPARENCY=0.392157, THICKEN=.TRUE., SURF_ID='steel'/ &OBST ID='FD.stl', XB=0.3,0.35,3.45,3.5,0.05,2.05, RGB=153,153,153, TRANSPARENCY=0.392157, THICKEN=.TRUE., SURF_ID='steel'/ &OBST ID='FD.stl', XB=0.3,0.35,2.3,3.35,0.15,0.25, RGB=153,153,153, TRANSPARENCY=0.392157, THICKEN=.TRUE., SURF_ID='steel'/ &OBST ID='FD.stl', XB=0.3,0.35,3.35,3.4,0.2,1.8, RGB=153,153,153, TRANSPARENCY=0.392157, THICKEN=.TRUE., SURF_ID='steel'/ &OBST ID='FD.stl', XB=0.3,0.35,2.3,3.35,1.75,1.85, RGB=153,153,153, TRANSPARENCY=0.392157, THICKEN=.TRUE., SURF_ID='steel'/ &OBST ID='FD.stl', XB=0.3,0.35,2.3,3.45,2.0,2.1, RGB=153,153,153, TRANSPARENCY=0.392157, THICKEN=.TRUE., SURF_ID='steel'/ &OBST ID='FD.stl', XB=0.3,1.15,2.3,3.45,0.0,0.05, RGB=153,153,153, TRANSPARENCY=0.392157, THICKEN=.TRUE., SURF_ID='steel'/ &OBST ID='FD.stl', XB=0.35,0.4,3.45,3.5,0.05,2.1, RGB=153,153,153, TRANSPARENCY=0.392157, THICKEN=.TRUE., SURF_ID='steel'/ &OBST ID='FD.stl', XB=0.35,0.4,3.35,3.4,0.15,1.9, RGB=153,153,153, TRANSPARENCY=0.392157, THICKEN=.TRUE., SURF_ID='steel'/ &OBST ID='FD.stl', XB=0.35,0.4,2.3,3.35,1.85,1.95, RGB=153,153,153, TRANSPARENCY=0.392157, THICKEN=.TRUE., SURF_ID='steel'/ &OBST ID='FD.stl', XB=0.35,0.4,2.3,3.45,2.1,2.15, RGB=153,153,153, TRANSPARENCY=0.392157, THICKEN=.TRUE., SURF_ID='steel'/ &OBST ID='FD.stl', XB=0.35,1.15,2.3,3.35,0.1,0.15, RGB=153,153,153, TRANSPARENCY=0.392157, THICKEN=.TRUE., SURF_ID='steel'/ &OBST ID='FD.stl', XB=0.4,0.45,3.45,3.5,0.05,2.2, RGB=153,153,153, TRANSPARENCY=0.392157, THICKEN=.TRUE., SURF_ID='steel'/ &OBST ID='FD.stl', XB=0.4,0.45,3.35,3.4,0.15,2.0, RGB=153,153,153, TRANSPARENCY=0.392157, THICKEN=.TRUE., SURF_ID='steel'/ &OBST ID='FD.stl', XB=0.4,0.45,2.3,3.35,1.95,2.05, RGB=153,153,153, TRANSPARENCY=0.392157, THICKEN=.TRUE., SURF_ID='steel'/ &OBST ID='FD.stl', XB=0.4,0.45,2.3,3.45,2.15,2.25, RGB=153,153,153, TRANSPARENCY=0.392157, THICKEN=.TRUE., SURF_ID='steel'/ &OBST ID='FD.stl', XB=0.45,0.5,3.45,3.5,0.05,2.25, RGB=153,153,153, TRANSPARENCY=0.392157, THICKEN=.TRUE., SURF_ID='steel'/ &OBST ID='FD.stl', XB=0.45,0.5,3.35,3.4,0.15,2.1, RGB=153,153,153, TRANSPARENCY=0.392157, THICKEN=.TRUE., SURF_ID='steel'/

&OBST ID='FD.stl', XB=0.2,0.25,2.3,3.35,1.4,1.6, RGB=153,153,153,

&OBST ID='FD.stl', XB=0.45,0.5,2.3,3.35,2.05,2.3, RGB=153,153,153, TRANSPARENCY=0.392157, THICKEN=.TRUE., SURF_ID='steel'/ &OBST ID='FD.stl', XB=0.45,0.5,3.35,3.45,2.15,2.3, RGB=153,153,153, TRANSPARENCY=0.392157, THICKEN=.TRUE., SURF_ID='steel'/ &OBST ID='FD.stl', XB=0.5,0.55,3.45,3.5,0.05,2.3, RGB=153,153,153, TRANSPARENCY=0.392157, THICKEN=.TRUE., SURF_ID='steel'/ &OBST ID='FD.stl', XB=0.5,0.55,3.35,3.4,0.15,2.15, RGB=153,153,153, TRANSPARENCY=0.392157, THICKEN=.TRUE., SURF_ID='steel'/ &OBST ID='FD.stl', XB=0.5,0.55,2.3,3.35,2.15,2.4, RGB=153,153,153, TRANSPARENCY=0.392157, THICKEN=.TRUE., SURF_ID='steel'/ &OBST ID='FD.stl', XB=0.5,0.55,3.35,3.45,2.25,2.4, RGB=153,153,153, TRANSPARENCY=0.392157, THICKEN=.TRUE., SURF_ID='steel'/ &OBST ID='FD.stl', XB=0.55,0.6,3.45,3.5,0.05,2.4, RGB=153,153,153, TRANSPARENCY=0.392157, THICKEN=.TRUE., SURF_ID='steel'/ &OBST ID='FD.stl', XB=0.55,0.6,3.35,3.4,0.15,2.2, RGB=153,153,153, TRANSPARENCY=0.392157, THICKEN=.TRUE., SURF_ID='steel'/ &OBST ID='FD.stl', XB=0.55,0.6,2.3,3.35,2.2,2.45, RGB=153,153,153, TRANSPARENCY=0.392157, THICKEN=.TRUE., SURF_ID='steel'/ &OBST ID='FD.stl', XB=0.55,0.6,3.35,3.45,2.3,2.45, RGB=153,153,153, TRANSPARENCY=0.392157, THICKEN=.TRUE., SURF_ID='steel'/ &OBST ID='FD.stl', XB=0.6,0.65,3.45,3.5,0.05,2.45, RGB=153,153,153, TRANSPARENCY=0.392157, THICKEN=.TRUE., SURF_ID='steel'/ &OBST ID='FD.stl', XB=0.6,0.65,3.35,3.4,0.15,2.3, RGB=153,153,153, TRANSPARENCY=0.392157, THICKEN=.TRUE., SURF_ID='steel'/ &OBST ID='FD.stl', XB=0.6,0.65,2.3,3.35,2.3,2.5, RGB=153,153,153, TRANSPARENCY=0.392157, THICKEN=.TRUE., SURF_ID='steel'/ &OBST ID='FD.stl', XB=0.6,0.65,3.35,3.45,2.4,2.5, RGB=153,153,153, TRANSPARENCY=0.392157, THICKEN=.TRUE., SURF_ID='steel'/ &OBST ID='FD.stl', XB=0.65,0.7,3.45,3.5,0.05,2.5, RGB=153,153,153, TRANSPARENCY=0.392157, THICKEN=.TRUE., SURF_ID='steel'/ &OBST ID='FD.stl', XB=0.65,0.7,3.35,3.4,0.15,2.35, RGB=153,153,153, TRANSPARENCY=0.392157, THICKEN=.TRUE., SURF_ID='steel'/ &OBST ID='FD.stl', XB=0.65,0.7,2.3,3.35,2.35,2.55, RGB=153,153,153, TRANSPARENCY=0.392157, THICKEN=.TRUE., SURF_ID='steel'/ &OBST ID='FD.stl', XB=0.65,0.7,3.35,3.45,2.45,2.55, RGB=153,153,153, TRANSPARENCY=0.392157, THICKEN=.TRUE., SURF_ID='steel'/ &OBST ID='FD.stl', XB=0.7,0.75,3.45,3.5,0.05,2.55, RGB=153,153,153, TRANSPARENCY=0.392157, THICKEN=.TRUE., SURF_ID='steel'/ &OBST ID='FD.stl', XB=0.7,0.75,3.35,3.4,0.15,2.4, RGB=153,153,153, TRANSPARENCY=0.392157, THICKEN=.TRUE., SURF_ID='steel'/ &OBST ID='FD.stl', XB=0.7,0.75,2.3,3.35,2.4,2.6, RGB=153,153,153, TRANSPARENCY=0.392157, THICKEN=.TRUE., SURF_ID='steel'/ &OBST ID='FD.stl', XB=0.7,0.75,3.35,3.45,2.5,2.6, RGB=153,153,153, TRANSPARENCY=0.392157, THICKEN=.TRUE., SURF_ID='steel'/ &OBST ID='FD.stl', XB=0.75,0.8,3.45,3.5,0.05,2.6, RGB=153,153,153, TRANSPARENCY=0.392157, THICKEN=.TRUE., SURF_ID='steel'/ &OBST ID='FD.stl', XB=0.75,0.8,3.35,3.4,0.15,2.45, RGB=153,153,153, TRANSPARENCY=0.392157, THICKEN=.TRUE., SURF_ID='steel'/ &OBST ID='FD.stl', XB=0.75,0.8,2.3,3.35,2.45,2.65, RGB=153,153,153, TRANSPARENCY=0.392157, THICKEN=.TRUE., SURF_ID='steel'/ &OBST ID='FD.stl', XB=0.75,0.8,3.35,3.45,2.55,2.65, RGB=153,153,153, TRANSPARENCY=0.392157, THICKEN=.TRUE., SURF_ID='steel'/

&OBST ID='FD.stl', XB=0.8,0.85,3.45,3.5,0.05,2.65, RGB=153,153,153, TRANSPARENCY=0.392157, THICKEN=.TRUE., SURF_ID='steel'/ &OBST ID='FD.stl', XB=0.8,0.85,3.35,3.4,0.15,2.5, RGB=153,153,153, TRANSPARENCY=0.392157, THICKEN=.TRUE., SURF_ID='steel'/ &OBST ID='FD.stl', XB=0.8,0.85,2.3,3.35,2.5,2.7, RGB=153,153,153, TRANSPARENCY=0.392157, THICKEN=.TRUE., SURF_ID='steel'/ &OBST ID='FD.stl', XB=0.8,0.85,3.35,3.45,2.6,2.7, RGB=153,153,153, TRANSPARENCY=0.392157, THICKEN=.TRUE., SURF_ID='steel'/ &OBST ID='FD.stl', XB=0.85,0.9,3.35,3.4,0.15,2.55, RGB=153,153,153, TRANSPARENCY=0.392157, THICKEN=.TRUE., SURF_ID='steel'/ &OBST ID='FD.stl', XB=0.85,0.9,2.3,3.35,2.55,2.75, RGB=153,153,153, TRANSPARENCY=0.392157, THICKEN=.TRUE., SURF_ID='steel'/ &OBST ID='FD.stl', XB=0.85,0.9,3.35,3.45,2.65,2.75, RGB=153,153,153, TRANSPARENCY=0.392157, THICKEN=.TRUE., SURF_ID='steel'/ &OBST ID='FD.stl', XB=0.85,0.95,3.45,3.5,0.05,2.7, RGB=153,153,153, TRANSPARENCY=0.392157, THICKEN=.TRUE., SURF_ID='steel'/ &OBST ID='FD.stl', XB=0.9,0.95,3.35,3.4,0.15,2.6, RGB=153,153,153, TRANSPARENCY=0.392157, THICKEN=.TRUE., SURF_ID='steel'/ &OBST ID='FD.stl', XB=0.9,0.95,2.3,3.35,2.6,2.75, RGB=153,153,153, TRANSPARENCY=0.392157, THICKEN=.TRUE., SURF_ID='steel'/ &OBST ID='FD.stl', XB=0.9,0.95,3.35,3.45,2.7,2.75, RGB=153,153,153, TRANSPARENCY=0.392157, THICKEN=.TRUE., SURF_ID='steel'/ &OBST ID='FD.stl', XB=0.95,1.0,3.45,3.5,0.05,2.75, RGB=153,153,153, TRANSPARENCY=0.392157, THICKEN=.TRUE., SURF_ID='steel'/ &OBST ID='FD.stl', XB=0.95,1.0,2.3,3.35,2.65,2.8, RGB=153,153,153, TRANSPARENCY=0.392157, THICKEN=.TRUE., SURF_ID='steel'/ &OBST ID='FD.stl', XB=0.95,1.0,3.35,3.45,2.75,2.8, RGB=153,153,153, TRANSPARENCY=0.392157, THICKEN=.TRUE., SURF_ID='steel'/ &OBST ID='FD.stl', XB=0.95,1.05,3.35,3.4,0.15,2.65, RGB=153,153,153, TRANSPARENCY=0.392157, THICKEN=.TRUE., SURF_ID='steel'/ &OBST ID='FD.stl', XB=1.0,1.05,2.3,3.35,2.65,2.85, RGB=153,153,153, TRANSPARENCY=0.392157, THICKEN=.TRUE., SURF_ID='steel'/ &OBST ID='FD.stl', XB=1.0,1.05,3.35,3.45,2.75,2.85, RGB=153,153,153, TRANSPARENCY=0.392157, THICKEN=.TRUE., SURF_ID='steel'/ &OBST ID='FD.stl', XB=1.0,1.1,3.45,3.5,0.05,2.8, RGB=153,153,153, TRANSPARENCY=0.392157, THICKEN=.TRUE., SURF_ID='steel'/ &OBST ID='FD.stl', XB=1.05,1.1,3.35,3.4,0.15,2.7, RGB=153,153,153, TRANSPARENCY=0.392157, THICKEN=.TRUE., SURF_ID='steel'/ &OBST ID='FD.stl', XB=1.05,1.1,2.3,3.35,2.7,2.85, RGB=153,153,153, TRANSPARENCY=0.392157, THICKEN=.TRUE., SURF_ID='steel'/ &OBST ID='FD.stl', XB=1.05,1.1,3.35,3.45,2.8,2.85, RGB=153,153,153, TRANSPARENCY=0.392157, THICKEN=.TRUE., SURF_ID='steel'/ &OBST ID='FD.stl', XB=1.1,1.15,3.45,3.5,0.05,2.85, RGB=153,153,153, TRANSPARENCY=0.392157, THICKEN=.TRUE., SURF_ID='steel'/ &OBST ID='FD.stl', XB=1.1,1.15,3.35,3.4,0.15,2.75, RGB=153,153,153, TRANSPARENCY=0.392157, THICKEN=.TRUE., SURF_ID='steel'/ &OBST ID='FD.stl', XB=1.1,1.15,2.3,3.35,2.75,2.9, RGB=153,153,153, TRANSPARENCY=0.392157, THICKEN=.TRUE., SURF_ID='steel'/ &OBST ID='FD.stl', XB=1.1,1.15,3.35,3.45,2.85,2.9, RGB=153,153,153, TRANSPARENCY=0.392157, THICKEN=.TRUE., SURF_ID='steel'/ &OBST ID='FD.stl', XB=1.15,1.2,0.1,0.15,0.0,2.8, RGB=153,153,153, TRANSPARENCY=0.392157, THICKEN=.TRUE., SURF_ID='steel'/

```
&OBST ID='FD.stl', XB=1.15,1.2,0.15,1.2,2.75,2.95, RGB=153,153,153,
TRANSPARENCY=0.392157, THICKEN=.TRUE., SURF_ID='steel'/
&OBST ID='FD.stl', XB=1.15,1.2,0.05,0.15,2.85,2.95, RGB=153,153,153,
TRANSPARENCY=0.392157, THICKEN=.TRUE., SURF_ID='steel'/
&OBST ID='FD.stl', XB=1.15,1.25,1.290634E-15,0.05,0.0,2.95, RGB=153,153,153,
TRANSPARENCY=0.392157, THICKEN=.TRUE., SURF_ID='steel'/
&OBST ID='FD.stl', XB=1.15,3.3,0.05,0.1,0.0,0.1, RGB=153,153,153,
TRANSPARENCY=0.392157, THICKEN=.TRUE., SURF_ID='steel'/
&OBST ID='FD.stl', XB=1.15,3.3,0.15,1.2,0.0,0.15, RGB=153,153,153,
TRANSPARENCY=0.392157, THICKEN=.TRUE., SURF_ID='steel'/
&OBST ID='FD.stl', XB=1.2,1.25,0.1,0.15,0.0,2.85, RGB=153,153,153,
TRANSPARENCY=0.392157, THICKEN=.TRUE., SURF_ID='steel'/
&OBST ID='FD.stl', XB=1.2,1.25,0.15,1.2,2.8,2.95, RGB=153,153,153,
TRANSPARENCY=0.392157, THICKEN=.TRUE., SURF_ID='steel'/
&OBST ID='FD.stl', XB=1.2,1.25,0.05,0.15,2.9,2.95, RGB=153,153,153,
TRANSPARENCY=0.392157, THICKEN=.TRUE., SURF_ID='steel'/
&OBST ID='FD.stl', XB=1.25,1.35,1.290634E-15,0.05,0.0,3.0, RGB=153,153,153,
TRANSPARENCY=0.392157, THICKEN=.TRUE., SURF_ID='steel'/
&OBST ID='FD.stl', XB=1.25,1.35,0.15,1.2,2.85,3.0, RGB=153,153,153,
TRANSPARENCY=0.392157, THICKEN=.TRUE., SURF_ID='steel'/
&OBST ID='FD.stl', XB=1.25,1.35,0.05,0.15,2.95,3.0, RGB=153,153,153,
TRANSPARENCY=0.392157, THICKEN=.TRUE., SURF_ID='steel'/
&OBST ID='FD.stl', XB=1.25,1.4,0.1,0.15,0.0,2.9, RGB=153,153,153,
TRANSPARENCY=0.392157, THICKEN=.TRUE., SURF_ID='steel'/
&OBST ID='FD.stl', XB=1.35,1.4,0.15,1.2,2.85,3.05, RGB=153,153,153,
TRANSPARENCY=0.392157, THICKEN=.TRUE., SURF_ID='steel'/
&OBST ID='FD.stl', XB=1.35,1.4,0.1,0.15,2.95,3.05, RGB=153,153,153,
TRANSPARENCY=0.392157, THICKEN=.TRUE., SURF_ID='steel'/
&OBST ID='FD.stl', XB=1.35,1.5,1.290634E-15,0.05,0.0,3.05, RGB=153,153,153,
TRANSPARENCY=0.392157, THICKEN=.TRUE., SURF_ID='steel'/
&OBST ID='FD.stl', XB=1.35,1.5,0.05,0.1,2.95,3.05, RGB=153,153,153,
TRANSPARENCY=0.392157, THICKEN=.TRUE., SURF_ID='steel'/
&OBST ID='FD.stl', XB=1.4,1.5,0.1,0.15,0.0,3.05, RGB=153,153,153,
TRANSPARENCY=0.392157, THICKEN=.TRUE., SURF_ID='steel'/
&OBST ID='FD.stl', XB=1.4,1.5,0.15,1.2,2.9,3.05, RGB=153,153,153,
TRANSPARENCY=0.392157, THICKEN=.TRUE., SURF_ID='steel'/
&OBST ID='FD.stl', XB=1.5,1.6,1.290634E-15,0.05,0.0,3.1, RGB=153,153,153,
TRANSPARENCY=0.392157, THICKEN=.TRUE., SURF_ID='steel'/
&OBST ID='FD.stl', XB=1.5,1.6,0.15,1.2,2.95,3.1, RGB=153,153,153,
TRANSPARENCY=0.392157, THICKEN=.TRUE., SURF_ID='steel'/
&OBST ID='FD.stl', XB=1.5,1.6,0.05,0.15,3.05,3.1, RGB=153,153,153,
TRANSPARENCY=0.392157, THICKEN=.TRUE., SURF_ID='steel'/
&OBST ID='FD.stl', XB=1.5,1.65,0.1,0.15,0.0,3.0, RGB=153,153,153,
TRANSPARENCY=0.392157, THICKEN=.TRUE., SURF_ID='steel'/
&OBST ID='FD.stl', XB=1.6,1.65,0.15,1.2,2.95,3.15, RGB=153,153,153,
TRANSPARENCY=0.392157, THICKEN=.TRUE., SURF_ID='steel'/
&OBST ID='FD.stl', XB=1.6,1.65,0.05,0.15,3.05,3.15, RGB=153,153,153,
TRANSPARENCY=0.392157, THICKEN=.TRUE., SURF_ID='steel'/
&OBST ID='FD.stl', XB=1.6,1.75,1.290634E-15,0.05,0.0,3.15, RGB=153,153,153,
TRANSPARENCY=0.392157, THICKEN=.TRUE., SURF_ID='steel'/
&OBST ID='FD.stl', XB=1.65,1.85,0.1,0.15,0.0,3.05, RGB=153,153,153,
TRANSPARENCY=0.392157, THICKEN=.TRUE., SURF_ID='steel'/
```

```
&OBST ID='FD.stl', XB=1.65,1.85,0.15,1.2,3.0,3.15, RGB=153,153,153,
TRANSPARENCY=0.392157, THICKEN=.TRUE., SURF_ID='steel'/
&OBST ID='FD.stl', XB=1.65,1.85,0.05,0.15,3.1,3.15, RGB=153,153,153,
TRANSPARENCY=0.392157, THICKEN=.TRUE., SURF_ID='steel'/
&OBST ID='FD.stl', XB=1.75,1.85,-0.05,1.290634E-15,0.05,3.1, RGB=153,153,153,
TRANSPARENCY=0.392157, THICKEN=.TRUE., SURF_ID='steel'/
&OBST ID='FD.stl', XB=1.75,1.85,1.290634E-15,0.05,3.1,3.15, RGB=153,153,153,
TRANSPARENCY=0.392157, THICKEN=.TRUE., SURF_ID='steel'/
&OBST ID='FD.stl', XB=1.75,3.3,1.290634E-15,0.05,0.0,0.05, RGB=153,153,153,
TRANSPARENCY=0.392157, THICKEN=.TRUE., SURF_ID='steel'/
&OBST ID='FD.stl', XB=1.85,2.05,0.1,0.15,0.0,3.1, RGB=153,153,153,
TRANSPARENCY=0.392157, THICKEN=.TRUE., SURF_ID='steel'/
&OBST ID='FD.stl', XB=1.85,2.65,-0.05,1.290634E-15,0.05,3.15, RGB=153,153,153,
TRANSPARENCY=0.392157, THICKEN=.TRUE., SURF_ID='steel'/
&OBST ID='FD.stl', XB=1.85,2.65,0.15,1.2,3.05,3.2, RGB=153,153,153,
TRANSPARENCY=0.392157, THICKEN=.TRUE., SURF_ID='steel'/
&OBST ID='FD.stl', XB=1.85,2.65,1.290634E-15,0.15,3.15,3.2, RGB=153,153,153,
TRANSPARENCY=0.392157, THICKEN=.TRUE., SURF_ID='steel'/
&OBST ID='FD.stl', XB=2.05,2.1,0.1,0.15,0.0,2.85, RGB=153,153,153,
TRANSPARENCY=0.392157, THICKEN=.TRUE., SURF_ID='steel'/
&OBST ID='FD.stl', XB=2.05,2.1,0.05,0.1,2.85,3.05, RGB=153,153,153,
TRANSPARENCY=0.392157, THICKEN=.TRUE., SURF_ID='steel'/
&OBST ID='FD.stl', XB=2.05,2.65,0.1,0.15,3.05,3.1, RGB=153,153,153,
TRANSPARENCY=0.392157, THICKEN=.TRUE., SURF_ID='steel'/
&OBST ID='FD.stl', XB=2.1,2.15,0.1,0.15,0.0,0.25, RGB=153,153,153,
TRANSPARENCY=0.392157, THICKEN=.TRUE., SURF_ID='steel'/
&OBST ID='FD.stl', XB=2.1,2.15,0.05,0.1,0.25,0.65, RGB=153,153,153,
TRANSPARENCY=0.392157, THICKEN=.TRUE., SURF_ID='steel'/
&OBST ID='FD.stl', XB=2.1,2.15,0.1,0.15,0.65,0.9, RGB=153,153,153,
TRANSPARENCY=0.392157, THICKEN=.TRUE., SURF_ID='steel'/
&OBST ID='FD.stl', XB=2.1,2.15,0.05,0.1,0.9,1.1, RGB=153,153,153,
TRANSPARENCY=0.392157, THICKEN=.TRUE., SURF_ID='steel'/
&OBST ID='FD.stl', XB=2.1,2.15,0.1,0.15,1.1,1.5, RGB=153,153,153,
TRANSPARENCY=0.392157, THICKEN=.TRUE., SURF_ID='steel'/
&OBST ID='FD.stl', XB=2.1,2.15,0.05,0.1,1.5,1.75, RGB=153,153,153,
TRANSPARENCY=0.392157, THICKEN=.TRUE., SURF_ID='steel'/
&OBST ID='FD.stl', XB=2.1,2.15,0.1,0.15,1.75,1.9, RGB=153,153,153,
TRANSPARENCY=0.392157, THICKEN=.TRUE., SURF_ID='steel'/
&OBST ID='FD.stl', XB=2.1,2.15,0.05,0.1,1.9,2.05, RGB=153,153,153,
TRANSPARENCY=0.392157, THICKEN=.TRUE., SURF_ID='steel'/
&OBST ID='FD.stl', XB=2.1,2.15,0.1,0.15,2.05,2.25, RGB=153,153,153,
TRANSPARENCY=0.392157, THICKEN=.TRUE., SURF_ID='steel'/
&OBST ID='FD.stl', XB=2.1,2.15,0.05,0.1,2.25,2.4, RGB=153,153,153,
TRANSPARENCY=0.392157, THICKEN=.TRUE., SURF_ID='steel'/
&OBST ID='FD.stl', XB=2.1,2.15,0.05,0.1,2.85,2.95, RGB=153,153,153,
TRANSPARENCY=0.392157, THICKEN=.TRUE., SURF_ID='steel'/
&OBST ID='FD.stl', XB=2.1,2.15,0.1,0.15,2.95,3.0, RGB=153,153,153,
TRANSPARENCY=0.392157, THICKEN=.TRUE., SURF_ID='steel'/
&OBST ID='FD.stl', XB=2.1,2.15,0.05,0.1,3.0,3.05, RGB=153,153,153,
TRANSPARENCY=0.392157, THICKEN=.TRUE., SURF_ID='steel'/
&OBST ID='FD.stl', XB=2.1,2.2,0.1,0.15,2.4,2.55, RGB=153,153,153,
TRANSPARENCY=0.392157, THICKEN=.TRUE., SURF_ID='steel'/
```

```
&OBST ID='FD.stl', XB=2.1,2.2,0.05,0.1,2.55,2.8, RGB=153,153,153,
TRANSPARENCY=0.392157, THICKEN=.TRUE., SURF_ID='steel'/
&OBST ID='FD.stl', XB=2.1,2.2,0.1,0.15,2.8,2.85, RGB=153,153,153,
TRANSPARENCY=0.392157, THICKEN=.TRUE., SURF_ID='steel'/
&OBST ID='FD.stl', XB=2.15,2.2,0.05,0.1,0.15,2.4, RGB=153,153,153,
TRANSPARENCY=0.392157, THICKEN=.TRUE., SURF_ID='steel'/
&OBST ID='FD.stl', XB=2.15,2.2,0.05,0.1,2.85,3.05, RGB=153,153,153,
TRANSPARENCY=0.392157, THICKEN=.TRUE., SURF_ID='steel'/
&OBST ID='FD.stl', XB=2.15,3.3,0.1,0.15,0.0,0.15, RGB=153,153,153,
TRANSPARENCY=0.392157, THICKEN=.TRUE., SURF_ID='steel'/
&OBST ID='FD.stl', XB=2.2,2.65,0.05,0.1,0.15,3.05, RGB=153,153,153,
TRANSPARENCY=0.392157, THICKEN=.TRUE., SURF_ID='steel'/
&OBST ID='FD.stl', XB=2.65,2.9,-0.05,1.290634E-15,0.05,3.1, RGB=153,153,153,
TRANSPARENCY=0.392157, THICKEN=.TRUE., SURF_ID='steel'/
&OBST ID='FD.stl', XB=2.65,2.9,0.05,0.1,0.15,3.0, RGB=153,153,153,
TRANSPARENCY=0.392157, THICKEN=.TRUE., SURF_ID='steel'/
&OBST ID='FD.stl', XB=2.65,2.9,0.1,1.2,3.0,3.15, RGB=153,153,153,
TRANSPARENCY=0.392157, THICKEN=.TRUE., SURF_ID='steel'/
&OBST ID='FD.stl', XB=2.65,2.9,1.290634E-15,0.1,3.1,3.15, RGB=153,153,153,
TRANSPARENCY=0.392157, THICKEN=.TRUE., SURF_ID='steel'/
&OBST ID='FD.stl', XB=2.9,3.0,0.05,0.1,0.15,2.95, RGB=153,153,153,
TRANSPARENCY=0.392157, THICKEN=.TRUE., SURF_ID='steel'/
&OBST ID='FD.stl', XB=2.9,3.0,0.1,1.2,2.95,3.1, RGB=153,153,153,
TRANSPARENCY=0.392157, THICKEN=.TRUE., SURF_ID='steel'/
&OBST ID='FD.stl', XB=2.9,3.0,1.290634E-15,0.1,3.05,3.1, RGB=153,153,153,
TRANSPARENCY=0.392157, THICKEN=.TRUE., SURF_ID='steel'/
&OBST ID='FD.stl', XB=2.9,3.05,-0.05,1.290634E-15,0.05,3.05, RGB=153,153,153,
TRANSPARENCY=0.392157, THICKEN=.TRUE., SURF_ID='steel'/
&OBST ID='FD.stl', XB=3.0,3.05,0.1,1.2,2.9,3.1, RGB=153,153,153,
TRANSPARENCY=0.392157, THICKEN=.TRUE., SURF_ID='steel'/
&OBST ID='FD.stl', XB=3.0,3.05,1.290634E-15,0.1,3.0,3.1, RGB=153,153,153,
TRANSPARENCY=0.392157, THICKEN=.TRUE., SURF_ID='steel'/
&OBST ID='FD.stl', XB=3.0,3.15,0.05,0.1,0.15,2.9, RGB=153,153,153,
TRANSPARENCY=0.392157, THICKEN=.TRUE., SURF_ID='steel'/
&OBST ID='FD.stl', XB=3.05,3.15,-0.05,1.290634E-15,0.05,3.0, RGB=153,153,153,
TRANSPARENCY=0.392157, THICKEN=.TRUE., SURF_ID='steel'/
&OBST ID='FD.stl', XB=3.05,3.15,0.1,1.2,2.9,3.05, RGB=153,153,153,
TRANSPARENCY=0.392157, THICKEN=.TRUE., SURF_ID='steel'/
&OBST ID='FD.stl', XB=3.05,3.15,1.290634E-15,0.1,3.0,3.05, RGB=153,153,153,
TRANSPARENCY=0.392157, THICKEN=.TRUE., SURF_ID='steel'/
&OBST ID='FD.stl', XB=3.15,3.25,-0.05,1.290634E-15,0.05,2.95, RGB=153,153,153,
TRANSPARENCY=0.392157, THICKEN=.TRUE., SURF_ID='steel'/
&OBST ID='FD.stl', XB=3.15,3.25,0.05,0.1,0.15,2.85, RGB=153,153,153,
TRANSPARENCY=0.392157, THICKEN=.TRUE., SURF_ID='steel'/
&OBST ID='FD.stl', XB=3.15,3.25,0.1,1.2,2.85,3.0, RGB=153,153,153,
TRANSPARENCY=0.392157, THICKEN=.TRUE., SURF_ID='steel'/
&OBST ID='FD.stl', XB=3.15,3.25,1.290634E-15,0.1,2.95,3.0, RGB=153,153,153,
TRANSPARENCY=0.392157, THICKEN=.TRUE., SURF_ID='steel'/
&OBST ID='FD.stl', XB=3.25,3.3,-0.05,1.290634E-15,0.05,2.9, RGB=153,153,153,
TRANSPARENCY=0.392157, THICKEN=.TRUE., SURF_ID='steel'/
&OBST ID='FD.stl', XB=3.25,3.3,0.05,0.1,0.15,2.8, RGB=153,153,153,
TRANSPARENCY=0.392157, THICKEN=.TRUE., SURF_ID='steel'/
```

&OBST ID='FD.stl', XB=3.25,3.3,0.1,1.2,2.8,2.95, RGB=153,153,153, TRANSPARENCY=0.392157, THICKEN=.TRUE., SURF_ID='steel'/ &OBST ID='FD.stl', XB=3.25,3.3,1.290634E-15,0.1,2.85,2.95, RGB=153,153,153, TRANSPARENCY=0.392157, THICKEN=.TRUE., SURF_ID='steel'/ &OBST ID='FD.stl', XB=1.15,3.3,2.2,2.3,0.0,0.05, RGB=153,153,153, TRANSPARENCY=0.392157, THICKEN=.TRUE., SURF_ID='steel'/ &OBST ID='FD.stl', XB=1.15,3.3,1.2,2.2,0.0,0.15, RGB=153,153,153, TRANSPARENCY=0.392157, THICKEN=.TRUE., SURF_ID='steel'/ &OBST ID='FD.stl', XB=1.15,3.3,2.2,2.3,0.1,0.15, RGB=153,153,153, TRANSPARENCY=0.392157, THICKEN=.TRUE., SURF_ID='steel'/ &OBST ID='FD.stl', XB=1.15,1.2,1.2,2.3,2.75,2.95, RGB=153,153,153, TRANSPARENCY=0.392157, THICKEN=.TRUE., SURF_ID='steel'/ &OBST ID='FD.stl', XB=1.2,1.25,1.2,2.3,2.8,2.95, RGB=153,153,153, TRANSPARENCY=0.392157, THICKEN=.TRUE., SURF_ID='steel'/ &OBST ID='FD.stl', XB=1.25,1.35,1.2,2.3,2.85,3.0, RGB=153,153,153, TRANSPARENCY=0.392157, THICKEN=.TRUE., SURF_ID='steel'/ &OBST ID='FD.stl', XB=1.35,1.4,1.2,2.3,2.85,3.05, RGB=153,153,153, TRANSPARENCY=0.392157, THICKEN=.TRUE., SURF_ID='steel'/ &OBST ID='FD.stl', XB=1.4,1.5,1.2,2.3,2.9,3.05, RGB=153,153,153, TRANSPARENCY=0.392157, THICKEN=.TRUE., SURF_ID='steel'/ &OBST ID='FD.stl', XB=1.5,1.6,1.2,2.3,2.95,3.1, RGB=153,153,153, TRANSPARENCY=0.392157, THICKEN=.TRUE., SURF_ID='steel'/ &OBST ID='FD.stl', XB=1.6,1.65,1.2,2.3,2.95,3.15, RGB=153,153,153, TRANSPARENCY=0.392157, THICKEN=.TRUE., SURF_ID='steel'/ &OBST ID='FD.stl', XB=1.65,1.85,1.2,2.3,3.0,3.15, RGB=153,153,153, TRANSPARENCY=0.392157, THICKEN=.TRUE., SURF_ID='steel'/ &OBST ID='FD.stl', XB=1.85,2.65,1.2,2.3,3.05,3.2, RGB=153,153,153, TRANSPARENCY=0.392157, THICKEN=.TRUE., SURF_ID='steel'/ &OBST ID='FD.stl', XB=2.65,2.9,1.2,2.3,3.0,3.15, RGB=153,153,153, TRANSPARENCY=0.392157, THICKEN=.TRUE., SURF_ID='steel'/ &OBST ID='FD.stl', XB=2.9,3.0,1.2,2.3,2.95,3.1, RGB=153,153,153, TRANSPARENCY=0.392157, THICKEN=.TRUE., SURF_ID='steel'/ &OBST ID='FD.stl', XB=3.0,3.05,1.2,2.3,2.9,3.1, RGB=153,153,153, TRANSPARENCY=0.392157, THICKEN=.TRUE., SURF_ID='steel'/ &OBST ID='FD.stl', XB=3.05,3.15,1.2,2.3,2.9,3.05, RGB=153,153,153, TRANSPARENCY=0.392157, THICKEN=.TRUE., SURF_ID='steel'/ &OBST ID='FD.stl', XB=3.15,3.25,1.2,2.3,2.85,3.0, RGB=153,153,153, TRANSPARENCY=0.392157, THICKEN=.TRUE., SURF_ID='steel'/ &OBST ID='FD.stl', XB=3.25,3.3,1.2,2.3,2.8,2.95, RGB=153,153,153, TRANSPARENCY=0.392157, THICKEN=.TRUE., SURF_ID='steel'/ &OBST ID='FD.stl', XB=1.15,1.2,3.35,3.4,0.15,2.75, RGB=153,153,153, TRANSPARENCY=0.392157, THICKEN=.TRUE., SURF_ID='steel'/ &OBST ID='FD.stl', XB=1.15,1.2,2.3,3.35,2.75,2.95, RGB=153,153,153, TRANSPARENCY=0.392157, THICKEN=.TRUE., SURF_ID='steel'/ &OBST ID='FD.stl', XB=1.15,1.2,3.35,3.45,2.85,2.95, RGB=153,153,153, TRANSPARENCY=0.392157, THICKEN=.TRUE., SURF_ID='steel'/ &OBST ID='FD.stl', XB=1.15,1.25,3.45,3.5,0.05,2.9, RGB=153,153,153, TRANSPARENCY=0.392157, THICKEN=.TRUE., SURF_ID='steel'/ &OBST ID='FD.stl', XB=1.15,3.3,2.3,3.45,0.0,0.05, RGB=153,153,153, TRANSPARENCY=0.392157, THICKEN=.TRUE., SURF_ID='steel'/ &OBST ID='FD.stl', XB=1.15,3.3,2.3,3.35,0.1,0.15, RGB=153,153,153, TRANSPARENCY=0.392157, THICKEN=.TRUE., SURF_ID='steel'/

&OBST ID='FD.stl', XB=1.2,1.25,3.35,3.4,0.15,2.8, RGB=153,153,153, TRANSPARENCY=0.392157, THICKEN=.TRUE., SURF_ID='steel'/ &OBST ID='FD.stl', XB=1.2,1.25,2.3,3.35,2.8,2.95, RGB=153,153,153, TRANSPARENCY=0.392157, THICKEN=.TRUE., SURF_ID='steel'/ &OBST ID='FD.stl', XB=1.2,1.25,3.35,3.45,2.9,2.95, RGB=153,153,153, TRANSPARENCY=0.392157, THICKEN=.TRUE., SURF_ID='steel'/ &OBST ID='FD.stl', XB=1.25,1.35,3.45,3.5,0.05,2.95, RGB=153,153,153, TRANSPARENCY=0.392157, THICKEN=.TRUE., SURF_ID='steel'/ &OBST ID='FD.stl', XB=1.25,1.35,2.3,3.35,2.85,3.0, RGB=153,153,153, TRANSPARENCY=0.392157, THICKEN=.TRUE., SURF_ID='steel'/ &OBST ID='FD.stl', XB=1.25,1.35,3.35,3.45,2.95,3.0, RGB=153,153,153, TRANSPARENCY=0.392157, THICKEN=.TRUE., SURF_ID='steel'/ &OBST ID='FD.stl', XB=1.25,1.4,3.35,3.4,0.15,2.85, RGB=153,153,153, TRANSPARENCY=0.392157, THICKEN=.TRUE., SURF_ID='steel'/ &OBST ID='FD.stl', XB=1.35,1.4,2.3,3.35,2.85,3.05, RGB=153,153,153, TRANSPARENCY=0.392157, THICKEN=.TRUE., SURF_ID='steel'/ &OBST ID='FD.stl', XB=1.35,1.5,3.45,3.5,0.05,3.0, RGB=153,153,153, TRANSPARENCY=0.392157, THICKEN=.TRUE., SURF_ID='steel'/ &OBST ID='FD.stl', XB=1.35,1.5,3.35,3.45,2.95,3.05, RGB=153,153,153, TRANSPARENCY=0.392157, THICKEN=.TRUE., SURF_ID='steel'/ &OBST ID='FD.stl', XB=1.4,1.5,3.35,3.4,0.15,2.9, RGB=153,153,153, TRANSPARENCY=0.392157, THICKEN=.TRUE., SURF_ID='steel'/ &OBST ID='FD.stl', XB=1.4,1.5,2.3,3.35,2.9,3.05, RGB=153,153,153, TRANSPARENCY=0.392157, THICKEN=.TRUE., SURF_ID='steel'/ &OBST ID='FD.stl', XB=1.5,1.6,3.45,3.5,0.05,3.05, RGB=153,153,153, TRANSPARENCY=0.392157, THICKEN=.TRUE., SURF_ID='steel'/ &OBST ID='FD.stl', XB=1.5,1.6,2.3,3.35,2.95,3.1, RGB=153,153,153, TRANSPARENCY=0.392157, THICKEN=.TRUE., SURF_ID='steel'/ &OBST ID='FD.stl', XB=1.5,1.6,3.35,3.45,3.05,3.1, RGB=153,153,153, TRANSPARENCY=0.392157, THICKEN=.TRUE., SURF_ID='steel'/ &OBST ID='FD.stl', XB=1.5,1.65,3.35,3.4,0.15,2.95, RGB=153,153,153, TRANSPARENCY=0.392157, THICKEN=.TRUE., SURF_ID='steel'/ &OBST ID='FD.stl', XB=1.6,1.65,2.3,3.35,2.95,3.15, RGB=153,153,153, TRANSPARENCY=0.392157, THICKEN=.TRUE., SURF_ID='steel'/ &OBST ID='FD.stl', XB=1.6,1.65,3.35,3.45,3.05,3.15, RGB=153,153,153, TRANSPARENCY=0.392157, THICKEN=.TRUE., SURF_ID='steel'/ &OBST ID='FD.stl', XB=1.6,1.85,3.45,3.5,0.05,3.1, RGB=153,153,153, TRANSPARENCY=0.392157, THICKEN=.TRUE., SURF_ID='steel'/ &OBST ID='FD.stl', XB=1.65,1.85,3.35,3.4,0.15,3.0, RGB=153,153,153, TRANSPARENCY=0.392157, THICKEN=.TRUE., SURF_ID='steel'/ &OBST ID='FD.stl', XB=1.65,1.85,2.3,3.35,3.0,3.15, RGB=153,153,153, TRANSPARENCY=0.392157, THICKEN=.TRUE., SURF_ID='steel'/ &OBST ID='FD.stl', XB=1.65,1.85,3.35,3.45,3.1,3.15, RGB=153,153,153, TRANSPARENCY=0.392157, THICKEN=.TRUE., SURF_ID='steel'/ &OBST ID='FD.stl', XB=1.85,2.65,3.45,3.5,0.05,3.15, RGB=153,153,153, TRANSPARENCY=0.392157, THICKEN=.TRUE., SURF_ID='steel'/ &OBST ID='FD.stl', XB=1.85,2.65,3.35,3.4,0.15,3.05, RGB=153,153,153, TRANSPARENCY=0.392157, THICKEN=.TRUE., SURF_ID='steel'/ &OBST ID='FD.stl', XB=1.85,2.65,2.3,3.35,3.05,3.2, RGB=153,153,153, TRANSPARENCY=0.392157, THICKEN=.TRUE., SURF_ID='steel'/ &OBST ID='FD.stl', XB=1.85,2.65,3.35,3.45,3.15,3.2, RGB=153,153,153, TRANSPARENCY=0.392157, THICKEN=.TRUE., SURF_ID='steel'/

```
&OBST ID='FD.stl', XB=2.65,2.9,3.45,3.5,0.05,3.1, RGB=153,153,153,
TRANSPARENCY=0.392157, THICKEN=.TRUE., SURF_ID='steel'/
&OBST ID='FD.stl', XB=2.65,2.9,3.35,3.4,0.15,3.0, RGB=153,153,153,
TRANSPARENCY=0.392157, THICKEN=.TRUE., SURF_ID='steel'/
&OBST ID='FD.stl', XB=2.65,2.9,2.3,3.35,3.0,3.15, RGB=153,153,153,
TRANSPARENCY=0.392157, THICKEN=.TRUE., SURF_ID='steel'/
&OBST ID='FD.stl', XB=2.65,2.9,3.35,3.45,3.1,3.15, RGB=153,153,153,
TRANSPARENCY=0.392157, THICKEN=.TRUE., SURF_ID='steel'/
&OBST ID='FD.stl', XB=2.9,3.0,3.35,3.4,0.15,2.95, RGB=153,153,153,
TRANSPARENCY=0.392157, THICKEN=.TRUE., SURF_ID='steel'/
&OBST ID='FD.stl', XB=2.9,3.0,2.3,3.35,2.95,3.1, RGB=153,153,153,
TRANSPARENCY=0.392157, THICKEN=.TRUE., SURF_ID='steel'/
&OBST ID='FD.stl', XB=2.9,3.0,3.35,3.45,3.05,3.1, RGB=153,153,153,
TRANSPARENCY=0.392157, THICKEN=.TRUE., SURF_ID='steel'/
&OBST ID='FD.stl', XB=2.9,3.05,3.45,3.5,0.05,3.05, RGB=153,153,153,
TRANSPARENCY=0.392157, THICKEN=.TRUE., SURF_ID='steel'/
&OBST ID='FD.stl', XB=3.0,3.05,2.3,3.35,2.9,3.1, RGB=153,153,153,
TRANSPARENCY=0.392157, THICKEN=.TRUE., SURF_ID='steel'/
&OBST ID='FD.stl', XB=3.0,3.05,3.35,3.45,3.0,3.1, RGB=153,153,153,
TRANSPARENCY=0.392157, THICKEN=.TRUE., SURF_ID='steel'/
&OBST ID='FD.stl', XB=3.0,3.15,3.35,3.4,0.15,2.9, RGB=153,153,153,
TRANSPARENCY=0.392157, THICKEN=.TRUE., SURF_ID='steel'/
&OBST ID='FD.stl', XB=3.05,3.15,3.45,3.5,0.05,3.0, RGB=153,153,153,
TRANSPARENCY=0.392157, THICKEN=.TRUE., SURF_ID='steel'/
&OBST ID='FD.stl', XB=3.05,3.15,2.3,3.35,2.9,3.05, RGB=153,153,153,
TRANSPARENCY=0.392157, THICKEN=.TRUE., SURF_ID='steel'/
&OBST ID='FD.stl', XB=3.05,3.15,3.35,3.45,3.0,3.05, RGB=153,153,153,
TRANSPARENCY=0.392157, THICKEN=.TRUE., SURF_ID='steel'/
&OBST ID='FD.stl', XB=3.15,3.25,3.45,3.5,0.05,2.95, RGB=153,153,153,
TRANSPARENCY=0.392157, THICKEN=.TRUE., SURF_ID='steel'/
&OBST ID='FD.stl', XB=3.15,3.25,3.35,3.4,0.15,2.85, RGB=153,153,153,
TRANSPARENCY=0.392157, THICKEN=.TRUE., SURF_ID='steel'/
&OBST ID='FD.stl', XB=3.15,3.25,2.3,3.35,2.85,3.0, RGB=153,153,153,
TRANSPARENCY=0.392157, THICKEN=.TRUE., SURF_ID='steel'/
&OBST ID='FD.stl', XB=3.15,3.25,3.35,3.45,2.95,3.0, RGB=153,153,153,
TRANSPARENCY=0.392157, THICKEN=.TRUE., SURF_ID='steel'/
&OBST ID='FD.stl', XB=3.25,3.3,3.45,3.5,0.05,2.9, RGB=153,153,153,
TRANSPARENCY=0.392157, THICKEN=.TRUE., SURF_ID='steel'/
&OBST ID='FD.stl', XB=3.25,3.3,3.35,3.4,0.15,2.8, RGB=153,153,153,
TRANSPARENCY=0.392157, THICKEN=.TRUE., SURF_ID='steel'/
&OBST ID='FD.stl', XB=3.25,3.3,2.3,3.35,2.8,2.95, RGB=153,153,153,
TRANSPARENCY=0.392157, THICKEN=.TRUE., SURF_ID='steel'/
&OBST ID='FD.stl', XB=3.25,3.3,3.35,3.45,2.85,2.95, RGB=153,153,153,
TRANSPARENCY=0.392157, THICKEN=.TRUE., SURF_ID='steel'/
&OBST ID='FD.stl', XB=3.3,3.35,-0.05,1.290634E-15,0.05,2.9, RGB=153,153,153,
TRANSPARENCY=0.392157, THICKEN=.TRUE., SURF_ID='steel'/
&OBST ID='FD.stl', XB=3.3,3.35,0.1,1.2,2.75,2.95, RGB=153,153,153,
TRANSPARENCY=0.392157, THICKEN=.TRUE., SURF_ID='steel'/
&OBST ID='FD.stl', XB=3.3,3.35,1.290634E-15,0.1,2.85,2.95, RGB=153,153,153,
TRANSPARENCY=0.392157, THICKEN=.TRUE., SURF_ID='steel'/
&OBST ID='FD.stl', XB=3.3,3.4,0.05,0.1,0.15,2.75, RGB=153,153,153,
TRANSPARENCY=0.392157, THICKEN=.TRUE., SURF_ID='steel'/
```

```
&OBST ID='FD.stl', XB=3.3,4.2,1.290634E-15,0.05,0.0,0.05, RGB=153,153,153,
TRANSPARENCY=0.392157, THICKEN=.TRUE., SURF_ID='steel'/
&OBST ID='FD.stl', XB=3.3,4.2,1.15,1.2,0.0,0.15, RGB=153,153,153,
TRANSPARENCY=0.392157, THICKEN=.TRUE., SURF_ID='steel'/
&OBST ID='FD.stl', XB=3.3,4.25,0.05,0.1,0.0,0.1, RGB=153,153,153,
TRANSPARENCY=0.392157, THICKEN=.TRUE., SURF_ID='steel'/
&OBST ID='FD.stl', XB=3.3,4.25,0.1,1.15,0.0,0.15, RGB=153,153,153,
TRANSPARENCY=0.392157, THICKEN=.TRUE., SURF_ID='steel'/
&OBST ID='FD.stl', XB=3.35,3.4,0.1,1.2,2.75,2.9, RGB=153,153,153,
TRANSPARENCY=0.392157, THICKEN=.TRUE., SURF_ID='steel'/
&OBST ID='FD.stl', XB=3.35,3.45,-0.05,1.290634E-15,0.05,2.85, RGB=153,153,153,
TRANSPARENCY=0.392157, THICKEN=.TRUE., SURF_ID='steel'/
&OBST ID='FD.stl', XB=3.35,3.45,1.290634E-15,0.1,2.85,2.9, RGB=153,153,153,
TRANSPARENCY=0.392157, THICKEN=.TRUE., SURF_ID='steel'/
&OBST ID='FD.stl', XB=3.4,3.45,0.1,1.2,2.7,2.9, RGB=153,153,153,
TRANSPARENCY=0.392157, THICKEN=.TRUE., SURF_ID='steel'/
&OBST ID='FD.stl', XB=3.4,3.5,0.05,0.1,0.15,2.7, RGB=153,153,153,
TRANSPARENCY=0.392157, THICKEN=.TRUE., SURF_ID='steel'/
&OBST ID='FD.stl', XB=3.45,3.5,-0.05,1.290634E-15,0.05,2.8, RGB=153,153,153,
TRANSPARENCY=0.392157, THICKEN=.TRUE., SURF_ID='steel'/
&OBST ID='FD.stl', XB=3.45,3.5,0.1,1.2,2.7,2.85, RGB=153,153,153,
TRANSPARENCY=0.392157, THICKEN=.TRUE., SURF_ID='steel'/
&OBST ID='FD.stl', XB=3.45,3.5,1.290634E-15,0.1,2.8,2.85, RGB=153,153,153,
TRANSPARENCY=0.392157, THICKEN=.TRUE., SURF_ID='steel'/
&OBST ID='FD.stl', XB=3.5,3.55,0.05,0.1,0.15,2.65, RGB=153,153,153,
TRANSPARENCY=0.392157, THICKEN=.TRUE., SURF_ID='steel'/
&OBST ID='FD.stl', XB=3.5,3.55,0.1,1.2,2.65,2.8, RGB=153,153,153,
TRANSPARENCY=0.392157, THICKEN=.TRUE., SURF_ID='steel'/
&OBST ID='FD.stl', XB=3.5,3.6,-0.05,1.290634E-15,0.05,2.75, RGB=153,153,153,
TRANSPARENCY=0.392157, THICKEN=.TRUE., SURF_ID='steel'/
&OBST ID='FD.stl', XB=3.5,3.6,1.290634E-15,0.1,2.75,2.8, RGB=153,153,153,
TRANSPARENCY=0.392157, THICKEN=.TRUE., SURF_ID='steel'/
&OBST ID='FD.stl', XB=3.55,3.6,0.05,0.1,0.15,2.6, RGB=153,153,153,
TRANSPARENCY=0.392157, THICKEN=.TRUE., SURF_ID='steel'/
&OBST ID='FD.stl', XB=3.55,3.6,0.1,1.2,2.6,2.8, RGB=153,153,153,
TRANSPARENCY=0.392157, THICKEN=.TRUE., SURF_ID='steel'/
&OBST ID='FD.stl', XB=3.6,3.65,-0.05,1.290634E-15,0.05,2.7, RGB=153,153,153,
TRANSPARENCY=0.392157, THICKEN=.TRUE., SURF_ID='steel'/
&OBST ID='FD.stl', XB=3.6,3.65,0.05,0.1,0.15,2.55, RGB=153,153,153,
TRANSPARENCY=0.392157, THICKEN=.TRUE., SURF_ID='steel'/
&OBST ID='FD.stl', XB=3.6,3.65,0.1,1.2,2.55,2.75, RGB=153,153,153,
TRANSPARENCY=0.392157, THICKEN=.TRUE., SURF_ID='steel'/
&OBST ID='FD.stl', XB=3.6,3.65,1.290634E-15,0.1,2.7,2.75, RGB=153,153,153,
TRANSPARENCY=0.392157, THICKEN=.TRUE., SURF_ID='steel'/
&OBST ID='FD.stl', XB=3.65,3.7,-0.05,1.290634E-15,0.05,2.65, RGB=153,153,153,
TRANSPARENCY=0.392157, THICKEN=.TRUE., SURF_ID='steel'/
&OBST ID='FD.stl', XB=3.65,3.7,0.05,0.1,0.15,2.5, RGB=153,153,153,
TRANSPARENCY=0.392157, THICKEN=.TRUE., SURF_ID='steel'/
&OBST ID='FD.stl', XB=3.65,3.7,0.1,1.2,2.5,2.7, RGB=153,153,153,
TRANSPARENCY=0.392157, THICKEN=.TRUE., SURF_ID='steel'/
&OBST ID='FD.stl', XB=3.65,3.7,1.290634E-15,0.1,2.65,2.7, RGB=153,153,153,
TRANSPARENCY=0.392157, THICKEN=.TRUE., SURF_ID='steel'/
```

```
&OBST ID='FD.stl', XB=3.7,3.75,-0.05,1.290634E-15,0.05,2.6, RGB=153,153,153,
TRANSPARENCY=0.392157, THICKEN=.TRUE., SURF_ID='steel'/
&OBST ID='FD.stl', XB=3.7,3.75,0.05,0.1,0.15,2.45, RGB=153,153,153,
TRANSPARENCY=0.392157, THICKEN=.TRUE., SURF_ID='steel'/
&OBST ID='FD.stl', XB=3.7,3.75,0.1,1.2,2.45,2.65, RGB=153,153,153,
TRANSPARENCY=0.392157, THICKEN=.TRUE., SURF_ID='steel'/
&OBST ID='FD.stl', XB=3.7,3.75,1.290634E-15,0.1,2.6,2.65, RGB=153,153,153,
TRANSPARENCY=0.392157, THICKEN=.TRUE., SURF_ID='steel'/
&OBST ID='FD.stl', XB=3.75,3.8,-0.05,1.290634E-15,0.05,2.55, RGB=153,153,153,
TRANSPARENCY=0.392157, THICKEN=.TRUE., SURF_ID='steel'/
&OBST ID='FD.stl', XB=3.75,3.8,0.05,0.1,0.15,2.4, RGB=153,153,153,
TRANSPARENCY=0.392157, THICKEN=.TRUE., SURF_ID='steel'/
&OBST ID='FD.stl', XB=3.75,3.8,0.1,1.2,2.4,2.6, RGB=153,153,153,
TRANSPARENCY=0.392157, THICKEN=.TRUE., SURF_ID='steel'/
&OBST ID='FD.stl', XB=3.75,3.8,1.290634E-15,0.1,2.5,2.6, RGB=153,153,153,
TRANSPARENCY=0.392157, THICKEN=.TRUE., SURF_ID='steel'/
&OBST ID='FD.stl', XB=3.8,3.85,-0.05,1.290634E-15,0.05,2.5, RGB=153,153,153,
TRANSPARENCY=0.392157, THICKEN=.TRUE., SURF_ID='steel'/
&OBST ID='FD.stl', XB=3.8,3.85,0.05,0.1,0.15,2.35, RGB=153,153,153,
TRANSPARENCY=0.392157, THICKEN=.TRUE., SURF_ID='steel'/
&OBST ID='FD.stl', XB=3.8,3.85,0.1,1.2,2.35,2.55, RGB=153,153,153,
TRANSPARENCY=0.392157, THICKEN=.TRUE., SURF_ID='steel'/
&OBST ID='FD.stl', XB=3.8,3.85,1.290634E-15,0.1,2.45,2.55, RGB=153,153,153,
TRANSPARENCY=0.392157, THICKEN=.TRUE., SURF_ID='steel'/
&OBST ID='FD.stl', XB=3.85,3.9,-0.05,1.290634E-15,0.05,2.45, RGB=153,153,153,
TRANSPARENCY=0.392157, THICKEN=.TRUE., SURF_ID='steel'/
&OBST ID='FD.stl', XB=3.85,3.9,0.05,0.1,0.15,2.3, RGB=153,153,153,
TRANSPARENCY=0.392157, THICKEN=.TRUE., SURF_ID='steel'/
&OBST ID='FD.stl', XB=3.85,3.9,0.1,1.2,2.3,2.5, RGB=153,153,153,
TRANSPARENCY=0.392157, THICKEN=.TRUE., SURF_ID='steel'/
&OBST ID='FD.stl', XB=3.85,3.9,1.290634E-15,0.1,2.4,2.5, RGB=153,153,153,
TRANSPARENCY=0.392157, THICKEN=.TRUE., SURF_ID='steel'/
&OBST ID='FD.stl', XB=3.9,3.95,-0.05,1.290634E-15,0.05,2.4, RGB=153,153,153,
TRANSPARENCY=0.392157, THICKEN=.TRUE., SURF_ID='steel'/
&OBST ID='FD.stl', XB=3.9,3.95,0.05,0.1,0.15,2.25, RGB=153,153,153,
TRANSPARENCY=0.392157, THICKEN=.TRUE., SURF_ID='steel'/
&OBST ID='FD.stl', XB=3.9,3.95,0.1,1.2,2.25,2.45, RGB=153,153,153,
TRANSPARENCY=0.392157, THICKEN=.TRUE., SURF_ID='steel'/
&OBST ID='FD.stl', XB=3.9,3.95,1.290634E-15,0.1,2.35,2.45, RGB=153,153,153,
TRANSPARENCY=0.392157, THICKEN=.TRUE., SURF_ID='steel'/
&OBST ID='FD.stl', XB=3.95,4.0,-0.05,1.290634E-15,0.05,2.35, RGB=153,153,153,
TRANSPARENCY=0.392157, THICKEN=.TRUE., SURF_ID='steel'/
&OBST ID='FD.stl', XB=3.95,4.0,0.05,0.1,0.15,2.15, RGB=153,153,153,
TRANSPARENCY=0.392157, THICKEN=.TRUE., SURF_ID='steel'/
&OBST ID='FD.stl', XB=3.95,4.0,0.1,1.2,2.15,2.4, RGB=153,153,153,
TRANSPARENCY=0.392157, THICKEN=.TRUE., SURF_ID='steel'/
&OBST ID='FD.stl', XB=3.95,4.0,1.290634E-15,0.1,2.25,2.4, RGB=153,153,153,
TRANSPARENCY=0.392157, THICKEN=.TRUE., SURF_ID='steel'/
&OBST ID='FD.stl', XB=4.0,4.05,-0.05,1.290634E-15,0.05,2.25, RGB=153,153,153,
TRANSPARENCY=0.392157, THICKEN=.TRUE., SURF_ID='steel'/
&OBST ID='FD.stl', XB=4.0,4.05,0.05,0.1,0.15,2.1, RGB=153,153,153,
TRANSPARENCY=0.392157, THICKEN=.TRUE., SURF_ID='steel'/
```

```
&OBST ID='FD.stl', XB=4.0,4.05,0.1,1.2,2.1,2.35, RGB=153,153,153,
TRANSPARENCY=0.392157, THICKEN=.TRUE., SURF_ID='steel'/
&OBST ID='FD.stl', XB=4.0,4.05,1.290634E-15,0.1,2.25,2.35, RGB=153,153,153,
TRANSPARENCY=0.392157, THICKEN=.TRUE., SURF_ID='steel'/
&OBST ID='FD.stl', XB=4.05,4.1,-0.05,1.290634E-15,0.05,2.2, RGB=153,153,153,
TRANSPARENCY=0.392157, THICKEN=.TRUE., SURF_ID='steel'/
&OBST ID='FD.stl', XB=4.05,4.1,0.1,1.2,2.05,2.25, RGB=153,153,153,
TRANSPARENCY=0.392157, THICKEN=.TRUE., SURF_ID='steel'/
&OBST ID='FD.stl', XB=4.05,4.1,1.290634E-15,0.1,2.1,2.25, RGB=153,153,153,
TRANSPARENCY=0.392157, THICKEN=.TRUE., SURF_ID='steel'/
&OBST ID='FD.stl', XB=4.05,4.15,0.05,0.1,0.15,2.05, RGB=153,153,153,
TRANSPARENCY=0.392157, THICKEN=.TRUE., SURF_ID='steel'/
&OBST ID='FD.stl', XB=4.1,4.15,-0.05,1.290634E-15,0.05,2.1, RGB=153,153,153,
TRANSPARENCY=0.392157, THICKEN=.TRUE., SURF_ID='steel'/
&OBST ID='FD.stl', XB=4.1,4.15,1.15,1.2,1.95,2.2, RGB=153,153,153,
TRANSPARENCY=0.392157, THICKEN=.TRUE., SURF_ID='steel'/
&OBST ID='FD.stl', XB=4.1,4.15,0.1,1.15,2.05,2.2, RGB=153,153,153,
TRANSPARENCY=0.392157, THICKEN=.TRUE., SURF_ID='steel'/
&OBST ID='FD.stl', XB=4.1,4.15,1.290634E-15,0.1,2.1,2.2, RGB=153,153,153,
TRANSPARENCY=0.392157, THICKEN=.TRUE., SURF_ID='steel'/
&OBST ID='FD.stl', XB=4.15,4.2,-0.05,1.290634E-15,0.05,2.05, RGB=153,153,153,
TRANSPARENCY=0.392157, THICKEN=.TRUE., SURF_ID='steel'/
&OBST ID='FD.stl', XB=4.15,4.2,0.05,0.1,0.15,2.1, RGB=153,153,153,
TRANSPARENCY=0.392157, THICKEN=.TRUE., SURF_ID='steel'/
&OBST ID='FD.stl', XB=4.15,4.2,1.15,1.2,1.85,2.1, RGB=153,153,153,
TRANSPARENCY=0.392157, THICKEN=.TRUE., SURF_ID='steel'/
&OBST ID='FD.stl', XB=4.15,4.2,1.290634E-15,0.05,2.0,2.1, RGB=153,153,153,
TRANSPARENCY=0.392157, THICKEN=.TRUE., SURF_ID='steel'/
&OBST ID='FD.stl', XB=4.15,4.2,0.1,1.15,2.05,2.1, RGB=153,153,153,
TRANSPARENCY=0.392157, THICKEN=.TRUE., SURF_ID='steel'/
&OBST ID='FD.stl', XB=4.2,4.25,1.290634E-15,0.05,0.0,0.1, RGB=153,153,153,
TRANSPARENCY=0.392157, THICKEN=.TRUE., SURF_ID='steel'/
&OBST ID='FD.stl', XB=4.2,4.25,1.15,1.2,0.0,0.25, RGB=153,153,153,
TRANSPARENCY=0.392157, THICKEN=.TRUE., SURF_ID='steel'/
&OBST ID='FD.stl', XB=4.2,4.25,-0.05,1.290634E-15,0.05,1.95, RGB=153,153,153,
TRANSPARENCY=0.392157, THICKEN=.TRUE., SURF_ID='steel'/
&OBST ID='FD.stl', XB=4.2,4.25,0.05,0.1,0.15,2.0, RGB=153,153,153,
TRANSPARENCY=0.392157, THICKEN=.TRUE., SURF_ID='steel'/
&OBST ID='FD.stl', XB=4.2,4.25,1.15,1.2,1.75,1.95, RGB=153,153,153,
TRANSPARENCY=0.392157, THICKEN=.TRUE., SURF_ID='steel'/
&OBST ID='FD.stl', XB=4.2,4.25,1.290634E-15,0.05,1.9,2.0, RGB=153,153,153,
TRANSPARENCY=0.392157, THICKEN=.TRUE., SURF_ID='steel'/
&OBST ID='FD.stl', XB=4.25,4.3,0.1,1.2,0.05,0.1, RGB=153,153,153,
TRANSPARENCY=0.392157, THICKEN=.TRUE., SURF_ID='steel'/
&OBST ID='FD.stl', XB=4.25,4.3,0.05,0.1,0.05,1.9, RGB=153,153,153,
TRANSPARENCY=0.392157, THICKEN=.TRUE., SURF_ID='steel'/
&OBST ID='FD.stl', XB=4.25,4.3,1.290634E-15,0.05,0.1,0.2, RGB=153,153,153,
TRANSPARENCY=0.392157, THICKEN=.TRUE., SURF_ID='steel'/
&OBST ID='FD.stl', XB=4.25,4.3,1.15,1.2,0.15,0.4, RGB=153,153,153,
TRANSPARENCY=0.392157, THICKEN=.TRUE., SURF_ID='steel'/
&OBST ID='FD.stl', XB=4.25,4.3,-0.05,1.290634E-15,0.15,1.8, RGB=153,153,153,
TRANSPARENCY=0.392157, THICKEN=.TRUE., SURF_ID='steel'/
```

```
&OBST ID='FD.stl', XB=4.25,4.3,1.15,1.2,1.55,1.85, RGB=153,153,153,
TRANSPARENCY=0.392157, THICKEN=.TRUE., SURF_ID='steel'/
&OBST ID='FD.stl', XB=4.25,4.3,1.290634E-15,0.05,1.8,1.9, RGB=153,153,153,
TRANSPARENCY=0.392157, THICKEN=.TRUE., SURF_ID='steel'/
&OBST ID='FD.stl', XB=4.3,4.35,1.290634E-15,0.05,0.2,0.55, RGB=153,153,153,
TRANSPARENCY=0.392157, THICKEN=.TRUE., SURF_ID='steel'/
&OBST ID='FD.stl', XB=4.3,4.35,0.05,0.1,0.25,1.75, RGB=153,153,153,
TRANSPARENCY=0.392157, THICKEN=.TRUE., SURF_ID='steel'/
&OBST ID='FD.stl', XB=4.3,4.35,1.15,1.2,0.3,0.7, RGB=153,153,153,
TRANSPARENCY=0.392157, THICKEN=.TRUE., SURF_ID='steel'/
&OBST ID='FD.stl', XB=4.3,4.35,-0.05,1.290634E-15,0.3,1.7, RGB=153,153,153,
TRANSPARENCY=0.392157, THICKEN=.TRUE., SURF_ID='steel'/
&OBST ID='FD.stl', XB=4.3,4.35,1.15,1.2,1.35,1.7, RGB=153,153,153,
TRANSPARENCY=0.392157, THICKEN=.TRUE., SURF_ID='steel'/
&OBST ID='FD.stl', XB=4.3,4.35,1.290634E-15,0.05,1.65,1.8, RGB=153,153,153,
TRANSPARENCY=0.392157, THICKEN=.TRUE., SURF_ID='steel'/
&OBST ID='FD.stl', XB=4.35,4.4,1.290634E-15,0.05,0.35,1.65, RGB=153,153,153,
TRANSPARENCY=0.392157, THICKEN=.TRUE., SURF_ID='steel'/
&OBST ID='FD.stl', XB=4.35,4.4,0.05,0.1,0.4,1.6, RGB=153,153,153,
TRANSPARENCY=0.392157, THICKEN=.TRUE., SURF_ID='steel'/
&OBST ID='FD.stl', XB=4.35,4.4,-0.05,1.290634E-15,0.45,1.55, RGB=153,153,153,
TRANSPARENCY=0.392157, THICKEN=.TRUE., SURF_ID='steel'/
&OBST ID='FD.stl', XB=4.35,4.4,1.15,1.2,0.45,1.55, RGB=153,153,153,
TRANSPARENCY=0.392157, THICKEN=.TRUE., SURF_ID='steel'/
&OBST ID='FD.stl', XB=4.4,4.45,1.290634E-15,0.05,0.55,1.45, RGB=153,153,153,
TRANSPARENCY=0.392157, THICKEN=.TRUE., SURF_ID='steel'/
&OBST ID='FD.stl', XB=4.4,4.45,0.05,0.1,0.65,1.35, RGB=153,153,153,
TRANSPARENCY=0.392157, THICKEN=.TRUE., SURF_ID='steel'/
&OBST ID='FD.stl', XB=4.4,4.45,-0.05,1.290634E-15,0.7,1.3, RGB=153,153,153,
TRANSPARENCY=0.392157, THICKEN=.TRUE., SURF_ID='steel'/
&OBST ID='FD.stl', XB=4.4,4.45,1.15,1.2,0.7,1.3, RGB=153,153,153,
TRANSPARENCY=0.392157, THICKEN=.TRUE., SURF_ID='steel'/
&OBST ID='FD.stl', XB=3.3,3.35,1.2,2.3,2.75,2.95, RGB=153,153,153,
TRANSPARENCY=0.392157, THICKEN=.TRUE., SURF_ID='steel'/
&OBST ID='FD.stl', XB=3.3,4.15,1.2,2.2,0.0,0.15, RGB=153,153,153,
TRANSPARENCY=0.392157, THICKEN=.TRUE., SURF_ID='steel'/
&OBST ID='FD.stl', XB=3.3,4.15,2.2,2.3,0.1,0.15, RGB=153,153,153,
TRANSPARENCY=0.392157, THICKEN=.TRUE., SURF_ID='steel'/
&OBST ID='FD.stl', XB=3.3,4.2,2.2,2.3,0.0,0.05, RGB=153,153,153,
TRANSPARENCY=0.392157, THICKEN=.TRUE., SURF_ID='steel'/
&OBST ID='FD.stl', XB=3.35,3.4,1.2,2.3,2.75,2.9, RGB=153,153,153,
TRANSPARENCY=0.392157, THICKEN=.TRUE., SURF_ID='steel'/
&OBST ID='FD.stl', XB=3.4,3.45,1.2,2.3,2.7,2.9, RGB=153,153,153,
TRANSPARENCY=0.392157, THICKEN=.TRUE., SURF_ID='steel'/
&OBST ID='FD.stl', XB=3.45,3.5,1.2,2.3,2.7,2.85, RGB=153,153,153,
TRANSPARENCY=0.392157, THICKEN=.TRUE., SURF_ID='steel'/
&OBST ID='FD.stl', XB=3.5,3.55,1.2,2.3,2.65,2.8, RGB=153,153,153,
TRANSPARENCY=0.392157, THICKEN=.TRUE., SURF_ID='steel'/
&OBST ID='FD.stl', XB=3.55,3.6,1.2,2.3,2.6,2.8, RGB=153,153,153,
TRANSPARENCY=0.392157, THICKEN=.TRUE., SURF_ID='steel'/
&OBST ID='FD.stl', XB=3.6,3.65,1.2,2.3,2.55,2.75, RGB=153,153,153,
TRANSPARENCY=0.392157, THICKEN=.TRUE., SURF_ID='steel'/
```

&OBST ID='FD.stl', XB=3.65,3.7,1.2,2.3,2.5,2.7, RGB=153,153,153, TRANSPARENCY=0.392157, THICKEN=.TRUE., SURF_ID='steel'/ &OBST ID='FD.stl', XB=3.7,3.75,1.2,2.3,2.45,2.65, RGB=153,153,153, TRANSPARENCY=0.392157, THICKEN=.TRUE., SURF_ID='steel'/ &OBST ID='FD.stl', XB=3.75,3.8,1.2,2.3,2.4,2.6, RGB=153,153,153, TRANSPARENCY=0.392157, THICKEN=.TRUE., SURF_ID='steel'/ &OBST ID='FD.stl', XB=3.8,3.85,1.2,2.3,2.35,2.55, RGB=153,153,153, TRANSPARENCY=0.392157, THICKEN=.TRUE., SURF_ID='steel'/ &OBST ID='FD.stl', XB=3.85,3.9,1.2,2.3,2.3,2.5, RGB=153,153,153, TRANSPARENCY=0.392157, THICKEN=.TRUE., SURF_ID='steel'/ &OBST ID='FD.stl', XB=3.9,3.95,1.2,2.3,2.25,2.45, RGB=153,153,153, TRANSPARENCY=0.392157, THICKEN=.TRUE., SURF_ID='steel'/ &OBST ID='FD.stl', XB=3.95,4.0,1.2,2.3,2.15,2.4, RGB=153,153,153, TRANSPARENCY=0.392157, THICKEN=.TRUE., SURF_ID='steel'/ &OBST ID='FD.stl', XB=4.0,4.05,1.2,2.3,2.1,2.35, RGB=153,153,153, TRANSPARENCY=0.392157, THICKEN=.TRUE., SURF_ID='steel'/ &OBST ID='FD.stl', XB=4.05,4.1,1.2,2.3,2.0,2.25, RGB=153,153,153, TRANSPARENCY=0.392157, THICKEN=.TRUE., SURF_ID='steel'/ &OBST ID='FD.stl', XB=4.1,4.15,1.2,2.3,1.9,2.0, RGB=153,153,153, TRANSPARENCY=0.392157, THICKEN=.TRUE., SURF_ID='steel'/ &OBST ID='FD.stl', XB=4.1,4.15,1.2,2.3,2.1,2.2, RGB=153,153,153, TRANSPARENCY=0.392157, THICKEN=.TRUE., SURF_ID='steel'/ &OBST ID='FD.stl', XB=4.15,4.2,1.2,2.3,0.15,0.25, RGB=153,153,153, TRANSPARENCY=0.392157, THICKEN=.TRUE., SURF_ID='steel'/ &OBST ID='FD.stl', XB=4.15,4.2,1.2,2.3,1.8,1.9, RGB=153,153,153, TRANSPARENCY=0.392157, THICKEN=.TRUE., SURF_ID='steel'/ &OBST ID='FD.stl', XB=4.15,4.2,1.2,2.3,2.0,2.1, RGB=153,153,153, TRANSPARENCY=0.392157, THICKEN=.TRUE., SURF_ID='steel'/ &OBST ID='FD.stl', XB=4.15,4.25,1.2,2.2,0.0,0.1, RGB=153,153,153, TRANSPARENCY=0.392157, THICKEN=.TRUE., SURF_ID='steel'/ &OBST ID='FD.stl', XB=4.2,4.25,2.2,2.3,0.0,0.1, RGB=153,153,153, TRANSPARENCY=0.392157, THICKEN=.TRUE., SURF_ID='steel'/ &OBST ID='FD.stl', XB=4.2,4.25,1.2,2.3,0.25,0.35, RGB=153,153,153, TRANSPARENCY=0.392157, THICKEN=.TRUE., SURF_ID='steel'/ &OBST ID='FD.stl', XB=4.2,4.25,1.2,2.3,1.65,1.8, RGB=153,153,153, TRANSPARENCY=0.392157, THICKEN=.TRUE., SURF_ID='steel'/ &OBST ID='FD.stl', XB=4.2,4.25,1.2,2.3,1.9,2.0, RGB=153,153,153, TRANSPARENCY=0.392157, THICKEN=.TRUE., SURF_ID='steel'/ &OBST ID='FD.stl', XB=4.25,4.3,1.2,2.2,0.05,0.2, RGB=153,153,153, TRANSPARENCY=0.392157, THICKEN=.TRUE., SURF_ID='steel'/ &OBST ID='FD.stl', XB=4.25,4.3,2.2,2.3,0.1,0.2, RGB=153,153,153, TRANSPARENCY=0.392157, THICKEN=.TRUE., SURF_ID='steel'/ &OBST ID='FD.stl', XB=4.25,4.3,1.2,2.3,0.35,0.55, RGB=153,153,153, TRANSPARENCY=0.392157, THICKEN=.TRUE., SURF_ID='steel'/ &OBST ID='FD.stl', XB=4.25,4.3,1.2,2.3,1.45,1.65, RGB=153,153,153, TRANSPARENCY=0.392157, THICKEN=.TRUE., SURF_ID='steel'/ &OBST ID='FD.stl', XB=4.25,4.3,1.2,2.3,1.8,1.9, RGB=153,153,153, TRANSPARENCY=0.392157, THICKEN=.TRUE., SURF_ID='steel'/ &OBST ID='FD.stl', XB=4.3,4.35,1.2,2.3,0.2,0.35, RGB=153,153,153, TRANSPARENCY=0.392157, THICKEN=.TRUE., SURF_ID='steel'/ &OBST ID='FD.stl', XB=4.3,4.35,1.2,2.3,0.55,0.85, RGB=153,153,153, TRANSPARENCY=0.392157, THICKEN=.TRUE., SURF_ID='steel'/

&OBST ID='FD.stl', XB=4.3,4.35,1.2,2.3,0.95,1.45, RGB=153,153,153, TRANSPARENCY=0.392157, THICKEN=.TRUE., SURF_ID='steel'/ &OBST ID='FD.stl', XB=4.3,4.35,1.2,2.3,1.65,1.8, RGB=153,153,153, TRANSPARENCY=0.392157, THICKEN=.TRUE., SURF_ID='steel'/ &OBST ID='FD.stl', XB=4.35,4.4,1.2,1.95,0.35,0.5, RGB=153,153,153, TRANSPARENCY=0.392157, THICKEN=.TRUE., SURF_ID='steel'/ &OBST ID='FD.stl', XB=4.35,4.4,1.95,2.3,0.35,0.55, RGB=153,153,153, TRANSPARENCY=0.392157, THICKEN=.TRUE., SURF_ID='steel'/ &OBST ID='FD.stl', XB=4.35,4.4,1.4,2.3,0.85,0.95, RGB=153,153,153, TRANSPARENCY=0.392157, THICKEN=.TRUE., SURF_ID='steel'/ &OBST ID='FD.stl', XB=4.35,4.4,1.2,1.4,0.85,1.65, RGB=153,153,153, TRANSPARENCY=0.392157, THICKEN=.TRUE., SURF_ID='steel'/ &OBST ID='FD.stl', XB=4.35,4.4,1.4,2.3,1.45,1.65, RGB=153,153,153, TRANSPARENCY=0.392157, THICKEN=.TRUE., SURF_ID='steel'/ &OBST ID='FD.stl', XB=4.4,4.45,1.2,1.95,0.5,0.85, RGB=153,153,153, TRANSPARENCY=0.392157, THICKEN=.TRUE., SURF_ID='steel'/ &OBST ID='FD.stl', XB=4.4,4.45,1.95,2.3,0.55,0.85, RGB=153,153,153, TRANSPARENCY=0.392157, THICKEN=.TRUE., SURF_ID='steel'/ &OBST ID='FD.stl', XB=4.4,4.45,1.2,1.4,0.95,1.45, RGB=153,153,153, TRANSPARENCY=0.392157, THICKEN=.TRUE., SURF_ID='steel'/ &OBST ID='FD.stl', XB=4.4,4.45,2.0,2.3,0.95,1.45, RGB=153,153,153, TRANSPARENCY=0.392157, THICKEN=.TRUE., SURF_ID='steel'/ &OBST ID='FD.stl', XB=4.4,4.45,1.4,2.0,1.0,1.45, RGB=153,153,153, TRANSPARENCY=0.392157, THICKEN=.TRUE., SURF_ID='steel'/ &OBST ID='FD.stl', XB=4.45,4.5,1.2,1.4,0.85,0.95, RGB=153,153,153, TRANSPARENCY=0.392157, THICKEN=.TRUE., SURF_ID='steel'/ &OBST ID='FD.stl', XB=4.45,4.5,2.0,2.3,0.85,0.95, RGB=153,153,153, TRANSPARENCY=0.392157, THICKEN=.TRUE., SURF_ID='steel'/ &OBST ID='FD.stl', XB=4.45,4.5,1.4,2.0,0.85,1.0, RGB=153,153,153, TRANSPARENCY=0.392157, THICKEN=.TRUE., SURF_ID='steel'/ &OBST ID='FD.stl', XB=3.3,3.35,3.45,3.5,0.05,2.9, RGB=153,153,153, TRANSPARENCY=0.392157, THICKEN=.TRUE., SURF_ID='steel'/ &OBST ID='FD.stl', XB=3.3,3.35,2.3,3.35,2.75,2.95, RGB=153,153,153, TRANSPARENCY=0.392157, THICKEN=.TRUE., SURF_ID='steel'/ &OBST ID='FD.stl', XB=3.3,3.35,3.35,3.45,2.85,2.95, RGB=153,153,153, TRANSPARENCY=0.392157, THICKEN=.TRUE., SURF_ID='steel'/ &OBST ID='FD.stl', XB=3.3,3.4,3.35,3.4,0.15,2.75, RGB=153,153,153, TRANSPARENCY=0.392157, THICKEN=.TRUE., SURF_ID='steel'/ &OBST ID='FD.stl', XB=3.3,4.15,2.3,3.35,0.1,0.15, RGB=153,153,153, TRANSPARENCY=0.392157, THICKEN=.TRUE., SURF_ID='steel'/ &OBST ID='FD.stl', XB=3.3,4.2,2.3,3.45,0.0,0.05, RGB=153,153,153, TRANSPARENCY=0.392157, THICKEN=.TRUE., SURF_ID='steel'/ &OBST ID='FD.stl', XB=3.35,3.4,2.3,3.35,2.75,2.9, RGB=153,153,153, TRANSPARENCY=0.392157, THICKEN=.TRUE., SURF_ID='steel'/ &OBST ID='FD.stl', XB=3.35,3.45,3.45,3.5,0.05,2.85, RGB=153,153,153, TRANSPARENCY=0.392157, THICKEN=.TRUE., SURF_ID='steel'/ &OBST ID='FD.stl', XB=3.35,3.45,3.35,3.45,2.85,2.9, RGB=153,153,153, TRANSPARENCY=0.392157, THICKEN=.TRUE., SURF_ID='steel'/ &OBST ID='FD.stl', XB=3.4,3.45,2.3,3.35,2.7,2.9, RGB=153,153,153, TRANSPARENCY=0.392157, THICKEN=.TRUE., SURF_ID='steel'/ &OBST ID='FD.stl', XB=3.4,3.5,3.35,3.4,0.15,2.7, RGB=153,153,153, TRANSPARENCY=0.392157, THICKEN=.TRUE., SURF_ID='steel'/

&OBST ID='FD.stl', XB=3.45,3.5,3.45,3.5,0.05,2.8, RGB=153,153,153, TRANSPARENCY=0.392157, THICKEN=.TRUE., SURF_ID='steel'/ &OBST ID='FD.stl', XB=3.45,3.5,2.3,3.35,2.7,2.85, RGB=153,153,153, TRANSPARENCY=0.392157, THICKEN=.TRUE., SURF_ID='steel'/ &OBST ID='FD.stl', XB=3.45,3.5,3.35,3.45,2.8,2.85, RGB=153,153,153, TRANSPARENCY=0.392157, THICKEN=.TRUE., SURF_ID='steel'/ &OBST ID='FD.stl', XB=3.5,3.55,3.35,3.4,0.15,2.65, RGB=153,153,153, TRANSPARENCY=0.392157, THICKEN=.TRUE., SURF_ID='steel'/ &OBST ID='FD.stl', XB=3.5,3.55,2.3,3.35,2.65,2.8, RGB=153,153,153, TRANSPARENCY=0.392157, THICKEN=.TRUE., SURF_ID='steel'/ &OBST ID='FD.stl', XB=3.5,3.6,3.45,3.5,0.05,2.75, RGB=153,153,153, TRANSPARENCY=0.392157, THICKEN=.TRUE., SURF_ID='steel'/ &OBST ID='FD.stl', XB=3.5,3.6,3.35,3.45,2.75,2.8, RGB=153,153,153, TRANSPARENCY=0.392157, THICKEN=.TRUE., SURF_ID='steel'/ &OBST ID='FD.stl', XB=3.55,3.6,3.35,3.4,0.15,2.6, RGB=153,153,153, TRANSPARENCY=0.392157, THICKEN=.TRUE., SURF_ID='steel'/ &OBST ID='FD.stl', XB=3.55,3.6,2.3,3.35,2.6,2.8, RGB=153,153,153, TRANSPARENCY=0.392157, THICKEN=.TRUE., SURF_ID='steel'/ &OBST ID='FD.stl', XB=3.6,3.65,3.45,3.5,0.05,2.7, RGB=153,153,153, TRANSPARENCY=0.392157, THICKEN=.TRUE., SURF_ID='steel'/ &OBST ID='FD.stl', XB=3.6,3.65,3.35,3.4,0.15,2.55, RGB=153,153,153, TRANSPARENCY=0.392157, THICKEN=.TRUE., SURF_ID='steel'/ &OBST ID='FD.stl', XB=3.6,3.65,2.3,3.35,2.55,2.75, RGB=153,153,153, TRANSPARENCY=0.392157, THICKEN=.TRUE., SURF_ID='steel'/ &OBST ID='FD.stl', XB=3.6,3.65,3.35,3.45,2.7,2.75, RGB=153,153,153, TRANSPARENCY=0.392157, THICKEN=.TRUE., SURF_ID='steel'/ &OBST ID='FD.stl', XB=3.65,3.7,3.45,3.5,0.05,2.65, RGB=153,153,153, TRANSPARENCY=0.392157, THICKEN=.TRUE., SURF_ID='steel'/ &OBST ID='FD.stl', XB=3.65,3.7,3.35,3.4,0.15,2.5, RGB=153,153,153, TRANSPARENCY=0.392157, THICKEN=.TRUE., SURF_ID='steel'/ &OBST ID='FD.stl', XB=3.65,3.7,2.3,3.35,2.5,2.7, RGB=153,153,153, TRANSPARENCY=0.392157, THICKEN=.TRUE., SURF_ID='steel'/ &OBST ID='FD.stl', XB=3.65,3.7,3.35,3.45,2.65,2.7, RGB=153,153,153, TRANSPARENCY=0.392157, THICKEN=.TRUE., SURF_ID='steel'/ &OBST ID='FD.stl', XB=3.7,3.75,3.45,3.5,0.05,2.6, RGB=153,153,153, TRANSPARENCY=0.392157, THICKEN=.TRUE., SURF_ID='steel'/ &OBST ID='FD.stl', XB=3.7,3.75,3.35,3.4,0.15,2.45, RGB=153,153,153, TRANSPARENCY=0.392157, THICKEN=.TRUE., SURF_ID='steel'/ &OBST ID='FD.stl', XB=3.7,3.75,2.3,3.35,2.45,2.65, RGB=153,153,153, TRANSPARENCY=0.392157, THICKEN=.TRUE., SURF_ID='steel'/ &OBST ID='FD.stl', XB=3.7,3.75,3.35,3.45,2.6,2.65, RGB=153,153,153, TRANSPARENCY=0.392157, THICKEN=.TRUE., SURF_ID='steel'/ &OBST ID='FD.stl', XB=3.75,3.8,3.45,3.5,0.05,2.55, RGB=153,153,153, TRANSPARENCY=0.392157, THICKEN=.TRUE., SURF_ID='steel'/ &OBST ID='FD.stl', XB=3.75,3.8,3.35,3.4,0.15,2.4, RGB=153,153,153, TRANSPARENCY=0.392157, THICKEN=.TRUE., SURF_ID='steel'/ &OBST ID='FD.stl', XB=3.75,3.8,2.3,3.35,2.4,2.6, RGB=153,153,153, TRANSPARENCY=0.392157, THICKEN=.TRUE., SURF_ID='steel'/ &OBST ID='FD.stl', XB=3.75,3.8,3.35,3.45,2.5,2.6, RGB=153,153,153, TRANSPARENCY=0.392157, THICKEN=.TRUE., SURF_ID='steel'/ &OBST ID='FD.stl', XB=3.8,3.85,3.45,3.5,0.05,2.5, RGB=153,153,153, TRANSPARENCY=0.392157, THICKEN=.TRUE., SURF_ID='steel'/

&OBST ID='FD.stl', XB=3.8,3.85,3.35,3.4,0.15,2.35, RGB=153,153,153, TRANSPARENCY=0.392157, THICKEN=.TRUE., SURF_ID='steel'/ &OBST ID='FD.stl', XB=3.8,3.85,2.3,3.35,2.35,2.55, RGB=153,153,153, TRANSPARENCY=0.392157, THICKEN=.TRUE., SURF_ID='steel'/ &OBST ID='FD.stl', XB=3.8,3.85,3.35,3.45,2.45,2.55, RGB=153,153,153, TRANSPARENCY=0.392157, THICKEN=.TRUE., SURF_ID='steel'/ &OBST ID='FD.stl', XB=3.85,3.9,3.45,3.5,0.05,2.45, RGB=153,153,153, TRANSPARENCY=0.392157, THICKEN=.TRUE., SURF_ID='steel'/ &OBST ID='FD.stl', XB=3.85,3.9,3.35,3.4,0.15,2.3, RGB=153,153,153, TRANSPARENCY=0.392157, THICKEN=.TRUE., SURF_ID='steel'/ &OBST ID='FD.stl', XB=3.85,3.9,2.3,3.35,2.3,2.5, RGB=153,153,153, TRANSPARENCY=0.392157, THICKEN=.TRUE., SURF_ID='steel'/ &OBST ID='FD.stl', XB=3.85,3.9,3.35,3.45,2.4,2.5, RGB=153,153,153, TRANSPARENCY=0.392157, THICKEN=.TRUE., SURF_ID='steel'/ &OBST ID='FD.stl', XB=3.9,3.95,3.45,3.5,0.05,2.4, RGB=153,153,153, TRANSPARENCY=0.392157, THICKEN=.TRUE., SURF_ID='steel'/ &OBST ID='FD.stl', XB=3.9,3.95,3.35,3.4,0.15,2.25, RGB=153,153,153, TRANSPARENCY=0.392157, THICKEN=.TRUE., SURF_ID='steel'/ &OBST ID='FD.stl', XB=3.9,3.95,2.3,3.35,2.25,2.45, RGB=153,153,153, TRANSPARENCY=0.392157, THICKEN=.TRUE., SURF_ID='steel'/ &OBST ID='FD.stl', XB=3.9,3.95,3.35,3.45,2.35,2.45, RGB=153,153,153, TRANSPARENCY=0.392157, THICKEN=.TRUE., SURF_ID='steel'/ &OBST ID='FD.stl', XB=3.95,4.0,3.45,3.5,0.05,2.35, RGB=153,153,153, TRANSPARENCY=0.392157, THICKEN=.TRUE., SURF_ID='steel'/ &OBST ID='FD.stl', XB=3.95,4.0,3.35,3.4,0.15,2.15, RGB=153,153,153, TRANSPARENCY=0.392157, THICKEN=.TRUE., SURF_ID='steel'/ &OBST ID='FD.stl', XB=3.95,4.0,2.3,3.35,2.15,2.4, RGB=153,153,153, TRANSPARENCY=0.392157, THICKEN=.TRUE., SURF_ID='steel'/ &OBST ID='FD.stl', XB=3.95,4.0,3.35,3.45,2.25,2.4, RGB=153,153,153, TRANSPARENCY=0.392157, THICKEN=.TRUE., SURF_ID='steel'/ &OBST ID='FD.stl', XB=4.0,4.05,3.45,3.5,0.05,2.25, RGB=153,153,153, TRANSPARENCY=0.392157, THICKEN=.TRUE., SURF_ID='steel'/ &OBST ID='FD.stl', XB=4.0,4.05,3.35,3.4,0.15,2.1, RGB=153,153,153, TRANSPARENCY=0.392157, THICKEN=.TRUE., SURF_ID='steel'/ &OBST ID='FD.stl', XB=4.0,4.05,2.3,3.35,2.1,2.35, RGB=153,153,153, TRANSPARENCY=0.392157, THICKEN=.TRUE., SURF_ID='steel'/ &OBST ID='FD.stl', XB=4.0,4.05,3.35,3.45,2.25,2.35, RGB=153,153,153, TRANSPARENCY=0.392157, THICKEN=.TRUE., SURF_ID='steel'/ &OBST ID='FD.stl', XB=4.05,4.1,3.45,3.5,0.05,2.2, RGB=153,153,153, TRANSPARENCY=0.392157, THICKEN=.TRUE., SURF_ID='steel'/ &OBST ID='FD.stl', XB=4.05,4.1,3.35,3.4,0.15,2.0, RGB=153,153,153, TRANSPARENCY=0.392157, THICKEN=.TRUE., SURF_ID='steel'/ &OBST ID='FD.stl', XB=4.05,4.1,2.3,3.35,2.0,2.25, RGB=153,153,153, TRANSPARENCY=0.392157, THICKEN=.TRUE., SURF_ID='steel'/ &OBST ID='FD.stl', XB=4.05,4.1,3.35,3.45,2.1,2.25, RGB=153,153,153, TRANSPARENCY=0.392157, THICKEN=.TRUE., SURF_ID='steel'/ &OBST ID='FD.stl', XB=4.1,4.15,3.45,3.5,0.05,2.1, RGB=153,153,153, TRANSPARENCY=0.392157, THICKEN=.TRUE., SURF_ID='steel'/ &OBST ID='FD.stl', XB=4.1,4.15,3.35,3.4,0.15,1.9, RGB=153,153,153, TRANSPARENCY=0.392157, THICKEN=.TRUE., SURF_ID='steel'/ &OBST ID='FD.stl', XB=4.1,4.15,2.3,3.35,1.9,2.0, RGB=153,153,153, TRANSPARENCY=0.392157, THICKEN=.TRUE., SURF_ID='steel'/

&OBST ID='FD.stl', XB=4.1,4.15,2.3,3.45,2.1,2.2, RGB=153,153,153, TRANSPARENCY=0.392157, THICKEN=.TRUE., SURF_ID='steel'/ &OBST ID='FD.stl', XB=4.15,4.2,3.45,3.5,0.05,2.05, RGB=153,153,153, TRANSPARENCY=0.392157, THICKEN=.TRUE., SURF_ID='steel'/ &OBST ID='FD.stl', XB=4.15,4.2,2.3,3.35,0.15,0.25, RGB=153,153,153, TRANSPARENCY=0.392157, THICKEN=.TRUE., SURF_ID='steel'/ &OBST ID='FD.stl', XB=4.15,4.2,3.35,3.4,0.2,1.8, RGB=153,153,153, TRANSPARENCY=0.392157, THICKEN=.TRUE., SURF_ID='steel'/ &OBST ID='FD.stl', XB=4.15,4.2,2.8,3.35,1.75,1.9, RGB=153,153,153, TRANSPARENCY=0.392157, THICKEN=.TRUE., SURF_ID='steel'/ &OBST ID='FD.stl', XB=4.15,4.2,2.3,2.8,1.8,1.9, RGB=153,153,153, TRANSPARENCY=0.392157, THICKEN=.TRUE., SURF_ID='steel'/ &OBST ID='FD.stl', XB=4.15,4.2,2.3,3.45,2.0,2.1, RGB=153,153,153, TRANSPARENCY=0.392157, THICKEN=.TRUE., SURF_ID='steel'/ &OBST ID='FD.stl', XB=4.2,4.25,2.3,3.45,0.0,0.1, RGB=153,153,153, TRANSPARENCY=0.392157, THICKEN=.TRUE., SURF_ID='steel'/ &OBST ID='FD.stl', XB=4.2,4.25,3.45,3.5,0.05,1.95, RGB=153,153,153, TRANSPARENCY=0.392157, THICKEN=.TRUE., SURF_ID='steel'/ &OBST ID='FD.stl', XB=4.2,4.25,2.3,3.35,0.25,0.35, RGB=153,153,153, TRANSPARENCY=0.392157, THICKEN=.TRUE., SURF_ID='steel'/ &OBST ID='FD.stl', XB=4.2,4.25,3.35,3.4,0.3,1.7, RGB=153,153,153, TRANSPARENCY=0.392157, THICKEN=.TRUE., SURF_ID='steel'/ &OBST ID='FD.stl', XB=4.2,4.25,2.8,3.35,1.65,1.75, RGB=153,153,153, TRANSPARENCY=0.392157, THICKEN=.TRUE., SURF_ID='steel'/ &OBST ID='FD.stl', XB=4.2,4.25,2.3,2.8,1.65,1.8, RGB=153,153,153, TRANSPARENCY=0.392157, THICKEN=.TRUE., SURF_ID='steel'/ &OBST ID='FD.stl', XB=4.2,4.25,2.3,3.45,1.9,2.0, RGB=153,153,153, TRANSPARENCY=0.392157, THICKEN=.TRUE., SURF_ID='steel'/ &OBST ID='FD.stl', XB=4.25,4.3,2.3,3.45,0.1,0.2, RGB=153,153,153, TRANSPARENCY=0.392157, THICKEN=.TRUE., SURF_ID='steel'/ &OBST ID='FD.stl', XB=4.25,4.3,3.45,3.5,0.2,1.8, RGB=153,153,153, TRANSPARENCY=0.392157, THICKEN=.TRUE., SURF_ID='steel'/ &OBST ID='FD.stl', XB=4.25,4.3,2.3,3.35,0.35,0.55, RGB=153,153,153, TRANSPARENCY=0.392157, THICKEN=.TRUE., SURF_ID='steel'/ &OBST ID='FD.stl', XB=4.25,4.3,3.35,3.4,0.45,1.5, RGB=153,153,153, TRANSPARENCY=0.392157, THICKEN=.TRUE., SURF_ID='steel'/ &OBST ID='FD.stl', XB=4.25,4.3,2.3,3.35,1.45,1.65, RGB=153,153,153, TRANSPARENCY=0.392157, THICKEN=.TRUE., SURF_ID='steel'/ &OBST ID='FD.stl', XB=4.25,4.3,2.3,3.45,1.8,1.9, RGB=153,153,153, TRANSPARENCY=0.392157, THICKEN=.TRUE., SURF_ID='steel'/ &OBST ID='FD.stl', XB=4.3,4.35,2.3,3.45,0.2,0.35, RGB=153,153,153, TRANSPARENCY=0.392157, THICKEN=.TRUE., SURF_ID='steel'/ &OBST ID='FD.stl', XB=4.3,4.35,3.45,3.5,0.3,1.7, RGB=153,153,153, TRANSPARENCY=0.392157, THICKEN=.TRUE., SURF_ID='steel'/ &OBST ID='FD.stl', XB=4.3,4.35,2.3,3.35,0.55,0.85, RGB=153,153,153, TRANSPARENCY=0.392157, THICKEN=.TRUE., SURF_ID='steel'/ &OBST ID='FD.stl', XB=4.3,4.35,3.35,3.4,0.7,1.3, RGB=153,153,153, TRANSPARENCY=0.392157, THICKEN=.TRUE., SURF_ID='steel'/ &OBST ID='FD.stl', XB=4.3,4.35,2.4,3.35,0.95,1.45, RGB=153,153,153, TRANSPARENCY=0.392157, THICKEN=.TRUE., SURF_ID='steel'/ &OBST ID='FD.stl', XB=4.3,4.35,2.3,2.4,0.95,1.8, RGB=153,153,153, TRANSPARENCY=0.392157, THICKEN=.TRUE., SURF_ID='steel'/

&OBST ID='FD.stl', XB=4.3,4.35,2.4,3.45,1.65,1.8, RGB=153,153,153, TRANSPARENCY=0.392157, THICKEN=.TRUE., SURF_ID='steel'/ &OBST ID='FD.stl', XB=4.35,4.4,2.3,3.45,0.35,0.55, RGB=153,153,153, TRANSPARENCY=0.392157, THICKEN=.TRUE., SURF_ID='steel'/ &OBST ID='FD.stl', XB=4.35,4.4,3.45,3.5,0.45,1.55, RGB=153,153,153, TRANSPARENCY=0.392157, THICKEN=.TRUE., SURF_ID='steel'/ &OBST ID='FD.stl', XB=4.35,4.4,2.3,3.35,0.85,0.95, RGB=153,153,153, TRANSPARENCY=0.392157, THICKEN=.TRUE., SURF_ID='steel'/ &OBST ID='FD.stl', XB=4.35.4.4.2.4.3.45.1.45.1.65, RGB=153.153.153. TRANSPARENCY=0.392157, THICKEN=.TRUE., SURF_ID='steel'/ &OBST ID='FD.stl', XB=4.35,4.4,2.3,2.4,1.45,1.7, RGB=153,153,153, TRANSPARENCY=0.392157, THICKEN=.TRUE., SURF_ID='steel'/ &OBST ID='FD.stl', XB=4.4,4.45,2.3,2.6,0.55,0.85, RGB=153,153,153, TRANSPARENCY=0.392157, THICKEN=.TRUE., SURF_ID='steel'/ &OBST ID='FD.stl', XB=4.4,4.45,2.6,3.45,0.55,1.45, RGB=153,153,153, TRANSPARENCY=0.392157, THICKEN=.TRUE., SURF_ID='steel'/ &OBST ID='FD.stl', XB=4.4,4.45,3.45,3.5,0.7,1.3, RGB=153,153,153, TRANSPARENCY=0.392157, THICKEN=.TRUE., SURF_ID='steel'/ &OBST ID='FD.stl', XB=4.4,4.45,2.3,2.6,0.9,1.45, RGB=153,153,153, TRANSPARENCY=0.392157, THICKEN=.TRUE., SURF_ID='steel'/ &OBST ID='FD.stl', XB=4.45,4.5,2.3,2.6,0.85,0.9, RGB=153,153,153, TRANSPARENCY=0.392157, THICKEN=.TRUE., SURF_ID='steel'/ &OBST ID='Obstruction', XB=1.8.2.7.1.3.2.2.0.45.0.65, RGB=255.0.51/ &OBST ID='leg', XB=2.0,2.05,1.4,1.45,0.0,0.6, RGB=255,0,51/ &OBST ID='leg', XB=2.0,2.05,1.9,1.95,0.0,0.6, RGB=255,0,51/ &OBST ID='leg', XB=2.45,2.5,1.4,1.45,0.0,0.6, RGB=255,0,51/ &OBST ID='leg', XB=2.45,2.5,1.9,1.95,0.0,0.6, RGB=255,0,51/

&VENT ID='Mesh Vent: MESH [XMAX]', SURF_ID='OPEN', XB=6.4,6.4,-1.55,4.65,0.0,6.0/ &VENT ID='Mesh Vent: MESH [XMIN]', SURF_ID='OPEN', XB=-1.8,-1.8,-1.55,4.65,0.0,6.0/ &VENT ID='Mesh Vent: MESH [YMAX]', SURF_ID='OPEN', XB=-1.8,6.4,4.65,4.65,0.0,6.0/ &VENT ID='Mesh Vent: MESH [YMIN]', SURF_ID='OPEN', XB=-1.8,6.4,-1.55,-1.55,0.0,6.0/ &VENT ID='Mesh Vent: MESH [ZMAX]', SURF_ID='OPEN', XB=-1.8,6.4,-1.55,4.65,6.0,6.0/ &VENT ID='fire', SURF_ID='Fire', XB=1.8,2.7,1.3,2.2,0.65,0.65/

&SLCF QUANTITY='TEMPERATURE', ID='Slice', PBY=0.65/
&SLCF QUANTITY='TEMPERATURE', ID='Slice01', PBY=1.75/
&SLCF QUANTITY='VOLUME FRACTION', SPEC_ID='OXYGEN', ID='Slice02', PBY=0.65/
&SLCF QUANTITY='VOLUME FRACTION', SPEC_ID='OXYGEN', ID='Slice03', PBY=1.75/
&SLCF QUANTITY='VELOCITY', VECTOR=.TRUE., ID='Slice04', PBY=0.65/
&SLCF QUANTITY='VELOCITY', VECTOR=.TRUE., ID='Slice05', PBY=1.75/
&SLCF QUANTITY='TEMPERATURE', ID='3D Slice', XB=-1.8,6.4,-1.55,4.65,0.0,6.0/
&SLCF QUANTITY='VELOCITY', VECTOR=.TRUE., ID='3D Slice', XB=-1.8,6.4,-1.55,4.65,0.0,6.0/
&SLCF QUANTITY='VOLUME FRACTION', SPEC_ID='OXYGEN', ID='3D Slice', XB=-1.8,6.4,-1.55,4.65,0.0,6.0/

```
Medium Scale fire test Curvilinear
```

Case_3_FD_Curvilinear_steel.fds Generated by PyroSim 2024.1.0702 Jan 16, 2025, 12:18:39 PM

&HEAD CHID='Case_3_FD_Curvilinear_steel'/
&TIME T_END=950.0/
&DUMP DT_RESTART=10.0, DT_SL3D=0.25/
&MISC TMPA=35.0/

&MESH ID='Mesh01-01-01', IJK=11,55,41, XB=-0.52,-0.3,-0.2,0.9,0.06,0.88/ &MESH ID='Mesh01-01-02', IJK=11,55,74, XB=-0.52,-0.3,-0.2,0.9,0.88,2.36/ &MESH ID='Mesh01-02-01', IJK=13,55,41, XB=-0.3,-0.04,-0.2,0.9,0.06,0.88/ &MESH ID='Mesh01-02-02', IJK=13,55,74, XB=-0.3,-0.04,-0.2,0.9,0.88,2.36/ &MESH ID='Mesh01-03-01', IJK=17,55,41, XB=-0.04,0.3,-0.2,0.9,0.06,0.88/ &MESH ID='Mesh01-03-02', IJK=17,55,74, XB=-0.04,0.3,-0.2,0.9,0.06,0.88/ &MESH ID='Mesh01-04-01', IJK=36,55,41, XB=0.3,1.02,-0.2,0.9,0.06,0.88/ &MESH ID='Mesh01-04-02', IJK=36,55,74, XB=0.3,1.02,-0.2,0.9,0.06,0.88/ &MESH ID='Mesh01-05-01', IJK=20,55,41, XB=1.02,1.42,-0.2,0.9,0.06,0.88/ &MESH ID='Mesh01-05-02', IJK=20,55,74, XB=1.02,1.42,-0.2,0.9,0.06,0.88/ &MESH ID='Mesh01-06-01', IJK=20,55,41, XB=1.42,1.82,-0.2,0.9,0.06,0.88/ &MESH ID='Mesh01-06-01', IJK=20,55,74, XB=1.42,1.82,-0.2,0.9,0.06,0.88/ &MESH ID='Mesh01-06-02', IJK=20,55,74, XB=1.42,1.82,-0.2,0.9,0.06,0.88/

&SPEC ID='N-HEPTANE'/
&SPEC ID='OXYGEN', LUMPED_COMPONENT_ONLY=.TRUE./

&REAC ID='FDS6 N-HEPTANE',

FYI='FDS6 Predefined',
FUEL='N-HEPTANE',
CO_YIELD=0.01,
SOOT_YIELD=0.037,
HEAT_OF_COMBUSTION=4.8059E+4,
RADIATIVE FRACTION=0.35/

&DEVC ID='1', QUANTITY='THERMOCOUPLE', XYZ=1.64,0.34,0.4/ &DEVC ID='2', QUANTITY='THERMOCOUPLE', XYZ=1.64,0.34,0.6/ &DEVC ID='3', OUANTITY='THERMOCOUPLE', XYZ=1.64.0.34.0.8/ &DEVC ID='4', QUANTITY='THERMOCOUPLE', XYZ=1.64,0.34,1.0/ &DEVC ID='5', QUANTITY='THERMOCOUPLE', XYZ=1.64,0.34,1.2/ &DEVC ID='6', QUANTITY='THERMOCOUPLE', XYZ=1.64,0.34,1.4/ &DEVC ID='7', QUANTITY='THERMOCOUPLE', XYZ=1.64,0.34,1.6/ &DEVC ID='101', QUANTITY='THERMOCOUPLE', XYZ=1.5,0.34,0.4/ &DEVC ID='201', QUANTITY='THERMOCOUPLE', XYZ=1.5,0.34,0.6/ &DEVC ID='301', QUANTITY='THERMOCOUPLE', XYZ=1.5,0.34,0.8/ &DEVC ID='401', QUANTITY='THERMOCOUPLE', XYZ=1.5,0.34,1.0/ &DEVC ID='501', QUANTITY='THERMOCOUPLE', XYZ=1.5,0.34,1.2/ &DEVC ID='601', QUANTITY='THERMOCOUPLE', XYZ=1.5,0.34,1.4/ &DEVC ID='701', QUANTITY='THERMOCOUPLE', XYZ=1.5,0.34,1.6/ &DEVC ID='Temperature Center Door 1', QUANTITY='THERMOCOUPLE', XYZ=1.34,0.34,0.4/ &DEVC ID='Velocity Center Door 1', QUANTITY='VELOCITY', XYZ=1.34,0.34,0.4/

```
&DEVC ID='T01', QUANTITY='THERMOCOUPLE', XYZ=-0.3,0.34,0.4/
&DEVC ID='T02', QUANTITY='THERMOCOUPLE', XYZ=-0.3,0.34,0.6/
&DEVC ID='T03', QUANTITY='THERMOCOUPLE', XYZ=-0.3,0.34,0.8/
&DEVC ID='T04', QUANTITY='THERMOCOUPLE', XYZ=-0.3,0.34,1.0/
&DEVC ID='T05', QUANTITY='THERMOCOUPLE', XYZ=-0.3,0.34,1.2/
&DEVC ID='T06', QUANTITY='THERMOCOUPLE', XYZ=-0.3,0.34,1.4/
&DEVC ID='T07', OUANTITY='THERMOCOUPLE', XYZ=-0.3.0.34.1.6/
&DEVC ID='FD 101', QUANTITY='THERMOCOUPLE', XYZ=-0.16,0.34,0.4/
&DEVC ID='FD 102', QUANTITY='THERMOCOUPLE', XYZ=-0.16,0.34,0.6/
&DEVC ID='FD 103', QUANTITY='THERMOCOUPLE', XYZ=-0.16,0.34,0.8/
&DEVC ID='FD 104', QUANTITY='THERMOCOUPLE', XYZ=-0.16,0.34,1.0/
&DEVC ID='FD 105', QUANTITY='THERMOCOUPLE', XYZ=-0.16,0.34,1.2/
&DEVC ID='FD 106', QUANTITY='THERMOCOUPLE', XYZ=-0.16,0.34,1.4/
&DEVC ID='FD 107', QUANTITY='THERMOCOUPLE', XYZ=-0.16,0.34,1.6/
&DEVC ID='Temperature Center Door 2 FD', QUANTITY='THERMOCOUPLE',
XYZ=6.175616E-16,0.34,0.4/
&DEVC ID='Velocity Center Door 2 FD', QUANTITY='VELOCITY', XYZ=6.175616E-
16.0.34.0.4/
&DEVC ID='Com. Temperature', QUANTITY='THERMOCOUPLE', XYZ=0.66,0.5,0.7/
&DEVC ID='Wall_temp_1', QUANTITY='WALL TEMPERATURE', XYZ=0.68,0.34,0.82, IOR=-
&DEVC ID='Wall temp_left', QUANTITY='WALL TEMPERATURE', XYZ=0.5,0.34,0.78,
&DEVC ID='Wall_temp_right', QUANTITY='WALL TEMPERATURE', XYZ=0.86,0.34,0.78,
IOR=-3/
&DEVC ID='inside_wall_temp_1_0.001', DEPTH=1.0E-3, QUANTITY='INSIDE WALL
TEMPERATURE', XYZ=0.68,0.34,0.82, IOR=-3/
&DEVC ID='inside_wall_temp_1_0.002', DEPTH=2.0E-3, QUANTITY='INSIDE WALL
TEMPERATURE', XYZ=0.68,0.34,0.82, IOR=-3/
&DEVC ID='inside wall temp 1 0.003', DEPTH=3.0E-3, QUANTITY='INSIDE WALL
TEMPERATURE', XYZ=0.68,0.34,0.82, IOR=-3/
&DEVC ID='inside_wall_temp_left_0.001', DEPTH=1.0E-3, QUANTITY='INSIDE WALL
TEMPERATURE', XYZ=0.5,0.34,0.78, IOR=-3/
&DEVC ID='inside_wall_temp_left_0.002', DEPTH=2.0E-3, QUANTITY='INSIDE WALL
TEMPERATURE', XYZ=0.5,0.34,0,78, IOR=-3/
&DEVC ID='inside_wall_temp_left_0.003', DEPTH=3.0E-3, QUANTITY='INSIDE WALL
TEMPERATURE', XYZ=0.5,0.34,0.78, IOR=-3/
&DEVC ID='inside wall temp_right_0.001', DEPTH=1.0E-3, QUANTITY='INSIDE WALL
TEMPERATURE', XYZ=0.86,0.34,0.78, IOR=-3/
&DEVC ID='inside_wall_temp_right_0.002', DEPTH=2.0E-3, QUANTITY='INSIDE WALL
TEMPERATURE', XYZ=0.86,0.34,0.78, IOR=-3/
&DEVC ID='inside_wall_temp_right_0.003', DEPTH=3.0E-3, QUANTITY='INSIDE WALL
TEMPERATURE', XYZ=0.86,0.34,0.78, IOR=-3/
&MATL ID='STEEL',
  FYI='Drysdale, Intro to Fire Dynamics - ATF NIST Multi-Floor Validation',
  SPECIFIC_HEAT=0.46,
  CONDUCTIVITY=45.8,
  DENSITY=7850.0.
```

EMISSIVITY=0.95/

&DEVC ID='Heat Flux Door 1', QUANTITY='GAUGE HEAT FLUX', XYZ=0.22,0.34,0.66,

```
&SURF ID='Wall',
  RGB=146,202,166,
  TMP_INNER=35.0,
  MATL ID(1,1)='STEEL',
  MATL_MASS_FRACTION(1,1)=1.0,
  THICKNESS(1)=3.0E-3/
&SURF ID='Burner',
  COLOR='RED'.
  HRRPUA=3125.0,
  RAMP_Q='Burner_RAMP_Q',
  TMP_FRONT=300.0/
&RAMP ID='Burner_RAMP_Q', T=0.0, F=0.0/
&RAMP ID='Burner_RAMP_Q', T=50.0, F=0.136054/
&RAMP ID='Burner_RAMP_Q', T=100.0, F=0.151578/
&RAMP ID='Burner_RAMP_Q', T=150.0, F=0.172382/
&RAMP ID='Burner_RAMP_Q', T=200.0, F=0.183673/
&RAMP ID='Burner_RAMP_Q', T=250.0, F=0.190476/
&RAMP ID='Burner_RAMP_Q', T=300.0, F=0.190215/
&RAMP ID='Burner_RAMP_Q', T=350.0, F=0.190476/
&RAMP ID='Burner_RAMP_Q', T=400.0, F=0.205076/
&RAMP ID='Burner_RAMP_Q', T=450.0, F=0.240741/
&RAMP ID='Burner_RAMP_Q', T=500.0, F=0.383402/
&RAMP ID='Burner_RAMP_Q', T=550.0, F=0.70068/
&RAMP ID='Burner_RAMP_Q', T=600.0, F=1.0/
&RAMP ID='Burner_RAMP_Q', T=630.0, F=0.959184/
&RAMP ID='Burner_RAMP_Q', T=650.0, F=0.47619/
&RAMP ID='Burner_RAMP_Q', T=700.0, F=0.421769/
&RAMP ID='Burner_RAMP_Q', T=720.0, F=0.244898/
&RAMP ID='Burner_RAMP_Q', T=750.0, F=0.238095/
&RAMP ID='Burner_RAMP_Q', T=800.0, F=0.068027/
&OBST ID='AcDb3dSolid - 2C0', XB=0.04,0.06,-2.081668E-17,0.2,0.1,0.36,
RGB=102,51,0, TRANSPARENCY=0.686275, SURF_ID='Wall'/
&OBST ID='AcDb3dSolid - 2C0', XB=0.04,0.06,0.5,0.7,0.1,0.36, RGB=102,51,0,
TRANSPARENCY=0.686275, SURF_ID='Wall'/
&OBST ID='AcDb3dSolid - 2C0', XB=0.04,0.3,0.2,0.5,0.1,0.16, RGB=102,51,0,
TRANSPARENCY=0.686275, SURF_ID='Wall'/
&OBST ID='AcDb3dSolid - 2C0', XB=0.06,0.08,-2.081668E-17,0.18,0.1,0.42,
RGB=102,51,0, TRANSPARENCY=0.686275, SURF_ID='Wall'/
&OBST ID='AcDb3dSolid - 2C0', XB=0.06,0.08,0.52,0.7,0.1,0.42, RGB=102,51,0,
TRANSPARENCY=0.686275, SURF_ID='Wall'/
&OBST ID='AcDb3dSolid - 2C0', XB=0.06,0.08,0.18,0.2,0.1,0.44, RGB=102,51,0,
TRANSPARENCY=0.686275, SURF_ID='Wall'/
&OBST ID='AcDb3dSolid - 2C0', XB=0.06,0.08,0.5,0.52,0.1,0.44, RGB=102,51,0,
TRANSPARENCY=0.686275, SURF_ID='Wall'/
&OBST ID='AcDb3dSolid - 2C0', XB=0.08,0.1,-2.081668E-17,0.06,0.1,0.48,
RGB=102,51,0, TRANSPARENCY=0.686275, SURF_ID='Wall'/
&OBST ID='AcDb3dSolid - 2C0', XB=0.08,0.1,0.66,0.7,0.1,0.48, RGB=102,51,0,
TRANSPARENCY=0.686275, SURF_ID='Wall'/
&OBST ID='AcDb3dSolid - 2C0', XB=0.08,0.1,0.06,0.2,0.3,0.48, RGB=102,51,0,
TRANSPARENCY=0.686275, SURF_ID='Wall'/
```

```
&OBST ID='AcDb3dSolid - 2C0', XB=0.08,0.1,0.5,0.52,0.3,0.48, RGB=102,51,0,
TRANSPARENCY=0.686275, SURF_ID='Wall'/
&OBST ID='AcDb3dSolid - 2C0', XB=0.08,0.1,0.52,0.66,0.32,0.48, RGB=102,51,0,
TRANSPARENCY=0.686275, SURF_ID='Wall'/
&OBST ID='AcDb3dSolid - 2C0', XB=0.08,0.3,0.06,0.2,0.1,0.16, RGB=102,51,0,
TRANSPARENCY=0.686275, SURF_ID='Wall'/
&OBST ID='AcDb3dSolid - 2C0', XB=0.08,0.3,0.5,0.66,0.1,0.16, RGB=102,51,0,
TRANSPARENCY=0.686275, SURF_ID='Wall'/
&OBST ID='AcDb3dSolid - 2C0', XB=0.1,0.12,-2.081668E-17,0.06,0.1,0.52,
RGB=102,51,0, TRANSPARENCY=0.686275, SURF_ID='Wall'/
&OBST ID='AcDb3dSolid - 2C0', XB=0.1,0.12,0.66,0.7,0.1,0.52, RGB=102,51,0,
TRANSPARENCY=0.686275, SURF_ID='Wall'/
&OBST ID='AcDb3dSolid - 2C0', XB=0.1,0.12,0.06,0.2,0.38,0.52, RGB=102,51,0,
TRANSPARENCY=0.686275, SURF ID='Wall'/
&OBST ID='AcDb3dSolid - 2C0', XB=0.1,0.12,0.5,0.66,0.38,0.52, RGB=102,51,0,
TRANSPARENCY=0.686275, SURF_ID='Wall'/
&OBST ID='AcDb3dSolid - 2C0', XB=0.12,0.14,-2.081668E-17,0.06,0.1,0.56,
RGB=102,51,0, TRANSPARENCY=0.686275, SURF_ID='Wall'/
&OBST ID='AcDb3dSolid - 2C0', XB=0.12,0.14,0.66,0.7,0.1,0.56, RGB=102,51,0,
TRANSPARENCY=0.686275, SURF_ID='Wall'/
&OBST ID='AcDb3dSolid - 2C0', XB=0.12,0.14,0.06,0.2,0.44,0.56, RGB=102,51,0,
TRANSPARENCY=0.686275, SURF_ID='Wall'/
&OBST ID='AcDb3dSolid - 2C0', XB=0.12,0.14,0.5,0.66,0.44,0.56, RGB=102,51,0,
TRANSPARENCY=0.686275, SURF_ID='Wall'/
&OBST ID='AcDb3dSolid - 2C0', XB=0.14,0.16,-2.081668E-17,0.06,0.1,0.58,
RGB=102,51,0, TRANSPARENCY=0.686275, SURF_ID='Wall'/
&OBST ID='AcDb3dSolid - 2C0', XB=0.14,0.16,0.66,0.7,0.1,0.58, RGB=102,51,0,
TRANSPARENCY=0.686275, SURF_ID='Wall'/
&OBST ID='AcDb3dSolid - 2C0', XB=0.14,0.16,0.06,0.2,0.48,0.58, RGB=102,51,0,
TRANSPARENCY=0.686275, SURF_ID='Wall'/
&OBST ID='AcDb3dSolid - 2C0', XB=0.14,0.16,0.5,0.66,0.48,0.58, RGB=102,51,0,
TRANSPARENCY=0.686275, SURF_ID='Wall'/
&OBST ID='AcDb3dSolid - 2C0', XB=0.16,0.18,-2.081668E-17,0.06,0.1,0.6,
RGB=102,51,0, TRANSPARENCY=0.686275, SURF_ID='Wall'/
&OBST ID='AcDb3dSolid - 2C0', XB=0.16,0.18,0.66,0.7,0.1,0.6, RGB=102,51,0,
TRANSPARENCY=0.686275, SURF_ID='Wall'/
&OBST ID='AcDb3dSolid - 2C0', XB=0.16,0.18,0.06,0.2,0.52,0.6, RGB=102,51,0,
TRANSPARENCY=0.686275, SURF_ID='Wall'/
&OBST ID='AcDb3dSolid - 2C0', XB=0.16,0.18,0.5,0.66,0.52,0.6, RGB=102,51,0,
TRANSPARENCY=0.686275, SURF_ID='Wall'/
&OBST ID='AcDb3dSolid - 2C0', XB=0.18,0.2,-2.081668E-17,0.06,0.1,0.64,
RGB=102,51,0, TRANSPARENCY=0.686275, SURF_ID='Wall'/
&OBST ID='AcDb3dSolid - 2C0', XB=0.18,0.2,0.66,0.7,0.1,0.64, RGB=102,51,0,
TRANSPARENCY=0.686275, SURF_ID='Wall'/
&OBST ID='AcDb3dSolid - 2C0', XB=0.18,0.2,0.6,0.66,0.54,0.64, RGB=102,51,0,
TRANSPARENCY=0.686275, SURF_ID='Wall'/
&OBST ID='AcDb3dSolid - 2C0', XB=0.18,0.2,0.06,0.2,0.56,0.64, RGB=102,51,0,
TRANSPARENCY=0.686275, SURF_ID='Wall'/
&OBST ID='AcDb3dSolid - 2C0', XB=0.18,0.2,0.5,0.6,0.56,0.64, RGB=102,51,0,
TRANSPARENCY=0.686275, SURF_ID='Wall'/
&OBST ID='AcDb3dSolid - 2C0', XB=0.2,0.22,-2.081668E-17,0.06,0.1,0.66,
RGB=102,51,0, TRANSPARENCY=0.686275, SURF_ID='Wall'/
```

```
&OBST ID='AcDb3dSolid - 2C0', XB=0.2,0.22,0.66,0.7,0.1,0.66, RGB=102,51,0,
TRANSPARENCY=0.686275, SURF_ID='Wall'/
&OBST ID='AcDb3dSolid - 2C0', XB=0.2,0.22,0.06,0.2,0.58,0.66, RGB=102,51,0,
TRANSPARENCY=0.686275, SURF_ID='Wall'/
&OBST ID='AcDb3dSolid - 2C0', XB=0.2,0.22,0.5,0.66,0.58,0.66, RGB=102,51,0,
TRANSPARENCY=0.686275, SURF_ID='Wall'/
&OBST ID='AcDb3dSolid - 2C0', XB=0.2,0.22,0.2,0.5,0.64,0.66, RGB=102,51,0,
TRANSPARENCY=0.686275, SURF_ID='Wall'/
&OBST ID='AcDb3dSolid - 2C0', XB=0.22,0.24,-2.081668E-17,0.06,0.1,0.68,
RGB=102,51,0, TRANSPARENCY=0.686275, SURF_ID='Wall'/
&OBST ID='AcDb3dSolid - 2C0', XB=0.22,0.24,0.66,0.7,0.1,0.68, RGB=102,51,0,
TRANSPARENCY=0.686275, SURF_ID='Wall'/
&OBST ID='AcDb3dSolid - 2C0', XB=0.22,0.24,0.06,0.2,0.6,0.68, RGB=102,51,0,
TRANSPARENCY=0.686275, SURF ID='Wall'/
&OBST ID='AcDb3dSolid - 2C0', XB=0.22,0.24,0.5,0.66,0.6,0.68, RGB=102,51,0,
TRANSPARENCY=0.686275, SURF_ID='Wall'/
&OBST ID='AcDb3dSolid - 2C0', XB=0.22,0.24,0.2,0.5,0.66,0.68, RGB=102,51,0,
TRANSPARENCY=0.686275, SURF_ID='Wall'/
&OBST ID='AcDb3dSolid - 2C0', XB=0.24,0.26,-2.081668E-17,0.06,0.1,0.7,
RGB=102,51,0, TRANSPARENCY=0.686275, SURF_ID='Wall'/
&OBST ID='AcDb3dSolid - 2C0', XB=0.24,0.26,0.66,0.7,0.1,0.7, RGB=102,51,0,
TRANSPARENCY=0.686275, SURF_ID='Wall'/
&OBST ID='AcDb3dSolid - 2C0', XB=0.24,0.26,0.06,0.2,0.62,0.7, RGB=102,51,0,
TRANSPARENCY=0.686275, SURF_ID='Wall'/
&OBST ID='AcDb3dSolid - 2C0', XB=0.24,0.26,0.5,0.66,0.62,0.7, RGB=102,51,0,
TRANSPARENCY=0.686275, SURF_ID='Wall'/
&OBST ID='AcDb3dSolid - 2C0', XB=0.24,0.26,0.2,0.5,0.66,0.7, RGB=102,51,0,
TRANSPARENCY=0.686275, SURF_ID='Wall'/
&OBST ID='AcDb3dSolid - 2C0', XB=0.26,0.28,0.06,0.2,0.64,0.72, RGB=102,51,0,
TRANSPARENCY=0.686275, SURF_ID='Wall'/
&OBST ID='AcDb3dSolid - 2C0', XB=0.26,0.28,0.5,0.66,0.64,0.72, RGB=102,51,0,
TRANSPARENCY=0.686275, SURF_ID='Wall'/
&OBST ID='AcDb3dSolid - 2C0', XB=0.26,0.3,-2.081668E-17,0.06,0.1,0.72,
RGB=102,51,0, TRANSPARENCY=0.686275, SURF_ID='Wall'/
&OBST ID='AcDb3dSolid - 2C0', XB=0.26,0.3,0.66,0.7,0.1,0.72, RGB=102,51,0,
TRANSPARENCY=0.686275, SURF_ID='Wall'/
&OBST ID='AcDb3dSolid - 2C0', XB=0.26,0.3,0.2,0.5,0.66,0.72, RGB=102,51,0,
TRANSPARENCY=0.686275, SURF_ID='Wall'/
&OBST ID='AcDb3dSolid - 2C0', XB=0.28,0.3,0.06,0.2,0.66,0.72, RGB=102,51,0,
TRANSPARENCY=0.686275, SURF_ID='Wall'/
&OBST ID='AcDb3dSolid - 2C0', XB=0.28,0.3,0.5,0.66,0.66,0.72, RGB=102,51,0,
TRANSPARENCY=0.686275, SURF_ID='Wall'/
&OBST ID='AcDb3dSolid - 2C0', XB=0.3,0.32,-2.081668E-17,0.06,0.1,0.74,
RGB=102,51,0, TRANSPARENCY=0.686275, SURF_ID='Wall'/
&OBST ID='AcDb3dSolid - 2C0', XB=0.3,0.32,0.66,0.7,0.1,0.74, RGB=102,51,0,
TRANSPARENCY=0.686275, SURF_ID='Wall'/
&OBST ID='AcDb3dSolid - 2C0', XB=0.3,0.32,0.06,0.66,0.68,0.74, RGB=102,51,0,
TRANSPARENCY=0.686275, SURF_ID='Wall'/
&OBST ID='AcDb3dSolid - 2C0', XB=0.3,1.02,0.06,0.66,0.1,0.16, RGB=102,51,0,
TRANSPARENCY=0.686275, SURF_ID='Wall'/
&OBST ID='AcDb3dSolid - 2C0', XB=0.32,0.36,-2.081668E-17,0.06,0.1,0.76,
RGB=102,51,0, TRANSPARENCY=0.686275, SURF_ID='Wall'/
```

```
&OBST ID='AcDb3dSolid - 2C0', XB=0.32,0.36,0.66,0.7,0.1,0.76, RGB=102,51,0,
TRANSPARENCY=0.686275, SURF_ID='Wall'/
&OBST ID='AcDb3dSolid - 2C0', XB=0.32,0.36,0.06,0.66,0.7,0.76, RGB=102,51,0,
TRANSPARENCY=0.686275, SURF_ID='Wall'/
&OBST ID='AcDb3dSolid - 2C0', XB=0.36,0.38,0.06,0.66,0.72,0.78, RGB=102,51,0,
TRANSPARENCY=0.686275, SURF_ID='Wall'/
&OBST ID='AcDb3dSolid - 2C0', XB=0.36,0.4,-2.081668E-17,0.06,0.1,0.78,
RGB=102,51,0, TRANSPARENCY=0.686275, SURF_ID='Wall'/
&OBST ID='AcDb3dSolid - 2C0', XB=0.36,0.4,0.66,0.7,0.1,0.78, RGB=102,51,0,
TRANSPARENCY=0.686275, SURF_ID='Wall'/
&OBST ID='AcDb3dSolid - 2C0', XB=0.38,0.4,0.06,0.66,0.74,0.78, RGB=102,51,0,
TRANSPARENCY=0.686275, SURF_ID='Wall'/
&OBST ID='AcDb3dSolid - 2C0', XB=0.4,0.42,0.06,0.66,0.74,0.8, RGB=102,51,0,
TRANSPARENCY=0.686275, SURF_ID='Wall'/
&OBST ID='AcDb3dSolid - 2C0', XB=0.4,0.44,-2.081668E-17,0.06,0.1,0.8,
RGB=102,51,0, TRANSPARENCY=0.686275, SURF_ID='Wall'/
&OBST ID='AcDb3dSolid - 2C0', XB=0.4,0.44,0.66,0.7,0.1,0.8, RGB=102,51,0,
TRANSPARENCY=0.686275, SURF_ID='Wall'/
&OBST ID='AcDb3dSolid - 2C0', XB=0.42,0.44,0.06,0.66,0.76,0.8, RGB=102,51,0,
TRANSPARENCY=0.686275, SURF_ID='Wall'/
&OBST ID='AcDb3dSolid - 2C0', XB=0.44,0.46,0.06,0.66,0.76,0.82, RGB=102,51,0,
TRANSPARENCY=0.686275, SURF_ID='Wall'/
&OBST ID='AcDb3dSolid - 2C0', XB=0.44.0.48,-2.081668E-17.0.06.0.1.0.82.
RGB=102,51,0, TRANSPARENCY=0.686275, SURF_ID='Wall'/
&OBST ID='AcDb3dSolid - 2C0', XB=0.44,0.48,0.66,0.7,0.1,0.82, RGB=102,51,0,
TRANSPARENCY=0.686275, SURF_ID='Wall'/
&OBST ID='AcDb3dSolid - 2C0', XB=0.46,0.48,0.06,0.66,0.78,0.82, RGB=102,51,0,
TRANSPARENCY=0.686275, SURF_ID='Wall'/
&OBST ID='AcDb3dSolid - 2C0', XB=0.48,0.54,0.06,0.66,0.78,0.84, RGB=102,51,0,
TRANSPARENCY=0.686275, SURF_ID='Wall'/
&OBST ID='AcDb3dSolid - 2C0', XB=0.48,0.56,-2.081668E-17,0.06,0.1,0.84,
RGB=102,51,0, TRANSPARENCY=0.686275, SURF_ID='Wall'/
&OBST ID='AcDb3dSolid - 2C0', XB=0.48,0.56,0.66,0.7,0.1,0.84, RGB=102,51,0,
TRANSPARENCY=0.686275, SURF_ID='Wall'/
&OBST ID='AcDb3dSolid - 2C0', XB=0.54,0.56,0.06,0.66,0.8,0.84, RGB=102,51,0,
TRANSPARENCY=0.686275, SURF_ID='Wall'/
&OBST ID='AcDb3dSolid - 2C0', XB=0.56,0.66,0.06,0.66,0.8,0.86, RGB=102,51,0,
TRANSPARENCY=0.686275, SURF_ID='Wall'/
&OBST ID='AcDb3dSolid - 2C0', XB=0.56,0.8,-2.081668E-17,0.06,0.1,0.86,
RGB=102,51,0, TRANSPARENCY=0.686275, SURF_ID='Wall'/
&OBST ID='AcDb3dSolid - 2C0', XB=0.56,0.8,0.66,0.7,0.1,0.86, RGB=102,51,0,
TRANSPARENCY=0.686275, SURF_ID='Wall'/
&OBST ID='AcDb3dSolid - 2C0', XB=0.66,0.72,0.06,0.66,0.82,0.86, RGB=102,51,0,
TRANSPARENCY=0.686275, SURF_ID='Wall'/
&OBST ID='AcDb3dSolid - 2C0', XB=0.72,0.8,0.06,0.66,0.8,0.86, RGB=102,51,0,
TRANSPARENCY=0.686275, SURF_ID='Wall'/
&OBST ID='AcDb3dSolid - 2C0', XB=0.8,0.84,0.06,0.66,0.8,0.84, RGB=102,51,0,
TRANSPARENCY=0.686275, SURF_ID='Wall'/
&OBST ID='AcDb3dSolid - 2C0', XB=0.8,0.88,-2.081668E-17,0.06,0.1,0.84,
RGB=102,51,0, TRANSPARENCY=0.686275, SURF_ID='Wall'/
&OBST ID='AcDb3dSolid - 2C0', XB=0.8,0.88,0.66,0.7,0.1,0.84, RGB=102,51,0,
TRANSPARENCY=0.686275, SURF_ID='Wall'/
```

```
&OBST ID='AcDb3dSolid - 2C0', XB=0.84,0.88,0.06,0.66,0.78,0.84, RGB=102,51,0,
TRANSPARENCY=0.686275, SURF_ID='Wall'/
&OBST ID='AcDb3dSolid - 2C0', XB=0.88,0.9,0.06,0.66,0.78,0.82, RGB=102,51,0,
TRANSPARENCY=0.686275, SURF_ID='Wall'/
&OBST ID='AcDb3dSolid - 2C0', XB=0.88,0.94,-2.081668E-17,0.06,0.1,0.82,
RGB=102,51,0, TRANSPARENCY=0.686275, SURF_ID='Wall'/
&OBST ID='AcDb3dSolid - 2C0', XB=0.88,0.94,0.66,0.7,0.1,0.82, RGB=102,51,0,
TRANSPARENCY=0.686275, SURF_ID='Wall'/
&OBST ID='AcDb3dSolid - 2C0', XB=0.9,0.94,0.06,0.66,0.76,0.82, RGB=102,51,0,
TRANSPARENCY=0.686275, SURF_ID='Wall'/
&OBST ID='AcDb3dSolid - 2C0', XB=0.94,0.96,0.06,0.66,0.76,0.8, RGB=102,51,0,
TRANSPARENCY=0.686275, SURF_ID='Wall'/
&OBST ID='AcDb3dSolid - 2C0', XB=0.94,0.98,-2.081668E-17,0.06,0.1,0.8,
RGB=102,51,0, TRANSPARENCY=0.686275, SURF_ID='Wall'/
&OBST ID='AcDb3dSolid - 2C0', XB=0.94,0.98,0.66,0.7,0.1,0.8, RGB=102,51,0,
TRANSPARENCY=0.686275, SURF_ID='Wall'/
&OBST ID='AcDb3dSolid - 2C0', XB=0.96,0.98,0.06,0.66,0.74,0.8, RGB=102,51,0,
TRANSPARENCY=0.686275, SURF_ID='Wall'/
&OBST ID='AcDb3dSolid - 2C0', XB=0.98,1.02,-2.081668E-17,0.06,0.1,0.78,
RGB=102,51,0, TRANSPARENCY=0.686275, SURF_ID='Wall'/
&OBST ID='AcDb3dSolid - 2C0', XB=0.98,1.02,0.66,0.7,0.1,0.78, RGB=102,51,0,
TRANSPARENCY=0.686275, SURF_ID='Wall'/
&OBST ID='AcDb3dSolid - 2C0', XB=0.98,1.02,0.06,0.66,0.72,0.78, RGB=102,51,0,
TRANSPARENCY=0.686275, SURF_ID='Wall'/
&OBST ID='AcDb3dSolid - 2C0', XB=1.02,1.06,-2.081668E-17,0.06,0.1,0.76,
RGB=102,51,0, TRANSPARENCY=0.686275, SURF_ID='Wall'/
&OBST ID='AcDb3dSolid - 2C0', XB=1.02,1.06,0.66,0.7,0.1,0.76, RGB=102,51,0,
TRANSPARENCY=0.686275, SURF_ID='Wall'/
&OBST ID='AcDb3dSolid - 2C0', XB=1.02,1.06,0.06,0.66,0.7,0.76, RGB=102,51,0,
TRANSPARENCY=0.686275, SURF_ID='Wall'/
&OBST ID='AcDb3dSolid - 2C0', XB=1.02,1.3,0.06,0.2,0.1,0.16, RGB=102,51,0,
TRANSPARENCY=0.686275, SURF_ID='Wall'/
&OBST ID='AcDb3dSolid - 2C0', XB=1.02,1.3,0.5,0.66,0.1,0.16, RGB=102,51,0,
TRANSPARENCY=0.686275, SURF_ID='Wall'/
&OBST ID='AcDb3dSolid - 2C0', XB=1.02,1.34,0.2,0.5,0.1,0.16, RGB=102,51,0,
TRANSPARENCY=0.686275, SURF_ID='Wall'/
&OBST ID='AcDb3dSolid - 2C0', XB=1.06.1.08.-2.081668E-17.0.06.0.1.0.74.
RGB=102,51,0, TRANSPARENCY=0.686275, SURF_ID='Wall'/
&OBST ID='AcDb3dSolid - 2C0', XB=1.06,1.08,0.66,0.7,0.1,0.74, RGB=102,51,0,
TRANSPARENCY=0.686275, SURF_ID='Wall'/
&OBST ID='AcDb3dSolid - 2C0', XB=1.06,1.08,0.06,0.66,0.68,0.74, RGB=102,51,0,
TRANSPARENCY=0.686275, SURF_ID='Wall'/
&OBST ID='AcDb3dSolid - 2C0', XB=1.08,1.1,-2.081668E-17,0.06,0.1,0.72,
RGB=102,51,0, TRANSPARENCY=0.686275, SURF_ID='Wall'/
&OBST ID='AcDb3dSolid - 2C0', XB=1.08,1.1,0.66,0.7,0.1,0.72, RGB=102,51,0,
TRANSPARENCY=0.686275, SURF_ID='Wall'/
&OBST ID='AcDb3dSolid - 2C0', XB=1.08,1.1,0.06,0.2,0.66,0.72, RGB=102,51,0,
TRANSPARENCY=0.686275, SURF_ID='Wall'/
&OBST ID='AcDb3dSolid - 2C0', XB=1.08,1.1,0.5,0.66,0.66,0.72, RGB=102,51,0,
TRANSPARENCY=0.686275, SURF_ID='Wall'/
&OBST ID='AcDb3dSolid - 2C0', XB=1.08,1.12,0.2,0.5,0.66,0.72, RGB=102,51,0,
TRANSPARENCY=0.686275, SURF_ID='Wall'/
```

```
&OBST ID='AcDb3dSolid - 2C0', XB=1.1,1.12,-2.081668E-17,0.06,0.1,0.7,
RGB=102,51,0, TRANSPARENCY=0.686275, SURF_ID='Wall'/
&OBST ID='AcDb3dSolid - 2C0', XB=1.1,1.12,0.66,0.7,0.1,0.7, RGB=102,51,0,
TRANSPARENCY=0.686275, SURF_ID='Wall'/
&OBST ID='AcDb3dSolid - 2C0', XB=1.1,1.12,0.06,0.2,0.64,0.72, RGB=102,51,0,
TRANSPARENCY=0.686275, SURF_ID='Wall'/
&OBST ID='AcDb3dSolid - 2C0', XB=1.1,1.12,0.5,0.66,0.64,0.72, RGB=102,51,0,
TRANSPARENCY=0.686275, SURF_ID='Wall'/
&OBST ID='AcDb3dSolid - 2C0', XB=1.12,1.14,-2.081668E-17,0.06,0.1,0.68,
RGB=102,51,0, TRANSPARENCY=0.686275, SURF_ID='Wall'/
&OBST ID='AcDb3dSolid - 2C0', XB=1.12,1.14,0.66,0.7,0.1,0.68, RGB=102,51,0,
TRANSPARENCY=0.686275, SURF_ID='Wall'/
&OBST ID='AcDb3dSolid - 2C0', XB=1.12,1.14,0.06,0.2,0.62,0.68, RGB=102,51,0,
TRANSPARENCY=0.686275, SURF_ID='Wall'/
&OBST ID='AcDb3dSolid - 2C0', XB=1.12,1.14,0.5,0.66,0.62,0.68, RGB=102,51,0,
TRANSPARENCY=0.686275, SURF_ID='Wall'/
&OBST ID='AcDb3dSolid - 2C0', XB=1.12,1.16,0.2,0.5,0.66,0.68, RGB=102,51,0,
TRANSPARENCY=0.686275, SURF_ID='Wall'/
&OBST ID='AcDb3dSolid - 2C0', XB=1.14,1.16,-2.081668E-17,0.06,0.1,0.66,
RGB=102,51,0, TRANSPARENCY=0.686275, SURF_ID='Wall'/
&OBST ID='AcDb3dSolid - 2C0', XB=1.14,1.16,0.66,0.7,0.1,0.66, RGB=102,51,0,
TRANSPARENCY=0.686275, SURF_ID='Wall'/
&OBST ID='AcDb3dSolid - 2C0', XB=1.14,1.16,0.06,0.08,0.6,0.66, RGB=102,51,0,
TRANSPARENCY=0.686275, SURF_ID='Wall'/
&OBST ID='AcDb3dSolid - 2C0', XB=1.14,1.16,0.62,0.66,0.66,0.66, RGB=102,51,0,
TRANSPARENCY=0.686275, SURF_ID='Wall'/
&OBST ID='AcDb3dSolid - 2C0', XB=1.14,1.16,0.08,0.2,0.6,0.68, RGB=102,51,0,
TRANSPARENCY=0.686275, SURF_ID='Wall'/
&OBST ID='AcDb3dSolid - 2C0', XB=1.14,1.16,0.5,0.62,0.6,0.68, RGB=102,51,0,
TRANSPARENCY=0.686275, SURF_ID='Wall'/
&OBST ID='AcDb3dSolid - 2C0', XB=1.16,1.18,-2.081668E-17,0.06,0.1,0.64,
RGB=102,51,0, TRANSPARENCY=0.686275, SURF_ID='Wall'/
&OBST ID='AcDb3dSolid - 2C0', XB=1.16,1.18,0.66,0.7,0.1,0.64, RGB=102,51,0,
TRANSPARENCY=0.686275, SURF_ID='Wall'/
&OBST ID='AcDb3dSolid - 2C0', XB=1.16,1.18,0.16,0.2,0.56,0.66, RGB=102,51,0,
TRANSPARENCY=0.686275, SURF_ID='Wall'/
&OBST ID='AcDb3dSolid - 2C0', XB=1.16,1.18,0.5,0.54,0.56,0.66, RGB=102,51,0,
TRANSPARENCY=0.686275, SURF_ID='Wall'/
&OBST ID='AcDb3dSolid - 2C0', XB=1.16,1.18,0.06,0.1,0.58,0.64, RGB=102,51,0,
TRANSPARENCY=0.686275, SURF_ID='Wall'/
&OBST ID='AcDb3dSolid - 2C0', XB=1.16,1.18,0.6,0.66,0.58,0.64, RGB=102,51,0,
TRANSPARENCY=0.686275, SURF_ID='Wall'/
&OBST ID='AcDb3dSolid - 2C0', XB=1.16,1.18,0.1,0.16,0.58,0.66, RGB=102,51,0,
TRANSPARENCY=0.686275, SURF_ID='Wall'/
&OBST ID='AcDb3dSolid - 2C0', XB=1.16,1.18,0.54,0.6,0.58,0.66, RGB=102,51,0,
TRANSPARENCY=0.686275, SURF_ID='Wall'/
&OBST ID='AcDb3dSolid - 2C0', XB=1.18,1.2,-2.081668E-17,0.06,0.1,0.62,
RGB=102,51,0, TRANSPARENCY=0.686275, SURF_ID='Wall'/
&OBST ID='AcDb3dSolid - 2C0', XB=1.18,1.2,0.66,0.7,0.1,0.62, RGB=102,51,0,
TRANSPARENCY=0.686275, SURF_ID='Wall'/
&OBST ID='AcDb3dSolid - 2C0', XB=1.18,1.2,0.06,0.2,0.54,0.62, RGB=102,51,0,
TRANSPARENCY=0.686275, SURF_ID='Wall'/
```

```
&OBST ID='AcDb3dSolid - 2C0', XB=1.18,1.2,0.5,0.66,0.54,0.62, RGB=102,51,0,
TRANSPARENCY=0.686275, SURF_ID='Wall'/
&OBST ID='AcDb3dSolid - 2C0', XB=1.2,1.22,-2.081668E-17,0.06,0.1,0.6,
RGB=102,51,0, TRANSPARENCY=0.686275, SURF_ID='Wall'/
&OBST ID='AcDb3dSolid - 2C0', XB=1.2,1.22,0.66,0.7,0.1,0.6, RGB=102,51,0,
TRANSPARENCY=0.686275, SURF_ID='Wall'/
&OBST ID='AcDb3dSolid - 2C0', XB=1.2,1.22,0.08,0.2,0.5,0.6, RGB=102,51,0,
TRANSPARENCY=0.686275, SURF_ID='Wall'/
&OBST ID='AcDb3dSolid - 2C0', XB=1.2,1.22,0.5,0.56,0.5,0.6, RGB=102,51,0,
TRANSPARENCY=0.686275, SURF_ID='Wall'/
&OBST ID='AcDb3dSolid - 2C0', XB=1.2,1.22,0.06,0.08,0.52,0.6, RGB=102,51,0,
TRANSPARENCY=0.686275, SURF_ID='Wall'/
&OBST ID='AcDb3dSolid - 2C0', XB=1.2,1.22,0.56,0.66,0.52,0.6, RGB=102,51,0,
TRANSPARENCY=0.686275, SURF_ID='Wall'/
&OBST ID='AcDb3dSolid - 2C0', XB=1.22,1.24,-2.081668E-17,0.06,0.1,0.58,
RGB=102,51,0, TRANSPARENCY=0.686275, SURF_ID='Wall'/
&OBST ID='AcDb3dSolid - 2C0', XB=1.22,1.24,0.66,0.7,0.1,0.58, RGB=102,51,0,
TRANSPARENCY=0.686275, SURF_ID='Wall'/
&OBST ID='AcDb3dSolid - 2C0', XB=1.22,1.24,0.18,0.2,0.46,0.58, RGB=102,51,0,
TRANSPARENCY=0.686275, SURF_ID='Wall'/
&OBST ID='AcDb3dSolid - 2C0', XB=1.22,1.24,0.5,0.6,0.46,0.58, RGB=102,51,0,
TRANSPARENCY=0.686275, SURF_ID='Wall'/
&OBST ID='AcDb3dSolid - 2C0', XB=1.22,1.24,0.06,0.18,0.48,0.58, RGB=102,51,0,
TRANSPARENCY=0.686275, SURF_ID='Wall'/
&OBST ID='AcDb3dSolid - 2C0', XB=1.22,1.24,0.6,0.66,0.48,0.58, RGB=102,51,0,
TRANSPARENCY=0.686275, SURF_ID='Wall'/
&OBST ID='AcDb3dSolid - 2C0', XB=1.24,1.26,-2.081668E-17,0.06,0.1,0.54,
RGB=102,51,0, TRANSPARENCY=0.686275, SURF_ID='Wall'/
&OBST ID='AcDb3dSolid - 2C0', XB=1.24,1.26,0.66,0.7,0.1,0.54, RGB=102,51,0,
TRANSPARENCY=0.686275, SURF_ID='Wall'/
&OBST ID='AcDb3dSolid - 2C0', XB=1.24,1.26,0.06,0.2,0.44,0.54, RGB=102,51,0,
TRANSPARENCY=0.686275, SURF_ID='Wall'/
&OBST ID='AcDb3dSolid - 2C0', XB=1.24,1.26,0.5,0.66,0.44,0.54, RGB=102,51,0,
TRANSPARENCY=0.686275, SURF_ID='Wall'/
&OBST ID='AcDb3dSolid - 2C0', XB=1.26,1.28,-2.081668E-17,0.06,0.1,0.5,
RGB=102,51,0, TRANSPARENCY=0.686275, SURF_ID='Wall'/
&OBST ID='AcDb3dSolid - 2C0', XB=1.26,1.28,0.66,0.7,0.1,0.5, RGB=102,51,0,
TRANSPARENCY=0.686275, SURF_ID='Wall'/
&OBST ID='AcDb3dSolid - 2C0', XB=1.26,1.28,0.06,0.2,0.36,0.5, RGB=102,51,0,
TRANSPARENCY=0.686275, SURF_ID='Wall'/
&OBST ID='AcDb3dSolid - 2C0', XB=1.26,1.28,0.5,0.66,0.36,0.5, RGB=102,51,0,
TRANSPARENCY=0.686275, SURF_ID='Wall'/
&OBST ID='AcDb3dSolid - 2C0', XB=1.28,1.3,-2.081668E-17,0.06,0.1,0.46,
RGB=102,51,0, TRANSPARENCY=0.686275, SURF_ID='Wall'/
&OBST ID='AcDb3dSolid - 2C0', XB=1.28,1.3,0.66,0.7,0.1,0.46, RGB=102,51,0,
TRANSPARENCY=0.686275, SURF_ID='Wall'/
&OBST ID='AcDb3dSolid - 2C0', XB=1.28,1.3,0.06,0.2,0.26,0.46, RGB=102,51,0,
TRANSPARENCY=0.686275, SURF_ID='Wall'/
&OBST ID='AcDb3dSolid - 2C0', XB=1.28,1.3,0.5,0.66,0.26,0.46, RGB=102,51,0,
TRANSPARENCY=0.686275, SURF_ID='Wall'/
&OBST ID='AcDb3dSolid - 2C0', XB=1.3,1.32,0.64,0.66,0.1,0.4, RGB=102,51,0,
TRANSPARENCY=0.686275, SURF_ID='Wall'/
```

```
&OBST ID='AcDb3dSolid - 2C0', XB=1.3,1.32,-2.081668E-17,0.2,0.1,0.42,
RGB=102,51,0, TRANSPARENCY=0.686275, SURF_ID='Wall'/
&OBST ID='AcDb3dSolid - 2C0', XB=1.3,1.32,0.5,0.64,0.1,0.42, RGB=102,51,0,
TRANSPARENCY=0.686275, SURF_ID='Wall'/
&OBST ID='AcDb3dSolid - 2C0', XB=1.3,1.32,0.66,0.7,0.1,0.42, RGB=102,51,0,
TRANSPARENCY=0.686275, SURF_ID='Wall'/
&OBST ID='AcDb3dSolid - 2C0', XB=1.32,1.34,-2.081668E-17,0.2,0.1,0.34,
RGB=102,51,0, TRANSPARENCY=0.686275, SURF_ID='Wall'/
&OBST ID='AcDb3dSolid - 2C0', XB=1.32,1.34,0.5,0.7,0.1,0.34, RGB=102,51,0,
TRANSPARENCY=0.686275, SURF_ID='Wall'/
&OBST ID='Fire', XB=0.54,0.74,0.24,0.44,0.16,0.26, SURF IDS='Burner', INERT', INERT'
&VENT ID='Mesh Vent: Mesh01-01 [XMIN]', SURF_ID='OPEN', XB=-0.52,-0.52,-
0.2,0.9,0.06,2.36/
&VENT ID='Mesh Vent: Mesh01-01 [YMAX]', SURF_ID='OPEN', XB=-0.52,-
0.36,0.9,0.9,0.06,2.36/
&VENT ID='Mesh Vent: Mesh01-01 [YMIN]', SURF ID='OPEN', XB=-0.52,-0.36,-0.2,-
0.2,0.06,2.36/
&VENT ID='Mesh Vent: Mesh01-01 [ZMAX]', SURF ID='OPEN', XB=-0.52,-0.36,-
0.2,0.9,2.36,2.36/
&VENT ID='Mesh Vent: Mesh01-01 [ZMIN]', SURF_ID='OPEN', XB=-0.52,-0.36,-
0.2,0.9,0.06,0.06/
&VENT ID='Mesh Vent: Mesh01-02 [YMAX]', SURF_ID='OPEN', XB=-
0.36,0.8,0.9,0.9,0.06,2.36/
&VENT ID='Mesh Vent: Mesh01-02 [YMIN]', SURF_ID='OPEN', XB=-0.36,0.8,-0.2,-
0.2,0.06,2.36/
&VENT ID='Mesh Vent: Mesh01-02 [ZMAX]', SURF_ID='OPEN', XB=-0.36,0.8,-
0.2,0.9,2.36,2.36/
&VENT ID='Mesh Vent: Mesh01-02 [ZMIN]', SURF_ID='OPEN', XB=-0.36,0.8,-
0.2,0.9,0.06,0.06/
&VENT ID='Mesh Vent: Mesh01-03 [YMAX]', SURF_ID='OPEN',
XB=0.8,1.56,0.9,0.9,0.06,2.36/
&VENT ID='Mesh Vent: Mesh01-03 [YMIN]', SURF_ID='OPEN', XB=0.8,1.56,-0.2,-
0.2,0.06,2.36/
&VENT ID='Mesh Vent: Mesh01-03 [ZMAX]', SURF_ID='OPEN', XB=0.8,1.56,-
0.2,0.9,2.36,2.36/
&VENT ID='Mesh Vent: Mesh01-03 [ZMIN]', SURF_ID='OPEN', XB=0.8,1.56,-
0.2,0.9,0.06,0.06/
&VENT ID='Mesh Vent: Mesh01-04 [XMAX]', SURF_ID='OPEN', XB=1.82,1.82,-
0.2,0.9,0.06,2.36/
&VENT ID='Mesh Vent: Mesh01-04 [YMAX]', SURF_ID='OPEN',
XB=1.56,1.82,0.9,0.9,0.06,2.36/
&VENT ID='Mesh Vent: Mesh01-04 [YMIN]', SURF_ID='OPEN', XB=1.56,1.82,-0.2,-
0.2,0.06,2.36/
&VENT ID='Mesh Vent: Mesh01-04 [ZMAX]', SURF_ID='OPEN', XB=1.56,1.82,-
0.2,0.9,2.36,2.36/
&VENT ID='Mesh Vent: Mesh01-04 [ZMIN]', SURF_ID='OPEN', XB=1.56,1.82,-
0.2,0.9,0.06,0.06/
&BNDF QUANTITY='WALL TEMPERATURE'/
```

&SLCF QUANTITY='TEMPERATURE', ID='Temp', PBY=0.34/

&SLCF QUANTITY='VOLUME FRACTION', SPEC_ID='OXYGEN', ID='Oxy', PBY=0.34/ &SLCF QUANTITY='VELOCITY', VECTOR=.TRUE., ID='Velocity', PBY=0.34/ &SLCF QUANTITY='TEMPERATURE', ID='Temp', PBX=1.3/ &SLCF QUANTITY='TEMPERATURE', ID='Temp', PBX=0.0/
&TAIL /